



Institut de Géophysique

**Development of a 3-D Very High-Resolution Seismic Reflection
System for Lacustrine Settings - a Case Study Over a Thrust Fault Zone
in Lake Geneva**

Thèse de doctorat

présentée à la

Faculté des Sciences de
l'Université de Lausanne

par

Maren Scheidhauer

Diplômée en Géophysique
Universität Karlsruhe (TH), Allemagne
Master of Science: Oregon State University, Les Etats Unis

Jury

Prof. Bernard Testa, Président
Prof. François Marillier, Directeur de thèse
Prof. Georges E. Gorin, Expert
Prof. Jean-Pierre Henriët, Expert
Dr. Bruno Marsset, Expert

LAUSANNE
2003

Imprimatur

Vu le rapport présenté par le jury d'examen, composé de

Président	Monsieur Prof. Bernard Testa
Directeur de thèse	Monsieur Prof. François Marillier
Rapporteur	
Experts	Monsieur Prof. Georges Gorin
	Monsieur Prof. Jean-Pierre Henriet
	Monsieur Dr Bruno Marsset

le Conseil de Faculté autorise l'impression de la thèse de

Madame Maren Scheidhauer

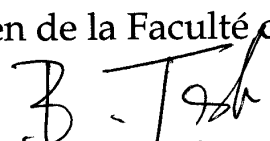
Géophysicienne diplômée de l'Université de Karlsruhe

intitulée

**Development of a 3-D Very High-Resolution Seismic
Reflection System for Lacustrine Settings - a Case Study
Over a Thurst Fault Zone in Lake Geneva**

Lausanne, le 27 juin 2003

pour Le Doyen de la Faculté des Sciences


Prof. Bernard Testa

In memory of my father

ABSTRACT

An efficient high-resolution three-dimensional (3-D) seismic reflection system for small-scale targets in lacustrine settings was developed. In Lake Geneva, near the city of Lausanne, Switzerland, past high-resolution two-dimensional (2-D) investigations revealed a complex fault zone, which was subsequently chosen for testing our system. Observed structures include a thin (<40 m) layer of subhorizontal Quaternary sediments that unconformably overlie southeast-dipping Tertiary Molasse beds and the Paudèze thrust zone, which separates Plateau and Subalpine Molasse units.

Two complete 3-D surveys have been conducted over this same test site, covering an area of about 1 km². In 1999, a pilot survey (Survey I), comprising 80 profiles, was carried out in 8 days with a single-streamer configuration. In 2001, a second survey (Survey II) used a newly developed three-streamer system with optimized design parameters, which provided an exceptionally high-quality data set of 180 common midpoint (CMP) lines in 9 days.

The main improvements include a navigation and shot-triggering system with in-house navigation software that automatically fires the gun in combination with real-time control on navigation quality using differential GPS (dGPS) onboard and a reference base near the lake shore. Shots were triggered at 5-m intervals with a maximum non-cumulative error of 25 cm. Whereas the single 48-channel streamer system of Survey I requires extrapolation of receiver positions from the boat position, for Survey II they could be accurately calculated (error <20 cm) with the aid of three additional dGPS antennas mounted on rafts attached to the end of each of the 24-channel streamers. Towed at a distance of 75 m behind the vessel, they allow the determination of feathering due to cross-line currents or small course variations. Furthermore, two retractable booms hold the three streamers at a distance of 7.5 m from each other, which is the same distance as the sail line interval for Survey I. With a receiver spacing of 2.5 m, the bin dimension of the 3-D data of Survey II is 1.25 m in in-line direction and 3.75 m in cross-line direction. The greater cross-line versus in-line spacing is justified by the known structural trend of the fault zone perpendicular to the in-line direction.

The data from Survey I showed some reflection discontinuity as a result of insufficiently accurate navigation and positioning and subsequent binning errors. Observed aliasing in the 3-D migration was due to insufficient lateral sampling combined with the relatively high-frequency (<2000 Hz) content of the water gun source (operated at 140 bars and 0.3 m depth). These results motivated the use of a double-chamber bubble-canceling air gun for Survey II. A 15 / 15 Mini G.I air gun operated at 80 bars and 1 m depth, proved to be better adapted for imaging the complexly faulted target area, which has reflectors dipping up to 30°. Although its frequencies do not exceed 650 Hz, this air gun combines a penetration of non-aliased signal to depths of 300 m below the water bottom (versus 145 m for the water gun) with a maximum vertical resolution of 1.1 m.

While Survey I was shot in patches of alternating directions, the optimized surveying time of the new three-streamer system allowed acquisition in parallel geometry, which is preferable when using an asymmetric configuration (single source and receiver array). Otherwise, resulting stacks are different for the opposite directions. However, the shorter streamer configuration of Survey II reduced the nominal fold from 12 to 6.

A 3-D conventional processing flow was adapted to the high sampling rates and was complemented by two computer programs that format the unconventional navigation data to industry standards. Processing included trace editing, geometry assignment, bin harmonization (to compensate for uneven fold due to boat/streamer drift), spherical divergence correction, bandpass filtering, velocity analysis, 3-D DMO correction, stack and 3-D time migration. A detailed semblance velocity analysis was performed on the 12-fold data set for every second in-line and every 50th CMP, i.e. on a total of 600 spectra.

According to this velocity analysis, interval velocities range from 1450-1650 m/s for the unconsolidated sediments and from 1650-3000 m/s for the consolidated sediments. Delineation of several horizons and fault surfaces reveal the potential for small-scale geologic and tectonic interpretation in three dimensions. Five major seismic facies and their detailed 3-D geometries can be distinguished in vertical and horizontal sections: lacustrine sediments (Holocene), (sub) glacio-lacustrine sediments (Pleistocene), Plateau Molasse, Subalpine Molasse and its thrust fault zone. Dips of beds within Plateau and Subalpine Molasse are $\sim 8^\circ$ and $\sim 20^\circ$, respectively. Within the fault zone, many highly deformed structures with dips around 30° are visible.

Preliminary tests with 3-D preserved-amplitude prestack depth migration demonstrate that the excellent data quality of Survey II allows application of such sophisticated techniques even to high-resolution seismic surveys. In general, the adaptation of the 3-D marine seismic reflection method, which to date has almost exclusively been used by the oil exploration industry, to a smaller scale and financial budget has helped pave the way for applying this technique to environmental and engineering purposes.

RESUME

Un système efficace de sismique tridimensionnelle (3-D) haute-résolution adapté à des cibles lacustres de petite échelle a été développé. Dans le Lac Léman, près de la ville de Lausanne, en Suisse, des investigations récentes en deux dimension (2-D) ont mis en évidence une zone de faille complexe qui a été choisie pour tester notre système. Les structures observées incluent une couche mince (<40 m) de sédiments quaternaires sub-horizontaux, discordants sur des couches tertiaires de molasse pentées vers le sud-est. On observe aussi la zone de faille de « La Paudèze » qui sépare les unités de la Molasse du Plateau de la Molasse Subalpine.

Deux campagnes 3-D complètes, d'environ d'un kilomètre carré, ont été réalisées sur ce site de test. La campagne pilote (campagne I), effectuée en 1999 pendant 8 jours, a couvert 80 profils en utilisant une seule flûte. Pendant la campagne II (9 jours en 2001), le nouveau système trois-flûtes, bien paramétrés pour notre objectif, a permis l'acquisition de données de très haute qualité sur 180 lignes CMP.

Les améliorations principales incluent un système de navigation et de déclenchement de tirs grâce à un nouveau logiciel. Celui-ci comprend un contrôle qualité de la navigation du bateau en temps réel utilisant un GPS différentiel (dGPS) à bord et une station de référence près du bord du lac. De cette façon, les tirs peuvent être déclenchés tous les 5 mètres avec une erreur maximale non-cumulative de 25 centimètres. Tandis que pour la campagne I la position des récepteurs de la flûte 48-traces a dû être déduite à partir des positions du bateau, pour la campagne II elle ont pu être calculées précisément (erreur <20 cm) grâce aux trois antennes dGPS supplémentaires placées sur des flotteurs attachés à l'extrémité de chaque flûte 24-traces. Il est maintenant possible de déterminer la dérive éventuelle de l'extrémité des flûtes (75 m) causée par des courants latéraux ou de petites variations de trajet du bateau. De plus, la construction de deux bras télescopiques maintenant les trois flûtes à une distance de 7.5 m les uns des autres, qui est la même distance que celle entre les lignes naviguées de la campagne II. En combinaison avec un espacement de récepteurs de 2.5 m, la dimension de chaque «bin» de données 3-D de la campagne II est de 1.25 m en ligne et 3.75 m latéralement. L'espacement plus grand en direction «in-line» par rapport à la direction «cross-line» est justifié par l'orientation structurale de la zone de faille perpendiculaire à la direction «in-line».

L'incertitude sur la navigation et le positionnement pendant la campagne I et le «binning» imprécis qui en résulte, se retrouve dans les données sous forme d'une certaine discontinuité des réflecteurs. L'utilisation d'un canon à air à double-chambre (qui permet d'atténuer l'effet bulle) a pu réduire l'aliasing observé dans les sections migrées en 3-D. Celui-ci était dû à la combinaison du contenu relativement haute fréquence (<2000 Hz) du canon à eau (utilisé à 140 bars et à 0.3 m de profondeur) et d'un pas d'échantillonnage latéral

insuffisant. Le Mini G.I 15/15 a été utilisé à 80 bars et à 1 m de profondeur, est mieux adapté à la complexité de la cible, une zone faillée ayant des réflecteurs pentés jusqu'à 30°. Bien que ses fréquences ne dépassent pas les 650 Hz, cette source combine une pénétration du signal non-aliasé jusqu'à 300 m dans le sol (par rapport au 145 m pour le canon à eau) pour une résolution verticale maximale de 1.1 m.

Tandis que la campagne I a été acquise par groupes de plusieurs lignes de directions alternées, l'optimisation du temps d'acquisition du nouveau système à trois flûtes permet l'acquisition en géométrie parallèle, ce qui est préférable lorsqu'on utilise une configuration asymétrique (une source et un dispositif de récepteurs). Si on ne procède pas ainsi, les stacks sont différents selon la direction. Toutefois, la configuration de flûtes, plus courtes que pour la campagne I, a réduit la couverture nominale, la ramenant de 12 à 6.

Une séquence classique de traitement 3-D a été adaptée à l'échantillonnage à haute fréquence et elle a été complétée par deux programmes qui transforment le format non-conventionnel de nos données de navigation en un format standard de l'industrie. Dans l'ordre, le traitement comprend l'incorporation de la géométrie, suivi de l'édition des traces, de l'harmonisation des «bins» (pour compenser l'inhomogénéité de la couverture due à la dérive du bateau et de la flûte), de la correction de la divergence sphérique, du filtrage passe-bande, de l'analyse de vitesse, de la correction DMO en 3-D, du stack et enfin de la migration 3-D en temps. D'analyses de vitesse détaillées ont été effectuées sur les données de couverture 12, une ligne sur deux et tous les 50 CMP, soit un nombre total de 600 spectres de semblance.

Selon cette analyse, les vitesses d'intervalles varient de 1450-1650 m/s dans les sédiments non-consolidés et de 1650-3000 m/s dans les sédiments consolidés. Le fait que l'on puisse interpréter plusieurs horizons et surfaces de faille dans le cube, montre le potentiel de cette technique pour une interprétation tectonique et géologique à petite échelle en trois dimensions. On distingue cinq faciès sismiques principaux et leurs géométries 3-D détaillées sur des sections verticales et horizontales: les sédiments lacustres (Holocène), les sédiments (sous) glacio-lacustres (Pléistocène), la Molasse du Plateau, la Molasse Subalpine de la zone de faille (chevauchement) et la Molasse Subalpine au sud de cette zone. Les couches de la Molasse du Plateau et de la Molasse Subalpine ont respectivement un pendage de ~8° et ~20°. La zone de faille comprend de nombreuses structures très déformées de pendage d'environ 30°.

Des tests préliminaires avec un algorithme de migration 3-D en profondeur avant sommation et à amplitudes préservées démontrent que la qualité excellente des données de la campagne II permet l'application de telles techniques à des campagnes haute-résolution. La méthode de sismique marine 3-D était utilisée jusqu'à présent quasi-exclusivement par l'industrie pétrolière. Son adaptation à une échelle et un budget plus petits a ouvert la voie d'appliquer cette technique à des objectifs d'environnement et du génie civil.

TABLE OF CONTENTS

ABSTRACT	I
RESUME	III
TABLE OF CONTENTS	V
LIST OF FIGURES	IX
LIST OF TABLES	XVII
ACKNOWLEDGMENTS	XX
LIST OF TERMS AND ABBREVIATIONS	XXIII
CHAPTER 1: INTRODUCTION	1
1.1 OBJECTIVE OF THIS WORK.....	1
1.2 2-D VERSUS 3-D.....	3
1.3 PROJECT MANAGEMENT	5
CHAPTER 2: 3-D SEISMIC THEORY	6
2.1 THE SEISMIC REFLECTION METHOD	6
2.1.1 The marine acquisition	6
2.1.2 The common-midpoint recording technique	6
2.1.3 Velocities and velocity analysis	8
2.1.3.1 <i>Single constant-velocity horizontal / dipping layer</i>	9
2.1.3.2 <i>Horizontally stratified earth</i>	10
2.1.3.3 <i>Hyperbolic assumption</i>	10
2.2 3-D DATA PROCESSING THEORY	11
2.2.1 Preprocessing and geometry	12
2.2.1.1 <i>3-D CMP binning or sorting</i>	12
2.2.2 Velocity analysis.....	12
2.2.3 Stacking / Migration	13
2.2.3.1 <i>NMO correction, stacking and post-stack migration</i>	13
2.2.3.2 <i>Prestack migration</i>	13
2.2.3.3 <i>Prestack partial migration (PSPM) or DMO</i>	14
2.2.3.4 <i>Azimuth, amplitude and offset considerations</i>	14
2.3 THEORY AND DESCRIPTION OF SEISMIC INSTRUMENTATION.....	15
2.3.1 Marine receiver systems	15
2.3.1.1 <i>Hydrophones</i>	15
2.3.1.2 <i>Streamers</i>	15
2.3.2 Data recording	16
2.3.2.1 <i>Temporal sampling theorem</i>	16
2.3.2.2 <i>Decibel scale and dynamic range</i>	16
2.3.2.3 <i>A/D conversion</i>	17
2.3.2.4 <i>Signal-to-noise ratio and instrument's resolution</i>	18
2.3.2.5 <i>Preamplification and instrument gain</i>	19
2.3.3 Seismic sources.....	19
2.3.3.1 <i>Air guns (explosive energy sources)</i>	20

2.3.3.2	<i>Bubble effect</i>	21
2.3.3.3	<i>G.I gun and Mini G.I</i>	21
2.3.3.4	<i>Water gun (implosive energy source)</i>	22
2.3.3.5	<i>Source signature</i>	22
2.3.3.6	<i>Far-field signature measurements</i>	25
2.3.4	Marine navigation and positioning	26
2.3.4.1	<i>Global positioning system (GPS)</i>	27
2.3.4.2	<i>Positional network</i>	28
2.3.4.3	<i>Acquisition preplots</i>	28
2.4	THREE-DIMENSIONAL SURVEY DESIGN	28
2.4.1	Seismic resolution.....	29
2.4.1.1	<i>Vertical resolution</i>	29
2.4.1.2	<i>Horizontal resolution</i>	29
2.4.2	Offset requirements	30
2.4.2.1	<i>Near offset</i>	31
2.4.2.2	<i>Far offset</i>	31
2.4.3	Spatial sampling	31
2.4.4	Acquisition Geometry.....	32
2.4.4.1	<i>Antiparallel geometry</i>	33
2.4.4.2	<i>Parallel geometry</i>	34
2.4.4.3	<i>Dip versus strike shooting</i>	34
2.4.4.4	<i>Streamer configuration</i>	35
2.4.4.5	<i>Streamer feathering</i>	35
2.4.5	Survey area	35
CHAPTER 3:	INSTRUMENT PARAMETERS	37
3.1	RESEARCH VESSEL	37
3.2	STREAMERS	37
3.2.1	Innovative Transducers Inc. solid streamer	37
3.2.2	S/N Technologies Inc. solid streamer	40
3.2.3	DC measurements on hydrophones	41
3.3	SEISMOGRAPHS	42
3.3.1	Signal amplification.....	43
3.3.2	Amplitude variations along streamers	47
3.3.3	Determination of the shot interval and shot distance	52
3.4	SEISMIC SOURCES	52
3.4.1	S15.02 Water Gun	54
3.4.2	Mini G.I Air Gun	54
3.4.3	Air consumption of all gun types – a comparison	55
3.4.4	Delay correction on seismic traces	58
3.4.4.1	<i>Recording delay</i>	59
3.4.4.2	<i>Mechanical delay</i>	59
3.4.5	The Generator-Injector (GI) delay.....	60
3.4.6	Signatures	64
3.4.6.1	<i>S15.02 Water Gun</i>	65
3.4.6.2	<i>Mini G.I G15 / I15</i>	67
3.4.6.3	<i>Mini G.I G30 / I30</i>	70

3.4.7	Concluding remarks.....	71
3.5	RETRACTABLE BOOMS FOR MULTI-STREAMER USE.....	72
3.6	NAVIGATION AND POSITIONING EQUIPMENT	76
3.6.1	Shot triggering for Survey I.....	78
3.6.2	Navigation software for Survey II.....	79
CHAPTER 4:	3-D TEST SITE AND SURVEY DESIGN	81
4.1	GEOLOGICAL SETTING.....	82
4.2	SELECTION OF TARGET AREA	83
4.3	2-D PROFILES IN TARGET AREA	85
4.3.1	2-D acquisition and processing.....	85
4.3.2	Large-scale seismic interpretation	91
4.3.3	2-D data results.....	94
4.3.3.1	<i>Vertical resolution</i>	94
4.3.3.2	<i>Penetration depth and trace length</i>	95
4.3.3.3	<i>Structural dip</i>	97
4.4	3-D SURVEY DESIGN PARAMETERS	97
4.4.1	Bin size (spatial sampling)	98
4.4.1.1	<i>Horizontal resolution</i>	99
4.4.2	Offsets.....	100
4.4.3	Survey area	100
CHAPTER 5:	3-D ACQUISITIONS	102
5.1	SURVEY I – OCTOBER 1999	102
5.1.1	Single-streamer configuration	102
5.1.2	Navigation and positioning.....	107
5.2	SURVEY II – AUGUST 2001	108
5.2.1	Multi-streamer configuration.....	109
5.2.2	Navigation and positioning.....	112
CHAPTER 6:	3-D DATA PROCESSING.....	118
6.1	PROCESSING FLOW.....	118
6.2	SEISMIC DATA INPUT AND FORMATTING (PROCESSING STEPS 1-4).....	119
6.3	PROCESSING OF NAVIGATION DATA (PROCESSING STEP 5A).....	120
6.3.1	Survey I.....	121
6.3.2	Survey II	124
6.4	GEOMETRY ASSIGNMENT (PROCESSING STEP 5B)	127
6.5	3-D BIN HARMONIZATION (PROCESSING STEP 6).....	134
6.6	VELOCITY ANALYSIS (PROCESSING STEP 7)	138
6.7	FILTERING, DMO AND STACK (PROCESSING STEP 8).....	144
6.8	POST-STACK TIME MIGRATION (PROCESSING STEP 9)	149
6.9	SUGGESTIONS FOR FURTHER PROCESSING	151

CHAPTER 7: RESULTS AND DATA EXAMPLES.....	153
7.1 COMPARISON OF SURVEY RESULTS	154
7.1.1 Penetration Depth	154
7.1.2 Vertical Resolution	157
7.1.3 Horizontal Resolution.....	160
7.1.3.1 <i>Navigation effects</i>	163
7.2 PRESERVED AMPLITUDE PRESTACK DEPTH MIGRATION	165
7.3 GEOLOGICAL INTERPRETATION	170
7.3.1 Paudèze Fault zone and Plateau Molasse	173
7.3.2 Plateau Molasse	184
7.3.3 Subalpine Molasse.....	185
7.3.4 Glacial and post-glacial sediments	186
CHAPTER 8: SUMMARY, CONCLUSIONS AND OUTLOOK	188
8.1 SUMMARY	188
8.1.1 Streamer configuration	188
8.1.2 Seismic source	189
8.1.3 Navigation and positioning.....	190
8.1.4 The test site	191
8.1.5 Survey area	191
8.1.6 Acquisition geometry	192
8.1.7 Survey direction.....	192
8.1.8 Data processing.....	193
8.1.9 Data quality.....	194
8.1.10 Geological interpretation	195
8.2 CONCLUSIONS	196
8.3 OUTLOOK	197
REFERENCES	200
APPENDIX.....	205
ACQUISITION STATISTICS.....	205
Survey I.....	205
Survey II	208

LIST OF FIGURES

- Fig. 1-1. 2-D seismic reflection method (a) and its extension to 3-D (b), adapted from Tacchini and Zingg (2000). _____ 4
- Fig. 1-2. Model demonstrating 3-D reflection effects on a single 2-D profile. _____ 4
- Fig. 2-1. CMP recording technique (a) shot gather showing different midpoints (M) between the same shot (S) and different geophones (G) along a profile; (b) CMP gather: traces from different shots and geophones sorted around their *common midpoint* (CMP = M). In case of a horizontal reflector, the *common depth point* (CDP) is the vertical projection of the CMP; adapted from Macfarlane et al. (1989). ____ 7
- Fig. 2-2. Scattering of reflection points due to dip ϕ , G = receiver location; S = source location; offset $x = \overline{SG}$; D = zero-offset depth point; D' = actual reflection point; M = midpoint at surface; M' = midpoint corresponding to reflection point D'; $d = \overline{DD'}$; $m = \overline{MM'}$; h = zero-offset distance to reflector; A = migration aperture; z = depth of reflection point D'. _____ 8
- Fig. 2-3. Conflicting dips: (a) Reflection raypaths of three source-receiver offsets from a flat event intersected by a dipping one at equal zero-offset distances h ; (b) zero-offset section (c) CMP gather around midpoint M with two hyperbolas at the same zero-offset traveltime t_0 (equation (2.1)) but different stacking velocities v and $v/\cos\theta$ for the horizontal and dipping reflector, respectively. _____ 9
- Fig. 2-4. Quantizing example: a 3-bit converter with a reference voltage of 8 V and a quantizer step of 1 V can represent 8 quantizing levels; from Dodds (2002). ____ 18
- Fig. 2-5. Schematic functioning of an air gun by M. Gros. _____ 21
- Fig. 2-6. Near field (left) and far-field (right) signature (pressure over time) by M. Gros. 23
- Fig. 2-7. Far-field signature test geometry. The time delay between the primary and ghost reflection arrival depends on water velocity and the distance ΔD , adapted from Fricke et al. (1985). _____ 24
- Fig. 2-8. Derivation of the first Fresnel zone's diameter ω for a coincident source and receiver and a horizontal reflector. The wavefront arrives first at reflection point O at the center and after a distance of $\lambda/4$ at A and A' at the edge of a disk where reflecting points cannot be distinguished, adapted from Yilmaz (1987). _____ 30
- Fig. 2-9. Two adjacent boat passes; solid lines indicate streamers, stippled lines source tracks; lines connecting sources with the farthest receivers are the shot-to-receiver offsets for the outer midpoint lines; dots represent CMP positions; (a) parallel geometry; (b) antiparallel geometry; from Vermeer (2001). _____ 33
- Fig. 2-10. Asymmetric recording (a) updip – wavefront arrives at similar times at receivers $G_1 - G_3$; (b) downdip – wavefront builds significant angle with surface and arrives at different times at receivers. _____ 34
- Fig. 2-11. The 3-D aperture window frame; A_i : aperture in in-line; A_c : aperture in cross-line direction. _____ 36
- Fig. 3-1. Research vessel “La Licorne”: (a) front view showing covered compressor; (b) rear view showing storage of streamers onboard and crane. _____ 37
- Fig. 3-2. Streamer sections: (a) deployment of ITI Stealtharray with floats (b) enlarged float; (c) orange Nexgen S/N Technologies section rolled on deck together with lead-ins (greenish), deck cable on roof (orange) and drogue rope (blue), two yellow ITI sections and yellow old lead-in; (d-e) configuration during streamer tests in March 2001: ITI sections towed port and starboard, S/N section in center; floats and GPS rafts keep streamers near surface; tail buoys are attached to each tail section. _____ 38

- Fig. 3-3. Estimation of streamer shape during 2-D acquisition in November 1998 using 55 m of lead-in cable, 120 m of total streamer and a tail buoy attached to the 2.5 m tail section. _____ 39
- Fig. 3-4. Schematic of DC measurements on each hydrophone. _____ 41
- Fig. 3-5. Seismographs: (a) 22-bit GEOMETRICS StrataView R series used for Survey I; (b) 20-bit BISON Spectra used for Survey II. _____ 43
- Fig. 3-6. Saturation induced by the presence of a DC. Dashed line indicates the instrument's saturation level; (a) no amplification; (b) amplified signal; (c) amplification with DC results in signal saturation. _____ 44
- Fig. 3-7. BISON saturation test with a DC pulse superimposed on a sinusoidal current. If the DC exceeds 15 mV at 60 dB, the BISON is saturated and no more measurement is possible. _____ 44
- Fig. 3-8. Signature measurements (section 3.4.6) with interconnected ITI streamer sections vertically below Mini G.I G30 / I30 Air Gun source (section 3.4.2). This shot gather was recorded at 60 dB and a GI delay of 48 ms (see section 3.4.5). Arrows and rectangles point at zones where signal clipping is visible. _____ 45
- Fig. 3-9. Constant gain test shots with Mini G.I G15 / I15 Air Gun source in multi-streamer configuration. Example gathers recorded at 24 dB with either (a) a 4 Hz or (b) a 40 Hz low-cut filter applied and (c) at 60 dB plus a low-cut at 40 Hz (saturation for direct wave). _____ 46
- Fig. 3-10. Noise tests with all three streamer sections in multi-streamer configuration recorded at 36 dB with (a) lead-in fixed directly to the vessel and (b) usage of bungee cord for lead-in attachment. Frequency spectra compare noise levels on both streamer types (c) of the data in (a) and on the S/N section (d) with and without bungee cord application on the data in (a) + (b). _____ 48
- Fig. 3-11. Mean absolute amplitude (blue line) of each hydrophone from both interconnected ITI streamers sections superimposed on common offset stack (fold 241) of bandpass filtered data set 1, calculated between (a) 0-130 ms: including the direct wave and (b) 120-250 ms: above the water bottom reflection. _____ 50
- Fig. 3-12. Mean absolute amplitude of each hydrophone superimposed on common offset stack (fold 306) of bandpass filtered data set 2 (multi-streamer acquisition), calculated between (a) 0-130 ms including the direct wave, (b) 120-250 ms: above the water bottom reflection and (c) 120-250 ms: without application of bandpass filter. _____ 51
- Fig. 3-13. S15.02 (15 in³) Water Gun (a); double chamber bubble canceling Mini G.I Air Gun with a total maximum volume of 60 in³ (b). _____ 53
- Fig. 3-14. Compressed air supply: (a) air production – Cirrus three phase compressor; (b) air storage at maximum 280 bars in four 50-l bottles placed inside the research vessel; (c) firing box that triggers the guns and is electrically connected to the seismograph; for details see Appendix Fig. A-3; (d) control panel for air supply regulation between (a), (b) and guns; for detailed description see Appendix Fig. A-2. _____ 53
- Fig. 3-15. Air consumption for a 3-D survey of 300 shots per in-line and a shot interval of 4 s; the total number of lines per day depends on ship turning time as in equation (3.5) for a 7 h working day (dark blue curve) and on the net air consumption as in equation (3.6); the three source types are shown: the water gun operated at 140 bars (green) and the Mini G.I G15 / I15 (red) and G30 / I30 (light blue) operated at 80 bars. Arrows in corresponding colors indicate how to find the maximum total number of lines for any turning time. Average values found for Survey I and II are highlighted (see Table A-3 and Table A-5). _____ 57

- Fig. 3-16. Recording delay Δt_{record} determined by the phase shift of the recorded sinusoid; table lists results of a test series with different sampling rates on the BISON seismograph. _____ 59
- Fig. 3-17. *GI delay* = time between electric trigger pulses; time between generator and injector blast as actually measured on the gun hydrophone, is a combination of the *mechanical delays* of generator (10 ms) and injector (6 ms) and should correspond to half the bubble period $T/2$, adapted from SODERA (1995). _____ 61
- Fig. 3-18. Amplitude spectrum up to 100 Hz measured on the gun hydrophone of the Mini G.I G15 / I15 with generator only. The inverse of the bubble frequency gives a bubble period of 50.8 ms. _____ 62
- Fig. 3-19. Pulse-to-bubble ratio (PBR) for Mini G.I G15 / I15 with respect to *GI delay* on the firing box. Measured values (at 106 m depth) are represented by blue triangles while the red curve indicates their mean. Signature was recorded at 12 dB. ____ 64
- Fig. 3-20. Pulse-to-bubble ratio (PBR) for Mini G.I G30 / I 30 with respect to *GI delay* set at firing box. Measured values (at 107 m depth) are represented by blue triangles while the red curve indicates their mean. Signature was recorded at 60 dB and signal is saturated even at greater depths. _____ 64
- Fig. 3-21. Far field *unfiltered* signature of the S15.02 Water Gun measured on trace 21 at 107 m depth with a recording gain of 24 dB (SI = 0.25 ms; GEOMETRICS): (a) time-domain signal and (b) its amplitude spectrum. Signature developed to 99.4%.
66
- Fig. 3-22. Near field *unfiltered* signature of Mini G.I G15 / I15 measured on gun hydrophone with a recording gain of 12 dB (SI = 0.5 ms, BISON) (a) with generator only, (b) with the optimum *GI delay* of 28 ms, (c) amplitude spectrum of (a) and (b). The difference in primary amplitude and amplitude levels in the spectrum are due to a reduced signal repetitivity in the near-field. _____ 68
- Fig. 3-23. Far field *unfiltered* signature of Mini G.I G15 / I15 measured on trace 23 at 106 m depth with a recording gain of 12 dB (SI = 0.5 ms, BISON) (a) with generator only, (b) with the optimum *GI delay* of 28 ms, (c) amplitude spectrum of (a) and (b). _____ 69
- Fig. 3-24. Far field *unfiltered* signature of Mini G.I G30 / I30 measured on trace 20 at 107 m depth with a recording gain of 60 dB (SI = 0.5 ms, BISON). Because the time-domain signal is clipped at peak amplitudes, an amplitude spectrum was not computed. _____ 71
- Fig. 3-25. Construction plan of (a) two retractable booms attached to each side of the ship with the aid of (b) a clutch and tow hook system and (c) whose outer ends are fixed on a raft. _____ 74
- Fig. 3-26. Retractable boom specially constructed for Survey II: (a) in acquisition mode, towing one of the three streamers; (b) close-up view of the raft that keeps the boom on the water surface and of the ropes that maintain it at a 90° angle relative to the side of the boat; (c) in transportation mode the booms are attached to the side of the boat. _____ 76
- Fig. 3-27. GPS antennas and navigation monitoring for Survey I (a) dGPS and radio receiver for boat position and GPS for navigation monitored on the Gamin GPS screen; and for Survey II (b) Leica dGPS antenna and radio receiver – current boat position is displayed by new navigation program on laptop (see section 3.6.2). _77
- Fig. 3-28. dGPS raft: (a) its dimension and (b) in use attached to the end of the streamer. _78
- Fig. 3-29. New navigation program GPS_shot v. 1.0; (a) acquisition preplot (see section 2.3.4.3) of all 60 navigation lines of Survey II and (b) navigation monitoring while aiming at target; top of window shows current ship speed and target

- bearing, lateral deviation from target line, number of satellites used and accuracy with which coordinates are determined. _____ 79
- Fig. 4-1. Simplified geological map of the area around Lake Geneva, Switzerland, showing a major thrust fault zone separating Plateau and Subalpine Molasse units; adapted from Weidmann (1988). _____ 81
- Fig. 4-2. Structure map and a schematic lithostratigraphic cross-section (vertical throw not considered) of the area around the city of Lausanne, modified from Weidmann (1988). Fault zone extensions into the lake are taken from Vernet et al. (1974). The conventional German abbreviations of the four listed molasse groups are given in parenthesis. _____ 82
- Fig. 4-3. Northwestern limit of the Paudèze Fault (red triangles) as interpreted by Morend (2000) on a grid of 2-D profiles acquired within the area indicated by a black rectangle; the average trend of the fault zone (solid red line) allows calculation of the future 3-D survey direction perpendicular to the average fault zone strike (dashed red line at 322.25° relative to geographical north); acquisition preplots of Survey I (yellow) and Survey II (black) are centered about the fault zone (for more details see chapter 5). _____ 84
- Fig. 4-4. Location of 2-D profile 140_30 (green, Fig. 4-7), lake traverse 140_15 a-d (red portions a and b are shown in Fig. 4-8) and 3-D survey site. Faults and structures on land are taken from the geological map of Weidmann (1988). Fault extensions into the lake (light blue) were interpreted by Vernet et al. (1974). _____ 86
- Fig. 4-5. Interval velocity distribution over in-line 142 extracted from the 3-D model in section 6.6. The 2-D profiles, which correspond to in-line 140, are located only 7.5 m southwest of in-line 142. _____ 87
- Fig. 4-6. 2-D profile 140_w (sail line 55 of Survey I), recorded with the S15.02 Water Gun. Real amplitudes were preserved and data are presented with a vertical exaggeration of 2 when using an average velocity of 2300 m/s for the imaged portion of the Plateau Molasse. Structural dips within the upper molasse beds and the Quaternary sediments (<350 ms) might thus be exaggerated while dips in the lower beds (>450 ms) might be too small. (a) Near-trace section, (b) stack and (c) post-stack time migration (Kirchhoff). For line location, see Fig. 4-4. _____ 88
- Fig. 4-7. 2-D post-stack time migrated (Kirchhoff) profiles 140_15a and 140_15b, recorded with the Mini G.I G15 / I15 Air Gun, showing the typical seismic signature observed in the 3-D survey area and much further to the southeast. CMP numbers are given relative to the 3-D survey grid for comparison. (a) Real amplitudes were preserved and data are presented with a vertical exaggeration of 2 when using an average velocity of 2300 m/s for the imaged portion of the Plateau Molasse. Structural dips within the upper Molasse beds and the Quaternary sediments (<350 ms) might thus be exaggerated while dips in the lower beds (>450 ms) might be too small. The signal at 590 ms is due to electrical noise of the BISON seismograph. (b) Interpretation of Plateau Molasse and Subalpine Molasse units separated by the Paudèze Fault zone and covered by glacial and post-glacial sediments. Within the Subalpine Molasse further southeast, the Lutrive Fault separates the steeply dipping "Molasse rouge" from the "Molasse à charbon". Still further southeast, lithology is not identified. The average fault dips as well as the dip of beds in all identified Molasse units are indicated in the interpreted section. For line location, see Fig. 4-4. Colors correspond to those in Fig. 4-2. Fig. 4-9 illustrates the interpretation in map view. _____ 89
- Fig. 4-8. 2-D post-stack time migrated (Kirchhoff) profile 140_30, recorded with the Mini G.I G30 / I30 Air Gun, showing the typical seismic signature observed in the 3-D

- survey area. CMP numbers are given relative to the 3-D survey grid for comparison. (a) Real amplitudes were preserved and data are presented without vertical exaggeration when using an average velocity of 2300 m/s for the imaged portion of the Plateau Molasse. Structural dips within the upper Molasse beds and Quaternary sediments (<350 ms) might thus be exaggerated while dips in the lower beds (>450 ms) might be too small. (b) Interpretation of Plateau Molasse and Subalpine Molasse units separated by the Paudèze Fault zone and covered by glacial and post-glacial sediments. The average dips for Plateau and Subalpine Molasse beds as well as the maximum fault dip are indicated below the interpreted section. For line location, see Fig. 4-4. Colors correspond to those in Fig. 4-2. Fig. 4-9 illustrates the interpretation in map view. _____ 90
- Fig. 4-9. Interpretation of fault locations from 2-D profiles and inferred lithostratigraphy. Colors on land correspond to those in Fig. 4-2 – their lighter counterparts signify the same lithology but extrapolated into the water. Black triangles indicate fault positions interpreted by Morend (2000) (see Fig. 4-3) and Chaudhary et al. (2002) (dashed grey profiles) while light blue lines designate fault locations from Vernet et al. (1974). The red triangles mark the position of faults as from profile 140_15a (Fig. 4-7). _____ 93
- Fig. 5-1. Single-streamer configuration of Survey I. _____ 103
- Fig. 5-2. Sketch of ship track pattern for Survey I including ship turns (dotted). Antiparallel geometry leads to patches of alternating direction. Colors indicate different acquisition days (see also Table A-2); patches of same color and same line thickness (thin lines from NW to SE, thick lines from SE to NW) were acquired under similar conditions – weather, currents, towing direction. _____ 106
- Fig. 5-3. Location map showing onboard dGPS position of every 2nd shot point for all 80 acquisition lines of Survey I; every 20th point is labeled. _____ 108
- Fig. 5-4. Multi-streamer configuration of Survey II. _____ 111
- Fig. 5-5. Ship tracks for Survey II with colors indicating different acquisition days (see also Table A-5); patches of same color were acquired under similar conditions – weather, currents; the towing direction is the same for all navigation lines due to full turns as shown on navigation line 60. _____ 113
- Fig. 5-6. Location map showing onboard dGPS position of every 2nd shot point for all 60 acquisition lines of Survey II; every 20th point is labeled. _____ 115
- Fig. 5-7. 3-D survey site showing navigated start and end points of each sail line (light blue and black) superimposed on theoretical preplots for Survey I (dark blue) and Survey II (red). Green line indicates location of 2-D profiles 140_15 and 140_30 located on sail line 55 (Survey I) or 37 (Survey II). _____ 116
- Fig. 6-1. Simplified 3-D processing flowchart used for Survey I and II. The number in front of each processing step indicates the corresponding Géovecteur job sequence. Details on modules and parameters used in those jobs are listed in Table A-18 for Survey I and in Table A-20 for Survey II. _____ 119
- Fig. 6-2. Chart showing streamer shapes for all 242 shots of a selected sail line (line 30). _____ 123
- Fig. 6-3. Shot positions (thin contour / red) and far offset receiver positions (heavy contour / green) for selected sail lines (even lines 26-46). Every 10th shot number is labeled along the source contour, and every 20th shot number is labeled (bold) along the receiver contour. Note how well the far offset hydrophone followed the course of the gun that was towed only 10 m behind the vessel when calculating receiver positions using imaginary compasses along the streamer. _____ 125

- Fig. 6-4. Stacking fold for each bin without (right) and with (left) application of flex binning for Survey I. Color palette was adapted to associate the nominal fold of 12 with green, low fold with yellow and high fold with red. _____ 137
- Fig. 6-5. Stacking fold for each bin without (right) and with (left) application of flex binning for Survey II. Color palette was adapted to associate the nominal fold of 6 with green, low fold with yellow and high fold with red. This way the improved navigation of Survey II compared to that of Survey I becomes obvious. _____ 138
- Fig. 6-6. Semblance velocity spectrum of CMP 420 on LINE 83 after DMO correction. Colors represent the semblance value from blue (low) to red (high). Superimposed on the spectrum are seven predefined velocity functions that serve as guides and the actually picked rms velocity function (squares). The corresponding interval velocities are shown on the right hand side (black line with squares). _____ 140
- Fig. 6-7. Representation of the rms velocity model in three dimensions composed of three in-lines (LINEs 42 - see Fig. 6-8 (a), 1st panel - 100 and 150), four cross-lines (CMPs 220, 400, 600 and 800) and two time slices (at 380 and 410 ms, see Fig. 6-9 (a), 1st and 4th panel). The model cube is oriented approximately with respect to geographical north. _____ 141
- Fig. 6-8. Example (a) rms and (b) interval velocity distributions along every 20th LINE. The superimposed black lines on in-line 42, 122 and 202 indicate the approximate northeastern limit of the fault zone and the inclination of molasse beds. Areas in white correspond to the water layer where no velocities were picked. See Fig. 6-9 for orientation of sections. _____ 142
- Fig. 6-9. Example (a) rms and (b) interval velocity distribution when cutting the 3-D model along constant times at intervals of 10 ms. The black line on slices 310, 360 and 410 ms indicates the approximate northeastern limit of the fault zone. Areas in white correspond to the water layer where no velocities were picked. Slices are oriented at the correct angle relative to geographic north. _____ 143
- Fig. 6-10. Frequency spectra of Survey I (S15.02 Water Gun) calculated on the entire trace from 250-470 ms at offset 7.5 m (black) and at offset 120 m (red), displayed in absolute amplitude (a), (b) and linear dB (c), (d). In (b) and (d) a low cut filter had been applied cutting off frequencies below 40 Hz and attenuating those between 40 and 60 Hz. _____ 146
- Fig. 6-11. Frequency spectra of Survey II (Mini G.I G15 / I15) calculated on the entire trace from 250-470 ms at offset 7.5 m (black) and at offset 60 m (red), displayed in absolute amplitude (a), (b) and linear dB (c), (d). In (b) and (d) a low cut filter had been applied cutting off frequencies below 40 Hz and attenuating those between 40 and 60 Hz. _____ 147
- Fig. 6-12. Final stacked section of LINE 102 of Survey I using the zero-dip velocity model and an accurate mute library (a) without and (b) with harmonized bins on input. Arrows indicate DMO artifacts due to a lack of coverage. _____ 148
- Fig. 6-13. Final stacked section of LINE 102 of Survey II using the zero-dip velocity model and an accurate mute library (a) without and (b) with harmonized bins on input. Arrows indicate DMO artifacts due to a lack of coverage. _____ 149
- Fig. 7-1. Interpretation of fault locations from 2-D and 3-D surveys and inferred lithostratigraphy (see Fig. 4-9). Black triangles indicate fault positions interpreted by Morend (2000) and Chaudhary et al. (2002) (dashed grey profiles). Small red triangles mark the limit of the Paudèze Fault zone as interpreted from Survey II while the large red triangle designates the position of the Lutrive Fault as deduced from profile 140_15a (Fig. 4-7). _____ 153

- Fig. 7-2. 3-D time migrated data cube of Survey I with several in-lines, cross-lines and times slices exposed. Vertical exaggeration 2. _____ 155
- Fig. 7-3. 3-D time migrated data cube of Survey II with several in-lines, cross-lines and times slices exposed. Vertical exaggeration 2. _____ 155
- Fig. 7-4. In-line 182 presents an example of penetration depth difference between (a) the S15 Water Gun (reflections in the Plateau Molasse beds down to 430 ms (~350 m)) and (b) the Mini G.I G15 / I15 Air Gun with reflections deeper than 500 ms (>430 m). _____ 156
- Fig. 7-5. In-line 96 shows an example of vertical resolution difference. Although the vertical resolution within the sediments for Survey I (a) is better than that for Survey II (b), the S15 Water Gun was not sufficiently energetic to clearly image the small thrust fault within the Plateau Molasse which is revealed by the Mini G.I G15 / I15. _____ 158
- Fig. 7-6. Time slices at 310 ms (a) and (b) and 340 ms (c) and (d) for Survey I and Survey II, respectively. The white dashed line in (d) indicates interpreted Paudèze Fault trace. _____ 159
- Fig. 7-7. The water bottom picked from the time migrated data of Survey II (a). The water bottom from Survey I (grey) is superimposed on the water bottom of (a) where it was picked at shallower depths and at less detail (b) than in Survey II. Location of LINE 74 (Fig. 7-8) and position of the trough centered about CMP 500 is indicated by the arrow and red rectangle. _____ 161
- Fig. 7-8. In-line 74 presents an example of horizontal resolution – the dashed rectangle frames an area with a channel that was not resolved during Survey I (a) but is visible in the data of Survey II (b). The location of LINE 74, the red arrow and the zone of the rectangle is indicated in Fig. 7-7. _____ 162
- Fig. 7-9. Zoom on a portion of 3-D time migrated LINE 58 (a) extracted from the data cube of Survey I and (b) from that of Survey II. The water bottom reflection picked in (b) was projected onto the section in (a). The true water bottom is indistinguishable from the earlier reflection energy due to incorrect 3-D migration. The black line indicates the location of cross-line 635 of Fig. 7-10. _____ 164
- Fig. 7-10. 3-D time migrated cross-line 635 (a) from the data cube of Survey I and (b) from that of Survey II. The water bottom reflection picked in (b) was projected onto the section in (a) where the water bottom is discontinuous and difficult to identify due to coarser spatial sampling. Incorrectly migrated energy, as was recognized on LINE 58 in Fig. 7-9, appears over a range of about 30 in-lines. Black line indicates location of in-line 58 of Fig. 7-9. _____ 166
- Fig. 7-11. Coverage for all 60 sail lines and each of the 24 offsets including the contribution of all three streamers of Survey II. Light blue indicates anomalously low coverage – those offsets contain weak or dead traces (trace 3 on S/N streamer section, trace 13 on ITI #2, and trace 24 on ITI #1, see section 3.3.2). _____ 167
- Fig. 7-12. The rms velocity model for stack and post-stack time migration has been converted to depth and surface distance, then smoothed, and finally padded beyond the survey area bounds (red dashed lines) in order to be used for prestack depth migration. _____ 168
- Fig. 7-13. Comparison of (a) post-stack time migration with (b) preserved amplitude prestack depth migration on in-line 125. _____ 169
- Fig. 7-14. Comparison of (a) post-stack time migration with (b) preserved amplitude prestack depth migration on cross-line 680 of Survey II. _____ 170
- Fig. 7-15. Comparison of three different migration algorithms applied to (a) profile 140_15 and LINE 140 of Survey II (b) and (c): (a) 2-D Kirchhoff time migration; (b) 3-D

- one-pass time migration in the frequency - space; and (c) 3-D preserved amplitude prestack depth migration (PAPsDM). All data are presented with a vertical exaggeration of 2. _____ 171
- Fig. 7-16. Time slice at 390 ms of Survey II (a), presenting the survey cube oriented with respect to the geographical north and location of all vertical sections displayed in Fig. 7-16 through Fig. 7-18 (solid black lines), as well as in previous figures (dashed lines). The orientation of the arbitrary line of Fig. 7-22 is indicated in blue. (b) Example of in-line 40 (uninterpreted and interpreted data). _____ 174
- Fig. 7-17. Example of in-line 80 (a) and 120 (b) (uninterpreted and interpreted data). See color scheme in Fig. 7-17 (a). _____ 175
- Fig. 7-18. Example of in-line 160 (a) and 200 (b) (uninterpreted and interpreted data). See color scheme in Fig. 7-17 (a). _____ 176
- Fig. 7-19. Times slices (uninterpreted) of Survey II taken every 10 ms. For orientation of the survey area, see Fig. 7-16 (a). _____ 177
- Fig. 7-20. Times slices of Survey II extracted every 10 ms with an interpretation of the different seismic facies. For survey orientation, colors and numbers, see Fig. 7-16 (a). _____ 178
- Fig. 7-21. Fault surfaces and horizon A (MGL) in 3-D representation (a) looking from west to east and (b) from east to west. The solid red line indicates the curved Paudèze Fault trace as seen on horizon A. The dashed red line highlights the axis along which the bedding dip changes – true dips are represented by red arrows. Numbers correspond to seismic facies. _____ 179
- Fig. 7-22. Arbitrary vertical section cut through the data cube perpendicular to the strike of MGL beds. The dip changes by about 5° along the axis indicated by the red dashed line. For line location, see Fig. 7-16 (a). _____ 181
- Fig. 7-23. Map of the top of the Plateau and Subalpine Molasse units in three dimensions with fault traces of the Paudèze Fault and fault B. Their map coordinates are shown in Fig. 7-1. Red arrows indicate the east-west trend of an escarpment and a topographic high and low. _____ 182
- Fig. 7-24. Contour maps at the top of the Plateau Molasse (PM) with location of the Paudèze Fault trace deduced from Survey II (red crosses) and from Morend (2000) beyond the survey limits (black triangles). The locations of the escarpment at the lake bottom and the interpreted axis of dip change in horizon A are superimposed on the PM contours. _____ 183
- Fig. A-1. Connections of batteries to deck cable (a) Survey I: single streamer configuration - both interconnected ITI streamer sections mounted on ITI deck cable; (b) Survey II: multi-streamer configuration – both ITI streamer sections and S/N section connected to each of the three branches of the S/N deck cable. Color code indicates which streamer (streamer position) corresponds to what channels on the recording seismograph, see also Fig. 5-4. _____ 211
- Fig. A-2. Detailed description of air flow through the control panel and its connection to the compressor, storage bottles and seismic sources. _____ 211
- Fig. A-3. The firing box (precision ~ 0.25 ms) and its connection to (a) the Geometrics or (b) the BISON seismograph and to either water (Survey I) or air gun (Survey II). _____ 212

LIST OF TABLES

Table 3-A. Results of DC measurements. The code refers to indications on the deck-cable pins that connect to the seismograph. Values behind the slash are results of repeated measurements after addition of capacitors to channels indicated in grey. 42	
Table 3-B. Air production / consumption and its influence on the total number of shots per single 2-D profile for all three gun types: S15.02 Water Gun and Mini G.I G15 / I15, G30 / I30 Air Gun. _____	56
Table 3-C. Arrival time delay $\Delta t_{arrival\ time}$ for each gun type determined using equation (3.7), in which arrival times were measured at 5 m distance from the source and a water velocity of 1450 m/s was used. _____	59
Table 3-D. Theoretical (equation (3.8)) and empirical bubble periods for different generator volumes, operating pressures and gun depths. _____	61
Table 3-E. Signal and bubble amplitude, pulse-to-bubble ratio (PBR), delay measured between generator and injector blast with respect to different <i>GI delays</i> during far-field signature tests with the Mini G.I G15 / I15. Last two columns present the measured <i>GI delay</i> using the relationship in Fig. 3-17 and its difference to the <i>GI delay</i> set on the firing box. Columns highlighted in grey are plotted in Fig. 3-19. 63	
Table 4-A. Frequency bandwidth of each type of seismic source after bandpass filtering (white), respective dominant frequency (grey), corresponding wavelength and vertical resolution within the post-glacial sediments. The wavelength was calculated assuming a velocity of 1500 m/s and no absorption of high frequencies. Values related to the dominant frequency are highlighted in grey. _____	95
Table 4-B. Penetration times and depth in three different zones for the water layer, the Quaternary (Q) sediments and the Molasse (M) unit. Depths were calculated using average interval velocities of 1450, 1550 and 2300 m/s, respectively. The penetration time/depth below the water bottom is indicated by Q+M (grey), while “Total” stands for the total penetration time/depth measured from the water surface. _____	96
Table 4-C. Largest possible bin size dX_{bin} or dY_{bin} (equations (2.21) or (2.22)) depending on structural dip α_{max} or β_{max} and highest unaliased frequency f_{max} . For a predefined bin size of 1.25 m, green indicates no aliasing, red aliasing for the air gun assuming frequencies beyond 650 Hz are filtered out; red and orange mean aliasing would occur for the water gun assuming frequencies beyond 1700 Hz are filtered out. _____	98
Table 4-D. Highest unaliased frequency f_{max} (equations (2.23) or (2.24)) depending on structural dip α_{max} or β_{max} and spatial sampling interval dX_{bin} or dY_{bin} . Red indicates combinations of interval and dip that would result in aliasing for both gun types while orange highlights aliasing only for the water gun; green stands for no aliasing. _____	98
Table 5-A. Acquisition parameters of Survey I. _____	117
Table 5-B. Acquisition parameters of Survey II. _____	117
Table 6-A. Trace header assignment at different processing stages. There is a total of 64 header words. Presented are only the most frequently used. It is indicated either whether a trace header content existed since recording (raw data) or if not, in which job it was firstly assigned. Either the newly assigned value is given or an X when the previously assigned value was kept . _____	120

Table 6-B. Table showing the correspondence between sail lines and CMP lines of Survey I and of Survey II after geometry assignment and grid origin definition. Highlighted is in-line 140, which corresponds to the location of the 2-D profiles in section 4.3.	133
Table 7-A. List of seismic facies analyzed within the 3-D survey area, adapted from Beres et al. (2003); PM = Plateau Molasse; SM = Subalpine Molasse, USM = Lower Freshwater Molasse.	172
Table 7-B. Geological timechart with lithology of the northern Alpine foreland basin and lithostratigraphy of Plateau and Subalpine Molasse as interpreted in the Lausanne area (Weidmann, 1988). Numbers in parenthesis refer to seismic facies of Table 7-A and colors correspond approximately to those already used in all previously interpreted sections.	173
Table A-1. Relationship between number of bits of the recording instrument (n), binary system level, total number of quantizing levels, theoretical dynamic range ($n*6\text{dB}$), and theoretical S/N ratio (in dB). Highlighted are the 20-bit and 22-bit values of the BISON and GEOMETRICS seismographs (section 3.3), respectively.	205
Table A-2. Accumulation of information concerned with line navigation time, turning time and compressed air consumption gathered from all acquisition sheets of Survey I. Exceptional turning times underlain in dark grey are not included in mean calculation. Air consumption is considered separately with the compressor off (dark grey) or on (light grey). Line names underlain in dark grey were repeated later.	207
Table A-3. Table showing statistics on acquisition time and total number of lines per day as well as the total and the mean of the whole Survey I (excluding values in grey).	208
Table A-4. Accumulation of information concerned with line navigation time, turning time and compressed air consumption gathered from all acquisition sheets of Survey II. Exceptional values underlain in dark grey are not included in mean calculations. Line names underlain in dark grey were repeated later.	209
Table A-5. Table showing statistics on acquisition time and total number of lines per day as well as the total and the mean of the whole Survey II (last day excluded from mean calculation).	210
Table A-6. Acquisition sheet of S15.02 Water Gun far-field signature test.	213
Table A-7. Acquisition sheet of Mini G.I G15 / I15 far- and near-field signature test including gun hydrophone measurements; page 1, 2 and 3.	214
Table A-8. Acquisition sheet of Mini G.I G30 / I30 far-field signature test including near-field measured on gun hydrophone; page 1 and 2.	215
Table A-9. Acquisition preplot: theoretical start and end points for all 80 sail lines of Survey I calculated perpendicular to the average fault zone direction – 322.25° relative to geographical north.	216
Table A-10. Acquisition preplot: theoretical start and end points for all 60 sail lines of Survey II calculated perpendicular to the average fault zone direction – 322.25° relative to geographical north.	217
Table A-11. Acquisition sheets of 2-D lake traverse, profile 140_15 portions a-d, shot with the Mini G.I G15 / I15 along extension of sail line 140 towards the southeast and northwest of Survey II.	220
Table A-12. Acquisition sheet of Mini G.I G30 / I30 2-D profile 140_30 along sail line 55 of Survey I.	221

-
- Table A-13. 2-D processing sheets for profile 140_30 using GéovecteurPlus. Gray areas indicate parameter differences between this profile and profile 140_15 and 140_w. 221
- Table A-14. Navigated start and end points for all 80 sail lines of Survey I, indicating acquisition direction between those points, corresponding shot point numbers and total number of shot points per line. 222
- Table A-15. Navigated start and end points for all 60 sail lines of Survey II, indicating acquisition direction between those points, corresponding shot point numbers and total number of shot points per line. 223
- Table A-16. Acquisition sheet of sail line 5, the first navigation line of 3-D Survey I. 224
- Table A-17. Acquisition sheet of sail line 1, the first navigation line of 3-D Survey II. 224
- Table A-18. 3-D processing sheets 1-6 for Survey I using GéovecteurPlus. Gray areas indicate parameter differences between Survey I and II. 227
- Table A-19. EGRID / HABIN coverage table for Survey I. For each sail line, the minimum and maximum CMP and LINE number are indicated that were assigned in EGRID. On this basis, the input files to the subsequent two bin harmonization jobs (job *habin*, step 6, Table A-18) were chosen. 228
- Table A-20. 3-D processing sheets 1, 2-6 for Survey II using GéovecteurPlus. Gray areas indicate parameter differences between Survey I and II. 231
- Table A-21. Example of a UKOOA P1/90 file showing the ship, tail buoy, shot and receiver positions for the first two shot points of Survey II. Line name and the shot number are highlighted in grey. This file is the result of processing step 5A in Table A-20. 232
- Table A-22. ASPRO spreadsheet for job *shift3D*, step 4 (Table A-20) of Survey II. The sail line number is represented by register #1#, the number of the last test shot to delete by register #2#. 233
- Table A-23. EGRID / HABIN coverage table for Survey II. For each sail line, the minimum and maximum CMP and LINE number are indicated that were assigned after EGRID. On this basis, the input files to the subsequent two bin harmonization jobs (job *habin3D*, step 6, Table A-20) were chosen. 234
- Table A-24. Navigation Processing for Survey I in form of a separate instruction document. 235
- Table A-25 Navigation processing for Survey II: FORTRAN 77 code *gvt3Dnav*. 255

ACKNOWLEDGMENTS

First of all, I would like to express my gratitude to my thesis advisor Prof. *François Marillier*, who gave me the opportunity to work on this fascinating and versatile subject, for his continuous support and constructive advice. Thank you very much to the three experts Prof. *Georges E. Gorin* from the University of Geneva, Prof. *Jean-Pierre Henriet* from the Renard Center of Geology (University of Gent, Belgium), Dr. *Bruno Marsset* from the French Institute for Marine Research and Exploitation (IFREMER, Brest, France) and the president Prof. *Bernard Testa* for accepting to be on my thesis committee.

I would like to acknowledge *Willem Versteeg* (University of Gent) for helping with the initial acquisition phases of the project and the F.-A. Forel Institute of the University of Geneva, for providing the ship (*La Licorne*), two pilots (*Ivan Christinet*, *Philippe Arpagaus*), their GEOMETRICS seismograph for Survey I, the dGPSs and access to some previous lake data (Dr. *Didier Morend*). Dr. *André Pugin* built the firing box, kindly provided the triggering software for Survey I, participated in some of the test measurements and was always at hand with good advise. *Philippe Logean* not only developed the new high-accuracy positioning and gun-firing system for Survey II as well as a program for later navigation processing, but he also was always immediately available to assist with every imaginable computer problem. *Pierre-Yves Gilliéron* from the Geomatic Institute of the Swiss Federal School of Technology, Lausanne (EPFL), generously lent us several dGPS receivers and *Yannick Levet* processed the raw navigation data. *Roger Wolfgang* designed and built together with *David Dupuy* the GPS rafts, the retractable booms and along with *André Rosselet* helped during numerous instrument testing, installation and maintenance of the seismic equipment. *Francis Perret* sketched or finalized some of the figures representing the 3-D system and the data cubes. I also thank *Imran Chaudhary*, *Mathieu Beck*, *Jochen Bihn*, *Emmanuel Marclay*, *Olivier Nigg*, *Gilles Tacchini* and *Olivier Zingg* for participating in the data acquisition.

A special thank you to all members of the Géovecteur user support group at the Compagnie Générale de Géophysique (CGG), i.e. *Pascal Thi Baolong*, *Nadine Gros*, *Agnès Moreau*, *Jean-Bernard Favreau*, *Laurent Baurens*, *Christian Maistorovitch*, *Brigitte Pruniaux*, *Christian Dheur*, *Kees Pabbuwee*, *Gilbert Pernot* and *François Rascalou*, as well as *Alain Thevenot* from SERCEL and the trainers from CEFOGA (*Luc Tondeur*, *Haydn Gould*, *David Williamson* and *Jean-Pierre Heberard*), who never became tired of answering my endless questions over the years. I am extremely grateful to *Pierre Pinvidic* (CGG) with whom I had the pleasure to collaborate and who invested numerous overtime hours to help me solve the problems with our non-conventional navigation data. Thank you to *Alain Le Bras* (Data processing & Reservoir Services, Senior Sales Director) and *Raoul Lehman* (Head of Massy Processing Center) for allowing my two stays at CGG's processing center in Massy in order to work with Pierre on the navigation data. The KINGDOM Suite that I used for 3-D

data interpretation was kindly provided free of charge by Micro Seismic Technology. Furthermore, I am very grateful to *Philippe Thierry* and the Ecole des Mines for making available and running their preserved amplitude prestack depth migration code (PAPsDM) on our 3-D data cube and the great collaboration. I owe a big thank you to *Michel Gros* from SODERA who not only helped throughout the design and acquisition phase with very useful advice, but who took the time to revise and comment the chapters on marine seismic sources. In *Christof Müller* from Kiel University I found a resourceful interlocutor on 3-D marine seismic acquisition. He developed a Matlab program to improve our onboard quality control. *Richard Pearce* and *Eric Boyer* from S/N Technologies contributed with their technical know-how in person and in personal communication to the success of this work.

Especially, I would like to thank Dr. *Milan Beres*, my office and project mate during Survey I. Together we tested our seismic equipment, learned Géovecteur and attended training courses in London and Lausanne. Milan performed the very tedious detailed velocity analysis. He has always been very patient and open for questions and continued helping even after the end of his post-doc at the University of Lausanne. The same special thanks are due to *David Dupuy*, my doctoral partner with whom I prepared and carried out Survey II and all related test measurements, who organized the GPS antennas, their raw data processing and who took big part in the planning and development of the retractable booms, its floats and the GPS rafts. His energetic involvement in all technical matters of the data acquisition was invaluable. He created the location and geological maps and some of the other figures, helped with poster presentations and was always available for discussion. *Claire Odello*, my new office mate, kindly and patiently spent her time finding solutions to several unconventional processing problems using Géovecteur. I am also very grateful to *Ludovic Baron* who wrote a Matlab program in order to visualize the three-dimensional velocity model.

The pleasant atmosphere at the Geophysical Institute made working here very agreeable. So thank you to Prof. *Raymond Olivier* and Prof. *Dominique-Marie Chapellier*, to Dr. *Pierre Gex*, *Bertrand Dumont*, *Michèle Ruf*, *Cristina Spillmann*, and *Pascale Zbinden*. My sincere gratitude also goes to all colleagues and friends who shared the time during my Ph.D. studies: *Francine Gass*, *Youcef Hacini*, *Issaka Issoufou*, *Laurent Marescot*, *Pedro Martinez*, *Régis Monnet*, *Manhiar Pasaribu*, *Steven Rochat*, *Alberto Rosselli*, and especially *Francesco Bruno* and *PierVittorio Radogna* – merci mille fois à tout le monde! A big thank you to *Gisèle Bazzuri-Delémont*, my French teacher for four years, who continuously improved my skills, which are so necessary for my work and life in “Suisse Romande”.

I would also like to address a word of gratitude to my friends from Lausanne and from all over the world for their continuous support and encouragement: *Laurence* and *Simon Bradley*, *Céline Dupuy*, *David* and *Diana Rueda*, *Carrie Hall*, *Lynne David*, *Tamara Pokrovskaja*, *Jörg Müller*, *Heidi Doose-Rolinski*, *Bärbel Traub*, *Hanna-Maria Rumpel* and *Alexander Goertz*, just to name a few. A special thank you goes to *Bernadette* and *Milan*

Beres as well as to *James DeRose* who in their spare time proofread several chapters. Very precious to me is the deep friendship to my sister *Ellen* and the unlimited trust and love I experience from my mother and the rest of my family (*Christa, Rüdiger, Charlotte, Renate, Helmut, Jochen, Irmgard, Volkmar, Christiane, Kai* and *Rolf*). Last but not least I owe a lot to *Jochen*. Without his love and patience, his advice and understanding even over long-distances, I could not have found the strength for the sacrifices and long working hours that have led to this thesis.

The Swiss National Science Foundation funded this project with grants 21-49710.96/1 and 20-54505.98/1. With financial aid from the “Fondation Herbette” of the University of Lausanne we purchased a more powerful SUN workstation which was used for processing (including 3-D migration) the data from survey II.

LIST OF TERMS AND ABBREVIATIONS

2-D	two-dimensional
3-D	three-dimensional
AGC	automatic gain control
AC	alternating current or air consumption of a seismic energy source (in NI/min or NI/shot)
AD	compressed air deposit in the storage bottles (in NI)
AVA	amplitude versus angle
AVO	amplitude versus offset
A/D converter	analog-to-digital converter
Antiparallel geometry	adjacent sail lines have opposite direction
AP	average air production rate of a compressor (in NI/min)
Arrival time delay = t_{delay}	The difference between the mechanical delay and the recording delay, which depends on gun type and recording instrument
Asymmetric system	single-source and receiver array
Bin	a bin is a rectangular area around one midpoint with the extensions dX_{bin} in in-line and dY_{bin} in cross-line direction
Bin harmonization	duplication of traces from neighboring bins into bins where they are missing
CDP	common depth point
CMP	common mid point
CMP-line = in-line	the line along which CMPs are situated that correspond to the same streamer – for a single-streamer survey sail line and <i>in-line</i> are identical, while for a multi-streamer survey, the <i>in-line</i> lies half way between streamer and source positions.
Cross-line	line perpendicular to the in-lines along the same CMP position
CVS	constant velocity stacks
DC	direct current
DGPS	differential GPS
DMO	dip moveout

Dominant frequency = f_{dom}	the reciprocal of the predominant period in the signature of a seismic source
Downdip	the streamer points in down dip direction
ENOB	Effective Number of Bits
G.I gun	a bubble-canceling air gun using two chambers: the generator (G) and the injector (I)
GI delay = t_{GI}	the time between electrical pulses that trigger the generator and the injector of the Mini G.I gun. It has to be adjusted to the generator's chamber volume, to the gun depth and to the operating pressure
GPS	global positioning system
Harmonic mode	generator and injector chambers of a G.I gun have the same volume
In-line = CMP-line	the line along which CMPs are situated that correspond to the same streamer – for a single-streamer survey sail line and <i>in-line</i> are identical, while for a multi-streamer survey, the <i>in-line</i> lies half way between streamer and source positions.
IFP	instantaneous floating point – a type of gain
Interval velocity = v_{int}	medium velocity between two reflectors
ITI	Innovative Transducers Inc., Texas, U.S.A., company that sold solid streamer sections
K-gain	preamplification: the amplification is set to a fixed amount so that the highest amplitude of interest in the received signal is recorded without being clipped
LSB	Least Significant Bit
Mechanical delay	A delay due to the reaction of the gun to the electrical trigger pulse. This time delay between triggering and actual firing is caused by mechanical friction of the gun components
Medium velocity = v_{medium}	velocity of the medium above the reflector
MC	Molasse à charbon
Mini G.I G15 / I15	SODERAs Mini G.I Air Gun with chamber volumes of 15 in ³
Mini G.I G30 / I30	SODERAs Mini G.I Air Gun with chamber volumes of 30 in ³

MGL	Molasse grise de Lausanne
Migration velocity	zero-dip velocity used within migration algorithm – equal to the <i>medium</i> (for one reflector) or <i>rms velocity</i> above the concerned reflector
NAC	net air consumption: air consumption (AC) of the energy source minus air production (AP) of the compressor
Navigated line = sail line	the line or profile along the ship track
Nl	normal liter; air flow is often stated in normal liters per minute (Nl/min). A normal liter is the volume of a liter of air at a pressure of about 1 atmosphere (\cong 1 bar) at a standard temperature of 0° or 20°C (Rowlett, 2001).
NMO	normal moveout
NMO velocity = v_{NMO}	velocity required to correct for normal moveout
Offset = x	distance between source and receiver
OMM	Upper Marine Molasse
Parallel geometry	all sail lines are in one direction
PBR = signal shape	pulse-to-bubble ratio; ratio between the main pulse and the bubble oscillation of an explosive energy source
PM	Plateau Molasse
Preplot	shows the beginning and ending coordinates for each planned sail line
PSPM	prestack partial migration
PAPsDM	preserved amplitude prestack depth migration
Pseudo 3-D	A dense grid of 2-D profiles not sufficiently close to adequately sample the first Fresnel zone
PTP = signal strength	the energy source's pulse peak-to-peak amplitude
Recording delay	a delay inherent to the seismograph
Rms velocity = v_{rms}	<i>NMO velocity</i> for zero-dip under the small-spread hyperbolic assumption
S15.02	SODERAs S15.02 Water Gun
Stacking velocity = $v_{stacking}$	dip dependant velocity derived directly from CMP data
Sail line = navigated line	the line or profile along the ship track
signal shape = PBR	pulse-to-bubble ratio; ratio between the main pulse and the bubble oscillation of an explosive energy source

Signal strength = PTP	the energy source's pulse peak-to-peak amplitude
SI	sampling interval
SM	Subalpine Molasse
S/N ratio	signal-to-noise ratio
Symmetric system	source and receiver array
True GI mode	the injector chamber of a G.I gun has about double the size (x 2.33) of the generator chamber
TWT	two-way traveltime
Updip	the streamer points in updip direction
UHR	ultra high-resolution – using frequencies of several kHz
UMM	Lower Marine Molasse
USM	Lower Freshwater Molasse
VHR	very high-resolution – using frequencies up to about 1000 Hz

CHAPTER 1: INTRODUCTION

1.1 Objective of this work

Very high resolution (VHR) marine seismics utilizes frequencies up to about 1000 Hz and reaches a vertical resolution of less than a meter. This technique is widely used both in the field of engineering geophysics as well as in geological and environmental site investigations. While two-dimensional (2-D) surveys became common practice, three dimensional (3-D) acquisitions, which involve complex field and processing procedures, are still mainly carried out by the exploration industry using much lower frequencies. From the geophysical point of view (acquisition and processing) but also from that of a geologist (interpretation), any target is in reality three dimensional and should be treated as such (see section 1.2). Numerous examples from hydrocarbon exploration proved that 3-D seismic reflection surveys, especially in geologically complex areas, are more appropriate than 2-D surveys for accurately imaging small-scale geological changes. A “true” 3-D survey adequately samples the target both in in-line and cross-line direction and allows migration in three dimensions of the whole data cube without spatial aliasing. Very often, even a dense grid of 2-D profiles only provides “pseudo” 3-D images, when profile spacing was too large for lateral continuity (Müller et al., 2002).

The adaptation of the 3-D marine technique to very high-frequency seismic investigations requires the down-scaling of the industry standard both geographically and financially and concerns the equipment, the survey design and the processing algorithms. Several institutes have been working on the development of such systems in recent years. At the beginning of the 1990s, the Renard Centre of Marine Geology (University of Gent, Belgium) constructed a relatively simple VHR acquisition system called “SEISCAT” composed of 12 dual-channel microstreamers attached to a catamaran, which is towed by a research vessel (Henriet et al., 1992). This system used a Boomer (EG&G Uniboom) and a modified water gun source (dominant frequencies of about 700 Hz) for imaging a small clay diapir (60 m in diameter) under the river Schelde in Antwerp. Due to tidal action with amplitudes of up to 5.5 m, special processing techniques were necessary and bin sizes of 1 m² required very accurate navigation (Marsset et al., 1998). Despite good results, the data were not of optimum quality due to a low sampling rate, coverage difficulties and positioning restrictions. A new compact 3-D ultra high resolution (UHR - multi-kHz) acquisition system (“Opus3D”) was designed for studies in shallow water (<30 m), providing limited penetration of less than 50 m below the water bottom (Missiaen et al., 2002). This system consists of a central rigid inflatable boat flanked by two inflated modular wings towing eight dual-channel 7.5 m long streamers and was tested on the same small diapir target using an electrodynamic Boomer source (SEISTEC) with a dominant frequency range of 2-3 kHz.

Marsset et al. (2002) from the French Institute for Marine Research and Exploitation (IFREMER) proposed a 3-D VHR acquisition system for sites of limited extent (2 km x 1 km), such as dams, artificial island sites, pipeline routes on the continental shelf in water depths up to 100 m and target vertical resolutions of 1 m. They used a Sparker and Boomer source in combination with four 6-channel streamers at 4 m distance and with a hydrophone spacing of 2 m. Due to the limited streamer length in this and also in the above SEISCAT and Opus3D systems, it is impossible to perform a velocity analysis directly on these data. An additional longer streamer 2-D survey is necessary to obtain the required detailed velocity model, especially important for complex targets.

The Institute of Marine Research at Kiel University (Germany) performed a high-frequency survey in the Baltic Sea using a system composed of a Boomer source (dominant frequency about 500 Hz) and two longer streamers towed with 15 m between them, one consisting of 12, the other of 48 channels with a group spacing of 3.8 m and 2 m, respectively (Müller et al., 2002). Their target was a fluvial channel system and shallow gas accumulations beneath unconsolidated sediments in the southern Kiel Bay. Due to limited maneuverability of the vessel at sea conditions, the inter-profile distances between two parallel ship tracks varied between 15 m and 35 m. This cross-line spacing was often inadequate with aliasing requirements which does not make it a “true” 3-D survey. Furthermore, it was difficult to stack the data because of the unconventional streamer geometry.

Whether high or ultra high-resolution short offset multi-streamer 3-D measurements in rivers or at shallow sea, or multi-channel dual-streamer surveys at high temporal resolution but of limited penetration, they represent configurations chosen with respect to the specific environment. The main objective of this work is to combine their advantages and to build a “true” 3-D multi-channel *and* multi-streamer system adapted to small-scale three-dimensional targets in lake environments such as river deltas, complex fault zones, etc. Because lakes have no tidal action, neither strong currents nor swell noise from waves and may have water depths of several hundred meters (late arrival of multiple energy), they form the ideal site in order to evaluate the capabilities of very high-resolution 3-D seismic reflection imaging while relative dimensions of design parameters come closest to those of the exploration realm. The system was designed to avoid spatial aliasing of the target horizons and to have a direct control on stacking and migration velocities. By using a lower frequency air gun (frequency bandwidth centered on 330 Hz), some of the vertical resolution of the above systems is traded off for a higher penetration down to several hundred meters below the water bottom. This reduces the risk of spatial aliasing for steeply dipping structures in the near surface, increases the required minimum distance between streamers and allows the imaging of targets at a wider range of depths.

Past high-resolution 2-D investigations (Morend, 2000) in Lake Geneva, Switzerland, revealed a complex thrust fault zone near the city of Lausanne that is well suited for 3-D

studies (see section 4.2), and which was chosen for testing our system. To resolve the stratigraphic and structural complexity within this fault zone and to demonstrate the interpretability of the acquired data cube represents a secondary goal of this project.

The work of this thesis is exceptionally versatile and challenging for it combines *all* different components of the seismic method:

- Dimensioning or design and construction of all necessary equipment
- Target selection and choice of instrumental parameters
- Instrument testing
- Data acquisition
- 3-D data processing
- Data interpretation.

In practice, the project's realization faces many obstacles, such as insufficient accuracy of vessel navigation, variable weather conditions, technical problems and construction imperfections of equipment, management of large seismic data volumes, adaptation of data processing and interpretation software to small sampling rates, just to mention some examples. However, these challenges were met by a large series of preparatory tests followed by the acquisition or development, adaptation and improvement of new components that were added to the pilot system.

As a first approach, we conducted a single-streamer 3-D survey (Survey I) on the chosen site in 1999. Less than two years later, in 2001, the newly developed "true" 3-D system with three 24-channel streamers and integrated differential GPS positioning was used for a second survey (Survey II) on the same site.

1.2 2-D versus 3-D

The seismic reflection method uses an energy source to produce an acoustic wave (Fig. 1-1 (a), more details in section 2.1). This wave travels first through water and is then transmitted and reflected at all interfaces of media with different densities and seismic velocities (acoustic impedance). The reflected waves of these layer interfaces are recorded at the water surface with receivers called hydrophones. A certain number of hydrophones are arranged at a fixed distance to each other inside a cable towed behind the research vessel. This cable is called a streamer. In general, the boat advances along a straight line, a so-called profile. Processing of the recorded data of one such profile allows to build a 2-D image of the subsurface under the assumption that all reflections came from the vertical plane below the acquisition line.

For 3-D measurements, we would also need data perpendicular (*cross-line*) to the direction of this profile, the *in-line* direction (Fig. 1-1 (b)). This can be done by shooting many closely spaced parallel 2-D profiles (see also section 2.1.1).

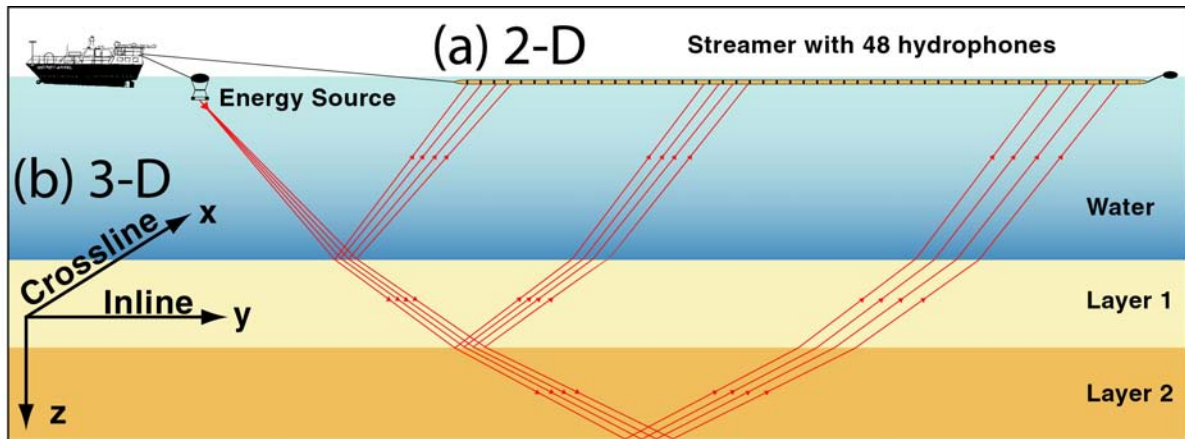


Fig. 1-1. 2-D seismic reflection method (a) and its extension to 3-D (b), adapted from Tacchini and Zingg (2000).

Fig. 1-2 demonstrates that recorded reflections do not always come from structures within the vertical plane of the profile. They can be caused by inclined surfaces on both sides of it. In this example, reflections come from a dome situated off-plane. If we had only this one 2-D profile, it would be impossible to correctly interpret reflections coming from this structure.

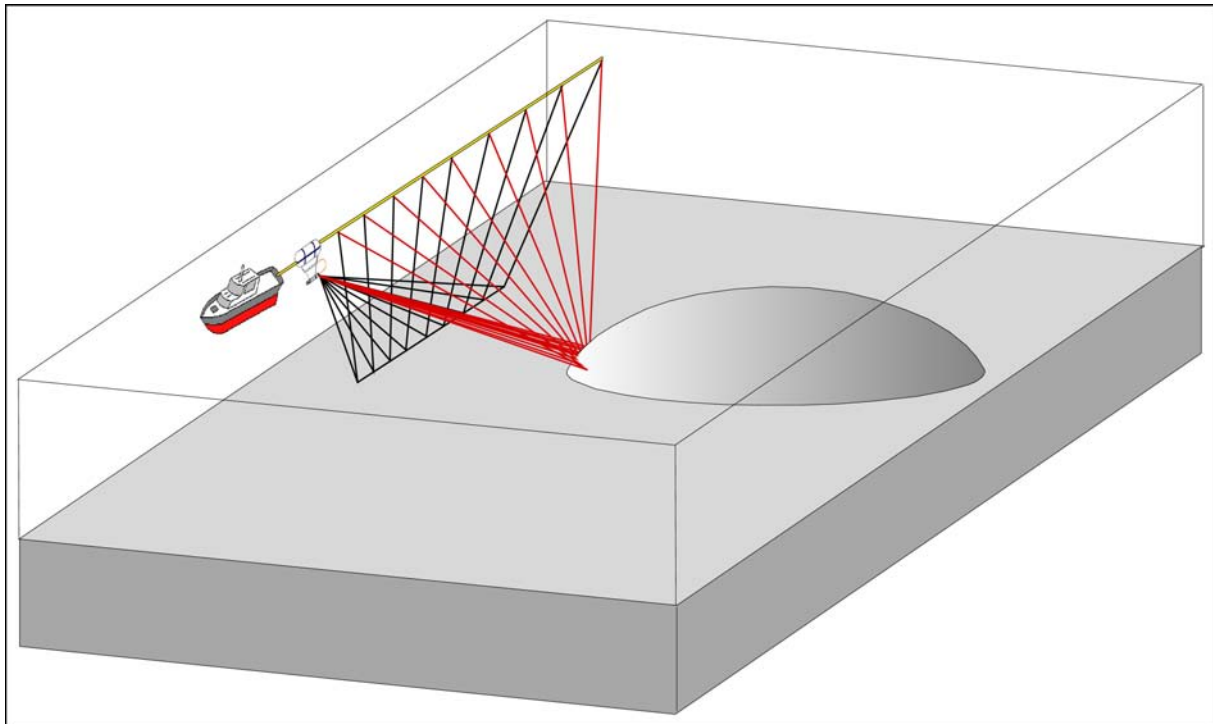


Fig. 1-2. Model demonstrating 3-D reflection effects on a single 2-D profile.

Migration is a data processing step (section 2.2.3) that repositions reflections to their true location in the subsurface. A 2-D migration, a process that considers only the 2-D plane, would interpret the side reflections from the dome as an existing structure beneath the profile. A 3-D migration instead would use the information from nearby parallel profiles, to find the

dome's true geometry. Here lies the main advantage of the 3-D seismic method since 3-D structures require 3-D measurements and 3-D migration for accurate imaging.

1.3 Project management

As mentioned above, this research project possesses exceptional versatility and requires expertise in a large spectrum of different domains. What normally is the work of a whole team of specialists in the exploration industry supported by consulting and service companies, is here united in the objective of one thesis: the development of a very high-resolution 3-D seismic reflection system for lake studies on a university budget. For the Institute of Geophysics at the University of Lausanne, this project meant not only extending the seismic method to the third dimension, but represented the beginning of applied marine or better lacustrine research within the seismic working group. Since this document focuses on the geophysical aspects of the developed 3-D system, it was often difficult to pay tribute to the other components that were crucial to the success of this project. Besides survey design, acquisition, processing, interpretation and presentation of the 3-D data, it was necessary to purchase or rent, test and improve the seismic equipment, design and construct parts of the system, choose, acquire, install and learn the appropriate software, handle and archive large volumes of data, upgrade hardware and adapt every element to non-standard dimensions. This multi-task work thus required much improvisation, management, problem solving and communication of ideas.

In the following chapter (*Chapter 2*), I summarize the most important theory utilized in this project before focusing on the seismic equipment and the instrument parameters in *Chapter 3*. *Chapter 4* presents the geological setting of Lake Geneva and the chosen 3-D test site as well as two 2-D profiles which link this area to the surrounding geology. The 3-D systems used for Survey I and Survey II are introduced in *Chapter 5* including a summary of all acquisition parameters and details on boat and streamer positioning. *Chapter 6* deals with the complete 3-D processing sequence of navigation and seismic data. The resulting two 3-D data cubes are presented in *Chapter 7*. They give examples of various aspects of data quality, a comparison of both surveys with respect to the changed acquisition design, some preliminary results of a prestack depth migration and a first geological interpretation of the surveyed area. Finally, a discussion and conclusions of the main results are given in *Chapter 8* followed by an outlook on the project's possible continuation. The Appendix offers some practical and very specific details on the employment of the instruments, on the acquisitions as well as on the complete processing sequence including the different codes for navigation data formatting.

CHAPTER 2: 3-D SEISMIC THEORY

2.1 The seismic reflection method

3-D seismic surveying involves four discrete stages: *survey design and planning*, *data acquisition*, *data processing* and *data interpretation*. The fundamentals of the marine seismic method, data processing and instrumental constraints are described first, in order to better understand their influence on the various components of survey design and planning an optimum acquisition. Often it is referred to exploration industry standard, representing the marine model of the seismic technique, to which we would like to down-scale and adapt our high-resolution lacustrine system.

2.1.1 The marine acquisition

In the marine environment data are commonly acquired using a parallel or anti-parallel geometry (see section 2.4.4.2), in which source and receiver lines are straight and parallel. The source is attached behind the research vessel and receivers (single or groups of hydrophones or traces) are arranged on one or several parallel cables (single or multi-streamer configuration) that are towed at a fixed offset with respect to the source. The ship's position is typically monitored by radionavigation or GPS (see section 2.3.4), so that shots can be fired at the desired location. Marine versus land records have the advantage of being relatively noise-free (no groundroll, no strong airwave, etc.) and thus have a high signal-to-noise ratio, although the presence of swell noise can severely reduce data quality. In lacustrine settings, however, this broad and deep undulation of the water surface plays generally no role.

During the early days of 3-D data acquisition, the exploration industry recorded data using a single vessel, a single streamer and a single energy source (Evans, 1997). Each *sail line* or *navigated line* produced one line of subsurface coverage, i.e. an *in-line* or *CMP-line*. If many closely spaced parallel lines are recorded, a 3-D volume of data is produced. Vessel turning between lines took almost the same time as the line shooting itself. In order to increase productivity, multi-streamer and multi-source surveys were introduced during the late 1980s (Evans, 1997).

2.1.2 The common-midpoint recording technique

The common midpoint method is the recording technique universally used in land seismic surveys. The same concept forms the basis for marine acquisitions although its realization is more delicate. The incident wave of a fired shot (S) is reflected from a subsurface boundary and recorded at several receivers (G) on the surface to form a *shot gather*. The point at half the distance between S and G is called *midpoint* M. When geologic layering is horizontal, reflection points lie midway between the source and the receiver position on the reflecting horizon (Fig. 2-1 (a)). As shown in Fig. 2-1 (b), a reflection point

can be the *common depth point* (CDP) for a whole family of source-receiver offsets, with the same *common midpoint* (CMP).

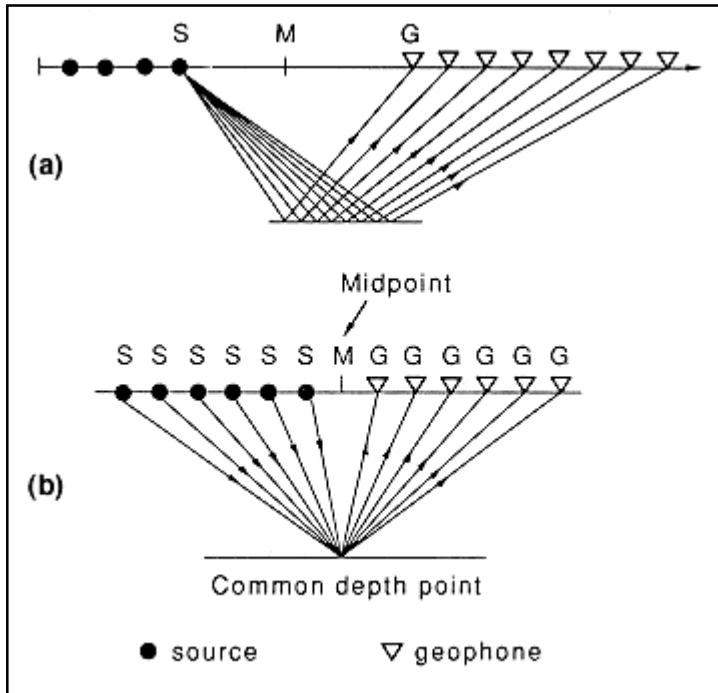


Fig. 2-1. CMP recording technique (a) shot gather showing different midpoints (M) between the same shot (S) and different geophones (G) along a profile; (b) CMP gather: traces from different shots and geophones sorted around their *common midpoint* (CMP = M). In case of a horizontal reflector, the *common depth point* (CDP) is the vertical projection of the CMP; adapted from Macfarlane et al. (1989).

The collection of traces having a *common midpoint* is called *CMP gather*. The number (N) of traces in such a gather is called its *fold*. During data

processing (section 2.2) when these traces are corrected for NMO (section 2.2.3.1) and then summed, the resulting stacked trace has a signal-to-noise ratio that is improved by the factor of \sqrt{N} , if noise is truly random (Sheriff and Geldart, 1982). The recording of shot gathers (shot-receiver coordinates) in a way that allows subsequent sorting into CMP gathers (midpoint-offset coordinates) is referred to as the *common midpoint recording technique*.

When layering is not horizontal, reflection points on the reflecting horizon projected to the surface no longer coincide with the midpoint (CMP). CDP gathers and CMP gathers are equivalent only when the earth is horizontally stratified. Fig. 2-2 shows a single dipping reflector and the reflection point of one source-receiver pair (S-G), while Fig. 2-3 illustrates its extension to a CMP gather of three pairs with different offsets around midpoint M. This midpoint remains common to all three pairs, while their depth points move up-dip with greater offset. D represents the zero-offset depth point (Fig. 2-2) that is assumed to be the reflection point for a whole gather around M in conventional NMO processing. Since D' is the real reflection point, M' should be the actual zero-offset surface position. Levin (1971) showed that the distance *d* along the dipping reflector between D and reflection point D', which depends on the source-receiver offset *x*, as well as the distance *m* between M and M' along the surface can be expressed as follows (see Fig. 2-2 for definition of variables):

$$d = \frac{x^2}{4h} \sin \phi \cos \phi \quad \text{and} \quad m = \frac{d}{\cos \phi} = \frac{x^2}{4h} \sin \phi$$

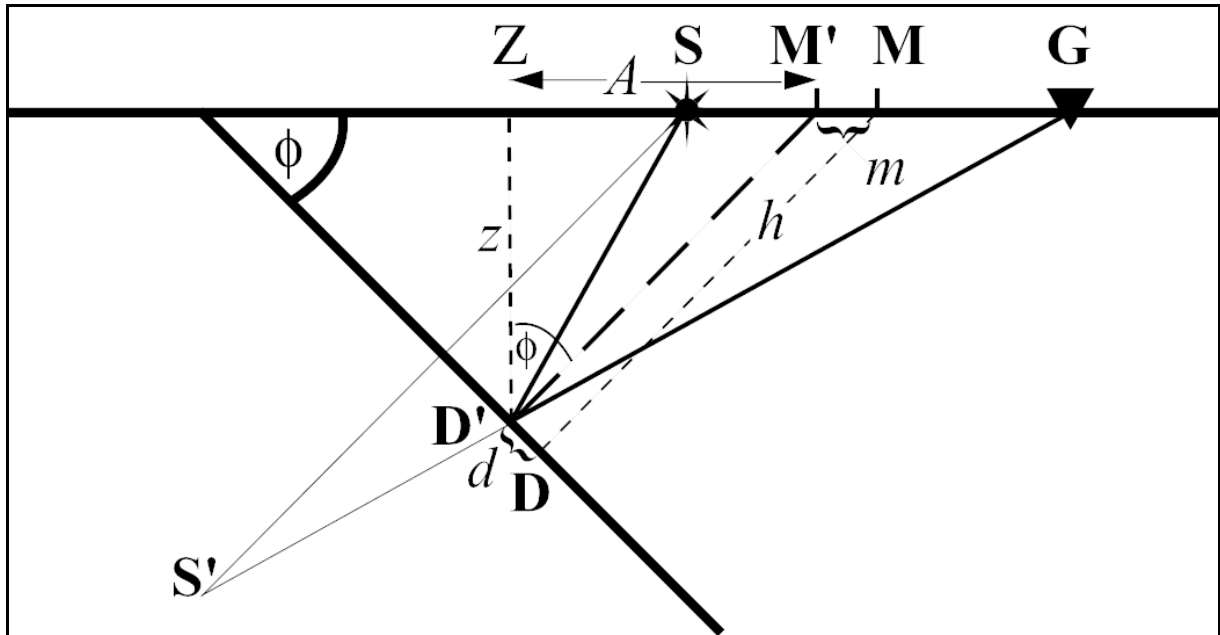


Fig. 2-2. Scattering of reflection points due to dip ϕ ; G = receiver location; S = source location; offset $x = \overline{SG}$; D = zero-offset depth point; D' = actual reflection point; M = midpoint at surface; M' = midpoint corresponding to reflection point D'; $d = \overline{DD'}$; $m = \overline{MM'}$; h = zero-offset distance to reflector; A = migration aperture; z = depth of reflection point D'.

In order to correct for this scattering of reflection points due to dip, prestack partial migration or *dip moveout* (DMO) is applied to the unmigrated section (section 2.2.3.3). DMO moves the data to the correct zero-offset trace, surface position or CMP gather, i.e. it moves the reflection energy to a trace at distance m from the original midpoint and eliminates reflection point dispersal.

2.1.3 Velocities and velocity analysis

It is generally true that seismic velocities increase with depth due to the increase in overburden (confining pressure). The first main requirement to estimate these velocities is to record data at nonzero-offsets using the *common midpoint recording technique* (section 2.1.2).

This technique uses time differences between the traveltime at a given offset and at zero-offset (called *normal moveout* – NMO) in order to determine the velocity of the medium above the reflector. The equations that build the foundation of *velocity analysis*, which is an important part of conventional seismic data processing, depend on the geometry of subsurface layers and the *hyperbolic assumption*.

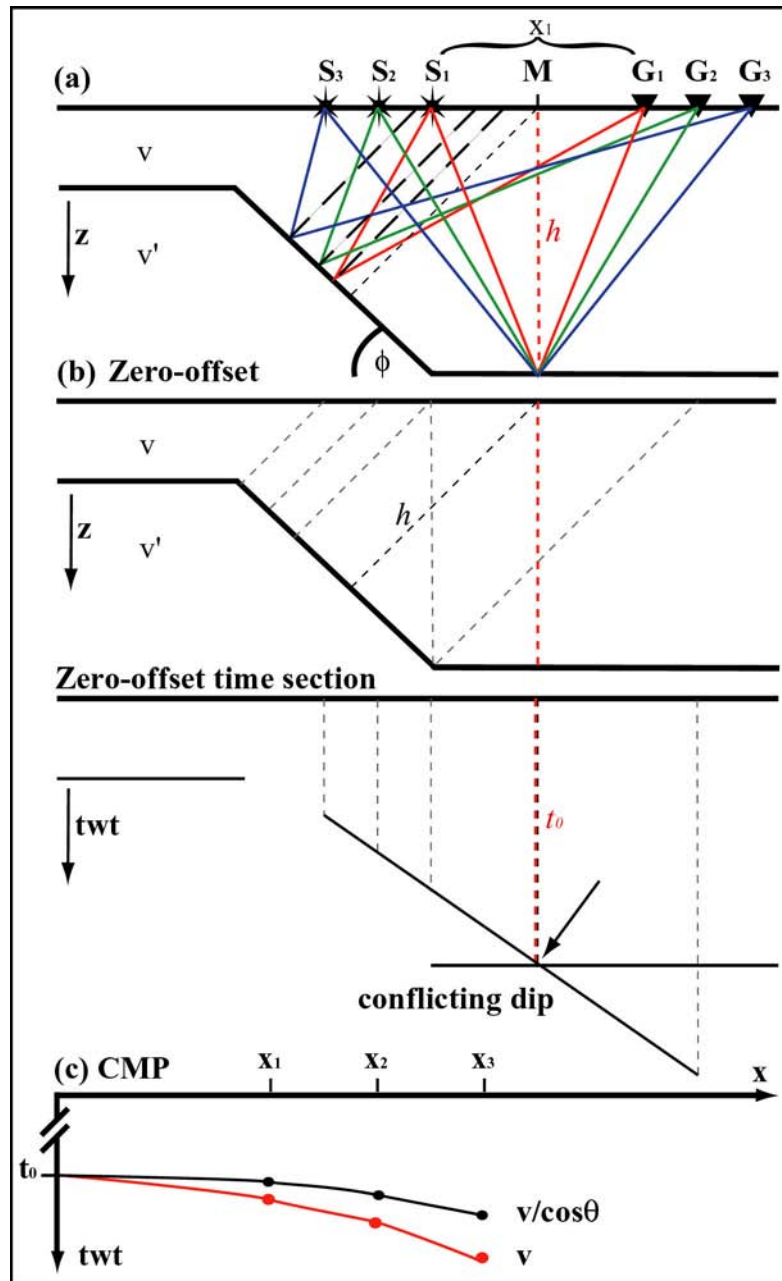


Fig. 2-3. Conflicting dips: (a) Reflection raypaths of three source-receiver offsets from a flat event intersected by a dipping one at equal zero-offset distances h ; (b) zero-offset section (c) CMP gather around midpoint M with two hyperbolas at the same zero-offset traveltime t_0 (equation (2.1)) but different stacking velocities v and $v/\cos\theta$ for the horizontal and dipping reflector, respectively.

2.1.3.1 Single constant-velocity horizontal / dipping layer

For a single constant-velocity horizontal layer of thickness h , the travel-time curve (t) as a function of offset (x) is a hyperbola (Yilmaz, 1987):

$$(2.1) \quad t^2(x) = t^2(0) + \frac{x^2}{v^2} \quad \text{with } v = v_{NMO} = v_{medium} \quad \text{and} \quad t(0) = t_0 = \frac{2h}{v}.$$

The velocity required to correct for normal moveout is called the *normal moveout velocity* (v_{NMO}) and is in this case equal to the velocity of the medium above the reflector (v_{medium}).

The 3-D travel-time curve for a constant-velocity dipping layer becomes a function of dip angle (ϕ) and azimuth (θ) (Yilmaz, 1987):

$$(2.2) \quad t^2(x) = t^2(0) + \frac{x^2}{v_{NMO}^2} = t^2(0) + \frac{x^2(1 - \sin^2 \phi \cos^2 \theta)}{v_{medium}^2}$$

$$\text{with } v_{NMO} = \frac{v_{medium}}{\sqrt{1 - \sin^2 \phi \cos^2 \theta}} \quad (3-D) \quad \text{or } v_{NMO} = \frac{v_{medium}}{\cos \phi} \quad (2-D).$$

Proper stacking of a single dipping event requires an *NMO velocity* that is greater than the *medium velocity* above the reflector!

2.1.3.2 Horizontally stratified earth

If the subsurface consists of several horizontal isovelocity layers $v_1, v_2, v_3, \dots, v_N$, the travelttime curve can be expressed as (Taner and Koehler, 1969):

$$(2.3) \quad t^2(x) = C_0 + C_1 x^2 + C_2 x^4 + C_3 x^6 + \dots = t^2(0) + \frac{x^2}{v_{rms}^2} + C_2 x^4 + C_3 x^6 + \dots$$

with C_2, C_3, \dots being complicated functions that depend on layer thickness and interval velocity and

$$v_{rms}^2 = \frac{1}{t(0)} \sum_{i=1}^N v_i^2 \Delta t_i(0) \quad \text{with } t(0) = \sum_{k=1}^i \Delta t_k$$

where Δt_i is the vertical two-way time through the i th layer.

The *interval velocity* between two parallel reflectors $n-1$ and n at two-way times t_{n-1} and t_n and with the *rms velocities* $v_{n \text{ rms}}$ to the n th reflector and $v_{n-1 \text{ rms}}$ to the reflector above it can be found by using Dix formula (Telford et al., 1990):

$$(2.4) \quad v_{n \text{ int}} = \left(v_{n \text{ rms}}^2 \sum_1^n t_i - v_{n-1 \text{ rms}}^2 \sum_1^{n-1} t_i \right) / t_n$$

2.1.3.3 Hyperbolic assumption

The assumption that equation (2.3) can be approximated by a hyperbola works well for offsets that are small compared to depth (z). For short offsets ($x \ll z$) and within a horizontally layered subsurface, the *NMO velocity* is equal to the *rms velocity* (v_{rms}) down to the layer boundary under consideration. The series can thus be truncated as follows (Yilmaz, 1987):

$$(2.5) \quad t^2(x) = t^2(0) + \frac{x^2}{v_{rms}^2}$$

In a medium composed of layers with arbitrary dips, the traveltine equation becomes complicated. But as long as dips are gentle and spread is small the hyperbolic assumption can still be made (Yilmaz, 1987). Under these conditions the more general form of equation (2.5) is given by:

$$t^2(x) = t^2(0) + \frac{x^2}{v_{NMO}^2}.$$

Dix hyperbolic normal moveout (Δt_{NMO}) is expressed as follows:

$$(2.6) \quad \Delta t_{NMO} = t(x) - t(0) = t(0) \left\{ \left[1 + \left(\frac{x}{v_{NMO} t(0)} \right)^2 \right]^{1/2} - 1 \right\}.$$

As previously described, *NMO velocity* depends on the geometry and number of layers above the reflector at $t(0)$ (see equations (2.1), (2.2), or (2.5)). However, the velocity that can reliably be derived from CMP seismic data is called *stacking velocity* ($v_{stacking}$) because it uses the hyperbola that best fits data over the entire spread length and thus yields the best stack:

$$t_{stacking}^2(x) = t_{stacking}^2(0) + \frac{x^2}{v_{stacking}^2}, \quad t_{stacking}(0) \neq t(0).$$

The difference between v_{NMO} and $v_{stacking}$ is called *spread-length bias* (Yilmaz, 1987) and increases with increasing offset. *Conventional velocity analysis* is based on the *small-dip and small-spread hyperbolic assumption* and uses *normal moveout* (see equation (2.6) to determine *stacking velocities* (e.g. with constant velocity stacks (CVS) or velocity spectra).

Velocities required by stacking and migration are only the same if no reflector dip is present. Stacking velocity is influenced by the dip angle while the migration velocity is simply the *medium* (for one reflector) or *rms velocity* above the concerned reflector (Yilmaz, 1987):

$$v_{stacking} \geq v_{migration}.$$

2.2 3-D data processing theory

The ultimate goal of conventional processing of 3-D survey data acquired using the CMP recording technique (section 2.1.2) is to obtain a 3-D seismic image of the subsurface. **Four primary stages** in processing seismic data are distinguished: *navigation*, *pre-processing/geometry*, *velocity analysis*, and *stacking / migration*.

2.2.1 Preprocessing and geometry

Deconvolution is a process that compresses the seismic wavelet and thereby increases temporal or *vertical resolution* (section 2.4.1.1). It acts on the time axis and removes the seismic wavelet from the recorded seismic trace (Yilmaz, 1987).

Several processing steps can be applied prior to deconvolution in order to make it more effective: a correction for geometric spreading is necessary to compensate for a loss of amplitude due to wavefront divergence; wide bandpass filtering removes very low and very high-frequency noise and dip filtering could reduce possible coherent noise in the data. These initial signal processing steps are also called preprocessing. Predictive deconvolution can be used to remove multiple energy in the data.

2.2.1.1 3-D CMP binning or sorting

In conventional mid-point analysis (see section 2.1.2), the subsurface is sampled at one-half the receiver spacing along the streamer, falling on common midpoints. Shot spacing influences the final fold of coverage of each CMP position. A bin is a rectangular area around one such midpoint with the extensions dX_{bin} in in-line and dY_{bin} in cross-line direction (definition see section 2.4.3). Theoretically, bin limits are found half-way between two adjacent midpoints. Midpoints are randomly scattered around the theoretical center point of the bin due to streamer feathering or inadequate positioning. The process of dividing the survey area into a number of discrete bins is called *CMP-binning* and can be viewed as if a virtual grid is placed onto this area. Smaller bins imply smaller receiver spacing; larger bins imply less resolution.

After preprocessing, the data are transformed from shot-receiver to midpoint-offset coordinates (section 2.1.2). All seismic traces whose midpoints fall into the same CMP bin are grouped. This sorting process requires field geometry or navigation information (section 2.3.4) and represents the most important part of the processing flow because the success of all subsequent steps depends on it. Based on the geometry information stored in the trace headers, each trace is assigned to a bin and all traces corresponding to the same bin build a CMP gather. This processing step is called “static” binning (Evans, 1997). If bin coverage is not evenly distributed it is common practice to use “dynamic” or “elastic” binning, a method that takes the desired traces from adjacent bins by changing bin size if necessary (Evans, 1997). This process, also called *bin harmonization*, duplicates traces from neighboring bins into bins where they are missing.

2.2.2 Velocity analysis

The multifold coverage of the CMP recording technique not only provides an improved S/N ratio (section 2.1.2) but most importantly yields velocity information about the subsurface (see theory in section 2.1.3). Velocity analysis is often performed on velocity

spectra of selected gathers and profiles in order to build a 3-D *stacking velocity* model. Signal coherency is measured along theoretical hyperbolas governed by velocity, offset and traveltime and allows determination of functions of velocity versus two-way zero-offset time. These velocity functions are then spatially interpolated between analyzed gathers across the entire survey.

2.2.3 Stacking / Migration

2.2.3.1 NMO correction, stacking and post-stack migration

In conventional processing, the stacking velocity model is used in normal moveout correction of CMP gathers (see theory in section 2.1.3) and reflection hyperbolas are flattened across the offset range. Hence, the offset effect is removed. Traces are then summed in order to obtain a zero-offset CMP stack.

Post-stack migration is a process that collapses diffractions and maps dipping events on a zero-offset section to their true subsurface locations. It is a spatial deconvolution process that improves spatial or *horizontal resolution* (section 2.4.1.2), (Yilmaz, 1987). The image quality from migration depends on stack quality and accuracy of the velocity model (see section 2.1.3) but also on the migration aperture (section 2.4.5) and spatial sampling (section 2.4.1.2), (Yilmaz, 2001). The last two criteria depend on the survey design (see section 2.4).

2.2.3.2 Prestack migration

The problem with a stack resulting from conventional NMO corrected data is *conflicting dips*, i.e. reflections occur at the same time with different stacking velocities. In section 2.1.3.1, equation (2.1), we saw that stacking velocities are dip dependent. Therefore, when a flat event is intersected by a dipping event (Fig. 2-3 (a)), there will be one CMP gather with two reflection hyperbolas but different stacking velocities at the same zero-offset time (Fig. 2-3 (c)). In velocity analysis, we can only choose a velocity in favor of one of these two events; the stacking quality of the other will be significantly degraded. This would not be the case for a real zero-offset section (Fig. 2-3 (b)), on which post-stack migration theory is based (Yilmaz, 1987). Thus, in the presence of conflicting dip, a conventional stack is no longer equivalent to a zero-offset section and migration after stack no longer valid.

Migration before stack, therefore, becomes necessary. As for any migration method, migration before stack requires knowledge of zero-dip or medium velocities, and thus is sensitive to the effect of velocity errors (Yilmaz, 1987). Instead of summing along the zero-offset diffraction hyperbolas on a stack, amplitudes are summed along the non zero-offset diffraction traveltime trajectories (Yilmaz, 1987) for each offset gather separately and makes *prestack migration* very demanding in time.

2.2.3.3 Prestack partial migration (PSPM) or DMO

Another less expensive possibility to handle the conflicting dip problem with conventional stacks is *prestack partial migration* after zero-dip NMO correction and before zero-offset *post-stack migration*. Equation (2.2) can be rewritten as follows (Yilmaz, 1987):

$$t^2(x) = t^2(0) + \frac{x^2}{v_{NMO}^2} = t^2(0) + \underbrace{\frac{x^2}{v_{medium}^2}}_{\text{zero-dip NMO}} - \underbrace{\frac{x^2 \sin^2 \theta}{v_{medium}^2}}_{\text{DMO}}$$

Comparing this equation with equation (2.2), we see that the first part of the moveout is associated with the *zero-dip moveout* (NMO), while the second part is related to reflector dip, and representing the *dip moveout* (DMO). In DMO processing, CMP gathers are first NMO corrected using zero-dip *rms velocities*, then sorted into common-offset sections, which are individually corrected for DMO. DMO becomes greater at increasingly shallower depths, large offsets and steep dips. Data are then sorted back into CMP gathers.

Since DMO correction is a migration-like process, it causes the energy to move from a CMP gather to neighboring gathers (bins) in the updip direction (Yilmaz, 1987). As we have seen in Fig. 2-2 and Fig. 2-3, dipping reflectors cause reflection point smearing (see section 2.1). DMO moves the data to the zero-offset surface location that corresponds to their true reflection point and lies updip of the source-receiver midpoint (Sheriff, 1991).

DMO requires a velocity model that consists of the medium (for one reflector) or *rms velocities* and not of the optimum *stacking velocities* which depend on dip and azimuth (3-D) (see section 2.1.3.1). However, the *stacking velocities* are the ones picked by conventional velocity analysis. In order to overcome this problem, a second velocity analysis is performed after conventional NMO correction, DMO and inverse NMO, using preliminary first-pick velocities. The second velocity analysis on dip corrected data then yields a dip-corrected velocity model suitable for post-stack migration. Using this DMO processing flow (see also Fig. 6-1) not only gives a better stack but also dip-corrected velocities that allow a better migration after stack. Ideally, if velocity gradients are low and lateral variations small, the imaging quality is similar to full time migration before stack (Yilmaz, 1987). Optimum full prestack migration, however, also needs a dip-independent velocity model and would thus require the same DMO velocity analysis as DMO processing plus full prestack migration.

2.2.3.4 Azimuth, amplitude and offset considerations

Conventional marine multi-streamer configurations have a minimum range of azimuths, the largest azimuth being that from the source to the near offset hydrophone. Vermeer (2001) states that this configuration is not suitable for the analysis of azimuth-dependent effects. Conventional DMO plus post-stack migration processing is much less sensitive to irregular sampling in azimuth and offset than prestack migration is (Canning and Gardner, 1996).

2.3 Theory and description of seismic instrumentation

2.3.1 Marine receiver systems

Geophones and cables on land are equivalent to hydrophones and streamers in marine surveys. Cables in water are called streamers because they “stream” behind the towing vessel (Evans, 1997). While geophones detect particle motion, hydrophones are sensitive to variations in pressure.

2.3.1.1 Hydrophones

Since liquids support only acoustic propagation (P-waves), seismic signal recording at the sea surface requires receivers capable of detecting pressure changes. A hydrophone is an electro-acoustic transducer that converts a pressure pulse into an electrical signal by means of the piezoelectric effect. The voltage produced is proportional to the amount of pressure (Evans, 1997).

Generally, each hydrophone consists of piezoelectric crystals. Several closely spaced hydrophones make up a *group* or an *array* and any number of groups make up the streamer. The stacked signal from a group of hydrophones connecting to one recording channel suppresses undesired coherent horizontal noise while enhancing the useful vertical signal. Although the manufacturer usually provides hydrophone calibrations, it is useful to compare hydrophone sensitivity between groups and also to a calibrated hydrophone if amplitude versus offset (AVO) analysis is an objective. Hydrophone sensitivity can be decreased by natural wear of the crystal (Evans, 1997). Since pressure amplitude of a seismic wave is linearly proportional to its frequency, a filter is necessary to guarantee a flat frequency response (Evans, 1997).

2.3.1.2 Streamers

A streamer cable is composed of several sections, which in turn contain one or more hydrophone groups. End connector couplings ensure interconnection of streamer sections in order to transport all information from one section to the next and finally via a lead-in and deck cable to the recording system onboard. The lead-in must be capable of withstanding high pressure from the energy source because it may come in contact with the energy source during vessel turns.

Ideally, the streamer should have neutral buoyancy, i.e. it can be placed at a particular depth and will remain there. One solution has been to fill the streamer with kerosene oil, which is lighter than water, to compensate its own weight. In the past couple of years, however, solid streamers became state of the art and the oil was replaced by a solid, yet flexible gel. This makes oil filling and emptying before and after each acquisition needless and removes the risk of oil seepage, which is especially important when working in lake environments and close to the shore. Apart from eliminating the environmental concerns,

solid streamer technology is said to provide improved operational performance and reduced noise levels. The new generation of solid streamers is even more flexible and easier to store onboard (see section 3.2).

2.3.2 Data recording

The seismic reflections to be recorded are produced by subsurface impedance contrasts and arrive as water pressure variations at the hydrophones situated near the sea surface. These pressure variations are converted (see section 2.3.1.1) into electrical voltage (mV), then preamplified and filtered. Numerical recording means digitization of the resulting analog electrical signal with the aid of an analog-to-digital (A/D) converter (section 2.3.2.3) within the seismic recording instrument (section 3.1). Important for this procedure are two main recording parameters, the sampling interval (SI, section 2.3.2.1), which depends on the frequency bandwidth of the seismic source, and the instrument's specific dynamic range or recording resolution (section 2.3.2.5). Other important parameters are the record length and therefore the total number of recorded samples per trace as well as the maximum recording speed of the instrument. For record length selection, factors such as the energy and penetration depth of the seismic source as well as the water depth and the occurrence of related strong multiples should be considered. Previously known geometries of the study site thus play an important role.

2.3.2.1 Temporal sampling theorem

The *Nyquist or sampling theorem* states that the minimum required sampling frequency (f_{SI}) needed in order to reconstruct a signal from equispaced (in time) data be double the maximum frequency (f_{\max}) in its spectrum. Half the frequency of sampling is called *Nyquist frequency* (f_N) (Sheriff, 1991). This results in a sampling interval (ΔT or SI) that must be small enough to fall twice or more often into the smallest cycle of the signal:

$$(2.7) \quad f_{\max} \leq f_N \leq \frac{f_{SI}}{2} = \frac{1}{2\Delta T} \Leftrightarrow \Delta T \leq \frac{1}{2f_N}$$

If there are fewer than two samples per period, frequency *aliasing* occurs, i.e. an input signal at $f_N + f$ yields the same sample values as a signal at $|(2m-1)f_N - f|$, where m is an integer such that the alias frequency is smaller than f_N (Sheriff, 1991; Yilmaz, 1987). To avoid frequency or temporal aliasing, an anti-aliasing filter before digitization removes frequencies above the *Nyquist frequency*.

2.3.2.2 Decibel scale and dynamic range

The dynamic range (D) in decibel scale of an analog signal is defined as the ratio of its maximum to minimum power (P):

$$D(dB) = 10 \log_{10} \frac{P_{\max}}{P_{\min}}$$

Since power is proportional to the amplitude (A) squared, the definition can be given in terms of an amplitude ratio:

$$(2.8) \quad D(dB) = 10 \log_{10} \frac{|A_{\max}|^2}{|A_{\min}|^2} \quad \text{or} \quad D(dB) = 20 \log_{10} \frac{|A_{\max}|}{|A_{\min}|}$$

A factor of 2 between two signal amplitudes corresponds to 1 *bit* in the binary system and is about 6 dB (relationships between amplitude ratios, bits and dynamic range are given in Table A-1 of the Appendix).

2.3.2.3 A/D conversion

The input electric voltage is analog and needs to be sampled with the aid of an analog-to-digital converter. Each discrete point in time is represented by a digital word. When written on magnetic tape, this seismic word or seismic sample represents one voltage or amplitude value. The greater the number of *bits* (n) in each word, the greater the range of amplitudes that can be converted without distortion and the greater the theoretical resolution of the A/D converter and the instrument.

An n -bit A/D converter allows the distinction of 2^n quantizing levels between the minimum and maximum amplitude. The best relative accuracy of quantization occurs when the signal is large enough to use all of these levels (Dodds, 2002). Therefore the input signal is normally amplified before digitization (see section 2.3.2.5). The smallest quantizing level is called *quantizer step* size (Δ) (Dodds, 2002) or the "Least Significant Bit" (LSB) (Durand, 2001). If, as shown in the example of Fig. 2-4, a 3-bit ($n=3$) converter can assume values between $-4V$ and $+4V$ ($V_{ref} = 8V$), the LSB (Δ) can be determined as follows:

$$(2.9) \quad \Delta = \frac{V_{ref}}{2^n} = \frac{8V}{2^3} = \frac{8V}{8} = 1V \quad (\text{Dodds, 2002}).$$

Hence, the peak-to-peak signal amplitude is $2^n \Delta$ (8 V), where Δ represents the voltage sampling interval (*quantizer step*) within the converter's reference voltage (here sampled into $2^3 = 8$ discrete values ranging from ± 0.5 to ± 3.5 ; Fig. 2-4 (a)). The instrument theoretical dynamic range can be calculated using equations (2.8) and (2.9) and is 18 dB in our example:

$$(2.10) \quad D(dB) = 20 \log_{10} \frac{V_{ref}}{2} \frac{2}{\Delta} = 20 \log_{10} \frac{V_{ref}}{\Delta} = 20 \log_{10} \frac{V_{ref} 2^n}{V_{ref}} = 20 \log_{10} 2^n \approx n * 6dB$$

In theoretical terms, there is an increase in the dynamic range by approximately 6 dB for each bit added to the word-length of an A/D converter. Note that the "6-dB-Per-Bit-Rule" is an approximation to calculating the actual dynamic range for a given word width.

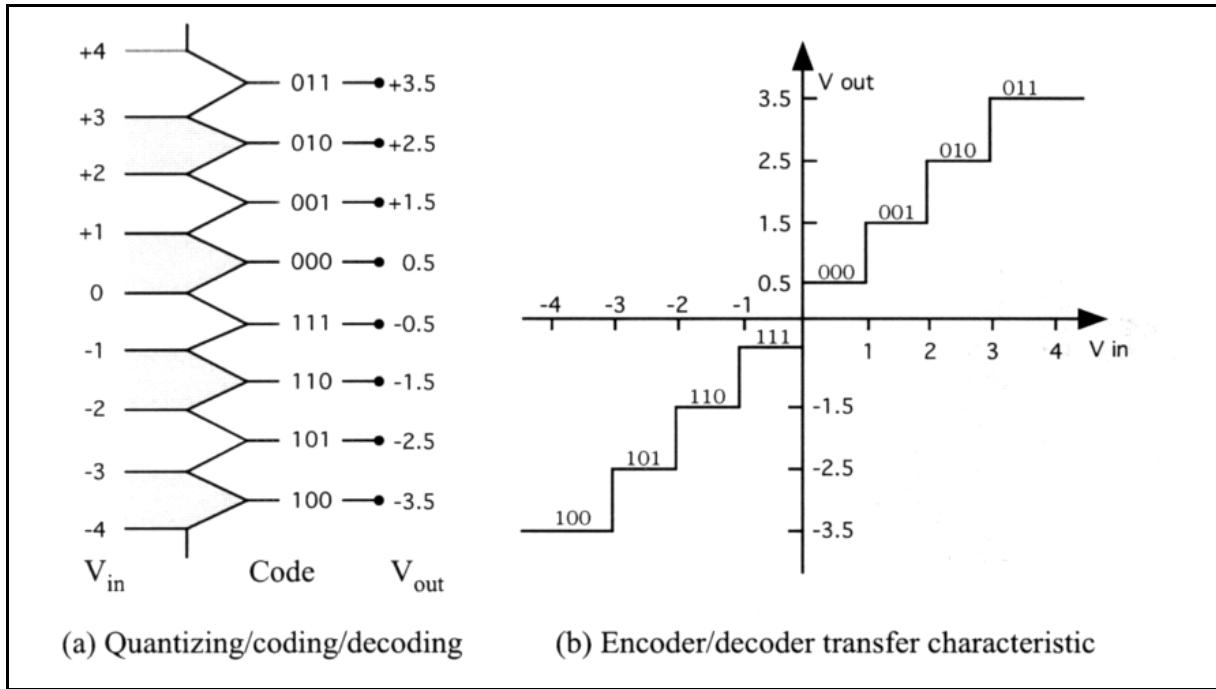


Fig. 2-4. Quantizing example: a 3-bit converter with a reference voltage of 8 V and a quantizer step of 1 V can represent 8 quantizing levels; from Dodds (2002).

2.3.2.4 Signal-to-noise ratio and instrument’s resolution

The difference between the analog incoming signal and its output numerical form is called *quantizing error (noise)* and cannot be greater than $\pm\frac{1}{2} \Delta$, given that the signal does not exceed the converter limits (Dodds, 2002; Durand, 2001). The accuracy of digitization is normally described in terms of “Signal-to-Noise Ratio” (S/N ratio), which is the ratio of signal power to quantizing noise power. In analog and digital terms, S/N ratio and *dynamic range* are often used synonymously.

Modeling quantizing noise as random noise that takes on all values between $\pm\frac{1}{2} \Delta$ with uniform probability and using a full load sinusoid input signal, the S/N ratio of its digital output can be approximated as:

$$(2.11) \quad S/N \text{ ratio}(dB) \approx 6n + 1.77dB \quad (\text{Durand, 2001; Dodds, 2002}).$$

The second term is influenced by waveshape and is 1.77 dB for a sinusoid, 0 dB for a triangular waveform and 4.77 dB for a square wave. Complex waveforms coupled with amplitude reduction result in an S/N ratio that is much less than that of a full load sinusoid (Dodds, 2002).

An instrument theoretical resolution can be expressed in dB as dynamic range or S/N ratio using equations (2.10) and (2.11) or simply by the number (*n*) of converter bits (see Table A-1). In practice, the actual S/N ratio never reaches this theoretical value. In order to measure the instrument’s “Effective Number of Bits” (ENOB) compared with the ideal resolution (*n*), the actually measured S/N ratio is put into equation (2.11) and transformed:

$$ENOB = \frac{S/N \text{ ratio actual} - 1.77}{6.02} \quad (\text{Sullivan, 1998})$$

The resolution of an A/D converter can be improved by using a technique called *oversampling*. In order to increase the effective number of bits, a signal is sampled at a rate f_{OS} (oversampling frequency) that is higher than the system's required sampling rate, which is at double the *Nyquist frequency* f_N (see section 2.3.2.1). For each additional bit (W) of resolution, the signal must be oversampled by a factor of four (Staller, 2002):

$$(2.12) \quad f_{OS} = 4^W * 2f_N.$$

The improvement is thus a function of the final sample interval chosen. Generally, one obtains about 6 dB dynamic range improvement for each additional bit gained through oversampling.

2.3.2.5 Preamplification and instrument gain

Received seismic signals often have a wide dynamic range. If they are outside of the instrument's range, they cannot be recorded faithfully. Signals that are too small are not recorded at all; too large signals are distorted or clipped. Seismic recording systems therefore contain an amplifier (gain control) that matches the amplitude of the received signal to the dynamic range of the seismograph's A/D converter (see section 2.3.2.3).

Gain control can be either *fixed* or *dynamic*, or a combination of both. In constant gain systems the amplification (*preamplifier* or *K-gain*) is set to a fixed amount so that the highest amplitude of interest in the received signal is recorded without being clipped. In such a system, small signals are lost if their voltage level falls below the recordable threshold, represented by the least significant bit (LSB). If the voltage level is too high, the signal will be saturated and the S/N ratio significantly reduced. The *gain-ranging* or *instantaneous floating point* (IFP) systems change the amplification factor on a sample-by-sample basis, so that the amplified signal falls within the dynamic range of the A/D converter. The total instrument gain is the amount of fixed plus dynamic gain. All incoming signals first have the constant gain applied to them followed by the variable gain. If, for example, the system noise level is 120 dB less than the maximum signal that can be recorded without amplification, and the fixed gain is set to 24 dB and gain-ranging to 36 dB, then the remaining theoretical dynamic range will be $120 - 24 - 36 = 60$ dB (e.g. Evans, 1997).

In order to determine the amount of fixed gain necessary, *gain-constant test shots* are performed at the start of each survey.

2.3.3 Seismic sources

Marine energy sources are classified into explosive (air guns) and implosive (water gun, Sparker or Boomer) types. For *explosive energy sources*, the initial peak, the explosive pulse or primary arrival, is created by the sudden release of high pressure gas in the water. It is

followed by a bubble-generated noise train from the subsequent expansion / compression phases of the generated bubble. *Implosive energy sources* are characterized by an outgoing wavefront generated by the collapse of a cavity in the water. Explosive and implosive sources are also called *impulsive*, because an explosion or an implosion is a sharp wave of very short duration, which somewhat simulates an impulse (Sheriff, 1991).

In general, marine energy sources should possess the following characteristics (Evans, 1997):

- (1) a maximum-output signal-to-noise ratio,
- (2) a high-output energy,
- (3) a high resolution,
- (4) a good signal repeatability both in time and in amplitude,
- (5) a good reliability,
- (6) a minimum disturbance of the environment,
- (7) a low capital and maintenance cost,
- (8) a convenience of re-supply.

Impulsive source signals are described by their frequency bandwidth, wavelet duration and consistency of wavelet shape. Seismic resolution can be improved as the seismic wavelet's amplitude spectrum becomes broader and smoother, as its duration becomes shorter and as its shape becomes more repeatable from shot to shot (Verbeek and McGee, 1995).

2.3.3.1 Air guns (explosive energy sources)

Air guns are the most common type of marine *impulsive* energy sources. The air gun's high-energy pulse is produced by the sudden release of a volume of high-pressure air. Compressed air first fills up the return chamber firing a hollow shuttle to close and seal the main chamber (Fig. 2-5, left). At the same time, the main chamber located between the casing and the shuttle starts to be pressurized. When the solenoid valve receives an electrical trigger impulse, the triggering chamber fills up allowing the shuttle to move and unseal the main chamber (Fig. 2-5, right). The lightweight shuttle quickly acquires a high velocity before uncovering the ports. High pressure air is then explosively released into the surrounding water to generate the main acoustic pulse. When the pressure within the main chamber drops, the air in the still fully pressurized return chamber returns the shuttle to its pre-firing position.

Air gun volumes typically range from 10-300 in³ while air-pressure levels are commonly operated between 34.5-345 bars (Evans, 1997). Other types of air guns are the *sleeve gun*, which allows air to escape in the form of an air annulus, or the *G.I gun* that cancels its own bubble oscillations.

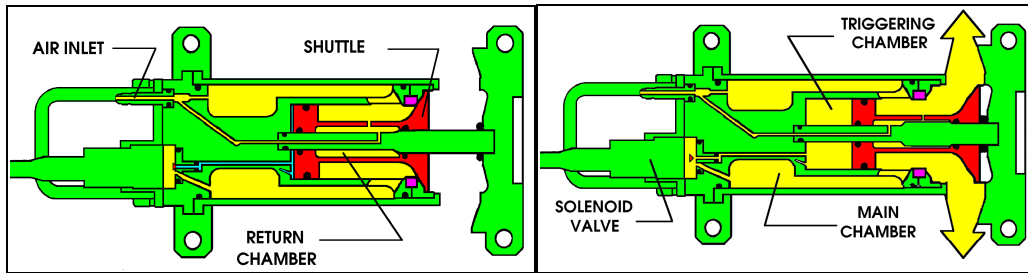


Fig. 2-5. Schematic functioning of an air gun by M. Gros.

2.3.3.2 Bubble effect

The bubble problem affects all types of marine *explosive energy sources*. After explosion, the outgoing wavefront creates the primary energy pulse and the air bubble starts to expand until its internal pressure is less than the hydrostatic pressure of the water around it (Evans, 1997). The hydrostatic pressure then compresses the bubble until the pressure reaches a level comparable to that of the initial explosion. The bubble again expands and produces another outgoing wave. It expands and collapses for several cycles until the oscillating bubble rises to the water surface. As a result, each recorded reflection event is composed of a primary followed by many bubble pulses. In order to resolve this problem, bubble canceling air guns (G.I guns) were invented. The use of *implosive energy sources* avoids bubble generation in the first place, but they have other disadvantages (see section 2.3.3.4).

2.3.3.3 G.I gun and Mini G.I

The *G.I gun* and its smaller counterpart the *Mini G.I* are pneumatic seismic sources that are constituted of two independent air guns within the same casing. The first air gun is called the “*generator*”, as it generates the primary pulse. The second one, the “*injector*”, injects air inside the bubble that was produced by the generator in order to control and to reduce the bubble oscillation. Each gun has its own reservoir, its own shuttle, its own set of exhaust ports, and its own solenoid valve. A common hydrophone provides both the time break and the shape of the near-field signal. This gun phone is located inside the bubble and therefore responds to the actual air blast of the *G.I gun* to which it is affixed, without being affected by neighboring guns.

When the *generator* is fired, the blast of compressed air produces the primary pulse and the bubble starts to expand. As soon as the bubble approaches its maximum size, it encompasses the *injector* ports, and its internal pressure is far below the outside hydrostatic pressure. At this time, the *injector* is fired, injecting air directly inside the bubble. Due to the quasi-static state of the bubble, the timing of the injection is not critical. The volume of air released by the *injector* increases the internal pressure of the bubble, and prevents its violent collapse. This way, the bubble oscillations and the resulting secondary pressure pulses are reduced and re-shaped (M. Gros, personal communication, 2003).

The *G.I gun* can be configured in "harmonic" or in "true GI" mode; i.e. the total volume of the gun is partitioned so that generator and injector have the same volume (harmonic mode) or the injector chamber has about double the size (x 2.33) of the generator chamber (true GI mode), (M. Gros, personal communication, 2000). The larger the percentage of total injection volume, the better will be the peak-to-bubble ratio. In true GI mode, the injection is optimally tuned to totally suppress the oscillation of the bubble (SODERA, 1995). However, for a fixed total volume this means that, in true mode, the generator is reduced to approximately half its harmonic volume and the pulse's peak-to-peak output will be 26% smaller (see section 2.3.3.5). The price of a good peak-to-bubble ratio is thus the reduction of the pulse's peak-to-peak amplitude (SODERA, 1997). As always, a trade-off between extremes has to be found.

2.3.3.4 Water gun (implosive energy source)

The water gun is an implosive energy source, that uses compressed air in an upper chamber to drive a shuttle that moves water through a lower chamber (Parkes and Hatton, 1986). This high-velocity water plug is violently ejected through several ports (precursor peak), forming a momentary void behind the jets. Implosion of the void generates the main outgoing pulse for seismic reflections. So basically, compressed air stored in the firing chamber is used to propel water jets that create vacuum cavities which, when they implode under the surrounding hydrostatic pressure, emit a strong bubble-free, high-frequency acoustic pulse.

Similar to air guns, water guns are operated at about 138 bars and they have comparable energy levels. Although water guns have no oscillating air bubble, their signature contains an undesirable precursor peak and implosion timing depends on gun depth.

2.3.3.5 Source signature

The shape of the pressure signal created by a marine source is called its *signature*. The source *signature* depends mainly upon three parameters that are the gun volume, the firing pressure and the firing depth. This *signature* can be measured either in the near-field or in the far-field. In the near-field, the time domain signature of an air gun source has three typical characteristics: a high-amplitude, narrow, positive peak followed by an almost half sinus negative portion, and another positive peak of smaller but wider amplitude (Fig. 2-6, left). In the far-field, the first positive peak is followed by a negative peak of almost the same amplitude and shifted in time (Fig. 2-6, right). This second peak is due to the "ghost effect" (see below). The remaining part of the signature is of course also affected by the bubble phenomenon.

In order to evaluate the signal emitted by the source, the *pulse's peak-to-peak amplitude* (PTP) or *signal strength* and the peak-to-peak amplitude of the bubble oscillation (Bubble PTP) is measured in bar-meters (see Fig. 2-6, right). The ratio between PTP and the bubble

oscillation is called the *peak-to-bubble ratio* (PBR) and describes the quality of the *signal shape*. The higher this dimensionless factor, the better generally is the measured signature. This criterion is also valid when the signal is looked at in the frequency domain. A high PBR will give a smooth amplitude spectrum.

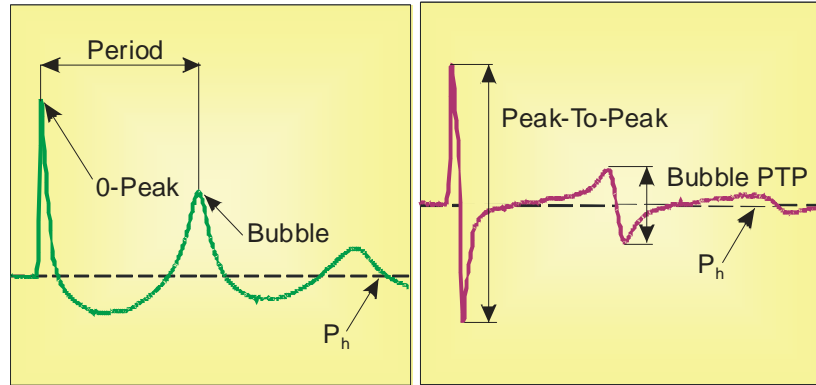


Fig. 2-6. Near field (left) and far-field (right) signature (pressure over time) by M. Gros.

In order to make direct comparison between different air guns or air gun arrays, it is more convenient to compare their performances in the frequency instead of the time domain. To do so, the amplitude spectrum should be absolutely calibrated in dB relative to $1 \mu\text{Pa} / \text{Hz}$ at 1 m (Dragoet, 1990). In the frequency domain, the *signal strength* is given by the maximum amplitude (in dB) of the spectrum, while the smoothness of the spectrum becomes a measure for good *signal shape* expressed also by the frequency bandwidth above a -6dB line.

For a given gun, *signal strength* is almost proportional to:

- the cube root of the gun volume. Doubling the gun volume will increase the PTP only by 26% (Dragoet, 1990).
- the two-third power of pressure. For example, increasing the firing pressure from 138 bars to 210 bars will increase the PTP by roughly 30% (M. Gros, personal communication, 2003).
- the two-third power of number of guns for a given total volume. Doubling the number of guns while the volume of each gun is halved will increase the PTP by 66% without using additional air. This is true if the guns are independent (M. Gros, personal communication, 2003). However, the more guns are used the higher is the directivity of the produced signal.
- thus the chamber volume is less important than the number of guns in an array in influencing the *Peak-To-Peak amplitude*.

The resolving power of a seismic source is related to its bandwidth, its directivity and its *dominant frequency*, which can be determined by measuring the predominant period in the

signature and taking the reciprocal (Sheriff, 1991). A large bandwidth ensures short signal duration and increases both temporal and spatial resolution (section 2.4.1).

Source and receiver depth (ghost effect)

The gun depth d_s and the receiver depth d_r govern the phenomenon called *ghost interference*. A ghost is created by the downward reflection of the primary pressure pulse from the water surface. Not only could the ghost cover true reflections but more importantly causes notching in the frequency spectrum. Since the reflection coefficient at the water surface is negative and close to 1, the ghost has a polarity opposite to that of the primary reflection. This 180° phase shift and the additional distance that it travels (ΔD in Fig. 2-7 or $2d_s$ for vertical raypaths) causes destructive interference if that distance is an integral number of wavelengths ($\Delta D = n\lambda$). Assuming the recording far-field hydrophone (see section below) is at great distance from the source ($D \gg d_s$, i.e. $\phi_1 \approx \phi_2$), the notch frequency f_{notch} is then given by:

$$(2.13) \quad f_{notch} = \frac{v_{water}}{\lambda} = \frac{nv_{water}}{\Delta D} = \frac{nv_{water}}{2d_s \cos \Phi}, \quad n = 0, 1, 2, \dots$$

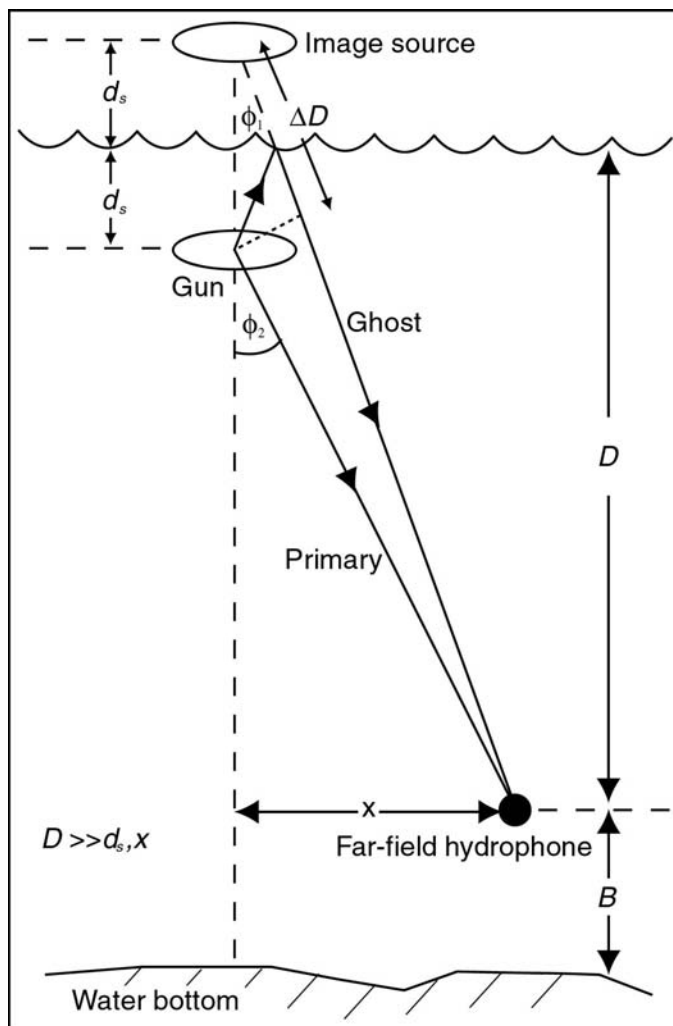


Fig. 2-7. Far-field signature test geometry. The time delay between the primary and ghost reflection arrival depends on water velocity and the distance ΔD , adapted from Fricke et al. (1985).

The deeper the gun location, the lower is the first notch frequency different from zero that affects the higher frequencies of the source's amplitude spectrum and thus influences the usable bandwidth. Furthermore, PTP strength increases with depth while the PBR decreases (Dragoet, 1990). Shallow guns work as a low-cut filter due to the less sloping zero-frequency notch. For this reason, Dragoet (1990) does not recommend improving the PBR by using shallow guns, except for high-resolution surveys that concentrate on higher frequencies.

The location of notches in the spectrum of reflected energy is not only influenced by the gun depth d_s , but also by the depth of the receivers d_r on the streamer. The first non-zero notch frequency is calculated as in equation (2.13) but using d_r and ϕ being the angle of incidence. The recorded signal is composed of the source's primary and ghost arrival plus the receiver ghost. Ideally, a streamer should be towed at a depth designed to minimize the impact of the received ghosts on the spectrum of the seismic data. The resulting signal bandwidth and hence the resolution is controlled by the deepest depth of either the source or the streamer. It is thus important to maintain both, source and receivers, at a constant depth.

2.3.3.6 Far-field signature measurements

Source signature can be measured in the *near-field* and in the *far-field*. The precise definition of these terms comes from the equation for particle velocity u , which can be derived using the solution (pressure) to the spherical wave equation (Parkes and Hatton, 1986). Particle velocity is a function of time t , radial distance r , phase velocity of wave propagation c (here sound velocity in water), density ρ and an unknown source-dependent function f .

$$(2.14) \quad u = \underbrace{\frac{1}{\rho r^2}}_{\text{near-field term}} f\left(t - \frac{r}{c}\right) + \underbrace{\frac{1}{\rho c r}}_{\text{far-field term}} f'\left(t - \frac{r}{c}\right)$$

The near-field is that region in which the $1/r^2$ term dominates and the far-field is the region far from the source in which the $1/r$ term dominates (Parkes and Hatton, 1986). A time-break hydrophone mounted directly on the gun allows display of the gun's near-field signature at almost zero distance. Since the shapes of the near-field signal (close vicinity) and the time-break hydrophone signal are very similar, it is much more convenient to use the time-break hydrophone during acquisition for optimized tuning and quality control at every shot (SODERA, 1997).

To a first approximation, the source wavefield can be characterized by the vertically traveling far-field signature. As mentioned above, this signature is then used to evaluate the performance of an energy source. The calibrated far-field hydrophone records the source's wavefield signature in the form of a voltage waveform $V(t)$ in the time-domain. Knowing the hydrophone's sensitivity S (V per bar) and the one-way distance of the source from the receiver ($D-d_s$), which can be determined from the travel time of the first arrival reception t_{first} and the water velocity v_{water} , the outgoing pressure $P(t)$ (bar-m) can be computed as follows (Evans, 1997):

$$P(t) = \frac{V(t) \times (D - d_s)}{S} = \frac{V(t) \times t_{first} \times v_{water}}{S}$$

Far-field hydrophone depth

To be in the far-field, the hydrophone has to be far enough from the source so that the pressure signature is indistinguishable from the signature that would be measured at infinity (Parkes and Hatton, 1986). At great distance, the ghost appears to have the same amplitude, opposite polarity and a slight delay with respect to the primary arrival. Both form the total signature which is the signal that enters the earth. At too short a distance from the source the hydrophone records a direct arrival that is larger than the ghost, which travels over a longer distance and has a smaller amplitude due to a larger spherical spreading loss. The ghost amplitude as a percentage of the primary arrival amplitude gives a measure of error. Since amplitude is inversely proportional to the traveled distance, the percent ghost G seen on a hydrophone vertically below the source can be expressed as (Fricke et al., 1985):

$$(2.15) \quad \boxed{G = 100 \frac{D - d_s}{D + d_s} \Leftrightarrow D = d_s \frac{100 + G}{100 - G}}$$

This equation helps to determine the optimum far-field hydrophone depth D depending upon the acceptable error tolerance G and the gun depth d_s (Fig. 2-7). For a gun at 1 m depth and a 99% ghost amplitude, the far-field hydrophone should be placed 199 m below the source, while 99 m are sufficient for a 98% ghost amplitude.

Hydrophone / water-bottom separation

A large enough distance (B) between the far-field hydrophone and the seabed (Fig. 2-7) is also important in preventing contamination by the sea-floor reflection (Evans, 1997). This distance must be such that the source signature is completely received before the water-bottom reflection arrives. Hence, the difference between water-bottom and direct arrival time must be greater than the wavelet duration Δt (Fricke et al., 1985):

$$(2.16) \quad \boxed{\frac{2B + (D - d_s) - (D - d_s)}{v_{water}} = \frac{2B}{v_{water}} \geq \Delta t \Rightarrow B \geq \frac{v_{water} \Delta t}{2}}$$

The hydrophone seabed separation B is completely independent of gun and hydrophone depths d_s and D . For an undisturbed signature measurement of 50 ms, the far-field hydrophone should be about 38 m above the water bottom.

2.3.4 Marine navigation and positioning

Accurate positioning of a seismic line is as important as having the best quality data. Locating the traces measured on the seismic streamer in order to combine them accurately within bins of common mid-points (see sections 2.1.2 and 2.2.1.1) is the basis of the multi-channel seismic method. This makes accurate positioning one of the most crucial requirements, especially for high-resolution surveys. Marine seismic navigation involves two main aspects: one is placing the research vessel at the desired position (piloting), which is a

so-called real-time activity, and the other is knowing exactly where the data have actually been recorded (source and streamer positioning). Knowing absolute position of source and sensor is necessary for returning to a certain surveying point later and tying the survey area into a geographical coordinate system. During a survey, it is the relative accuracy that plays a more important role, i.e. the accurate relative locations of midpoints. The accuracies obtained in a survey depend upon the equipment used, the configuration of the reference station on land and the position of the mobile stations with respect to the reference stations (Sheriff and Geldart, 1995). Especially 3-D acquisitions, with their complexity and large number of shot and receiver stations, need precise positioning. The design of a 3-D survey is impossible without knowledge of the types and limitations of positioning equipment. Standard navigation techniques used by the oil exploration industry rely mainly on radiopositioning, satellite observations, acoustic measurements, compasses and increasingly on the Global Positioning System (Sheriff and Geldart, 1995).

2.3.4.1 Global positioning system (GPS)

The NAVSTAR (Navigation System with Time and Ranging) *Global Positioning System* (GPS) is operated by the U.S. Government and is by far the most accurate global navigation system ever devised (Hurn, 1989). It is based on a constellation of 25 satellites (since 1994) orbiting the earth at elevations of 22 200 km, with four satellites in each of six orbital planes (Sheriff and Geldart, 1995). This ensures that four to seven satellites are visible from any point on earth at all times (Evans, 1997). Each satellite orbits the earth in about 12 hours and broadcasts on two carrier frequencies of 1575.42 (L1) and 1227.6 MHz (L2) modulated with a precision (P) code (Sheriff and Geldart, 1995). This P code allows determination of the signal transit time and, when multiplied by the velocity of light, of the range from the satellite to the GPS receiver of the user (Evans, 1997). The simultaneous solution of range information of four satellites determines the receiver clock error and the user's position in latitude, longitude and elevation by trilateration. The precision of this position was purposefully degraded by the Department of Defense using an operational mode called "Selective Availability" or "S/A" (Hurn, 1989). It was the largest component of GPS error until May 2nd 2000, when it had been switched off. With the remaining orbital and timing errors depending on atmospheric and equipment conditions, this *point-position mode* can now have an accuracy of 5 to 10 m (Evans, 1997).

However, *translocation* (or usage in *differential-operation mode*) can significantly improve this accuracy by using variations in observations measured simultaneously at a fairly close fixed station (base or *reference station* onshore) of known coordinates (Sheriff and Geldart, 1995). This station acts as a static reference point and transmits an error correction message via low-frequency radio waves to any other receiver in the local area. *Differential GPS* (dGPS) utilizes these error readings to remove short-term satellite perturbations (or the

S/A) from the mobile station, thereby obtaining precisions of better than a meter (Hurn, 1989). The closer one is to the reference point, the smaller becomes the error. If the user's receiver is stationary for 30 minutes, its position can be determined with an accuracy of 5 mm plus 1 mm per kilometer of separation (Evans, 1997).

GPS coordinates have to be transformed into local coordinates. Accuracy achieved thereby depends on measurement duration, whether the receiver is static or in motion, whether locations are required in real time or later for postprocessing, whether absolute locations or only relative ones are required and, most importantly, whether or not the translocation correction has been applied (Sheriff and Geldart, 1995).

2.3.4.2 Positional network

If GPS is the primary operational navigation system the vessel's position and heading, the latter usually measured with a gyrocompass, might be well known. However, sources and streamers can drift considerably. This is why they often have transponders or pingers mounted along their length allowing computation of their relative positions to the ship (Evans, 1997). Magnetic cable compasses additionally measure the streamer orientation, and tail buoys may have satellite receivers and transmitters on them providing their location with respect to the streamer and towing ship (e.g. Evans, 1997). GPS receivers may also be mounted on the tail buoy in order to determine its absolute position. All this information of the positional network has to be processed and combined to finally give the coordinates of the midpoints and to find the corresponding bin. On the large vessels of the exploration industry powerful workstations onboard carry out this data inversion in real-time and compute CMP coverage maps (see section 2.2.1.1) for quality control. Coverage shortcomings can thus be immediately fixed by line in-fill (Evans, 1997). The only way of quality controlling small-scale surveys with limited onboard facilities often is restricted to real-time ship navigation. Positioning irregularities of source and receivers will not be visible until postprocessing has been done.

2.3.4.3 Acquisition preplots

Prior to every survey, it is important to prepare a theoretical acquisition plan or *preplot*. It normally contains all useful information with regard to the acquisition, either in graphical or tabular form (Evans, 1997). *Preplots* show at least the beginning and ending coordinates for each planned sail line. The onboard navigation system controls the ship's speed, its direction and the shot firing interval to match as well as possible this theoretical acquisition plan.

2.4 Three-dimensional survey design

The primary goal of 3-D survey design is to ensure that field acquisition parameters produce an interpretable image of the exploration target. A secondary goal is to minimize the acquisition and processing time and the cost of the necessary equipment. Unfortunately, those two principle goals are at odds with each other. Hence, as with all 3-D seismic design

problems, the proposed solution to imaging the target will involve compromises among instrumental limits and geophysical parameters. Parameters have to be selected to meet the requirements of spatial continuity, resolution, mapping of shallowest and deepest horizons of interest and noise suppression. A number of formulas and criteria help to estimate their relative importance and are shown in section 4.4 to calculate seismic acquisition parameters from known properties of the geophysical target, set objectives and given technical limitations.

2.4.1 Seismic resolution

Resolution determines how close two points can get, yet be distinguishable. In reflection seismics, the vertical and lateral resolution of marine subsurface structures strongly depends on the seismic source and the streamer system. *Vertical resolution* is controlled by the dominant frequency and bandwidth of the reflected signals and can be improved by using higher frequency sources. The first Fresnel zone is taken as a measure of the *horizontal resolution* of unmigrated data (Sheriff and Geldart, 1995).

2.4.1.1 Vertical resolution

Rayleigh's $\lambda/4$ -wavelength resolution analysis is based on the ability to resolve reflection events from the top and bottom of a layer. His criterion (same polarity) defines the resolution limit as one-quarter wavelength of the dominant frequency f_{dom} (Lansley, 2000):

$$(2.17) \quad \boxed{\frac{\lambda_{dom}}{4} = \frac{v_{int}}{4f_{dom}}} \quad \text{with}$$

v_{int} : interval velocity of the target layer.

The smaller the interval velocity of the target layer and the higher the dominant frequency of the source, the better is the vertical resolution. Thus, with respect to the same target velocity and neglecting any frequency absorption or attenuation, theoretical vertical resolution depends only on the source's frequency content. Deconvolution tries to improve the vertical resolution by increasing the bandwidth (section 2.2.1).

2.4.1.2 Horizontal resolution

The first Fresnel zone is that part of a reflecting interface which returns energy to the receiver within half the dominant period of the first reflection. Because the wave must travel from source to reflector and back to the receiver, energy from the wavefront one-quarter of a wavelength ($\lambda/4$) behind the first wavefront is delayed by half a cycle when reflected back to the receiver (Fig. 2-8). The energy from all the points within the reflecting disk of radius $\overline{OA'}$ interfere constructively and are considered indistinguishable. The extent of this first Fresnel zone is used to describe the *horizontal resolution* of an unmigrated seismic section (Sheriff, 1991).

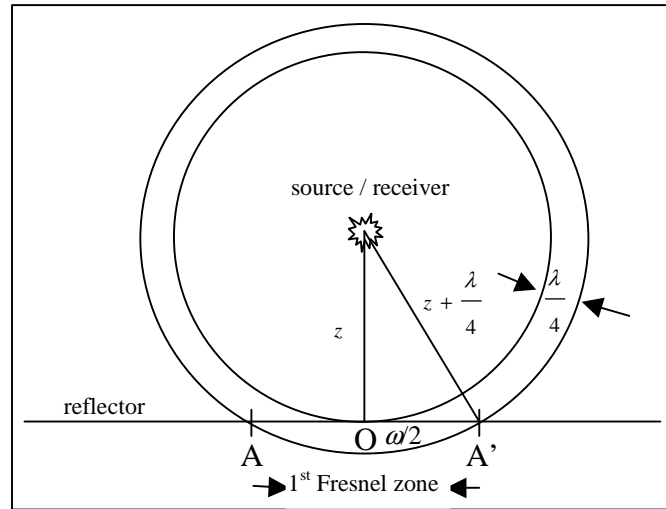


Fig. 2-8. Derivation of the first Fresnel zone's diameter ω for a coincident source and receiver and a horizontal reflector. The wavefront arrives first at reflection point O at the center and after a distance of $\lambda/4$ at A and A' at the edge of a disk where reflecting points cannot be distinguished, adapted from Yilmaz (1987).

The diameter of the Fresnel zone ω depends on the depth z of the reflector, on the velocity above the reflector v and the dominant frequency f_{dom} . The triangle in Fig. 2-8 leads to the following equation that can be solved for ω

$$(2.18) \quad \left(z + \frac{\lambda_{dom}}{4}\right)^2 = z^2 + \left(\frac{\omega}{2}\right)^2$$

$$\omega^2 = 4\left(z^2 + \frac{z\lambda_{dom}}{2} + \frac{\lambda_{dom}^2}{16} - z^2\right) \Rightarrow \omega = \sqrt{2z\lambda_{dom} + \frac{\lambda_{dom}^2}{4}} = \sqrt{\frac{2zv}{f_{dom}} + \frac{v^2}{4f_{dom}^2}}$$

Migration tends to collapse the Fresnel zone ($\overline{AA'}$) to approximately the dominant wavelength (Yilmaz, 1987). However, if the velocity field used in migration has an error of 0.5%, it can degrade this ideal horizontal resolution by a factor or more than 5 (Deregowski et al., 1997 in Lansley, 2000). Migration in two dimensions shortens the Fresnel zone only in the direction parallel to the in-line direction. Cross-line resolution is not affected unless a 3-D migration is performed.

2.4.2 Offset requirements

The position of the target horizons to be imaged plays an important role in determining the spread size of the receivers. There is a well-founded rule of thumb developed by field operations that relates horizon depths to offset (Stone, 1994). The nearest offset (x_{min}) should be smaller than the shallowest horizon of interest and the farthest offset (x_{max}) should be greater than the deepest one. In order to estimate the depth (z_{sh} and z_d) of these horizons, their rms-velocities (v_{sh} and v_d) and approximate arrival times (t_{sh} and t_d) are needed and can be calculated by:

$$(2.19) \quad x_{\min} < z_{sh} = v_{sh} \frac{t_{sh}}{2} \quad \text{and} \quad z_d = v_d \frac{t_d}{2} < x_{\max}.$$

If horizons are dipping, then the far offset should be extended as a function of dip (ϕ) by the distance $z_d \tan \phi$ (Stone, 1994) (see also migration aperture in section 2.4.5).

2.4.2.1 Near offset

In marine situations the uniform water layer would allow much larger nearest offsets than are necessary to overcome static problems in land surveys. However, other difficulties are inherent to marine acquisitions only, such as streamer feathering and variations in ship track. The closer the receivers are to the research vessel, the smaller will be the influence of these effects on data quality. Another consideration is the hyperbolic assumption (section 2.1.3.3) that would not be valid anymore if offsets approach or exceed horizon depths.

Since zero-offset represents the least distorted image of the earth in time coordinates, the nearest offset should be chosen as small as noise conditions allow in order to record a good approximation to zero-offset (Stone, 1994). Data processing is largely dedicated to correcting offsets to approximate zero-offset for stacking and noise reduction, and good data in the shallow part is needed for analyzing velocities with confidence. Therefore, sufficient coverage of the near offsets is important.

2.4.2.2 Far offset

Large offsets are important not only to allow a stable determination of stacking velocities but also to overcome multiple problems. To ensure a good quality velocity analysis a certain amount of normal moveout is required. The transformation of Dix hyperbolic normal moveout (see equation (2.6)) allows an estimation of the maximum necessary offset with respect to target depth and a certain desired normal moveout:

$$(2.20) \quad x_{\max} = v_{NMO} \sqrt{\Delta t_{NMO}^2 + 2t(0)\Delta t_{NMO}} \quad \text{with}$$

v_{NMO} : normal moveout velocity of the target layer

Δt_{NMO} : normal moveout

$t(0)$: zero-offset time of the target layer

For conventional oil-industry marine surveys, Musser (2000) suggests a value of 200 ms for Δt_{NMO} .

2.4.3 Spatial sampling

The maximum dip is an important geophysical parameter because it governs the spatial sampling of the survey and may cause production of reflected energy at the surface in regions beyond the target edges (section 2.4.5). If such energy is not recorded, then migration (section 2.2.3) cannot focus it back toward the target location (Evans, 1997). Thus, the amount of dip

in an area ultimately determines the physical size of a survey needed to properly image the area.

As described in section 2.2.1.1, bin sizes depend on CMP spacing. Thus, shot and receiver positioning must be chosen in a way to ensure that spatial aliasing for the resulting CMP interval is not a problem for the steep dip events. Antialiasing calculations for bin sizes are related to the maximum signal frequency or sampling interval (SI, i.e. temporal sampling; section 2.3.2.1) required to avoid aliasing and are typically based on the following formulas (Musser, 2000):

$$(2.21) \quad dX_{bin} = \frac{v_{avg}}{4f_{max} \sin \alpha_{max}} \geq \frac{SI v_{avg}}{2 \sin \alpha_{max}} \quad \text{in in-line and}$$

$$(2.22) \quad dY_{bin} = \frac{v_{avg}}{4f_{max} \sin \beta_{max}} \geq \frac{SI v_{avg}}{2 \sin \beta_{max}} \quad \text{in cross-line direction with}$$

dX_{bin} : maximum unaliased bin size in in-line direction

dY_{bin} : maximum unaliased bin size in cross-line direction

v_{avg} : average seismic velocity to the target reflector

f_{max} : highest unaliased seismic frequency in the wavelet

α_{max} : maximum dip in in-line direction to be imaged without aliasing

β_{max} : maximum dip in cross-line direction to be imaged without aliasing

A simple transformation yields an equation for the maximum unaliased frequency:

$$(2.23) \quad f_{max} = \frac{v_{avg}}{4dX_{bin} \sin \alpha_{max}} \quad \text{or}$$

$$(2.24) \quad f_{max} = \frac{v_{avg}}{4dY_{bin} \sin \beta_{max}}$$

Although spatial sampling may be adequate to permit unaliased migration of data, there could be significant attenuation of the higher frequencies due to mid-point or zero-offset-point scattering (section 2.2.1.1) within the bin (Lansley and Stupel, 2000). DMO (section 2.2.3.3) moves reflection points of data with finite source to receiver offsets to the zero-offset point, which may or may not be at the center of the output bin. If the bin size is too large and a dip is present, attenuation of high frequencies will result. The amount of attenuation depends on frequency, dip and the dimension of the bin in dip direction (Lansley and Stupel, 2000).

2.4.4 Acquisition Geometry

Acquisition geometry in marine 3-D seismics is primarily constrained by the available equipment. Most 3-D marine surveys using a towed gun and streamer configuration record a sequence of closely spaced parallel 2-D lines (in contrast to circle shooting or recording with bottom cables). Except for the tight line spacing, this type of marine 3-D acquisition is similar

to 2-D acquisition and many of the techniques already developed for 2-D processing can be applied (Vermeer, 2001). The sequence of 2-D lines can be shot in several ways. Although the minimization of the time spent moving from the end of one line to the start of the next is an important economic aspect, other scientific criteria may influence geometry decisions.

2.4.4.1 Antiparallel geometry

Antiparallel geometry reverses the shooting direction of every line. If subsurface dip is present, the smaller the number of midpoint lines (streamers) in one boat pass and the shorter the offset, the less irregular becomes illumination, i.e. reflection points are more evenly distributed (Vermeer, 2001). Fig. 2-9 demonstrates that adjacent boat passes should be antiparallel to minimize these illumination irregularities. Whereas for two parallel acquisition lines, the adjacent midpoints in the center of Fig. 2-9 (a) have opposite cross-line offset, hence different shot-to-receiver azimuth, for antiparallel shooting (Fig. 2-9 (b)), adjacent midpoints have opposite cross-line and in-line offset, hence identical shot-to-receiver azimuth. Only the single-source single-streamer configuration samples the subsurface in a regular way (Vermeer, 2001).

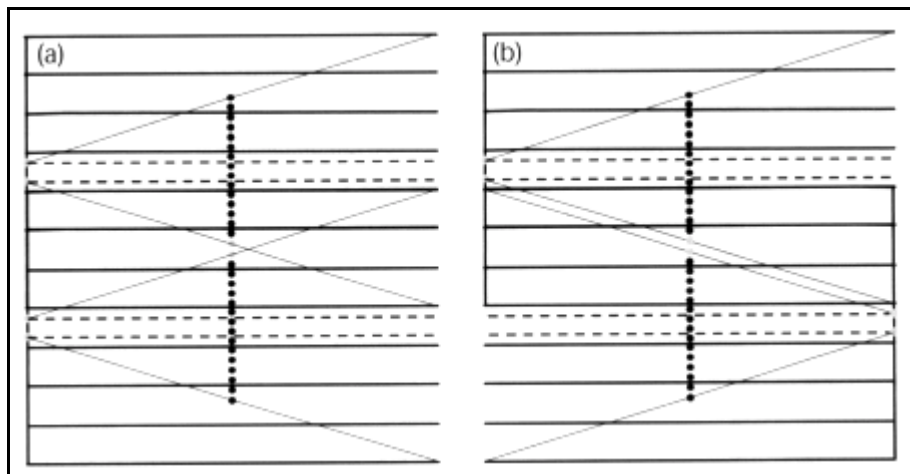


Fig. 2-9. Two adjacent boat passes; solid lines indicate streamers, stippled lines source tracks; lines connecting sources with the farthest receivers are the shot-to-receiver offsets for the outer midpoint lines; dots represent CMP positions; (a) parallel geometry; (b) antiparallel geometry; from Vermeer (2001).

Antiparallel geometry combined with asymmetric recording causes static effects when dipping structures are present. Asymmetric recording uses only one point-source and a receiver array, while in symmetric recording there are arrays of sources and receivers (Vermeer, 1991). An *updip* shot from a single energy source has the reflections arriving nearly vertically and at similar times (Fig. 2-10 (a)). *Downdip* shooting, however, produces reflections at an acute angle and at different times (Fig. 2-10 (b)). This results in a different stack for the updip versus downdip direction (Evans, 1997). In order to avoid this problem, an

asymmetric survey should be recorded in *parallel geometry*: either completely *updip* or completely *downdip*.

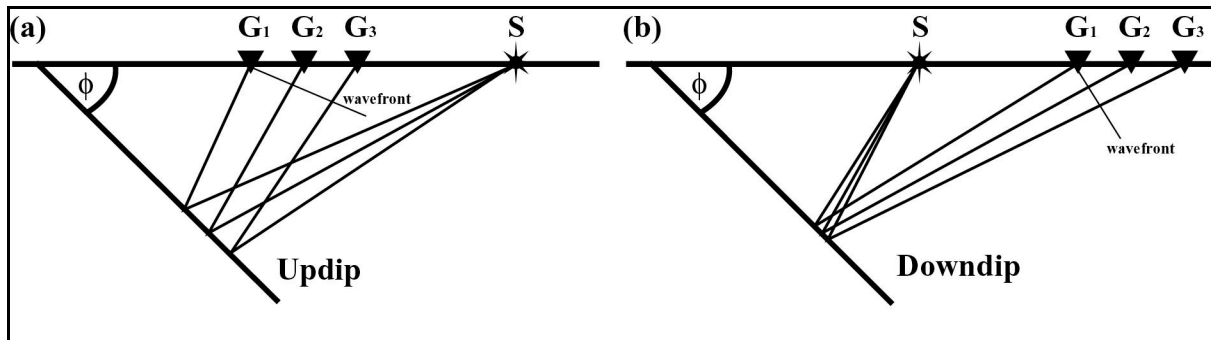


Fig. 2-10. Asymmetric recording (a) *updip* – wavefront arrives at similar times at receivers $G_1 - G_3$; (b) *downdip* – wavefront builds significant angle with surface and arrives at different times at receivers.

2.4.4.2 Parallel geometry

In *parallel geometry* acquisition lines are all shot in the same direction (Fig. 2-9 (a)). Apart from avoiding static effects, a great advantage of this technique is that survey area boundaries are smooth and the fold of coverage varies only slightly at the beginning and end of adjacent sail lines. For high-resolution studies, it is also easier to align CMP locations in the cross-line direction, to organize the survey grid in advance and to coordinate navigation of the vessel during acquisition. The turning time is double the time of antiparallel shooting. This extra time, however, could be used to produce compressed air, if the compressor power and the compressed air storage is limited.

Parallel shooting raises the question of whether the survey in-line direction should be *updip* or *downdip*. Lansley and Stupel (2000) favor *updip* for minimizing high-frequency attenuation that results from array effects: “The array with the longest effective array length should be *updip*.”

2.4.4.3 Dip versus strike shooting

The *strike direction* of a geologic section is the direction marked by the intersection of a horizontal plane with the geological unit; the *dip direction* is perpendicular to this direction. The geology of beds is easier to understand when the seismic profile is shot in dip direction and data tend to be of better quality (Evans, 1997). In addition, since aliasing considerations ask for finer sampling in steep dips, most seismic lines of a 3-D survey using a parallel acquisition geometry are recorded parallel to the dip direction (Evans, 1997) while the distance between CMP lines is chosen at an interval larger than the receiver spacing.

2.4.4.4 Streamer configuration

Two main configurations have been described in section 2.1: the single (example in Fig. 5-1) and the multi-streamer configuration (example in Fig. 5-4). While a single streamer and a single source can easily be attached to the center rear deck of the research vessel, two approaches can be used to position additional streamers with a desired separation distance. One approach is to tow the equipment from paravanes and the other is to use solid booms swung out from the vessel's sides (Evans, 1997).

2.4.4.5 Streamer feathering

Whether the ship is towing a single streamer or many of them, the position of the towed system is always subject to currents. A phenomenon called *streamer feathering* occurs when a current or wind with a component in cross-line direction is present. Feathering influences the distribution of CMPs on the survey area, and drift of the streamer causes a subsurface coverage that is different from the one designed. During data processing the location of each trace's actual position (CMP) must be known, so that it can be assigned to the correct bin (section 2.2.1.1). Thus, accurate source and receiver positioning (section 2.3.4) is very important to ensure good imaging quality. In order to provide continuous monitoring of streamer and boat position during acquisition, it is necessary to have real-time navigation information.

2.4.5 Survey area

A major step in 3-D survey design is deciding for the extent of surface coverage needed to obtain a desired subsurface image (Evans, 1997). The surface area should always be larger than the area to be mapped because of the fold-taper zone and the radius of the migration operator (Vermeer, 2001).

Fold taper is a zone added to the edges of the area of interest to ensure full fold. Therefore, a tail end of data (half the streamer length) needs to be recorded at the beginning and end of each sail line. This way, stacked full fold coverage is obtained at the desired last full fold CMP or bin (Evans, 1997).

Migration is a processing step that returns reflection and diffraction energy to their true location (section 2.2.3). Summation along diffraction hyperbolas in order to focus energy on diffracting events at target limits requires additional coverage beyond the area intended to be mapped.

As we have seen in section 2.1, reflection points move when dip is present. The distance A in Fig. 2-2 is called the *migration aperture* and depends on dip angle ϕ (or α in in-line and β in cross-line direction) and target depth z . With the aid of the right-angle triangle $D'ZM'$, depth z and dip ϕ , the aperture A can be derived as follows (Evans, 1997):

$$(2.25) \quad \tan \alpha = \frac{A_i}{z} \Leftrightarrow A_i = z \tan \alpha \quad \text{with } A_i: \quad \text{aperture in in-line direction}$$

$$(2.26) \quad \tan \beta = \frac{A_c}{z} \Leftrightarrow A_c = z \tan \beta \quad \text{with } A_c: \quad \text{aperture in cross-line direction.}$$

In order to allow for migration effects, each sail line should be increased at each end by the aperture length A_i and as many sail lines must be added so that aperture length A_c is reached (Fig. 2-11). Additionally, the recording time must be long enough to include diffraction tails and all of the dipping events of interest.

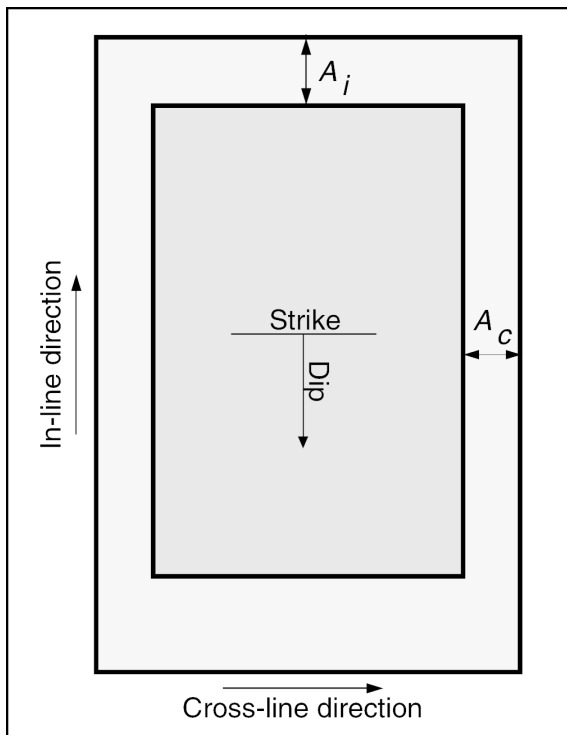


Fig. 2-11. The 3-D aperture window frame; A_i : aperture in in-line; A_c : aperture in cross-line direction.

The required migration radius or migration aperture is often described in terms of Fresnel zone radius (see section 2.4.1.2), which is calculated by using the dominant frequency or wavelength of the wavelet. This Fresnel zone has a very specific meaning and does not quite express the zone around the imaging point that is required for complete imaging with correct phase and amplitude. For broadband data, the Fresnel radius is not large enough. It is better to define a larger *zone of influence* for migration by including the start and end of the wavelet and not only its dominant wavelength and to

use the radius of that zone (Vermeer, 2002).

CHAPTER 3: INSTRUMENT PARAMETERS

3.1 Research vessel

The research vessel forms the basis of every marine acquisition. For each of the two surveys, we rented over a period of two weeks a 13-m long and 3.5-m wide boat (Fig. 3-1) from the “Institut Forel” of the University of Geneva. This boat served as working platform during acquisition on Lake Geneva, i.e. for compressed air production, gun and streamer deployment, data quality control and positioning reference of source and receivers. Thus, the vessel represents a storage area for all seismic equipment during measurements and during ship-down time at night. Fig. 3-1 shows “La Licorne” in Ouchy harbor, Lausanne: the compressor is placed on the front deck (Fig. 3-1 (a)) while the streamers are stored on the rear deck (Fig. 3-1 (b)). The recording and navigation instrumentation as well as the seismic sources are located in the boat’s interior. The guns can be deployed via the back door (closed in Fig. 3-1 (b)) with aid of an onboard crane.

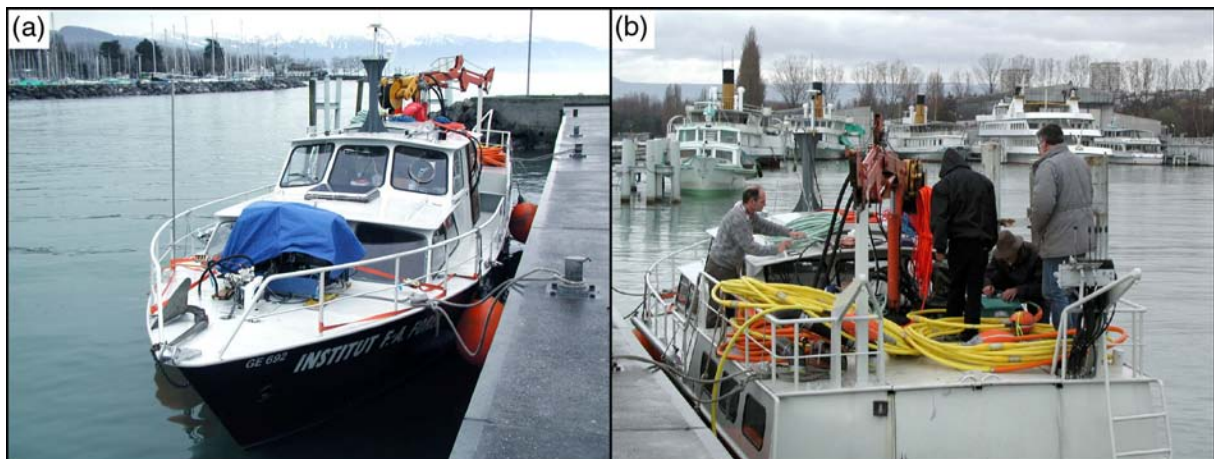


Fig. 3-1. Research vessel “La Licorne”: (a) front view showing covered compressor; (b) rear view showing storage of streamers onboard and crane.

3.2 Streamers

3.2.1 Innovative Transducers Inc. solid streamer

Our first streamer consisted of two interconnectable solid units (see section 2.3.1.2), one lead-in, one deck cable and one tail section. Innovative Transducers Inc. (ITI) constructed the ensemble under the name Stealtharray in 1997 in Texas, U.S.A. (Fig. 3-2 (a)). Each streamer section contains 24 groups of one hydrophone spaced at 2.5 m and two bird coils added between groups towards the end of the section. Including twice the 1.25 m-distance between connector and first / last hydrophone the total section length amounts to 60 m. The lead-in measures 60 m, the deck cable 20 m and the tail section 2.5 m. A tail buoy can be attached to the stainless eye hook and swivel at the end of the tail section in order to provide a reference

on the cable position and to ensure that the cable has straightened out after pre-line ship maneuvers.



Fig. 3-2. Streamer sections: (a) deployment of ITI Stealtharray with floats (b) enlarged float; (c) orange Nexgen S/N Technologies section rolled on deck together with lead-ins (greenish), deck cable on roof (orange) and drogue rope (blue), two yellow ITI sections and yellow old lead-in; (d-e) configuration during streamer tests in March 2001: ITI sections towed port and starboard, S/N section in center; floats and GPS rafts keep streamers near surface; tail buoys are attached to each tail section.

Although this non-fluid filled flotation cable with contoured hydrophone nodes was constructed to float in fresh water, a 2-D survey conducted in November 1998 (Zingg et al., 2003) revealed severe buoyancy problems by ghost reflections in the data. Connectors and lead-in were obviously too heavy and only the positive buoyancy of the tail buoy kept the streamer from sinking completely (Fig. 3-3). Further details about this construction problem and the results of streamer / lead-in buoyancy tests (June 1999), which were carried out in the lake and in the laboratory's pool, are described by Tacchini and Zingg (2000). ITI later confirmed that the lead-in is a non-flotation type and that the measured streamer weight in water does not correspond to construction specifications. In order to guarantee that the two streamer sections stay horizontal below the water surface, orange syntactic foam cable floats

are fixed around each connector (Fig. 3-2 (a-b)). These floats keep the streamers at an approximate depth between 10 and 20 cm. In spite of the close vicinity to the water surface, noise from wave action did not visibly affect the shot gathers. The advantage of a shallow streamer for high resolution studies is, that receiver ghost notching does not occur for frequencies below 3000 Hz (see section 2.3.3.5). This way, the recorded bandwidth will mainly depend on the gun, which is usually located at depths greater than 20 cm (see section 3.4.1 and 3.4.2). A special 45-m long drogue rope attached to the tail section of the streamer should give the appropriate tension to keep the array straight when towed at 4-5 km/h.

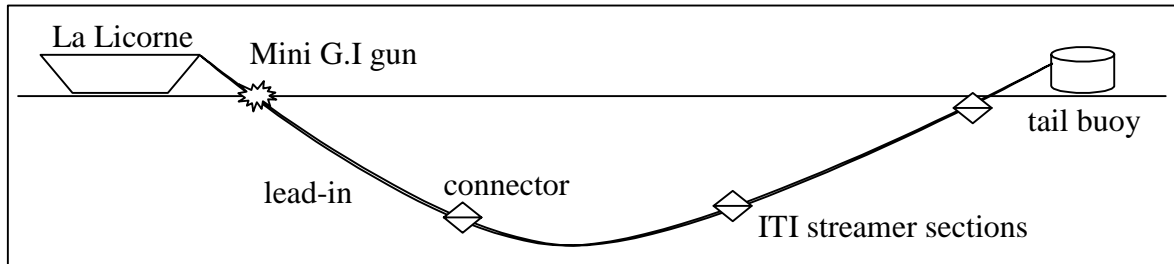


Fig. 3-3. Estimation of streamer shape during 2-D acquisition in November 1998 using 55 m of lead-in cable, 120 m of total streamer and a tail buoy attached to the 2.5 m tail section.

During the acquisition of November 1998, we noticed that several hydrophones recorded only noise or changed their recording characteristics from shot to shot. In order to distinguish problems due to the hydrophone itself from problems related to the connectors, two sets of tests were conducted in the laboratory pool. For the first test, section #1 was connected via lead-in to the deck cable and section #2 to the end of section #1. For test two, section #1 and #2 were interchanged. Kicking on the pool's side represented the source and data were recorded with 60 dB of gain on the BISON seismograph (see section 3.3). In both tests, traces 9 and 24 on section #1 and trace 13 on section #2 recorded no signal at all. This could either mean that the hydrophone of those traces is completely dead or that their preamplifier introduces a high direct current (see following section). Traces 22, 31 and 37 had strange characteristics no matter what streamer configuration was chosen, thus pointing at a connector defect (which was later repaired at ITI).

The Stealtharray houses ISOSENSTM piezo polymer (PVDF) type hydrophones with one preamplifier per group. Hydrophone voltage sensitivity is 22 V/bar, which preamplified by 5 dB of gain gives a final sensitivity of about 40 V/bar (see section 2.3.1.1). The preamplifiers need to be powered by 12 V DC and draw an average current of 1 mA per amplifier. Experience shows that the consumption significantly increases after longer use, when streamers are subjected to increased water pressure during vertical signature measurements or when water penetrates the connectors. To prevent a short coming of battery power during daily measurements and to provide for the necessary -12 V, 0 V and +12 V

voltage levels, we used two 12 V batteries. Three amplifier powering cables from the ITI deck cable are connected to the battery series as indicated in Fig. A-1 (a).

The recordable hydrophone bandwidth ranges from 6 Hz to 4.7 kHz. At frequencies higher than 30 Hz, the hydrophone has a flat response, which then decreases to low amplitudes towards the 6 Hz band-limit. A calibration was performed in April 2001 by S/N Technologies in Texas, U.S.A., on the 4-year-old streamer cable #2, which we sent there in order to guide the construction of a new streamer section for Survey II.

3.2.2 S/N Technologies Inc. solid streamer

The new third streamer section, which we acquired from S/N Technologies Inc. in 2001, should have the same characteristics as the other two sections from ITI since they were to be used simultaneously in a multi-streamer 3-D acquisition. ITI was sold to Syntron / Sercel in 1997 and does not manufacture high-resolution streamers of needed dimensions anymore. S/N Technologies, Inc. was founded by the former ITI president who designed a new generation of polymer hydrophones (Nexgen) that address the manufacturing and performance limitations of previous designs. The new solid array features extreme flexibility (minimum bend radius of 46 cm and a diameter of 51 mm), reduced S/N ratio and no hydrophone nodes. The hydrophones of the same PVDF polymer type and their preamplifiers are completely encapsulated with a two-part urethane material, which provides the first of many watertight seals. Hydrophone sensitivity is, as that for the ITI sections, 22 V/bar. The preamplifiers though are different and have a voltage regulator located at the preamplifier locations to prevent problems with an individual preamplifier getting into different channels. Each amplifier draws an average current of 7 mA. Hydrophone bandwidth ranges from 3 Hz – 4 kHz and a pre-amp low cut is set to 10 Hz.

We purchased one Nexgen analog-active section with 24-channels of 2.5-m trace spacing, an integrated 2.5 m tail section and three 40-m long Nexgen analog lead-ins connecting to a 72 channel deck cable (Fig. 3-2 (c)). All hydrophone preamplifiers are powered via this deck cable (see Fig. A-1(b) for battery connection). For our multi-streamer measurements, a color code simplifies connecting each 24-channel deck cable branch to the corresponding connector on the seismograph (Fig. A-1): ITI section #2 attaches to the starboard side of the ship (starboard = green = channels 1-24), the new S/N section is towed directly behind the vessel (center = blue = channels 25-48) and ITI streamer section #1 occupies the port side (port = red = channels 49-72). This configuration is shown in Fig. 5-4 with the same colors indicating each section's GPS raft. This color code will be maintained throughout the whole thesis.

The three streamers were first tested in March 2001 with the connection scheme as described above (see Fig. 3-2 (d-e)). Fig. 3-2 (a) shows the deployment of the ITI streamer while Fig. 3-2 (c) illustrates on deck storage of all cables, GPS rafts (see section 3.6 and Fig.

3-28) and tail buoys. Note the difference in bend radius between the two streamer types. The ITI sections were easily visible on the water's surface (Fig. 3-2 (d-e)) since we attached the orange foam cable floats to their front connectors while the GPS rafts were fixed close to the connectors at their end. Not only did we notice a lack in buoyancy of the Nexgen streamer but, more importantly, a severe amplification problem: dead traces, traces with large amplitude variations from shot to shot and a much higher noise level than on the old sections. After a series of tests, S/N Technologies found that this problem was based on an error during modifications on the gain of the preamplifiers. They built a new active section that was delivered end of May 2001 and immediately tested in Lake Geneva together with Richard Pearce, the president of S/N Technologies. Although the new streamer is still negatively buoyant, the amplifiers work well and the signal-to-noise ratio is significantly better than that of the ITI streamer sections (see section 3.3.1). S/N Technologies was sold to Input / Output in July 2002.

3.2.3 DC measurements on hydrophones

The PVDF of each hydrophone (2.3.1.1) produces a voltage that is proportional to the pressure amplitude of the seismic / acoustic wave. In an ideal noise-free environment no voltage would be measurable. This defines zero amplitude and is equivalent to the zero-crossing of the measured signal. Voltage differences in seismic measurements are so small that they need to be amplified. An imperfection in the construction of such amplifier in the hydrophone can lead to the introduction of a *direct current (DC)*, which can vary in each channel. Very high DC voltages could lead to signal saturation during recording (see section 3.3.1).

Fig. 3-4 shows a schematic of how we carried out DC measurements (April 2001) on each channel of all three streamer sections. The results are listed in Table 3-A, where channels highlighted in grey show elevated DC voltages. Remarkable is the correspondence of three of these channels to those four hydrophones that were found to be dead or have a possible amplifier defect (see section 3.2.1).

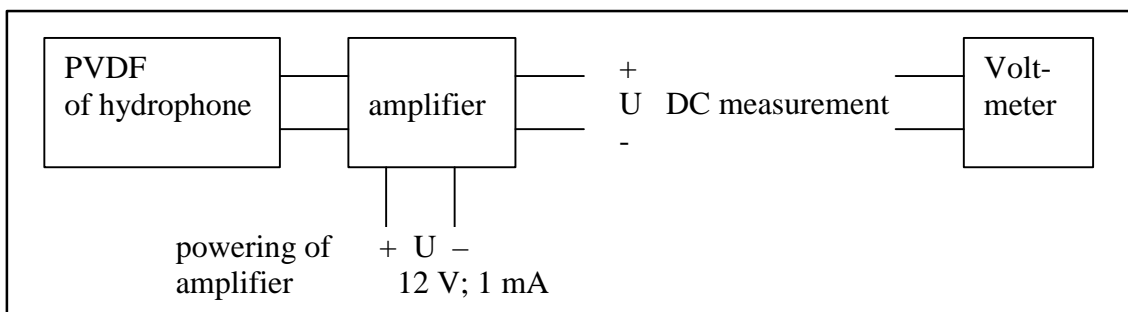


Fig. 3-4. Schematic of DC measurements on each hydrophone.

Trying to correct for a potential amplifier problem, André Rosselet, our electrical engineer, added capacitors to each of the indicated channels in the deck-cable. A repetition of

the same DC measurements (values after the slash) shows that the direct current on those corrected channels is now significantly reduced. Values on the remaining channels are remarkably similar when comparing both measurements. In May 2001, the functioning of those capacitors was verified during gain-constant test shots (section 3.3.1). While trace 24 on streamer section #1 and trace 13 on section #2 remain dead, traces 9 (#1) and 12 (#2) work well when setting constant gains at 24 dB or less.

Trace number	Code	DC voltage (mV) ITI streamer #1	DC voltage (mV) ITI streamer #2	DC voltage (mV) S/N streamer
1	A-B	+0.2 / -0.3	0 / 0	+13.3
2	C-D	+0.2 / +0.1	+0.2 / +0.2	-2.8
3	E-F	+0.2 / 0	0 / 0	-4.4
4	G-H	-0.2 / -0.2	+0.2 / +0.2	-13.4
5	J-K	0 / 0	-0.1 / -0.1	-6.3
6	L-M	0 / 0	+0.3 / +0.3	-21
7	N-P	-0.1 / -0.1	0 / 0	+17.8
8	R-S	-0.2 / 0	+0.6 / +0.6	-13.0
9	T-U	+8.0 / +1.5	-0.1 / 0	-10.3
10	V-W	-0.2 / -0.2	+0.3 / +0.3	-16.6
11	X-Y	-1.1 / -1.1	0 / +0.1	+11.9
12	Z-a	-0.3 / -0.3	+2600 / +1018	-20.6
13	b-c	-0.3 / -0.3	+14700 / +700	-19.6
14	d-e	-0.4 / -0.4	0.6 / +1.6	-10.2
15	f-g	0 / 0	-0.7 / -0.7	-11.2
16	n-i	0 / 0	0 / 0	-32.0
17	j-k	-0.4 / -0.4	+0.2 / +0.2	+6.0
18	m-n	-0.4 / -0.4	+0.1 / 0.1	+33.3
19	p-q	0 / 0	0 / 0	-11.1
20	r-s	+0.1 / +0.1	-0.1 / -0.1	+13.2
21	t-u	+0.4 / +0.2	-0.2 / -0.2	-3.4
22	v-w	-0.4 / -0.5	+0.3 / +0.3	+9.6
23	x-y	-0.2 / -0.2	+0.4 / +0.4	-10
24	z-AA	-0.25 / -2.0	-7.4 / -3.6	-64.7

Table 3-A. Results of DC measurements. The code refers to indications on the deck-cable pins that connect to the seismograph. Values behind the slash are results of repeated measurements after addition of capacitors to channels indicated in grey.

3.3 Seismographs

Two different seismographs were used for the recording of seismic signals. A GEOMETRICS StrataView R series (Fig. 3-5 (a)), 48-channel seismograph with a 4-bit instantaneous floating point (IFP, section 2.3.2.5) gain-ranging system followed by an 18-bit A/D converter using 32 kHz oversampling (equivalent to 22 bits of resolution or more if the sampling frequency is less than 32 kHz or the sample interval is larger than 31.25 μ s; see section 2.3.2.4) served as a recording unit for the first 3-D acquisition. Included is a standard 36 dB preamplifier gain followed by the 24 dB floating point amplifier (section 2.3.2.5). Data were saved directly on hard disk and transferred later via a SUN Workstation onto tape. Survey II was conducted using a BISON Spectra 96-channel instrument (Fig. 3-5 (b)) with Jupiter system software and an external DAT tape drive (HP SureStore DAT24). The BISON's 20/20 VISION A/D Seismic Data Acquisition Board provides a maximum of 60 dB gain (steps of 12 dB) selectable for each channel, a sampling rate of up to 20 μ s and 20 bits of dynamic range with oversampling software algorithms (Delta-Sigma) allowing resolutions of

up to 24 bits. For both instruments an *anti-aliasing filter* (see section 2.3.2.1) is applied before analog-to-digital (A/D) conversion, which varies automatically with sampling rate. Data were recorded in IBM floating point 32-bit SEG-Y format. Either of the two seismographs available for this project was designed for land seismic surveys where shot recurrence rate (see section 3.3.3) is not a constraint that influences acquisition strategy.

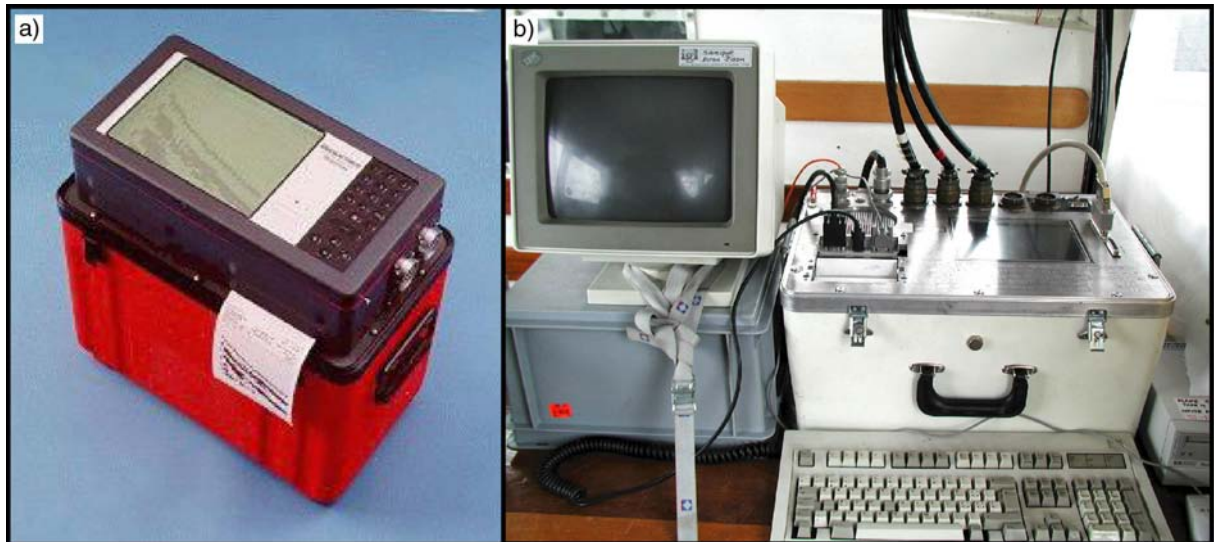


Fig. 3-5. Seismographs: (a) 22-bit GEOMETRICS StrataView R series used for Survey I; (b) 20-bit BISON Spectra used for Survey II.

Using equation (2.10), the 20-bit A/C converter of the BISON has a theoretical dynamic range of about 120 dB, while the 22-bit GEOMETRICS can reach up to 132 dB (see also Table A-1). However, considering the instrument's internal sampling frequency (f_{os}) of 32 kHz and Nyquist frequencies of 2 kHz for Survey I and 1 kHz for Survey II, we can get oversampling up to a factor of 8 and 16, respectively (equation (2.12)). This improves resolution by 1.5 / 2 bits or 9 / 12 dB and thus increases the theoretical dynamic range of the GEOMETRICS to 141 / 144 dB. Actual or measured dynamic ranges as given by the constructors lie far below the theoretical values and depend on the chosen sampling rate and recorded bandwidth. Although the theoretical dynamic range of both seismographs differ by more than 20 dB, the recorded range for a sampling interval of 2 ms and signal between 3 to 150 Hz was found to be almost identical: the BISON reaches 110 dB (ENOB = 18 bits, see section 2.3.2.4) and the GEOMETRICS up to 113 dB (ENOB = 18.5 bits).

3.3.1 Signal amplification

Survey I was conducted with a standard 36 dB preamplifier (K) gain automatically set in the GEOMETRICS recording instrument.

For Survey II, a number of tests were conducted with the BISON seismograph in order to determine (1) the BISON's saturation level and (2) the optimum recording gain via constant-gain test shots (section 2.3.2.5).

(1) BISON saturation test

An *AC coupled* seismograph excludes *DC voltages* by employing a series capacitive element. Such *DC voltages* can be induced by hydrophone amplifiers (section 3.2.3). If the recording instrument is not *AC coupled*, the signal may be saturated much more easily. This effect is illustrated in Fig. 3-6. Signals without amplification (Fig. 3-6 (a)) lie far below the instrument's saturation level. Amplified signals such as the one shown in Fig. 3-6 (b) will be saturated if the *DC* exceeds the difference between saturation level and maximum amplified input amplitude (Fig. 3-6 (c)).

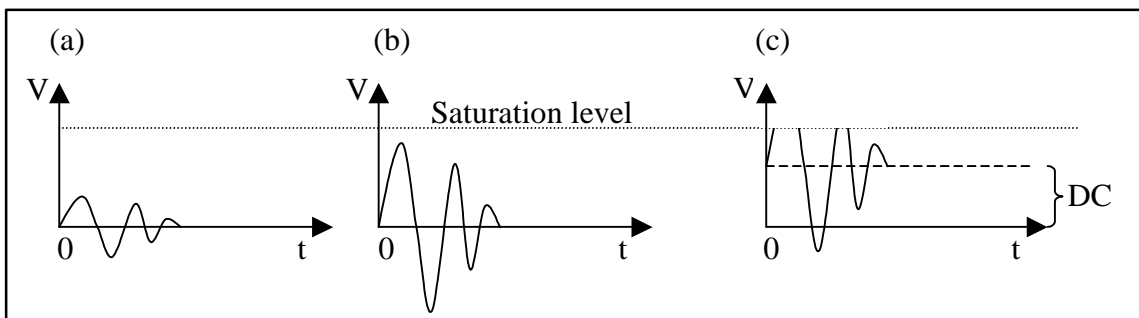


Fig. 3-6. Saturation induced by the presence of a DC. Dashed line indicates the instrument's saturation level; (a) no amplification; (b) amplified signal; (c) amplification with DC results in signal saturation.

It is thus important to determine the BISON's saturation level. To do so, we send a sinusoidal current onto pins A and B of the connector for channels 1 through 24, then superimpose a direct current. We record over a time of 5 seconds at a sampling rate of 0.5 ms and a gain of 60 dB. At some time during these 5 seconds, the *DC* pulse is added and with every new measurement its amplitude increased (Fig. 3-7).

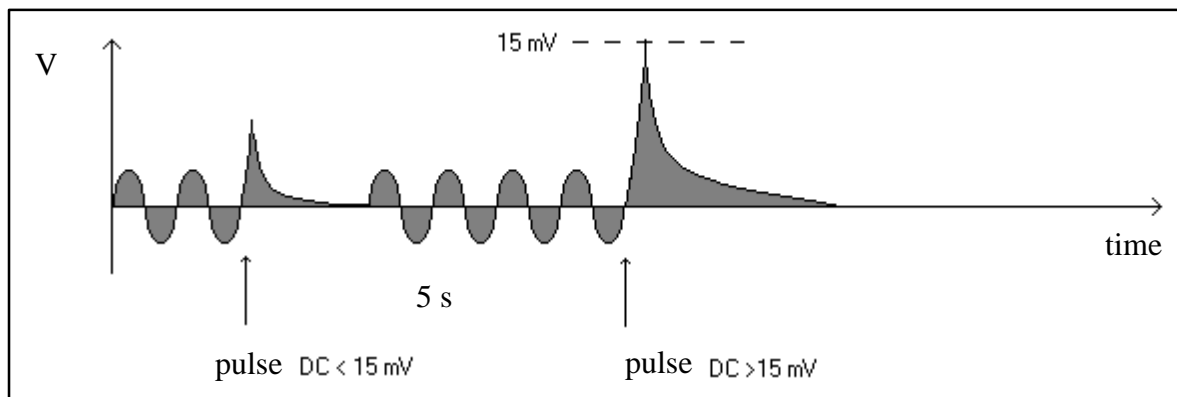


Fig. 3-7. BISON saturation test with a DC pulse superimposed on a sinusoidal current. If the DC exceeds 15 mV at 60 dB, the BISON is saturated and no more measurement is possible.

If this amplitude is small, the sinusoidal current will appear again after the pulse, but if it passes a threshold of 15 mV, the BISON is saturated and no more measurement is possible. This means that the maximum recordable amplitude of an incoming signal without gain must

be smaller than 15 V. At the same time this experiment showed that the BISON is not AC coupled.

(2) BISON gain test

During signature measurements in September 1999 (see also 3.4.6) using the double chamber Mini G.I Air Gun (section 3.4.2), we noticed a signal saturation on the BISON seismograph at a gain of 60 dB. Fig. 3-8 shows one shot gather recorded with both ITI streamers placed vertically below the source, focusing on the direct wave at the nearest 24 traces (section #2). Indicated are areas where signal saturation is easily detectable by the clipping of high amplitudes.

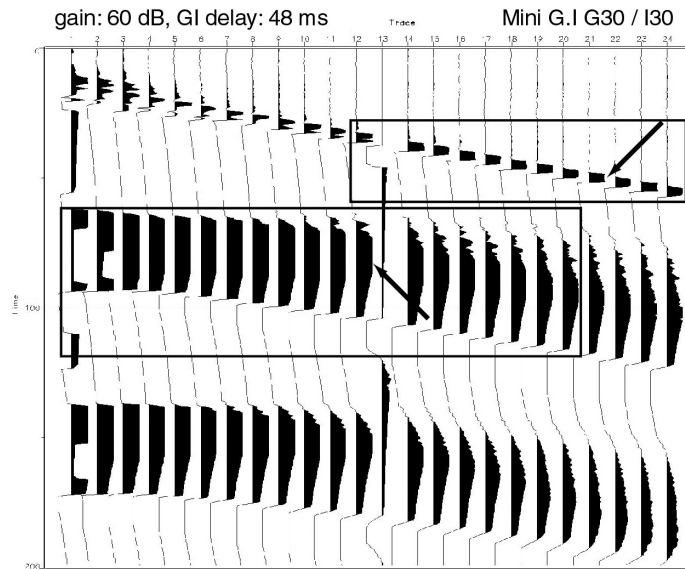


Fig. 3-8. Signature measurements (section 3.4.6) with interconnected ITI streamer sections vertically below Mini G.I G30 / I30 Air Gun source (section 3.4.2). This shot gather was recorded at 60 dB and a GI delay of 48 ms (see section 3.4.5). Arrows and rectangles point at zones where signal clipping is visible.

In order to avoid this problem and to determine the correct amount of recording gain, also with regard to saturation due to amplifier DC, a series of constant-gain test shots was conducted in May 2001 during streamer testing with the air gun using the multi-streamer configuration. For each shot the gain was increased in steps of 12 dB from 12 dB to 60 dB. Fig. 3-9 (a) and (b) show example shot gathers at 24 dB with either a 4 Hz or 40 Hz low-cut filter applied. In (c) the same 40 Hz filter is combined with a recording gain of 60 dB. Overall, the signal shape shows no clipping of high amplitudes except for the direct wave close to the source in Fig. 3-9 (c). Dead traces 13 (#2) and 24 (#1) of the ITI streamer sections correspond to defect hydrophones, but traces 9 (#1) and 12 (#2), as mentioned in section 3.2.3, saturate due to amplifier DC at gains larger than 24 dB (Fig. 3-9 (c)). The elimination of high-amplitude, low-frequency noise superimposed on the signal reduces this effect. While trace 12 is dead because of saturation at a gain of 24 dB and full bandwidth (a), it is properly recorded when cutting frequencies below 40 Hz (b).

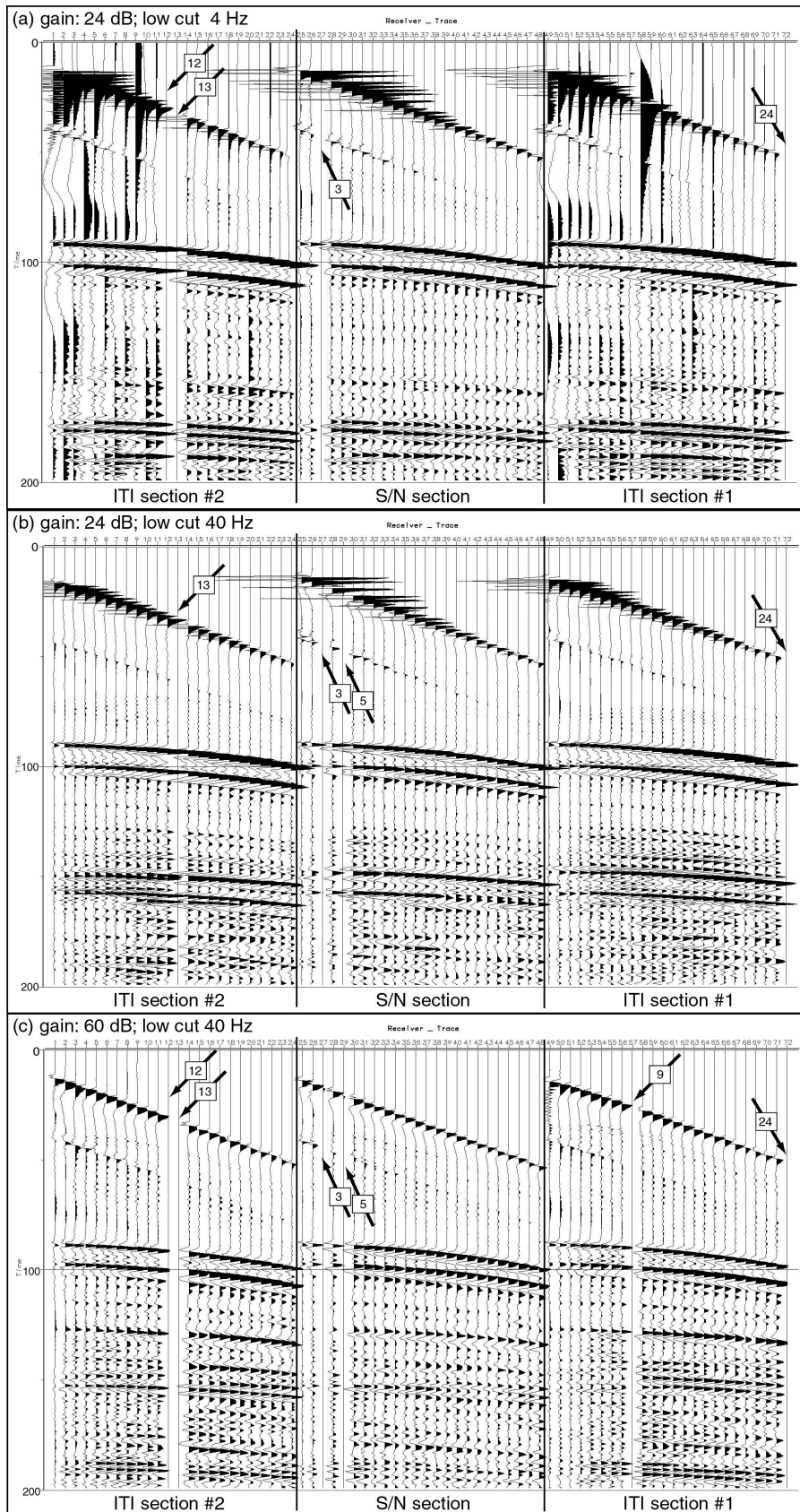


Fig. 3-9. Constant gain test shots with Mini G.I G15 / I15 Air Gun source in multi-streamer configuration. Example gathers recorded at 24 dB with either (a) a 4 Hz or (b) a 40 Hz low-cut filter applied and (c) at 60 dB plus a low-cut at 40 Hz (saturation for direct wave).

It is also important to study the noise distribution on all three streamer sections, in order to determine low-frequency filter limits for data processing (section 6.7). For this purpose, data were recorded without firing the gun (Fig. 3-10 (a)). The strikingly lower noise level on the centered S/N streamer section compared to its neighbors is confirmed by their noise spectra (Fig. 3-10 (c)). The noise level recorded on ITI streamer #2 at frequencies below 10 Hz is more than sixteen times larger but decreases rapidly and becomes very low between 50 and 70 Hz. If the observed noise is seismic noise, this would mean that the hydrophone sensitivity of the ITI streamers is higher at frequencies below 50 Hz. If the noise is mainly of electronic origin, the S/N streamer simply has a better signal-to-noise ratio. As described in the previous section, the nominal hydrophone sensitivity of both streamer types is the same, although their pre-amp low cut filters vary from 6 Hz (ITI) to 10 Hz (S/N). This explains the sensitivity difference below 10 Hz while a better shield against electronic noise of the S/N section would be an explanation for the difference above 10 Hz.

On the S/N hydrophones of shot gather Fig. 3-10 (a), significant noise with a spectral peak of 30 Hz (d) could be due to boat-vibration noise transmitted to the streamers. Attaching a bungee cord between the lead-in and vessel or lead-in and boom rafts significantly reduces the noise level in the data (Fig. 3-10 (b) and (d)). The spectrum (d), calculated only on traces from the S/N streamer section without (a) and with (b) the cord, illustrates this noise reduction by the elimination of the 30 Hz peak. Bungee cords were thus used throughout Survey II. The optimum recording gain was set to 24 dB using a low-cut filter of 25 Hz during acquisition.

3.3.2 Amplitude variations along streamers

Fig. 3-9 shows that amplitudes vary significantly within the first traces of the new S/N streamer section. Traces 3 and sometimes 5 seem to have recorded no signal at all. Nevertheless, the application of an automatic gain control (AGC) using a 50 ms operator length reveals that the hydrophone pre-amplification must have been set too small and that data have only been recorded with much lower amplitudes. Ideally, a hydrophone calibration is necessary to determine such variations in amplification levels between receivers. Only with this knowledge is it possible to properly correct individual traces and keep real amplitude information for future amplitude versus offset (AVO) studies. Hydrophone calibrations have not been provided by S/N Technologies and, since these measurements require special technical equipment, they have not been conducted at our Institute. Consequently, real amplitudes are not available and an AVO analysis can not be performed at this state of the project. However, studying relative variations in hydrophone sensitivity allows application of a corrective scalar to weak traces. This will at least make all traces in a CMP gather contribute evenly to the stack.

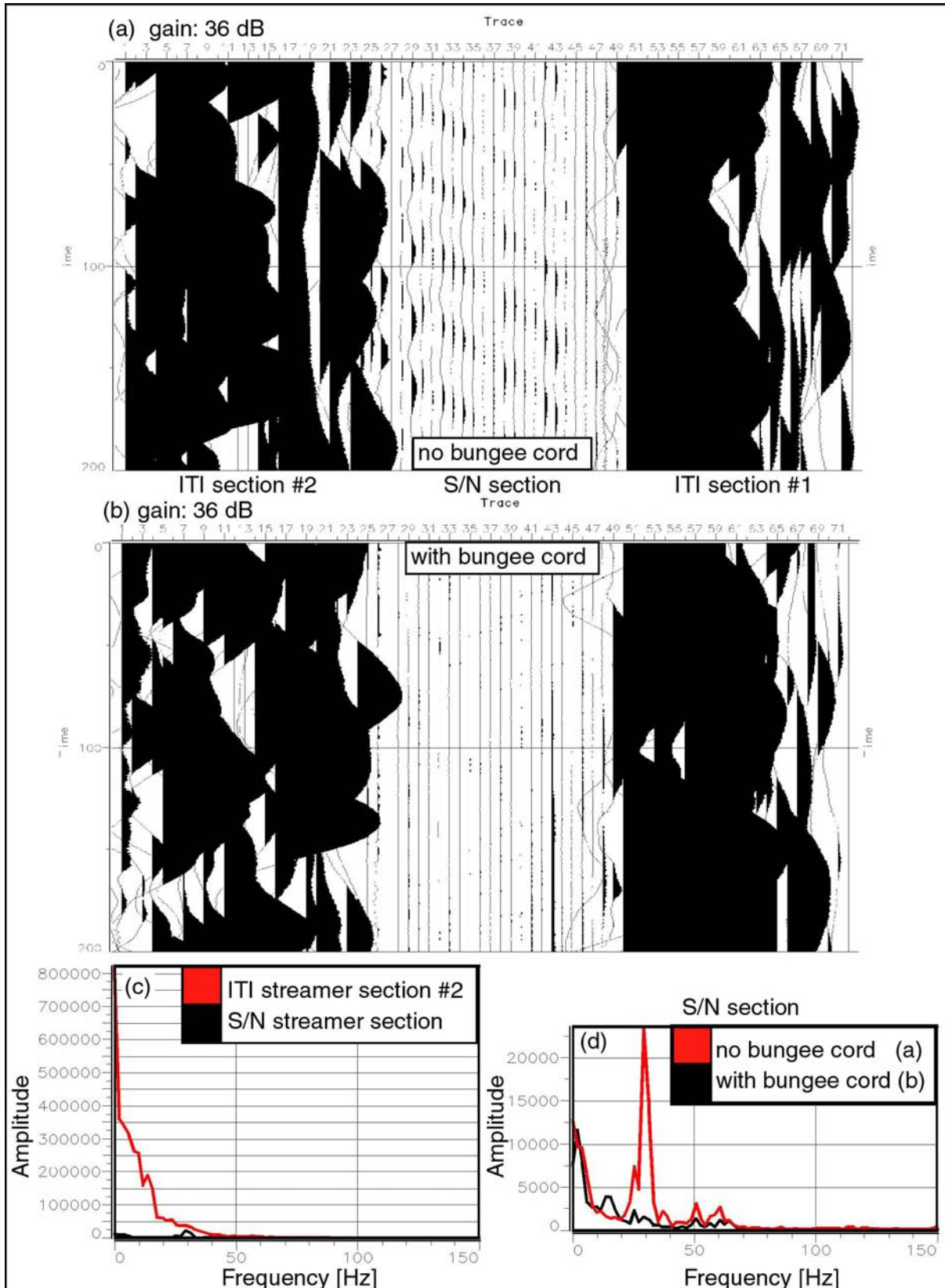


Fig. 3-10. Noise tests with all three streamer sections in multi-streamer configuration recorded at 36 dB with (a) lead-in fixed directly to the vessel and (b) usage of bungee cord for lead-in attachment. Frequency spectra compare noise levels on both streamer types (c) of the data in (a) and on the S/N section (d) with and without bungee cord application on the data in (a) + (b).

In order to get an idea of hydrophone sensitivity along all three streamer sections, the following analysis of two different data sets was carried out. Data set 1 consists of 241 shot gathers from a profile acquired during a 2-D survey in October 2000 (Chaudhary et al., 2002; Chaudhary, 2002, see also Fig. 4-7). The position of the chosen gathers of this profile also correspond to a portion of line 140 (306 shots) of 3-D multi-streamer Survey II that will serve as data set 2. While the three streamers of Survey II were parallel (Fig. 5-4), the 2-D profile was recorded in single-streamer configuration (Fig. 5-1, but sections #1 and #2 exchanged). For each data set, the traces of the entire profile were sorted into common offset (hydrophone) gathers and a bandpass filter and stack applied. The result are 48 traces of fold 241 for data set 1 (Fig. 3-11) and 72 traces of fold 306 for data set 2 (Fig. 3-12). Subsequently, the mean absolute amplitude was calculated for every stacked trace of all samples within a pre-defined time window. The type of seismic signal recorded in this window is important to detect real differences in hydrophone sensitivity.

Fig. 3-11 (a) shows mean amplitudes calculated between 0-130 ms superimposed on the common offset stack of data set 1. The energy of the direct wave decays due to spherical divergence. Although this effect is strongly reflected in the trend of the curve, amplitudes seem to increase again beyond hydrophone 27. This could be due to sensitivity variations or amplification differences. In order to eliminate all source or boat-inherent amplitude variations, a window was chosen between the direct arrival and above the water bottom reflection (120-250 ms, Fig. 3-11 (b)). Besides the air wave (hydrophones are close to the water surface and no hydrophone groups are used), coherent electrical noise with high amplitudes every 200 ms and remnants of the source bubble oscillation at near offsets, this window contains only seismic noise. Mean stacked amplitudes here show very few variations and follow a slight linear decrease towards larger offsets. Although influenced by the presence of electronic noise, which should not be different for different hydrophones but might be more important than the seismic noise even with its low-frequency component filtered out (bandpass 40-650 Hz), hydrophone sensitivity seems relatively constant along the two ITI sections.

Fig. 3-12 shows the same analysis for data set 2, with the difference that corresponding offsets of each streamer here were recorded simultaneously, thus allowing additional comparison of sensitivity variations from section to section. In Fig. 3-12 (a), the S/N streamer records higher amplitudes of the direct wave at near offsets, whereas both ITI sections show similar hydrophone sensitivity per offset, section #1 being slightly less sensitive. This difference could be due to the fact, that the centered S/N section is closer to the seismic source, which is especially important for short offsets. For example, the first hydrophone of the S/N section has an offset of 5 m while the first hydrophone of the ITI sections is 9 m. For the 15th hydrophone, the offset difference is reduced to only 70 cm. Similar to Fig. 3-11 (b), all three sections in Fig. 3-12 (b) record random noise at about the same amplitude level. This

also supports the explanation that the higher recorded amplitudes of the direct wave on the S/N section in Fig. 3-12 (a) are due to the difference in distance towards the source. If no bandpass filter is applied (Fig. 3-12 (c)), the S/N section demonstrates a much lower sensitivity to high-amplitude low frequencies, as was shown in Fig. 3-10 and attributed to the different pre-amp low cut filters of both streamer types and the better shield against electrical noise of the S/N section. The first mean amplitude peak at small offsets is due to the high-amplitude low-frequency component of the air gun bubble oscillation, while the second mean amplitude peak starting at hydrophone 14 could be explained by the high-amplitude low-frequency component of the air wave that enters the time window at trace 14 (better seen on Fig. 3-11 (b)).

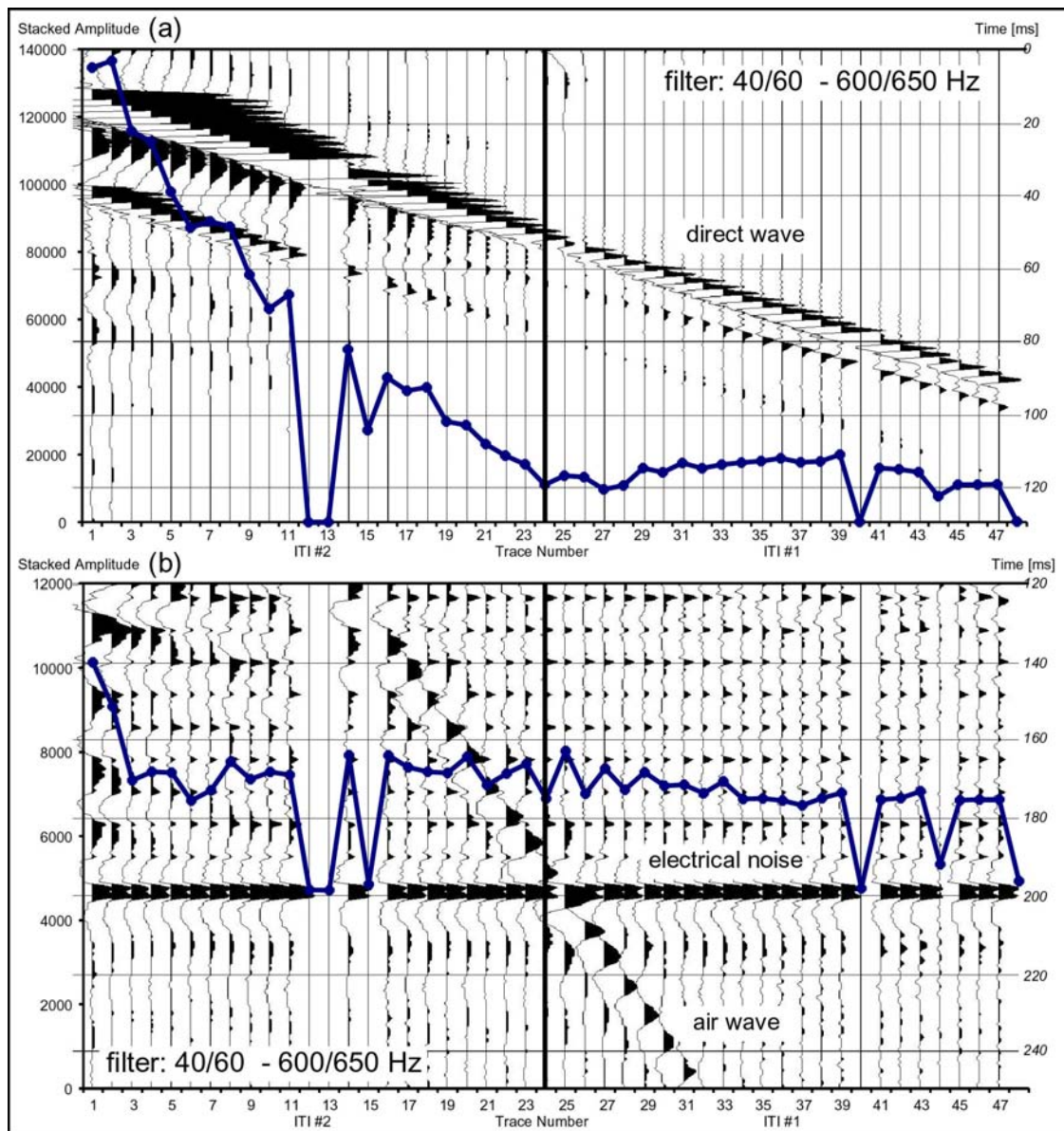


Fig. 3-11. Mean absolute amplitude (blue line) of each hydrophone from both interconnected ITI streamer sections superimposed on common offset stack (fold 241) of bandpass filtered data set 1, calculated between (a) 0-130 ms: including the direct wave and (b) 120-250 ms: above the water bottom reflection.

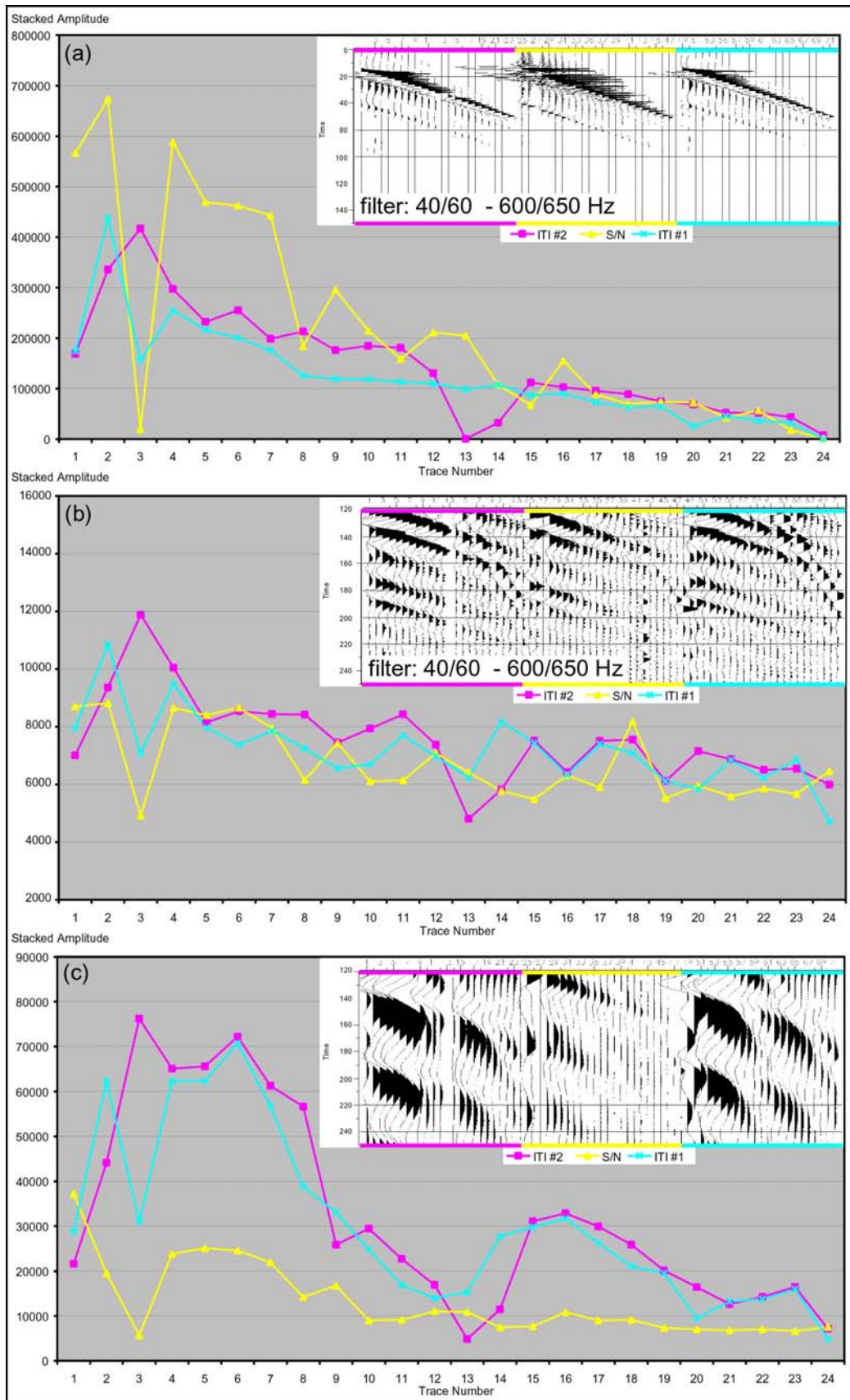


Fig. 3-12. Mean absolute amplitude of each hydrophone superimposed on common offset stack (fold 306) of bandpass filtered data set 2 (multi-streamer acquisition), calculated between (a) 0-130 ms including the direct wave, (b) 120-250 ms: above the water bottom reflection and (c) 120-250 ms: without application of bandpass filter.

Besides these observations of general sensitivity trends, some traces, as described in section 3.2.3 and 3.3.1, are always exceptionally low in amplitude. The presented analysis, therefore, allows systematic determination of these problematic traces for trace editing. A quality control of this kind prior to processing is crucial in order to evaluate recording conditions at all offsets for real amplitude stacking or subsequent AVO studies. It confirms the previously mentioned lack in amplification on trace 3 of the S/N section although the same low levels of mean amplitude are found on dead traces 13 (#2) and 24 (#1). It is thus still necessary to verify whether such selected traces are only weak and need to be scaled or whether they are completely dead and should be eliminated (see also description of trace editing in section 6.4). However, the above analysis is a rather qualitative measure of hydrophone sensitivity and cannot replace a thorough hydrophone calibration.

3.3.3 Determination of the shot interval and shot distance

The recording speed of the seismograph and the total number of samples recorded during one shot cycle place a limit on the minimum shot interval. For a record length of 1 s (Survey II), a sampling interval of 0.5 ms and 72 traces in a gather, 144000 samples need to be written to tape between one shot and the next. Tests with both instruments and tape drive showed that at least a 4-s *shot interval* is needed (~36000 samples / second). On the other hand, since homogenous coverage is an objective for conventional NMO/DMO processing (see section 6.7), the streamer's hydrophone spacing constrains *shot distance* (pop interval) to a multiple of 2.5 m. A pop interval of 2.5 m would require a vessel speed of only 2.25 km/h (0.625 m/s), a speed that is difficult to maintain and that can evoke steering problems and great instability in the ship track. A 5-m *shot distance* requires a vessel speed of 4.5 km/h (1.25 m/s) – fast enough to allow good steering and straight ship tracks, if the weather conditions are optimal.

3.4 Seismic sources

Two different types of energy sources were purchased from Seismic Systems Inc. (Houston, TX, U.S.A.) via SODERA (Société pour le Développement de la Recherche Appliquée, Toulon, France) in July 1998: the T WATER GUN *S15 Model 02* (section 2.3.3.4) and the *MINI G.I GUN*, which is a small bubble-canceling air gun (section 2.3.3.1). Both guns (Fig. 3-13) are compatible with the same shipboard equipment. The compressed air is generated onboard with a three-phase compressor of three cylinders (type S 2.33, Cirrus S.A., France; Fig. 3-1 (a) and Fig. 3-14 (a)). Air flow is often stated in normal liters per minute (NL/min). A normal liter is the volume of a liter of air at a pressure of about 1 atmosphere (\cong 1 bar) at a standard temperature of 0° or 20°C (Rowlett, 2001). Cirrus indicates a nominal air compressor capacity of 16 m³/h (~270 NL/min). However, the actual production rate depends on the purge interval set to empty condensed water from the interior which slows down the process. By experience from Survey II (Table A-4), the average air production (AP) rate

amounts to $15 \text{ m}^3/\text{h}$, ($250 \text{ NI}/\text{min}$) when purging every 15-20 minutes. The produced air is then stored in four 50-l bottles (Fig. 3-14 (b)) placed inside the research vessel. A control panel (Fig. 3-14 (d)) regulates the air supply between the gun and the bottles and between the bottles and the compressor. Fig. A-2 in the Appendix illustrates its detailed functioning. Maximum storage pressure should not exceed 280 bars.

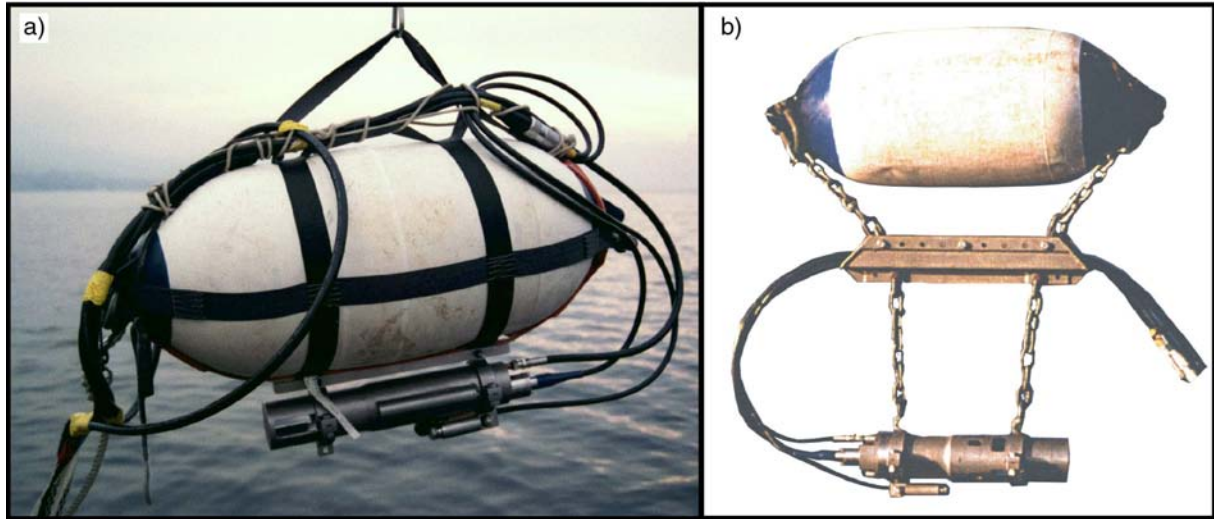


Fig. 3-13. S15.02 (15 in^3) Water Gun (a); double chamber bubble canceling Mini G.I Air Gun with a total maximum volume of 60 in^3 (b).

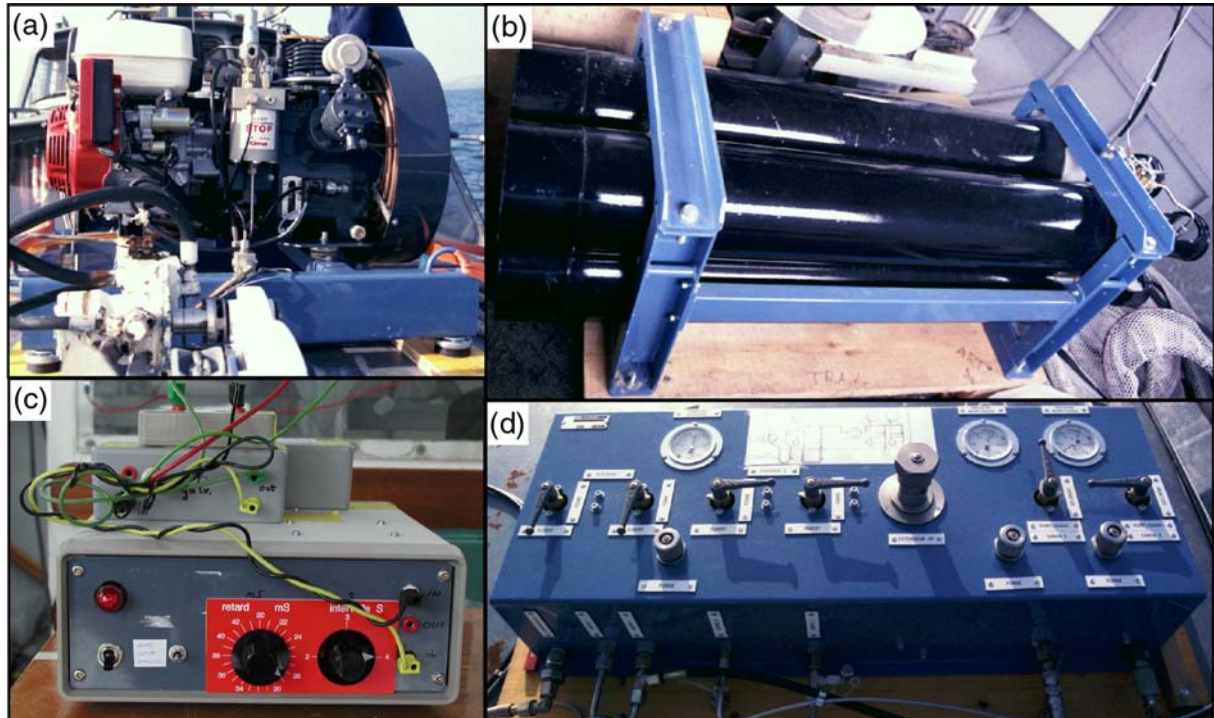


Fig. 3-14. Compressed air supply: (a) air production – Cirrus three phase compressor; (b) air storage at maximum 280 bars in four 50-l bottles placed inside the research vessel; (c) firing box that triggers the guns and is electrically connected to the seismograph; for details see Appendix Fig. A-3; (d) control panel for air supply regulation between (a), (b) and guns; for detailed description see Appendix Fig. A-2.

3.4.1 S15.02 Water Gun

The S15.02 Water Gun consists of a 10 in³ air chamber and a 15 in³ chamber filled with water. Operating pressure may range from 20 bars to 210 bars and the minimum firing depth is 0.22 m below the water surface. Per shot this gun needs about 10 in³ (or 0.164 l) of air at firing pressure. Its air consumption in normal liters per shot or per minute depends on gun volume (V in l), firing pressure (p in bars) and shot interval (Δt_s in seconds) and is estimated as follows (SODERA, 1990):

$$(3.1) \quad \boxed{\text{air consumption [Nl/shot]} \approx V \times p \quad \text{or} \quad \text{air consumption [Nl/min]} \approx \frac{60s \times V \times p}{\Delta t_s}}$$

For the recommended operating pressure of 140 bars and a shot interval of 4 s determined in section 3.3.3, only about 23 Nl of air per shot or 344 Nl per minute are consumed. Survey I was conducted using the S15 Water Gun.

3.4.2 Mini G.I Air Gun

Upon delivery, the Mini G.I Gun was fully equipped for harmonic mode 60 in³ (see section 2.3.3.3), that is generator (G) and injector (I) each have chamber volumes of 30 in³. In the following, this mode will be called G30 / I30. A change of both air chamber sizes is possible by means of plastic volume reducers, which allow adjustment to 15 in³. Smaller chambers reduce air consumption but also decrease the primary pulse's peak-to-peak amplitude (section 2.3.3.3). One 2-D line was shot across the 3-D survey site with the Mini G.I Gun in harmonic mode G30 / I30 operated at 90 bars (section 4.3 and Fig. 4-8). The whole 3-D Survey II and a complete lake traverse, 13 km in length (sections 4.3 and 5.2 and Fig. 4-7), were acquired using the reduced volume configuration G15 / I15 at 80 bars.

Operating pressure may range from 70 to 210 bars and the minimum firing depth is 0.6 m. The volume of air needed per shot corresponds to the sum of generator and injector chamber volumes. Thus, as for the water gun, the compressor delivery for the Mini G.I Gun or air requirement in normal liters per shot or minute depends on firing pressure (p in bar), shot interval (Δt_s in seconds) and on the total air volume (V in l) emitted into the water (SODERA, 1995):

$$(3.2) \quad \boxed{\text{air consumption [Nl/shot]} \approx 1.15 \times V \times p} \quad \text{or}$$

$$\boxed{\text{air consumption [Nl/min]} \approx \frac{69s \times V \times p}{\Delta t_s}} \quad \text{or}$$

$$\boxed{\text{air consumption [Nl/min]} \approx \frac{1.13077 \times V[\text{in}^3] \times p}{\Delta t_s}}$$

Because of design differences, the Mini G.I uses slightly more air (x 1.15) than its nominal volume. This is not the case for the S15, hence it is essential to use the two different formulas (3.1) and (3.2) for the correct calculation of air consumption.

3.4.3 Air consumption of all gun types – a comparison

In the following table are listed the compressor delivery requirements (equation (3.2)) for both Mini G.I Gun configurations at different operating pressures. For the same operating pressure, the G30 / I30 consumes seven times and the G15 / I15 three and a half times as much compressed air as the water gun (last line, equation (3.1)).

air consumption [Nl/min]	p [bar]	V_{total} [cu. in.]	V_{total} [l]	shot interval [s]
1527.66	90	60	0.984	4
678.96	80	30	0.492	4
2376.36	140	60	0.984	4
1188.18	140	30	0.492	4
344.40	140	10	0.164	4

Using the compressed air production rate of the compressor (AP) as well as the air consumption (AC) of these three source types at a shot interval of 4 s, the following investigates how their employment during a 2-D and a 3-D survey influences survey time and ship track design. If the four storage bottles (200 l) are filled to their maximum (280 bars) and the compressor is running during acquisition, operating pressure and gun type are the only variables for determining the possible total number of shots fired along a single 2-D profile before the pressure level falls below the operating pressure. The available air deposit in the bottles (AD) in normal liters is the difference between their maximum storage pressure (280 bars) and the operating pressure (in bar) multiplied by the volume (in liter). For a shot interval of 4 s, the compressor produces $AP = 16.67$ Nl/shot and the net air consumption (NAC) during measurements is the air consumed by one shot minus the air produced during one shot cycle. The total number of possible shots is determined by dividing the air deposit (AD) by the net air consumption (NAC) per shot. All calculations are done in normal liters or normal liters per shot and the results are listed in Table 3-B.

Not surprisingly, it is the water gun that can shoot the longest acquisition line non-stop. With an operating pressure of 80 bars, air production is even greater than air consumption, allowing any profile lengths to be shot at 5 m shot distances (section 3.3.3). However, water gun operation is recommended at 140 bars (SODERA, 1990). With a lower operating pressure, the input energy level decreases, which causes weakening of lower frequencies and, therefore, less penetration (Verbeek and McGee, 1995). But even when operated at 140 bars, the water gun can be used continuously for 4.9 hours, while the air gun at only 80 bars reaches air supply limits after 1.6 hours (G15 / I15) or 36 minutes (G30 / I30). Thus, with respect to air consumption, the water gun is the optimal source for 3-D acquisitions when a great number of sail lines is required, i.e. single-streamer surveys (see section 5.1.1).

2-D profile	S 15.02	G15 / I15	G30 / G30	pressure p [bars]
V [cu. in.]	10	30	60	
V [l]	0.164	0.492	0.984	
shot interval [s]	4	4	4	
AP - air production [NI/shot]	16.67	16.67	16.67	compressor
AD - air deposit in bottles [NI]	28000	28000	28000	140
(200l x (280 bars - p))	40000	40000	40000	80
air consumption AC [NI/shot]	22.96	79.21	158.42	140
equations (3.1) and (3.2)	13.33	45.26	90.53	80
net air consumption [NI/shot]	6.29	62.55	141.76	140
NAC (AC -AP)	-3.33	28.60	73.86	80
total number of shots	4449	448	198	140
(AD / NAC)	infinite	1399	542	80
total possible survey time	296.61	29.85	13.17	140
at 4s shot interval [min]	infinite	93.25	36.10	80
total possible survey time	4.94	0.50	0.22	140
at 4s shot interval [hours]	infinite	1.55	0.60	80
total possible profile length	22.25	2.24	0.99	140
at 5m shot distance [km]	infinite	6.99	2.71	80

Table 3-B. Air production / consumption and its influence on the total number of shots per single 2-D profile for all three gun types: S15.02 Water Gun and Mini G.I G15 / I15, G30 / I30 Air Gun.

Specifying further, it is useful to determine for each gun type the optimum time between two consecutive sail lines and the possible total number of navigated lines per day during a 3-D survey with a certain line length. Experience from our survey site shows that a typical working day consists of approximately 7 hours of acquisition time. This value as well as the number of shots per sail line and the shot cycle (Δt_s) are constants, although they can vary from one survey to another. Assuming a *shot interval of 4 s*, one sail line of *300 shots* would take about *20 minutes*. The total number of sail lines per day (Y) and the ship turning time (X) have two mutual dependencies. On the one hand, the longer the time is between two consecutive acquisition lines, the fewer total lines (here in-line plus turning) can be shot in the limit of *7 hours* (equation (3.3)). On the other hand, since longer ship turning means more time for air production by the compressor, hence less total air consumption per line, a higher total number of lines (equation (3.4)) can be shot within the limits of a fixed air deposit (AD). These two relationships can be expressed as follows:

$$(3.3) \quad Y(X) = \frac{\text{working day}}{\text{duration of one sail line} + X}$$

$$(3.4) \quad Y(X) = \frac{\text{air deposit}}{\text{shots per line} \times \text{net air consumption per shot} - \text{air production per min} \times X}$$

Selected values of operating pressure p and chamber volume V from Table 3-B demonstrate the equations' dependency on these gun properties:

$$(3.5) \quad Y(X) = \frac{420}{20 + X}$$

$$(3.6) \quad Y(X) = \frac{AD}{\text{shots per line} \times NAC - AP \times X} \approx \frac{200(280 - p)}{300 \times (V \times p - 16.67) - 250 \times X}$$

Obviously, the curves of equations (3.5) and (3.6) have opposite trends. The optimum turning time for each gun configuration is thus found at their intersection. Fig. 3-15 shows the total number of lines per day over turning times of up to 70 minutes for all three gun types, using the recommended 140 bars for the water gun and 80 bars for both air gun configurations.

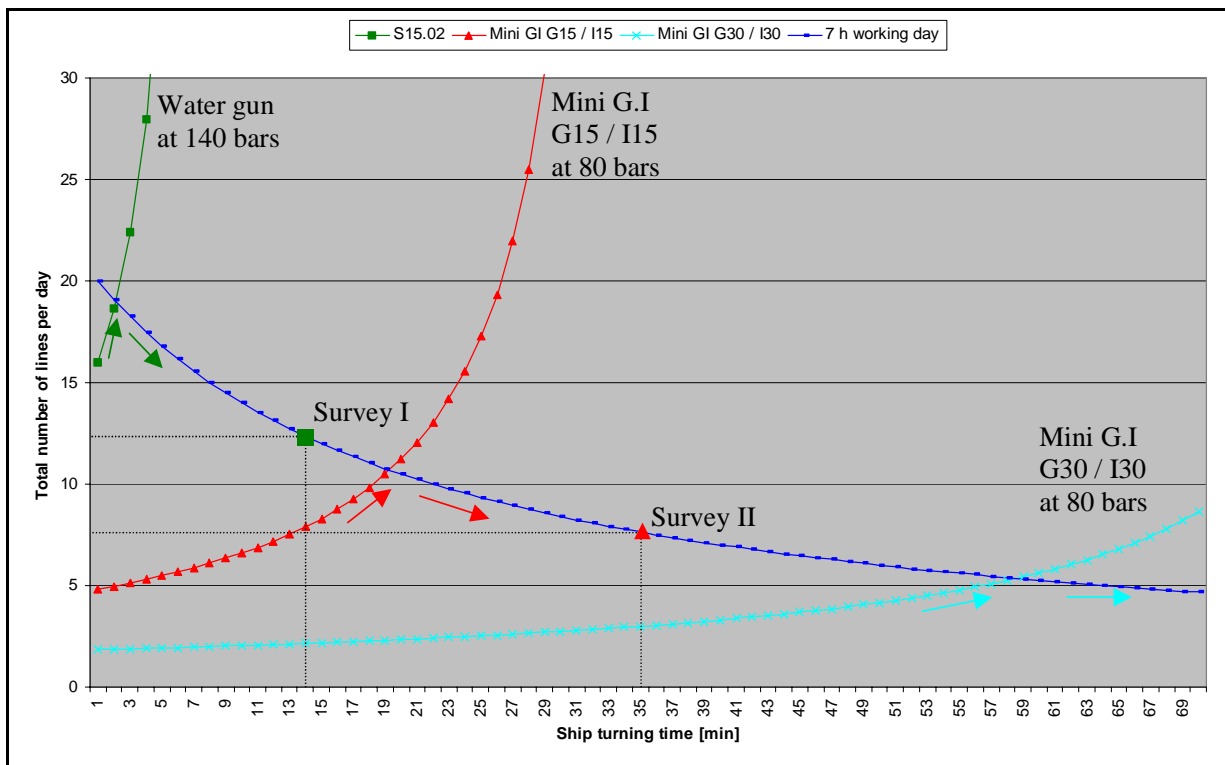


Fig. 3-15. Air consumption for a 3-D survey of 300 shots per in-line and a shot interval of 4 s; the total number of lines per day depends on ship turning time as in equation (3.5) for a 7 h working day (dark blue curve) and on the net air consumption as in equation (3.6); the three source types are shown: the water gun operated at 140 bars (green) and the Mini G.I G15 / I15 (red) and G30 / I30 (light blue) operated at 80 bars. Arrows in corresponding colors indicate how to find the maximum total number of lines for any turning time. Average values found for Survey I and II are highlighted (see Table A-3 and Table A-5).

For an optimum usage, the water gun requires a ship turning time of about 2 minutes in order to navigate 19 lines per day, while the air gun needs about 19 min (G15 / I15) or even 59 min (G30 / I30) to shoot a total of 10-11 or 5 lines, respectively. Of course, a certain minimum amount of turning time is required for simple turning (180°, as in Survey I, see Fig. 5-2) or for a whole circle (360°, as in Survey II, see Fig. 5-5) when shooting parallel. This depends on the length of the streamer and the research vessel. Experience with “La Licorne”

shows, that at least 10 minutes are necessary for a “U-turn” (antiparallel survey) with a radius large enough to allow for streamer to straighten before starting the new line (Table A-2). In parallel geometry, it was possible to return to the beginning of all lines in only 22 minutes (Table A-4). If the optimum turning time cannot be achieved, the maximum total number of lines corresponding to any other turning time is found by following both curves along the arrows indicated in Fig. 3-15. The average measured turning times and corresponding total number of lines of Surveys I (14 min, 12 lines, see Table A-3) and II (35 min, 8 lines, see Table A-5) are highlighted and confirm the theory. Of course, these calculations could be made with any other operating pressure or chamber volume to find the corresponding best turning time between consecutive acquisition lines. So for a 3-D survey with certain limits on time and spacing between CMP-lines, the water gun would be the best energy source in a single-streamer case. Multi-streamers on the other hand, would also allow the employment of air guns, since total acquisition time can be divided by the number of streamers.

3.4.4 Delay correction on seismic traces

Two different delays influence the arrival time of a seismic signal as it is recorded. The first is due to the reaction of the gun to the electrical trigger pulse. This time delay between triggering and actual firing is caused by mechanical friction of the gun components (*mechanical delay*). The second one is a *recording delay* inherent to the seismograph. Together they result into the *arrival time delay*, which thus depends on gun type and recording instrument. Knowledge of the actual arrival time allows application of a correcting time shift to all recorded traces prior to processing (see section 6.2). The *arrival time delay* $\Delta t_{arrival\ time}$ can be easily determined by using the direct wave. The difference between its measured arrival time $t_{measured}$ at one of the hydrophones at a known distance x and the theoretical arrival time calculated using the water velocity v_{water} gives the delay to an accuracy of the sampling rate:

$$(3.7) \quad \Delta t_{arrival\ time} = t_{measured} - \frac{x}{v_{water}} = \Delta t_{mechanical} - \Delta t_{record.}$$

The water velocity depends on temperature and may vary as well. However, a change of ± 50 m/s causes an arrival time difference of only ± 0.1 ms at 5 m offset, which is smaller than the sampling rates of 0.25 ms or 0.5 ms used in Surveys I and II, respectively. Table 3-C lists delays for all different gun types measured from both 3-D surveys (a, d) as well as from 2-D profile 140_30 (c, section 4.3, Fig. 4-8). The arrival time delay for b) was taken from Tacchini and Zingg (2000). All other delays were calculated from sample arrival times measured at 5 m from the source and assuming a water velocity of 1450 m/s. These values are used in section 6.2 as delay correction.

Gun Type	Gun Depth	Op. Pressure	Seismograph	t_{measured} [ms]	$\Delta t_{\text{arrival time}}$ [ms]
a) G15 / I15	1.0 m	80 bars	BISON	11.0	7.6
b) G30 / I30	1.5 m	100 bars	BISON		7.5
c) G30 / I30	1.5 m	100 bars	Geometrics	13.5	10.1
d) S15.02	0.3 m	140 bars	Geometrics	28.5	25.1

Table 3-C. Arrival time delay $\Delta t_{\text{arrival time}}$ for each gun type determined using equation (3.7), in which arrival times were measured at 5 m distance from the source and a water velocity of 1450 m/s was used.

3.4.4.1 Recording delay

The *recording delay* is inherent to the recording instrument. For its determination, we conducted the following test series on our BISON seismograph: A generated sinusoidal signal of 40 Hz (or 100 Hz) was simultaneously sent to trigger the instrument at the rising edge (see Fig. 3-16) and directly to one of the channels where it was then recorded for 100 ms using sampling rates of 0.1, 0.25, 0.5 and 1 ms, respectively. The seismograph is triggered at a certain voltage level. Since this level lies close to our input signal's zero amplitude, the phase delay of the sinusoid on the recorded trace indicates the BISON's approximate intrinsic delay (Fig. 3-16). Because the moment of triggering depends on the steepness of the signal's onset, i.e. its frequency, a box-car signal would have been preferable in order to avoid the change in measured delay with varying frequency.

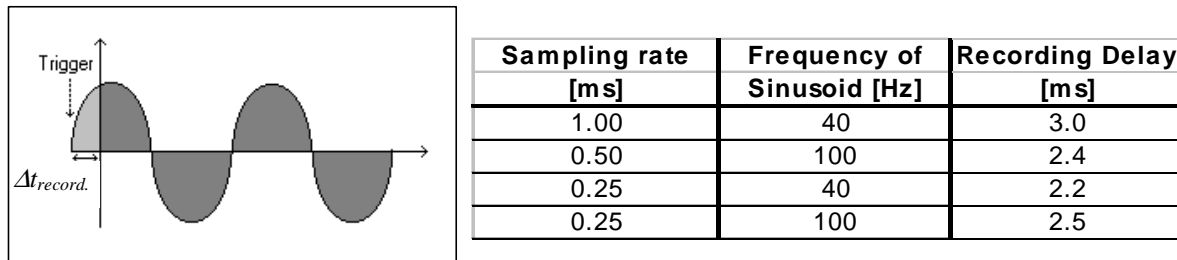


Fig. 3-16. Recording delay $\Delta t_{\text{record.}}$ determined by the phase shift of the recorded sinusoid; table lists results of a test series with different sampling rates on the BISON seismograph.

As the table in Fig. 3-16 shows, the BISON's *recording delay* lies between 2.2 and 2.5 ms for sampling rates under 1 ms. Unfortunately, we did not conduct the same test series on the GEOMETRICS seismograph, which was borrowed from the University of Geneva for Survey I.

3.4.4.2 Mechanical delay

SODERA (SODERA, 1995; M. Gros, personal communication, 2000) determined a *mechanical delay* of 10 ms for the generator of the Mini G.I and the S15 Water Gun and a 6 ms delay for the air gun's injector. In the absence of a recording delay, the mechanical delay can easily be measured with the aid of the time break hydrophone.

Taking now the difference of the 10 ms *mechanical delay* and the *recording delay* (3.7) of the BISON (~2.5 ms) leads to an *arrival time delay* of 7.5 ms, which corresponds

very well to the values found in the first two rows of Table 3-C. This confirms the *mechanical delay* of about **10 ms** for the Mini G.I Gun and allows deduction of a **zero recording delay** for the GEOMETRICS from Table 3-C c). Consequently, we would expect for the water gun (Table 3-C d) the same *arrival time delay* as its *mechanical delay*, but this is not the case. Yet, the water gun is not a "minimum phase" gun, i.e. some energy is emitted before the main pulse (see signature Fig. 3-21). The time between the trigger and the blast here also depends upon gun depth and operating pressure and includes the mechanical delay and the precursor of the main acoustic pulse (see section 2.3.3.4). Hence, the *arrival time delay* for the water gun will be greater than for the Mini G.I, as is confirmed in Table 3-C.

3.4.5 The Generator-Injector (GI) delay

The time between electrical pulses that trigger the generator and the injector of the Mini G.I gun is called *GI delay* and has to be adjusted to the generator's chamber volume, the gun depth and the operating pressure. These three parameters directly influence the bubble oscillation period, which is used to determine the *GI delay*. If the *GI delay* is set to the optimum value, the injected air largely cancels the bubble pulse, thus enhancing the pulse-to-bubble ratio and signal shape (see section 2.3.3.5). Theoretically, the bubble period T (in ms) depends on the hydrostatic pressure $P = \rho g d$ (in bars) and gun depth d (M. Gros, personal communication, 2000).

$$(3.8) \quad T = 5 \frac{\sqrt[3]{V \times p}}{P^{0.833}}$$

V : generator chamber volume (in in³)

p : operating pressure (in bars)

Empirical determination of the bubble period should be done without injector usage on the time break hydrophone (called RT58 on SODERA's Mini G.I Gun), which is situated close to the generator port and within the bubble right after its generation (section 2.3.3.3). If the injector fires half the bubble period after the generator blast, it optimally cancels the oscillation (M. Gros, personal communication, 2000). Ideally, the *GI delay* would thus be $T/2$. In practice, however, the *mechanical delay* (see section above) of the Mini G.I Gun requires a small correction. Fig. 3-17 illustrates that the combination of the 10 ms delay of the generator blast with a 6 ms delay of the injector blast results in a difference of 4 ms between the *GI delay* and half the bubble period (*mechanical delays* determined by the constructor, see section above).

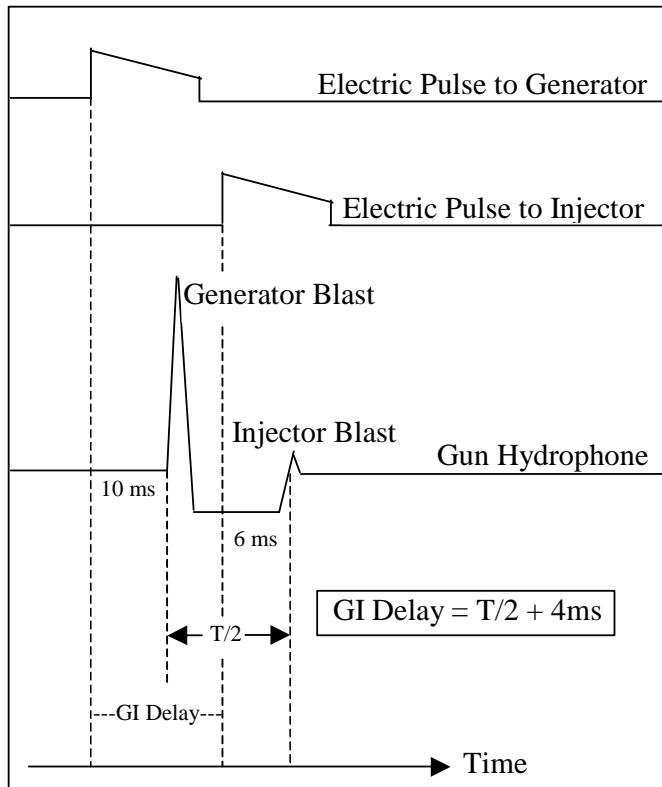


Fig. 3-17. *GI delay* = time between electric trigger pulses; time between generator and injector blast as actually measured on the gun hydrophone, is a combination of the *mechanical delays* of generator (10 ms) and injector (6 ms) and should correspond to half the bubble period $T/2$, adapted from SODERA (1995).

Table 3-D lists the theoretical bubble period calculated with equation (3.8) and the resulting *GI delay* from the relationship in Fig. 3-17. A shallow gun at small hydrostatic pressure produces a longer bubble period than a deeper gun. As equation (3.8) states, the bubble oscillation is proportional to the cube root of both the chamber volume and the operating pressure. The

gun configuration used for Survey II is highlighted in grey.

Generator Volume V [cu. in.]	Op. Pressure p [bars]	Depth d [m]	Hydrost. Pressure P [bars]	Theoretical		Empirical	
				Bubble Period T [ms]	GI delay $T/2 + 4$ [ms]	Bubble Period T [ms]	GI delay $T/2 + 4$ [ms]
15	80	1.0	1.10	49.08	28.5	50.76	29.38
15	80	1.5	1.15	47.29	27.6		
15	100	1.5	1.15	50.95	29.5		
30	80	1.0	1.10	61.83	34.9		
30	100	1.0	1.10	66.61	37.3		
30	100	1.5	1.15	64.19	36.1		

Table 3-D. Theoretical (equation (3.8)) and empirical bubble periods for different generator volumes, operating pressures and gun depths.

Two types of *GI delay* tests were conducted as part of far-field signature determinations (section 3.4.6) for the Mini G.I Gun G15 / I15 prior to Survey II. The first couple of shots were fired with the generator only, in order to measure the bubble oscillation period T . Afterwards, the injector was used for bubble cancellation, and the firing box (Fig. 3-14 (c) and Fig. A-3) was set to *GI delays* ranging from 20 to 42 ms. This second test allowed an evaluation of signature shape and the degree of bubble canceling from the various delay times (pulse-to-bubble ratio - PBR). From the bubble oscillation frequency ($f_{bubble} = 19.7$ Hz) measured with the gun hydrophone on the generator shots only, I determined a bubble period of 50.8 ms (see Fig. 3-18). The corresponding *GI delay* is **29.4 ms** using the relationship of Fig. 3-17, which corresponds well to the theoretical value of **28.5 ms** in Table 3-D.

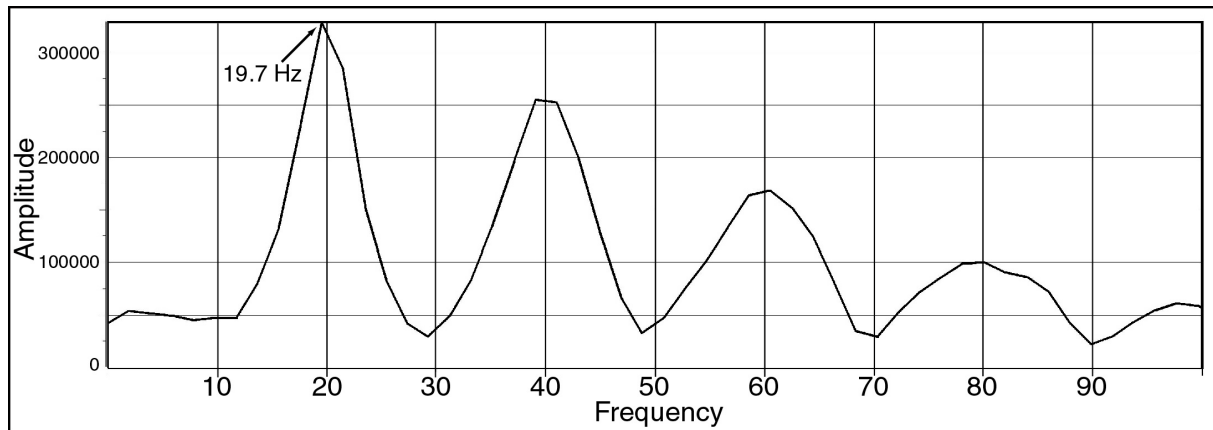


Fig. 3-18. Amplitude spectrum up to 100 Hz measured on the gun hydrophone of the Mini G.I G15 / I15 with generator only. The inverse of the bubble frequency gives a bubble period of 50.8 ms.

For the following 33 shots, different *GI delays* were set on the firing box, and two or three shots were fired with the same delay. Table 3-E lists the signal and bubble peak amplitudes measured in the unfiltered far-field on a hydrophone at 106 m depth. The corresponding PBRs are plotted for the delay time in Fig. 3-19, with the curve of the mean ratio per *GI delay* superimposed. Between 25 and 28 ms, the PBR seems to be highest with a peak at about **27 ms**, although standard deviations are relatively large. Furthermore, the delay between the peaks of the generator and injector blast on the gun hydrophone was measured (Table 3-E, column 5), which should correspond to half the bubble period ($T/2$) and, when adding 4 ms, to the *GI delay* (Table 3-E, column 6; Fig. 3-17). It is important to take this measurement as close to the gun as possible since generator and injector pulses may not travel with the same group velocity, causing errors of a few milliseconds. The last column of Table 3-E shows that the difference between the *GI delay* measured on the gun hydrophone and the set *GI delay* has an average discrepancy of only 0.5 ms. This discrepancy corresponds to the precision of sampling in the time domain ($SI = 0.5$ ms), i.e. the maximum possible error to determine each peak's position is 0.25 ms. This is one of the reasons why signature measurements should be recorded with as high a sampling rate as possible. The precision of the firing box is 0.25 ms. Other sources of error could be varying mechanical delays of the injector and differing build-up times to reach the energy peaks.

Similar *GI delay* tests have been conducted for the Mini G.I gun G30 / I30, although no shots exist with the generator fired separately, and the *GI delay* sampling was very coarse due to a less detailed calibration of the firing box than was available for Survey II. The measured PBR over the five different *GI delay* settings are plotted again in Fig. 3-20. Main pulse amplitude determination was very difficult and PBRs have great deviations from their superimposed mean. The reason for this large scattering and the very low ratios compared to those in Fig. 3-19 is an excessive recording gain that saturated the pulse's peak amplitudes (see also Fig. 3-8 and Fig. 3-24). Nevertheless, the trend shows that the optimum recording

delay for this gun configuration must lie somewhere between 30 and 40 ms. The theoretical delay in Table 3-D suggests a value close to 36 ms.

set GI delay [ms]	Signal amplitude	Bubble amplitude	PBR	measured T/2 [ms]	T/2 + 4 [ms]	T/2 + 4 - set GI delay [ms]
20	143508	11411	12.6	17	21	1.0
20	127827	7470	17.1	16.5	20.5	0.5
22	158939	12910	12.3	18.5	22.5	0.5
22	150544	8755	17.2	17.5	21.5	-0.5
24	159875	10051	15.9	20.5	24.5	0.5
24	140751	12450	11.3	20	24	0.0
26	159977	9745	16.4	22.5	26.5	0.5
26	156800	8648	18.1	23	27	1.0
27	149131	7706	19.4	23.5	27.5	0.5
27	152282	8644	17.6	22.5	26.5	-0.5
28	156439	13150	11.9	24.5	28.5	0.5
28	153713	7751	19.8	24.5	28.5	0.5
29	152650	9917	15.4	26	30	1.0
29	160399	10604	15.1	25	29	0.0
29	155606	13558	11.5	25	29	0.0
30	157441	14664	10.7	26	30	0.0
30	147814	9638	15.3	26.5	30.5	0.5
30	159897	9718	16.5	26.5	30.5	0.5
31	148790	12042	12.4	27.5	31.5	0.5
31	160252	12123	13.2	28	32	1.0
31	149745	11047	13.6	28	32	1.0
32	160945	13751	11.7	28	32	0.0
32	148824	12751	11.7	28.5	32.5	0.5
34	145572	10414	14.0	30.5	34.5	0.5
34	144401	12928	11.2	31	35	1.0
36	150633	12677	11.9	33	37	1.0
36	153068	9478	16.1	32.5	36.5	0.5
38	149521	14502	10.3	34.5	38.5	0.5
38	157006	13794	11.4	33.5	37.5	-0.5
40	157773	16721	9.4	36.5	40.5	0.5
40	156769	18520	8.5	36.5	40.5	0.5
42	154429	18102	8.5	40.5	44.5	2.5
42	147766	19752	7.5	38.5	42.5	0.5
Mean:						0.5

Table 3-E. Signal and bubble amplitude, pulse-to-bubble ratio (PBR), delay measured between generator and injector blast with respect to different *GI delays* during far-field signature tests with the Mini G.I G15 / I15. Last two columns present the measured *GI delay* using the relationship in Fig. 3-17 and its difference to the *GI delay* set on the firing box. Columns highlighted in grey are plotted in Fig. 3-19.

In summary, the *GI delay* time has been determined in three different ways: theoretically by using equation (3.8), (Table 3-D) and empirically by measuring the bubble period of the generator (Fig. 3-18) as well as by evaluating signal shape (Table 3-E and Fig. 3-19). The respective values for the Mini G.I G15 / I15 vary slightly from between 29.4 to 27 ms with a mean of 28.3 ms. By choosing 28 ms as the *GI delay* for Survey II, an optimum solution is found within the error tolerance (The resulting near and far-field signatures using this delay of 28 ms are shown in Fig. 3-22 and Fig. 3-23 (b) and can be compared to the signatures with no bubble canceling injection in (a). The bubble oscillation in (b) almost completely disappears.

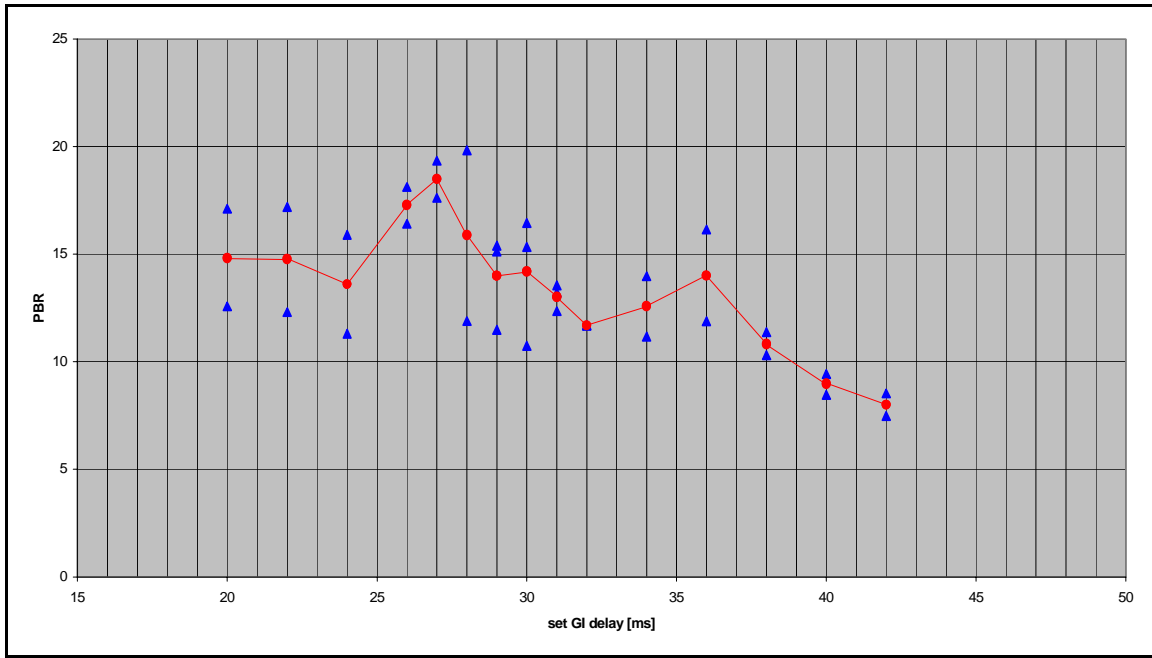


Fig. 3-19. Pulse-to-bubble ratio (PBR) for Mini G.I G15 / I15 with respect to *GI delay* on the firing box. Measured values (at 106 m depth) are represented by blue triangles while the red curve indicates their mean. Signature was recorded at 12 dB.

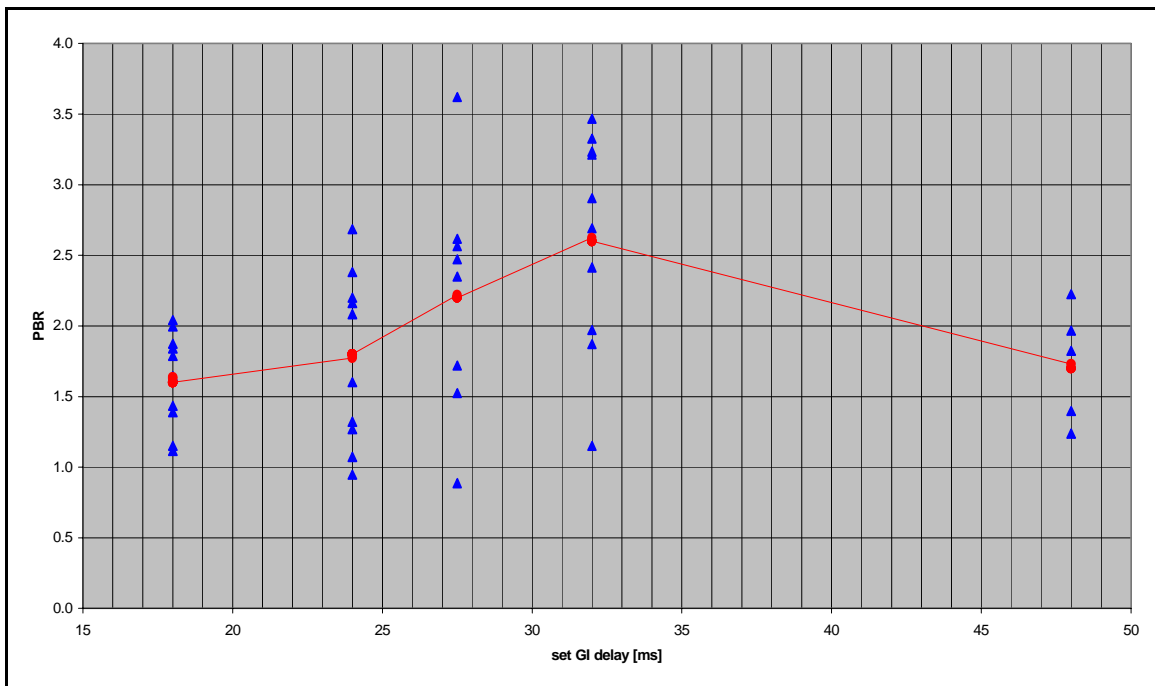


Fig. 3-20. Pulse-to-bubble ratio (PBR) for Mini G.I G30 / I 30 with respect to *GI delay* set at firing box. Measured values (at 107 m depth) are represented by blue triangles while the red curve indicates their mean. Signature was recorded at 60 dB and signal is saturated even at greater depths.

3.4.6 Signatures

Signature measurements are essential in order to evaluate signal characteristics and to determine important parameters such as the source’s resolving power for survey design. As

already mentioned above, the energy source's performance can be expressed in the pulse's peak-to-peak amplitude and the pulse-to-bubble ratio. These amplitudes are measured in the time domain. In the frequency domain signal strength and shape are expressed by the peak dB level and the amplitude spectrum's smoothness.

We conducted near and far-field signature tests in the center of the lake (300 m water depth) with all three gun types at their survey configurations for comparison. While the gun hydrophone detected the signal in the near-field, the far-field signature was recorded with the aid of one or both ITI streamer sections, weighted at the end by the vessel's anchor and hung vertically below the energy source. The first streamer section was attached to a lead-in cable that either placed the nearest hydrophone directly underneath the gun or at about 50 m below the water surface. In this way, a large span of distances could be covered ranging between 5 and 170 m depth, which correspond roughly to a signature development between 60 and 98.5% (equation (2.15) in section 2.3.3.5).

Signature tests for the Mini G.I G15 / I15 have been conducted with one streamer only, in which the deepest hydrophone was located at a depth of 106.25 m. At this distance from the energy source, the far-field signature is developed already to 98.1% and thus allows a good evaluation. Since the far-field hydrophone is located almost 200 m above the water bottom, 270 ms will elapse between the direct arrival and the detection of the first reflection (see equation (2.16), which is enough time to estimate wavelet shape and remaining bubble oscillations. Hence, this depth was chosen for the following signature comparisons of all three gun types.

3.4.6.1 S15.02 Water Gun

SODERA's S15 Water Gun is capable of producing frequencies of up to 2250 Hz and higher (SODERA, 1990). Choosing a sampling interval of 0.25 ms, it is necessary to apply an analogue high-cut filter at the Nyquist frequency (equation (2.7)) of 2000 Hz prior to digitization (see section 2.3.2.1) in order to avoid aliasing.

The water gun signature was recorded with the GEOMETRICS at 36 dB preamplifier gain, a sampling interval of 0.25 ms and an operating pressure of 140 bars. The acquisition sheet is attached to the Appendix (Table A-6). Fig. 3-21 (a) presents the far-field signature measured on trace 21 of shot 15 (Table A-6) at 107.25 m depth. The first part of the signal is composed of the precursor, typical for the water gun's water ejection, followed by the main pulse, the implosion of the generated void (see section 2.3.3.4). The source's ghost reflection arrives shortly thereafter with opposite polarity. Destructive interference with this ghost causes notches in the corresponding amplitude spectrum. Notch frequencies and ghost arrival time depend on gun depth (section 2.3.3.5) as expressed in equation (2.13). Hence, the gun depth should be chosen such that the first non-zero notch will occur outside the bandwidth of the desired spectrum. Using a water velocity of 1500 m/s and a first non-zero notch frequency

of 2000 Hz, equation (2.13) gives a maximum gun depth of 37.5 cm. A deeper gun would cause loss of the very high frequencies due to notching. Although complete destructive interference occurs only at the notch frequency itself, frequencies around this notch have reduced amplitudes. In order to keep as many of the highest frequencies at reasonable amplitudes, the water gun was put at 30 cm below the water surface (first non-zero notch at 2500 Hz).

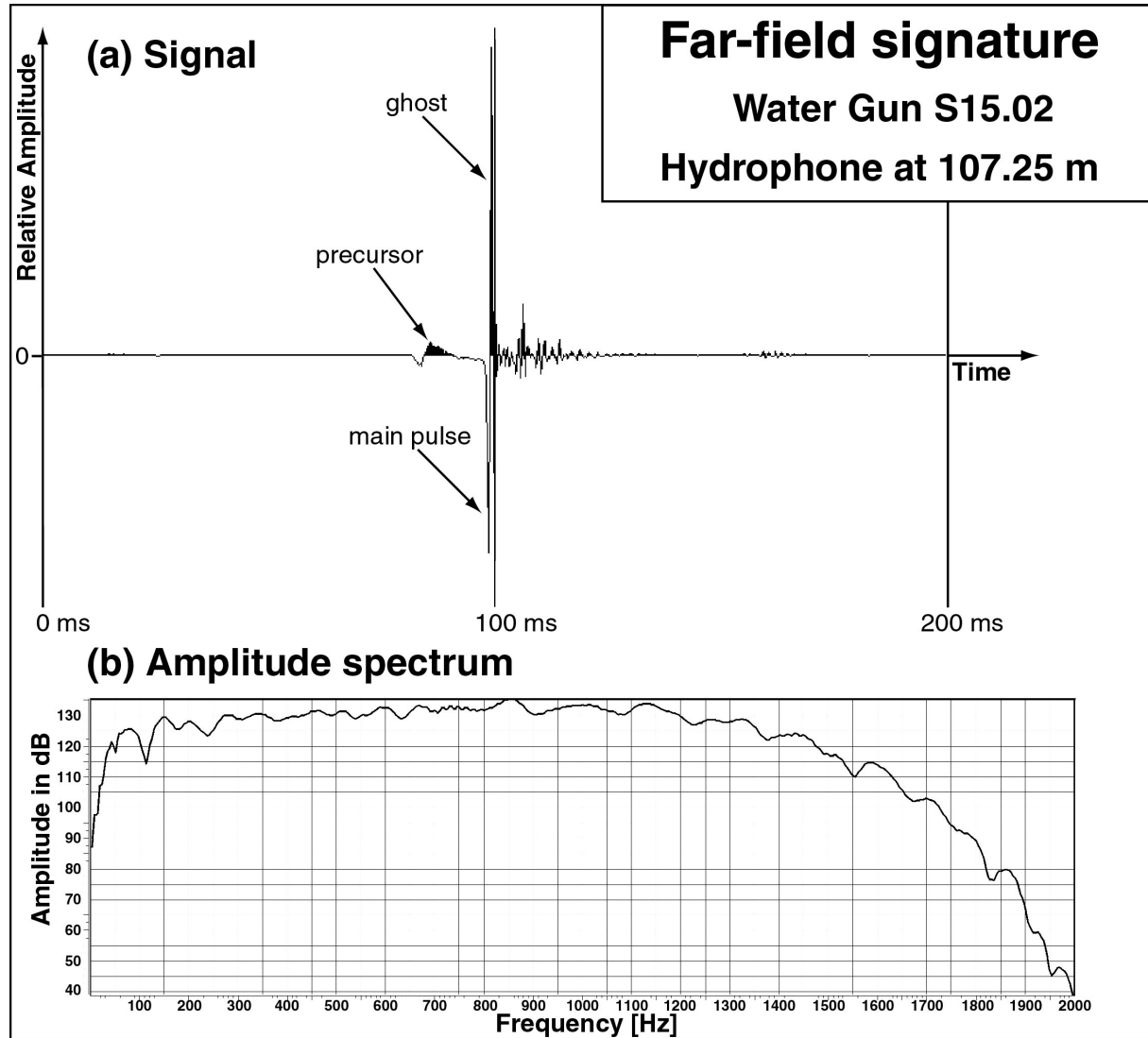


Fig. 3-21. Far field *unfiltered* signature of the S15.02 Water Gun measured on trace 21 at 107 m depth with a recording gain of 24 dB (SI = 0.25 ms; GEOMETRICS): (a) time-domain signal and (b) its amplitude spectrum. Signature developed to 99.4%.

The steepness with which the amplitudes slope down to zero at the notch frequency also depends on gun depth: the deeper the gun, the steeper is the slope. Shallow guns work as low-cut filters (Dragoset, 1990), since amplitudes at the zero-frequency notch increase only slowly. This has the positive effect of weakening the low-frequency bubble oscillation and, therefore, increasing the PBR. However, reduced low frequencies decrease signal strength and result in lower penetration. For high-resolution surveys such as ours, the loss of some low

frequencies within a very broad spectrum is less significant, since targets are usually at shallower depth. The emphasis here is placed on a clean signal allowing good temporal resolution of detailed structures. Consequently, it is important that the energy source produces a superior signal shape and as high a dominant frequency (see section 2.3.3.5) as possible. The amplitude spectrum (Fig. 3-21 (b)) of the water gun is relatively flat between 150 and 1350 Hz with a peak frequency that lies at about 850 Hz. To get an estimate of the signal's dominant frequency (section 2.3.3.5), the inverse of twice the time measured between primary and ghost reflection peaks ($1/(2*0.75 \text{ ms})$) gives a value of ~ 670 Hz (see Table A-6). A higher sampling rate would have been desirable for more accuracy. Despite the undesired precursor that makes the signal non-minimum-phase, the water gun has no bubble oscillation and only some minor reverberations shortly after the main pulse. The resulting smooth amplitude spectrum and the broad bandwidth are characteristic of an energy source with high resolving power, although the shallow gun depth limits signal strength and penetration.

3.4.6.2 Mini G.I G15 / I15

SODERA's Mini G.I G15 / I15 produces frequencies of up to about 650 Hz (M. Gros, personal communication, 2000). The signature can thus be recorded at a lower sampling rate than that of the water gun. A sampling interval of 0.77 ms would guarantee unambiguous reconstruction of the full bandwidth. Since our seismographs only accept digitization at intervals of 0.25, 0.5, 1 ms or larger, we used 0.5 ms combined with an automatic anti-aliasing high-cut filter set to the corresponding Nyquist frequency of 1000 Hz.

The signature tests with the Mini G.I G15 / 15 were recorded with the BISON at 12 dB recording gain, a sampling interval of 0.5 ms and a gun operating pressure of 80 bars. The acquisition sheets are attached to the Appendix (Table A-7). Fig. 3-22 presents an example of the near-field signature measured on the gun hydrophone with (a) generator use only (shot 2) and (b) in harmonic mode (shot 21). Here again, the ghost surface reflection comes closely behind the main pulse, whose arrival time delay of 7.5 ms confirms the calculations in Table 3-C. The difference in primary amplitudes and amplitude levels in the spectrum (c) are due to a reduced signal repetitivity in the near-field. While in (a) the following sequence of smaller bubble pulses at period T is undisturbed, it is canceled almost completely in (b) by the injector blast, which is optimally delayed by half the bubble period using a GI delay set to 28 ms (see section 3.4.5). Fig. 3-23 shows the signature of the same gun configuration but recorded in the far-field on trace 23 at 106.25 m depth. Spherical divergence attenuated both generator and injector amplitudes as well as the bubble oscillation while the signature developed to 98%. The amplitude spectra (c) in both Figures demonstrate how well the bubble oscillation in (a) has been canceled in (b) and how the bubble is dominated by frequencies below 200 Hz.

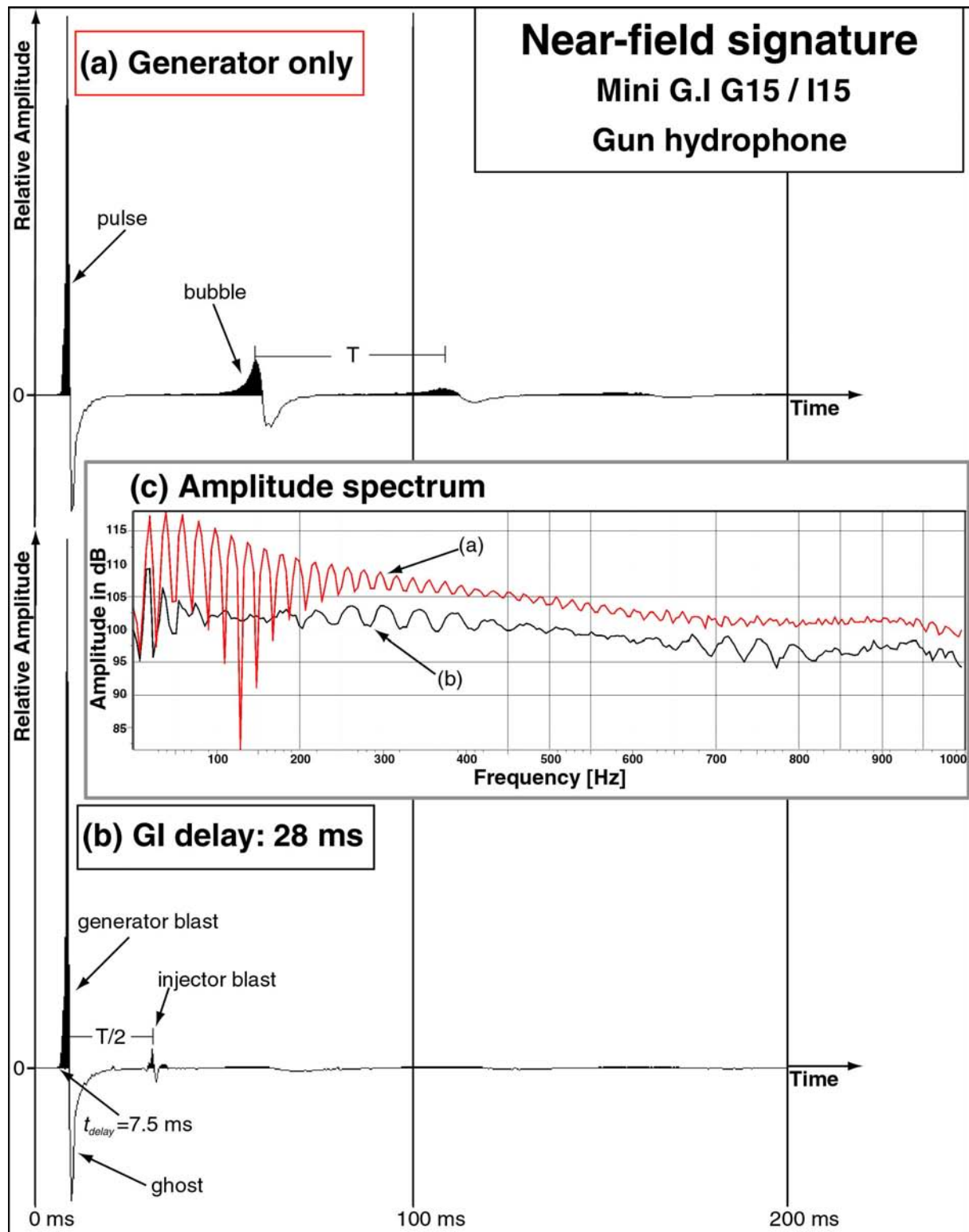


Fig. 3-22. Near field *unfiltered* signature of Mini G.I G15 / I15 measured on gun hydrophone with a recording gain of 12 dB (SI = 0.5 ms, BISON) (a) with generator only, (b) with the optimum GI delay of 28 ms, (c) amplitude spectrum of (a) and (b). The difference in primary amplitude and amplitude levels in the spectrum are due to a reduced signal repetitivity in the near-field.

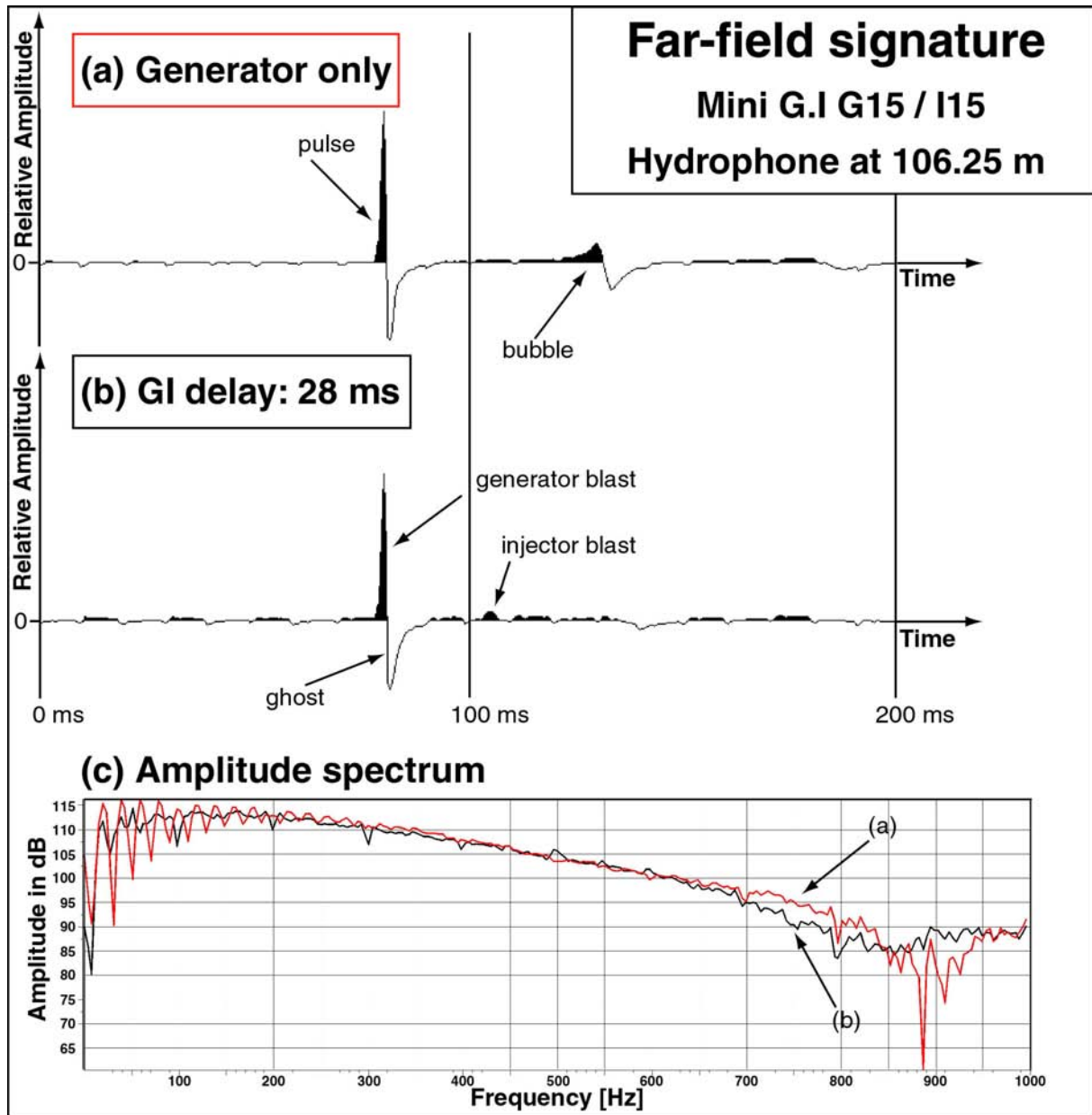


Fig. 3-23. Far field *unfiltered* signature of Mini G.I G15 / I15 measured on trace 23 at 106 m depth with a recording gain of 12 dB (SI = 0.5 ms, BISON) (a) with generator only, (b) with the optimum GI delay of 28 ms, (c) amplitude spectrum of (a) and (b).

For the first non-zero notch to occur beyond 650 Hz, the gun depth should not exceed 1.15 m. To be on the safe side and to take into account the gentle amplitude decay towards the notch frequency at shallow depths, the gun was put at 1 m below the surface ($f_{notch} = 750$ Hz). The amplitude spectrum in Fig. 3-23 (c) suggests, however, that the gun must have been situated even a bit closer to the surface (at about 80 cm) because notching occurs at more than 800 Hz. No ghost notching is observed on the gun hydrophone spectrum in Fig. 3-22 (c), where wavefield interference might be hindered by the close vicinity to the gun and buoy. The spectrum of the well developed far-field signature is relatively flat between 70 and 350 Hz, and lower frequencies are better preserved than for the water gun due to the greater gun depth.

Comparison of absolute amplitudes in dB levels is not possible since receivers were not calibrated, although slope steepness and smoothness of the spectrum can still be evaluated.

The greater importance of low frequencies of the Mini G.I G15 / I15 implies higher signal strength and deeper penetration, but temporal resolution suffers. The dominant frequency measured in the time domain lies at about 330 Hz (see Table A-7) – here again a higher sampling rate would have been desirable in order to better determine the dominant period of the signal. This energy source has less than half the bandwidth of that of the water gun but a higher signal strength and, when used with the correct GI delay, a smoother spectrum which is also expressed in the pulse-to-bubble ratio of almost 20. In addition, the wavelet's energy is concentrated at its onset (minimum phase) and no precursor pulse hinders determination of accurate reflection times.

3.4.6.3 Mini G.I G30 / I30

SODERA's Mini G.I G30 / I30 specification sheet indicates a spectral limit at about 500 Hz (M. Gros, personal communication, 2000). Although a sampling interval of 1 ms would be sufficient for exact signal recovery, the same interval (0.5 ms) was chosen as for the smaller air gun type. The corresponding 1000 Hz high-cut anti-aliasing filter makes detection of frequencies higher than the expected 500 Hz still possible. The signature of the Mini G.I G30 / I30 was recorded with the BISON at 60 dB recording gain and an operating pressure of 100 bars. The acquisition sheets are attached in the Appendix (Table A-8).

Fig. 3-24 (a) presents the signature measured on a far-field hydrophone (trace 20, shot 118, Table A-8) at 106.75 m depth using a GI delay of 32 ms. This delay came closest to the estimated optimum GI delay of 36 ms (see section above). The amplitude of the generator blast seems to be cut, even the injector blast is flattened. The recording gain of 60 dB obviously saturated the dynamic range of the seismograph. Determination of the main pulse's amplitude is thus impossible and PBRs are much lower than expected (compare Fig. 3-20 to Fig. 3-19). The spectrum in Fig. 3-24 (b) does not present the real frequency content of the signal, since large amplitudes were clipped. Especially the higher frequencies are underrepresented, since they compose the short primary pulse.

If the first non-zero notch is to occur at 500 Hz, the gun should be placed at a depth of 1.5 m. Tests with a slightly shallower gun should be undertaken in order to verify the actual spectral bandwidth when the first non-zero notch frequency lies beyond 500 Hz. A recording gain reduced to 0 or 12 dB would then allow proper evaluation of the amplitude spectrum. The theory in section 2.3.3.5 indicates that the doubled chamber size and the slightly higher operating pressure would cause an increase in signal strength of about 25-30% with respect to the G15 / I15 configuration. The deeper gun position favors lower frequencies. However, the bubble oscillation is also composed of lower and stronger frequencies that modulate the signal's spectrum and make it less smooth. The actual strength gain decreases because these

larger air bubbles interact more. Despite the saturated main peaks, the dominant frequency can still be measured from the zero-crossings in the time domain and lies at about 150 Hz (see Table A-8). Temporal resolution is thus half of that of the Mini G.I G15 / I15. A doubled air consumption and a halved resolving power are worth a maximum 30% strength gain if signal penetration is more important than resolution. Otherwise, for relatively shallow targets, the Mini G.I with two 15 in³ chambers presents an economic and still powerful high-resolution energy source that will be ideal for many small-scale 3-D surveys.

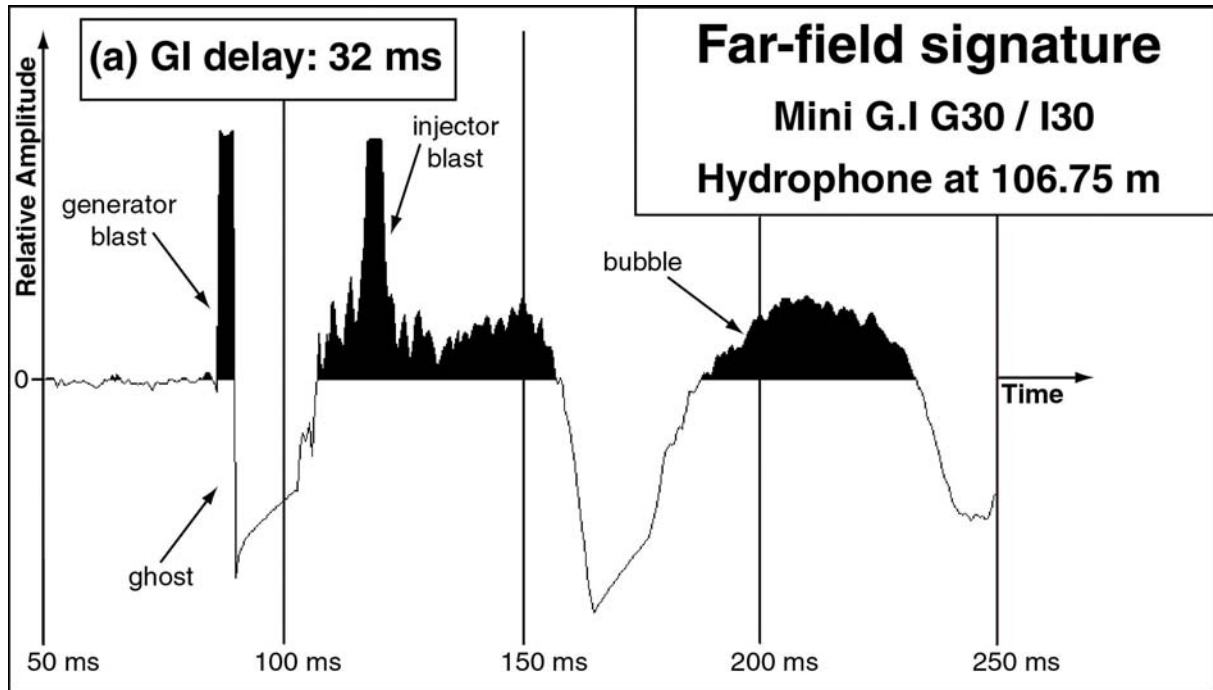


Fig. 3-24. Far field *unfiltered* signature of Mini G.I G30 / I30 measured on trace 20 at 107 m depth with a recording gain of 60 dB (SI = 0.5 ms, BISON). Because the time-domain signal is clipped at peak amplitudes, an amplitude spectrum was not computed.

3.4.7 Concluding remarks

It is very important to conduct signature measurements prior to any seismic survey in order to evaluate gun characteristics. Signature interpretation is easiest when using the smallest possible sampling rate and a low recording gain to prevent signal saturation. For double chamber air guns the GI delay should be determined empirically by recording the bubble oscillation period when shooting with the generator only or by using the gun in its actual GI mode, shooting about ten times per set delay and changing delay time with the smallest possible interval. This way, the mutual influence of all participating instruments and their components (mechanical delay, recording delay) is included in optimum signal shaping, and acquisition parameters are then adapted to this individual configuration.

Besides far-field signature interpretation on the direct arrival, it is equally important to examine the frequency spectra of the reflected signal. We can look at the earth as a filter of seismic energy. Ideally, the signal that we record would simply be the source signal

convolved with the impulse response of the earth. However, in practice, there are not only primary reflections, but also multiples, diffractions, etc., all modified by filtering because of absorption and other causes, and with random noise superimposed. So, studying the signal arriving after reflection at the water bottom can help estimate the earth's filtering effect. Since it is this same wave that will arrive at the receiver array (streamer) with limited spatial sampling property, the resulting gather or section will be subjected to aliasing of steep dips and high frequencies. If the highest frequencies in the source spectrum are already filtered out by the water bottom reflection, there is no need in trying to record them and the sampling interval whether in time or space might be chosen accordingly.

If possible it is thus recommended to conduct a test line across a typical portion of the target site itself (see section 4.3.1). By looking at selected traces one learns about signal penetration and absorption as a function of depth and about the highest frequencies actually in the reflected wave (see section 6.7). After having considered all parameter constraints, those of the target area and of the used equipment, e.g. deepest structural dip and minimum in-line and cross-line bin size (see section 4.3.3.3 and 4.4.1), it might be better to use an additional high-cut filter prior to digitization in order to avoid aliasing of frequencies below the Nyquist frequency.

3.5 Retractable booms for multi-streamer use

In a multi-streamer system, several streamers are towed behind the research vessel. How many streamers can be towed depends on the capacity of the recording instrument, on the number of channels per streamer, on the size of the research vessel and the way of streamer attachment. The BISON seismograph has a total of 96 recording channels separated into four connectors of groups of 24 traces (see section 3.3). Three possibilities thus present themselves for multi-streamer use with this instrument: two interconnected streamer sections of 48 channels each or either three or four streamers of 24 channels each.

Further to consider are the instrument recording speed of 36000 samples per second (section 3.3.3) and a minimum required ship speed of about 4 km/h for navigation stability. At a shot spacing of 5 m, 162000 samples can be recorded between two triggers. Traces of 2000 samples (as in Survey I, see section 5.1.1) on 96 channels make the recording of 192000 samples/shot necessary - too many for this combination of ship speed and shot distance. Consequently, if 96 channels were to be used, either the sampling interval has to be increased or the trace length reduced. This configuration is thus inappropriate to be used with the water gun, as its high-frequency content requires a sampling interval of 0.25 ms and the target needs a trace length of about 500 ms (see section 4.3.3.2). However, a three-streamer system of 72 channels, which requires recording of only 144000 samples per shot, would still work.

Another system consideration is the attachment of the streamers to the ship. However, the most important constraint is the cross-line spacing that has to be chosen according to

spatial sampling requirements with respect to the structural dip of the target (see section 4.3.3.3). The data of Survey I (see section 7.1.3) proved that structural dip even in fault strike direction can reach values of more than 5° due to the complex topography. These dips require a cross-line bin size of less than 7.5 m depending on the bandwidth of the source (see Table 4-C in section 4.4.1). Since a multi-streamer configuration has the advantage of needing as many times fewer boat passes as streamers are used to acquire the same number of CMP lines, it is now possible to improve the cross-line resolution of a single-streamer survey without increasing total acquisition time. If we halved the cross-line spacing of Survey I from 7.5 to 3.75 m, a two-streamer system would need the same time to acquire double the number of in-lines over the same survey area, while a three-streamer system would need two thirds and a four-streamer system only half the time. A cross-line spacing of 3.75 m, thus, reduces the risk of spatial aliasing in the target's strike direction (unaliased dips below 9° instead of 2° when using the air gun) and requires smaller streamer separation. The two and four streamers would have to be arranged symmetrically around the source: the inner two streamers at a distance of 3.75 m and the outer two at 11.25 m from the source. The center streamer of the asymmetrical three-streamer configuration would be towed directly behind the gun, the other two at 7.5 m to both sides.

As stated in section 2.4.4.4, there are two commonly applied methods to hold multiple streamers in place outboard of the research vessel: paravanes and booms swung out from the vessel's sides. Because we are limited to a maximum of four streamers and those streamers are not distributed over a large lateral distance, it seemed thus easier to construct booms for each side of the boat (Fig. 3-25 (a)) instead of using paravanes that would be much more sensitive to varying ship speed and relatively small turning radii.

These booms were designed and built by our technician Roger Wolfgang in collaboration with David Dupuy. Our research vessel "La Licorne" is only 3.5 m wide. Hence for a four-streamer system and a CMP-line spacing of 3.75 m, it is necessary to construct two booms of 2-m length to hold the inner streamers at a distance of 7.5 m to each other and centered around the energy source. For the outer two streamers, the booms would need a length of 9.5 m for four versus 5.75 m for three total streamers. Numerous calculations and tests were conducted with respect to the type of material and the construction feasibility, which showed that due to weight and stability considerations the booms could not exceed a length of about 6 m. Even when using hollow aluminum tubes, 9.5 m turned out to be too long a distance to keep the boom light enough and the construction stable. A four-streamer system would thus only be feasible when cross-line spacing was further reduced. In order to be able to compare results of Survey II with those of Survey I and for simplicity in processing it is preferable to keep the cross-line spacing a multiple of the in-line bin dimension of 1.25 m. This way, some of the in-lines of Survey II will always directly fall on the in-lines of Survey I. The next smaller cross-line spacing is 2.5 m, which would require the same distance

of 5.75 m between the outer streamers and the boat as the three-streamer system would and a length of 0.75 m for the booms of the inner streamers and the boat. With this configuration, we would need a similar number of boat passes as for the three-streamer system, but would further increase horizontal resolution.

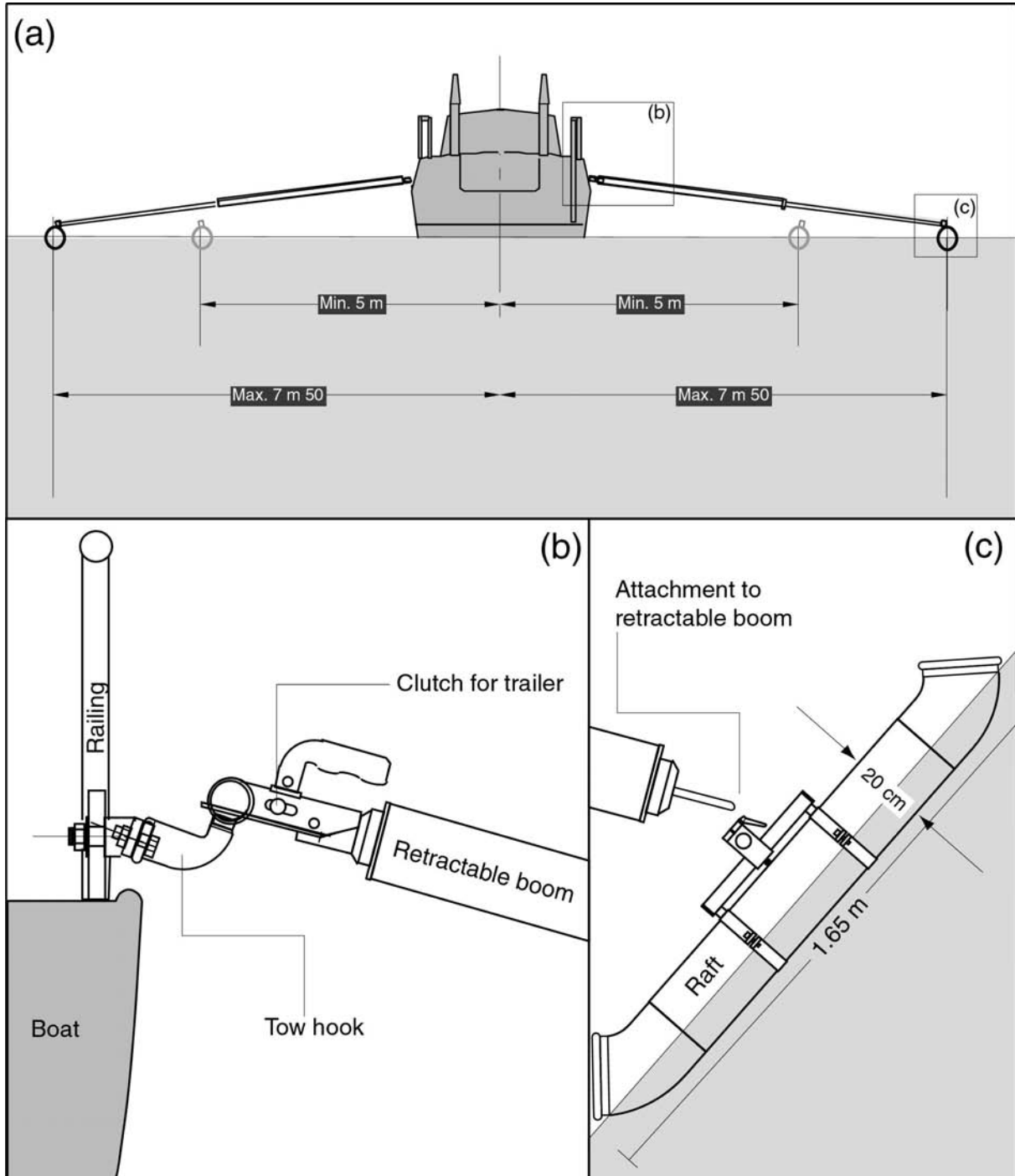


Fig. 3-25. Construction plan of (a) two retractable booms attached to each side of the ship with the aid of (b) a clutch and tow hook system and (c) whose outer ends are fixed on a raft.

Three reasons made us decide for the three-streamer system. The first is that it will be more economic on acquisition time than the two-streamer configuration at 3.75 m cross-line spacing. The second is that the four-streamer system would require the purchase of a fourth streamer section and the construction of two additional booms. And finally, the asymmetric system allows recording of zero-azimuth traces on the center streamer. This way it will be possible to directly compare every sixth in-line of Survey II with an in-line of Survey I that both have zero-azimuth traces in the same bins.

Fig. 3-25 (a) presents the construction plan of two retractable booms attached to each side of the boat building the basis of the future three-streamer system. Those booms have to be constructed in a way to combine the following four criteria. First, their attachment to the boat needs to be flexible to allow adaptation to minor vertical wave movement. Second, the booms have to be attached in a way to limit the drag force from boat advancement so it would not change their angle towards the boat nor apply extreme horizontal tear to the boom's attachment. Third, the booms should be easy to maneuver and easy to transport from the harbor to the survey site. And finally, they must tow the lead-ins at a stable position just below the water's surface.

In order to meet these requirements a simple but effective attachment system has been conceived based on the combination of a tow hook and the clutch of a trailer - the former fixed to a metal plank to the side of the boat and the latter to one end of the boom (Fig. 3-25 (b)). This way, a joint is built between ship and boom that allows free rotation in all directions and cushions possible movement due to wave motion. The boom itself consists of two hollow aluminum shells one of which can be slid out of the other to reach the required total distance of 7.5 m from the boat center (see section 5.2.1 and Fig. 3-25 (a)). In order to assure the stable position of the lead-in and to prevent the boom from sinking into the water, its outer end was fastened to a specially developed raft of sufficient buoyancy (Fig. 3-25 (c)) and Fig. 3-26 (a) and (b)).

Fig. 3-26 shows some pictures of how boom, raft and lead-in are placed with respect to each other and to "La Licorne". With a system of three ropes, each boom is kept at a right angle to the side of the ship (see Fig. 3-26 (a) and (b)). During deployment, the booms are first attached to the ship and then retracted along its side. As a next step, the raft is fastened to the boom's free end and ropes are fixed as shown in Fig. 3-26 (b). The lead-ins of the two outer ITI streamer sections are then hooked to the back side of the raft and taped along the corresponding boom to be connected to the onboard deck cable (see Fig. 3-26 (a)). Finally, the boom is put into its place by pulling on the two front ropes until a right angle is reached. Once the acquisition day is over, these ropes also serve as aid to pull the booms back in. After having pushed both shells into each other, they are fastened to the side of the ship for better transportation (see Fig. 3-26 (c)).

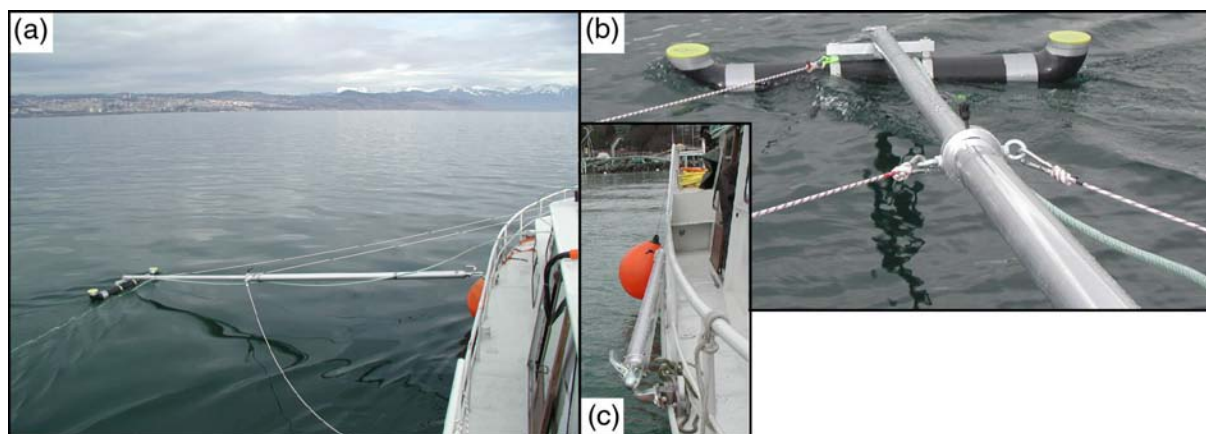


Fig. 3-26. Retractable boom specially constructed for Survey II: (a) in acquisition mode, towing one of the three streamers; (b) close-up view of the raft that keeps the boom on the water surface and of the ropes that maintain it at a 90° angle relative to the side of the boat; (c) in transportation mode the booms are attached to the side of the boat.

3.6 Navigation and positioning equipment

Section 2.3.4 explained how important precise positioning is for 3-D surveys, especially for those of high or very high-resolution. Having the advantage of a lacustrine setting with shorelines always in close vicinity, the most accurate positioning tool, the differential GPS, was chosen for both our acquisitions. Since the survey site is located less than five kilometers offshore from the city of Lausanne, reference stations could easily be set up and employed with minimal error for differential correction.

During Survey I, we used a differential GPS receiver (Ashtech SCA-12) from the “Institut Forel” in order to record the position of the center of the boat at the time of each shot. A second GPS antenna served uniquely for navigation purposes (Fig. 3-27 (a)). The GPS displayed the boat position and the lines to navigate on a small screen for the pilot to consult as guideline (Fig. 3-27 (a)). The differential correction was obtained by an additional onboard antenna that received signals from a PTT (Swisscom) antenna in the lake vicinity (~40 km). A computer program (see section 3.6.1) on a laptop uses the transmitted dGPS coordinates for gun triggering and directly records those boat coordinates that correspond to the most recent reading before the shot time. The dGPS has a maximum precision of 0.5 m while the GPS could reach 2-3 m at best (see also 2.3.4.1). Navigation and positioning were thus two independent processes and recorded positions could neither be displayed nor used for quality control during the acquisition of one sailed line.

Multi-streamer Survey II with half the cross-line spacing required even more accurate navigation. A reference station (Leica GPS SR 530) was set up on the biology building of the University of Lausanne at an altitude of about 50 m above the lake surface and at a distance of less than five kilometers from any position of the survey area. It recorded the coordinates of this reference position on disk non-stop during the entire length of the survey. The error corrections transmitted via radio waves were received right next to the mobile dGPS antenna

(same Leica GPS System 500) mounted to a pole on the roof top at the vessel center (Fig. 3-27 (b)). The position of the antenna can be determined to a precision that lies between 2 and 5 cm. Our newly developed navigation program (see 3.6.2) made it possible to display this precise boat position in real-time on a laptop (Fig. 3-27 (b) and Fig. 3-29) allowing immediate quality control of line straightness and heading correction by the pilot. Navigation and recording of boat positions at shot time are based on coordinate calculations from error corrected signals received by the same dGPS antenna.

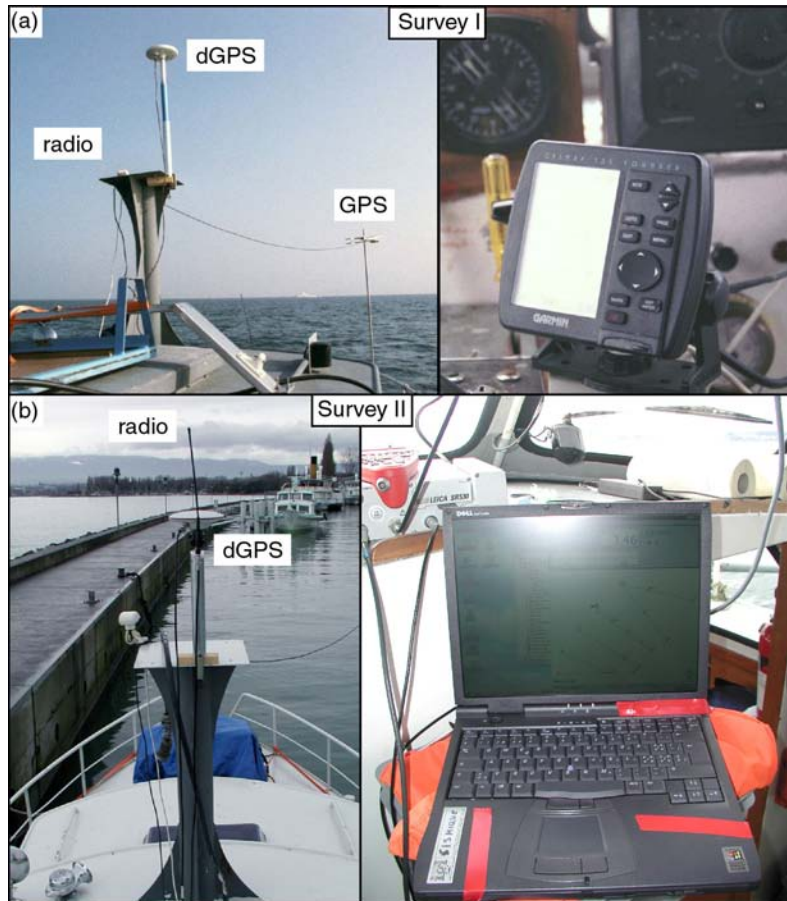


Fig. 3-27. GPS antennas and navigation monitoring for Survey I (a) dGPS and radio receiver for boat position and GPS for navigation monitored on the Garmin GPS screen; and for Survey II (b) Leica dGPS antenna and radio receiver – current boat position is displayed by new navigation program on laptop (see section 3.6.2).

Besides this onboard dGPS, three other dGPS receivers were mounted to the end of each streamer section. For this purpose we constructed three rafts onto which a waterproof case was fixed that housed the antenna (Trimble or Leica) and an Ashtech dGPS instrument

(Fig. 3-28). This raft was then attached between the second last and last hydrophone.

The receivers were switched on when the streamers were put in water. From that time till the end of the acquisition day, the dGPS recorded raft positions in two-second intervals on mini disk. In the evening, the raw data were downloaded on PC using Ashtech Version 2.0 Receiver Communication Software and were subsequently converted from Ashtech into Rinex format. The Rinex data together with the recordings of the base station were postprocessed into Swiss rectangular coordinates by Yannick Levet at the Swiss Federal Institute of Technology. Processing was done with GrafNav Version 6.03 to an accuracy of at least 20 cm and data were converted from the datum of the World Geodetic System of 1984 (WGS84) to the Swiss datum. The boat position at shot time and the location of the three

streamer tails now allowed more precise calculation of each receiver position at the corresponding shot time (see section 6.3.2).

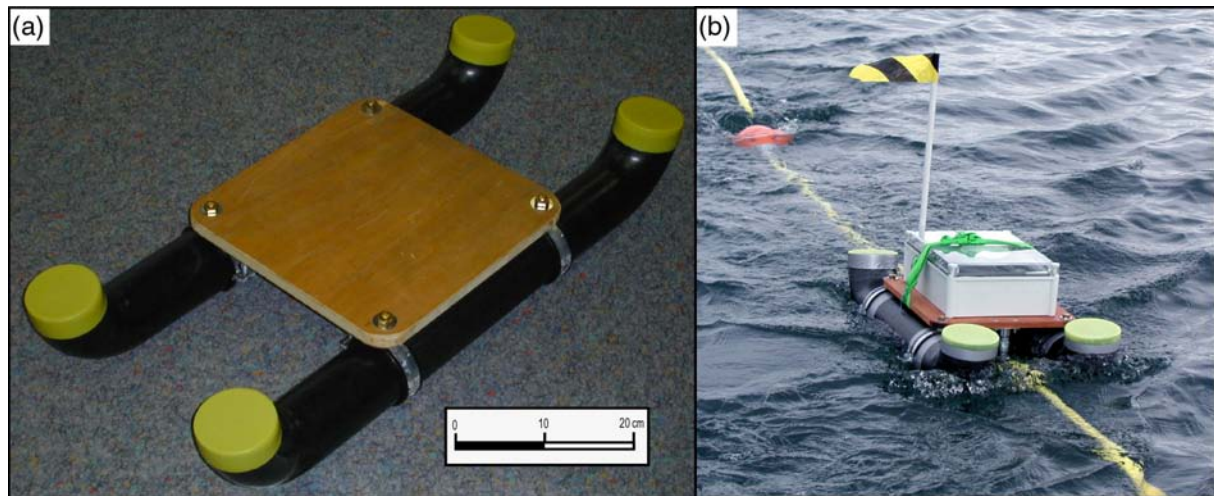


Fig. 3-28. dGPS raft: (a) its dimension and (b) in use attached to the end of the streamer.

3.6.1 Shot triggering for Survey I

The program used for shot triggering in Survey I has been developed by André Pugin, Institut Forel, University of Geneva (Pugin et al., 1999). It runs under MS-DOS and requires an initialization file (dts.ini) that contains the desired shot spacing, the shot interval and the first shot number. Computer and dGPS times are synchronized before the beginning of measurements. This process is repeated several times a day. At the start of the navigation line, shots are triggered at the initial shot interval. The program then calculates boat speed from coordinates of two dGPS readings at an interval chosen by the user. The desired shot spacing divided by the so measured speed gives the corresponding new shot interval. At the end of each line an ASCII file is output that contains for each shot, the shot time as well as the time, latitude and longitude of the most recent dGPS reading before that shot. Coordinates are calculated about as often in a minute as is shot. While the shot time is output to an accuracy of 10 ms (~ 5 cm), the coordinate time is rounded to the full second. An error of 0.5 s in coordinated time would thus produce a coordinate shift of 2.25 m. In addition, the dGPS antenna position at shot time has to be interpolated from the time difference to coordinates measured before and after triggering – a postprocessing step that further propagates the error (see section 6.3.2). So on the one hand there is the inaccuracy of the interpolated antenna position itself. On the other hand, this program is a dead-reckoning system, that is, it determines position with respect to a starting point by measuring and integrating the ship's velocity. Although boat speed is adjusted regularly it is unavoidable that small errors in actual shot distance accumulate in the integration towards the end of each navigated line. Thus, the measured position of the last shot point could be many meters away from the predetermined theoretical position.

3.6.2 Navigation software for Survey II

For Survey II navigation and distance shooting was significantly improved with the aid of a navigation program (GPS_shot) specially developed for this project by Philippe Logean from the Institute of Geophysics at the University of Lausanne. GPS_shot version 1.0 is a Windows based software, which requires two input files: an initialization file containing initial settings such as desired shot distance, baud rate and streamer length and a survey file with all the navigation line names, shot distance, start and end coordinates. Fig. 3-29 (a) shows the display of these theoretical navigation lines before the beginning of Survey II. The start and end point of the first line to shoot then have to be selected by mouse click. As soon as the program receives the antenna positions, which are determined from dGPS readings five times a second, the ship track is monitored in real-time on the monitoring window (Fig. 3-29 (b)). Between the time of signal reception and availability of corresponding coordinates lies a systematic delay of 100 ms for transmission and 50 ms for calculation. At a boat speed of 4.5 km/h this means a systematic absolute coordinate shift of about 19 cm.

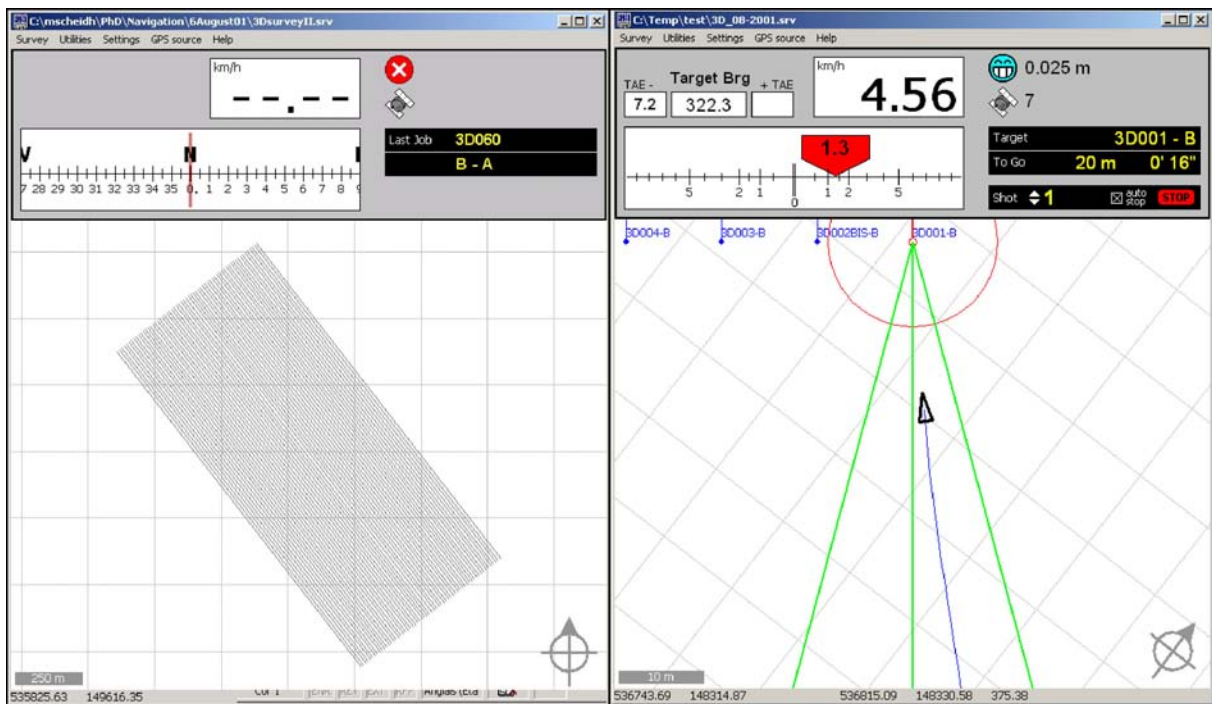


Fig. 3-29. New navigation program GPS_shot v. 1.0; (a) acquisition preplot (see section 2.3.4.3) of all 60 navigation lines of Survey II and (b) navigation monitoring while aiming at target; top of window shows current ship speed and target bearing, lateral deviation from target line, number of satellites used and accuracy with which coordinates are determined.

Fig. 3-29 (b) shows a zoom on the starting points of sail lines 1 through 4, line 1 being the selected target in red. The first shot position of this target line is surrounded by a red circle of a radius twice the shot distance (set in initialization file). The ship has to enter into this circle in the defined survey direction in order to activate shot triggering. A green 30°-triangle

pointing at the starting point of the target line helps the pilot to approach the circle with a straight streamer. The program places virtual grid lines on the survey area that have intervals of the desired shot spacing and are perpendicular to the survey direction. Every time the boat crosses one of these virtual grid lines, a shot is triggered. Due to the 5 Hz dGPS coordinate reading rate, the maximum possible error of triggering behind the grid line is 25 cm. Since grid lines are equidistant and triggering depends on real coordinates instead of shot intervals, the error is not cumulative and varies only slightly with changes in ship velocity. This navigation program thus presents a powerful tool for high-resolution marine acquisitions that performs automatic shot sampling in combination with real-time control on navigation quality.

CHAPTER 4: 3-D TEST SITE AND SURVEY DESIGN

Shallow seismic surveys have been carried out in numerous lakes, perialpine and others, in order to study the stratigraphy of glacial and post-glacial deposits as well as the geometry of the underlying bedrock (e.g. Finckh et al., 1984; Pugin et al., 1999; Zingg et al., 2003). In Lake Geneva, western Switzerland (Fig. 4-1), high-resolution seismic data have been acquired over extensive areas but could not provide detailed information on deeper structures (e.g. Vernet et al., 1974; Loizeau, 1991; Chapron, 1999). Furthermore, these mostly single-channel surveys consisted of widely-spaced grids that made it difficult to correlate complex features from line to line.

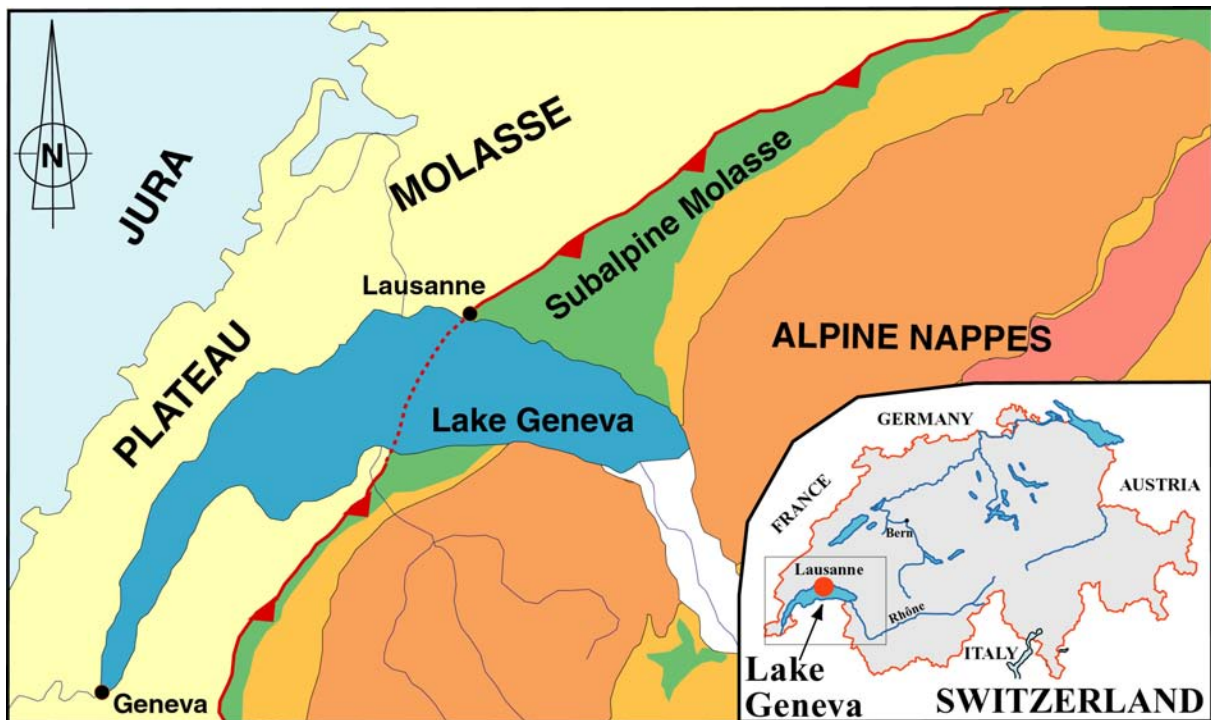


Fig. 4-1. Simplified geological map of the area around Lake Geneva, Switzerland, showing a major thrust fault zone separating Plateau and Subalpine Molasse units; adapted from Weidmann (1988).

In north-central Lake Geneva, just offshore the city of Lausanne (Fig. 4-1), recent surveying of a tight grid of 2-D multi-channel seismic lines attained a generally deeper signal penetration and a higher signal-to-noise ratio than those of the earlier studies (Morend, 2000; Morend et al., 2002). The authors presented high-resolution images of shallow Quaternary sediments as well as deeper incised-valley fill within the consolidated molasse units in the vicinity of a major thrust fault zone – La Paudèze. Surprisingly, even a line spacing as low as 50 m was insufficient to allow correlation of some of the complex geological structures. Hence, this portion of the lake seems well-suited for 3-D studies and was chosen to be the test site for our 3-D system.

4.1 Geological setting

The northern Alpine foreland basin, spanning a distance of ~700 km from the French Savoy area in the west to Linz (Austria) in the east, is filled with molasse deposits, which are subdivided into two shallowing-upward megasequences by the Aquitanian / Burdigalian unconformity (Homewood et al., 1986). The sedimentary succession comprises four lithostratigraphic groups (Fig. 4-2, bottom): Lower Marine Molasse (UMM, Rupelian), Lower Freshwater Molasse (USM, Rupelian?-Chattian-Aquitanian), Upper Marine Molasse (OMM, late Aquitanian-Burdigalian), and Upper Freshwater Molasse (OSM, Langhian-Serravalian).

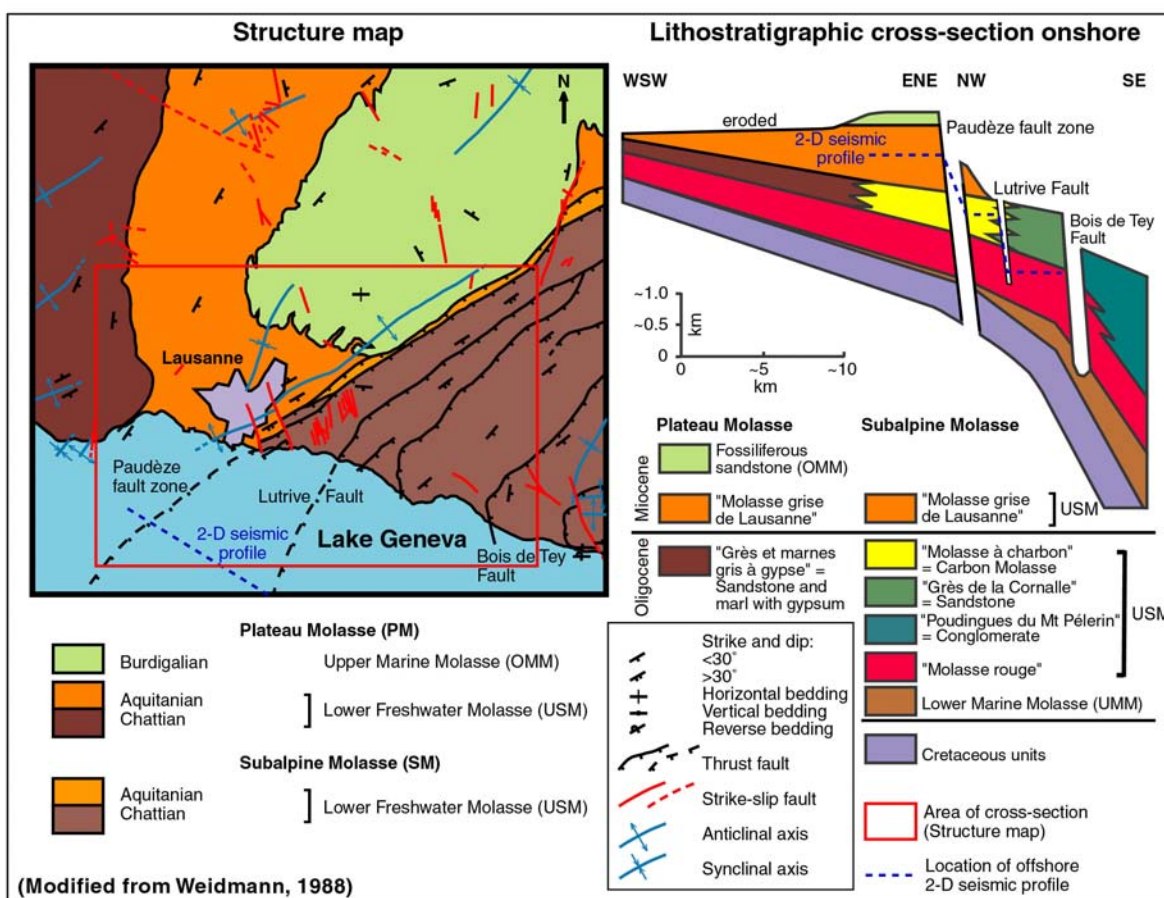


Fig. 4-2. Structure map and a schematic lithostratigraphic cross-section (vertical throw not considered) of the area around the city of Lausanne, modified from Weidmann (1988). Fault zone extensions into the lake are taken from Vernet et al. (1974). The conventional German abbreviations of the four listed molasse groups are given in parenthesis.

The chosen study area is located in the western part of the Swiss Molasse Basin, which comprises two tectonic units: the relatively undeformed, southeast-dipping *Plateau Molasse* (PM) and the *Subalpine Molasse* (SM), a complex assemblage of imbricated thrust slices (Gorin et al., 1993). These units are separated by the "Paudèze" fault zone, a major thrust fault system with a total vertical throw of ~1 km and a southwest-northeast trend (Weidmann, 1988; Fig. 4-2). It runs through the city of Lausanne, presumably across the whole lake and reappears on the French shore (Fig. 4-1).

Lake Geneva, Europe's biggest perialpine lake, formed in a glacial trough that was carved in the PM and SM units along the western part of Switzerland (Fig. 4-1). Pleistocene glacial deposits and Holocene fluvio-lacustrine deposits in the eastern part of the lake are more than 350 m thick, but have thicknesses of less than 40 m along the steep northern slope of the lake (Vernet et al., 1974; Morend et al., 2002). In the area offshore Lausanne, this Quaternary lake fill overlies unconformably the upper part of the Lower Freshwater Molasse (USM), i.e. the Aquitanian "*Molasse grise de Lausanne*" (MGL) Formation and the Chattian "*Molasse à charbon*" (MC) Formation (Fig. 4-2). It is characterized by eskers, till / (sub) glacio-lacustrine sequences of four glacial fluctuations and thick deltaic deposits (Moscariello et al., 1998). Among the authors that describe the stratigraphy and sedimentology of the MGL are Bersier (1958a), Bersier (1958b), Rigassi (1977), Weidmann (1988), Morend et al. (2002) and Weidmann and Morend (2002). This formation is a thick succession (800-1100 m) of laterally discontinuous, channelized sequences composed of coarse sandstone bodies with concave-upward erosional bases (channels), fine-grained sandstones, silty marls, and scarce clays. The depositional environment of this formation is depicted as a wide, low-relief floodplain with meandering rivers that was locally invaded by tidal channels at the end of the Aquitanian (Berger in Weidmann, 1988; Berger, 1992).

The Subalpine Molasse is made up of five major tectonic slices of the Chattian Lower Freshwater Molasse (Fig. 4-2), each bordered to the north by a thrust fault. The northernmost two slices (including the Paudèze thrust zone) comprise the "*Molasse à charbon*" while the next slice separated by the Lutrive Fault is composed of "*Molasse rouge*" (Weidmann, 1988, Fig. 4-2). Internal tectonic deformations, lithologies and dip values are highly variable from one slice to another.

4.2 Selection of target area

The investigations of Morend et al. (2002) revealed complex geological structures offshore Lausanne, just 800-4000 m southwest of Ouchy harbor (Fig. 4-3). Many of their north - south and northwest – southeast 2-D profiles image the northwestern limit of the thrust fault zone ("La Paudèze" accident), which Morend (2000) accurately picked at the abrupt termination of continuous reflections in the MGL of the Plateau Molasse. Its location approximately confirms the interpretation of Vernet et al. (1974), who studied the extension of the frontal thrust into Lake Geneva based on single-channel seismic data that were acquired in the early 1970's with an analog recording system, and that of Weidmann (1988), who mapped the fault zone onshore (Fig. 4-4). Morend et al. (2002) suggest that a continuous 3-D seismic survey with a higher penetration depth would be the best way to interpret the onshore structures into Lake Geneva and might as well allow accurate mapping of the channel system they recognized. Such prospect, the excellent signal penetration and clearness of reflectors observed on the 2-D profiles as well as the close vicinity to Ouchy, the harbor of Lausanne,

make this study site well suited to test our 3-D system. Since a 3-D survey is composed of a large quantity of navigated lines, and our research vessel cannot operate at night, it is very important to keep the transit time to the survey area as short as possible. With the knowledge of the exact position of the fault limit and the approximate strike of the Plateau Molasse beds parallel to this limit, it now is a simple task to outline a 3-D area that includes the frontal thrust and is oriented perpendicularly to it. The resulting data set will complement the seismic work of Morend et al. (2002) by producing a deeper but still very high-resolution continuous three-dimensional image, especially of the highly deformed fault zone.

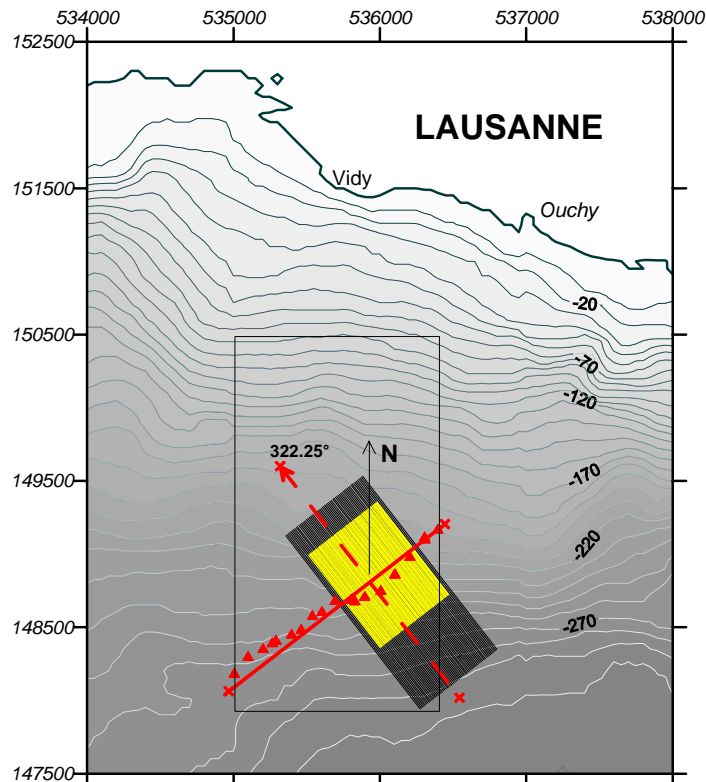


Fig. 4-3. Northwestern limit of the Paudèze Fault (red triangles) as interpreted by Morend (2000) on a grid of 2-D profiles acquired within the area indicated by a black rectangle; the average trend of the fault zone (solid red line) allows calculation of the future 3-D survey direction perpendicular to the average fault zone strike (dashed red line at 322.25° relative to geographical north); acquisition preplots of Survey I (yellow) and Survey II (black) are centered about the fault zone (for more details see chapter 5).

Didier Morend kindly provided the position of the northwestern limit of the Paudèze thrust fault extracted from their grid of interpreted 2-D lines, giving a relatively accurate location of the fault strike over a length of about 2 km. The fault limit on each line is indicated by a red triangle in Fig. 4-3. The principal direction of the future 3-D survey (dashed red line) was determined as that perpendicular to the average trend through those data points (solid red line). Start and end points of all theoretical acquisition lines were then calculated by adding half the required line length in survey direction (322.25° relative to geographical north) to both sides of equidistant points along the fault strike. The theoretical start and end points of both 3-D surveys that were carried out on this study site are listed in Table A-9 and Table A-10 of the Appendix. Fig. 4-3 shows the corresponding acquisition line preplots (definition see section 2.3.4.3). The longer lines for Survey II and their additional extension towards the southeast is based on experience from Survey I (see sections 5.1.1 and 5.2.1).

4.3 2-D profiles in target area

In order to get a good idea of the overall geological situation in the lake close to the chosen 3-D test site, a 2-D profile across the whole lake was acquired that crosses the Paudèze Fault zone and forms the extension of one of the center in-lines of the 3-D survey area (sail line 55 for Survey I or sail line 37 for Survey II corresponding to CMP line 140 - Table 6-B - when using the common grid defined in section 6.4). This complete lake traverse was shot in four parts (profiles 140_15 a-d, Table A-11) before and during Survey II using the Mini G.I Gun in harmonic mode G15 / I15 (section 3.4.2). At the end of Survey I, another 2-D line slightly longer to the northwest and southeast than in-line 140 had been acquired with the Mini G.I Air Gun in G30 / I30 configuration (profile 140_30, Table A-12). Processing the S15.02 Water Gun data from sail line 55 of Survey I (see section 5.1) in 2-D allows the comparison of all three different source types under the same subsurface conditions where profiles coincide. Their location with respect to the 3-D survey area are shown in Fig. 4-4.

4.3.1 2-D acquisition and processing

Profile 140_30 and portions (a) and (b) of profile 140_15 were acquired using the single-streamer configuration as described in section 5.1.1 (Fig. 5-1). Their acquisition sheets can be found in Table A-11 and Table A-12. Portions 140_15 (c) and (d), which build the northwest extension of sail line 37, were shot as part of Survey II using the multi-streamer configuration (see section 5.2.1, Fig. 5-4). Acquisition parameters are identical to those for the 3-D surveys, with the difference that the recording gain for profile 140_30 was set to 36 dB (GEOMETRICS seismograph) and for 140_15 (a) and (b) to 60 dB (BISON seismograph) instead of 24 dB. Gain tests were conducted as a result of the observed signal saturation on individual traces (section 3.3.1). Since profile 140_30 and sail line 55 of 3-D Survey I (profile 140_w) were recorded with the GEOMETRICS seismograph, gain ranging was used in combination with the instrument's standard 36 dB preamplifier gain (section 3.3).

Profiles 140_30, 140_w and portions (a) and (b) of profile 140_15 were processed into time migrated sections while portions (c) and (d) so far exist only as near trace plots. The 2-D processing flow used is a simplified version of that applied to the 3-D surveys (chapter 6). After data format conversion and an arrival time correction appropriate to the corresponding gun (section 3.4.4), geometry was assigned by assuming that shots had been triggered at exact 5 m intervals. In order to bypass the merge of navigation data with seismic trace headers, each profile was tied to geographical coordinates with the aid of its starting point and the average acquisition direction. After trace editing, sorting into CMP gathers and velocity analysis, data were bandpass filtered, spherical divergence corrected, NMO corrected and stacked. Due to the multi-fold coverage, the stacks reveal a deeper penetration and a better signal-to-noise ratio than single-channel sections from the same location (example in Fig. 4-6 (a) and (b)). The CMP gathers permitted accurate determination of stacking velocities. Corresponding

interval velocities range from 1450-1600 m/s for the unconsolidated sediments and from 1600 to more than 3000 m/s for the consolidated sediments.

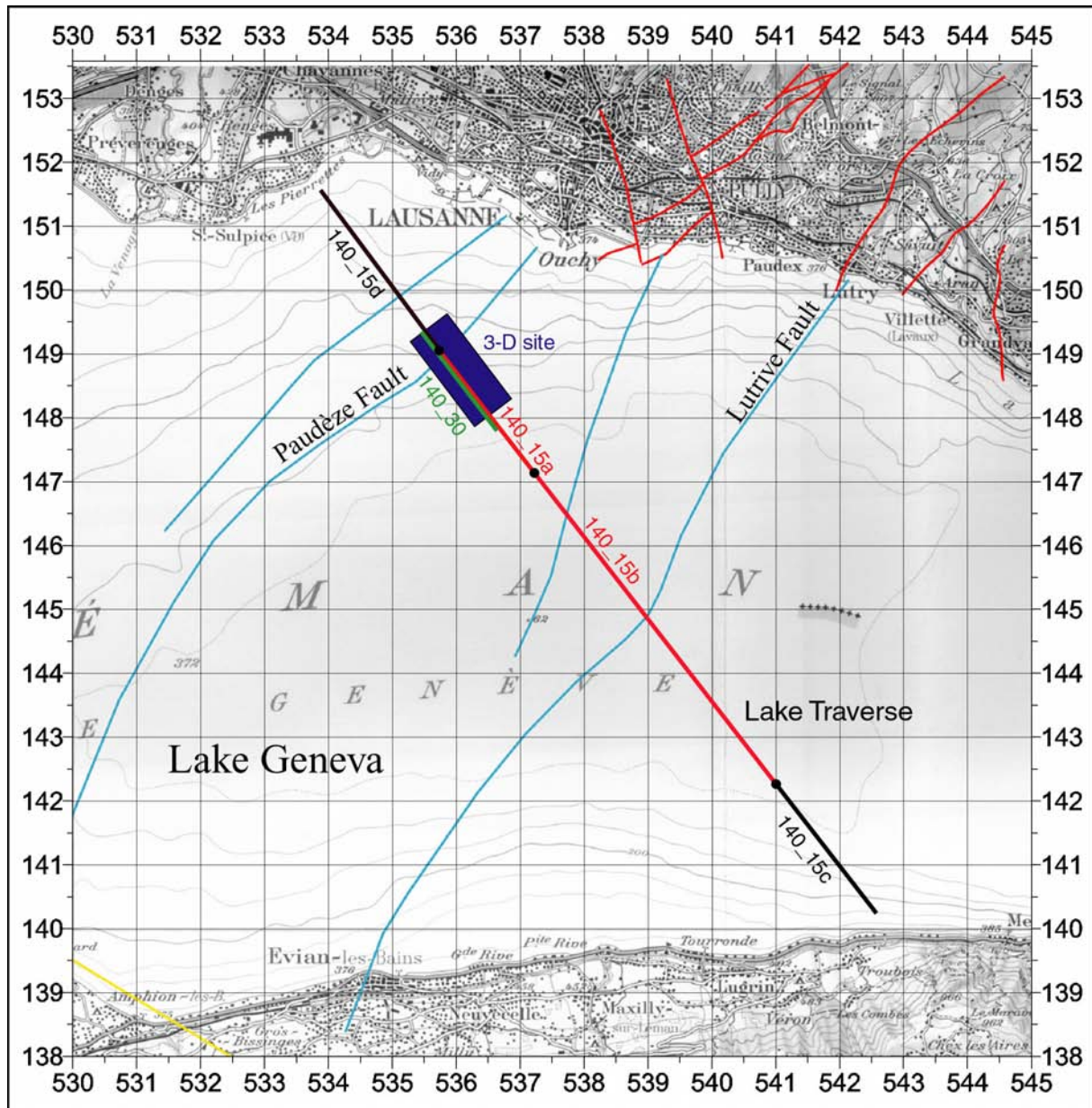


Fig. 4-4. Location of 2-D profile 140_30 (green, Fig. 4-7), lake traverse 140_15 a-d (red portions a and b are shown in Fig. 4-8) and 3-D survey site. Faults and structures on land are taken from the geological map of Weidmann (1988). Fault extensions into the lake (light blue) were interpreted by Vernet et al. (1974).

An example 2-D processing flow of profile 140_30 using the processing software Géovecteur is listed in Table A-13 of the Appendix. Except for filtering and velocity analysis, the same parameters were used for all three profiles. Filter bands were set according to gun signatures (section 3.4.6) to 40/60 – 500/550 Hz for profile 140_30, to 40/60-600/650 Hz for profile 140_15 (a) and (b) and to 100/200-1500/1700 Hz for profile 140_w. In order to better

compare the effects of different source types and penetration, traces of all three profiles were brought up to the same mean amplitude level using a constant scale factor (no AGC).

Since no DMO correction had been applied, the 2-D velocity analysis produced a stacking velocity model that is affected by dip and out-of-plane reflections. For this reason, the 3-D zero-dip rms velocity model (see section 6.6 and Fig. 6-8) was used to determine an average interval velocity (equation (2.4)) with which the corresponding horizontal to vertical aspect ratio of the time sections could be calculated. The velocity distribution over in-line 142 (Fig. 4-5), which lies only 7.5 m southwest of the 2-D profiles, shows that interval velocities within the Plateau Molasse (left side of panel) range from 1600 to 2700 m/s between 300 and 410 ms while velocities within the Subalpine Molasse further southeast are much lower for the same time interval. This apparent lateral change in velocity is mainly due to the deepening topography and the thicker layer of quaternary sediments overlying the Subalpine Molasse fault zone. Since the signal in profiles 140_15 and 140_30 (Fig. 4-7 and Fig. 4-8) penetrates the Plateau Molasse down to at least 530 ms before the multiple superimposes the primary reflections and where velocities might exceed the 3000 m/s, an interval velocity of 2300 m/s was chosen to represent the molasse average velocity over the 3-D survey extent. With respect to this velocity, the 2-D migrated sections are displayed in Fig. 4-6 and Fig. 4-7 with an exaggeration of 2 and in Fig. 4-8 with no exaggeration at all.

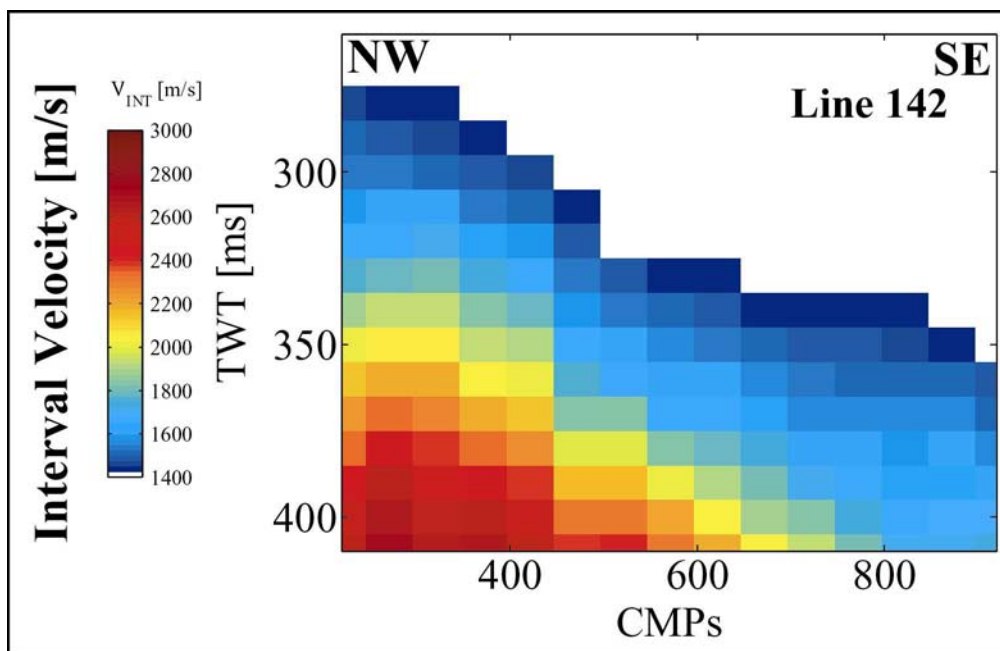


Fig. 4-5. Interval velocity distribution over in-line 142 extracted from the 3-D model in section 6.6. The 2-D profiles, which correspond to in-line 140, are located only 7.5 m southwest of in-line 142.

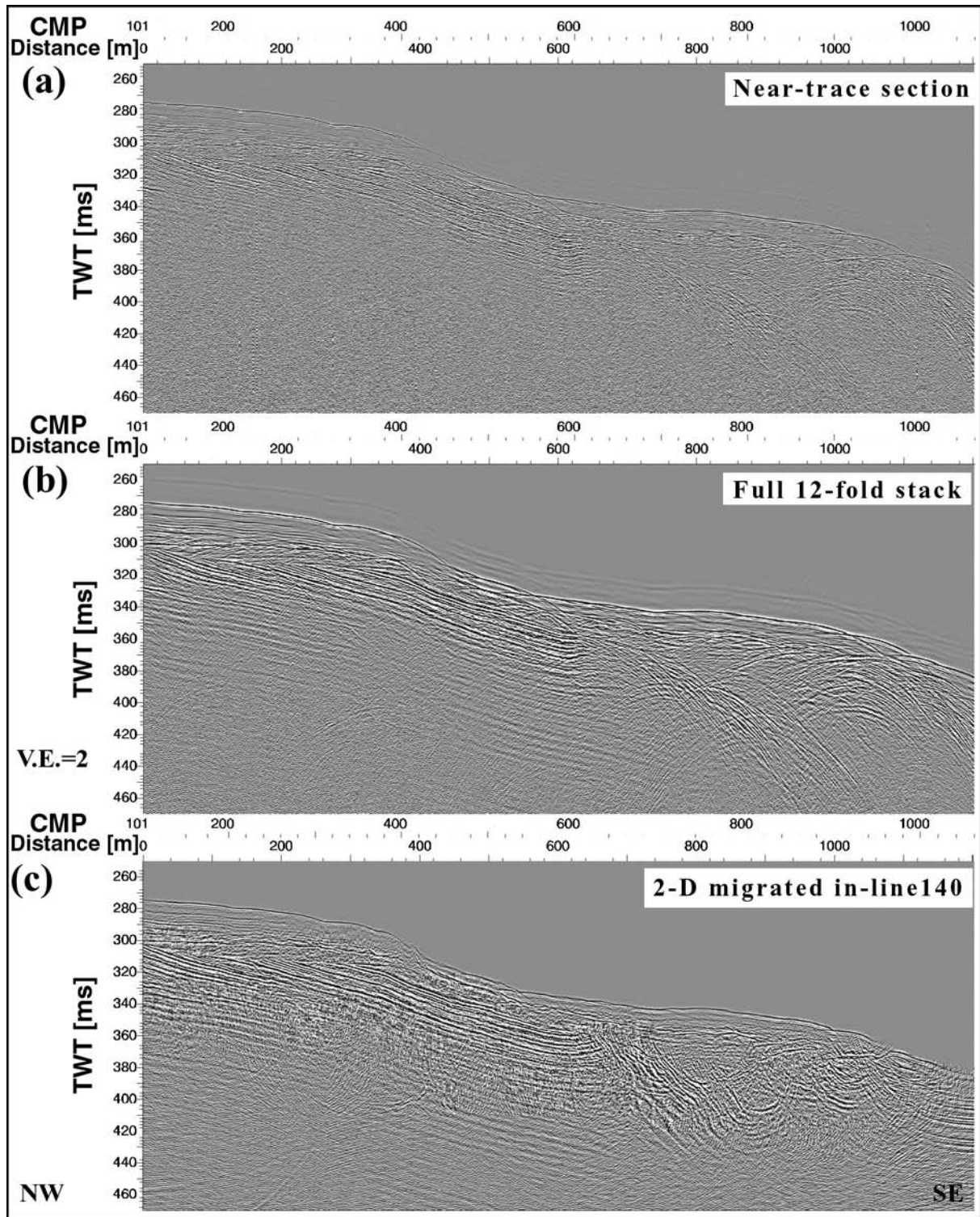


Fig. 4-6. 2-D profile 140_w (sail line 55 of Survey D), recorded with the S15.02 Water Gun. Real amplitudes were preserved and data are presented with a vertical exaggeration of 2 when using an average velocity of 2300 m/s for the imaged portion of the Plateau Molasse. Structural dips within the upper molasse beds and the Quaternary sediments (<350 ms) might thus be exaggerated while dips in the lower beds (>450 ms) might be too small. (a) Near-trace section, (b) stack and (c) post-stack time migration (Kirchhoff). For line location, see Fig. 4-4.

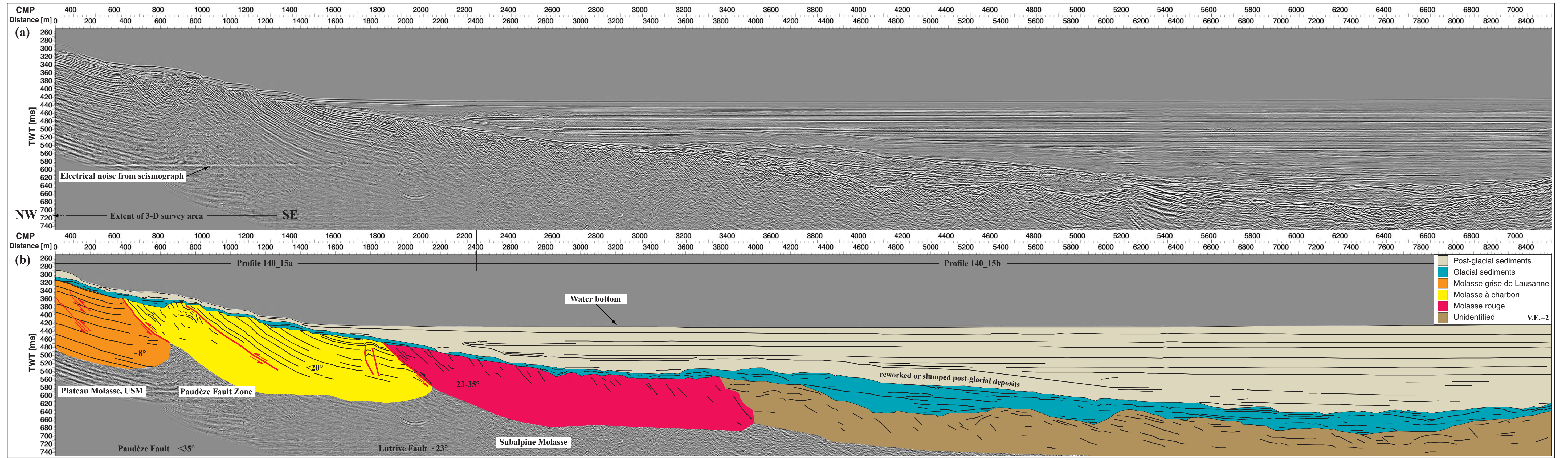


Fig. 4-7. 2-D post-stack time migrated (Kirchhoff) profiles 140_15a and 140_15b, recorded with the Mini G.I G15 / I15 Air Gun, showing the typical seismic signature observed in the 3-D survey area and much further to the southeast. CMP numbers are given relative to the 3-D survey grid for comparison. (a) Real amplitudes were preserved and data are presented with a vertical exaggeration of 2 when using an average velocity of 2300 m/s for the imaged portion of the Plateau Molasse. Structural dips within the upper Molasse beds and the Quaternary sediments (<350 ms) might thus be exaggerated while dips in the lower beds (>450 ms) might be too small. The signal at 590 ms is due to electrical noise of the BISON seismograph. (b) Interpretation of Plateau Molasse and Subalpine Molasse units separated by the Paudèze Fault zone and covered by glacial and post-glacial sediments. Within the Subalpine Molasse further southeast, the Lutrive Fault separates the steeply dipping "Molasse rouge" from the "Molasse à charbon". Still further southeast, lithology is not identified. The average fault dips as well as the dip of beds in all identified Molasse units are indicated in the interpreted section. For line location, see Fig. 4-4. Colors correspond to those in Fig. 4-2. Fig. 4-9 illustrates the interpretation in map view.

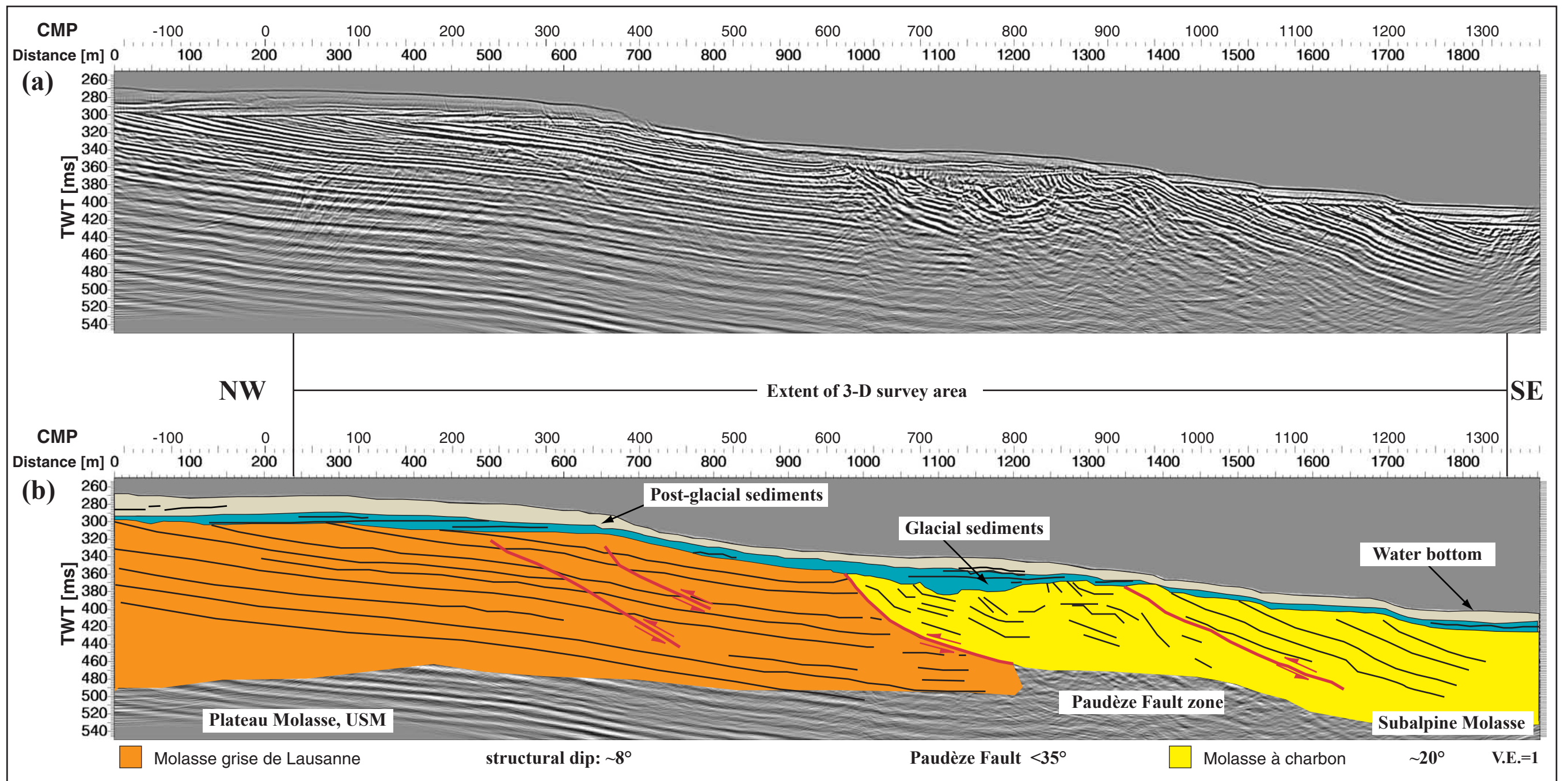


Fig. 4-8. 2-D post-stack time migrated (Kirchhoff) profile 140_30, recorded with the Mini G.I G30 / I30 Air Gun, showing the typical seismic signature observed in the 3-D survey area. CMP numbers are given relative to the 3-D survey grid for comparison. (a) Real amplitudes were preserved and data are presented without vertical exaggeration when using an average velocity of 2300 m/s for the imaged portion of the Plateau Molasse. Structural dips within the upper Molasse beds and Quaternary sediments (<350 ms) might thus be exaggerated while dips in the lower beds (>450 ms) might be too small. (b) Interpretation of Plateau Molasse and Subalpine Molasse units separated by the Paudèze Fault zone and covered by glacial and post-glacial sediments. The average dips for Plateau and Subalpine Molasse beds as well as the maximum fault dip are indicated below the interpreted section. For line location, see Fig. 4-4. Colors correspond to those in Fig. 4-2. Fig. 4-9 illustrates the interpretation in map view.

4.3.2 Large-scale seismic interpretation

A large-scale lithostratigraphic interpretation is superimposed on the time migrated sections in Fig. 4-7 (b) and Fig. 4-8 (b). The two tectonic units - Plateau Molasse and Subalpine Molasse - can be easily distinguished for two reasons. First, because they are separated by the about 350 m broad Paudèze Fault zone and second because of their very different degrees of deformation and inclination. The northwestern limit of the fault zone, the Paudèze Fault, is a distinct feature and can be accurately picked on all three profiles at the abrupt termination of the continuous reflections in the Plateau Molasse. Its dip increases towards the eroded surface of the USM to a maximum value of 35° . This dip change might be partially due to the increase in velocity as a function of depth. To the southeast, the fault zone is limited by another fault that separates the discontinuous, steeply dipping bedding planes from again very continuous reflectors. Both 2-D air gun profiles allowed accurate delineation of these two most external structural slices within the Subalpine Molasse because of their sufficient extent and a high enough energy level. On profile 140_30 (Fig. 4-8), the Paudèze Fault can be traced as deep as 100 ms two-way travelttime (TWT) below the top molasse surface, which is equivalent to a penetration of approximately 115 m.

Extending the known lithostratigraphical units on land (Weidmann, 1988; Fig. 4-2) into the lake helps interpreting the different seismic facies along the 2-D profiles, at least in close vicinity to the shoreline. Morend et al. (2002) identified the USM “*Molasse grise de Lausanne*” (MGL) northwest of the fault zone limit. Reflections in the MGL are of relatively high amplitude, very continuous and dip approximately 8° towards the southeast within the studied area. The large-scale tectonic map of Fig. 4-2 shows that these dipping reflectors are part of the southeast flank of the Lausanne anticline, whose apex is almost parallel to the Paudèze Fault zone in its vicinity. Consequently, this measured dip represents the true inclination of beds in the shallow portion of the imaged MGL, as will be confirmed later by the 3-D data (section 7.3).

Based on onshore structural data and geological cross-sections, the northernmost two slices of Subalpine Molasse on the other side of the Paudèze Fault are very likely composed of “*Molasse à charbon*”. While reflectors in the fault zone slice are contorted and chaotic and it is difficult to determine their actual dip, the seismic facies in the second main slice is parallel, continuous and steeply inclined ($\sim 20^\circ$ southeast dip) although flattening towards the southeast. The paleosurface of the “*Molasse à charbon*” has a highly irregular relief (nearly 100 ms range, see Fig. 4-7) probably because of the presence of steep-dipping beds of alternating sandstones and shales with differential erosion rates.

In Fig. 4-7 (b), another thrust fault further to the southeast separates an additional main slice whose chaotic seismic facies and steep inclination ($< 35^\circ$ southeast dip) is similar to the appearance of the “*Molasse rouge*” as mapped by Weidmann (1988) onshore. On his geological cross-section number 4, which is oriented almost parallel to our 2-D profiles, the

“*Molasse à charbon*” and the “*Molasse rouge*” are separated by the Lutrive Fault, suggesting it being the fault observed on profile 140_15 at CMP 1800 (Fig. 4-7). Still further south (CMPs >3200) the eroded USM surface becomes progressively more hummocky and reflectors within this unit less clear because the thickening glacial and post-glacial sedimentary layer and the internal deformations prevent sufficient signal penetration. Faults there are difficult to identify, which makes the exact extent of the “*Molasse rouge*”-slice uncertain.

The folded and faulted USM was eroded by Pleistocene glaciers. Along the processed portion of the lake traverse, the total thickness of Quaternary sediments varies from 7 m to 170 m in the deeper part of the lake, when using an average velocity of 1550 m/s (see velocity model of Fig. 6-8). Because of its general structural dip, the surface of the USM is a distinct unconformity (Fig. 4-7 and Fig. 4-8 (a)) beneath the glacial sediments. Two main seismic facies characterize the sediments of the Quaternary overburden. Immediately overlying the molasse units is a facies with a generally discontinuous to chaotic reflection pattern, interpreted as glacial sediments. According to Chapron (1999), these sediments are composed of waterlain till and (sub) glacio-lacustrine deposits. The interface between both is only distinguishable on the northwest portion of the water gun profile 140_w in Fig. 4-6 and between CMP 3800 and CMP 4600 of profile 140_15 in Fig. 4-7. The uppermost stratigraphic sequence is interpreted as post-glacial lacustrine sediments (Chapron, 1999) and contains continuous, parallel and low-amplitude reflections. In the deep lake portion of profile 140_15, the glacial sediments are covered by an up to 40 ms (~30 m) thick low-amplitude facies, which might contain reworked or slumped post-glacial sediments. Its top forms a discontinuity with the onlapping very continuous, horizontal, overlying sediments. The 2-D data do not indicate any faulting within the Quaternary sediments. This observation is consistent with that of relatively recent seismic work in Lake Geneva (Finckh et al., 1984; Moscariello et al., 1998; Chaudhary et al., 2002; Morend et al., 2002).

Fig. 4-9 shows a map that gathers all available information on fault locations and lithology based on the above observations (red triangles) and all previously collected data in the area (black triangles, light blue lines). In combination with the well-known geology onshore (Weidmann, 1988), recent multi-channel 2-D measurements (Morend et al., 2002; Chaudhary et al., 2002; this work) allow an update of the large-scale tectonic image in the close vicinity of the 3-D test site offshore the city of Lausanne. It seems obvious to connect the northwest fault zone limit, as interpreted by Morend (2000), with the Paudèze Fault onshore, which is consistent with the interpretation of profiles 140_15a and 140_30. Two 2-D profiles from Chaudhary et al. (2002) located between the lake traverse and the shore line help delineate the extent of the fault zone towards the southeast.

However, the position of the Lutrive Fault and the distribution of the “*Molasse à charbon*” is less evident. For comparison, the interpretation by Vernet et al. (1974) (light blue

lines) of a number of single-channel profiles shot in the 1970s was digitized and put on Fig. 4-9. If the Lutrive Fault was correctly interpreted on all three multi-channel profiles - and the observed seismic facies speaks for it - then some additional faulting must have taken place in the area marked by question marks. A sign of the complexity of the indicated zone is given by a possible strike-slip fault identified on the northernmost - but not on the southern - profiles (Chaudhary et al., 2002) and which could be the extension of the onshore strike-slip fault. A denser grid of 2-D profiles would certainly give more insight into the tectonics of the area between Paudèze and Lutrive Faults. Even a 3-D survey might be necessary to fully understand its complicated structure.

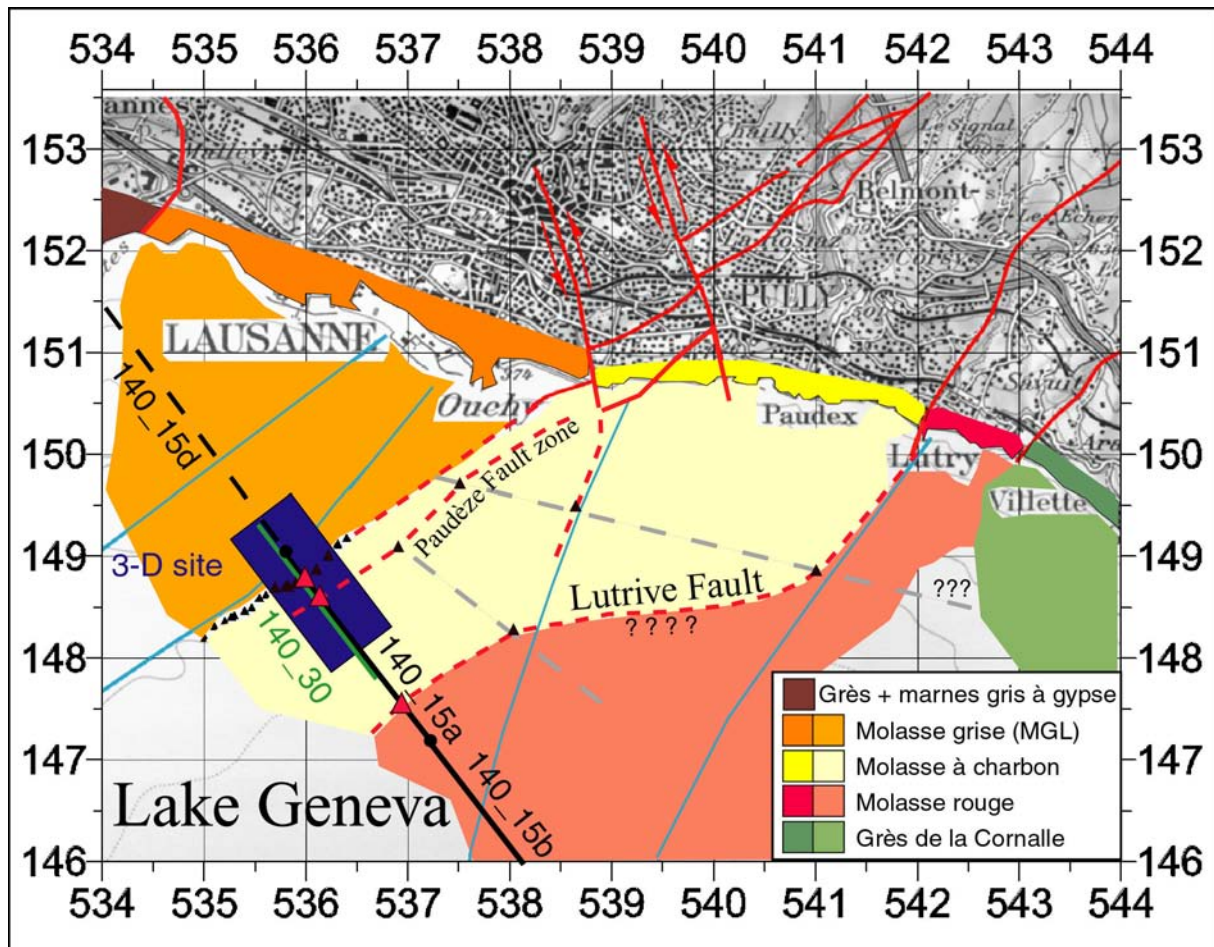


Fig. 4-9. Interpretation of fault locations from 2-D profiles and inferred lithostratigraphy. Colors on land correspond to those in Fig. 4-2 – their lighter counterparts signify the same lithology but extrapolated into the water. Black triangles indicate fault positions interpreted by Morend (2000) (see Fig. 4-3) and Chaudhary et al. (2002) (dashed grey profiles) while light blue lines designate fault locations from Vernet et al. (1974). The red triangles mark the position of faults as from profile 140_15a (Fig. 4-7).

All dip values indicated in this chapter and on the presented sections were determined relative to the average velocity of 2300 m/s, which was taken from the 3-D velocity model in the Plateau Molasse. Thus, structural dips within the upper Molasse beds (>350 ms) may be exaggerated while those in the lower beds (>450 ms) may appear too small. Morend et al.

(2002) calculated dips in the offshore Plateau Molasse beds using an average velocity of 3200 m/s, which was derived from velocity measurements from the Bois-Genoud outcrop close to Lausanne. They found variations in dip ranging from 17° close to the shore to 10° in the vicinity of the Paudèze Fault. If the scale of the time axis in our 2-D profiles were calculated with the same higher average velocity, beds within the MGL would also dip about 10°, the fault zone even 45° and the beds of the “*Molasse à charbon*” 27°. Since the portion close to the Paudèze Fault is composed of the upper part of the MGL (Morend et al., 2002) it is possible that, because of its anticlinal structure, velocity measurements onshore might have taken place in a lower portion of the thick (>1000 m) MGL unit. As the 3-D velocity model shows and as is confirmed by other measurements onshore (e.g. Baron (2001)), velocity is highly variable, especially within the upper molasse beds. This might be due to weathering and deformation close to the thrust zone - see folds and faults within the MGL in Fig. 4-6 and Fig. 4-7. Thus, it is believed that 2300 m/s represents the proper average velocity for the small portion close to the fault zone, whereas for large-scale corrections of units with great age differences 3200 m/s might be a more appropriate value.

4.3.3 2-D data results

The three presented profiles give a high-resolution image of excellent quality in two dimensions of the geological structure and tectonic environment across the 3-D test site. Each profile was shot with a different source type, which allows comparison of their performance in the target zone by using all other equipment in the same single-streamer configuration as planned for the first 3-D survey (Fig. 5-1). The most important aspect of these measurements is that the processed results will help evaluate those acquisition parameters for 3-D survey design that directly depend on the target area, e.g. migration aperture due to structural dip, recorded frequency bands after reflection, and especially rms velocities, obtained vertical resolution, maximum signal penetration depth and corresponding required trace length.

4.3.3.1 Vertical resolution

In order to calculate data resolution, it is necessary to know the approximate interval velocity of the imaged layer and the dominant frequency of the seismic signal (see equation (2.17)). The dominant frequency of the reflected wavelet changes as a function of depth due to absorption of the higher frequencies. In order to get an estimate of the best vertical resolution achieved in the 2-D profiles calculations are made for the uppermost sedimentary section close to the water bottom where the velocity is only slightly bigger than that of the water and the signal has not yet degraded. Consequently, an interval velocity of 1500 m/s was used for the post-glacial sediments. Table 4-A lists the range of wavelengths with respect to each source signature's bandwidth after bandpass filtering (section 4.3.1), their dominant frequency (determined in section 3.4.6) and the corresponding theoretical vertical resolution,

using Rayleigh's criterion (section 2.4.1.1). To determine the signal resolution at deeper levels it would be necessary to know how the dominant frequency changes with depth.

The best vertical resolution in the upper sedimentary section with respect to the dominant frequency of the seismic signal is 60 cm for the water gun and 1.1 m and 2.5 m for the air gun sources, respectively. In order to provide the dominant frequency (sections 2.3.3 and 2.3.3.5) of 150 Hz / 330 Hz / 670 Hz for each of these sources, it is necessary for the seismic wavelet to contain unaliased frequencies of the whole spectrum up to approximately 550 Hz/ 650 Hz / 1700 Hz, respectively (see section 3.4.6). This illustrates the importance of maintaining the maximum possible frequencies in the seismic wavelet. Consequently, all frequencies over the full bandwidth of the source spectrum are to be checked for potential aliasing problems with respect to the chosen bin size (section 4.4.1).

Source Profile	Water gun water_w	Mini G.I G15 / I15 140_15	Mini G.I G30 / I30 140_30
Bandwidth [Hz]	100/200 - 1500/1700	40/60 - 600/650	40/60 - 500/550
Dom. Frequency	670 Hz	330 Hz	150 Hz
Wavelength λ [m]	0.9/1 - 7.5/15 2.2 m	2.3/2.5 - 25/37.5 4.5 m	2.7/3 - 25/37.5 10 m
Vertical Resolution $\lambda/4$ [m]	0.2/0.3 - 1.9/3.8 0.6 m	0.6 - 6.3/9.4 1.1 m	0.7/0.8 - 6.3/9.4 2.5 m

Table 4-A. Frequency bandwidth of each type of seismic source after bandpass filtering (white), respective dominant frequency (grey), corresponding wavelength and vertical resolution within the post-glacial sediments. The wavelength was calculated assuming a velocity of 1500 m/s and no absorption of high frequencies. Values related to the dominant frequency are highlighted in grey.

4.3.3.2 Penetration depth and trace length

Different to vertical resolution, calculation of the signal's penetration depth requires the average velocity of the medium above the deepest recognizable reflector and is often given relative to the water surface. This might be less instructive than indicating a penetration depth below the water bottom. For this reason, layer thicknesses will be computed separately by using the average interval velocities, firstly, of the water layer, secondly of the Quaternary sediments and thirdly of the molasse unit from its top down to the deepest imaged reflector. The sum of the latter two thicknesses will result into the maximum penetration depth below the water bottom at a specific location. However, it will already be sufficient to decide on the trace length for recording when knowing the maximum total penetration time. Water bottom arrival times automatically determine the arrival time of the first multiple, which might be difficult to eliminate and places a constraint on data quality. If record length is to be spared for reasons of seismograph recording speed, number of traces and minimum ship velocity (section 3.3.3), then the multiple arrival time would be a good criterion to define the recording limit.

In the following, the extent of the 3-D survey area will be divided into three zones from northwest to southeast: the one that images the Plateau Molasse (zone 1), the fault zone itself (zone 2) and the southeast portion of the “*Molasse à charbon*” slice (zone 3). For every gun type (profile), Table 4-B lists the penetration times measured at the same CMP location of each zone for the water layer, the Quaternary sediments and the molasse unit. Using average interval velocities of 1450, 1550 and 2300 m/s, respectively, the corresponding partial and maximum penetration depths are calculated. The distinction of three vertical layers in three horizontal zones of the section allows an evaluation of how the maximum penetration depth was composed.

Layer	Zone, CMP	Water gun 140_w		Mini G.I G15/I15 140_15		Mini G.I G30/I30 140_30	
		[ms]	[m]	[ms]	[m]	[ms]	[m]
Water	1, 400	300	218	300	218	306	222
Q-sediments	1, 400	23	18	18	14	16	12
Molasse	1, 400	110	127	250	288	250	288
Q + M	1, 400	133	144	268	301	266	300
Total	1, 400	433	362	568	519	572	522
Water	2, 800	345	250	346	251	344	249
Q-sediments	2, 800	28	22	36	28	30	23
Molasse	2, 800	59	68	76	87	82	94
Q+ M	2, 800	87	90	112	115	112	118
Total	2, 800	432	340	458	366	456	367
Water	3, 1200	N/A	N/A	390	283	394	286
Q-sediments	3, 1200	N/A	N/A	15	12	16	12
Molasse	3, 1200	N/A	N/A	104	120	116	133
Q + M	3, 1200	N/A	N/A	119	131	132	146
Total	3, 1200	N/A	N/A	509	414	526	431

Table 4-B. Penetration times and depth in three different zones for the water layer, the Quaternary (Q) sediments and the Molasse (M) unit. Depths were calculated using average interval velocities of 1450, 1550 and 2300 m/s, respectively. The penetration time/depth below the water bottom is indicated by Q+M (grey), while “Total” stands for the total penetration time/depth measured from the water surface.

As expected, the penetration of the water gun is significantly lower than that of both air gun sources. However, the water gun has double the vertical resolution (Table 4-A) than the Mini G.I G15 / I15. This increase in resolvable detail was traded off against a signal penetration that is more than halved within the Plateau Molasse and much reduced within the fault zone. While in zone 1, the Mini G.I’s signal reaches depths of more than 300 m below the water bottom, the water gun records reflections only down to 144 m.

Surprisingly, the reduction to half the total air gun chamber size from 60 to 30 in³ affected penetration only slightly. Since the zone that images the Plateau Molasse is shallower than the remaining part of the 3-D survey extent, the signal of both air guns penetrates below the first multiple arrival time to an undetermined depth. In the fault zone and zone 3, penetration depth for the Mini G.I G30 / I30 increases by less than 10%. The question asked

in section 3.4.6, whether a doubled air consumption and a halved resolving power is worth the increase in strength can, at least for this target zone, be answered with no. The little gain in signal strength is worthless in zone 1 and does not reveal any additional structures in zone 2 and 3. Instead, as profile 140_15 demonstrated, the Mini G.I G15 / I15 visibly and theoretically (Table 4-A) increased vertical seismic resolution by a spectacular amount.

The shallowest portion of the 3-D survey area has a minimum water depth of 270 ms (196 m). Hence, the earliest multiple appears at 540 ms. Table 4-B shows that the total penetration time for the water gun does not exceed 430 ms. A trace length of 500 ms would thus be sufficient to record all reflected primary arrivals but no multiples. For the air gun profiles, the maximum penetration within the Plateau Molasse is deeper than the arrival of the first multiple. Penetration depth indicated in Table 4-B refers to this limit since it is not sure how much deeper the signal penetrated. Consequently, the record length for air gun profiles should be chosen at least as long as the latest multiple arrival time within the Plateau Molasse (~680 ms), if not significantly longer in case multiples can be successfully removed.

4.3.3.3 Structural dip

The structural dip of the target beds (“*Molasse grise de Lausanne*”: ~8° and “*Molasse à charbon*”: ~20°, see section 4.3.2 and Fig. 4-7) is not the only dipping seismic signal that must be accurately imaged. The fault zone causes truncations on beds that will generate diffraction events with an apparent dip that is significantly steeper than that of the Molasse beds themselves. The 2-D test profiles showed dips of up to 30° in the fault zone and at fault zone limits, culminating to about 35° close to the erosional surface. Since our system favors a higher sampling rate in in-line than in cross-line direction (section 3.5), the largest dip should occur in in-line direction (see section 2.4.4.3). The direction of the 3-D survey will thus be oriented perpendicularly to the strike of the fault zone (dip shooting). In the following 3-D survey design, a steep dip of $\alpha_{max} \approx 30^\circ$ will be used for all sampling calculations.

4.4 3-D survey design parameters

As stated in the first two chapters, one of the objectives of this thesis is to design a survey for high-resolution lake studies with parameters allowing geophysical interpretation of small 3-D targets in the most ideal way but with the equipment available. The first step has been the selection, acquisition and testing of all necessary instruments as well as the determination of their constraints (chapter 3). The determination of the survey target was set in this chapter. The final step for designing the survey is to combine instrument parameters with the depth and areal extent of the target image in consideration of the largest dip (α_{max}) that will contribute to the final image in order to determine all remaining survey parameters.

4.4.1 Bin size (spatial sampling)

With the aid of equations (2.21) - (2.24) and assuming a lowest possible average velocity within the post-glacial sediments of ≈ 1500 m/s, it is possible to summarize the influence of varying structural dip and signal frequency on the maximum unaliased bin size (Table 4-C) or varying structural dip and bin size on the maximum unaliased frequency (Table 4-D). The same equations also express the relationship to the sampling interval (*SI*).

FREQUENCY f_{max} [Hz]	STRUCTURAL DIP α_{max} or β_{max} [°]								
	5	10	15	20	25	30	35	40	45
250	17.21	8.64	5.80	4.39	3.55	3.00	2.62	2.33	2.12
500	8.61	4.32	2.90	2.19	1.77	1.50	1.31	1.17	1.06
650	6.62	3.32	2.23	1.69	1.37	1.15	1.01	0.90	0.82
750	5.74	2.88	1.93	1.46	1.18	1.00	0.87	0.78	0.71
1000	4.30	2.16	1.45	1.10	0.89	0.75	0.65	0.58	0.53
1250	3.44	1.73	1.16	0.88	0.71	0.60	0.52	0.47	0.42
1500	2.87	1.44	0.97	0.73	0.59	0.50	0.44	0.39	0.35
1700	2.53	1.27	0.85	0.64	0.52	0.44	0.38	0.34	0.31
1750	2.46	1.23	0.83	0.63	0.51	0.43	0.37	0.33	0.30
2000	2.15	1.08	0.72	0.55	0.44	0.38	0.33	0.29	0.27

Table 4-C. Largest possible bin size dX_{bin} or dY_{bin} (equations (2.21) or (2.22)) depending on structural dip α_{max} or β_{max} and highest unaliased frequency f_{max} . For a predefined bin size of 1.25 m, green indicates no aliasing, red aliasing for the air gun assuming frequencies beyond 650 Hz are filtered out; red and orange mean aliasing would occur for the water gun assuming frequencies beyond 1700 Hz are filtered out.

dX_{bin} or dY_{bin} [m]	STRUCTURAL DIP α_{max} or β_{max} [°]								
	5	10	15	20	25	30	35	40	45
1.25	3442	1728	1159	877	710	600	523	467	424
2.5	1721	864	580	439	355	300	262	233	212
3.75	1147	576	386	292	237	200	174	156	141
5	861	432	290	219	177	150	131	117	106
6.25	688	346	232	175	142	120	105	93	85
7.5	574	288	193	146	118	100	87	78	71

Table 4-D. Highest unaliased frequency f_{max} (equations (2.23) or (2.24)) depending on structural dip α_{max} or β_{max} and spatial sampling interval dX_{bin} or dY_{bin} . Red indicates combinations of interval and dip that would result in aliasing for both gun types while orange highlights aliasing only for the water gun; green stands for no aliasing.

If the source’s spectrum is not high-cut filtered or strictly band-limited at one maximum frequency, as is the case for the Mini G.I G15 / I15 (see Fig. 3-23), the highest possible frequency that could be recorded will be the Nyquist frequency. It is thus according to the sampling interval, that aliasing calculations should be made unless a high-cut filter was applied before digitization (frequency aliasing) or before migration (spatial aliasing). For signature measurements in section 3.4.6, the sampling interval for the water gun was set to 0.25 ms and for the Mini G.I to 0.5 ms. Corresponding Nyquist frequencies are 2000 and 1000 Hz respectively. However, after having been reflected at the water bottom or deeper discontinuities, the earth might have filtered (absorbed) some of the higher frequencies of the source signal (see 3.4.7). Because the higher end of the spectrum close to the Nyquist frequency even before reflection is of low amplitude, the following tables only consider

frequencies up to $f_{max} = 1700$ Hz for the water gun and $f_{max} = 650$ Hz for the Mini G.I G15 / I15. The data will be high-cut filtered at these frequencies prior to stacking (for more details see section 6.7). Table 4-C illustrates how frequencies that are present in the gun's source spectra influence the bin size for dips between 5 and 45 degrees. Table 4-D chooses multiples of the smallest possible in-line spatial sampling interval ($dX_{bin} = 1.25$ m) constrained by the seismic streamer (section 3.2) to calculate the highest unaliased frequency (f_{max}) with respect to the mentioned range of structural dips.

Areas in green indicate parameter combinations that lead to no spatial aliasing. In orange zones, aliasing occurs only for the higher frequencies of the water gun ($f > 650$ Hz) while areas in red are aliased for both source types. Taking the highest effective frequencies present in each source spectrum ($f_{air\ gun} \approx 650$ Hz, $f_{water\ gun} \approx 1700$ Hz – as highlighted in Table 4-C; see also section 3.4.7), and a steep dip of $\alpha_{max} = 30^\circ$, the maximum bin size in in-line direction without aliasing would be $dX_{bin} = 0.44$ m for the water gun and 1.15 m for the Mini G.I G15 / I15. Because our smallest possible spatial sampling interval in in-line direction is 1.25 m, we see in both tables that for the water gun, spatial aliasing theoretically occurs down to a structural dip of almost 10° while with the air gun, we can image dips up to almost 30° . The fact that average velocities within the fault zone are generally higher than 1500 m/s gives a bit of free play.

For our target, bin size in cross-line direction may be larger since dip is less significant. At 7.5 m intervals, which equals six times the in-line bin size, aliasing occurs for all dips exceeding 5° (Table 4-D). At a cross-line spacing of 3.75 m, dips greater than 2° are aliased when shooting with the water gun. The Mini G.I, however, allows unaliased imaging of dipping structures in cross-line direction of up to 9° . It thus becomes obvious that with a high-frequency source even very small dips require small sampling intervals. Within the constraints of the streamer dimension, the Mini G.I presents the more appropriate source in order to image the relatively steep fault zone of our target area. For the sake of unaliased imaging, some vertical resolution has to be sacrificed. In cross-line direction dips are known to be much smaller (Morend, 2000). Unless CMP line spacing is as fine as 2.5 m or less it is thus safer to use the Mini G.I source since inclinations of more than 2° are likely to occur. However, employing the water gun on this study site could still give good results since high frequencies are more rapidly absorbed, the low velocity Quaternary sediments are horizontally stratified and cover the molasse beds and the fault zone of velocities higher than those with which the above estimates were made. Furthermore, dips are mostly smaller than 30° .

4.4.1.1 Horizontal resolution

As stated in section 2.4.1.2, horizontal resolution of an unmigrated section is described by the extent of the first Fresnel zone, which depends on the average velocity above the

reflector and the dominant frequency in the reflected seismic wavelet. Equation (2.18) gives the diameter of the reflecting disk within which reflected points seem indistinguishable. Horizontal resolution decreases with increasing depth and average velocity and increases with increasing dominant frequency. In order to estimate the highest possible horizontal resolution for the water gun and the Mini G.I G15 / I15, the smallest average rms velocity ($v_{water} \approx 1500$ m/s) was used at the shallowest water bottom (~200 m) and the unfiltered dominant frequencies of both source types as in the section above. Hence, the maximum resolution to image horizontal variations along the water bottom amounts to 30 m for the water gun and 43 m for the air gun. However, after migration this resolution can be significantly improved; ideally to the signal's dominant wavelength at that depth (Yilmaz, 1987). This would thus be 2.2 m and 4.5 m, respectively.

4.4.2 Offsets

The shallowest horizon of our test site is the water bottom closest to the shore at approximately 270 ms two-way traveltime. The deepest target was set approximately to the deepest reflections recorded on profile 140_15 within and close to the fault zone in the Subalpine Molasse (see Table 4-B), which corresponds to an rms velocity of about 1800 m/s at 450 ms. Using a water velocity of 1450 m/s, equation (2.19) gives a depth of 196 m for the shallowest and 405 m for the deepest target horizon, which should be taken as nearest and farthest recommended offset. Far offset calculations using equation (2.20) and 200 ms for Δt_{NMO} , as suggested by Musser (2000), result in even larger far offsets of more than 800 m.

In order to work within the hyperbolic assumption (section 2.1.3.3) as well as for reasons indicated in section 2.4.2.1 and especially for streamer stability considerations, we decided for a very short near offset of 5 m, equal to double the hydrophone spacing. Receivers in even closer vicinity to the energy sources (water gun and Mini G.I, section 3.4) were overpowered during signature tests (section 3.4.6).

Since our 24-channel streamer sections (section 3.2) have a fixed receiver spacing of 2.5 m, the far offset is automatically determined once the near offset is set. Hence, the 48-channel single-streamer configuration that will be used for Survey I provides a maximum source-receiver distance of 122.5 m, while the farthest receiver of the three 24-channel streamers of Survey II will be towed at an average distance of 62.5 m. This difference in far offsets and fold for both streamer configurations allows comparison of resulting velocity spectra quality (see section 6.5).

4.4.3 Survey area

In order to determine the minimum required extent of the survey area necessary to correctly image the complete fault zone, a steep dip of $\alpha_{max} = 30^\circ$ and a deep target at 400 m depth (see section above) were substituted into equation (2.25). Perpendicular to fault strike

(in-line), a migration aperture of $A_i = 230$ m was found while along the fault trace (cross-line), dip is much smaller. Assuming a β_{max} of 10° , we would get an aperture A_c of 70 m (equation (2.26)). Thanks to the 2-D profiles shot across the fault zone, we know that its extension in dip direction amounts to approximately 350 m. In cross-line direction there is no specific limit since the Paudèze Fault runs from onshore into the lake and its position across the chosen survey site is accurately known (Morend et al. , 2002) to an extent of almost 2 km (see Fig. 4-3 and Fig. 4-9). Thus, the survey area limit in cross-line direction depends only upon the total of sail lines and the distance between them. In in-line direction, however, the survey area would have to be extended at least by 460 m, i.e. twice the migration aperture A_i , in order to migrate the fault zone correctly. This way the minimum sail line will have a length of 810 m. Of course it is not only the fault zone that is of interest alone, but as well the structure of the different molasses to both sides. So in-lines will be extended at least by additional 200 m to both sides (see sections 4.2, 5.1.1 and 5.2.1).

CHAPTER 5: 3-D ACQUISITIONS

Chapter 4 was mainly devoted to the selection, purchase and testing of all necessary seismic equipment as well as to the survey design that defines acquisition parameters and limitations depending on this equipment. Many parameter combinations are possible of which some are more suitable for the selected study site than others. In this chapter, I will use all the gathered information from chapter 4, discuss their mutual influence and choose the survey parameters for the two 3-D acquisitions that have been carried out as part of this thesis project. Both acquisitions combine very different parameters, which are very interesting to compare. Survey I was the first 3-D survey ever conducted on Lake Geneva and thus has more the status of an experiment. Based on the results of this first acquisition, new seismic equipment was constructed or bought, and already existing components were improved. It was tried to take advantage of this previously gained experience to change some of the acquisition parameters in order to find an even better design for Survey II. However, each of the two acquisitions focuses on different design aspects and depending on the main objective and with regard to instrumental constraints both have their pros and cons.

5.1 Survey I – October 1999

Survey I presents the beginning of a whole series of instrumental and software developments. Several 2-D profiles (see section 4.3) and many test measurements have been carried out prior to this acquisition. The simplest approach has thus been to extend the same basic single-streamer 2-D set-up to the third dimension by navigating along many closely spaced parallel 2-D lines (section 2.1.1). Survey I was carried out in October 1999 and we acquired a total of 80 sail lines in 8 days, covering an area of 1200 m by 600 m and giving an in-line to cross-line length ratio of 2:1. Details on the acquisition and some statistical observations are given in the Appendix on page 205.

5.1.1 Single-streamer configuration

The single-streamer configuration represents the standard acquisition set-up for marine 2-D profiling. “La Licorne”, our research vessel (section 3.1), tows the two interconnected ITI streamer sections (section 3.2.1) and one energy source. Fig. 5-1 shows the lay-out and the dimensions of this system (section 2.4.4). The streamer has a total length of 120 m with the first hydrophone located at an offset of 5 m to the source, which is towed 10 m behind the ship. The minimum offset of 5 m has been determined in section 4.4.2. With the 48 hydrophones arranged at 2.5 m-intervals, the far offset is then constrained to 122.5 m.

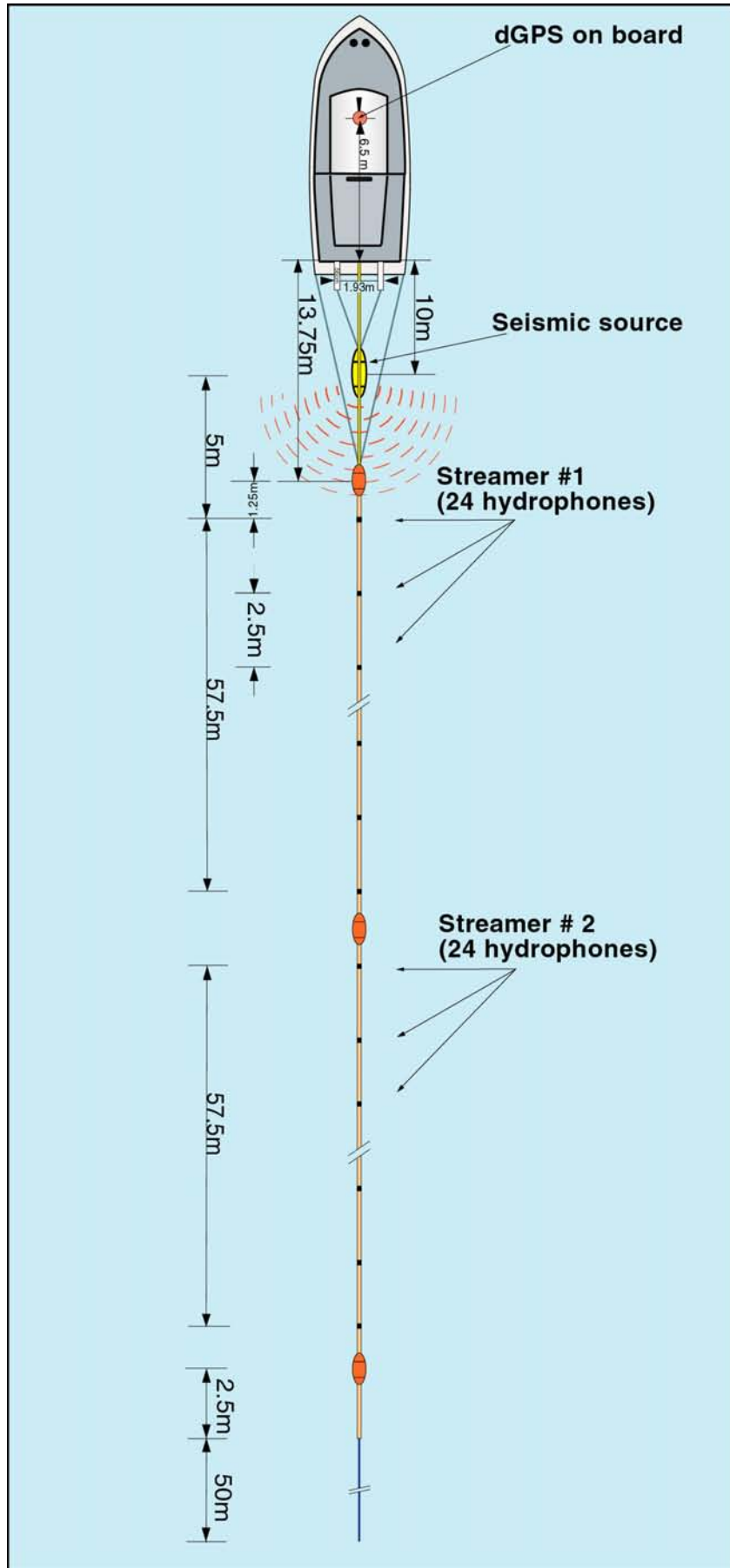


Fig. 5-1. Single-streamer configuration of Survey I.

At identical cross-line spacing, a single-streamer survey would need as many times more sail lines to cover the same survey area as a multi-streamer survey has streamers. The discussion in section 3.4.3 (Fig. 3-15) demonstrated that the S15 Water Gun represents the most appropriate source for the single-streamer configuration with regard to air consumption and maximum total number of lines that can be shot per day when using the Cirrus air compressor and a 200 l air tank. In addition to the low air consumption, the water gun's high dominant frequency allows very accurate imaging. Theoretically, a maximum vertical resolution of 60 cm can be reached (section 4.3.3.1). Horizontal resolution after migration is possible down to 2.2 m given that the bin size is sufficiently small (section 4.4.1.1). Anyhow, while the advantage of a broad frequency spectrum is high resolution, its disadvantage is a greater risk of spatial and temporal aliasing. Temporal aliasing can be prevented by choosing a smaller sampling interval at the recording instrument, although constraints are imposed by the necessary record length and the number of traces that have to be recorded during one shot cycle. From 2-D tests on the target site (section 4.3.3) we know, that the first multiple appears at 540 ms and that, when using the water gun, penetration within the fault zone is limited to less than 430 ms. Thus, as discussed for the source signature measurements in section 3.4.6, a sampling interval of 0.25 ms is sufficient to record frequencies up to 2000 Hz without aliasing. Using this interval, a record length of 500 ms would thus mean 2000 samples per trace and 96000 per shot. Since the maximum recording speed of the GEOMETRICS seismograph is 36000 samples per second (section 3.3.3), a minimum ship speed of about 4 km/h as needed for navigation stability allows recording of 81000 samples/shot at 2.5 m shot spacing and 162000 samples/shot at a shot spacing of 5 m. Thus, 2.5 m is too short a shot spacing to record traces of 500 ms length. But with a shot spacing of 5 m and a sampling interval of 0.25 ms, even a record length up to 800 ms would guarantee no recording problems and no temporal aliasing. However, as the tables in section 4.4.1 demonstrate, spatial aliasing at water velocity will occur for dips greater than 10° in in-line direction. Even at average velocities as high as 1800 m/s, dips of more than 12° will be aliased. Only if all frequencies higher than 600 Hz were absorbed, dips up to 30° will be correctly imaged. So with the water gun source, we risk paying for a possible higher vertical resolution in shallower flatter parts, such as the upper sedimentary section of the target zone, with aliased higher dips in the fault zone. Since the shot spacing was set to 5 m, the expected nominal fold for bin sizes of 1.25 m in in-line direction is 12.

As stated in section 2.4.4.3, receiver spacing on streamers is often smaller than CMP line spacing. It is therefore recommended to shoot in target dip direction since this way finer spatial sampling is applied to the steepest dip, which will prevent aliasing during migration. Consequently, the target fault zone width plus twice the migration aperture for the steepest dipping fracture (810 m, section 4.2) represents our minimum in-line length. In order to get a reasonably sized 3-D data cube, about the same length should be covered in cross-line

direction. Since in a single-streamer survey every navigation line means one CMP line, many boat passes are needed. A spacing of 3.75 m would require a total of 224 navigation lines to obtain 840 m in fault strike direction. Ship time on hand plays an important role in determining survey geometry and line spacing. For Survey I, “La Licorne” and its pilot were available for no more than two weeks, i.e. 10 working days minus at least a day for loading and unloading the boat. Fig. 3-15 illustrated that the maximum possible total number of lines per day is 14 when using the minimum necessary turning time of 10 minutes between consecutive antiparallel sail lines. Hence, a maximum of 126 lines can be shot in 9 days covering a distance of only 468.75 m. I thus decided to double the cross-line spacing to 7.5 m, although by doing so the risk of spatial aliasing parallel to the fault zone considerably increases. If all 9 acquisition days will be optimally used and no lines have to be repeated, it is possible to obtain 937.5 m of cross-line data, which would permit construction of a nice 3-D data cube. In order to gain acquisition time, we were forced to conduct the survey in alternating shooting direction. Since parallel acquisition geometry is more appropriate for asymmetric systems (see section 2.4.4) a compromise was to leave several sail lines between consecutively navigated in-lines. This way the ship follows an oval pattern as illustrated in Fig. 5-2 creating patches of sail lines with the same direction. Due to the necessary straightening of the streamer it is even of advantage to skip several lines than U-turning directly to the adjacent one at a distance of only 7.5 m. Fig. 5-2 does not present the real acquisition preplot but a representation of the 80 actually navigated lines during Survey I. Thick lines were passed from the southeast to the northwest while thin lines indicate the opposite direction. Due to several line repetitions patches of identical line direction are not always coherent (see more detail in following section).

Prior to Survey I, the start and end points of 120 acquisition lines of 800 m length were calculated according to section 4.2 and 4.4.3 and then saved in the onboard GPS instrument (section 3.6). During navigation we further extended those theoretical lines 200 m to each side to make sure enough of both molasse structures were included. The acquisition preplot of the 80 navigated sail lines at a cross-line spacing of 7.5 m is shown in Fig. 4-3; their corresponding theoretical start and end points are listed in Table A-9.



Fig. 5-2. Sketch of ship track pattern for Survey I including ship turns (dotted). Antiparallel geometry leads to patches of alternating direction. Colors indicate different acquisition days (see also Table A-2); patches of same color and same line thickness (thin lines from NW to SE, thick lines from SE to NW) were acquired under similar conditions – weather, currents, towing direction.

5.1.2 Navigation and positioning

Fig. 5-2 illustrates how lines that were navigated on the same day are distributed over the survey area and what influence the survey direction has on coverage at their limits. Since theoretical start and end points of each acquisition line had been calculated as antenna position at shot time, the effect of varying shooting direction is, that corresponding reflection points could lie on different sides of those positions. If a line was shot from southeast to northwest, the last reflection point lies half the maximum offset plus the distance between antenna and source southeast of the calculated end point, and if it was shot in the opposite direction, the first reflection point lies the same distance but northwest of the start point. This way the actually imaged surface gets the dented pattern as seen in Fig. 5-2. In these figures, acquisition lines connect all possible reflection points and show very well the uneven coverage at line limits. Thick lines were sailed from SE to NW and thin lines from NW to SE.

Ideally, all lines shot on the same day cover one coherent zone as planned in the acquisition preplot. However, this is not always as simple a task, since the total number of lines per day may vary or some lines have to be repeated due to recording problems or other ships crossing our course (lines indicated in dark grey in Table A-2). Those lines were filled-in at a later acquisition day. If weather conditions, such as direction of wind and currents, played an important role and assuming they did not change significantly during the 7 h of an acquisition day, all lines with the same color in Fig. 5-2 were recorded under similar conditions. This might be taken into account when navigation data are processed and could explain differences in streamer feathering from one day to another. Badly navigated lines influence bin coverage and furthermore noise from wave motion could have decreased overall data quality.

It is thus important to know under what conditions data have been acquired and what has been the survey direction. A change in survey direction causes, on the one hand, that the streamer is feathered to opposite sides, which could produce areas of no bin coverage and others of trace abundance; on the other hand, antiparallel lines in an asymmetric survey as ours are subject to static effects when dipping structures are present (see section 2.4.4.1). In order to avoid these problems we tried to arrange as many navigation lines as possible in groups of the same direction (see Fig. 5-2).

As discussed in section 3.6, we used an onboard GPS antenna for ship navigation while shots were triggered with the aid of a computer program that calculated ship speed and shot interval from coordinate calculations of a dGPS. Ship position was thus at best accurate to 2 or 3 m, although recorded antenna positions at shot time could have a precision of 0.5 m. Fig. 5-3 shows this antenna position of every second shot for all 80 acquisition lines. Compared to Fig. 5-2, here the boat position is always in line at survey area boundaries. Navigation irregularities show itself in two ways. Lines are not equispaced, some are closer and some are

further apart, and when looking at adjacent sail lines, shot points with the same number are not aligned. This becomes obvious when looking at every 20th labeled shot point.

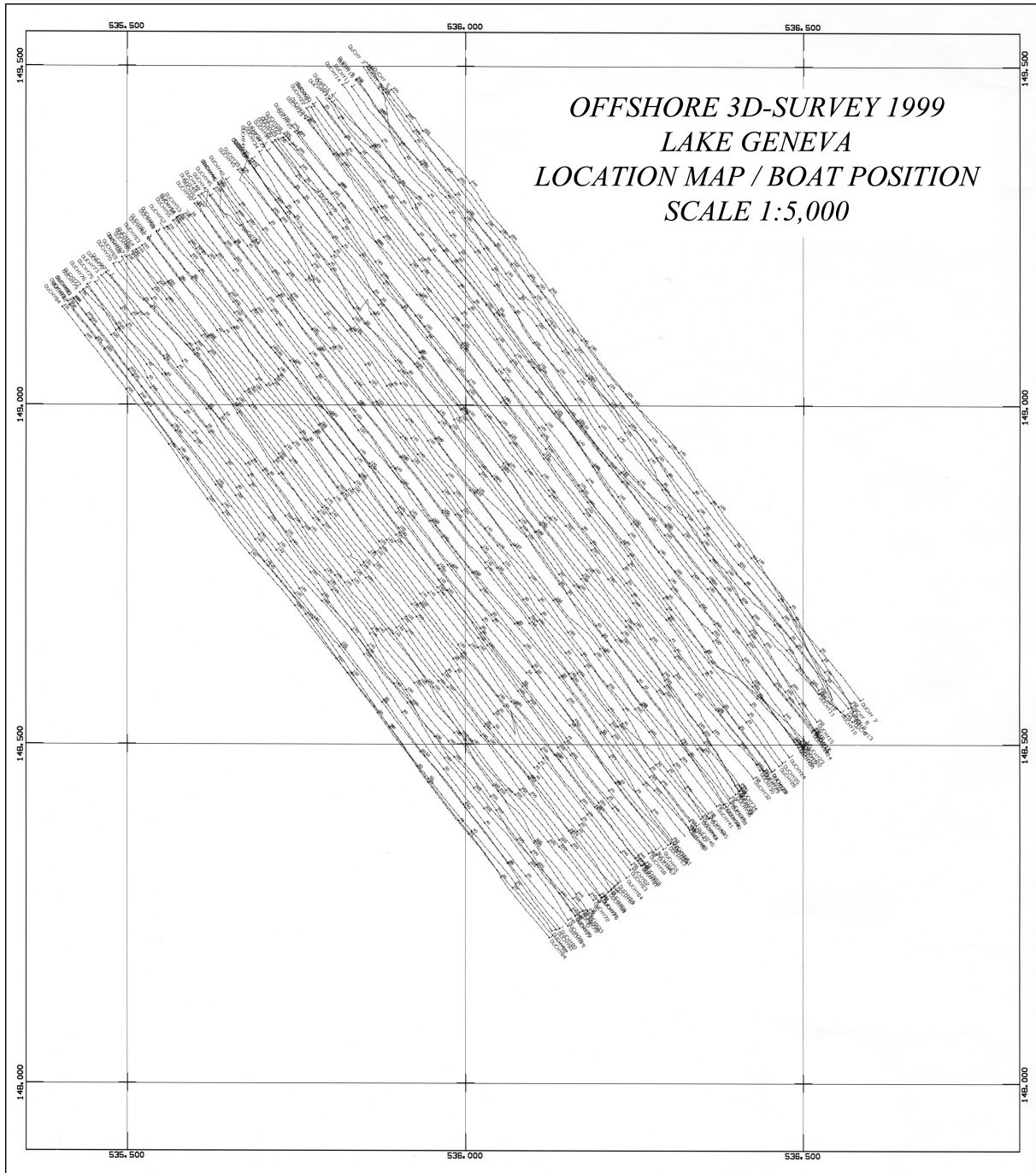


Fig. 5-3. Location map showing onboard dGPS position of every 2nd shot point for all 80 acquisition lines of Survey I; every 20th point is labeled.

5.2 Survey II – August 2001

Survey I provided an abundance of seismic and navigation data to be processed (chapter 6) and to be interpreted for the effect the chosen design parameters have on data quality (chapter 7). These results were then used to improve the parameter choice. The ultimate project goal, the development of a true multi-streamer 3-D system, firstly demanded the

acquisition or construction of all necessary lacking equipment (such as additional streamer sections, booms and GPS rafts), which had to be adapted to the existing components. But secondly and most importantly, the system had to be built in a way which allowed the improved design parameters to be applicable or vice versa, the design parameters are often constrained by the seismic instrumentation (seismograph capacities and total number of channels, vessel speed and nominal fold, boom length and cross-line spacing, etc., section 5.2.1). The new components were continuously tested and further enhanced. Finally, our second 3-D survey was carried out in August 2001 on the same site as Survey I. This way the multi-streamer configuration, the improved navigation software as well as the changed source type could be directly compared. We acquired 60 sail or 180 CMP-lines in 9 days, covering a surface of about 1500 m by 675 m, an area bigger than that of Survey I but sampled at half the cross-line interval. Details on the acquisition and some statistical observations are given in the Appendix on page 208.

5.2.1 Multi-streamer configuration

Fig. 5-4 shows the lay-out and all the dimensions of the three-streamer configuration that was used for Survey II. The retractable booms (see section 3.5) keep the two outer streamers at a distance of 7.5 m to the center streamer, whose first hydrophone is located at a minimum offset of 5 m behind the energy source. Therefore, the 24-channel streamer at 2.5 m trace spacing gives a far offset of 62.5 m only. At the same 5 m shot spacing the nominal fold for this survey will be reduced from 12 to 6, a not unimportant draw-back compared to a single or double-streamer configuration. As described in section 3.2.2, a color code was applied to each streamer section, each lead-in, the deck-cable connectors and the connectors to the seismograph. In this way, the same streamer was always placed at the same position and connected to the same channels. Green stands for starboard, ITI streamer #2 and channels 1-24. The S/N technology streamer is put in the center for symmetry reasons and is labeled with blue for channels 25-48. ITI streamer #1 is attached to the port boom and their traces are recorded on channels 49-72 of the seismograph. These colors also correspond to those indicated on the GPS rafts at the end of each streamer section (Fig. 5-4). Fig. 5-4 shows a cross-section and a plan view of how boom, raft and lead-in are placed with respect to each other and to “La Licorne”.

As has been discussed before, the S15 Water Gun represents the most economic energy source for a single-streamer configuration with regard to air consumption and total number of navigated lines per day when being constrained to a compressor that produces about 250 NI/min and a storage of 200 l. Instead of one single streamer we now have three and instead of 7.5 m the cross-line spacing is halved. As a result, line navigation will take about two thirds of the time that was necessary for Survey I. It would thus be possible to use a source that consumes more air than the water gun and to still cover about the same survey

area. The Mini G.I G15 / I15 double-chamber bubble canceling air gun as described in section 3.4.6 combines several advantages. Lower frequencies are better preserved than for the water gun and give higher signal strength and possible penetration. If the GI delay is optimally set, the spectrum is smoother and the signal is minimum phase – contrary to the precursor in the water gun wavelet. Although temporal and spatial resolution will be reduced to a maximum of 1.25 m and 4.5 m after migration due to a dominant frequency of only 330 Hz, penetration will increase as well as the dips that can be imaged without aliasing. The much lower maximum frequency (~650 Hz) in the source signal prevents aliasing in in-line direction for dips up to almost 30° and in cross-line direction for dips up to 10° (see Table 4-C and Table 4-D). So basically, by using the Mini G.I G15 / I15, no aliasing will occur within our target fault zone. Another good reason for trying this air gun is that the lower frequencies in the source spectrum allow temporal sampling at intervals of 0.5 ms instead of 0.25 ms for the water gun. Record length could thus be increased from 500 to 1000 ms allowing to record more deeply penetrating signals and to check whether any reflections are present shortly above and maybe below the water bottom multiple. Since in the deepest part of the survey area water has a depth of almost 400 ms, reflections above the multiple could be recorded down to 800 ms.

In Survey I, we acquired a total of 80 sail lines, corresponding to about 600 m along the fault strike. In order to cover at least the same distance, about 160 CMP lines are necessary at a cross-line spacing of 3.75 m, corresponding to about 53 sail lines (two sail lines for our three-streamer system are 11.25 m apart if shooting with no overlap). For Survey II, “La Licorne and its pilot were available for a total of 2 ½ weeks, i.e. 13 working days minus two days for loading and unloading the boat and another two for recording the Mini G.I G15 / I15 signature and GI delay tests plus additional 2-D profiles (e.g. profile 140_15 (c), see section 4.3 and Table A-11, as well as section 3.4.6 and Table A-7).

As discussed for the single-streamer survey, the partly antiparallel acquisition technique was not the most favorable solution with respect to feathering and static effects at dipping structures. Since air consumption is significantly increased with the Mini G.I G15 / I15 (see Table 3-B), the optimum turning time will be much longer and the total possible number of navigation lines per day reduced. Fig. 3-15 suggests a turning time of 19 minutes for a total of about 11 lines a day. At this long a turning time it would not take much longer to make a complete circle and to always return to the same side of the survey area for line start. A line consisting of 300 shots takes 20 minutes at a shot interval of 4 seconds, but could be sailed much faster as part of the turning process. Average U-turning for Survey I took 14 minutes, so a total of 30 minutes for a complete circle is a reasonable assumption. At this turning time of 30 minutes between consecutive parallel sail lines, a total of 9 lines could be navigated per day (Fig. 3-15), which amounts to a maximum of 81 in 9 days covering a cross-line distance of about 900 m. So even if weather conditions force us to skip an acquisition day and some of

the sail lines have to be repeated we will be sure to cover at least the same survey area along strike than we did in Survey I.

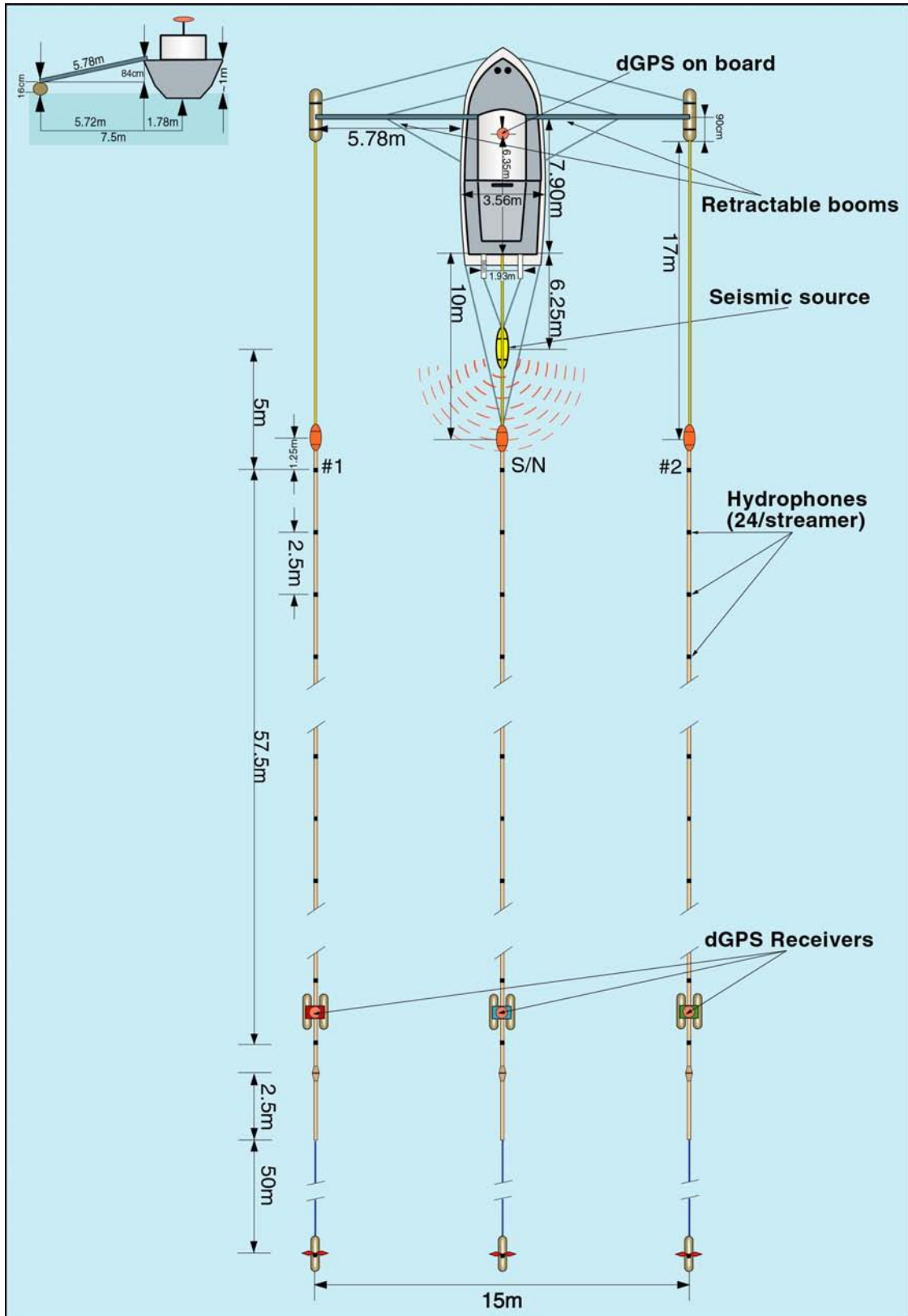


Fig. 5-4. Multi-streamer configuration of Survey II.

Prior to Survey II, as has been described in section 4.2, the start and end points of 120 theoretical acquisition lines have been calculated. Experience from Survey I showed, that the use of the northwest limit of the fault zone as center reference of the survey area lead to almost no recording of the Subalpine Molasse beyond the heavily fractured Paudèze Fault zone to the southeast. For this reason, overall line length was extended to 1500 m, padding another 300 m to the southeast end of the navigated lines of Survey I (sections 4.2, 4.4.3 and 5.1.1). All theoretical start and end points of the boat antenna were then saved in the form of a survey file to be entered into our new navigation software (see 3.6.2 and Appendix, page 208). The acquisition preplot of the 60 actually navigated sail lines at a cross-line spacing of 3.75 m is illustrated in Fig. 4-3; their theoretical start and end points are listed Table A-10.

5.2.2 Navigation and positioning

Fig. 5-5 illustrates how lines that were navigated on the same day are distributed over the survey area. As is typical for parallel surveying, the ship follows complete circles always shooting in one direction. Survey II was conducted in down-dip direction from the southeast to the northwest. Since theoretical start and end points of each acquisition line had been calculated as ship antenna positions at shot time, corresponding reflection points are now always on the same side of the antenna position. This way all lines are perfectly aligned at survey area limits avoiding the uneven coverage that has been present in Survey I. This is illustrated in Fig. 5-5, where acquisition lines connect all possible reflection points.

Ideally, all lines shot on the same day cover one coherent zone as planned in the acquisition preplot. Although this is not always as simple a task since some lines have to be repeated due to recording problems or other ships crossing the course (lines indicated in dark grey in Table A-4), Fig. 5-5 and Fig. 5-2 demonstrate that better coherency was achieved with parallel compared to partly anti-parallel line geometry. For Survey II, only four lines had to be repeated, all the remaining ones form groups of lines acquired on the same day (indicated by the same color) and in the same direction (indicated by the same line thickness). Those lines that were filled-in at a later acquisition day might have been recorded under different weather conditions but they are still all in parallel geometry. In a survey acquired this way, streamer feathering normally occurs always in the same direction unless winds radically change from one day to the next. Consequently, bins should be more evenly filled, in particular because streamer feathering is less pronounced with cables having only half the length of those used in Survey I. Furthermore static effects due to dipping structures measured by an asymmetric system of gun and streamer array should be identical on neighboring lines.

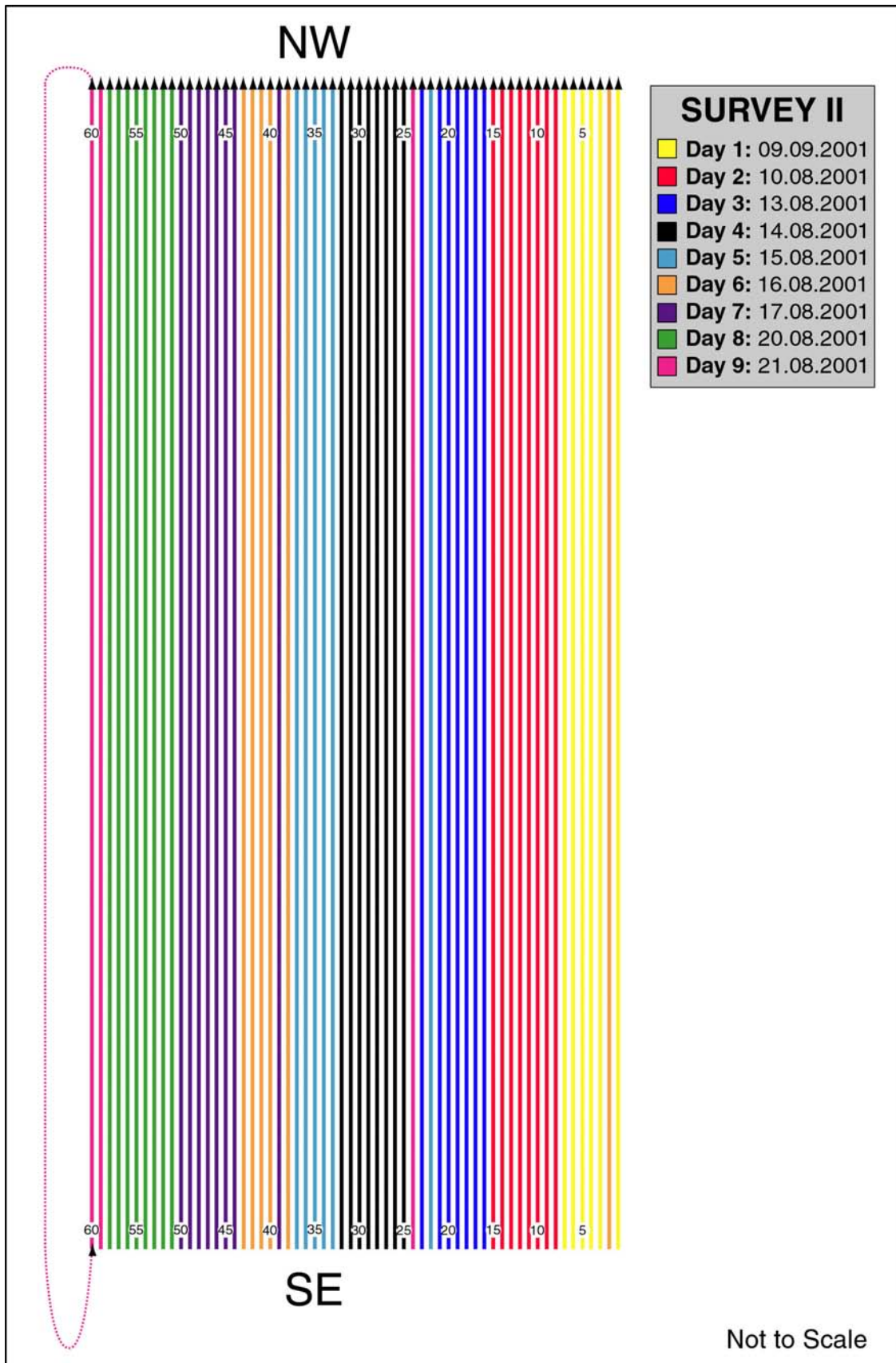


Fig. 5-5. Ship tracks for Survey II with colors indicating different acquisition days (see also Table A-5); patches of same color were acquired under similar conditions – weather, currents; the towing direction is the same for all navigation lines due to full turns as shown on navigation line 60.

As described in section 3.6, we used a new navigation and positioning system for Survey II. On the one hand, the additional dGPS instruments housed on top of the three GPS rafts (Fig. 3-28) recorded the position of the three streamer ends every 2 seconds (Fig. 5-4); on the other hand, the newly developed navigation program using more precise onboard antenna coordinates, provided by a GPS with differential correction in real-time received from a base station at less than 5 km distance, allowed boat navigation and automatic shot triggering that can be monitored for quality control (for details see 3.6.2).

The absolute positioning error of the ship's onboard antenna during navigation is only 19 cm, while the relative error made to trigger a shot at 5 m distances between pre-defined grid lines is at the most 25 cm. The combined maximum possible absolute error of the ship antenna at shot time with respect to its theoretical position is thus 44 cm. However, important for seismic data quality and binning accuracy is only the variation of maximally 25 cm.

With the aid of this new positioning system, the ship navigation has significantly improved. Fig. 5-6 shows the measured onboard antenna position of every second shot for all 60 acquisition lines. Sail lines have been navigated almost perfectly straight and at constant 11.25 m distances, while shots have been not only triggered at very regular 5 m-intervals but line up along a virtual grid contour in the survey's cross-line direction. This can be easily verified in Fig. 5-6 since every 20th shot point of all lines is labeled.

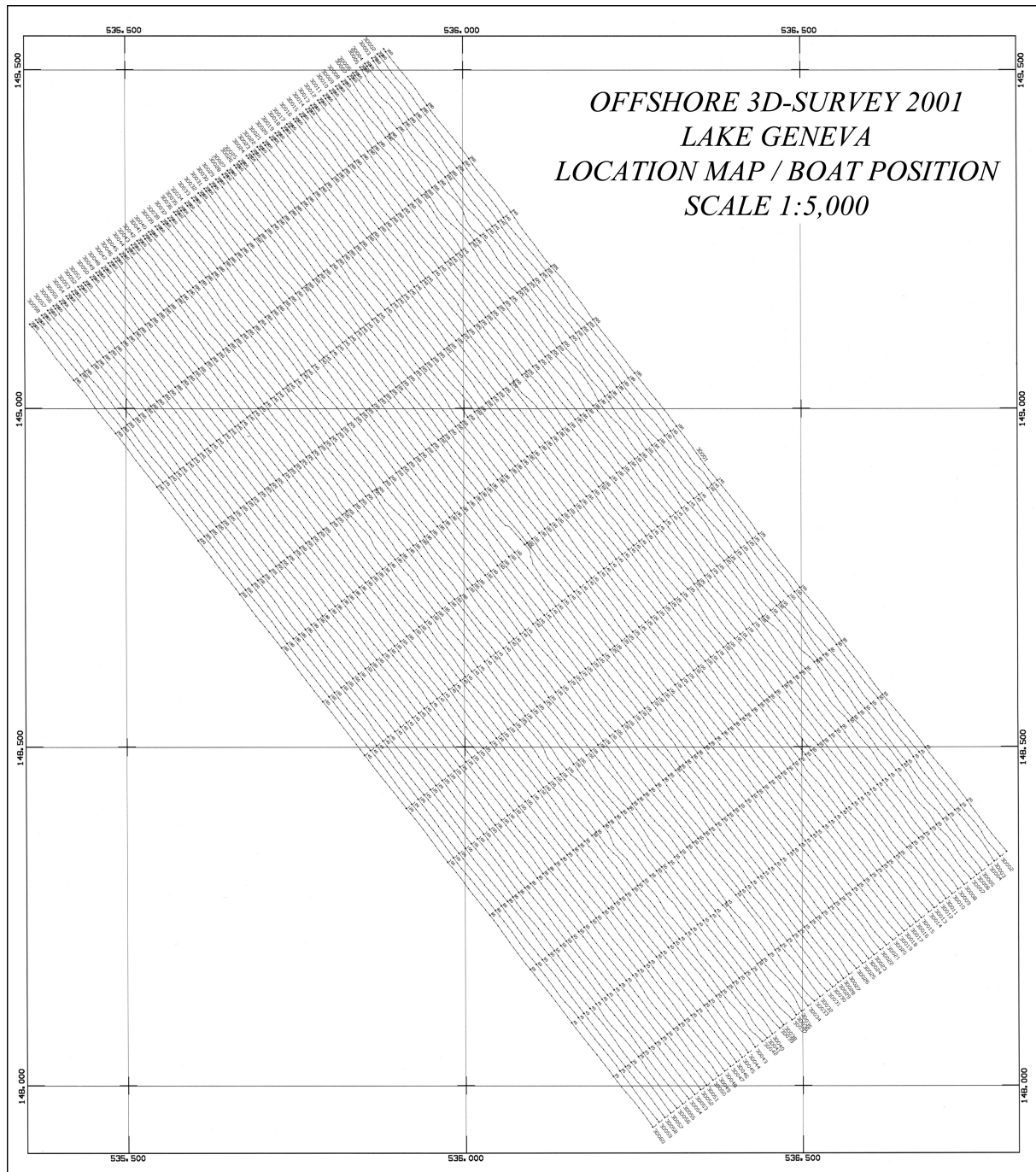


Fig. 5-6. Location map showing onboard dGPS position of every 2nd shot point for all 60 acquisition lines of Survey II; every 20th point is labeled.

As a summary, Fig. 5-7 presents the navigated first and last sail line as well as start and end points of all other lines of Survey I and II (Table A-14 and Table A-15 list those values) superimposed on their theoretical positions (Table A-9 and Table A-10). For Survey II, the navigated antenna positions at the time of the first and last shot point fall exactly on the ones predicted while those of Survey I are scattered about the imaginary location when extending the theoretical points 200 m to the northwest and to the southeast. Our new navigation

software significantly improves acquisition quality and will facilitate subsequent binning (section 2.2.1.1 and 6.4) process.

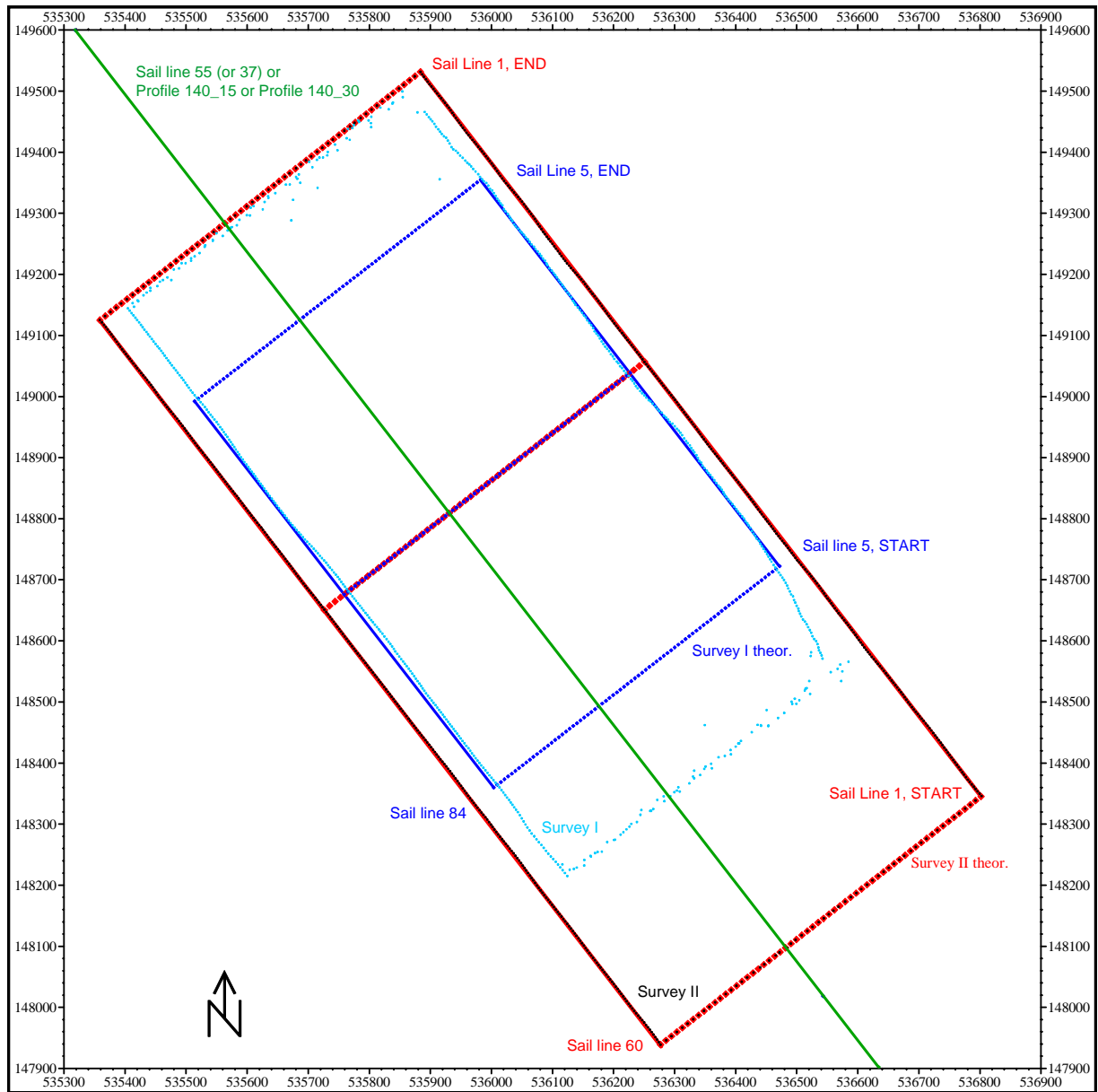


Fig. 5-7. 3-D survey site showing navigated start and end points of each sail line (light blue and black) superimposed on theoretical preplots for Survey I (dark blue) and Survey II (red). Green line indicates location of 2-D profiles 140_15 and 140_30 located on sail line 55 (Survey I) or 37 (Survey II).

Table 5-A and Table 5-B contain a summary of all acquisition and design parameters of both surveys.

A Single-Streamer System			
No. of streamers:	1	Seismograph:	GEOMETRICS, 48 channels
No. of receivers per streamer:	48		Strataview R series, 18.5 ENOB
Receiver spacing:	2.5 m	Recording at:	36 dB, 4-2000 Hz
Total number of receivers per acquisition line:	48	Source:	S15 Water Gun, SODERA
Shot spacing:	5 m	Air consumption:	350 NI/min
Min. offset:	5 m	Depth:	0.3 m
Max. offset:	122.5 m	Chamber size:	15 cu. in.
Nominal fold:	12	Nominal pressure:	140 bars
B Acquisition Parameters		C Navigation	
Sample interval:	0.25 ms / rate 4000Hz	● dGPS on board (accuracy of 0.5 m).	
Trace length /recording length:	512 ms	● Base station 40 km away. Shot was triggered using average ship speed that predicts shooting interval.	
Source frequency range:	100 - 1700 Hz	● Error in shot distance accumulates towards the end of each line.	
Dominant frequency:	670 Hz		
Nyquist frequency:	2000 Hz	Survey area:	600 x 1350 m 0.81 km ²
Inline aliasing:	for dips > 10°	Acquisition lines:	80 at 7.5 m spacing
Cross-line aliasing:	for dips > 2°	CMP lines	80
Max. penetr. depth below water:	~145 m	Bin size	7.5 m x 1.25 m
Best vertical resolution:	0.6 m	Survey time:	8 days = 0.1 km ² per day 10 CMP lines per day
Lateral resolution (before and after migration):	30 m (diameter) max. 2.2 m or bin	Av. vessel speed:	4.5 km/h
Migration aperture:	230 m (in-line)	Shot interval:	4 s
Max. dip / target depth:	30° / 400 m		

Table 5-A. Acquisition parameters of Survey I.

A Multi-Streamer System			
No. of streamers:	3	Seismograph:	BISON Spectra, 96 channels
No. of receivers per streamer:	24		Jupiter/Galileo, 18 ENOB
Receiver spacing:	2.5 m	Recording at:	24 dB, 25-1000 Hz
Total number of receivers per acquisition line:	72	Source:	Mini G.I Air Gun, SODERA
Shot spacing:	5 m	Air consumption:	678.5 NI/min
Min. offset:	5 m	Depth:	1 m
Max. offset:	62.5 m	Chamber size:	Generator 15 cu. in. Injector 15 cu. in.
Nominal fold:	6	GI delay:	28 ms
		Nominal pressure:	80 bars
B Acquisition Parameters		C Navigation	
Sample interval:	0.5 ms / rate 2000Hz	● dGPS on board and 3 dGPS on rafts at the end of each streamer (accuracy of 0.2 m).	
Trace length /recording length:	1000 ms	● Base station is located on a University building (~4 km away). Shots were triggered every 5 m in absolute position.	
Source frequency range:	40 - 650 Hz	● No error accumulation.	
Dominant frequency:	330 Hz		
Nyquist frequency:	1000 Hz	Survey area:	675 x 1530 m 1.03 km ²
Inline aliasing:	for dips > 27.5°	Acquisition lines:	60 at 11.25 m spacing
Cross-line aliasing:	for dips > 9°	CMP lines	180
Max. penetr. depth below water:	>300 m	Bin size	3.75 m x 1.25 m
Best vertical resolution:	1.1 m	Survey time:	9 days = 0.12 km ² per day 20 CMP lines per day
Lateral resolution (before and after migration):	43 m (diameter) max. 4.5 m or bin	Av. vessel speed:	4.5 km/h
Migration aperture:	230 m (in-line)	Shot interval:	4 s
Max. dip / target depth:	30° / 400 m		

Table 5-B. Acquisition parameters of Survey II.

CHAPTER 6: 3-D DATA PROCESSING

Data acquired during both 3-D surveys (as described in chapter 5) have been processed using the commercial software package *GéovecteurPlus* from the Compagnie Générale de Géophysique (CGG). While for Survey I processing of the navigation data was performed with *GéovecteurPlus Version 6.2*, the more complex navigation data available for Survey II required creation of an additional computer program that calculates shot coordinates and receiver positions for all three streamers and outputs them in *Géovecteur* compatible UKOOA90 format. The newer *Version 8.1* of *GéovecteurPlus* was then employed for geometry assignment and seismic data processing.

Within *GéovecteurPlus*, processing is carried out using a set of commands grouped in a seismic job. This job consists of libraries containing parameters such as mute or velocity functions and of seismic processing commands, called modules. *GéovecteurPlus* runs on UNIX machines either interactively using the XJOB graphic editor, which automatically converts the job to *Géovecteur* Seismic Language (GSL) prior to execution, or in batch mode where jobs are directly written in GSL. The software package has been developed for exploration industry standards and includes approximately 250 program modules covering algorithms in 2-D and 3-D (for both land and marine) as well as algorithms for vertical seismic profiling (VSP). With this vast variety of algorithms, libraries and parameter combinations *Géovecteur* is an extremely powerful tool although it is this complexity that makes mastering it rather difficult. Since processing of data at industry standard represents the main application of this software, algorithms had been programmed according to that standard's scale. In the course of establishing a suitable processing flow for our 3-D surveys, I realized that some of the modules were not adapted to very-high-resolution imaging, i.e. that the minimum temporal sampling interval was fixed to integer values in milliseconds (see section 6.8). Consequently, these modules could not be used for data sampled at intervals smaller than 1 ms and alternatives had to be found. Another finding was that coordinates and offsets saved in the trace headers are rounded to 1 m. So even when an accuracy of more than 20 cm was reached for receiver positioning, it will not be considered in the processing flow following the merge of navigation and seismic data.

6.1 Processing flow

Being aware of these software limitations I tried to find the best possible (feasible) 3-D processing flow for Survey I and Survey II on the basis of conventional pre- and post-stack routines using data organized in bins of common midpoints and in-lines. Fig. 6-1 shows a simplified representation of this sequence, which consists of three major components: data preparation, pre- and post-stack processing. Data preparation includes the formatting and arrival time delay correction (see section 3.4.4) of the seismic data, the processing of the navigation files in order to locate the position of each seismic trace and the merging of both.

After geometry assignment (see section 2.2.1.1), bad traces are edited and finally binning is harmonized. Two velocity analyses are performed before NMO and DMO correction (section 2.2.3.3) prestack. Post-stack processing comprises a 3-D time migration and water bottom mute. Each of these processing steps, which make up the three components, is organized in jobs composed of different Géovecteur modules. The number in front of the processing steps in Fig. 6-1 indicates the sequence of corresponding jobs - details on those jobs and the modules and parameters used within them are summarized in Table A-18 for Survey I and in Table A-20 for Survey II and will be referred to throughout the following descriptions. This relatively basic processing flow proved to work very well on both data cubes, favored by the excellent quality of the data. Nevertheless, since a depth migrated section is the more desirable basis for geological interpretation, a prestack depth migration has already been tested and preliminary results are presented in section 7.2.

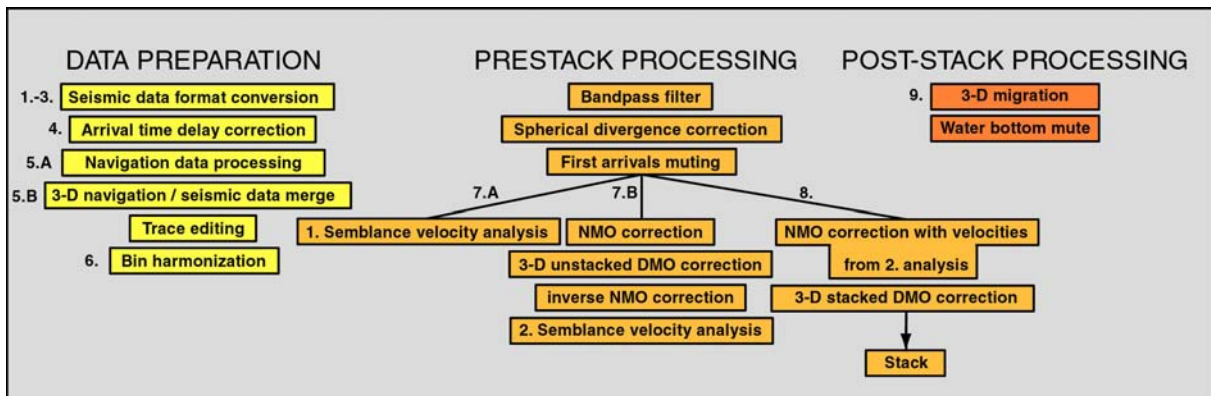


Fig. 6-1. Simplified 3-D processing flowchart used for Survey I and II. The number in front of each processing step indicates the corresponding Géovecteur job sequence. Details on modules and parameters used in those jobs are listed in Table A-18 for Survey I and in Table A-20 for Survey II.

In the following, I will first describe the seismic data input and arrival time delay correction (steps 1-4), then continue with the processing of the navigation data for Survey I and Survey II (step 5A) and the definition of a common survey grid for geometry assignment and easy comparison (step 5B). Afterwards, I will introduce all remaining processing steps, modules and parameters applied while discussing their direct influence on data quality leading to suggestions for further improvement.

6.2 Seismic data input and formatting (processing steps 1-4)

Initially, the SEG-Y data are read from tape and written to disk. Each sail line of Survey I produced a SEG-Y file of about 100 MB (~250 shots with 48 traces of 2000 samples each). The total raw data of all 80 lines thus occupy about 8 GB of disk. For Survey II, the size of each SEG-Y file amounts to 180 MB (~301 shots with 72 traces of 2000 samples each), which lead to 10.8 GB for the total of 60 sail lines. In processing step 1, those SEG-Y files are converted to Géovecteur format and sorted into shot gathers. A few of the 64 trace header

words are automatically filled, as indicated in Table 6-A. Though, the sequence number (WORD 17) of each trace within a shot gather has to be explicitly defined as well as the shot number (WORD 2) for data recorded with the GEOMETRICS seismograph (job *input*, step 1).

WORD	Content	Before Geometry	After Geometry	After Stack
1	Time of the last non zero sample [ms]	raw data	X	X
2	Shot point number	job <i>input</i> , step 1	X	X
4	CMP number		job <i>egrid</i> , step 5	X
6	Time of the first non zero sample - mute [ms]	0	0	mute
8	Stacking fold			job <i>stack</i> , step 8
9	Sample interval [microseconds]	raw data	X	X
10	Trace length [ms]	raw data	X	X
11	0 for non valid trace; 7 for valid trace	raw data; 7	7	X
16	Delay [ms]	job <i>shift</i> , step 4	X	X
17	Trace number in gather	job <i>input</i> , step 1	X	
19	LINE number		job <i>egrid</i> , step 5	X
20	Offset [m]		job <i>egrid</i> , step 5	
30	sail line number	job <i>shift</i> , step 4	X	X
43	X-coordinate: midpoint or bin center		midpoint	bin center
44	Y-coordinate: midpoint or bin center		midpoint	bin center
60	X-coordinate: receiver		job <i>egrid</i> , step 5	
61	Y-coordinate: receiver		job <i>egrid</i> , step 5	
62	X-coordinate: shot		job <i>egrid</i> , step 5	
63	Y-coordinate: shot		job <i>egrid</i> , step 5	

Table 6-A. Trace header assignment at different processing stages. There is a total of 64 header words. Presented are only the most frequently used. It is indicated either whether a trace header content existed since recording (raw data) or if not, in which job it was firstly assigned. Either the newly assigned value is given or an X when the previously assigned value was kept .

As a first quality control, trace 4 with an offset of 12.5 m (close to the near trace, but less noisy) was plotted for every sail line (job *neartrace*, step 2). Since the GEOMETRICS' deck cable inverses the first half of its 48 channels, traces 1-24 have to be renamed in the opposite order (job *inversion*, step 3). Processing step 4 takes care of the arrival time delay correction and applies to all traces a constant shift of 25 ms to Survey I and of 8 ms to Survey II (see values in Table 3-C and section 3.4.4). As a result, the water bottom reflection of both surveys is brought to the same arrival times. Also in this job (*shift*, step 4), but only for Survey II, WORD 30 is set to the navigation line number and bad shot gathers are deleted, as will be explained in more detail in section 6.4.

6.3 Processing of navigation data (processing step 5A)

Navigation data processing means to combine the complete existing information on ship, gun and streamer positioning to determine all shot and receiver coordinates at the moment of every shot in a format accessible by the processing software. In GéovecteurPlus it is a module called EGRID (step 5B) that performs marine 3-D geometry assignment (see next section), i.e. that merges navigation with seismic data. To use EGRID, the navigation data of the whole survey need to be available in the form of one single ASCII file in UKOOA P1/90

format. This is a standard industry format consisting of a header part and a data part, which is already processed – in the exploration industry by navigation specialists on board the recording vessel. This format requires for each shot the sail line with coordinates (latitude/longitude and rectangular coordinates) corresponding to the ship antenna, the tail buoys and the shot point followed by a block with numbers and coordinates of all receivers in this shot gather. An example of the UKOOA P1/90 file header and the data block of the first two shots of the first sail line of Survey II for all 72 hydrophones on three streamers is shown in Table A-21 of the Appendix.

While for Survey I, the UKOOA P1/90 navigation file was constructed by using a FORTRAN 77 computer program that creates a number of necessary libraries to be applied within a long series of Géovecteur radionavigation modules, for Survey II it was directly output from a C++ computer program written for this purpose. In the following, I will describe in detail, how this UKOOA P1/9090 file was obtained in both cases.

6.3.1 Survey I

As explained in detail in section 3.6, there was only one dGPS antenna on board that was used for ship navigation during Survey I. Consequently, all shot and receiver positions have to be extrapolated from that antenna position. The shot triggering software (section 3.6.1) recorded for each shot the shot time (in seconds after midnight) as well as the time, latitude and longitude of the most recent dGPS reading before that shot (in hours, minutes and seconds after midnight). As a first step, it was necessary to search in the output file of each navigated line, the coordinate times that were recorded closest before and after each shot time. The corresponding coordinates were then linearly interpolated in order to find the antenna position at the moment of gun firing. From this position are now derived all remaining coordinates for the source and every receiver.

In order to do those calculations, I wrote a FORTRAN 77 computer program that reads in all shot and coordinate times as well as the latitude/longitude readings from each dGPS data file (OUCHY05.OBS – OUCHY84.OBS). The complete navigation processing sequence, as it has been applied to Survey I, is attached as a separate document to the end of the Appendix (Table A-24), including the program code “*gvtlibrary*”. Figure 1 at the end of this document illustrates how the program searches for each shot (m) the correct coordinate time before ($coortime(loc1(m))$) and after ($coortime(loc2(m))$) the shot time ($shottime(m)$) and how it performs the interpolation for antenna coordinates ($antn(m)$ and $ante(m)$) after having converted latitude/longitudes into Swiss rectangular coordinates.

Géovecteur’s radionavigation modules have been developed to process and combine all information from standard industry 3-D positional networks (section 2.3.4.2) and to finally output the standard UKOOA P1/90 navigation file that is needed for geometry assignment. For these modules to function properly, it is necessary to provide a minimum of navigation

data in addition to the ship's antenna position. One requirement is the theoretical heading usually given by the Gyro-compass onboard and measured relative to geographical north. A second requirement is directional data from at least three compasses along the streamer length. Those compass readings are always made relative to magnetic north and then corrected to be used in geographical coordinates. Another requirement is that the position of source and streamer head relative to the origin of the ship's coordinate system must be known for every shot. This origin generally represents the position of an onboard reference station, such as the ship's antenna. The system's x-axis points to geographic east, the y-axis to geographic north. All this information has to be provided in the form of navigation libraries accessible by the different radionavigation modules or input as an ASCII file in NAVP1 format for the vessel's reference station or other directly measured coordinates.

In order to create the NAVP1 input file along with the navigation libraries for each shot and sailed line, I extended the above computer program. As a first step the boat course between all consecutive antenna positions was determined and then smoothed to predict the current *vessel heading* (variable *VHDG* in library) for each shot by averaging over 5 preceding shot points. The angle α in the triangle between two consecutive antenna positions is the arctangent of the ratio of the differences between their x (east) and y (north) coordinates (Δx and Δy , see Table A-24: Figure 2). Depending on the ship's direction of advancement, each quadrant in the geographical coordinate system produces a different combination of signs of Δx and Δy . Since the variable *VHDG* is defined relative to geographical north, these four cases have to be distinguished in order to calculate the correct heading, as illustrated in Table A-24: Figure 2.

Gun and streamer head had been towed at relative distances of 16.5 m and 20.25 m to the ship antenna, followed by the 120 m long streamer, tail and drogue rope (see Fig. 5-1). In addition to these relative distances, only the vessel heading is needed to determine those positions relative to the ship's coordinate system. Table A-24: Figure 3 illustrates how this system is defined with respect to geographical coordinates and how those positions are determined according to the same four cases of Figure 2. The resulting relative coordinates of the source (*DXSOUR*, *DYSOUR*) and the streamer head (*DXHEAD*, *DYHEAD*) at each shot are written in two different libraries and accessed by radionavigation modules to calculate absolute gun and receiver positions using the streamer shape derived from the readings of at least three compasses.

Simulating non-existing compass readings along the streamer required the assumption that the streamer drift mimics approximately the boat drift and that no significant cross-line currents are present. For this purpose, three imaginary compasses B11, B12 and B13 were placed at distances of 50 m along the streamer (sketch on page 2 of Table A-24). As a first approximation, the vessel heading was assigned to them, as it had been when the ship passed their respective location 6, 16 and 26 shots ago. This boat course was written into libraries

using variables *BSL1-3*. When read by radionavigation modules their content was then passed through temporal and spatial filtering, which increased gradually with offset (job4b, Table A-24, page 10) taking into account the smoothing effect of the boat course at greater distance. Once all libraries were created, read and used by the sequence of radionavigation jobs presented in Table A-24, the UKOOA P1/90 file was output and could be used for quality control.

Fig. 6-2 shows the streamer shape for every shot of sail line 30 as it has been deduced from those three virtual compasses. For most shots the streamer is almost straight and feathers slightly to the left by less than 15 m. Where streamer shapes of different shots converge or diverge, the cable feathered more or less strongly or even in opposite directions; where streamer drift is almost constant they are close to parallel. It speaks for correct compass simulation that streamer shape always changes gradually from one shot to the next.

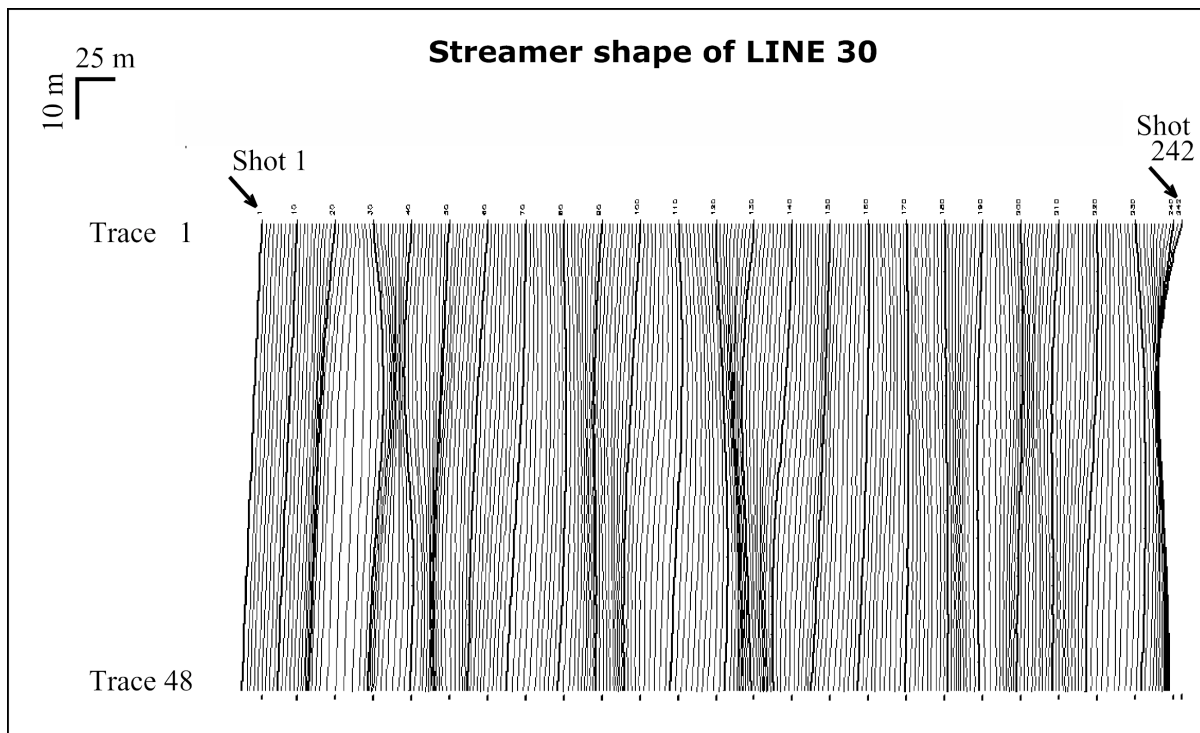


Fig. 6-2. Chart showing streamer shapes for all 242 shots of a selected sail line (line 30).

Nevertheless, there is no means of estimating the actual error made in receiver positioning since all positions were derived from the vessel's antenna position only and more or less strongly mimic its course. The farther the offset, the less control there is - since cross-line currents have more influence - and the greater is the danger of missing the correct position. Assuming an error of 15 m in estimating the position of a far offset trace feathered by cross-currents results in placing the corresponding reflection point 7.5 m away from its correct position, i.e. misplacing it by one bin or CMP line opposite to feathering direction. However, if the lake is relatively calm and the streamer not too long, cross-current feathering might not be too important and far offset feathering due to ship track curvature remains the

main influence on streamer shape. This type of feathering is believed to be reasonably well approximated by the compass simulation. So under these conditions and since streamer feathering seems seldom greater than 15° m, as seen in Fig. 6-2, it could be assumed that the error in determining the streamer position does not exceed this maximum deflection, yielding a reflection point positioning error of less than 7.5 m or one lateral bin size for Survey I.

Generally, with the above positioning system and in the presence of cross-line currents, long streamers combined with small cross-line bin spacing are likely to have reflection points distributed several bins away from their assumed bin while with larger lateral bin sizes the gathered reflection points lie at great ranges of distances around its midpoint and cause smearing effects if data were not migrated prestack. In Survey I, the streamer had double the length of that in Survey II, hence reflection points might have been determined with double the error for far offsets. With the same positioning network, both surveys would have the same far offset positioning error within their bins since the lateral bin size in Survey II was half of that in Survey I.

In Fig. 6-3, shot and far offset receiver positions were superimposed for every second sail line taken from the UKOOA P1/90 output file. For sail line 40 the shot positions are highlighted in red while the far offset receiver positions, calculated using the imaginary compasses along the streamer, are connected in green. This example of a line demonstrates well how close the end of the streamer followed the track of the gun, which was towed at a distance of only 10 m behind the vessel. The temporal and spatial filters made the course of the far offsets smoother explaining why this curve is less pronounced than that of the source position, a phenomenon that one would expect intuitively. The navigated line 40 deviated more than average from the theoretical course and thus presents a good example to show the maximum deviation in source and far offset receiver positions (or feathering) due to ship track curvature. For an ideally navigated line, the far offset receiver would always fall on the same track as the source had traveled. Hence, streamer feathering due to cross-line currents cannot be considered when the only navigation data come from the ship antenna. Consequently, the absolute positioning error will be the greater the stronger those currents were. The only possibility to determine actual streamer feathering is to have at least one more device on the streamer itself that measures either streamer direction, relative coordinates with respect to the ship's reference system or absolute coordinates as has been done for Survey II.

6.3.2 Survey II

In order to actually measure streamer feathering, three additional dGPS antennas were mounted on rafts attached to the streamer tails for Survey II. As has been described in section 3.6, the absolute raft position was recorded on disk at two-second intervals, downloaded every evening and post-processed at a later time. The streamer tail positioning thus did not improve

real-time quality control on ship navigation and bin coverage but allowed much more precise determination of receiver positions.

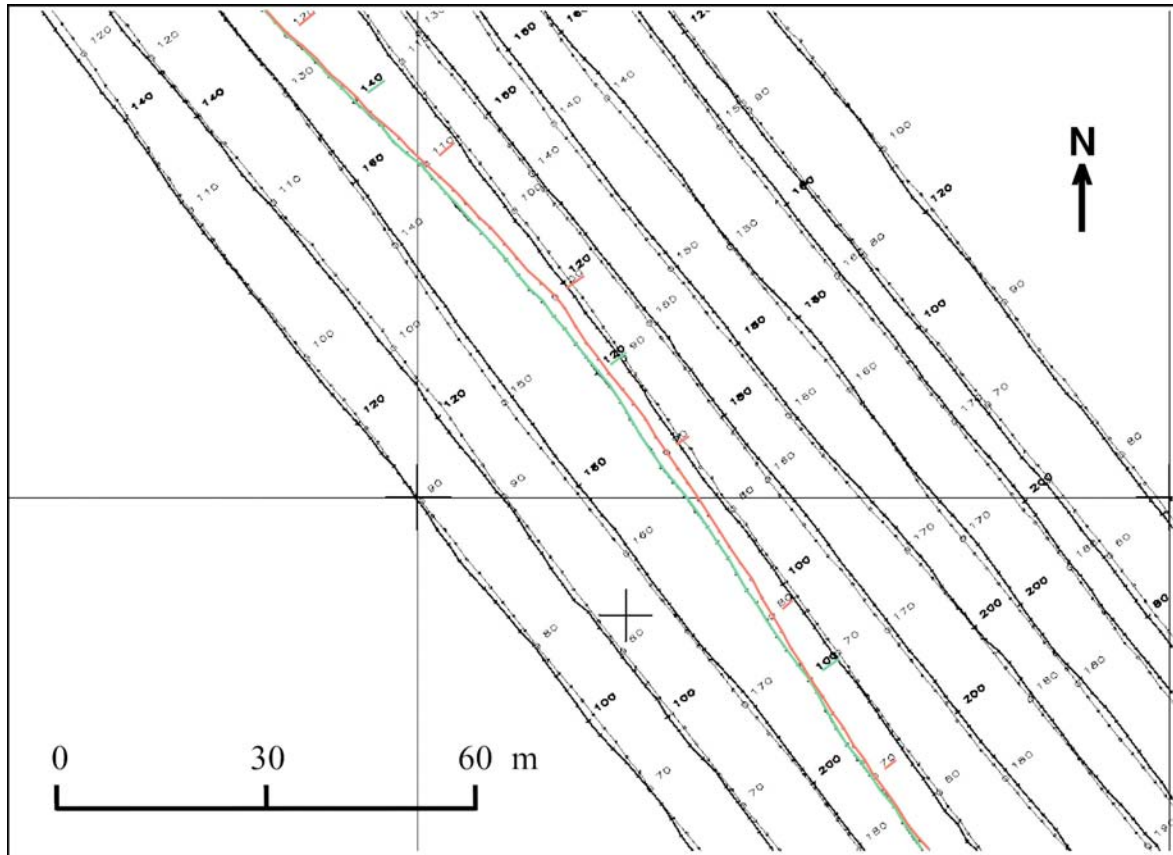


Fig. 6-3. Shot positions (thin contour / red) and far offset receiver positions (heavy contour / green) for selected sail lines (even lines 26-46). Every 10th shot number is labeled along the source contour, and every 20th shot number is labeled (bold) along the receiver contour. Note how well the far offset hydrophone followed the course of the gun that was towed only 10 m behind the vessel when calculating receiver positions using imaginary compasses along the streamer.

While we depended for Survey I entirely on the assumption that the streamer mimicked the boat course, we now have real control on streamer behavior, though restricted to one point on each cable. Anyhow, calculation of actual streamer shape still depends on an assumption about how the streamer behaves between its attachment to the ship and the dGPS raft at its end. Based on observations of streamer behavior during acquisition of Survey I using a streamer of yet 122.5 m, it seemed not appropriate to suppose that the streamer was always straight with respect to the current vessel heading. Although smoothed, the vessel heading could change by more than one degree from one shot to another, which would mean abrupt deflection of the last receiver by about 2 m per degree. By mimicking the boat course and by filtering the far offsets, a solution was found that made the relatively long streamer vary only gradually its shape (see section above).

For Survey II, the situation has changed significantly. The streamer had only half the length and we now know exactly where its end was located. Using Géovecteur's radionavigation modules would require a whole series of libraries, that need to be conform with the course of both the ship antenna and the respective streamer end, three compass readings per cable and the position of the three streamer heads relative to the ship's coordinate system. There are too much data to make the invention of imaginary navigation devices trivial, and there are not enough to take full advantage of the modules' capacities. Providing the necessary information for the modules while constrained by the additional three data points per shot seemed far more complicated than writing an independent computer program that makes the necessary calculations itself.

This computer code was written in C++ by Philippe Logean of the Institute of Geophysics at the University of Lausanne. Before entering the navigation data into the program they have to be prepared and edited, as have been those of Survey I. A great advantage of the dGPS data file available from the new triggering software (section 3.6.2) is that it directly provides shot time and corresponding antenna coordinates in Swiss rectangular coordinates. For data preparation, it thus remains to find the dGPS raft coordinates at the same shot times as the antenna coordinates. For this purpose, I modified the program "*gvtlibrary*" into a new program "*gvt3Dnav*" that now reads in all four data files together and searches for the times closest before and after the shot time, to linearly interpolate corresponding coordinates and to produce one file per line and raft that includes raft positions for each of the 301 shots. This modified program is also attached to the Appendix in Table A-25.

Ideally, the dGPS instruments in the waterproof boxes on the rafts should have recorded non-stop during a whole acquisition day. However, it sometimes happened that no satellite data were received for a certain duration of time, at the worst for up to 20 minutes. Fortunately, this lack of navigation data did not always occur during line shooting and if so, raft positions could be reconstructed using recordings from the other two dGPS rafts assuming a fixed distance of 7.5 m between them. In order to determine where data was missing, I integrated into the program code a quality control criteria that outputs all line and shot numbers at which the difference between the raft coordinate time closest before and after the shot time was greater than 60 seconds. To those line and shot numbers, I assigned a distant coordinate point far outside the survey area, then plotted for each shot, ship antenna and raft positions on a map and connected consecutive points. This way it was easy to spot the data holes and to evaluate whether it was necessary to reconstruct them by using adjacent raft positions or whether a simple linear interpolation between closest recordings was sufficient. For data holes of less than 60 seconds such linear interpolation was automatically applied.

The new navigation C++ computer code now assumes that the streamer is approximately straight between the measured raft position and the points of lead-in attachment, i.e. the float on the booms for the outer streamers and the rear of "La Licorne" for

the one in the center (see Fig. 5-4). This assumption can be made at a lower risk as for Survey I since first the streamer has only half the length (62.5 m), second it was observed to never have more than slight curvature in one direction and third, determination of streamer orientation here does not depend on the ship heading alone but in addition on measured locations of each streamer's end. Using ship heading and antenna positions as well as the known relative distances from the antenna reference point to the lead-in attachments, which are fixed in the ship coordinate system, allowed calculation of the geographical coordinates of these attachment points for each shot. As a next step, the position of each of the 24 hydrophones was determined along the line that connects each lead-in attachment with the corresponding raft (located between the last two receivers of each streamer). If the streamer was curved, the direct connection between its end points builds the chord length of this curve, which is shorter than the actual streamer and lead-in length. The error (in the order of several meters) made by assuming the chord instead of the real streamer shape is distributed evenly over all receiver positions resulting in slightly shortened lead-in cables and distances between receivers. Coordinates are then directly output into UKOOA P1/90 format (see Table A-21) and subsequently used for geometry assignment.

6.4 Geometry assignment (processing step 5B)

Before merging the seismic with the navigation data, it is very important to verify whether each shot recorded by the triggering software was also recorded by the seismograph and vice versa. Generally, several test shots were made at the beginning of each line, in order to write the file header on tape and to check whether the equipment functions properly. Moreover, the triggering software might have recorded some shots that have never fired the gun. All such shots have to be eliminated from the seismic data and the UKOOA P1/90 navigation file prior to data merge.

This editing process turned out to be much easier for Survey II than for Survey I, since the improved triggering software ensured that always the exact same number of 301 shots was triggered over the 1500 m between the defined start and end points of the acquisition preplot (see section 3.6.2 and Appendix, page 208). Hence, only the additional test shots had to be deleted or missing shots duplicated. To do so, a model job (*shift3D*, step 4) was created for ASPRO. ASPRO is a data base within Géovecteur that simplifies processing if the same job structure has to be applied to many input files with varying parameters - very practical for 3-D processing. These varying parameters are called registers and ASPRO manages their assignment from one job to the next by accessing a table that contains the corresponding values. Here for example, model job *shift3D* is applied to all 60 sail lines (see Table A-20 for complete processing flow) changing the sail line number (register #1#) and the number of shots to be deleted (register #2#) at the beginning of each line accordingly (Table A-22).

During Survey I, every line had a different total number of shots ranging from 226 to 253, demonstrating that shot distance must have varied not only within one acquisition line but also from one line to another. Since the distance between start and end point always remained 1200 m, the average shot spacing thus lay between 4.7 and 5.3 m. Due to the reduced navigation quality control of Survey I, several shots at the beginning of some of the acquisition lines were too far off the theoretical course to be consistent with the general ship heading. Those shots had to be eliminated in order to avoid too abrupt changes in streamer shape (see section 6.3.1). Page 8 of Table A-24 lists all parameters of the shot editing process for Survey I, such as the total number of shots recorded by the triggering software (*SPGPS*) and by the seismograph (*SPTOTAL*) as well as the selected first shot point of good quality in the navigation data (*NAVSTSP*) and in the seismic data (*SEISSTSP*). For sail lines underlain in black, the shot point number in the navigation file is not the same as in the seismic and had to be renamed accordingly during navigation data processing (see radionavigation job 5b in Table A-24).

While the seismic data have been recorded in one file per sail line and in groups of shot gathers (see section 6.2), the UKOOA P1/90 navigation file combines shot and receiver coordinates of all sail lines and is sorted first by line and then by shot number (see example in Table A-21). In order to merge each seismic file with the correct portion of this one navigation file, the sail line number has to be assigned to word 30 in the seismic trace headers (job *shift*, step 4 in Fig. 6-1 and Table A-18 and Table A-20) and to word 12 for the navigation data, once the UKOOA P1/90 ASCII file was transformed to Géovecteur binary format with trace headers (Seismic Navigation Tape - radionavigation job6 in Table A-24 for Survey I and job *wiloc3D*, step 4 in Table A-20 for Survey II).

With all these preparations done, it is the module EGRID (job *egrid*, step 5) that finally performs the data merge. It not only assigns the receiver and shot positions to designated trace header words 60 through 63 (receiver-x, receiver-y, shot-x, shot-y), it also calculates the actual shot distance or offset (header word 20) and the midpoint coordinates (header words 43 and 44) between shot and receiver; but most importantly, it carries out the CMP-binning process, described in section 2.2.1.1. In order to be able to assign a CMP bin to each seismic trace it is necessary to place a virtual grid upon the survey area that defines for each rectangular bin a CMP and a LINE number, and then to determine what CMP and LINE number correspond to the trace's midpoint coordinates. CMP-binning thus represents a midpoint coordinate transformation from the original geographical coordinate system to the CMP-LINE system, in which seismic data are conventionally processed when using post-stack migration algorithms. After this transformation, each trace possesses the CMP (header word 4) and the LINE (header word 19) number of that bin into which its midpoint fell. The spacing between grid lines in in-line direction usually is half the receiver spacing and in cross-line direction the CMP line spacing. The position of the origin of the CMP-LINE system,

however, needs to be defined in geographical coordinates and should lie outside the survey area to not produce negative values.

Correct seismic trace header assignment is the most crucial step in data processing, especially in three dimensions. An error in shot and receiver coordinates will propagate through all processing stages beginning with the calculation of midpoints and CMP binning over offset dependent NMO and DMO corrections to the migration algorithm itself. Table 6-A summarized all important trace headers, which have been used during different stages of processing. Data quality from trace to trace can only be compared with respect to a header word reference system. This is why it is extremely important to choose a CMP-LINE system that is appropriate to directly compare results of Survey I and Survey II.

In order to determine the origin for such a CMP-LINE system it is necessary to verify, how midpoints are distributed over the survey area. With the grid's origin and the bin size in CMP or LINE direction, all variables of this new coordinate system are defined. The position of the origin fixes its location relative to the acquired data. Ideally, the midpoints between source and receiver should lie at the center of the bin, since when common midpoint traces are once stacked the resulting stacked trace will be assigned to the bin center coordinates. When structural dip is present, the actual reflection point for different offsets (or depth points – CDPs, see section 2.1.2), will not fall on the same subsurface position. This problem can be corrected by prestack migration or by DMO and post-stack migration (see sections 2.2.3.2 and 2.2.3.3). However, if no full prestack migration is applied, which would migrate the energy of traces whose midpoints are scattered about the bin center to the correct position, those scattered midpoints will be considered coincident with the bin center. For conventional processing it is thus important that theoretical midpoint positions are as close to the bin center as possible and that variations in distance to the bin center are not systematic, i.e. induced by acquisition or survey direction. If the midpoints are distributed evenly around the center due to random errors in navigation, the mean position will still be the center point, if, however, midpoints always fall a certain distance away from the midpoint, the stacked trace will have the wrong coordinates. Correct positioning of the survey grid can eliminate these systematic errors.

For Survey II, as has been described in section 3.6.2, the navigation software allowed very accurate positioning and the error in shot distance was not cumulative, thus the actual shot position varied only slightly relative to the theoretical one. For this reason, we can refer to the theoretical grid of sail lines and shot positions, in order to define a grid of bins centered about the corresponding theoretical midpoint positions. For Survey I, the situation is more complicated. Due to the less precise triggering and navigation software (section 3.6.1), errors in shot distance accumulated towards the end of the line and in addition, the lines were not always shot in the same direction. This change in direction means not only, that the error accumulated in different sides of the survey area, but also, that theoretical midpoint positions

of adjacent lines that were sailed in opposite direction only coincide, if the distance between boat antenna and source was a multiple of the bin size (see Fig. 5-2 for how directions distributed over the survey area). The distances from the antenna to the gun and to the first theoretical CMP were 16.5 m and 19 m, respectively, as indicated in Fig. 5-1. Hence, when the boat antenna arrived at the end of the line, the last theoretical midpoint position is located 19 m away (nearest offset = 5 m). If the boat turned around and started a new line, the first midpoint would be placed at the same distance to the antenna but in the opposite direction. Both midpoints would thus be 38 m apart, which makes 30.4 bins, with a bin size of 1.25 m in in-line direction. Consequently, the theoretical bin centers of those two lines are shifted by 0.4 bin sizes or 50 cm relative to each other. A distance of 16.25 m instead of 16.5 m between antenna and source would have prevented this shift.

This relative shift in bin centers for lines shot in opposite directions and the additional error accumulation towards their respective opposite ends makes it impossible to find a grid of bins, that could compensate these effects. Either a grid could be chosen whose bin centers fall between midpoint accumulations of both directions (always 0.25 cm off) or a grid that favors one direction over the other (0 or 50 cm off). Since the purpose is to find a coordinate system that would allow binning of both surveys to the same LINE and CDP numbers, the best solution would be to apply to Survey I the grid that is ideal to Survey II, under the condition that the shift does not exceed the 50 cm already made within Survey I.

For both our acquisitions, navigation and positioning were always made relative to the ship coordinate system's origin, the dGPS reference antenna, since it represented the only known position in real-time. If real-time positioning were possible for the near offset, this would be the most appropriate reference in order to obtain good binning for antiparallel surveys and would have facilitated acquisition and processing also with regard to coverage at survey area boundaries (see chapter 5). However, for future surveys that are to be acquired in antiparallel geometry with our positioning system, it is important to define a distance between reference antenna and energy source that is a multiple of the bin size in in-line direction. As soon as two or more surveys are supposed to be compared on the same study site, this criterion is necessary even for parallel surveys.

Since ship antenna coordinates for the theoretical starting and end point of each sail line had been determined relative to the average fault direction (section 4.2), Survey I and Survey II have identical theoretical ship antenna positions at shot time. The only difference is that for Survey II one additional CMP line lies between two CMP lines of Survey I and that they are longer by 300 m. At one such theoretical antenna position, the midpoints for Survey II would be shifted by 35 cm with respect to those of Survey I when both streamer systems pointed in opposite directions and by 15 cm when they pointed in the same. This is because for Survey II the distance between antenna and source was 12.6 m instead of 16.5 m, so that the sum of both gives 23.28 bin sizes (equal to a shift of 35 cm) and their difference 3.12 bin sizes (equal

to a shift of 15 cm), respectively. These shifts are both within the limit of 50 cm and almost correspond to the shift of the grid that was first suggested for Survey I where bin centers fall half way between midpoint accumulations of both directions. So it is a good solution for both surveys to choose a grid that coincides with theoretical midpoint positions of Survey II.

Sail line numbers increased from east to west. Hence, it is logical to start counting LINE numbers east of the survey area (see Fig. 5-7 for orientation). As for the CMP numbers, I decided to have them increase from northwest to southeast. In order to define the grid origin, we now need to find the X/Y coordinates of the theoretical boat position closest to the northeast. This is the theoretical end point of sail line 1 from Survey II (see Table A-10). Using this reference point and the known survey direction of 322.25° it is possible to calculate the position of the midpoint furthest to the northeast. Since for Survey I the acquisition direction can be reversed, it is the midpoint that corresponds to the far offset (trace 48) of the single-streamer configuration when pointing towards the northwest, that yields this position. When shifted 90 cm (one in-line bin size minus -35 cm) to the northeast, it becomes midpoint position -74 in the relative coordinate system of Survey II where midpoint 1 corresponds to the near offset (streamers for Survey II always point to the southeast). This position represents the outer northeastern corner of the combined survey area and falls on a theoretical midpoint of Survey II. Since negative values are not allowed, it is necessary to rename this point according to the new CMP-LINE coordinate system. Sail line 1 of Survey II corresponds to its second CMP line. So any LINE number greater than 2 and any CMP number greater than 0 can be chosen for the above determined reference point.

Later in the processing sequence, a post-stack time migration will be performed, for which padding of additional LINES and CMPs is required. In order to avoid another renaming of all traces' header words 19 and 4, sufficiently high minimum LINE and CMP number were chosen. Tests with the migration algorithm showed that adding 30 LINES and 30 CMPs to all sides of the survey area, results in good migration without significant edge effects. The outer northeastern reference point (535836.299 E and 149592.625 N) was thus determined to lie on CMP 30 and LINE 32 with respect to the new CMP-LINE coordinate system. The grid's origin can now be calculated with the aid of "*grillth*", a GEOUNIX utility within Géovecteur (job *egrid*, step 5B). The X/Y coordinates of the grid's origin, the definition of the orientation of the CMP and LINE axes with respect to the geographical coordinate system as well as the bin dimensions are written into a grid library that will be called by the binning module EGRID. Since the bin dimension in cross-line direction for Survey II is half of that of Survey I, it is necessary to define two different grid libraries (*grid1.lgr* and *grid2.lgr*) with two different origins to make geometry assignment feasible. Given that for both surveys, the first CMP of sail line 1 was placed onto the above reference point (CMP = 30, LINE = 32), CMP numbers are identical and every second CMP line of Survey II will fall on a CMP line of Survey I. CMP line correspondence between both surveys is shown in Table 6-B. After post-

stack migration the LINE numbers for Survey I will be changed to match those of Survey II. This way, the final data cubes can be directly compared by referring to the same CMP-LINE coordinate system. Before migration, comparisons can be made with the aid of Table 6-B.

The module EGRID performs the coordinate transformation and assigns the appropriate bin (job *egrid*, step 5B) to each trace's calculated midpoint coordinates. As a result, header words 19 and 4 (see Table 6-A) are filled with the respective LINE and CMP number and an EGRID coverage table is output (Table A-19 and Table A-23). In this table, we find for each input sail line the respective minimum and maximum CMP and LINE numbers of the filled bins. For Survey I, CMPs range from 31 to 1112 and LINEs from 35 to 115, whereas for Survey II, CMPs vary from 102 to 1328 and LINEs from 29 to 210.

Only after geometry assignment, it is possible to edit traces, i.e. eliminate those that are permanently dead or to apply a corrective scalar when amplitudes (not real one since hydrophones were not calibrated) are anomalously high (energy spikes) or low (lack in amplifier gain). Section 3.3.2 described how to search for irregularities in hydrophone sensitivity by using the stacked mean of all traces with the same offset at times of random noise recording. A similar procedure was used to develop a job, which consists of a two-step process, for automatically despiking all traces. As a first step, anomalous traces have to be searched for and selected among all traces in the data cube. As a second step, the samples of such selected traces that are considered spiky according to a chosen criterion, will be attenuated. In practice, each trace's maximum amplitude, mean and corresponding standard deviation is calculated on all samples recorded 50 ms after the water bottom reflection (to exclude the high-amplitude water bottom reflection). If the difference between maximum amplitude and mean passes the standard variation by a factor of more than 25 or if the mean itself is exceptionally high, the trace is selected. A sample of such a trace will be considered spiky, if its amplitude is higher than 40 times the median of the whole trace and will be attenuated along with the neighboring samples. This job has already been tested but not yet applied to the whole data cube. A similar job needs to be established in order to bring up the gain of those traces whose hydrophone sensitivity was weaker than average, i.e. trace 3 on the S/N section. Nevertheless, the dead hydrophones that have been determined in section 3.2.3, trace 24 on ITI streamer section #1 and trace 13 on ITI streamer section #2, were systematically deleted on all shot gathers in job *egrid* (step 5B).

SURVEY I (1999)		SURVEY II (2001)		Common Grid	SURVEY I (1999)		SURVEY II (2001)		Common Grid
Sail LINE	CMP LINE	Sail LINE	IN-LINE	CMP LINE	Sail LINE	CMP LINE	Sail LINE	CMP LINE	CMP LINE
			1	31				91	121
1	32	1	2	32	46	77	31	92	122
			3	33				93	123
2	33		4	34	47	78		94	124
		2	5	35			32	95	125
3	34		6	36	48	79		96	126
			7	37				97	127
4	35	3	8	38	49	80	33	98	128
			9	39				99	129
5	36		10	40	50	81		100	130
		4	11	41			34	101	131
6	37		12	42	51	82		102	132
			13	43				103	133
7	38	5	14	44	52	83	35	104	134
			15	45				105	135
8	39		16	46	53	84		106	136
		6	17	47			36	107	137
9	40		18	48	54	85		108	138
			19	49				109	139
10	41	7	20	50	55	86	37	110	140
			21	51				111	141
11	42		22	52	56	87		112	142
		8	23	53			38	113	143
12	43		24	54	57	88		114	144
			25	55				115	145
13	44	9	26	56	58	89	39	116	146
			27	57				117	147
14	45		28	58	59	90		118	148
		10	29	59			40	119	149
15	46		30	60	60	91		120	150
			31	61				121	151
16	47	11	32	62	61	92	41	122	152
			33	63				123	153
17	48		34	64	62	93		124	154
		12	35	65			42	125	155
18	49		36	66	63	94		126	156
			37	67				127	157
19	50	13	38	68	64	95	43	128	158
			39	69				129	159
20	51		40	70	65	96		130	160
		14	41	71			44	131	161
21	52		42	72	66	97		132	162
			43	73				133	163
22	53	15	44	74	67	98	45	134	164
			45	75				135	165
23	54		46	76	68	99		136	166
		16	47	77			46	137	167
24	55		48	78	69	100		138	168
			49	79				139	169
25	56	17	50	80	70	101	47	140	170
			51	81				141	171
26	57		52	82	71	102		142	172
		18	53	83			48	143	173
27	58		54	84	72	103		144	174
			55	85				145	175
28	59	19	56	86	73	104	49	146	176
			57	87				147	177
29	60		58	88	74	105		148	178
		20	59	89			50	149	179
30	61		60	90	75	106		150	180
			61	91				151	181
31	62	21	62	92	76	107	51	152	182
			63	93				153	183
32	63		64	94	77	108		154	184
		22	65	95			52	155	185
33	64		66	96	78	109		156	186
			67	97				157	187
34	65	23	68	98	79	110	53	158	188
			69	99				159	189
35	66		70	100	80	111		160	190
		24	71	101			54	161	191
36	67		72	102	81	112		162	192
			73	103				163	193
37	68	25	74	104	82	113	55	164	194
			75	105				165	195
38	69		76	106	83	114		166	196
		26	77	107			56	167	197
39	70		78	108	84	115		168	198
			79	109				169	199
40	71	27	80	110			57	170	200
			81	111		CMPcom=		171	201
41	72		82	112		CMP LINE		172	202
		28	83	113		* 2 - 32	58	173	203
42	73		84	114				174	204
			85	115				175	205
43	74	29	86	116			59	176	206
			87	117				177	207
44	75		88	118				178	208
		30	89	119			60	179	209
45	76		90	120				180	210

Table 6-B. Table showing the correspondence between sail lines and CMP lines of Survey I and of Survey II after geometry assignment and grid origin definition. Highlighted is in-line 140, which corresponds to the location of the 2-D profiles in section 4.3.

6.5 3-D bin harmonization (processing step 6)

An important part of 3-D processing is bin harmonization (see section 2.2.1.1). Due to navigation inaccuracies and streamer feathering, traces were not always evenly distributed over the bins, i.e. the nominal fold of 12 for Survey I or 6 for Survey II was not always reached. Low fold bins mean, that it is very likely that some of the offset classes are not represented at all, which in turn has an effect on DMO processing, in which reflection energy of dipping reflectors is moved to adjacent bins within the same offset class. For large navigation errors, it even sometimes happened that after geometry assignment, bins were completely empty. If in the same offset class, several adjacent bins have no data the DMO operator does not function properly. Fig. 6-12 and Fig. 6-13 (a) in section 6.7 present the stacked section of LINE 102 of both surveys, exhibiting areas of DMO artifacts due to bins with empty offset classes. It is thus important to avoid areas with no or even low fold.

Two processes (as described in section 2.2.1.1) are distinguished for harmonizing offsets within each bin: “static” and “dynamic” binning. The aim of *static binning* is to have one single trace per offset class and bin in order to keep the amplitude level constant for subsequent stack. If the offset class of the same bin is represented by N traces, either the amplitude of each trace is divided by N or one trace is selected to criteria such as minimum distance to the studied bin center or minimum offset. *Dynamic binning* or *flex binning* seeks those traces in the neighboring bins that represent the offset classes missing from the bin being studied. For this purpose, a rectangular macro-bin is defined, which is centered on the current bin. The trace missing from one class of the current bin is sought among the same class of the neighboring bins within a circle or an ellipse whose radius can vary as a function of offset class, and which is limited by the macro-bin size. If several traces are present in the neighboring bins, selection or rejection criteria can be defined. If still several traces are left after application of these criteria, these traces are weighted and then duplicated at the center of the studied bin.

Both, *static* and *dynamic binning* were applied to Surveys I and II using the Géovecteur module HABIN (job *habin*, step 6, Table A-18 and Table A-20). As a first step, offset classes have to be defined. Since the goal of offset harmonization is to have one trace per offset class, it is reasonable to define class dimension in a way to make sure we keep the nominal fold. If offset class increments are chosen too large, more than one trace might be placed in each class and fold may be reduced, if the increment is too small, some classes risk to stay empty. With a receiver spacing of 2.5 m and a shot spacing of 5 m, the total of 48 receivers in Survey I gives a nominal fold of 12 while the total of 24 receivers in Survey II results in a nominal fold of 6. The minimum possible offset is 5 m and the maximum offset 62.5 m or 122.5 m, respectively. Considering the stacking chart, there are four theoretically possible offset distributions (sets) over four consecutive bins (bin n , $n+1$, $n+2$, $n+3$ and $n+4 = n$) with 5, 7.5, 10 or 12.5 m as the respective smallest offset as listed in the following table. Those four

smallest offsets represent the first offset class, offsets between 15 and 25 m, the second and so forth up to class 6 for Survey I and class 12 for Survey II. If offsets are grouped at increments of 10 m starting at an offset of 5 m, theoretically there should always be one trace per class and bin.

Offset Class	Set 1	Set 2	Set 3	Set 4
1	5 m	7.5	10	12.5
2	15 m	17.5	20	22.5
3	25 m	27.5	30	32.5
4	35 m	37.5	40	42.5
5	45 m	47.5	50	52.5
6	55 m	57.5	60	62.5

As a second step, macro-bin and search radius have to be defined. Since navigation inaccuracies and streamer feathering predominantly occur perpendicularly to the sail line, duplication was limited to the cross-line direction only. According to streamer shape simulations for the longer streamer of Survey I (see Fig. 6-2), feathering did not exceed 15 m and never did the vessel cross more than the adjacent sail line. This is why the macro-bin was set to one CMP spacing in in-line and three LINE spacings in cross-line direction, i.e. traces for duplication will only come from one bin to the left and one to the right of the studied bin center, which equals a distance of 11.25 m for Survey I and 5.625 m for Survey II. The search radius was set to 20 m and 10 m, respectively, greater than the extent of the macro-bin to ensure that only traces from those two adjacent bins are considered.

Géovecteur limits the size of data that can be sorted at a time to about 6 GB. Since the input data to HABIN have to be sorted in the same job (module BSORT - either into CMP / LINE order or vice versa) to correctly set the Y-flags, it is necessary to split bin harmonization into two jobs (step 6, Table A-18 and Table A-20; total size of data from step 5B, job *egrid*, are about 8 GB for Survey I and 10 GB for Survey II). In order to harmonize half of the LINE numbers in the first job, those sail lines need to be input whose traces were assigned to the selected LINES. The EGRID coverage in Table A-19 and Table A-23 indicated the CMP and LINE numbers that had been covered by each sail line and allow verification of correct grid origin choice. Those tables also list the sail lines necessary for the chosen subsurface lines of both HABIN jobs. This is an important step since otherwise coverage will be reduced at file edges. The created two output files are each bigger than 4 GB, too big to be examined in Géovecteur's display software EXAM. Selected LINES thus have to be output separately in order to be studied in more detail for quality control. During industry processing, the splitting of jobs and the search for corresponding input sail lines is automated by accessing large data bases, which contain the contents of such coverage tables and other useful information.

Bin harmonization was applied with great success to both surveys. Following velocity analysis (step 7, next section), both surveys were NMO and DMO corrected (step 8, see

section 6.7) and stacked by (a) inputting files directly after geometry assignment and (b) by using the harmonized bins as input (steps 8A and 8). The example stacks of LINE 102 (Fig. 6-12 and Fig. 6-13 (b) in section 6.7) from both surveys demonstrate, how bin harmonization improves DMO performance. Fig. 6-4 and Fig. 6-5 show fold before stack in every bin represented at scale for the 80 and 60 sail lines of Survey I and II, respectively, with and without *flex binning* applied. Since the nominal fold of Survey II was half of that of Survey I, the color palettes for both surveys was adapted to associate no fold (blue), low fold (yellow), nominal fold (green) and high fold (red) with the same colors in order to facilitate comparison with respect to navigation effects.

In Fig. 6-4, the change in acquisition direction every 6-8 lines is clearly visible causing irregular boundaries to the data cube of Survey I. In great contrast, CMP coverage at survey area limits of Fig. 6-5 is perfectly straight, as could have been assumed from the exact same number of 301 shots fired per line (compare Table A-15 to Table A-14). The new navigation software proves to be well adapted for high precision navigation.

When comparing stacking charts without bin harmonization, the improved line navigation of Survey II strikes the eye. While for Survey I, an important portion of the survey area has no data at all, bins with no fold are almost lacking for Survey II. If low fold areas occur it is obvious that they are always due to a deviation of the navigated ship track from the straight theoretical course, causing uneven coverage exclusively in cross-line direction. As a consequence, systematically there are red bins with very high fold next to no-fold areas in blue (Fig. 6-4) indicating that two sail lines must have been superimposed when the correct sail line heading had been missed. Hence, this very uneven distribution of fold is the effect of important navigation errors. The fold map of Survey II on the other hand exhibits much larger coherent green areas of nominal coverage showing that here navigation errors play a much smaller role than in Survey I.

As demonstrated in both examples, bin harmonization worked very well even when trace duplication is allowed only from one bin to either side of the studied bin. For Survey I, the empty bins could be filled to a low, at places almost nominal coverage. Only very few bins remain without data. Areas with exceptionally high coverage were reduced to bring the total amplitude to a common level. The same effects can be observed for Survey II. Since line navigation had been much better in the first place, the overall result is also much improved. Bin coverage for Survey II after bin harmonization is almost perfectly homogeneous! However, at a nominal coverage of only 6, lower fold areas possess double the probability of having several adjacent bins lacking the same offset class – there are 6 offset classes for Survey II while there are 12 for Survey I. The effect will show in partial or prestack migration, processes that are performed in the common offset domain and which create traces whose energy will be either constructively or destructively stacked. Furthermore, the overall lower fold will influence the quality of velocity analysis.

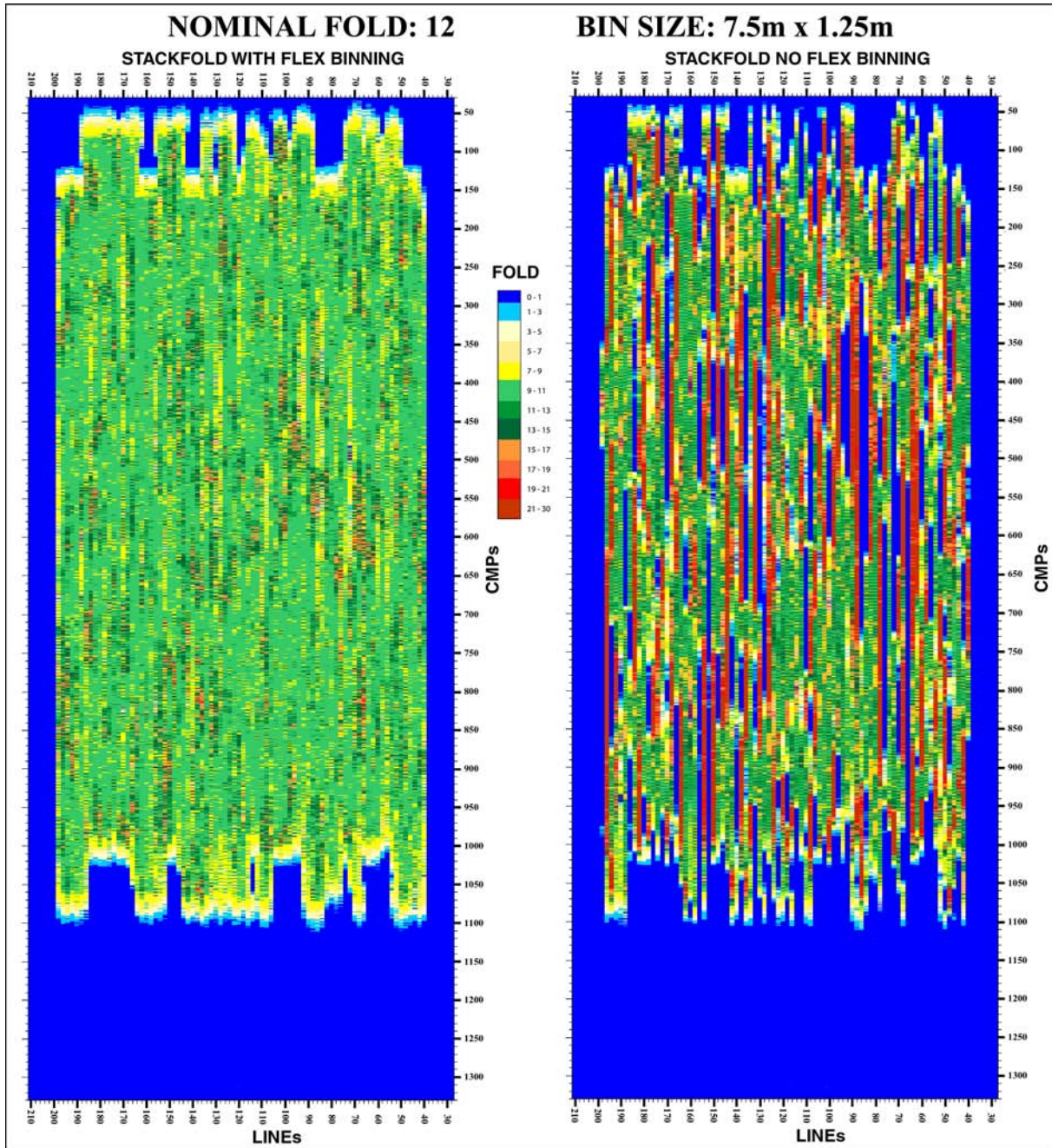


Fig. 6-4. Stacking fold for each bin without (right) and with (left) application of flex binning for Survey I. Color palette was adapted to associate the nominal fold of 12 with green, low fold with yellow and high fold with red.

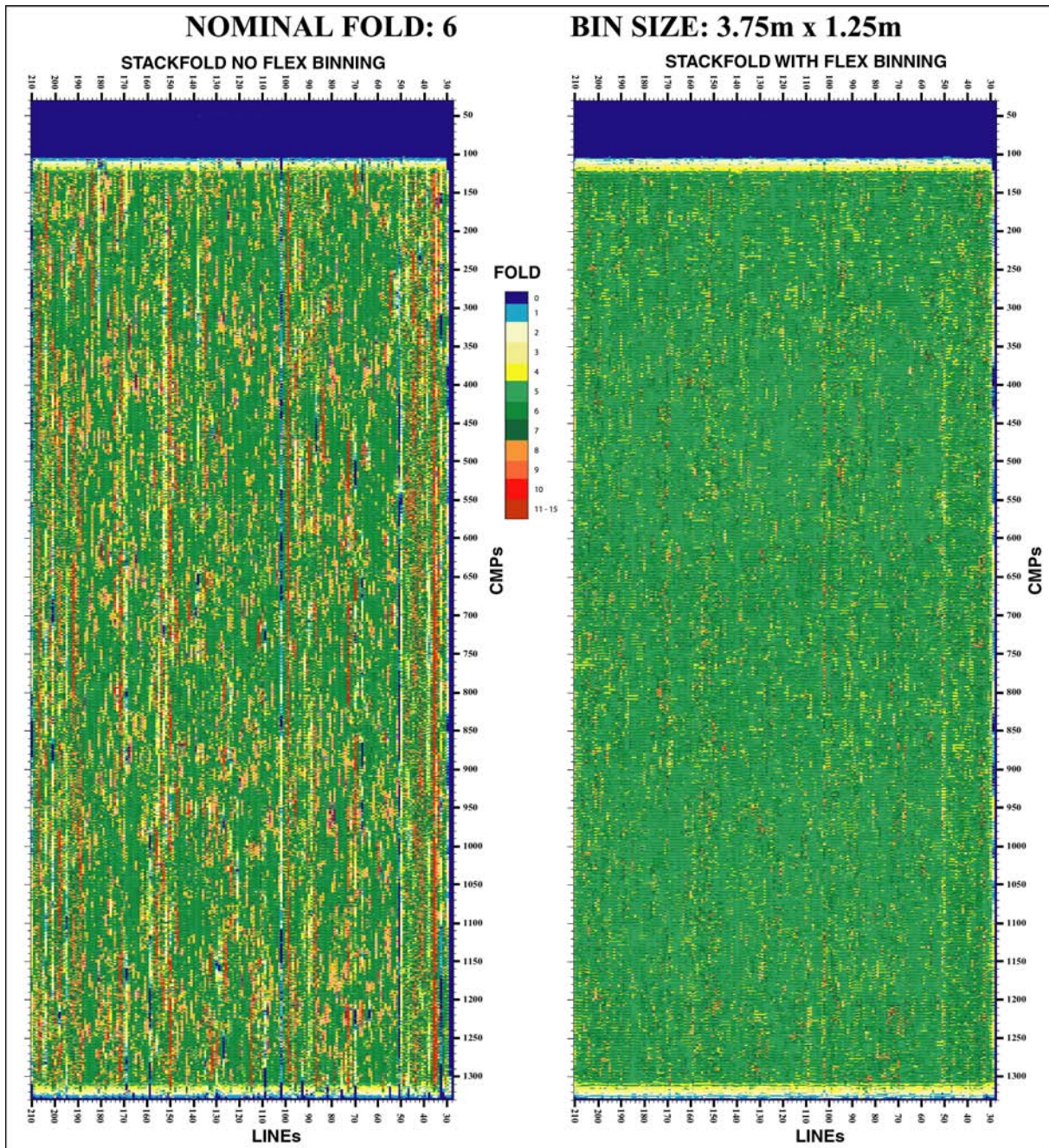


Fig. 6-5. Stacking fold for each bin without (right) and with (left) application of flex binning for Survey II. Color palette was adapted to associate the nominal fold of 6 with green, low fold with yellow and high fold with red. This way the improved navigation of Survey II compared to that of Survey I becomes obvious.

6.6 Velocity analysis (processing step 7)

The main part of the prestack processing flow (Fig. 6-1) consists of the construction of a 3-D velocity model. As has been described in section 2.1.2 and 2.2.3.2, there are two effects, both from the presence of dipping structures, that degrade the quality of a stack resulting from conventionally NMO corrected data: one is the conflicting dip problem, the other reflection point smearing. The solution to both problems is migration before stack or at least a prestack partial migration or DMO that migrates energy from dipping reflectors back to the correct

zero-offset. Conventional NMO correction uses *stacking velocities* (see section 2.1.3.3) picked during velocity analysis. These stacking velocities might be the zero-dip *rms velocity* (section 2.1.3.2) of the medium above the reflector or, much more likely, at the presence of structural dip, a dip and azimuth dependent velocity, which is greater. DMO requires a velocity model that consists of the zero-dip rms velocities only (see section 2.2.3.3). In order to obtain this model, velocity analysis is divided into two steps (step 7A and 7B in Fig. 6-5). The first step is a conventional velocity analysis (see section 2.2.2) performed on a coarser grid of LINES and CMPs in order to determine a stacking velocity model that will approximately remove the effect of offset for subsequent DMO correction in step two. The DMO operator works in the domain of common offset and removes the effect of dip. Subsequently, the previously corrected NMO is reapplied to the CMP gathers and zero-dip velocities can be picked.

The initial semblance velocity analysis was performed on every fourth LINE and every 100th CMP (a total of 140 spectra) on the data of Survey I. For this purpose the input bin-harmonized CMP gathers were sorted into LINE-CMP order. After application of a bandpass filter, amplitude recovery, muting of the water column and automatic gain control (see job *vespai*, step 7A, and next section), semblance spectra were calculated between 1300 and 3000 m/s. For the second step (job *dmoforvespa*, step 7B), the data were again filtered, the amplitudes recovered and then NMO corrected using the preliminary velocity field picked in the above initial analysis. After 3-D Kirchhoff DMO (module KIDMO), a water bottom mute and inverse NMO correction, a total of 600 semblance spectra were computed, this time, on every second LINE and every 50th CMP (job *vespa*, step 7B).

Before doing the zero-dip velocity analysis on all 600 semblance spectra, it was first performed only on those CMP/LINE positions that had been chosen for the initial analysis. The stack, which used the resulting velocity model, showed that the distance between adjacent velocity functions, especially in cross-line direction, was not appropriate for the lateral structural variations present in the data. While stacking quality was convincing on those LINES on which velocity functions were picked, it degraded towards adjacent LINES with interpolated values. Only when the velocity analysis was performed on all 600 semblance spectra, the density of velocity picks was sufficiently high to have overall good stacking throughout the whole data cube. Since LINES have a spacing of 7.5 m and CMPs a distance of 1.25 m, we can conclude that for our survey site and our type of data, detailed velocity information is necessary in intervals not bigger than 15 m in fault strike and 62.5 m in fault dip direction.

Creation of semblance spectra in Géovecteur is done with the aid of the module VESPA. The sampling interval for computation outputs is limited to 10 ms and 20 m/s, which means that for data of Survey I, only one semblance value every 40th sample is calculated. Hence, VESPA represents one of those modules that is not adapted to very high-resolution

surveys and makes it impossible to pick velocities more accurately than to this computational threshold. The output semblance spectra are read into an interactive Géovecteur application called VELCOM that allows display of the spectra along with uncorrected or corrected reflection hyperbolas, corresponding to the picked velocity function, as well as a stack of several neighboring CMPs. Fig. 6-6 shows an example of the spectrum of LINE 83 and CMP 420 as it appeared in VELCOM after DMO dip correction. Superimposed is the respective picked zero-dip rms velocity function and to the right the corresponding interval velocities.

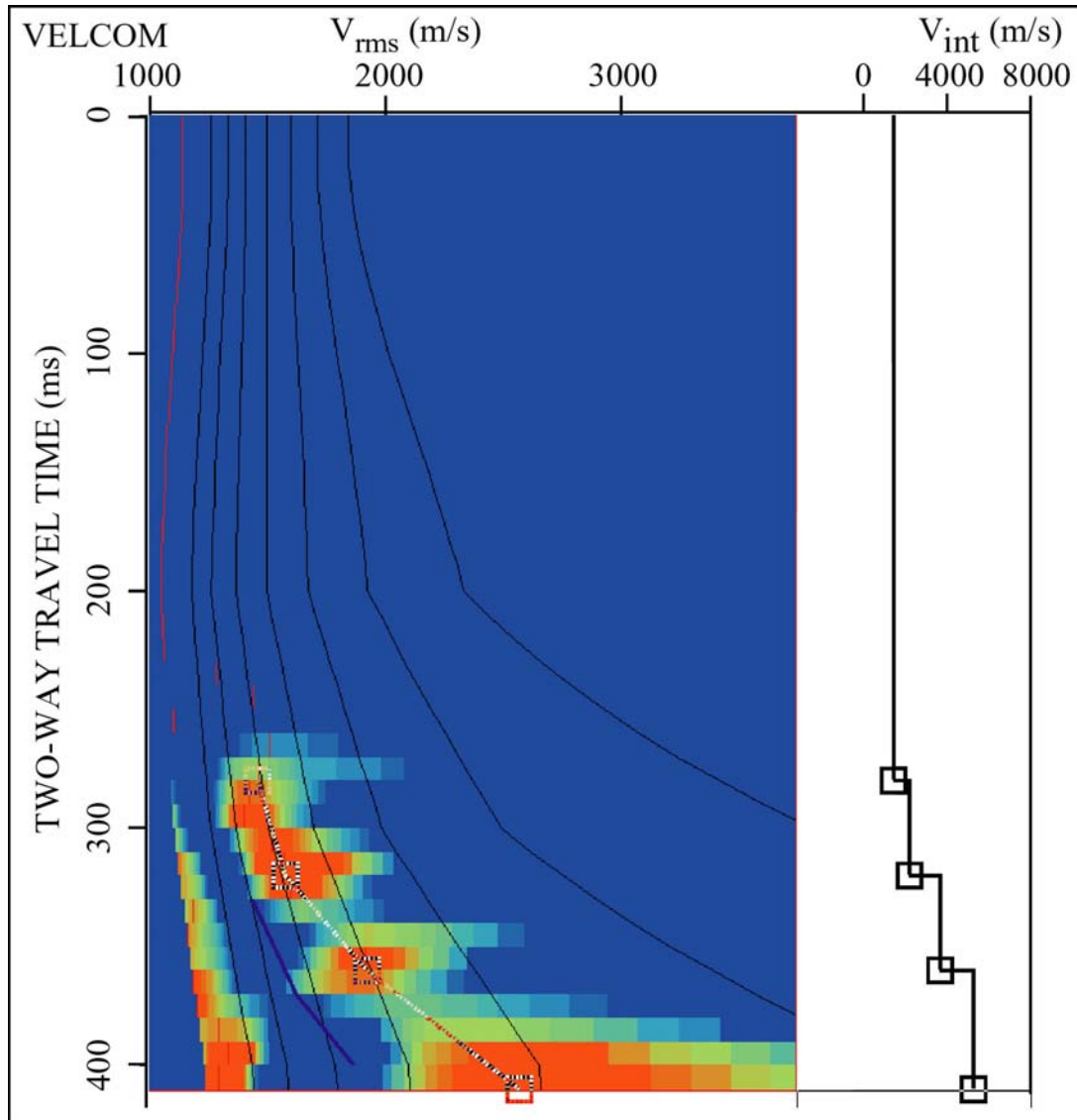


Fig. 6-6. Semblance velocity spectrum of CMP 420 on LINE 83 after DMO correction. Colors represent the semblance value from blue (low) to red (high). Superimposed on the spectrum are seven predefined velocity functions that serve as guides and the actually picked rms velocity function (squares). The corresponding interval velocities are shown on the right hand side (black line with squares).

A representation of the final 3-D zero-dip rms velocity model is shown in Fig. 6-7. LINE and CMP numbers were chosen relative to the grid common to both surveys. Consequently, the velocity functions picked on every 2nd sail line of Survey I correspond here

to every 4th LINE starting at number 42 (sail line 6, see Table 6-B). Thus, the dimension of each color block on a time slice represents the interval between adjacent velocity functions. The three dimensional structure of the geology within the study site is obvious: rms velocities not only increase with time (depth) but also from the south to the north for the same time intervals mainly due to the effect of the deepening lake, as illustrated by the respective slices along LINES 42, 100 and 150 and along CMPs 220, 400, 600 and 800. Since velocity functions were picked on CMP gathers organized LINE by LINE, the picking coherency is higher in in-line than in cross-line direction or at constant times.

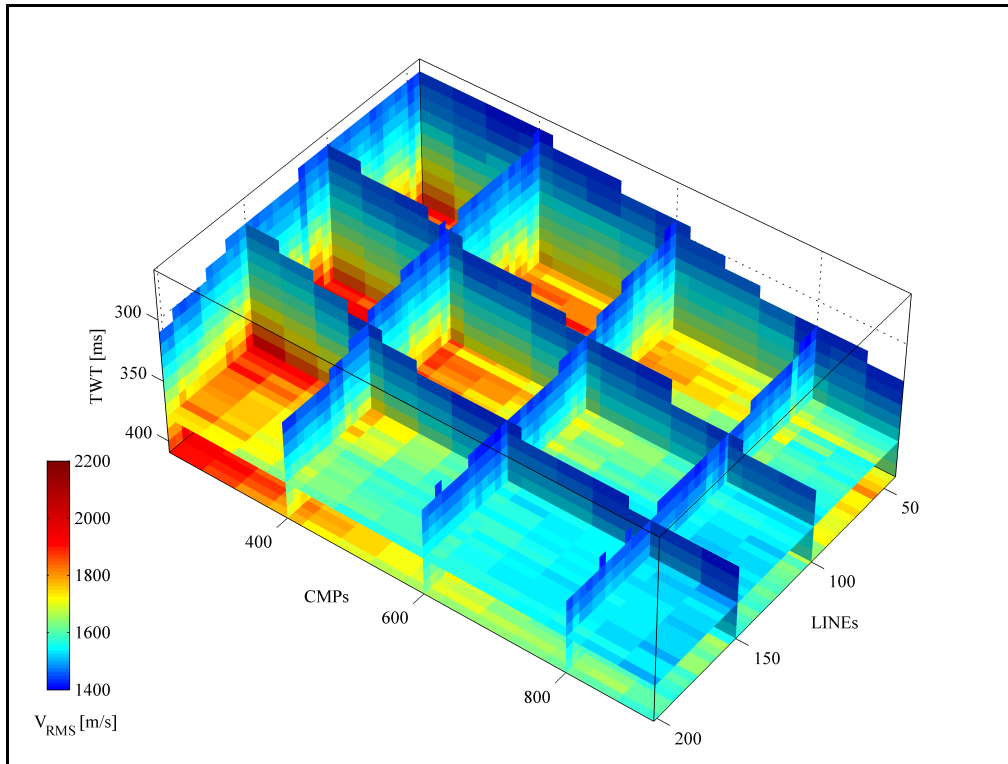


Fig. 6-7. Representation of the rms velocity model in three dimensions composed of three in-lines (LINEs 42 - see Fig. 6-8 (a), 1st panel - 100 and 150), four cross-lines (CMPs 220, 400, 600 and 800) and two time slices (at 380 and 410 ms, see Fig. 6-9 (a), 1st and 4th panel). The model cube is oriented approximately with respect to geographical north.

Fig. 6-8 (a) presents 9 example velocity distributions in in-line direction on every 20th LINE, while Fig. 6-9 (a) shows 16 such distributions when cutting the model at constant times of 10-ms intervals. It is on these time slices that the three dimensional velocity variations become most striking. Rms velocities range from 1420 m/s at the water bottom reflection (260-330 ms) to a maximum of 2180 m/s at a depth of 400 ms towards the northern side of the survey area. At the same depth but in the area's southernmost corner, rms velocities are found to be as low as 1550 m/s. This variation from north to south exactly mimics the bathymetry as shown in Fig. 7-7. While, for example, the northern portion of time slice 370 ms is overlain by 80 ms of reflection data from Quaternary sediments and upper molasse, the southern portion still measures the water velocity.

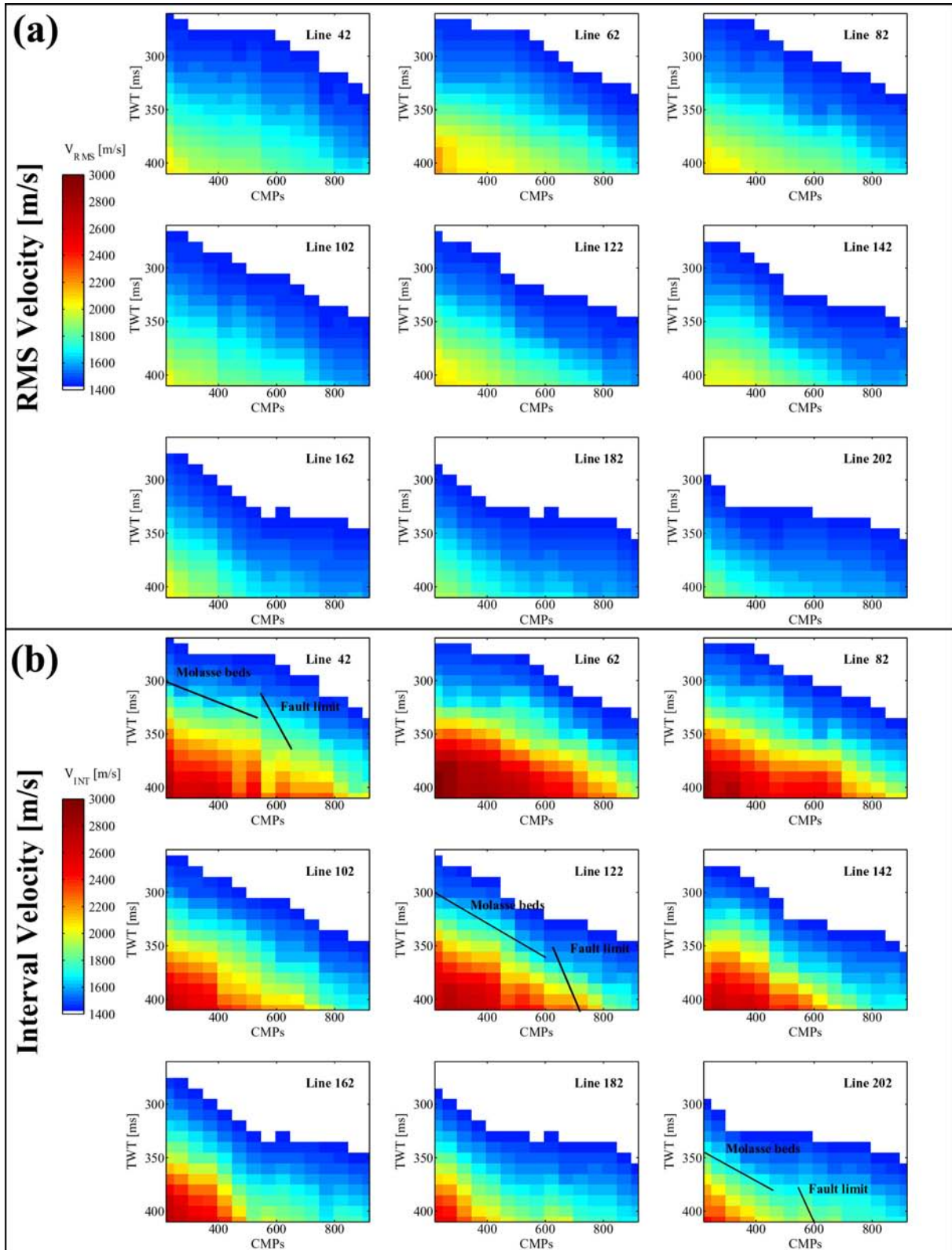


Fig. 6-8. Example (a) rms and (b) interval velocity distributions along every 20th LINE. The superimposed black lines on in-line 42, 122 and 202 indicate the approximate northeastern limit of the fault zone and the inclination of molasse beds. Areas in white correspond to the water layer where no velocities were picked. See Fig. 6-9 for orientation of sections.

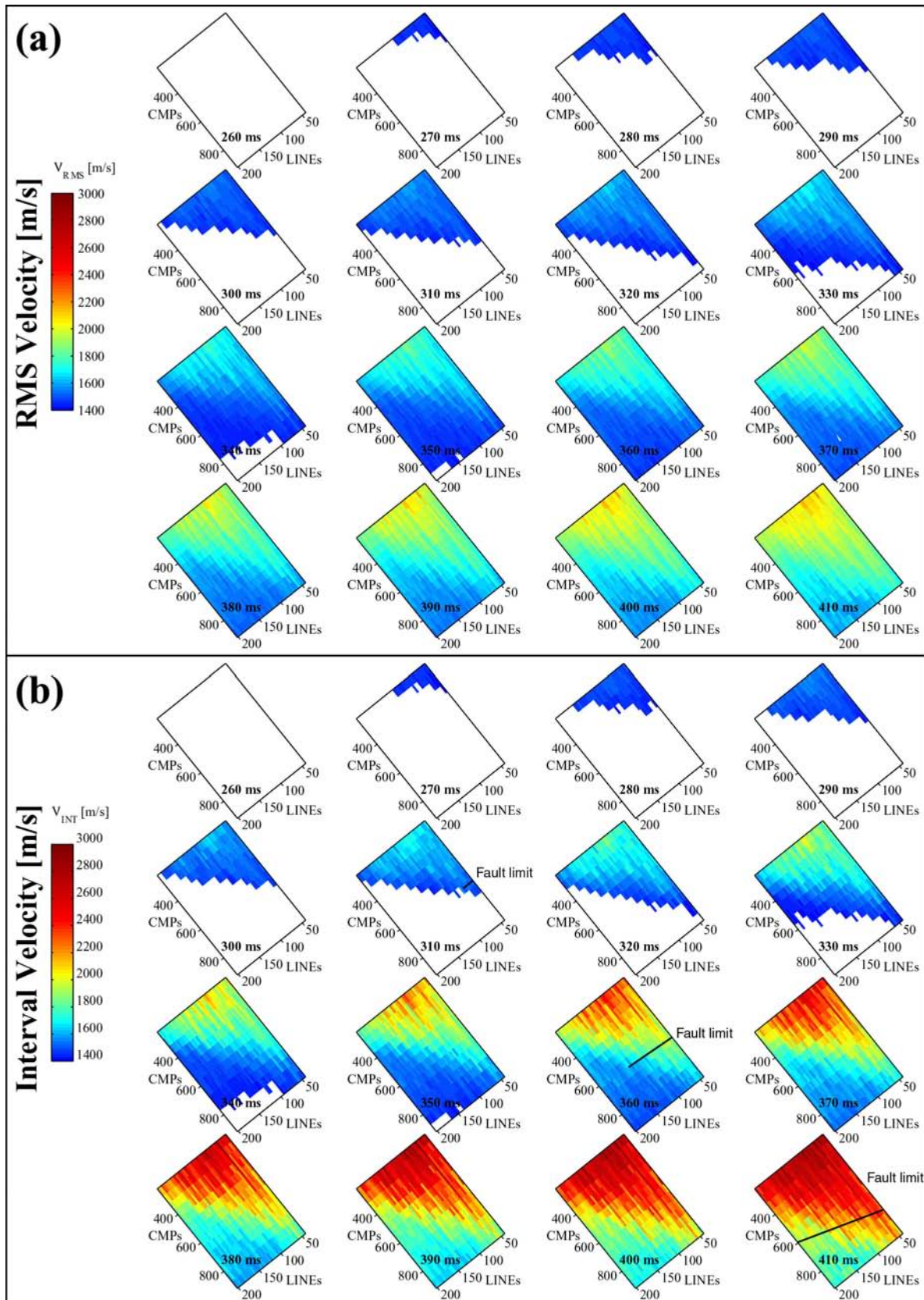


Fig. 6-9. Example (a) rms and (b) interval velocity distribution when cutting the 3-D model along constant times at intervals of 10 ms. The black line on slices 310, 360 and 410 ms indicates the approximate northeastern limit of the fault zone. Areas in white correspond to the water layer where no velocities were picked. Slices are oriented at the correct angle relative to geographic north.

The first in-line sections of Fig. 6-8 (a) show well how isovelocity lines follow the trend of the water bottom. However, higher in-line numbers demonstrate that it is mainly the angle of Plateau Molasse beds northwest of the fault zone limit that influences the velocity distribution.

Interval velocities were calculated between all picked rms velocities in each function. Subsequent interpolation along the time axis produced velocity distributions in in-line direction (Fig. 6-8 (b)) and at constant times (Fig. 6-9 (b)) that are comparable to those in Fig. 6-8 (a) and Fig. 6-9 (a). The generally larger interval velocities range from 1420 m/s at the water bottom up to 3000 m/s at a maximum depth of 410 ms and represent values that have an approximate geological significance. At times greater than 410 ms, no more velocity picking was possible due to the limited signal penetration and number of semblance values that could be calculated from input data of 475 ms traces length (after arrival time correction).

A similar detailed and time consuming velocity analysis as conducted for Survey I has not yet been performed on the data of Survey II. Instead, the velocity model of Survey I was simply adapted to match the LINE numbers of Survey II (see LINE correspondence Table 6-B) and extrapolated to the CMPs at survey area boundaries – another great advantage of having assigned the geometry to a common grid of bins. A velocity analysis on the data of Survey II would be very interesting since a different type of energy source had been employed and the streamers had only half the offset. While the larger penetration of the lower frequency air gun (see section 3.4.6) used in Survey II will facilitate velocity analysis at depth, half the maximum offset will make velocity distinction more difficult due to the lack of moveout. The reduced fold might also cause limitations during semblance calculations. With this respect, tests have been conducted prior to Survey II and semblance spectra calculated by using only the 24 nearest offset traces of the single 48-channel streamer of Survey I. The semblance spectra as well as the velocity functions picked were almost identical to those using the full offset range, which made us all the more determined in developing the multi-streamer configuration that was feasible only by sacrificing half the offset and half the fold (see section 5.2.1).

6.7 Filtering, DMO and stack (processing step 8)

After detailed velocity analysis, all information is available for DMO correction and stack. Before doing so, the data were bandpass filtered and spherical divergence corrected. In order to distinguish between usable signal and noise, amplitude spectra were studied on a great number of shot gathers from both data cubes. Noise tests (Fig. 3-10) showed that the main portion of undesirable signal is recorded in the low-frequency range between 0 and 40-60 Hz. The same very high peak of low-frequency noise is visible on Fig. 6-10 and Fig. 6-11 (a) and (c). These figures present the amplitude spectrum calculated over a time window from 250-470 ms on a shot gather whose near trace at 7.5 m offset falls into the same bin for

Survey I and Survey II. This way, variations in the form of the spectrum due to a change of reflectivity at different locations is eliminated. While in (a) and (c) the spectrum was calculated with no filter applied, the data in (b) and (d) were filtered cutting off frequencies below 40 Hz and attenuating those between 40 and 60 Hz in order to better scale the remaining signal.

In addition to offset 7.5 m, the spectrum of a far offset trace was calculated for comparison of the influence of incidence angle in (b) and (d). The far offset at 120 m for Survey I exhibits lower amplitudes and a reduced content of higher frequencies whereas the far offset at 60 m of Survey II shows higher amplitudes at lower frequencies than the near trace, although it was not even corrected for spherical divergence. This phenomenon was detected on the water bottom reflection of many shot gathers: first, its amplitude increases with increasing offset, then it decreases again until the amplitude falls below that of the near trace. However, a detailed hydrophone calibration is necessary before really interpreting these amplitude versus offset variations. They would only be taken into account during AVO analysis or when the data are migrated prestack while preserving true amplitudes (section 7.2).

The spectra in Fig. 6-10 and Fig. 6-11 (d) can be compared to those of the water gun (Fig. 3-21) and the Mini G.I G15 / I15 (Fig. 3-23) signatures. After elimination of the high-amplitude low-frequency noise, the reflected spectra are very similar in shape to the respective gun's signature although amplitudes are attenuated. In Fig. 6-10 (b) or (d) amplitudes fall below the minimum amplitude level of the lower frequencies (95 dB) for frequencies above 1700 Hz while in Fig. 6-11 (b) or (d) they fall below this level (at 75 dB) for frequencies above 650 Hz. For Survey I, the low cut filter at 40/60 Hz (Fig. 6-10 (b)) still did not completely eliminate the noise peak in (a). Since frequencies up to 200 Hz are not well represented in the water gun signal anyways, a bandpass filter was used with the corner frequencies at 100/200 and 1500/1700 for Survey I, but at 40/60 and 600/650 for Survey II.

The module REFOR performs amplitude recovery for spherical divergence using the following factor c as a scalar for the sample amplitude at time t :

$$c = \left(\frac{t}{250} \right)^e$$

The exponent e was determined by testing a range of different values. The best stack was obtained with an exponent of 5. Amplitudes at 250 ms thus stay unchanged while those at 500 ms are multiplied by 32. Since the amplitude of a signal decreases by a factor of 32 due to spherical divergence ($\sim 1/\sqrt{r}$) when it propagated for 500 ms in a medium of 2000 m/s average velocity, this value seems a reasonable estimate.

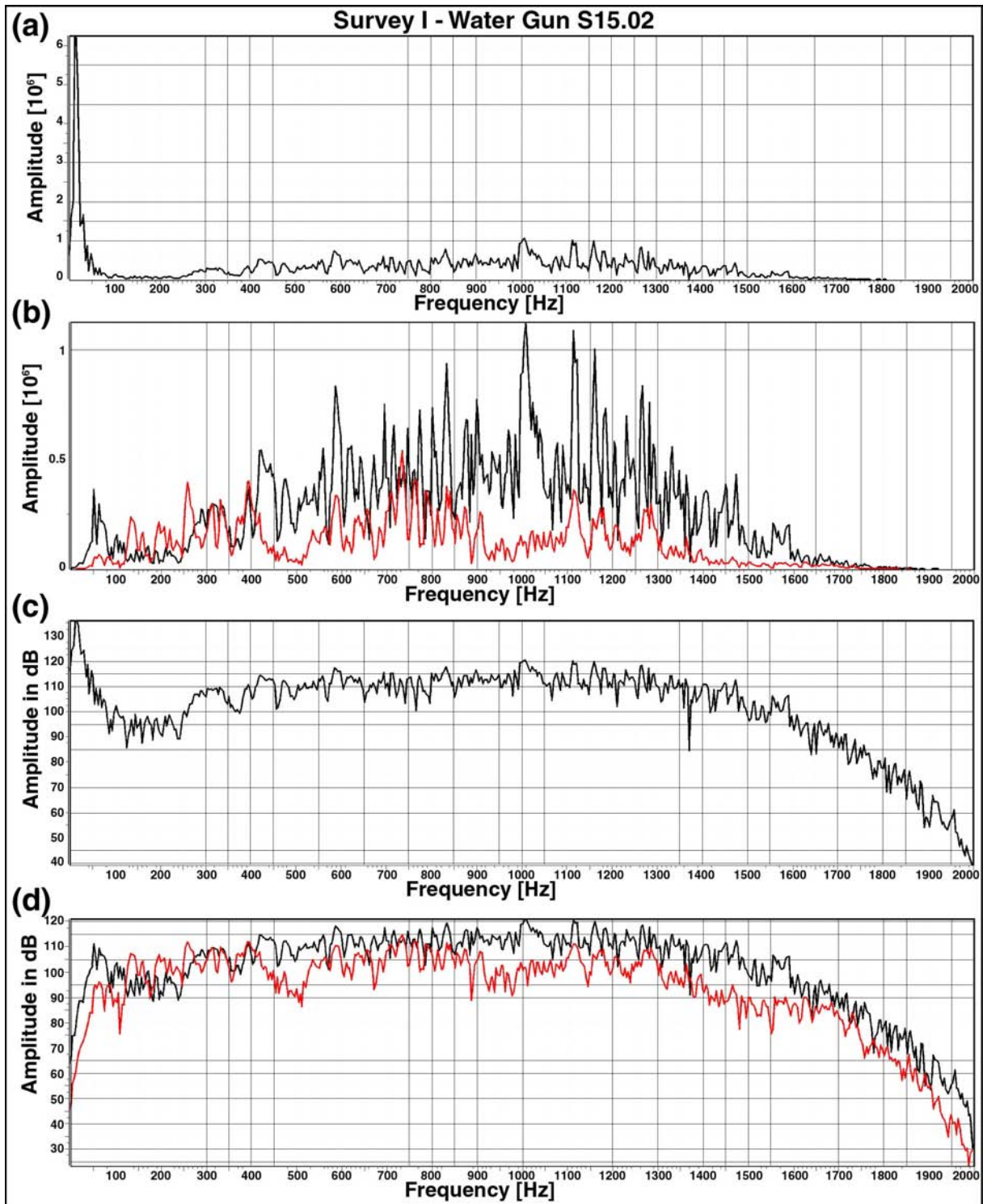


Fig. 6-10. Frequency spectra of Survey I (S15.02 Water Gun) calculated on the entire trace from 250-470 ms at offset 7.5 m (black) and at offset 120 m (red), displayed in absolute amplitude (a), (b) and linear dB (c), (d). In (b) and (d) a low cut filter had been applied cutting off frequencies below 40 Hz and attenuating those between 40 and 60 Hz.

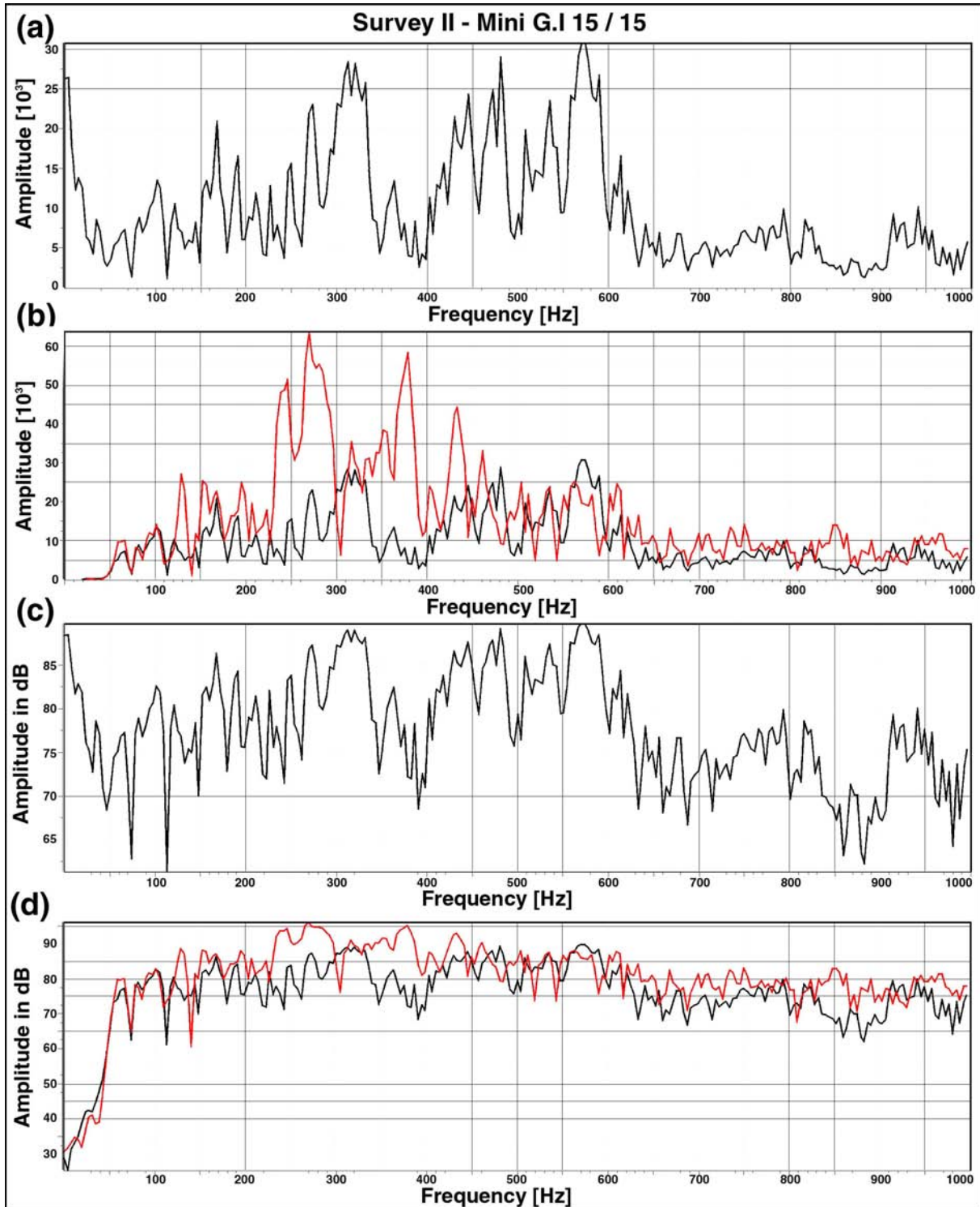


Fig. 6-11. Frequency spectra of Survey II (Mini G.I G15 / I15) calculated on the entire trace from 250-470 ms at offset 7.5 m (black) and at offset 60 m (red), displayed in absolute amplitude (a), (b) and linear dB (c), (d). In (b) and (d) a low cut filter had been applied cutting off frequencies below 40 Hz and attenuating those between 40 and 60 Hz.

At the beginning, the filtered and amplitude recovered data were NMO corrected by using the initial stacking velocity field (job *stacki*, step 8A), then DMO corrected and stacked. This stack is used on the one hand to get a first impression of stacking quality, and on the

other to pick a water bottom library, which will be applied in the DMO process before final stack to mute the noise above the water bottom reflection. After stack, the water bottom library is used to remute the noise in the water column and to delete the multiples at twice the water bottom arrival time (job *stackmute*, step 8). Amplitudes of all traces are then brought up to the same mean for better display. As shown in Fig. 6-12 and Fig. 6-13, a final stack with zero-dip velocities and an accurate mute library was run using input data without (a) and with (b) bin harmonization (jobs *stacknohabin* and *stack*, step 8B and 8). In-line 102 was chosen for this purpose since the fold distribution maps without flex binning of Fig. 6-4 and Fig. 6-5 both exhibit several bins with no coverage at all. For Survey II, this in-line together with in-line 51 even represent the worst case scenario. Comparing the non-harmonized stacks to the fold distribution maps, we see the relationship between low fold or no fold bins on LINE 102 and DMO artifacts indicated by arrows in (a). With bin harmonization those artifacts almost completely disappear.

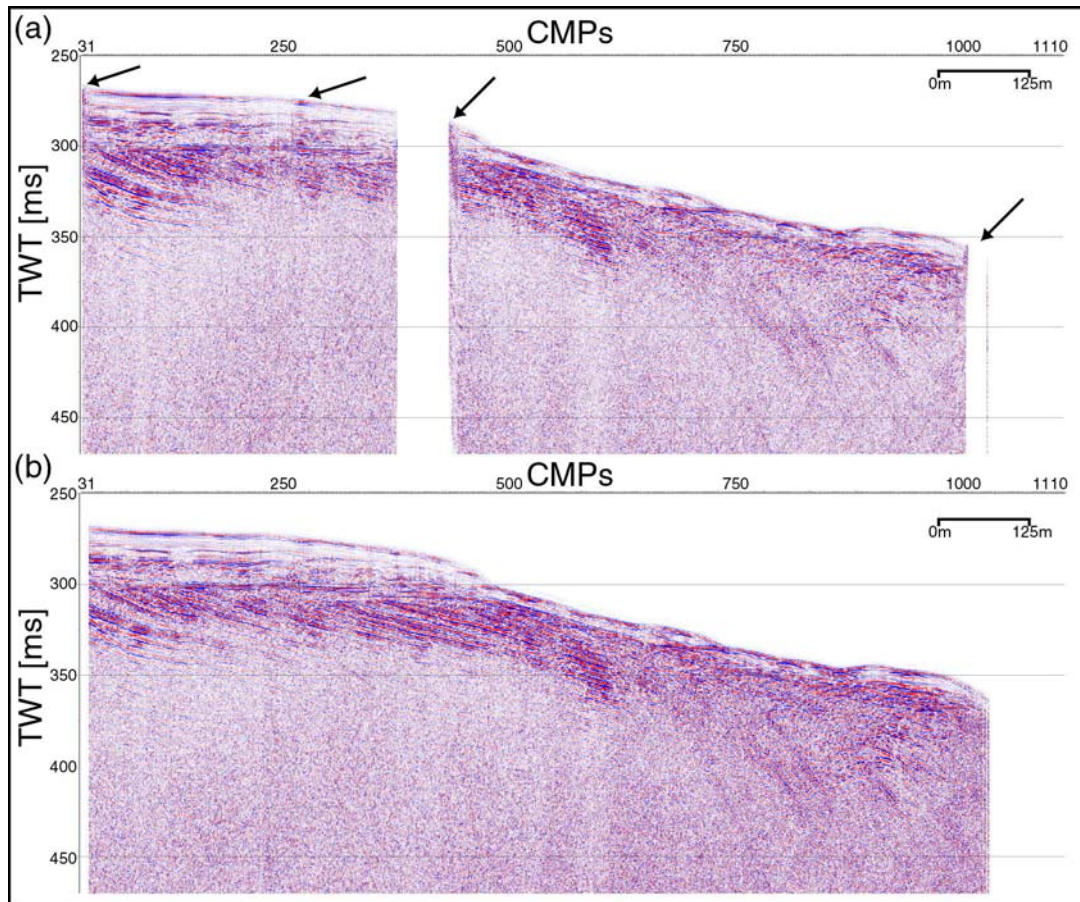


Fig. 6-12. Final stacked section of LINE 102 of Survey I using the zero-dip velocity model and an accurate mute library (a) without and (b) with harmonized bins on input. Arrows indicate DMO artifacts due to a lack of coverage.

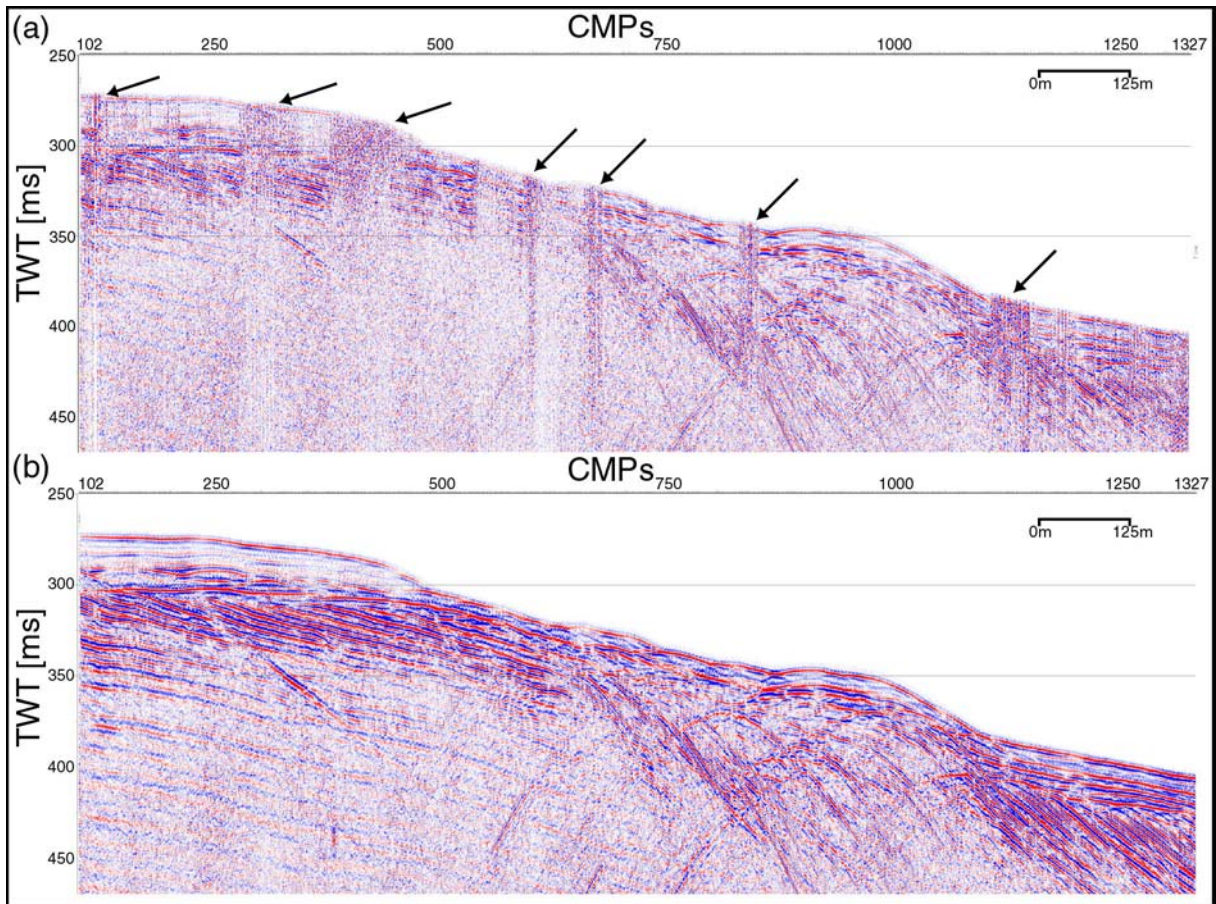


Fig. 6-13. Final stacked section of LINE 102 of Survey II using the zero-dip velocity model and an accurate mute library (a) without and (b) with harmonized bins on input. Arrows indicate DMO artifacts due to a lack of coverage.

6.8 Post-stack time migration (processing step 9)

Post-stack time migration in two dimensions worked well with *Géovecteur* (see section 4.3) on lines 140_30 and 140_15. Nevertheless, the module that performs time migration (GTMIG or GTMIP) in three dimensions is limited to input data sampled at intervals of integer values only. A resampling of our data to 1 ms is out of the question since we would lose all frequencies above 500 Hz. Especially for the data of Survey I, this would destroy the high-resolution aspect of this work. An alternative solution around the problem was to make *Géovecteur* “believe” that the data were sampled at 1-ms intervals. However, instead of actually resampling the data by selecting every fourth (Survey I) or every second (Survey II) sample, all samples are kept while changing the header words (corresponding to sampling interval and trace length) as well as the velocity model and the used frequency range accordingly. As a consequence, the new sampling interval of 1 ms requires trace lengths that are four times (Survey I) or twice (Survey II) as long as the original one. The following table lists the three header words that had to be changed before migration (job *migrphase1*, step 9).

WORD	Content	Survey I	Survey II	for Migration
1	Time of the last non zero sample [ms]	499	999	1000
9	Sample interval [microseconds]	250	500	1000
10	Trace length [ms]	500	1000	2000

Given that the velocity model from DMO velocity analysis in section 6.6 was picked on dip corrected data, it is suitable for post-stack migration as well. Since keeping the number of total samples while increasing the trace length changes all dips in the stacked section by the same factor as the increase in trace length, velocities in the velocity library have to be divided by this factor, whereas corresponding times have to be multiplied by it (job *librimod*, step 9).

GTMIP works in combination with the input module INMIG and the output module OUMIG in a job series of four phases. In phase one (job *migrphase1*, step 9), INMIG creates a 3-D frequency volume, whose frequencies are reduced by the same factor as the velocities, and in phase two (job *migrphase2*, step 9), it creates a 3-D velocity volume interpolated from the velocity functions at time intervals τ . Phase three (job *migrphase3*, step 9) carries out the actual 3-D one-pass phase-shift time migration after stack using a wave equation in the frequency-space domain (f, x, y) where τ represents the extrapolation step of the wave field. The larger τ is, the more accurate calculations are but the longer will take the migration process. For a τ set to 24 ms, this third migration phase ran between 5 and 6 hours for each survey. In order to reduce edge effects during the migration process, the data were padded with additional traces at all sides of the survey area. By running several tests with different numbers of padded traces, good migration results were obtained with a pad of more than 25 traces. For the final migration, 30 CMPs were added to the beginning and end of each LINE and 30 LINES to each side of all cross-lines. It is important that the velocity model is extended to match this padding of the input data. During phase four (job *migrphase4*, step 9) the resulting frequency volume planes are transposed again into a volume of traces, the header words 1, 9, and 10 are changed back to their original values and the LINE numbers for Survey I are reassigned to match those of Survey II (see Table 6-B).

The time migrated data cubes (see Fig. 7-2 and Fig. 7-3) present the final result of this processing sequence. A mute of multiples and noise in the water column was reapplied after creation of a new water bottom library on the migrated data with correct reflector geometry (job *migrmute*, step 9). Differences in line navigation and positioning or small errors in arrival time delay correction may be the cause for a small constant shift of 2 ms between the migrated water bottom of Survey I with respect to that of Survey II. Ideally, at least one calibration point would be needed for each survey, where water depth is precisely known. The depth and coordinates of this point could help to determine the arrival time delay with greater precision. However, accuracy is limited to the sampling rate and to possible variations in water velocity. At a water velocity of 1450 m/s and a sampling interval of 0.5 ms, any depth variations of more than 40 cm can not be accounted for. With respect to these considerations, the 2 ms time shift, which corresponds to a distance of 1.5 m in water, already proves a

remarkable correspondence of two 3-D seismic data cubes measured over the exact same area but two years apart.

After shifting the data of Survey II 2 ms up, amplitudes of all traces were scaled to the same mean for better display (job *migrmute*, step 9) – no AGC had been used during the whole processing sequence – and the data can now be output in SEG-Y format and read into any interpretation software (job *segout3DTKS*, Table A-18 and Table A-20). An interpretation of the high quality data cubes will be shown in section 7.3. Since interpretation is preferable on depth migrated data and because it is uncertain whether the algorithms offered by Géovecteur can cope with the high-resolution sampling intervals, a prestack depth migration code (Thierry et al., 1999), which is adaptable to all types of input data, was tested on our data and will be described in section 7.2.

6.9 Suggestions for further processing

Based on the experience with both 3-D data sets, some suggestions can be made for further improving the above processing flow. Given that Géovecteur will be used as the processing software for high-resolution data sampled at intervals below 1 ms, which is an issue to reevaluate, it would be preferable to multiply all positioning information (from UKOOA P1/90 file) by a factor of 100 in order to keep the decimals of the navigation data in the trace headers (see beginning of this chapter). As a consequence, all subsequently calculated distances, such as offset, bin dimensions, etc., would change as well and the whole processing sequence following the data and navigation merge has to be adapted accordingly. As done for the post-stack migration in section 6.8, the time sampling interval should be changed to 1 ms or more. The best solution would be to multiply sampling interval and trace length by the same factor of 100, which keeps the velocities at their original values. With a sampling interval larger or equal to 1 ms, semblance computations during velocity analysis can be made at a sufficiently high density (see section 6.6) and velocities can be determined with a greater precision, which is needed for shallow seismic data. In theory, these suggestions may seem rather easy to implement, but great care has to be taken with respect to every algorithm used and default parameters set in it, when redimensioning offset and time axes, since this might change velocities, frequencies or dips.

The despiking job, described in section 6.4, will find and eliminate short energy bursts from otherwise normal traces. In order to account for a lack of sensitivity of certain hydrophones in a shot gather, a job needs to be composed that will scale the mean of these traces to an average mean of the others at the same offset before stack. A detailed velocity analysis on the data of Survey II will allow comparison of semblance spectra and might extend the velocity model to greater depths.

Other processing steps not yet included in the described flow might further improve data quality, such as deconvolution and multiple removal. Tests on spiking deconvolution

showed that without the integration of the source signature, the resulting deconvolved traces have a less good quality than the original ones. Predictive deconvolution did not produce satisfactory results either. Anyhow, the lack of moveout in both of our systems will make the reduction of strong multiple energy very difficult. F-k filtering of coherent noise coming from other ships on the lake has been applied as part of the preprocessing prior to prestack depth migration (see section 7.2) and might as well be beneficial to the conventional processing flow.

Although there still is some work to be done to find the ideal processing sequence for both data cubes, the results presented in this and the following chapter already show the exceptionally good data quality that could be achieved thanks to the design of the developed acquisition system and the data processing that was subsequently applied.

CHAPTER 7: RESULTS AND DATA EXAMPLES

As stated at the end of the last chapter, time migration indicates the final stage of the processing sequence that was intended to be applied in the course of this project. After having assigned geometry to a common grid (section 6.4), LINE (in-lines) and CMP (cross-lines) numbers range from 40-198 and 31-1112 for Survey I and from 29-210 and 102-1328 for Survey II, respectively. The exact position of the data limits of both surveys can be found in Fig. 7-1, superimposed on the interpreted map of Fig. 4-9. The location of the fault zone as deduced from Survey II (see section 7.3) is added to the results of all previous 2-D studies.

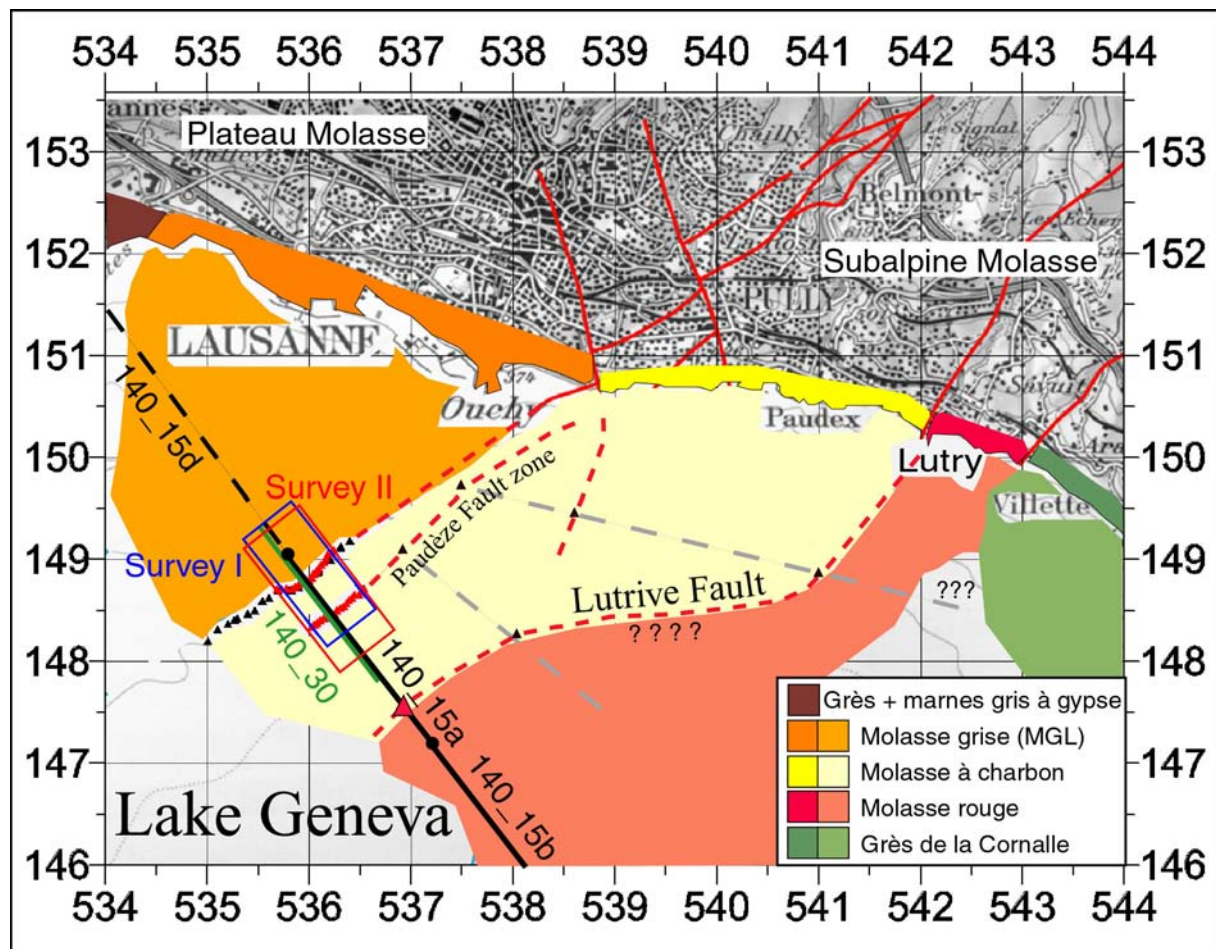


Fig. 7-1. Interpretation of fault locations from 2-D and 3-D surveys and inferred lithostratigraphy (see Fig. 4-9). Black triangles indicate fault positions interpreted by Morend (2000) and Chaudhary et al. (2002) (dashed grey profiles). Small red triangles mark the limit of the Paudèze Fault zone as interpreted from Survey II while the large red triangle designates the position of the Lutrive Fault as deduced from profile 140_15a (Fig. 4-7).

Fig. 7-2 and Fig. 7-3 show three dimensional representations of the final two data cubes which are oriented northwest to southeast. To visualize the data in all directions, three time slices (constant time), three in-lines (constant LINE number) and four cross-lines (constant CMP number) were extracted and the water layer cut away. In Survey I, recorded traces had a

length of only 512 ms and the subsequent arrival time correction eliminated another 25 ms, thus, both cubes are represented by 470 ms for comparison. Data have a vertical exaggeration of 2 when using an average velocity of 2300 m/s.

Although both cubes show excellent data quality, even at this small scale, they exhibit striking differences in vertical resolution, signal penetration and fold distribution at the survey boundaries. In section 7.1, these differences will be presented in more detail. Because it is preferable to use prestack depth migrated over post-stack migrated data for subsequent interpretation, section 7.2 introduces some examples from tests using a prestack depth migration code (Thierry et al., 1999) that was applied to the data of Survey II in collaboration with Philippe Thierry at the Ecole des Mines, Fontainebleau, France. Preliminary results already show further improvement in the final interpretable image. At the end of this chapter (section 7.3), a detailed analysis of the time migrated data of Survey II gives an idea of the spectacular potential this excellent data set offers for complex geologic and tectonic interpretation in three dimensions. Visualization of various structural surfaces with respect to each other allow an estimation of the possible accuracy of future high-resolution 3-D surveys in lacustrine settings.

7.1 Comparison of survey results

7.1.1 Penetration Depth

Fig. 7-4 presents in-line 182 over almost the complete northwest - southeast extent of the 3-D survey area down to the maximum recorded time of Survey I after migration. When comparing this extracted seismic section with 2-D profile 140_15 in Fig. 4-7, the following large-scale geological units can be recognized: the continuous beds of the Plateau Molasse in the northwest, the Paudèze Fault that separates Plateau from Subalpine Molasse and the fault zone of fractured Subalpine Molasse to the southeast; the erosional surface of the molasse is covered by glacial and post-glacial sediments. This example in-line illustrates the difference in signal penetration between the water gun of Survey I in (a) and the air gun of Survey II in (b). While reflections within the Plateau Molasse are visible even beyond 470 ms in (b), the signal-to-noise ratio in (a) is sufficient only until 430 ms. Similarly, reflections within the fault zone are much stronger in (b), although the 3-D migration worked less well and left numerous artifacts at the discontinuity between the steeply dipping Subalpine Molasse fractures and the overlying glacial sediments. Data quality should be compared again when a velocity model has been determined directly with the data of Survey II.

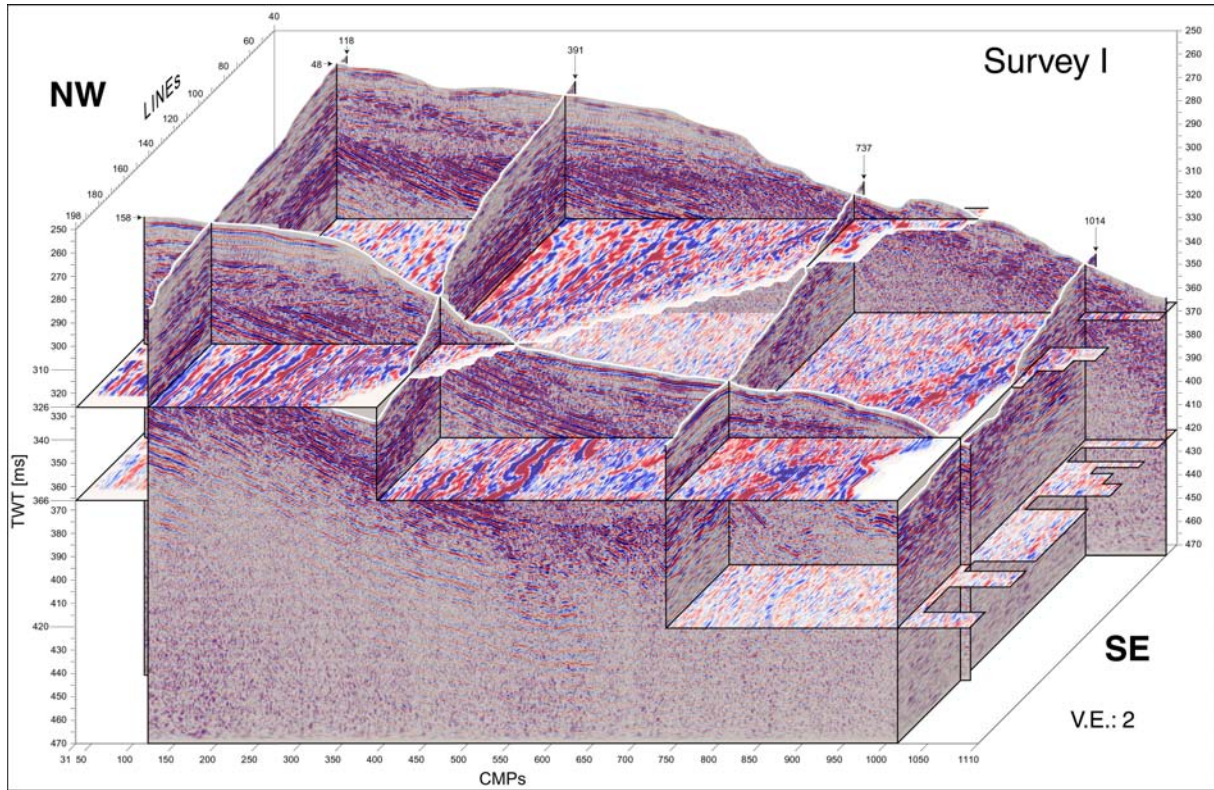


Fig. 7-2. 3-D time migrated data cube of Survey I with several in-lines, cross-lines and times slices exposed. Vertical exaggeration 2.

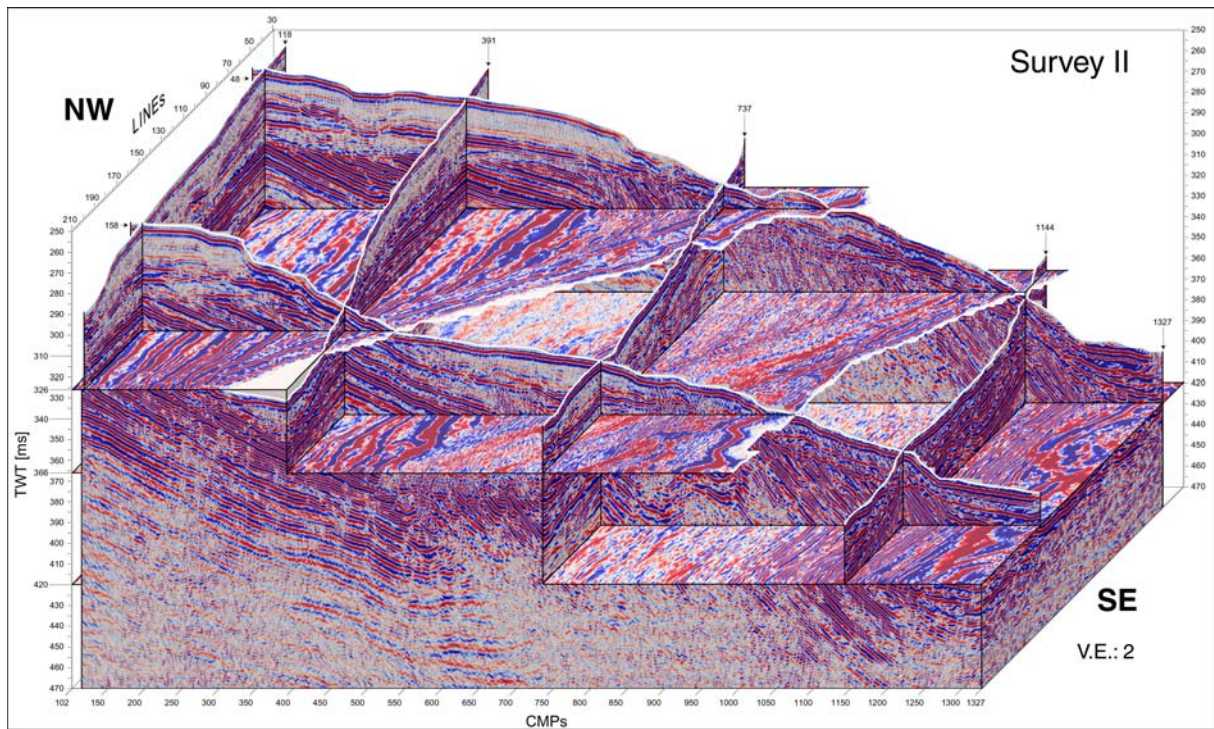


Fig. 7-3. 3-D time migrated data cube of Survey II with several in-lines, cross-lines and times slices exposed. Vertical exaggeration 2.

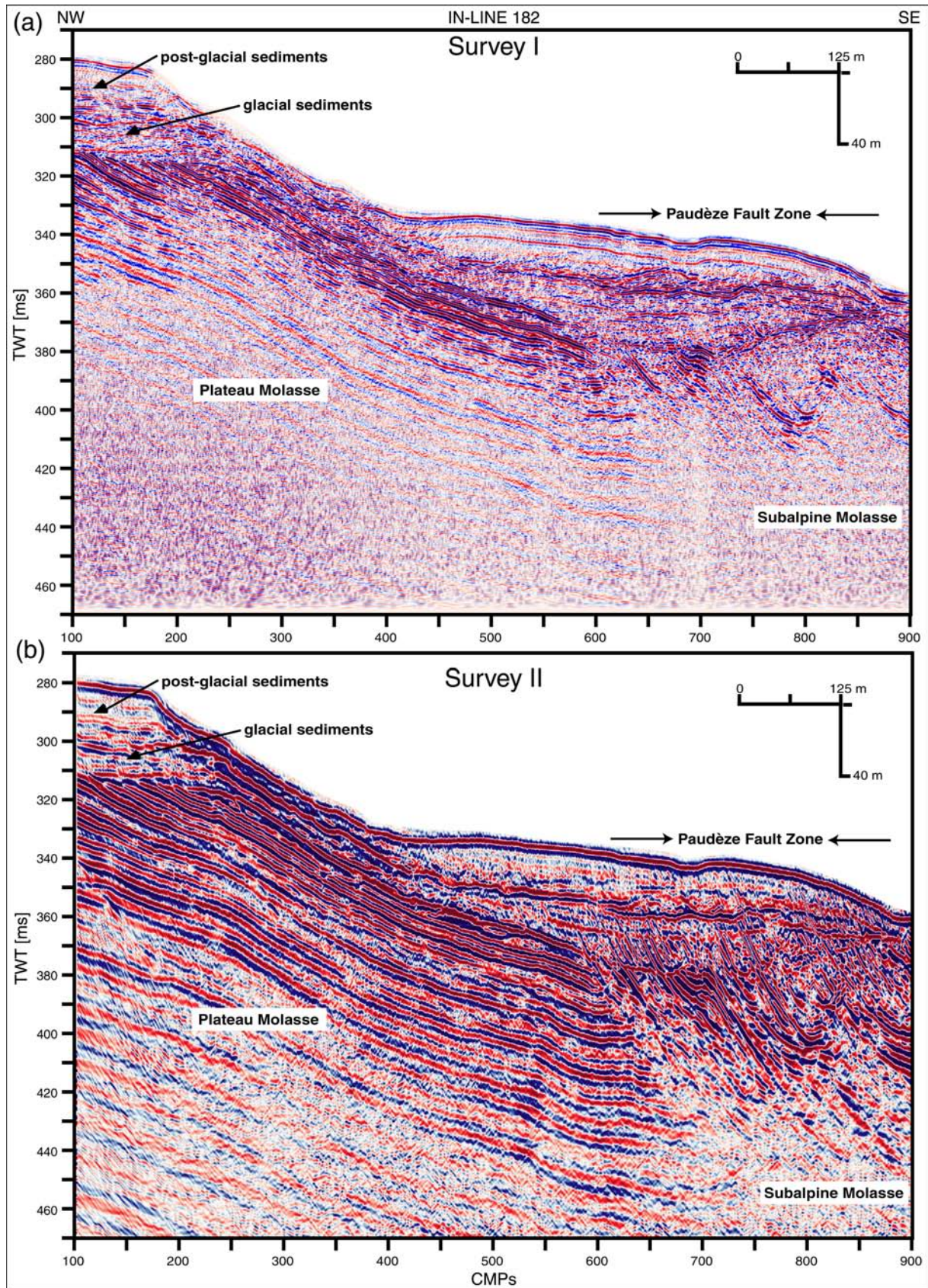


Fig. 7-4. In-line 182 presents an example of penetration depth difference between (a) the S15 Water Gun (reflections in the Plateau Molasse beds down to 430 ms (~350 m)) and (b) the Mini G.I G15 / I15 Air Gun with reflections deeper than 500 ms (>430 m).

7.1.2 Vertical Resolution

The vertical resolution that can be achieved with the water gun (2-D profiles - section 4.3.3.1 - Survey I) is about twice as good as that of the Mini G.I G15 / I15 (Table 4-A). Within the Quaternary sediments, a theoretical resolution of 60 cm might be possible. Fig. 7-5 focuses on the glacial and post-glacial sediments that cover the Plateau Molasse in the northwest portion of the survey area (in-line 96). Fig. 7-5 (a) presents the water gun data of Survey I and Fig. 7-5 (b) the air gun data of Survey II. The higher vertical resolution in (a) is evident, especially in the Quaternary sediments and at the angular unconformity along the erosional surface of the Plateau Molasse. However, reflectors seem more discontinuous and difficult to trace, while in (b) a bright reflector separates low-amplitude post-glacial from higher amplitude glacial sediments. This interface is much less prominent in (a).

Another example of an imaging difference is illustrated by a smaller thrust fault within the Plateau Molasse beds. This fault is more difficult to detect in (a), whereas its location and even displacement direction (inverse) can be easily determined in (b). This is a surprising phenomenon. One possible explanation could be the inferior signal-to-noise level of the Survey I data knowing the fact that the air gun of Survey II releases a higher energy signal (see signature tests in 3.4.6). Aliasing during 3-D migration due to higher frequencies in the signal in areas of steeply dipping fractures could be another. Occasionally, fault planes generate reflections themselves. In the lower portion of Fig. 7-5 (b), between 310 and 360 ms, such fault plane reflections are visible. The much shorter wavelengths of the water gun signal (~3.4 m in the molasse) might see the fault plane as a variable reflector while for the longer wavelengths of the air gun signal (~7 m) it presents a homogeneous surface. A similar explanation might work for the shallower portion of the fault where reflectors seem well displaced in (b) but only more discontinuous in (a). The greater variability in geological structure that the higher resolution source resolves, can make it more difficult to interpret a level of structural continuity that we are often looking for.

Another example of the difference in continuity of reflectors encountered when comparing both surveys is given in Fig. 7-6 on a set of two time slices, the first at 310 ms and the second at 340 ms. The slice at 310 ms cuts through the upper portion of the Plateau Molasse just below its erosional surface and exhibits glacial and post-glacial sediments close to the water bottom. Reflectors in (b) seem extremely continuous and make it easy to determine the interface between the molasse and Quaternary sediments. This is not the case in (a). Slice two at 340 ms is deep enough to cut through the Paudèze Fault zone on the northeastern half of the cube (LINEs 29-110) where the Plateau is juxtaposed against Subalpine Molasse. Although not simple, it is possible to delineate the fault trace on the data of Survey II, indicated by a white dashed line on (d). The reflectors of the Plateau Molasse can be distinguished from those of the Subalpine Molasse by their different seismic facies. Due to their steeper dip, beds in the Subalpine Molasse appear at a higher frequency than the

gently dipping Plateau Molasse beds. On the corresponding slice in (c), these variations cannot be detected for two reasons: (1) because of the smaller signal penetration of the water gun (compare the amplitude level at 340 ms from Fig. 7-4 with Fig. 7-5) and (2) because of the generally smaller reflector continuity and the larger cross-line spacing.

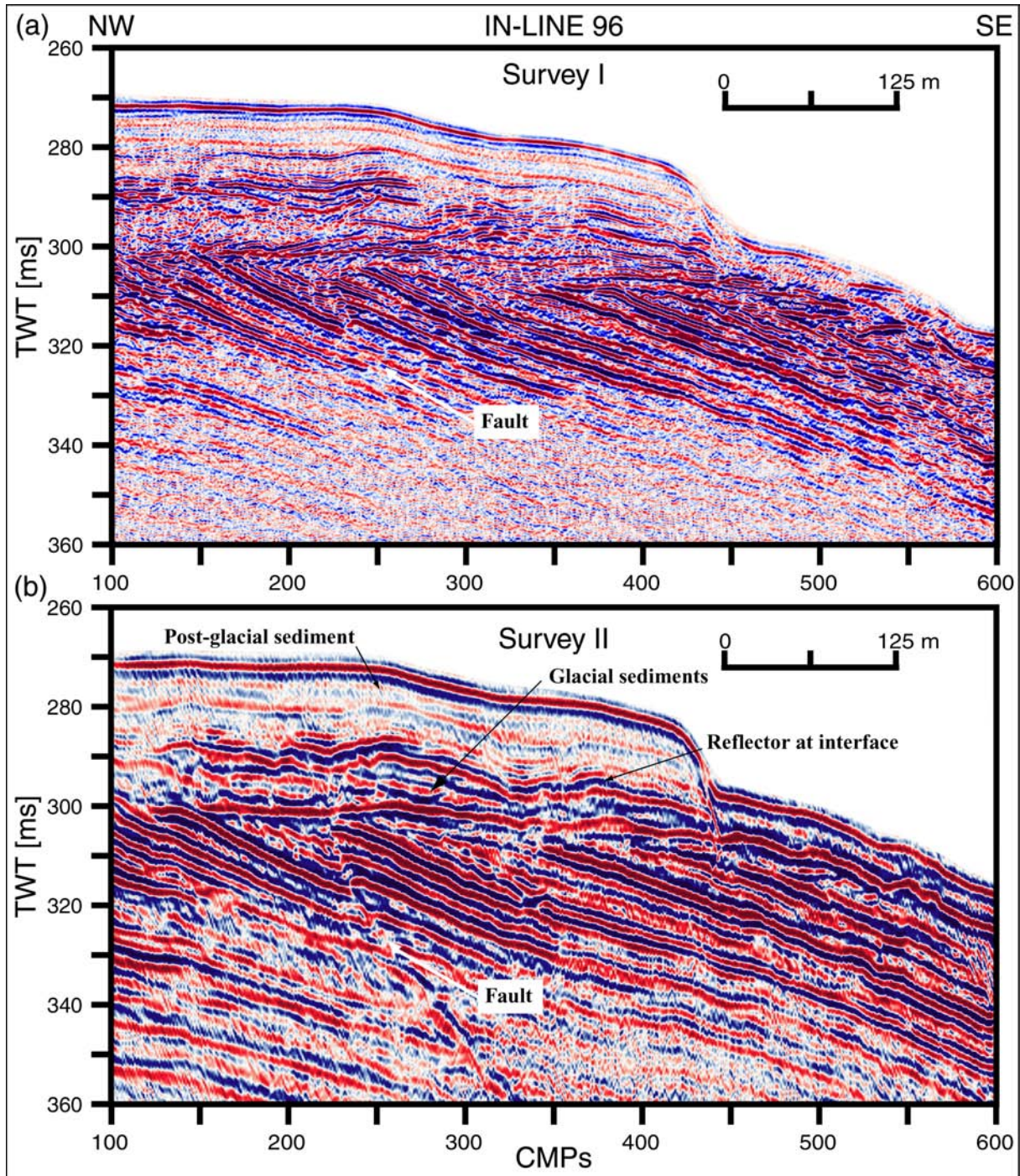


Fig. 7-5. In-line 96 shows an example of vertical resolution difference. Although the vertical resolution within the sediments for Survey I (a) is better than that for Survey II (b), the S15 Water Gun was not sufficiently energetic to clearly image the small thrust fault within the Plateau Molasse which is revealed by the Mini G.I G15 / I15.

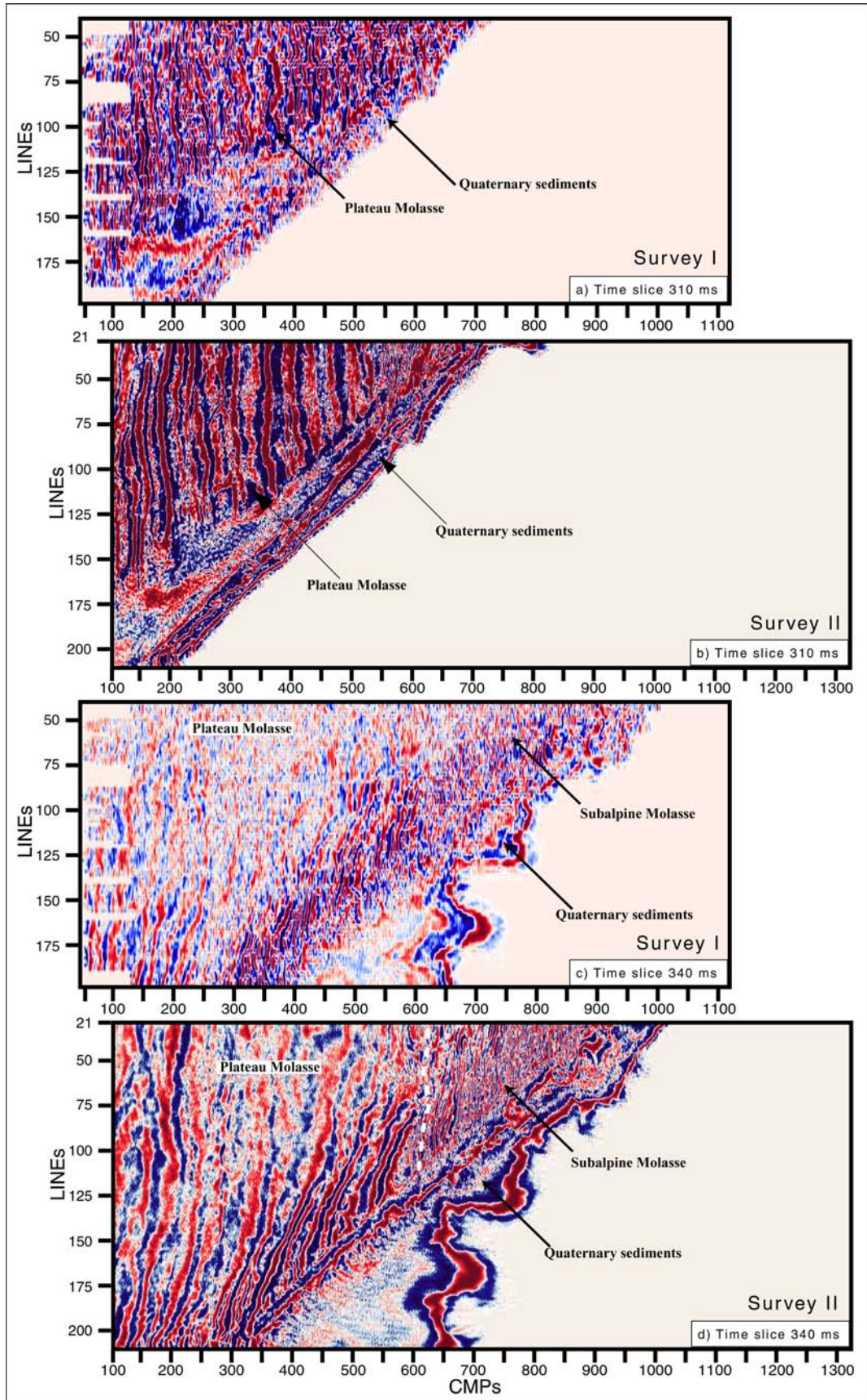


Fig. 7-6. Time slices at 310 ms (a) and (b) and 340 ms (c) and (d) for Survey I and Survey II, respectively. The white dashed line in (d) indicates interpreted Paudèze Fault trace.

This is an illustration that a seismic source should always be adapted to the main objective of the work. Is it more important to detect detailed structural variations in shallow beds or to delineate discontinuities of larger scale that bound different geological units over a more extended depth range? If the budget allows, the best solution of course would be to perform a higher AND lower resolution survey on the same site. As the data examples demonstrate, the system developed here with accurate positioning allows such repetition of measurements.

7.1.3 Horizontal Resolution

Theoretically, migration can shorten the Fresnel zone down to the dominant wavelength assuming perfect sampling, i.e. a continuous wavefield. When sampling takes place, the integrands of the migration formulas are sampled. If this sampling is not rapid enough (aliased), resolution will suffer (Vermeer, 2002). Consequently, the effective horizontal resolution of the migrated data depends upon two different factors: the dominant frequency of the reflected seismic signal and the spatial sampling or bin size.

The shallowest reflection in the data cubes is that of the water bottom at a velocity of 1450 m/s. For this reflection, the dominant wavelength amounts to 2.2 m when using the water gun (Survey I) and to 4.4 m when using the Mini G.I G15 / I15. These values correspond to the theoretically possible horizontal resolution in in-line direction. In cross-line direction, however, the bin dimension of Survey I is larger than the dominant wavelength resulting in a resolution that can not be better than 7.5 m while it still is 4.4 m for Survey II. Hence the resolution along cross-lines is higher than for Survey I, despite the fact that a source of lower dominant frequency was used.

Obviously, a resolution of 7.5 m is not sufficient to resolve the topographic detail of the water bottom reflection within the survey area. Fig. 7-7 (a) shows the water bottom reflector as it was picked on the data of Survey II. The red rectangle on the shown surface outlines an area of highly variable topographic relief at the location where the slope of the lake bottom changes. In this area, a channel less than 70 m wide and 10 m deep (red arrow points to its center) was carved into the post-glacial sediments (Fig. 7-8). This channel is visible between LINE 68 and 82 where its southeastern edge disappears and merges with the steep slope. As an example, Fig. 7-8 presents in-line 74 (location indicated at 250 ms in Fig. 7-7) which crosses this channel at about CMP 500 (Fig. 7-8 (b)). Yet, on the data of Survey I (Fig. 7-8 (a)), the channel is not visible at all. This phenomenon appears over the complete range of LINES within the marked area, as well in many other locations of extremely complex bathymetry.

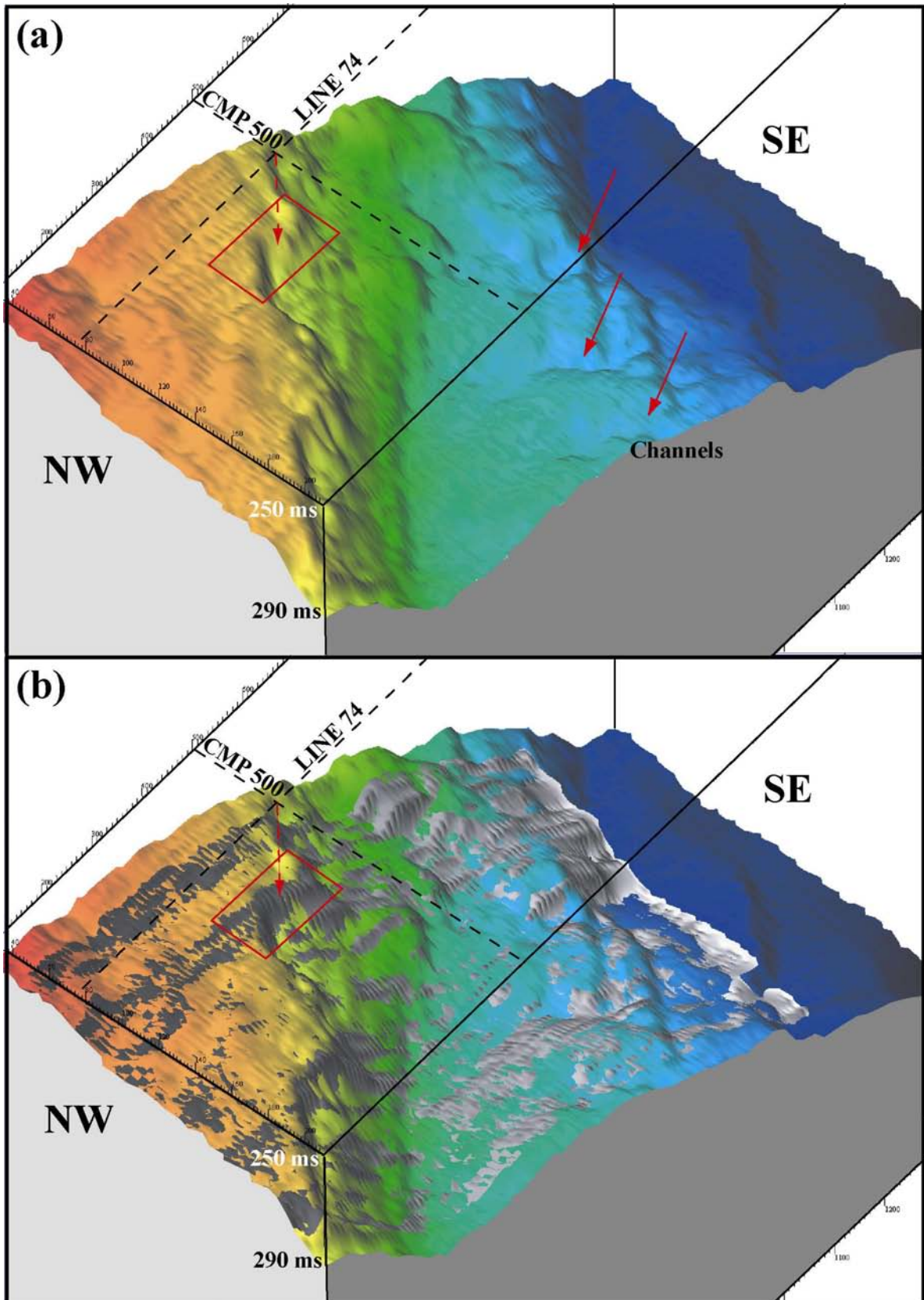


Fig. 7-7. The water bottom picked from the time migrated data of Survey II (a). The water bottom from Survey I (grey) is superimposed on the water bottom of (a) where it was picked at shallower depths and at less detail (b) than in Survey II. Location of LINE 74 (Fig. 7-8) and position of the trough centered about CMP 500 is indicated by the arrow and red rectangle.

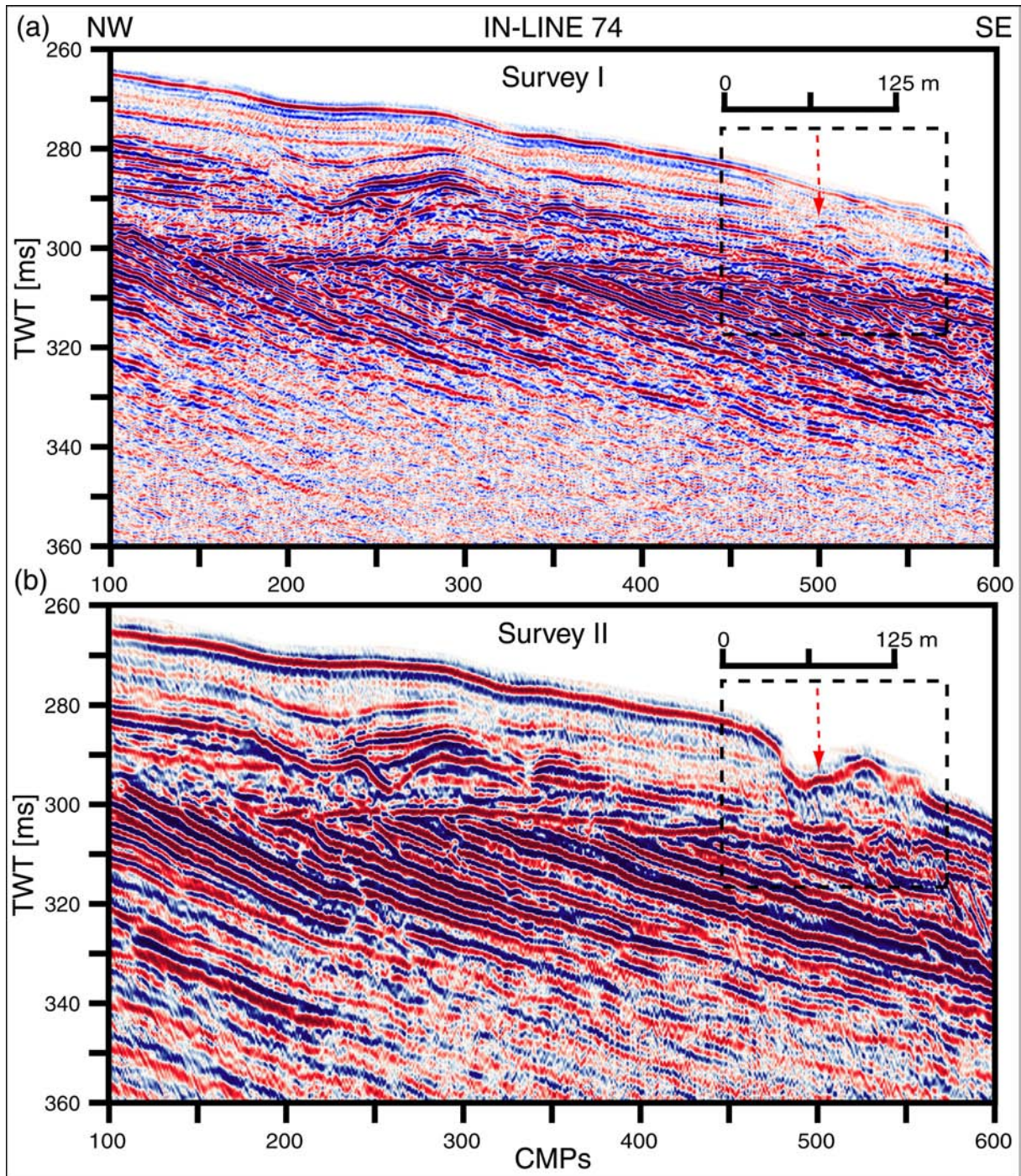


Fig. 7-8. In-line 74 presents an example of horizontal resolution – the dashed rectangle frames an area with a channel that was not resolved during Survey I (a) but is visible in the data of Survey II (b). The location of LINE 74, the red arrow and the zone of the rectangle is indicated in Fig. 7-7.

In Fig. 7-7 (b), the water bottom arrival times (grey) picked from the time migrated data of Survey I were superimposed upon those shown in (a), when they arrive earlier than those picked from the data of Survey II. Some of the small depressions, troughs and channels visible in (a) are filled and could not be imaged. The interpretation of the water bottom from data of Survey I seems as if bathymetry had been filtered and large slopes had been smoothed.

This demonstrates the observed decrease in horizontal resolution. The reason is insufficient lateral sampling for 3-D migration combined with navigation inaccuracies that result in uneven bin coverage. So what happens? First of all, the marked channel on Fig. 7-7 (a) was imaged on 16 in-lines during Survey II, which correspond to only 8 in-lines for Survey I. Because the channel is located on a steep slope, its reflections were originally recorded on in-lines further downdip, i.e. at greater LINE numbers. When looking at the stacked data, the channel is visible between LINEs 75 and 89 for BOTH surveys. During 3-D migration of data cube II, the channel was then shifted updip to LINEs 68 through 82 while it disappeared in data cube I.

For Survey I, however, half of the in-lines have empty bins at the location of the channel before bin harmonization and data had to be duplicated from adjacent cross-line bins. This is one reason for the observed smoothing effect. Nevertheless, bow-ties, the typical appearance for a buried focus on a seismic record section, appear on the stacked data where bins are filled. The Fresnel zone diameter of 30-43 m before migration (see Table 5-A and Table 5-B) is thus sufficiently small to detect the 70 m wide channel. But, in the course of the one-pass 3-D migration algorithm, it is the spatial sampling in the cross-line direction that influences the accuracy of the migration process each time the structures have larger dip and vary not only in-line but cross-line as well. This way it is impossible for the 3-D extrapolation operator to properly migrate the available, rapidly changing information in the cross-line direction independently for each downward-continuation step (Yilmaz, 2001). Because sampling is a way of approximating the migration integration formulas, invalid migration results are obtained as soon as the integrand in those formulas varies more rapidly than sampling can follow, thus, the data are aliased along the migration paths (Vermeer, 2002). In other words, sampling should be dense enough to allow accurate evaluation of the integrals involved in migration.

7.1.3.1 Navigation effects

This difference in horizontal resolution between both surveys is also observed in the definition of the water bottom reflection and supposedly of many other horizons. Whereas in Survey II the water bottom is marked by a strong continuous reflection, in Survey I it is much less pronounced and not always easy to identify because of ambiguous reflections. This is why detecting the water bottom becomes more difficult. As an example, Fig. 7-9 shows a zoom on a portion of the 3-D migrated in-line 58 for Survey I in (a) and for Survey II in (b). While the water bottom can be easily traced in (b), there is a second reflection of similar amplitude in (a) that arrives earlier than the real water bottom reflection (yellow dashed line). Without the aid of the data from Survey II, it would be almost impossible to pick the correct horizon. To better interpret the water bottom in Survey I, the picking results of Survey II were projected onto the data of Survey I. After identification of the correct horizon, its reflector

was traced across the whole survey area, resulting in the bathymetry presented in Fig. 7-7 (b). The remaining erroneous energy in the water layer was muted for subsequent data presentation.

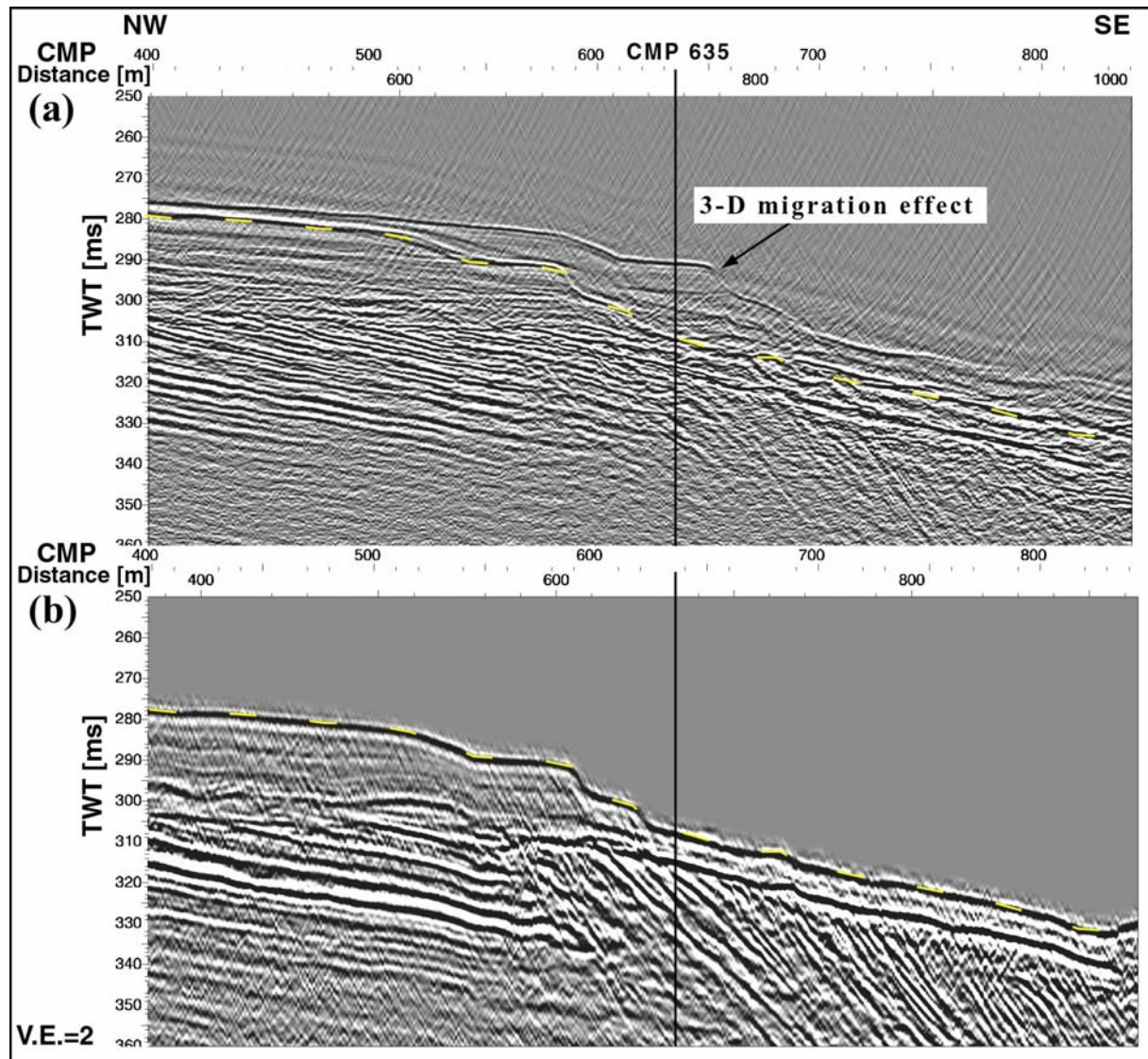


Fig. 7-9. Zoom on a portion of 3-D time migrated LINE 58 (a) extracted from the data cube of Survey I and (b) from that of Survey II. The water bottom reflection picked in (b) was projected onto the section in (a). The true water bottom is indistinguishable from the earlier reflection energy due to incorrect 3-D migration. The black line indicates the location of cross-line 635 of Fig. 7-10.

This additional reflection in the water layer is also observed on some of the stacked in-lines prior to bin harmonization and thus cannot be entirely due to an effect of incorrect migration of lateral reflection energy onto a wrong LINE. It is more likely due to a combination of coarse sampling and insufficient accuracy in ship navigation and streamer positioning. As has been described in section 3.6, the control on ship navigation and shot triggering for Survey I was less accurate. Comparison of Fig. 5-3 and Fig. 5-6 demonstrates how much the positioning of the sail lines improved in Survey II thanks to the newly

developed navigation software. Because the only reference of the single-streamer configuration was the dGPS antenna on board, all receiver positions had to be derived relative to this reference during post-processing (section 6.3.2). Consequently, the error made by placing the reflection point of a trace into its corresponding correct bin is far greater for Survey I, especially because the streamer had double the offset. Therefore, the appearance of more than one water bottom reflection on the same in-line in areas of complex topography and steeper slopes is a result of incorrect binning. This problem is worsened by the frequent occurrence of data holes, the necessary trace duplication over a coarser cross-line spacing and finally by 3-D migration effects.

The effect of having false lateral energy migrated into a seismic section – whether through navigation errors or aliasing along the migration path as a consequence of too coarse spatial sampling - might severely degrade interpretation results. Whereas data quality in in-line direction, disregarding the additional reflection in the water, still seems fairly similar when comparing data of Survey I and II, in cross-line direction the influence of coarser spatial sampling becomes evident. Fig. 7-10 shows cross-line 635 whose location is indicated on Fig. 7-9. Besides the 3-D migration effect in the water (compare with in-line 58 in Fig. 7-9), the reflection of the water bottom in the data of Survey I (Fig. 7-10 (a)) is extremely discontinuous in the steeper northeastern portion. The overall continuous water bottom horizon interpreted in Survey II (Fig. 7-10 (b)) was transferred to the data of Survey I (yellow dashed line). Again, this interpretation would have been very difficult without the aid of the air gun data of Survey II.

Based on the experience of this work, it is recommended for future surveys over a similarly complex topographic relief to choose bin dimensions that are in any case smaller than the dominant wavelength of the selected signal at the shallowest target depth. Furthermore, the employment of the improved navigation software as well as the additional dGPS rafts along the single-streamer configuration is essential in avoiding positioning errors that result in degradation of data quality of the stacked and migrated results.

7.2 Preserved amplitude prestack depth migration

Prestack depth migration is a processing step usually devoted to “oil-industry targets” and has rarely been applied to high-resolution seismic data. As the target gets closer to the surface, data pre-processing becomes more and more difficult and final processing seldom goes further than DMO and post-stack time migration. Hence, only near-surface data of exceptionally high quality are suitable for the very sensitive prestack depth migration algorithm. While the data of Survey I were not considered appropriate for the reasons explained in the previous section, the data acquired during Survey II using the multi-streamer configuration, the air gun source and the newly developed navigation and positioning system have very promising initial conditions.

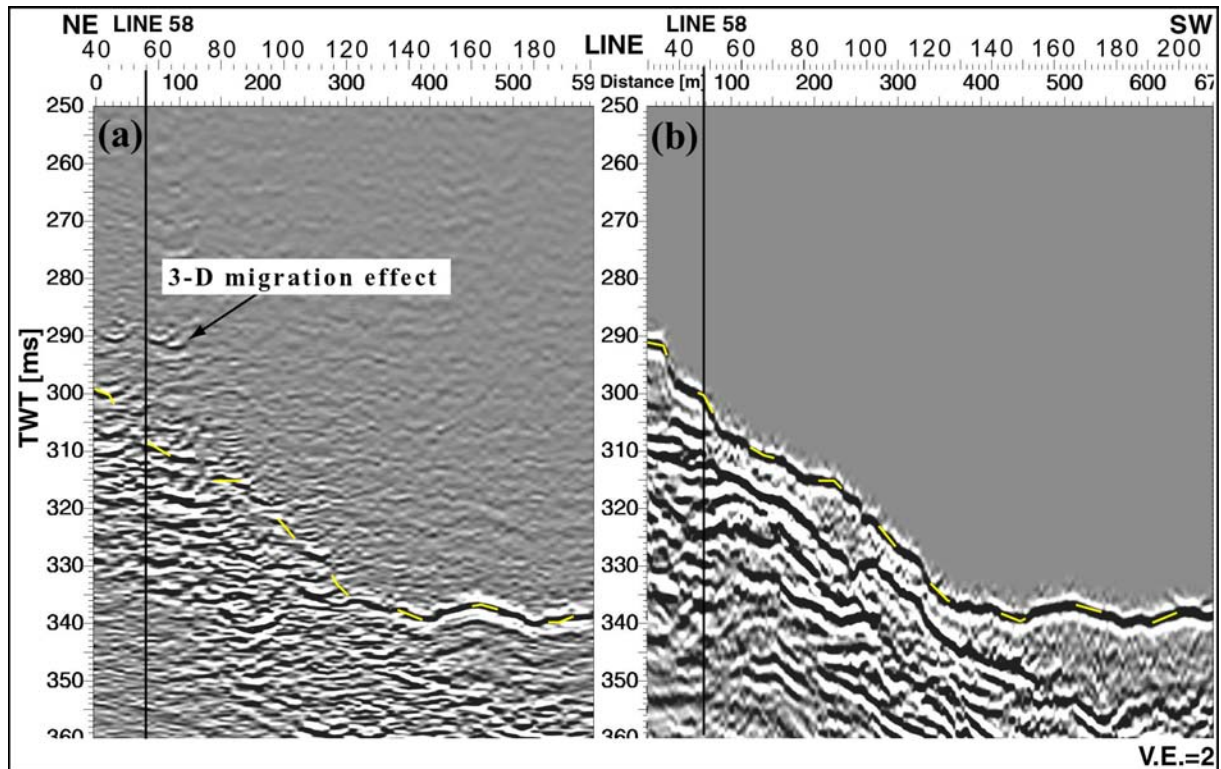


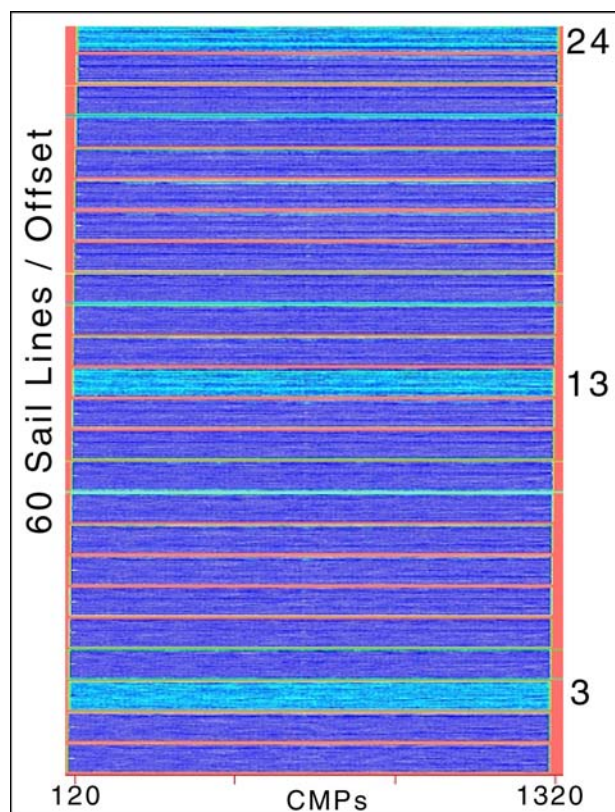
Fig. 7-10. 3-D time migrated cross-line 635 (a) from the data cube of Survey I and (b) from that of Survey II. The water bottom reflection picked in (b) was projected onto the section in (a) where the water bottom is discontinuous and difficult to identify due to coarser spatial sampling. Incorrectly migrated energy, as was recognized on LINE 58 in Fig. 7-9, appears over a range of about 30 in-lines. Black line indicates location of in-line 58 of Fig. 7-9.

A 3-D Preserved Amplitude Prestack Depth Migration code (PAPsDM) was developed by Thierry et al. (1999) at the Ecole des Mines de Paris. PAPsDM is an inversion method used in the oil industry for 3-D quantitative estimation of subsurface reflectivity (Baina et al., 2002). Using dynamic ray tracing to account for 3-D propagation effects within the migration kernel, PAPsDM requires prestack data without the amplitude corrections, which are commonly applied during time processing, and which damage raw amplitude variations. Three dimensional PAPsDM allows both structural imaging and a quantitative recovery of the reflectivity dedicated to amplitude versus angle (AVA) inversion. Because AVA inversion needs noise free inputs along the maximum available offset or angle range, it is normally not suitable for shallow seismics (short offset, noisy panels). Collaboration with Philippe Thierry made it possible to test the capacity of this 3-D imaging algorithm to handle the change of scales and the resulting damage to the reflected signal. However, it is important to keep in mind that due to the lack in appropriate hydrophone calibrations, real amplitude assumptions are not justified. For application to our very high-resolution 3-D data set, he adapted the algorithm, which is based on the Kirchhoff approximation for 3-D preserved amplitude prestack depth migration of seismic reflection data, to small sampling intervals and high frequencies.

With respect to the limited offset range and penetration depth of the multi-streamer VHR system, the lake bottom at about 200 m causes similar multiple problems as encountered by the oil industry in deep-water environments (lake bottom multiple occurs at >500 ms). The velocity model estimation, on the other hand, cannot be as precise as in the industry because the ratio between offset (62.5 m) and target depth (<400 m) is significantly reduced. This is why a simple down-scaling of the classical pre-processing technique is not straightforward. Due to this pre-processing stage, most of the shallow seismic data in complex geological settings are processed conventionally in time before and after stack using the CDP / LINE domain. Few examples prove that more sophisticated velocity estimation and migration methods can be used when the signal-to-noise ratio increases (Pasasa et al., 1998).

In comparison with other near surface seismic measurements, our lacustrine data set exhibits an exceptionally good signal-to-noise ratio, especially when compared to land shallow seismics (Steeple and Miller, 1998). Because a detailed velocity model could be obtained during conventional processing, the PAPsDM code was applied to study the possible benefits of prestack depth imaging in a VHR context within the favorable lacustrine environment studied here.

As a first step within the 3-D PAPsDM flowchart, an acquisition QC was performed with respect to the given target. For this purpose, trace density was calculated along all 60 sail lines



lines and for each of the 24 offset classes separately (Fig. 7-11). In confirmation with results of section 6.5, Survey II exhibits a very regular coverage for each individual offset range, except for those influenced by the anomalously weak or dead hydrophones identified in section 3.3.2. Offset class 3 contains weak trace 3 of the S/N streamer section, offset class 13, the dead hydrophone of ITI section #2 and offset class 24 the dead hydrophone of ITI section #1.

Fig. 7-11. Coverage for all 60 sail lines and each of the 24 offsets including the contribution of all three streamers of Survey II. Light blue indicates anomalously low coverage – those offsets contain weak or dead traces (trace 3 on S/N streamer section, trace 13 on ITI #2, and trace 24 on ITI #1, see section 3.3.2).

After checking the records that are supposed to contribute to the target, the second step is to perform the Green's function computations via dynamic and parallel ray tracing. For this

purpose, the 3-D rms-velocity model used for post-stack time migration (see section 6.6) was converted to depth and surface distance, smoothed, and finally padded beyond the survey area limits (Fig. 7-12). Finally, migration of the 24 offset ranges was distributed to 24 R10000 (195 MHz) processors of an Origin 2000. After several tests done on independent in-line and cross-line sections, in-line and cross-line image sampling intervals were fixed to 2.5 and 5 m, respectively. Furthermore, depth sampling was fixed to a maximum value of 0.25 m (equivalent to about 0.35 ms at water velocity) to give good resolution of dipping events. Due to this down-scaling of the image sampling, the resulting migrated image of the whole survey required 5.4 GB disk space (plus two images computed for AVA purposes). A smaller first run on a 1.8 GB target (a third of the data cube: 1.5 x 0.3 x 0.2 km) provided a clear improvement compared to the time processing (Fig. 7-13 and Fig. 7-14). Assuming that the reflectivity is constant, the 24 migrated common offset gathers were stacked to obtain structural (or cinematic) images.

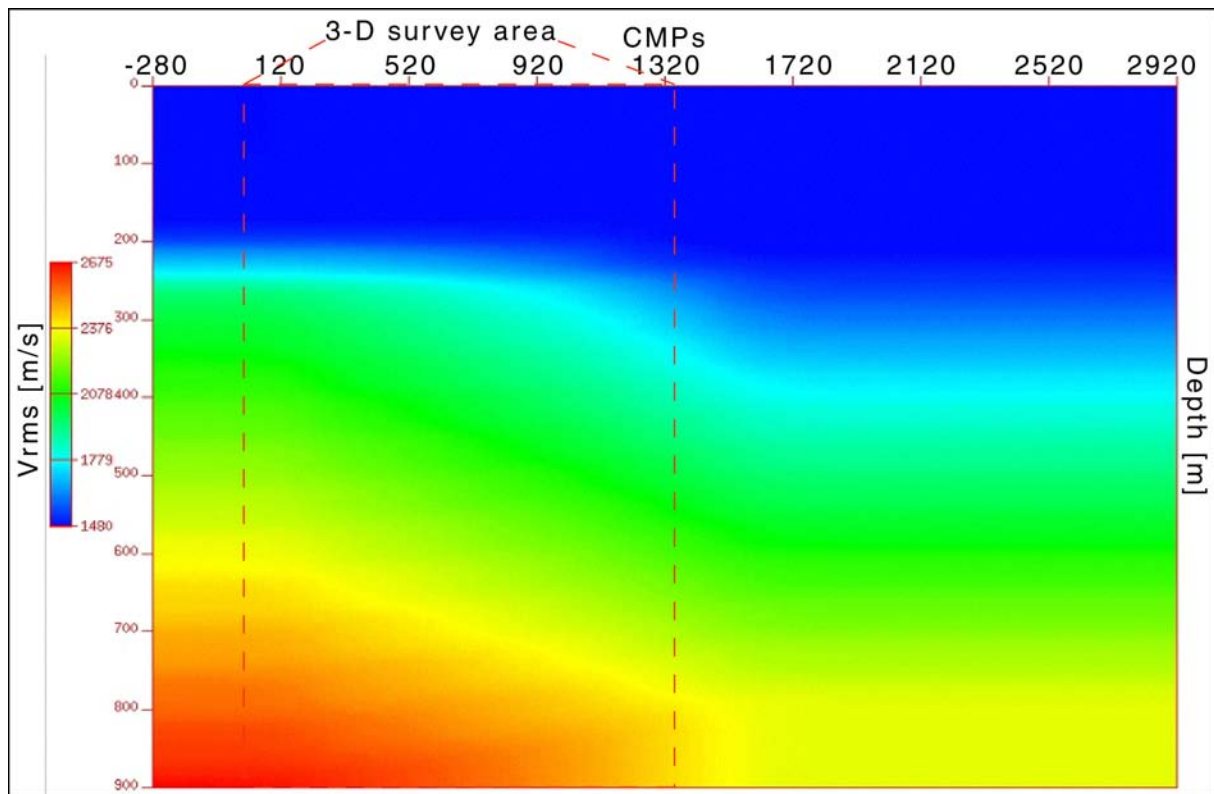


Fig. 7-12. The rms velocity model for stack and post-stack time migration has been converted to depth and surface distance, then smoothed, and finally padded beyond the survey area bounds (red dashed lines) in order to be used for prestack depth migration.

Fig. 7-13 and Fig. 7-14 show examples of in-line 125 and cross-line 680, both post-stack time migrated (a) and prestack depth migrated (b). The result is very promising. Many of the time migration artifacts in the fault zone disappeared. As the energy is focused onto fewer real reflectors, the depth image becomes much easier to interpret. The good data quality of the 3-D VHR Survey II is a rare example that demonstrates the successful application of

3-D prestack depth imaging to near surface seismics. Additional pre-processing will be needed to limit artifacts that can be present on migrated images, but were reduced on a simple NMO-stack. Once such a pre-processing routine is established and the prestack depth migration algorithm further adapted to the developed 3-D acquisition system presented in this work, it will become a very powerful tool for the imaging and subsequent interpretation of three dimensional complex targets in lacustrine settings.

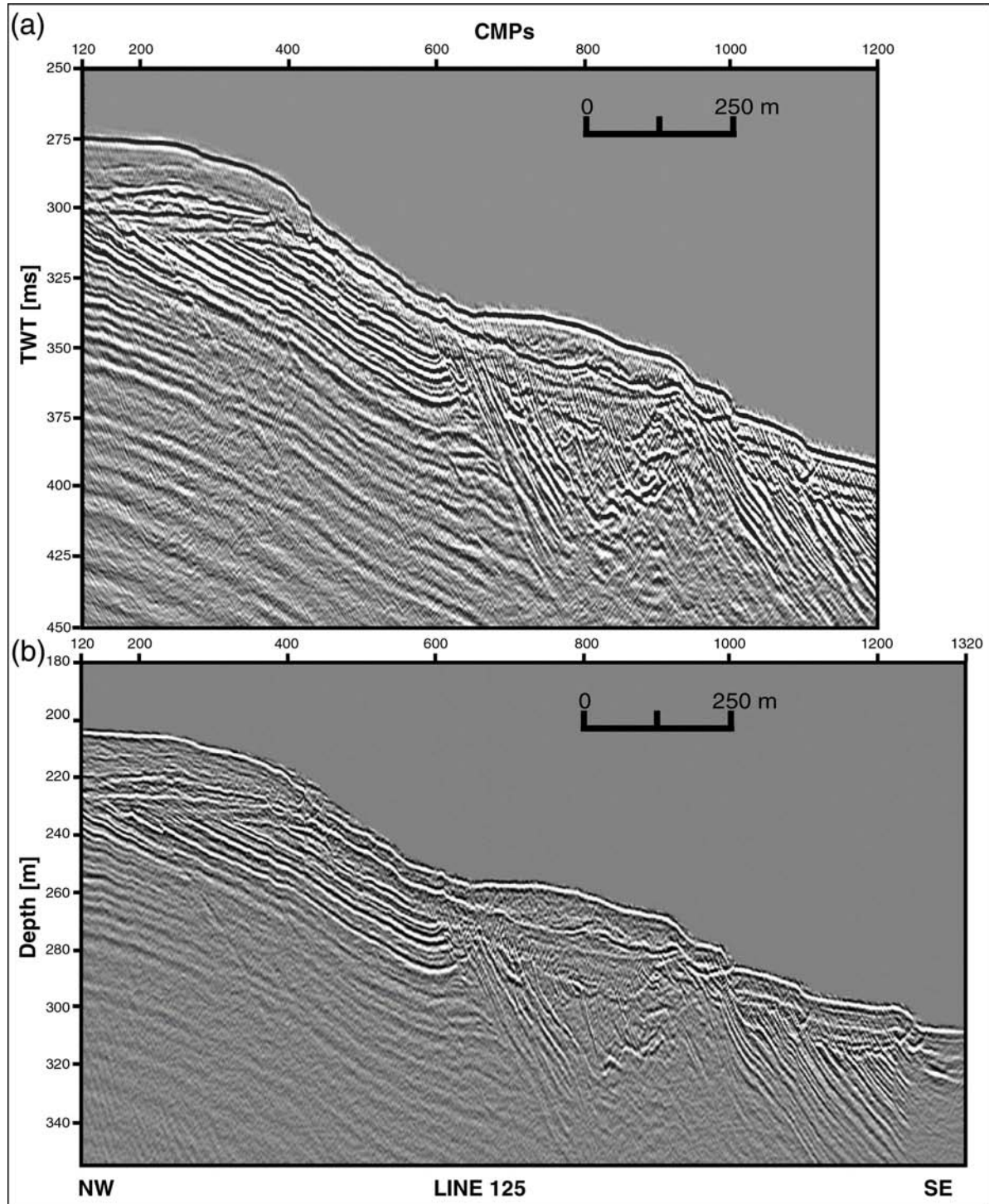


Fig. 7-13. Comparison of (a) post-stack time migration with (b) preserved amplitude prestack depth migration on in-line 125.

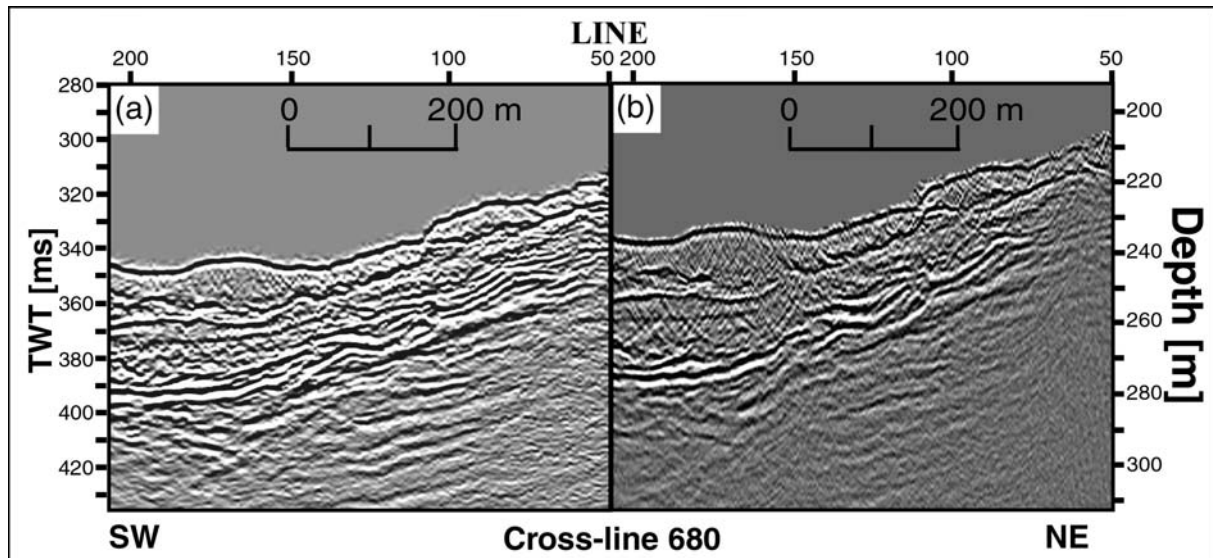


Fig. 7-14. Comparison of (a) post-stack time migration with (b) preserved amplitude prestack depth migration on cross-line 680 of Survey II.

The acquisition and processing of two 2-D profiles (140_15 and 140_30) have been described in chapter 4 (Fig. 4-7 and Fig. 4-8). These profiles crossed the 3-D survey area approximately at in-line 140 which now allows a comparison between 2-D and 3-D results. Profile 140_15 was shot with the Mini G.I G15 / I15 Air Gun, the same used for the 3-D Survey II. Fig. 7-15 presents that portion of profile 140_15 that corresponds to the 3-D survey extent in (a), as well as LINE 140 extracted from the final 3-D time migrated data cube in (b) and the corresponding 3-D depth migrated image in (c). Generally, the 3-D migrated data seem less contaminated by lateral reflection energy as is visible within the northwest Plateau Molasse in (a). However, the section in (b) shows various migration artifacts at the top of the Subalpine Molasse unit in the fault zone. Velocity probably changes abruptly at the transition from glacial sediments to steeply dipping molasse beds and, if the velocity field was not defined precisely enough, the 3-D migration algorithm might produce these migration artifacts. Some of the discrepancies could also be due to the different geometry assignment and time migration algorithms: 2-D Kirchhoff post-stack time migration in (a) and a 3-D one-pass post-stack time migration using a wave equation in the frequency-space domain (f, x, y) in (b). The preserved amplitude depth migration code produces a clean image that contains less lateral reflection energy than either in (a) or (b). This is not the only reason why this depth section will be easier to interpret geologically. There is especially no distortion in the data due to laterally and horizontally varying velocities. Dip angle and dimensions can be directly measured on the depth migrated image.

7.3 Geological interpretation

Even without the complicated and time consuming prestack depth migration, the 3-D time migrated data show the remarkable complexity and three-dimensionality of the survey

area. A series of four LINE slices (Fig. 7-16, Fig. 7-17 and Fig. 7-18) and twelve time slices (Fig. 7-19 and Fig. 7-20) extracted from the cube of Survey II give an idea of the system's ability to capture rapid structural changes in all directions.

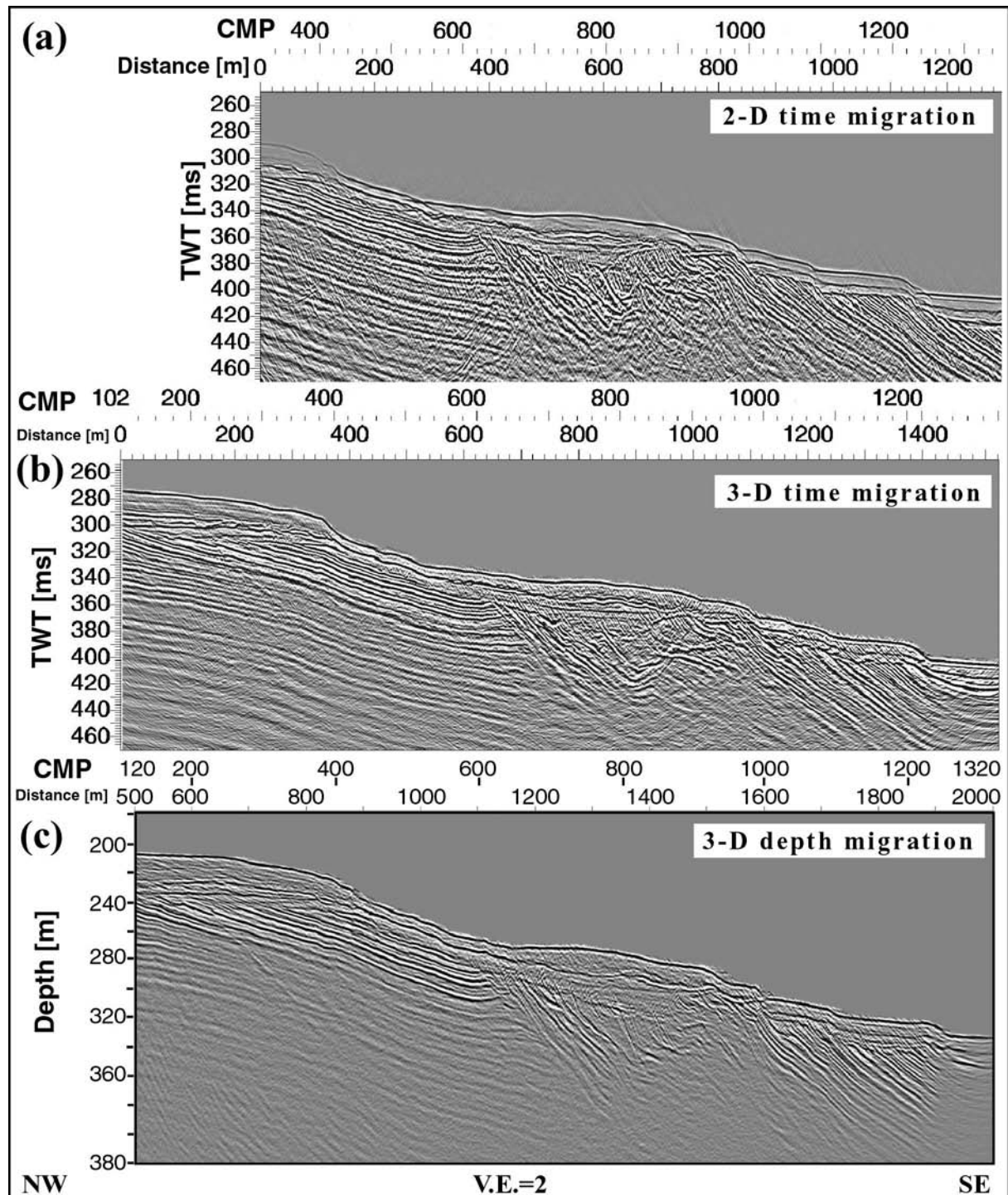


Fig. 7-15. Comparison of three different migration algorithms applied to (a) profile 140_15 and LINE 140 of Survey II (b) and (c): (a) 2-D Kirchhoff time migration; (b) 3-D one-pass time migration in the frequency - space; and (c) 3-D preserved amplitude prestack depth migration (PAPsDM). All data are presented with a vertical exaggeration of 2.

In chapter 4, a preliminary geological interpretation has been performed on the 2-D profiles of Fig. 4-7 and Fig. 4-8. The same five major seismic facies can be distinguished throughout the 3-D data cube (Fig. 7-16 - Fig. 7-20): **1** – Plateau Molasse (PM); **2** - highly deformed Subalpine Molasse (SM) within the fault zone; **3** – less deformed SM southeast of the fault zone; **4** – glacial sediments; and **5** – post-glacial sediments. Table 7-A summarizes these different facies. The Plateau Molasse within the survey area is considered as being the *Molasse grise de Lausanne*, whereas the Subalpine Molasse is made of *Molasse à Charbon* (see also Fig. 7-1). Each lithostratigraphic unit is represented by a specific color (see Fig. 4-2) which is consistently used in all interpreted vertical and horizontal sections and maps. Table 7-B relates those colors and seismic facies to the lithostratigraphy of the two structural units of Plateau and Subalpine Molasse – as interpreted by Weidmann (1988).






Seismic Facies	Reflection Character = Seismic Facies	Stratigraphy and Sedimentology	Lithostratigraphic Unit	Age	
1	oblique, parallel, wavy, high amplitude, sub-continuous		PM, channel-fill and floodplain	Molasse grise de Lausanne (USM)	Aquitainian
2	contorted to chaotic, variable amplitude		SM, deformed channel-fill and floodplain	Molasse à charbon (USM)	Chattian
3	oblique, parallel (steep), high amplitude, sub-continuous		SM, channel-fill and floodplain	Molasse à charbon (USM)	Chattian
4	parallel discontinuous to chaotic, hummocky		glacial sediments, waterlain till, (sub) glacio-lacustrine		Pleistocene
5	parallel continuous, low amplitude		post-glacial sediments, lacustrine		Holocene

Table 7-A. List of seismic facies analyzed within the 3-D survey area, adapted from Beres et al. (2003); PM = Plateau Molasse; SM = Subalpine Molasse, USM = Lower Freshwater Molasse.

Comparison of Fig. 6-8 and Fig. 6-9 with Fig. 7-16 through Fig. 7-20 allows to draw a relation between lithostratigraphic units and interval velocities: high velocities for the Molasse grise (1650-3000 m/s), intermediate velocities for the Molasse à charbon (1600-2400 m/s), which was imaged down to shallower depths below the water bottom than the Molasse grise, and low velocities for the water column and the Quaternary sediments (1450-1600 m/s).

So far, data have been shown mostly in two dimensions. In order to demonstrate the potential for detailed geological and tectonic interpretation, some horizons and fault surfaces (water bottom, top of the molasse, horizon A, Paudèze Fault, fault B and C, see Fig. 7-16 (b)) were traced over all in-lines and cross-lines of Survey II using the interpretation software “The KINGDOM SUITE” version 7.1 of Seismic Micro-Technology, Inc. Those horizon and fault surfaces can then be presented in three dimensional models. With the delineation of such

major boundaries, new insight into small-scale geomorphological features and geological processes is possible.

Era	Period	Sub-period	Epoch	Age	Lithology of Alpine foreland	Lithostratigraphy of Plateau Molasse	Lithostratigraphy of Subalpine Molasse	Ma	Intervals, My				
Cenozoic	Tertiary	Paleogene	Quaternary	Holocene	Post-Molasse	post-glacial sediments (5)		0.01	0.01				
				Pleistocene	sediments	glacial sediments (4)		1.64	1.63				
			Neogene	Miocene	Pliocene	Piacenzian					3.4	3.6	
						Zanclian					5.2		
					Oligocene	Messinian						6.7	7
						Tortonian						10.4	
						Serravallian	OSM - Upper					14.2	
						Langhian	Freshwater M.					16.3	
						Burdigalian	OMM - Upper	"Burdigalian"			21.5		
						Late Aquitanian	Marine Molasse						
						Aquitanian	USM - Lower	"Molasse grise de Lausanne" (1)	"Molasse grise de Lausanne"	23.3	6		
						Chatthian	Freshwater Molasse	"Molasse à charbon"	"Molasse à charbon" (2),(3)	29.3			
			Eocene	Oligocene	Early Chattian			"Grès et marnes gris à gypse"	"Grès de la Cornalle"				
					Rupelian?			"Molasse rouge"	"Molasse rouge"				
					Rupelian	UMM - Lower				35.4	6.1		
					Priabonian	Marine Molasse							
					Bartonian					38.6	3.2		
					Lutetian					42.1			
			Paleocene	Eocene	Ypresian					50	11.4		
					Thanetian					56.5	6.5		
					Danian					60.5	4		
										65	4.5		

Table 7-B. Geological timechart with lithology of the northern Alpine foreland basin and lithostratigraphy of Plateau and Subalpine Molasse as interpreted in the Lausanne area (Weidmann, 1988). Numbers in parenthesis refer to seismic facies of Table 7-A and colors correspond approximately to those already used in all previously interpreted sections.

7.3.1 Paudèze Fault zone and Plateau Molasse

The northwestern fault of the Paudèze thrust zone (Fig. 7-1), the Paudèze Fault, can be easily distinguished on all in-lines (Fig. 7-16 through Fig. 7-18) by the abrupt termination of the continuous reflections in the Plateau Molasse. Its distinction is also possible on time slices deeper than 310 ms (Fig. 7-19) when following the corresponding change in seismic facies from 1 to 2. A dip of about 30° is visible on the vertical sections, whereas time slices show that the fault strike varies from nearly parallel to the cross-lines at shallower depths (<350 ms) to a shape slightly concave towards the northwest.

The fault can generally be traced down to 430 / 440 ms, and deeper in places. This corresponds to a total depth of about 360 m, i.e. 120 m below the lake bottom. Although the Paudèze Fault is associated with many minor faults along both sides of the main trace (see for example faulting within facies 1 in Fig. 7-17 (b)), only the main fault was picked. This simplification allowed the construction of one coherent fault surface, represented in 3-D (Fig. 7-21), as it cuts horizon A, which lies within the *Molasse grise de Lausanne* (MGL) of the Plateau Molasse. Similar fault surfaces were generated for faults B and C. All three surfaces seem more or less parallel to each other and perpendicular to the survey direction and show slight undulations. These undulations are also indicated in the in-line profiles of Fig. 7-16 through Fig. 7-18 and in the time slices (Fig. 7-20).

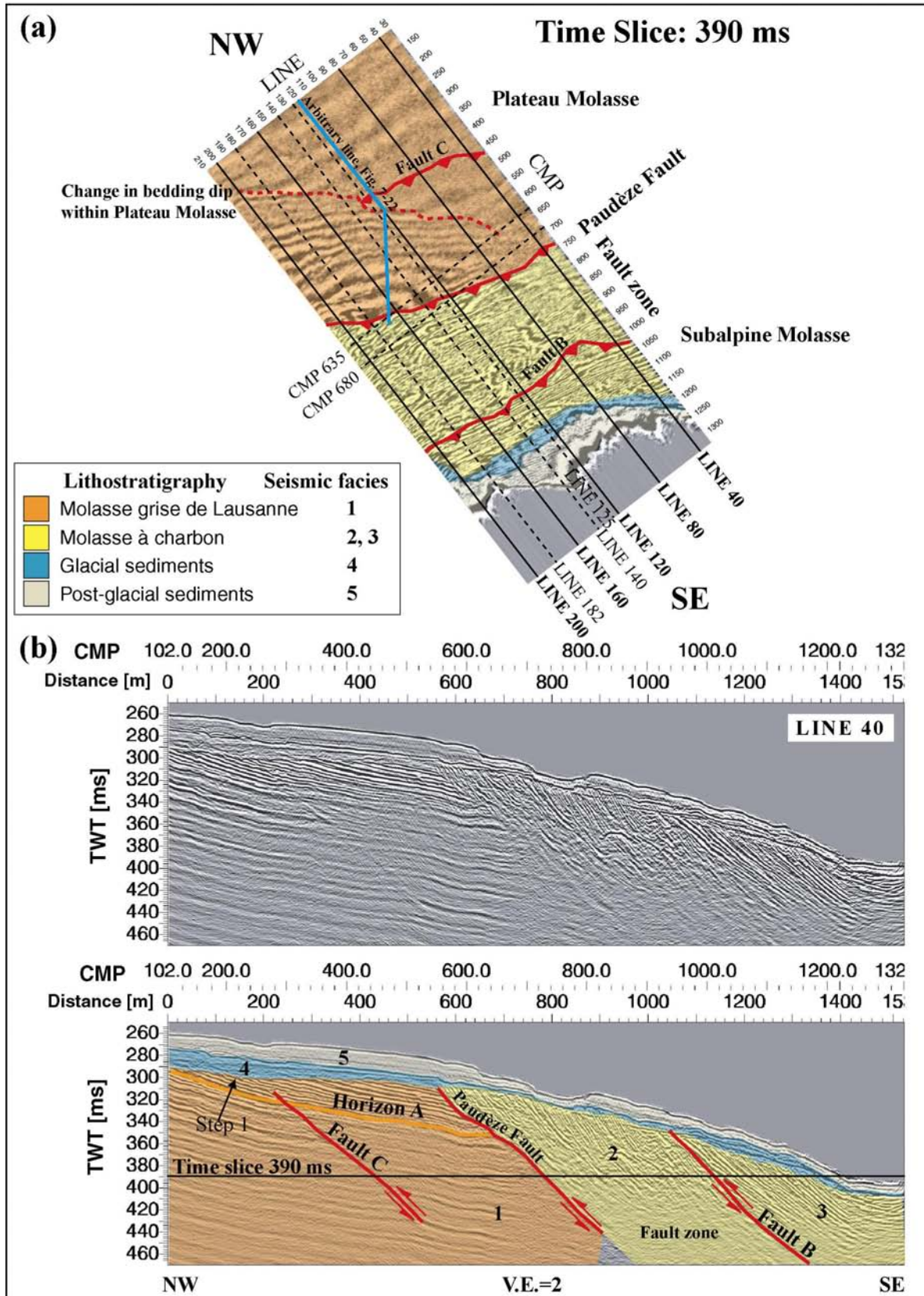


Fig. 7-16. Time slice at 390 ms of Survey II (a), presenting the survey cube oriented with respect to the geographical north and location of all vertical sections displayed in Fig. 7-16 through Fig. 7-18 (solid black lines), as well as in previous figures (dashed lines). The orientation of the arbitrary line of Fig. 7-22 is indicated in blue. (b) Example of in-line 40 (uninterpreted and interpreted data).

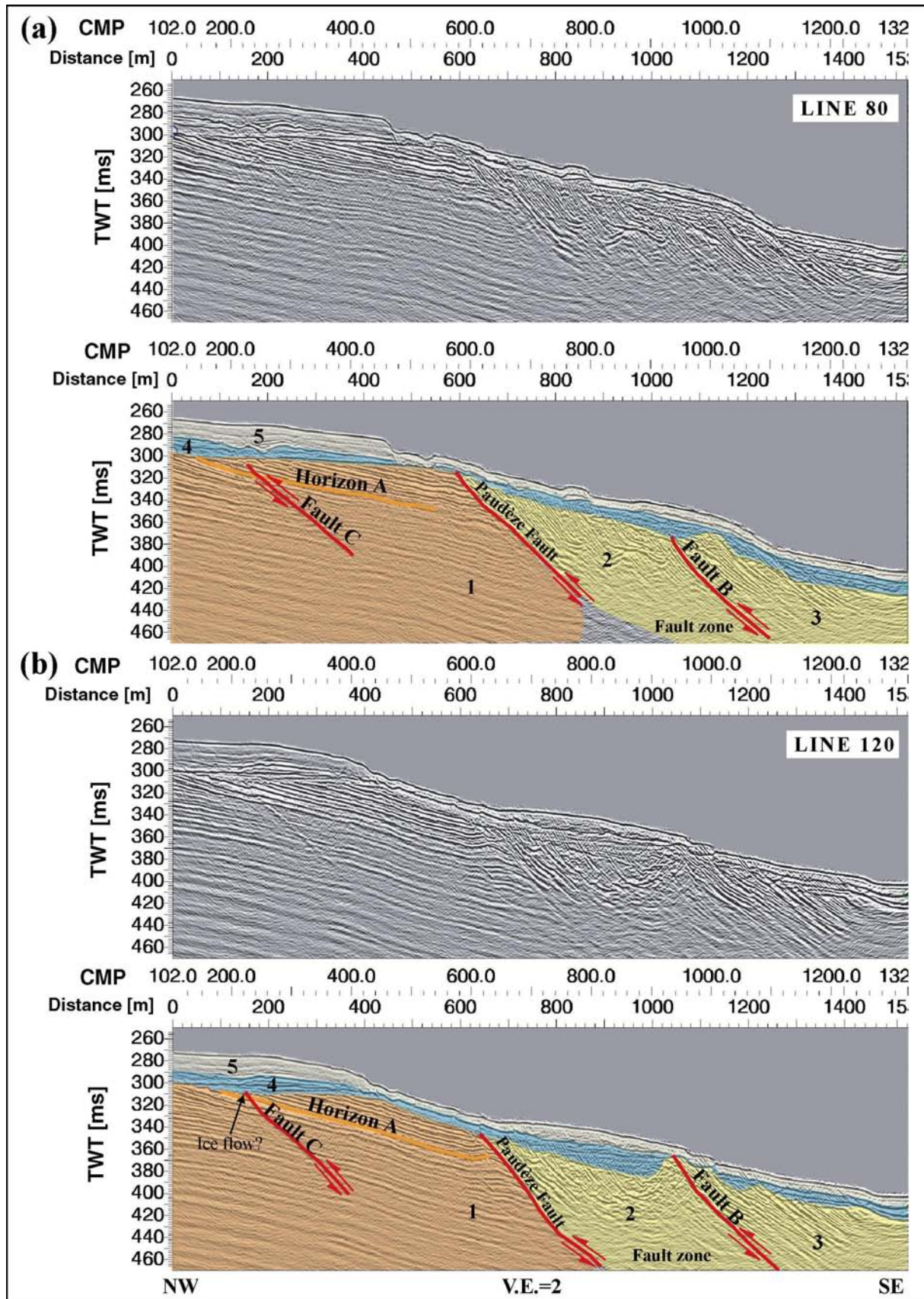


Fig. 7-17. Example of in-line 80 (a) and 120 (b) (uninterpreted and interpreted data). See color scheme in Fig. 7-17 (a).

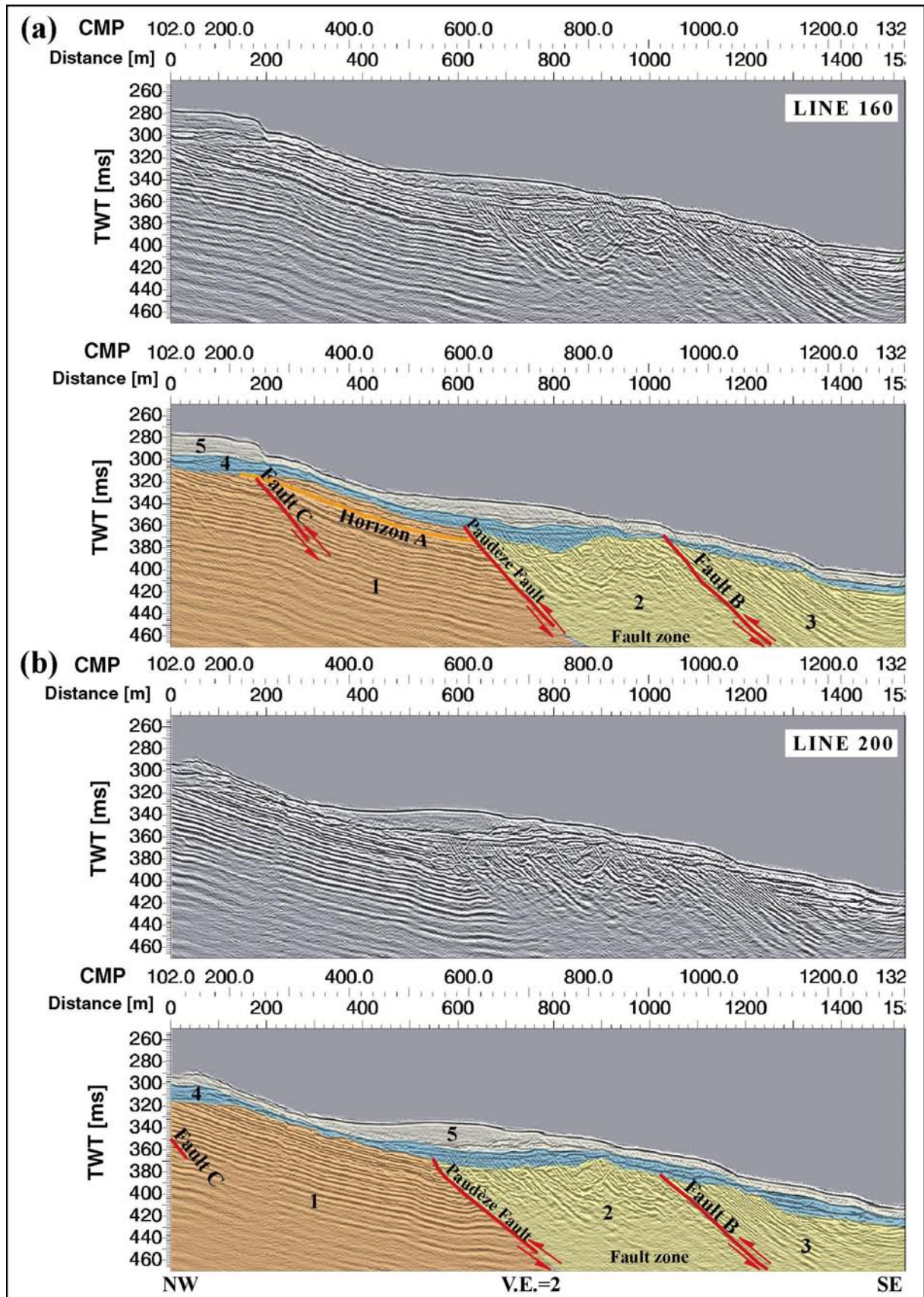


Fig. 7-18. Example of in-line 160 (a) and 200 (b) (uninterpreted and interpreted data). See color scheme in Fig. 7-17 (a).

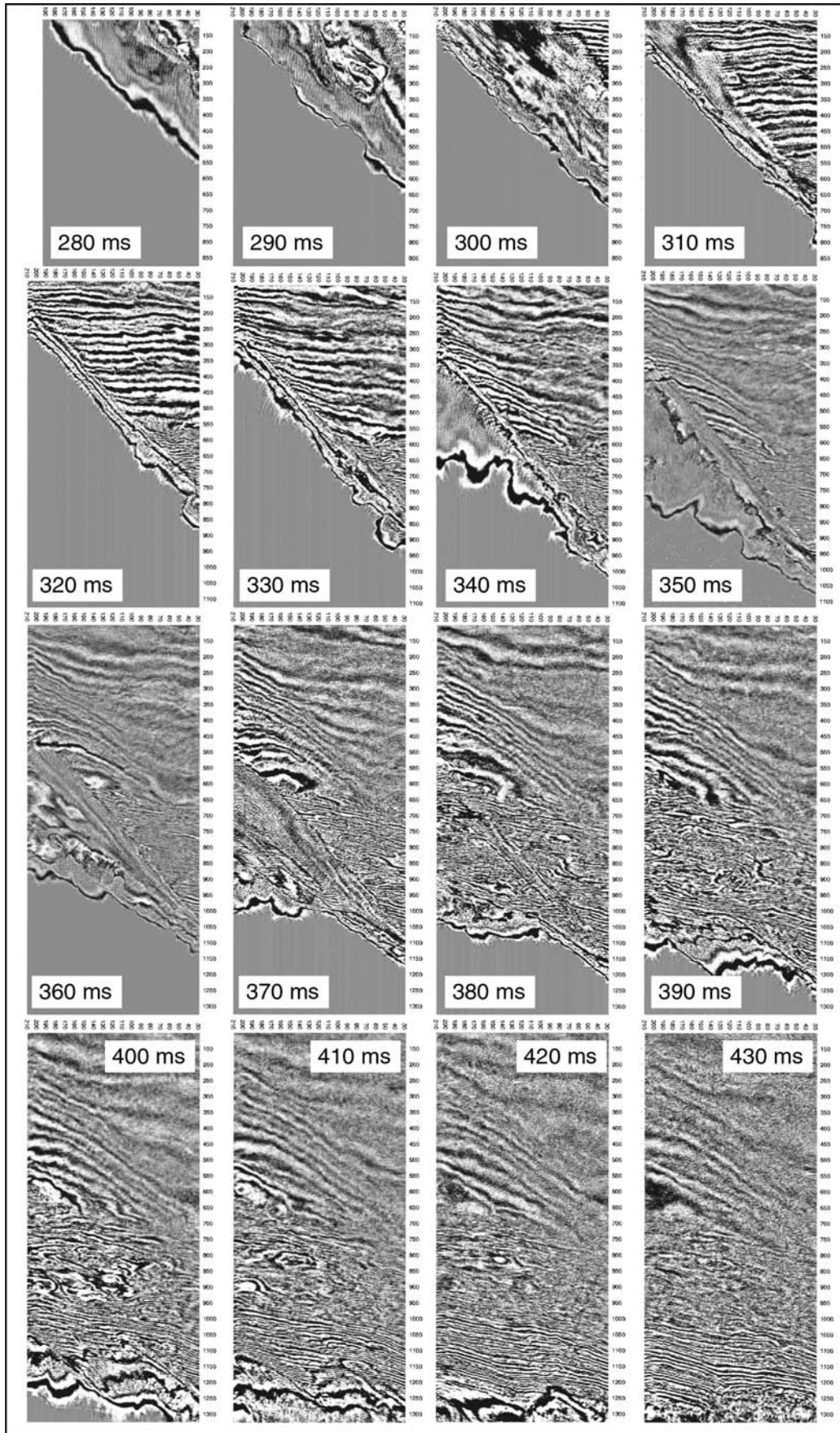


Fig. 7-19. Times slices (uninterpreted) of Survey II taken every 10 ms. For orientation of the survey area, see Fig. 7-16 (a).

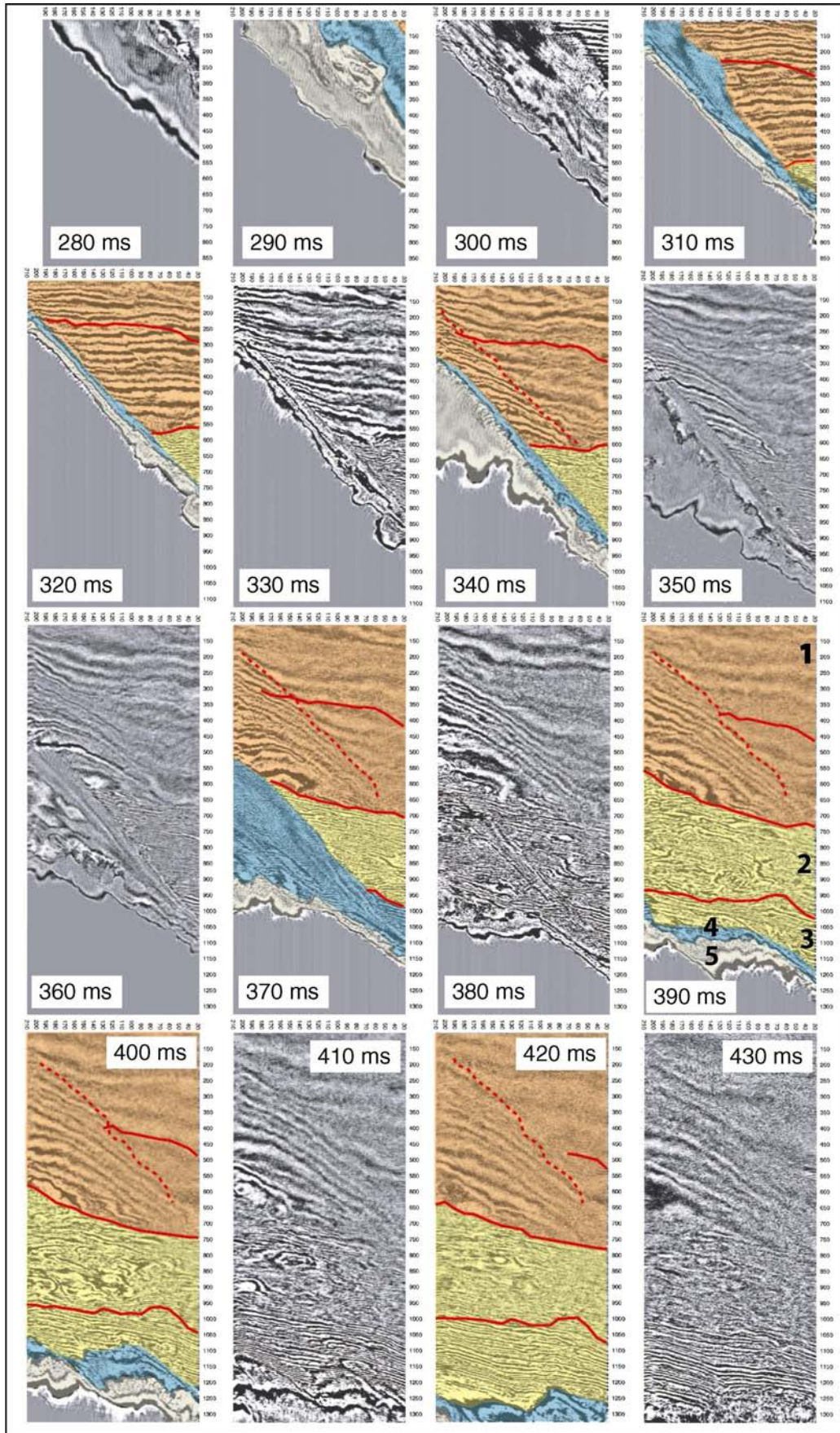


Fig. 7-20. Times slices of Survey II extracted every 10 ms with an interpretation of the different seismic facies. For survey orientation, colors and numbers, see Fig. 7-16 (a).

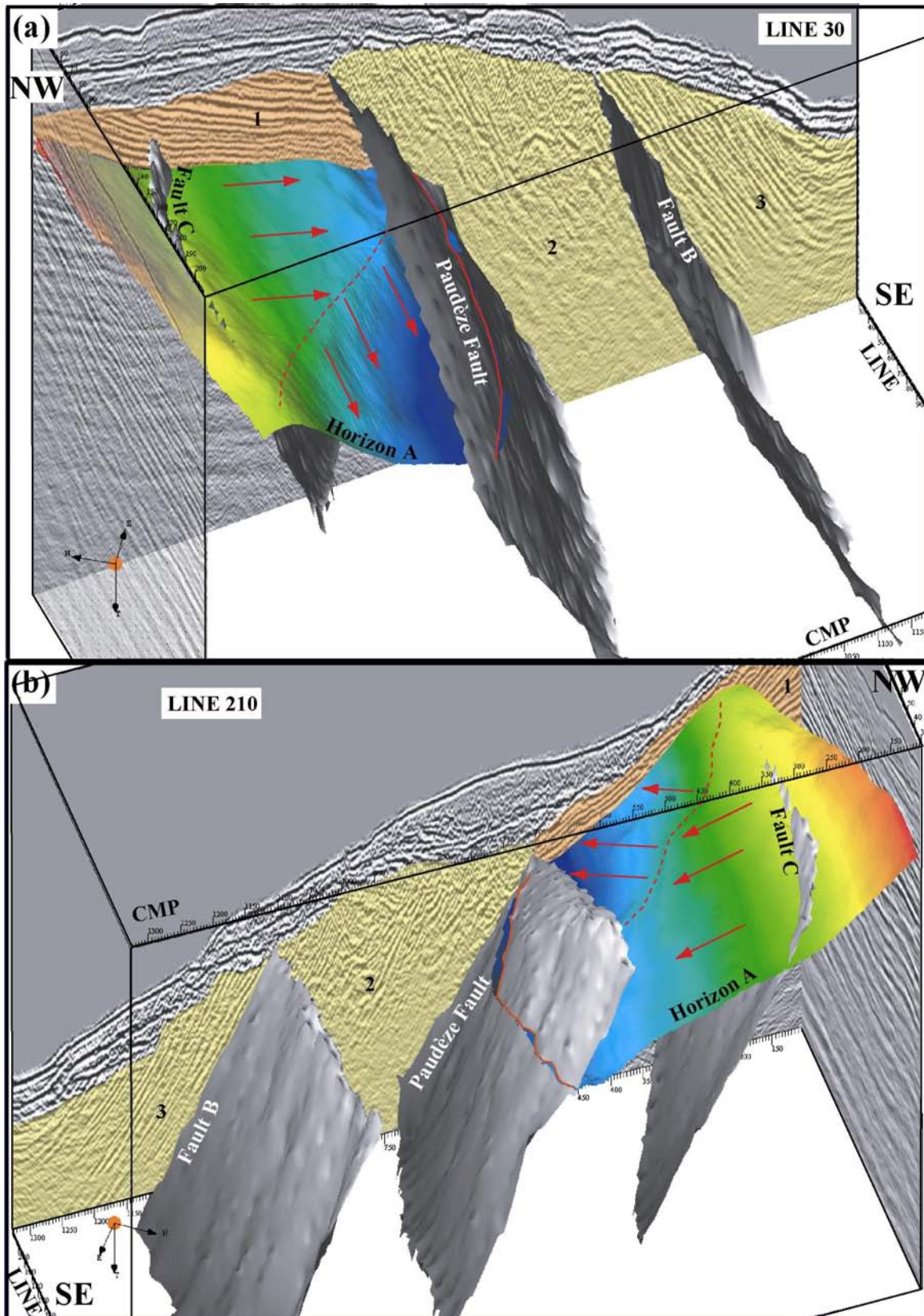


Fig. 7-21. Fault surfaces and horizon A (MGL) in 3-D representation (a) looking from west to east and (b) from east to west. The solid red line indicates the curved Paudèze Fault trace as seen on horizon A. The dashed red line highlights the axis along which the bedding dip changes – true dips are represented by red arrows. Numbers correspond to seismic facies.

However, the trace of the Paudèze Fault on horizon A (Fig. 7-21) has the same concave shape as that observed in the deeper time slices (Fig. 7-20) within that part of the survey area where a local change in direction of bedding dip occurred within the MGL from north to south. While in the northern part of horizon A the bedding strike is predominantly parallel to the cross-lines (SW-NE), its trend changes towards a W-E orientation further south. This phenomenon can only be observed in the 3-D visualization of horizon A (Fig. 7-21) and in the time slices of Fig. 7-20. Red arrows mark the two different true dip directions (NW-SE and N-S) of the bedding in this area (Fig. 7-21).

Although Morend (2000) detected the fault trace curvature on the dense grid of 2-D seismic profiles (see Fig. 4-3), it was impossible to observe the local change in dip direction of the MGL beds in separate vertical sections only. In Fig. 7-16 through Fig. 7-18, the apparent dip of horizon A appears constant. However, when selecting an arbitrary vertical section through the data cube that is perpendicular to the strike of reflectors in the Plateau Molasse, as marked in time slice 390 ms of Fig. 7-16 (a), the change in true dip of the MGL beds becomes obvious (Fig. 7-22). Fig. 7-22 also shows that the axis along which the dip of horizon A and deeper reflectors change by about 5° (dashed red line) is almost vertical. This result and the fact that fault C is never observed south of the dip change implies that it might not only be a fold, but even a fault with strike-slip movement which is generally very difficult to detect in vertical sections.

Usually, a fault trace on a map indicates the intersection of a fault with a mapped horizon. Because the Paudèze Fault does not cut the glacial and post-glacial sedimentary layer, its fault trace in Fig. 7-1 was projected vertically to the lake bottom. It indicates the fault position when glacial erosion stopped. Fig. 7-23 shows the Paudèze Fault trace as the boundary between the erosional surfaces of the Plateau and Subalpine Molasse in three dimensions. In Fig. 7-24, this trace was superimposed on the contour map at the top of the Plateau Molasse. The fault coordinates correspond perfectly to those interpreted by Morend (2000) (see Fig. 7-1). His interpretation of the fault location beyond the 3-D survey area was added to Fig. 7-24 where it seems to be fairly straight. When comparing bathymetry (Fig. 7-7 (a)) with the morphology of the erosional surface of the top molasse, one notices a similar east-west trending escarpment. This escarpment, which is too small to have been mapped in past large-scale bathymetric studies of the lake, is not parallel to the Paudèze Fault trace (see Fig. 7-23). However, it corresponds to the orientation of the fold axis or strike-slip fault interpreted in horizon A (Fig. 7-21).

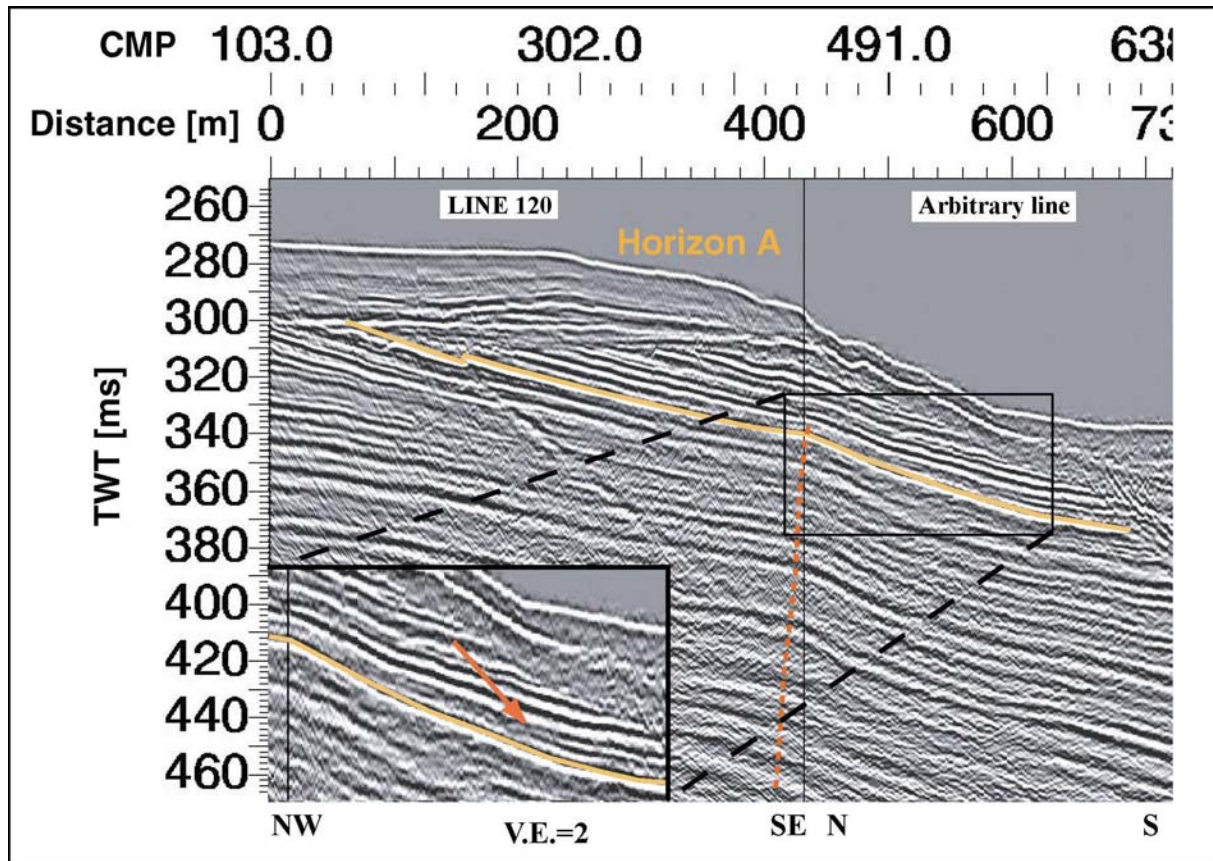


Fig. 7-22. Arbitrary vertical section cut through the data cube perpendicular to the strike of MGL beds. The dip changes by about 5° along the axis indicated by the red dashed line. For line location, see Fig. 7-16 (a).

In summary, four structural phenomena are observed within the limits of the 3-D survey area. Firstly, the otherwise straight Paudèze Fault trace exhibits a concave curvature towards the northwest. Secondly, in the close vicinity of this curvature, there is a steep east-west striking escarpment visible at both the water bottom and on the erosional surface of the top molasse that crosses the fault obliquely (see Fig. 7-24). Thirdly, the trend of this escarpment coincides with the axis of a dip change observed in the bedding of the MGL (horizon A). The steeper sloping part south of this axis approximately mimics the dip of the escarpment. Fourthly, a topographic high and low within the erosional surface of the Subalpine Molasse fault zone (Fig. 7-23) show again the same west-east orientation.

Is this escarpment a feature related merely to glacial erosion which continues its orientation parallel to the lake shore further to the west and east of the survey area (Fig. 7-24)? If the answer were yes, this would mean that the fault's convexity at the location of this escarpment is pure coincidence. A satisfactory answer to this question can be found only with the aid of additional 3-D data. The inclusion of interpreted bathymetry and molasse top horizons from the high-resolution work of Morend (2000) may also help.

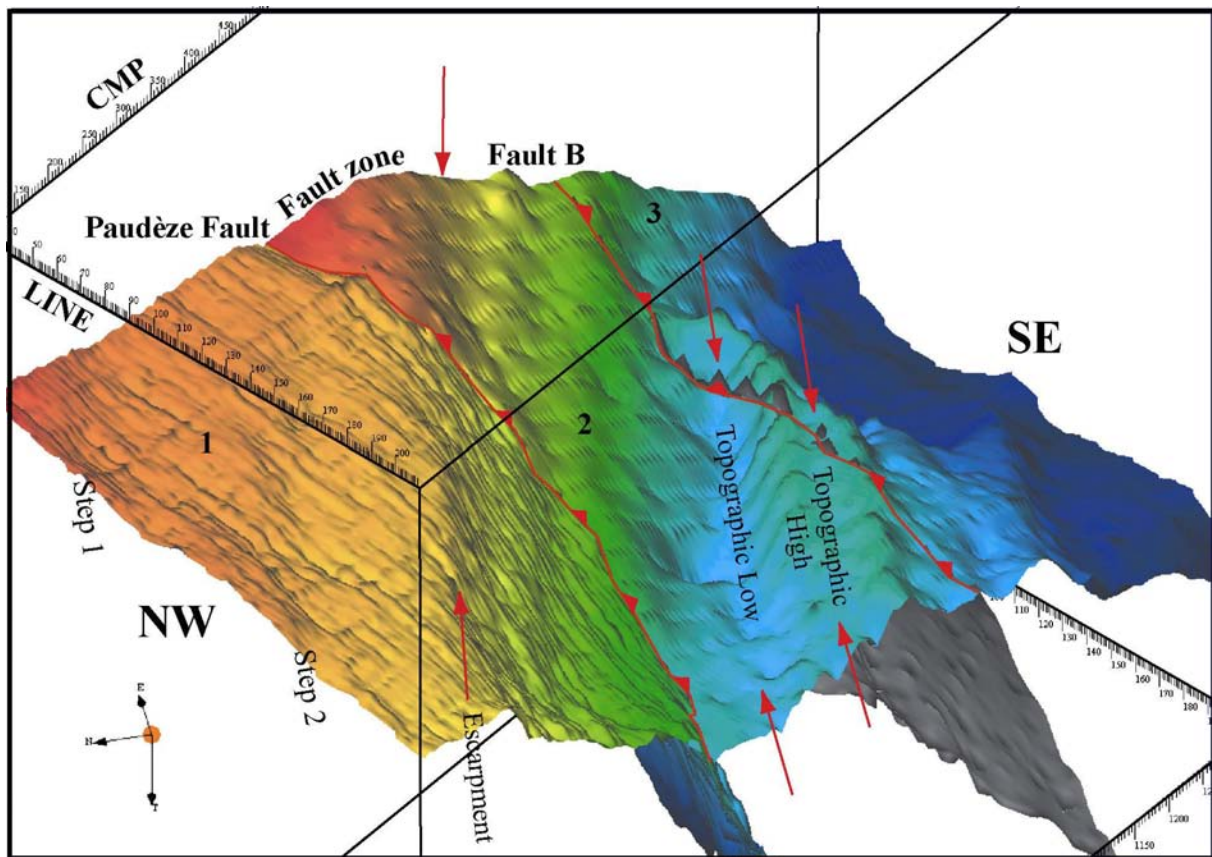


Fig. 7-23. Map of the top of the Plateau and Subalpine Molasse units in three dimensions with fault traces of the Paudèze Fault and fault B. Their map coordinates are shown in Fig. 7-1. Red arrows indicate the east-west trend of an escarpment and a topographic high and low.

Anyhow, the orientation of glacial erosion in the vicinity of Lausanne is approximately west-east (see bathymetry contours in Fig. 4-4) and coincides with the trend of the escarpment, the topographic high and low and the step-like relief of the Plateau Molasse top (Fig. 7-23). However, large-scale bedding dip within the PM is related to the Lausanne anticline (see Fig. 4-2), whose strike is oriented approximately parallel to the fault zone (Weidmann, 1988). Bed competence should thus vary predominantly perpendicularly to this strike in in-line direction and could not have influenced the west-east trending steps. Furthermore, when looking at in-line 40 in Fig. 7-16 (b), there seems to be no remarkable slope change on the molasse top and only a little depression carved into the Quaternary sediments. The escarpment seems to die out in the east where it would affect Subalpine instead of Plateau Molasse. Consequently, it seems more likely that the existence of the escarpment and the change in fault strike are somehow related to a pre-existing structure within the PM and that it is only a regional structure in close vicinity of the 3-D survey site.

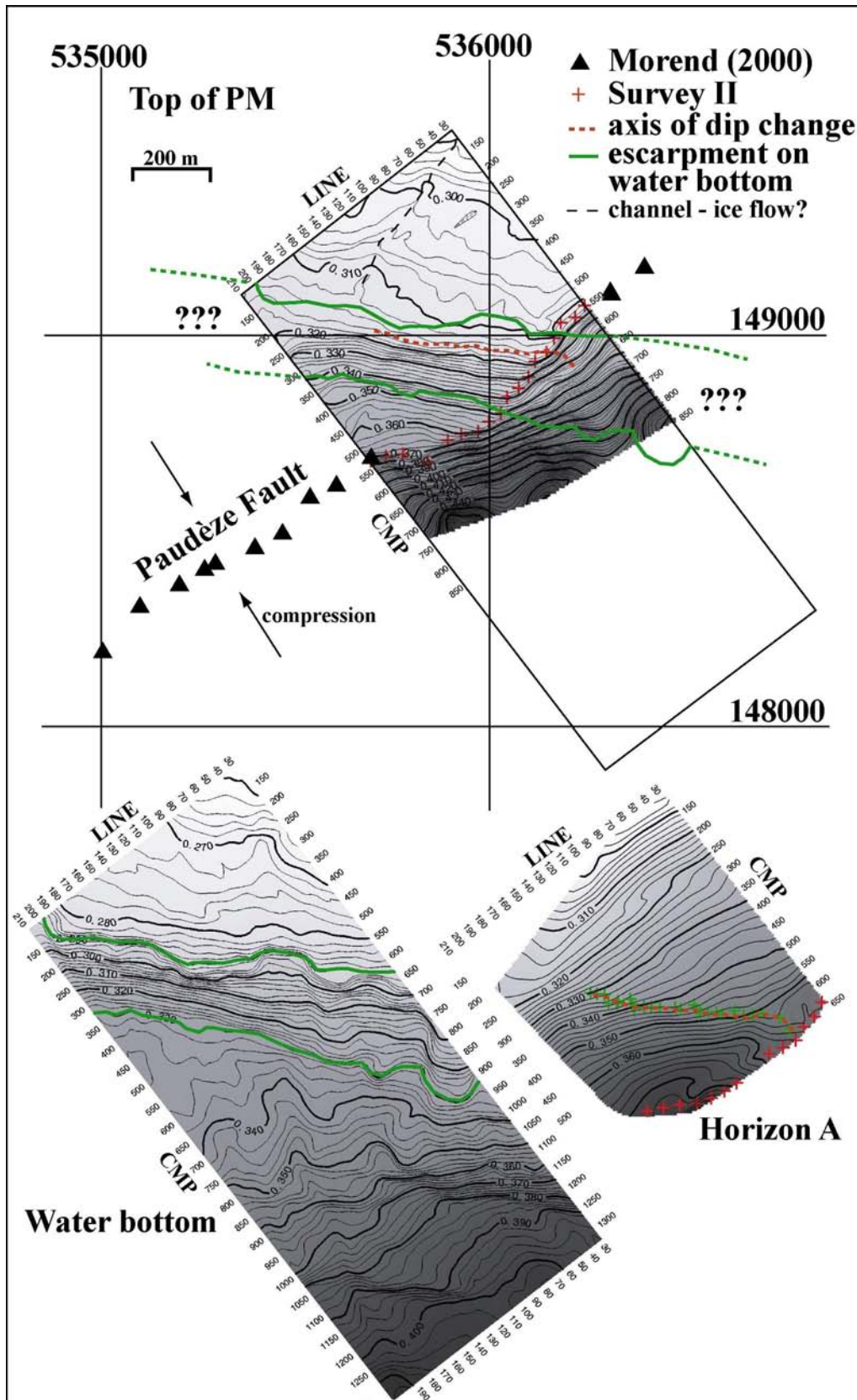


Fig. 7-24. Contour maps at the top of the Plateau Molasse (PM) with location of the Paudèze Fault trace deduced from Survey II (red crosses) and from Morend (2000) beyond the survey limits (black triangles). The locations of the escarpment at the lake bottom and the interpreted axis of dip change in horizon A are superimposed on the PM contours.

Interestingly, the deformation within the MGL beds is not observed at depths shallower than 330 ms. This is visible in the time slices (Fig. 7-20), but also in the arbitrary vertical section of Fig. 7-22. The dip of reflections observed above horizon A seems to be the same as that in the northwest and folding or faulting disappears, i.e. no dip change or deformation occurred in the overlying molasse beds which on-lap the older ones (see zoom window in Fig. 7-22) and form an unconformity. So assuming that after or during deposition of these older MGL beds, the (local) stress regime was different from that responsible for the creation of the Paudèze Fault zone and fault C, strike-slip movement combined with a component of compression might have formed a fault / fold that was later cut by the Paudèze accident. This preexisting structure oriented obliquely to the current principle stress axis must have influenced the regional stress regime and, with it, the development of the curved fault trace in the area of intersection. Glacial erosion might have been guided by this pre-existing zone of weakness and by the steeply inclined beds so favorably oriented.

When inspecting time slices deeper than 350 ms (Fig. 7-20), reflections seem to be curved. A trough was formed by the upward bending of MGL beds due to compression and additional faulting close to the main fault. This kind of minor faulting is visible for example on in-line 120 in Fig. 7-17 (b) and a synclinal structure can be observed in Fig. 7-18 (b) at about 400 ms. These might be indications of local variations in stress due to the changing curvature of the Paudèze Fault trace. Such a change under compression leads to a lateral component of movement either to the right or to the left depending upon the angle of the fault trace relative to the stress axis. The region would be under transtension or transpression or both, which form shear zones (Sanderson and Marchini, 1984). Anyhow, a more detailed geological interpretation is needed, especially with respect to the western limit of the survey area. More data for this region might help to explain the complex environment close to the fault curvature and the impressive structural and morphological variations. In any case, no previously published geological or structural maps show such detail in the PM-SM boundary, even on land (Vernet et al., 1974). Moreover, this study has determined the location of this boundary within the site up to an accuracy of a few meters.

7.3.2 Plateau Molasse

Reflections in the PM, which comprise a large portion of the seismic data set along the northwest, are inclined, relatively high-amplitude and generally very continuous (facies 1). The inclination represents an $\sim 8^\circ$ dip towards the southeast in the northern portion and a dip of up to 13° towards the south in the southern portion. Although interpreted as one single facies, a cyclic pattern of reflections of variable amplitude and frequency is visible in both vertical sections (Fig. 7-16 and Fig. 7-17) and time slices (Fig. 7-19) representing the alternating shale (high-amplitude, low-frequency) and sandstone (moderate-amplitude, variable frequency) sequence of the Lower Freshwater Molasse (Morend et al., 2002).

Although generally flat, the PM paleosurface (Fig. 7-23, Fig. 7-24) is characterized by a step-like relief with slight irregularities. In Fig. 7-23, two less than 10 m high steps bound three plateaus before getting to the steeply sloping escarpment. Due to their small scale, the steps are difficult to recognize on the in-lines presented at a vertical exaggeration of only 2. The shallowest one is indicated in Fig. 7-16 (b). Both steps are more distinct in the 3-D representation of Fig. 7-23. As mentioned in the previous section, the trend of this stepping relief, as well as the escarpment, are oriented west-east. Because the strike of MGL beds is approximately parallel to the fault zone (NW-SE), it is not the varying bed competence that could have led to the described morphology, but more likely glacial erosion influenced by pre-existing deformation. However, the small channel-like morphology visible on the PM contour map of Fig. 7-24 is oriented approximately parallel to the strike of MGL beds and shows a relief of several meters. It might be interpreted as a trace of former ice flow during glaciation resulting from small-scale differential erosion throughout areas of inclined bedding planes with different lithologies (see also Fig. 7-17 (b)), i.e. sandstone-shale cycles.

7.3.3 Subalpine Molasse

Seismic images of the Subalpine Molasse are dramatically different from those of the Plateau Molasse (Fig. 7-16 through Fig. 7-20). Seismic facies within this unit range from contorted and chaotic (facies **2**, see Table 7-A) to steeply-inclined ($\sim 20^\circ$ southeast dip, see Fig. 7-20), parallel, and relatively continuous (facies **3**), although difficult to trace over larger distances. Facies **2** is generally lower amplitude with bright reflections and indicates intense folding and faulting. Facies **3** is high-amplitude and is concentrated at the southeast margin of the data set. Because much of the diffraction energy of these steeply dipping reflectors was not recorded within the survey area, migration did not work satisfactorily over a range of at least 150 CMPs at this margin (compare southeast portion of 3-D in-lines in Fig. 7-16 - Fig. 7-18 with that of 2-D profile 140_15 in Fig. 4-7). The two facies are separated by fault B which bounds the thrust zone to the southeast and which is roughly parallel to the northwestern Paudèze Fault (Fig. 7-1 and Fig. 7-23).

The paleosurface of the SM within the survey area has a highly irregular relief of nearly 130-m range (~ 130 m) mainly because of the presence of numerous thrust slices and steep-dipping beds with various competence. A large topographic high oriented approximately parallel to the escarpment in the west-east direction extends from within the fault zone at the western survey limit and ends shortly after the intersection with fault B (Fig. 7-23). Between this ridge and the major fault plane, an elongated topographic low represents a large trough predominantly eroded into the upper surface of facies **2** (see LINEs 80, 120 and 160 in Fig. 7-17 (b) and Fig. 7-18). The maximum topographic relief between both structures amounts to 25 m. The trough is about 150 m wide close to fault B (LINE 80), widens to 300 m in the center of the fault zone (LINE 120, 160) and seems to disappear towards the survey boundary

(see LINE 200). Smaller relief structures, apparently representing more resistant thrust blocks within facies 2, are located throughout this trough and correlate positively with higher amplitude zones.

A possible interpretation for the formation of this trough and topographic high would be that faulted blocks within the *Molasse à charbon* with different lithologies or tectonic fracturation were preferentially eroded during Quaternary glaciations. Similar observations of tectonics controlling subsequent drainage patterns have been made with 2-D high-resolution seismic reflection profiling in Lake Neuchâtel, Switzerland (Gorin et al., 2001). The fact that these morphologic features seem to exist only within the limits of the thrust zone supports the above interpretation. However, it does not explain why it is oriented obliquely to the strike of the Paudèze Fault and why differential erosion does not follow the general bedding trend as observed southeast of fault B. The angle between the trough axis and the Paudèze Fault is 40°. In transpressional regimes, thrusting and strike-slip movement may occur at such angles relative to each other (Sanderson and Marchini, 1984). As the preexisting deformation within the Plateau Molasse might have influenced the shape of the fault plane in this area (see section 7.3.1), it might also be responsible for a change in stress regime across the fault zone with possible shearing, rotation, and tilting of fractured blocks and the resulting preferential erosion along these zones of weakness from west to east. The chaotic facies within the thrust fault zone, as visible in the time slices at 390 ms and deeper (Fig. 7-20), supports this theory and little highs and troughs filled with glacial sediments demonstrate a lack in reflection coherency.

7.3.4 Glacial and post-glacial sediments

Although a variety of seismic facies characterizes the sediments of the Quaternary overburden, only the boundary between glacial and post-glacial sediments was interpreted for the whole data cube. Immediately overlying the molasse units is the low-amplitude facies of glacial sediments with a generally discontinuous to chaotic reflection pattern (facies 4, Table 7-A). According to Chapron (1999), Moscariello et al. (1998), Van Rensbergen et al. (1998) and Van Rensbergen et al. (1999), this facies contains waterlain till and (sub) glacio-lacustrine deposits. It underlies a continuous, parallel and low-amplitude reflection package (facies 5) which is up to 18 ms (~15 m) thick in the southeast and northwest portion and is interpreted as post-glacial lacustrine sediments (Chapron, 1999).

Post-glacial and glacial sediments are separated by a relatively strong reflection (see Fig. 7-16 through Fig. 7-18) that disappears where glacial sediments are thin or absent. This reflection approximately mimics bathymetry. While on eastern LINES with relatively low topographic relief at the top of the molasse (Fig. 7-16 (b) and Fig. 7-17 (a)), the layer of post-glacial deposits has a relatively uniform thickness except for some erosion in the area of the fault zone, thickness variation is more pronounced along the changing slopes of the western

LINES (Fig. 7-17 (b), Fig. 7-18). The entire Quaternary overburden is thickest (up to 46 ms thick - ~40 m) in the large west-east trending trough shown in Fig. 7-23 which was first filled by glacial sediments and then covered by a post-glacial layer (Fig. 7-17 (b), Fig. 7-18). Post-glacial sediments above the trough are thicker due to the almost horizontal top of its in-fill. The differential erosion of the Subalpine Molasse top (lower boundary) and the irregular bathymetry (Fig. 7-7, upper boundary) create a high variability of the entire trough-fill thickness. Bathymetry (Fig. 7-7) as well as the contour map in Fig. 7-24 show three elongated channels converging from the hinge of the escarpment towards the deep-water portion of the data cube.

Neither the 3-D data of Survey I nor those of Survey II indicate any evidence for faulting within the Quaternary sediments. This observation is consistent with the relatively recent seismic work in Lake Geneva (Finckh et al., 1984). However, the low reflectivity within the glacial sedimentary layer above the fault zone and minor faults within the PM make it extremely difficult to detect possible vertical displacement. Future preserved amplitude prestack depth migration images after finalization of processing parameters (see section 7.2) may help provide more definitive conclusions about neotectonics within the survey site.

CHAPTER 8: SUMMARY, CONCLUSIONS AND OUTLOOK

8.1 Summary

The past seven chapters presented a detailed description of the 3-D marine seismic reflection method as it has been adapted to near-surface lacustrine settings from instrument considerations, system development, acquisition, processing and data interpretation. In the following, the most important aspects that influenced the system and survey design will be discussed.

8.1.1 Streamer configuration

Two different acquisition systems have been conceived and used to survey the same target site for comparison of design parameters. The first system (used for Survey I) combined a single 48-channel streamer with a high-frequency water gun source and represented a preliminary development stage towards the more advanced multi-streamer configuration of the second system (used for Survey II). This final 72-channel three-streamer configuration was designed according to the following instrumentational limitations: the total number of 96 channels of the seismograph, which was designed for land seismic surveys, and its inherent slowness in recording, a minimum possible ship speed of about 4 km/h for navigation stability, as well as streamers organized in sections of 24 channels. Furthermore, spatial aliasing which depends also on the structural dip of the survey area and the gun's frequency bandwidth, guided the selection of streamer separation. Two retractable booms were constructed in order to separate the two outer streamers from the one in the center by a distance of 7.5 m, resulting in a cross-line spacing of 3.75 m. The ends of these light and hollow aluminum booms rest on floats while an elaborate attachment system to each side of the research vessel allows adaptation to minor vertical and horizontal wave movement and prevents abrupt course changes of the connected lead-ins.

In order to simplify data processing, bin sizes in cross-line direction were chosen as a multiple of the distance between CMPs, which in turn is dictated by the fixed hydrophone spacing of 2.5 m. At a shot spacing of 5 m, the first system obtained a nominal fold of 12, whereas the reduction to 24-channels per streamer in Survey II, permitted a nominal fold of only 6. Sail lines in Survey I were 7.5 m apart – equal to 6 CMP intervals. Because a multi-streamer configuration has the advantage of needing as many times fewer boat passes as used streamers in order to acquire the same number of CMP lines (in-lines), it is possible to improve cross-line resolution without increasing total acquisition time. Hence, when halving the cross-line spacing of Survey I to 3.75 m (3 CMP intervals), the three-streamer system of Survey II needed only two thirds of the time to acquire double the number of in-lines over the same survey area. This gain in lateral resolution reduced the risk of spatial aliasing perpendicular to survey direction.

8.1.2 Seismic source

Not only for aliasing considerations but also for questions of resolution and signal penetration does the choice of the seismic source present one of the most important parameters in survey design. For this reason, far-field signature measurements and 2-D tests on the target site were conducted with the three different gun types available in order to determine their bandwidth, signal strength and dominant frequency - parameters that directly influence the necessary temporal and spatial sampling rate, resolving power and signal penetration depth. The high-frequency S15.02 water gun possesses a bandwidth between 100-1700 Hz and a dominant frequency of 670 Hz while the Mini G.I double chamber air gun was operated in two harmonic mode configurations with total volumes of either 30 in³ (G15 / I15) or 60 in³ (G30 / I30). While their signal strengths and frequency spectra are almost identical (40-650 Hz versus 40-550 Hz), their air consumption and resolving power differ by a factor of 2 (dominant frequency of 330 Hz versus 150 Hz).

Air consumption turned out to be another critical design parameter, especially when limited to a relatively small rate of compressed air production. A detailed study showed how the total number of acquired lines per working day depends upon the chosen ship turning time and the air consumption of each. When using the optimum turning time between two consecutive sail lines with respect to a fixed production rate, operating pressure, number of shots per line and shot interval, the water gun (operated at 140 bars) can shoot about twice as many lines as the Mini G.I G15 / I15 and four times as many as the Mini G.I G30 / I30 (the latter two operated at 80 bars).

Considering the specific characteristics of the guns, but also the influence of steep dips in the survey area on spatial and temporal aliasing helped evaluate the source configuration for the planned survey. The low air consumption of the water gun seemed more appropriate for the single-streamer configuration because the short optimum ship turning time allowed acquisition of a greater number of sail lines per day than possible with the Mini G.I G15 / I15. The multi-streamer system, however, made the use of the air gun more economic in surveying time. In addition, its longer duration of optimum ship turning favored the preferred acquisition geometry in one direction only. Comparison of the processed 2-D air gun profiles with those of the water gun showed that, although vertical resolution was halved, signal penetration increased by a factor of 2. Due to much lower frequencies in the spectrum, the signal is not aliased in in-line direction for dips smaller than 30° (versus ~10° for the water gun). Hence, compared with the water gun, the Mini G.I G15 / I15 proved to be better adapted to complex areas of steeply dipping structures, especially at shallow depths where velocities are low, given the fixed minimum spatial sampling interval of the streamer sections (1.25 m) and the available instruments (seismograph, boat).

8.1.3 Navigation and positioning

The higher the recorded frequencies and the smaller the spatial sampling intervals are in a high-resolution survey, the more accurate the ship navigation and shot and receiver positioning need to be. Having the advantage of a lacustrine setting with shorelines always in close vicinity allowed application of the most accurate positioning tool, the differential GPS, with a reference station set up onshore. Two separate GPS antennas onboard built the first system of navigation and ship positioning during Survey I. Because differential correction was available only for the recording of the ship coordinates and resulted in a maximum precision of 0.5 m, ship navigation did not reach an accuracy of more than 2-3 m. Thus, navigation and positioning represented two independent processes and recorded positions could neither be displayed nor used for quality control onboard. The shot triggering program determined position with respect to a starting point by measuring the ship's velocity. Although boat speed was adjusted regularly, it was unavoidable that small errors in actual shot distance accumulated in the integration towards the end of each navigated line. There is no means to estimate the actual error made in shot and receiver positioning if all positions have to be extrapolated during data processing from the vessel's antenna position - the only recorded reference during Survey I. These extrapolated positions more or less strongly mimic the ship course, depending upon the amount of ship track curvature. Hence, streamer feathering due to cross-line currents could not be considered at all. The only possibility to determine the actual total feathering is to have at least one more device on the streamer itself.

For these reasons, navigation and positioning needed to be greatly improved. For Survey II, three other dGPS receivers, besides the onboard dGPS antenna, measured absolute coordinates at the end of each streamer. Rafts were constructed that carried these antennas as well as mini disks for data storage during one acquisition day. The recorded data were unloaded every evening for subsequent postprocessing. Combined with the boat location at shot time, calculation of each receiver position was then possible. Furthermore, navigation and distance shooting significantly improved with the aid of a newly developed navigation and triggering program. This program places virtual grid lines on the survey area at intervals of the desired shot spacing and perpendicular to survey direction. Every time the boat crosses one of these grid lines, a shot is triggered. As soon as the antenna position is received, the ship track can be monitored in real-time on the onboard PC. Due to the 5 Hz dGPS coordinate reading rate, the maximum possible error of triggering behind the grid line is 25 cm. Since grid lines are equidistant and triggering depends on real coordinates instead of shot intervals, the error is not cumulative and varies only slightly with changes in ship velocity. A systematic coordinate shift of 19 cm, due to a delay in transmission and calculation, combined with the triggering inaccuracy, gives a maximum absolute error between theoretical and measured boat position of no more than 44 cm. However, only the variation of maximally 25 cm is important for seismic data quality and binning accuracy. Thus, this new navigation program presents a

powerful tool for high-resolution marine acquisition: it performs automatic shot sampling in combination with real-time control on navigation quality.

A comparison of measured onboard antenna positions of both surveys showed a remarkable improvement when using the new software. Whereas sail lines in Survey II have been navigated almost perfectly straight and shot points lined up at 5 m intervals along virtual grid contours, ship positions for Survey I had an accuracy of maximally 2 to 3 m, sail lines were not equidistant and identical shot point numbers not aligned. Examples within the 3-D data cube of Survey I showed that the use of the improved navigation software as well as the additional dGPS rafts along the single-streamer configuration would have been necessary to avoid positioning errors that resulted in degradation of data quality of the stacked and migrated images.

8.1.4 The test site

In Lake Geneva, offshore the Ouchy harbor of Lausanne, recent high-resolution 2-D investigations (Morend, 2000) revealed a complex fault zone. This major thrust fault system has a total vertical throw of ~1 km and trends southwest – northeast. It separates two tectonic units, the Plateau Molasse and the Subalpine Molasse. Its northwestern limit was accurately picked by Morend (2000), and very likely represents the extension of the Paudèze Fault mapped onshore by Weidmann (1988). Morend et al. (2002) noted the difficulty to correlate complex geological structures across seismic lines only 50 m apart. They suggested that a continuous 3-D seismic survey with a higher penetration depth would be the best way to extrapolate onshore structures into Lake Geneva. Moreover, such a survey might as well allow accurate mapping of a channel system they recognized in the area northwest of the fault zone. Such prospect and the close vicinity to the harbor make this study site well suited to test our 3-D acquisition systems. Knowing the exact position of the fault limit and the approximate strike of the Plateau Molasse strata (parallel to this limit), it was easy to outline a 3-D area that centers the frontal thrust perpendicular to survey direction. The resulting data sets complement the seismic work of Morend et al. (2002) by producing a deeper, but still very high-resolution continuous three-dimensional image of the highly deformed fault zone.

8.1.5 Survey area

Thanks to 2-D profiles shot across the survey site, the extension of the fault zone in dip direction was known down to approximately 350 m. For a 30° dip and a 400 m deep target within the fault zone, the migration aperture in in-line direction amounted to 230 m. In order to migrate the complete fault zone, the survey area needed to include at least twice this migration aperture, resulting in a minimum length of 810 m per sail line. Since the structure within the molasse on both sides of the fault zone is of interest as well, in-lines were set to a total length of 1200 m for Survey I, and to 1500 m for Survey II. This additional extension is

the consequence of an observed difficulty during Survey I to image enough of the Subalpine Molasse southeast of the fault zone to get an idea of its characteristics.

8.1.6 Acquisition geometry

Several criteria influenced the choice of acquisition geometry. In Survey I, a mixture between parallel and antiparallel geometry was used in order to minimize the time spent moving from the end of one sail line to the start of the next. Whereas consecutively navigated lines were antiparallel (with opposite direction) and about 8 lines apart, the acquisition pattern resulted in patches of parallel (same direction) lines in alternating direction - with a total of up to 13 lines recorded during a single acquisition day. When using the single-streamer configuration, one boat pass meant one CMP line and it was important to shoot a great number of lines to obtain a reasonably squared survey area in a limited number of survey days. A total of 80 sail lines was recorded over 8 days, covering an area of 1200 x 600 m.

Survey II was acquired in parallel geometry for several reasons: firstly, the three-streamer configuration obtained three CMP lines per boat pass, accounting for the required extra acquisition time; secondly, the chosen Mini G.I G15 / I15 Air Gun required a turning time of at least 19 minutes to have the necessary amount of air produced by the compressor; and thirdly, because antiparallel shooting with an asymmetric system (one source, many receivers) would produce different stacks and unlike attenuation of high frequencies for opposite directions. Accounting for the halved cross-line spacing (3.75 m) and the slightly longer line length, Survey II covered the same cross-line distance of 85 m in one day as in Survey I. A total of 60 sail lines (or 180 CMP lines) was recorded in 9 days, covering an area of 1500 x 675 m. The parallel geometry in combination with our navigation system that references boat position instead of the first CMP had two advantages: 1) having more uniformly stacked data in cross-line direction and 2) it produced an evenly distributed fold at survey boundaries and facilitated subsequent data processing. Both, navigation quality and acquisition geometry have been significantly improved in Survey II.

8.1.7 Survey direction

The survey direction (downdip or updip) becomes important when shooting with an asymmetric system in parallel geometry. The largest array length (the streamer), should be placed in updip direction, because in this way, reflections are recorded almost vertically and high-frequency attenuation is minimized. Survey II should have been ideally shot completely in updip direction, i.e. from the coast to the deep lake, thereby reducing the effect of steep dip on the reflection character. However, the difference is only visible through careful inspection of two neighboring lines acquired in opposite directions and, because the streamer of Survey II had a length of only 62.5 m, this effect will be negligible. Anyhow, in order to have the best possible data quality, future surveys should always be shot with parallel geometry and updip with respect to target inclination.

8.1.8 Data processing

The new navigation and positioning software not only improved ship maneuvering and shot triggering during acquisition, but resulted in a better navigation data quality. The latter influenced subsequent processing steps, such as geometry assignment and bin harmonization. For both surveys computer programs were written to undertake necessary coordinate interpolations and format the output navigation data for merge with the seismic traces. Because the commercial processing software has been developed for exploration industry standards, algorithms are programmed according to that standard's scale and are not always adapted to very high-resolution imaging. So, in addition to having non-conventional navigation data that needed to meet industry format, it was required to adjust seismic trace header words to a classical use within processing routines. Although this worked well for 3-D post-stack migration, semblance calculations within velocity analysis and all distance calculations were limited to industry orders of magnitude.

A conventional processing flow has been applied using data organized in bins of common midpoints and line numbers. After data formatting and arrival time delay corrections, processed navigation data were merged with the seismic traces and geometry was assigned. Further prestack processing included trace editing, bin harmonization and a detailed velocity analysis on DMO corrected gathers before final DMO and NMO correction and stack. Post-stack processing comprised a 3-D one-pass time migration in the frequency-space domain. The raw data volumes ranged between 8 and 11 GB and were reduced to 670 and 1.8 GB after stack.

During geometry assignment, great care was taken to find a reference grid that allowed the definition of the same CMP and line numbers for both surveys. However, since distances between ship antenna and energy source were different and had not been chosen as a multiple of the in-line bin size, the defined bin centers deferred by 35 cm or 15 cm from the ideal midpoint positions of Survey I, depending upon the survey direction of the line. If any future surveys were to be acquired with our positioning system in antiparallel geometry, it would be important to define the distance between reference antenna and energy source as a multiple of the bin size, or otherwise adjacent cross-line bins would contain systematically shifted midpoints. As soon as two or more surveys are supposed to be compared on the same study site, this becomes a necessary criterion even for parallel surveys. Only then do theoretical midpoints fall on the same bin center and are assigned to the correct coordinates when stacked.

Bin harmonization represented an important part of the 3-D processing sequence, because navigation accuracies and streamer feathering caused uneven coverage, especially during Survey I. Aiming at having only one trace per offset class and bin, bins were harmonized for both surveys by duplicating those traces within the same offset class that come from either one of the two adjacent cross-line bins. This method was successful in the

way that only very view bins remained empty and the overall fold became close to nominal. Bin harmonization also improved the performance of later DMO correction, a process in which reflection energy of dipping reflectors is moved to adjacent bins.

In order to obtain a zero-dip rms velocity model, a detailed two-step analysis was performed on a total of 600 semblance spectra of the data of Survey I computed on every second in-line and every 50th CMP. Velocity picking on subsets of those semblance spectra showed that the complexity of the chosen survey site required detailed velocity information at intervals not bigger than 15 m in fault strike and about 60 m in fault dip direction. Interval velocities range from 1420 m/s at the water bottom to 3000 m/s at about 410 ms. Below this time, no more velocity picking was possible due to the limited signal penetration of the water gun and a lack of semblance values. A velocity analysis on the data of Survey II has not yet been performed. Although the larger penetration of the lower frequency air gun will facilitate velocity analysis at depth, half the maximum offset will make velocity distinction more difficult due to the limited moveout. Test analyses on semblance spectra, calculated on the 24 nearest offset traces of Survey I, showed that velocity functions could be picked with almost the same accuracy as on the full range of all 48 offsets. However, these tests can not replace velocity analysis on the data of a different source.

The post-stack time migrated data cubes represented the final result of the conventional processing sequence. Although there is still room for improvement, the exceptionally good data quality of the final images of both cubes shows the potential of 3-D high-resolution acquisition design and conventional processing techniques.

8.1.9 Data quality

The data quality of both surveys varies significantly with respect to vertical and horizontal resolution as well as to signal penetration and fold distribution at survey boundaries (see summary of all parameters in Table 5-A and Table 5-B). Whereas during Survey II, the lower frequency signal of the air gun penetrated the Plateau Molasse to more than 300 m below the water bottom, the higher frequency water gun of Survey I reaches maximally 145 m. Thus, higher penetration in Survey II was traded off against lower vertical resolution (at best 1.1 m versus 60 cm), although reflections in Survey I seem much less continuous and difficult to trace. This latter difference influences the potential of tracing a smaller thrust fault within the Plateau Molasse or the fault zone limits in time slices. This might be due to a lack in signal-to-noise ratio or simply to the fact that the shorter wavelengths of the water gun might not see the fault plane as a homogeneous reflective surface. The greater variability of geological structure resolved by this source and the resulting lack in reflector continuity seem to make it more difficult to delineate larger scale discontinuities that frame geological units over a more extended depth range.

The effective horizontal resolution of migrated data depends upon the dominant frequency of the reflected signal but also on the spatial sampling or bin size. Although the theoretical horizontal resolution after migration of Survey I (2.2 m) is higher than that of Survey II (4.4 m), the bin size in cross-line direction places the resolution limit to 7.5 m. This spatial sampling interval was obviously not sufficient to resolve the topographic details within the survey area. Bathymetry in Survey I seemed as if filtered and smoothed. On the one hand, it makes duplication distance across data holes over complex zones too large; on the other hand, it influences the correctness of the migration process. Moreover, the appearance of more than one water bottom reflection on stacks of the same in-line in areas of complex topography can be explained by incorrect binning in Survey I. Due to the combination of too coarse sampling and insufficient accuracy of ship navigation and streamer positioning, the binning error was far more elevated than in Survey II, especially because the streamer had double the length. Based on this experience, it is recommended for future surveys over similarly complex topographic relief to choose bin dimensions that are smaller than the dominant wavelength of the selected signal at the shallowest target depth.

The effect of having false lateral energy migrated into a seismic section – whether through navigation errors or aliasing along the migration path as a consequence of too coarse spatial sampling – might severely degrade interpretation results. Consequently, the acquisition parameters of the multi-streamer system are better adapted to the remarkable complexity and three-dimensionality of the survey area. The excellent data quality of Survey II was used for tests on depth migration with very promising results showing that more sophisticated processing techniques can further improve the final interpretable image. This very high-resolution data set is a rare example to demonstrate that 3-D prestack depth imaging can be applied to near surface seismics. But even without this complicated and time-consuming processing step, the 3-D time migrated data are well interpretable and give an idea of the ability of the system to capture rapid structural changes in all directions.

8.1.10 Geological interpretation

In order to demonstrate the potential for detailed geological and tectonic interpretation, data were loaded into an interpretation software and several horizons and fault surfaces were traced through the complete data cube. Even with the delineation of only some such boundaries over the survey area, new insight into small-scale geomorphological features and geological processes was possible. Besides the detection of some minor thrust faults within the Plateau Molasse, the concave three dimensional shape of the Paudèze Fault surface could be visualized and possibly related to a regional rapid morphological change in bathymetry but also in the morphology of the erosional surface and an internal horizon of the Plateau Molasse. Three dimensional imaging of such structures revealed changes in dip direction within the same horizon and time slices allowed easy determination of true dip directions.

Although only larger-scale morphological aspects of the 3-D data cube were interpreted, smaller-scale features, such as on-lapping reflectors and differential erosion could be observed. A complete geological interpretation of this and maybe also of the second data cube remains one of the future perspectives.

8.2 Conclusions

The main objective of this project, the development of an efficient high-resolution 3-D multi-channel seismic reflection system that is adapted to small-scale three-dimensional targets in lake environments has been reached with great success. The final system allows acquisition of high quality data, which already after conventional 3-D time processing show particularly clean, interpretable images of complex subsurface structure in all directions. In order to achieve this goal, the whole sequence of different components of the seismic method has been worked through: it extends from the acquisition and construction of all necessary equipment, over instrument testing, target selection and survey design to data acquisition, processing and interpretation.

Two complete 3-D surveys, covering an area of about 1 km², have been carried out over the same target site, a complex thrust fault zone in Lake Geneva near the city of Lausanne. Having first utilized a single, then a multi-streamer configuration with different source types, Survey II represented the advanced version of Survey I, which was conducted using a start-up experimental composition of the equipment as it was available at the beginning of this work. The main improvements were the development of an accurate navigation and positioning system, including a new navigation software that performs automatic shot sampling in combination with real-time control on navigation quality, as well as the conception of three independent dGPS streamer positioning units. Furthermore, design parameters were better adapted to small scale three dimensional morphological variations in areas of steeply dipping (<30°) structures as present in the study site.

The high-frequency (<2000 Hz) water gun source was considered inadequate to cope with this type of target when used as in Survey I with the old navigation system and a cross-line spacing of 7.5 m. Despite the theoretically greater vertical resolutions, it has a reduced horizontal resolving power. This is related to problems with insufficient lateral sampling and positioning accuracy that caused incorrect binning and aliasing in the 3-D migration algorithm. It resulted in a lack of reflector continuity and made it more difficult to delineate larger-scale discontinuities between different lithologies. The still high-resolution Mini G.I Air Gun with each chamber reduced to 15 in³ and frequencies below 650 Hz proved to be the more appropriate source both with respect to aliasing considerations and signal strength. However, combination of the water gun with the improved navigation and positioning system and the smaller cross-line sampling of Survey II might also produce satisfactory results in very shallow targets.

Another important development represented the change from the single- to a three-streamer system through the construction of two retractable booms that hold the streamers at the required distance of 7.5 m for the desired cross-line spacing of 3.75 m. Although the three-streamer system decreased acquisition time by a factor of three, the reduced cable lengths halved the maximum offset and the nominal fold.

If acquisition time and cost did not play a role, the ideal survey design using the available equipment would be the single-streamer, zero-azimuth configuration using all 72 channels. However, since the effect of small azimuth variations and the reduced fold and offset still produced excellent data results, the developed three-streamer system presents itself as the more economic compromise and as an overall very powerful 3-D acquisition tool for lake studies in complex areas.

Processing of very high-resolution data sampled in time intervals below 1 ms and space intervals of less than a meter turned out to be a complicated task because the available exploration industry software was often not adapted to high-resolution imaging. Nevertheless, a 3-D conventional processing flow has been tailored to work around the software's sampling requirements and was complemented by two computer programs that format the unconventional navigation data to industry standards.

Delineation of several horizons and fault surfaces in the time-migrated data of Survey II revealed the potential for detailed small-scale geological and tectonic interpretation in three dimensions. Preliminary tests with a 3-D preserved amplitude prestack depth migration algorithm demonstrate that the excellent quality of this data set allows application of such sophisticated techniques even to shallow seismic surveys.

The adaptation of the 3-D marine seismic reflection method, which to date has almost exclusively been used by the oil exploration industry, to a smaller scale and financial budget has smoothed the way of this technique into university research and might also be used for civil engineering purposes in the future.

8.3 Outlook

This work has developed an efficient high-resolution 3-D seismic reflection system for lake studies in complex areas. It also established a conventional time processing sequence that allowed subsequent detailed geological interpretation of the resulting data cube in all directions. Although the main target was reached with great success, there remain many possibilities to improve and complement this pioneer research. Here are some suggestions and recommendations for future surveys concerned firstly with the design and acquisition process, secondly with the processing of the data and thirdly with its interpretation.

Design and acquisition:

1. A thorough calibration of all three streamer sections is needed.

2. Streamer positioning of future acquisitions might still be improved by adding at least one more dGPS raft to each streamer. If the single-streamer configuration is used, three or more such positioning units should be attached to the longer and more feathered streamer.
3. Preferably, acquisitions ought to be conducted in parallel geometry and in updip direction. If time lapse studies were an objective, the distance between antenna and first hydrophone should be a multiple of the chosen in-line bin dimension.
4. Future surveys will be acquired with the aid of the recently purchased faster Geometrics Geode 96-channel seismograph, whose output SEG-Y format contains precise information on missing shots and whose more sophisticated onboard control and better recording quality will much improve the output raw data.
5. A cross-line bin size of 3.75 m or less is essential to guarantee no spatial aliasing and fine enough sampling for subsequent 3-D migration. The purchase of another 24-channel streamer section and the construction of two additional shorter 2-m long booms would allow four-streamer acquisitions. This configuration with a cross-line bin size of 2.5 m produces an even better horizontal resolution in about the same surveying time as when using three streamers.

Processing:

6. Given that Géovecteur version 8100 will be used as the processing software for high-resolution data sampled at intervals below 1 ms, it would be preferable to multiply all distances in the navigation data by a factor of 100 in order to preserve the decimals in the seismic trace headers or otherwise to choose a more adapted software.
7. The already conceived despiking job, which finds and eliminates short energy bursts that are present especially in the data recorded with the BISON seismograph, should be applied to the raw data of both surveys and the whole processing sequence repeated. Additionally, the overall data quality and signal-to-noise ratio could be further enhanced by scaling to an average mean those traces that show a lack in hydrophone sensitivity. However, for future amplitude versus offset (AVO) studies or for application of a preserved amplitude prestack depth migration, a thorough hydrophone calibration has to be performed.
8. Detailed velocity analysis on the data of Survey II will allow comparison of semblance spectra of both sources and might extend velocity model to greater depths.
9. Inclusion of other processing steps such as deconvolution and multiple removal, steps not yet considered in the current processing flow, might further improve data quality and reveal previously masked reflections at depth. Because tests on spiking deconvolution showed that the resulting deconvolved traces have a less good quality than the original ones and predictive deconvolution did not produce satisfactory

results either, it seems essential to integrate the previously measured source signature into these processes. Anyhow, the lack of moveout in both our systems will make the reduction of strong multiple energy very difficult.

Interpretation:

10. Although the delineation of larger-scale morphological aspects showed the great potential for a detailed geological analysis of the data of Survey II, a complete structural and tectonic interpretation remains one of the future perspectives.
11. Since geologists prefer to work on subsurface images as realistic as possible, i.e. represented in depth instead of time, and to better account for true reflection point positions and AVO, first steps have been undertaken to apply a 3-D preserved amplitude prestack depth migration code to the high quality data of Survey II. After some modifications of the algorithm by Philippe Thierry, preliminary tests have been run at the Ecole des Mines de Paris with very promising results. However, before interpreting results an appropriate pre-processing sequence on calibrated real amplitude input data will first have to be established. A proposal for post-doctoral research that promotes a continuation of this collaboration in the direction of adapting such sophisticated imaging algorithms to shallow seismic marine data has been submitted and will be one of the main objectives for future endeavors towards high-resolution imaging techniques in university research.

REFERENCES

- Baina, R., Thierry, P., Calandra, H. and Devaux, V., 2002. 3-D preserved amplitude PsDM & AVA relevance. *The Leading Edge*, **21** (12): 1237-1241.
- Baron, L., 2001. Détermination dans les forages de l'élasticité des sols à l'aide de sondes. *Ph.D. Thesis*, University of Lausanne, Lausanne, Switzerland: 268 pp.
- Beres, M., Scheidhauer, M. and Marillier, F., 2003. Imaging Perialpine Structures in Lake Geneva, Switzerland, with 3-D High-Resolution Seismic Reflection Methods. *Eclogae Geologicae Helveticae*, **Supplement 1** (Lake Systems - From Ice Age to Industrial Time): 31-38.
- Berger, J.-P., 1992. Correlative chart of the European Oligocene and Miocene: application to the Swiss Molasse Basin. *Eclogae Geologicae Helveticae*, **85**: 573-609.
- Bersier, A., 1958a. Exemples des sédimentation cyclothématique dans l'Aquitainien de Lausanne. *Eclogae Geologicae Helveticae*, **51**: 842-853.
- Bersier, A., 1958b. Séquence détritiques et divagations fluviales. *Eclogae Geologicae Helveticae*, **51**: 854-893.
- Canning, A. and Gardner, G.H.F., 1996. Another look at the question of azimuth. *The Leading Edge*, **15** (7): 821-823.
- Chapron, E., 1999. Contrôles climatique et sismo-tectonique de la sédimentation lacustre dans l'avant-pays alpin (Lac du Bourget, Léman) durant le Quaternaire récent. Géologie Alpine Mémoire 30. *Ph.D. Thesis*, University of Joseph Fourier, Grenoble, France: 261 pp.
- Chaudhary, I., 2002. 2D-high resolution seismic survey in Lake Geneva across the Molasse transition zone in South-West of Switzerland. *Diplôme Thesis*, University of Lausanne, Lausanne, Switzerland: 63 pp.
- Chaudhary, I., Dupuy, D., Scheidhauer, M. and Marillier, F., 2002. The Molasse Fault Zone in Lake Geneva, South-West Switzerland, From High-Resolution Seismic Reflection Data. *Proceedings of 8th Meeting of Environmental & Engineering Geophysical Society*, European Section, Sept. 8-12, Aveiro, Portugal.
- Deregowski, S., Bloor, R. and Koeninger, C., 1997. Increasing lateral resolution. *59th Conference: European Association of Geoscientists & Engineers*, Extended Abstracts, Geneva, Switzerland: A024.
- Dodds, D.E., 2002. Quantization and Coding. *Course notes for Communication Systems EE352*, University of Saskatchewan, Saskatoon, Canada, <http://128.233.12.252/Web-EE352/HomePage352.html>: Chapter 5, 85-111 pp.
- Dragoset, W.H., 1990. Air-gun array specs: A tutorial. *The Leading Edge*, **9** (1): 24-32.
- Durand, J., 2001. La numérisation d'un signal. *DEA Thesis*, Université Louis Pasteur Strassbourg, Strassbourg, France, http://phineas.u-strasbg.fr/~marquis/Enseignement/Public/DEA/Numer/Numerisation_2001_b.html: 9 pp.

- Evans, B.J., 1997. A Handbook for Seismic Data Acquisition in Exploration. In: Dragoset Jr., W. H. (Ed.), *geophysical monograph series*, 7. Society of Exploration Geophysicists, Tulsa, OK, 305 pp.
- Finckh, P., Kelts, K. and Lambet, A., 1984. Seismic stratigraphy and bedrock forms in perialpine lakes. *Geological Society of America Bulletin*, **95**: 1118-1128.
- Fricke, J.R., Davis, J.M. and Reed, D.H., 1985. A standard quantitative calibration procedure for marine seismic sources. *Geophysics*, **50** (10): 1525-1532.
- Gorin, G.E., Signer, C. and Amberger, G., 1993. Structural configuration of the western Swiss Molasse Basin as defined by reflection seismic data. *Eclogae Geologicae Helvetiae*, **86** (3): 693-716.
- Gorin, G.E., Dupont, G., Morend, D. and Pugin, A., 2001. Paleofaults, glacial erosion and Quaternary sediments in Lake Neuchâtel, as derived from high-resolution seismic reflection. *Program and Abstracts of 181st Congress of Swiss Academy of Sciences (Lake systems from ice age to industrial time)*, Oct. 17-20, Yverdon-Les-Bains, Switzerland.
- Henriet, J.-P., Verschuren, M. and Versteeg, W., 1992. Very high resolution 3D seismic reflection imaging of small-scale structural deformation. *First Break*, **10** (3): 81-88.
- Homewood, P.A., Allen, P.A. and Williams, G.D., 1986. Dynamics of the Molasse Basin of western Switzerland. In: Allen, P. A. and Homewood, P. A. (Eds), *Foreland basins*, **8**. Special Publication of the International Association of Sedimentologists, Blackwell, Oxford, 199-217 pp.
- Hurn, J., 1989. GPS - A Guide to the Next Utility. Trimble Navigation Ltd., Sunnyvale, CA, U.S.A., 76 pp.
- Lansley, R.M., 2000. 3D seismic survey design: a solution. *First Break*, **18** (5): 162-166.
- Lansley, R.M. and Stupel, M., 2000. Planning and Executing a Marine 3-D Seismic Survey, *Continuing Education Workshop*. Society of Exploration Geophysicists, Calgary, Canada.
- Levin, F.K., 1971. Apparent velocities from dipping interface reflections. *Geophysics*, **36** (3): 510-516.
- Loizeau, J.L., 1991. La sédimentation récente dans le delta du Rhône, Léman: processus et évolution. *Ph.D. Thesis*, University of Geneva, Geneva, Switzerland: 209 pp.
- Macfarlane, P.A., Whittemore, D.O., Townsend, M.A., Doveton, J.H., Hamilton, V.J., Coyle III, W.G., Wade, A., Macpherson, G.L. and Black, R.D., 1989. The Dakota Aquifer Program Annual Report, FY 1989. *Open-file Report 90-27*, Kansas Geological Survey, <http://www.kgs.ukans.edu/Dakota/vol3/fy89/index.htm>.
- Marsset, B., Missiaen, T., De Roeck, Y.-H., Noble, M., Versteeg, W. and Henriët, J.-P., 1998. Very high resolution 3D marine seismic data processing for geotechnical applications. *Geophysical Prospecting*, **46**: 105-120.

- Marsset, T., Marsset, B., Thomas, Y. and Didaieller, S., 2002. Sismique très haute résolution 3D: une nouvelle méthode d'imagerie des sols superficiels. *C. R. Geoscience*, **334** (6): 403-408.
- Missiaen, T., Versteeg, W. and Henriët, J.-P., 2002. A new 3D seismic acquisition system for very high and ultra high resolution shallow water studies. *First Break*, **20** (4): 227-232.
- Morend, D., 2000. High-resolution seismic facies of alluvial depositional systems in the Lower Freshwater Molasse (Oligocene - early Miocene, western Swiss Molasse Basin). *Ph.D. Thesis*, University of Geneva, Geneva, Switzerland: Vol. 23, 97 pp.
- Morend, D., Pugin, A. and Gorin, G.E., 2002. High-resolution seismic imaging of outcrop-scale channels and an incised-valley system within the fluvial-dominated Lower Freshwater Molasse (Aquitainian, western Swiss Molasse Basin). *Sedimentary Geology*, **149**: 245-264.
- Moscariello, A., Pugin, A., Wildi, W., Beck, C., Chapron, E., De Batist, M., Girardclos, S., Ochs, S.I., Rachoud-Schneider, A.-M., Signer, C. and Van Clauwenberghe, T., 1998. Déglaciation würmienne dans des conditions lacustres à la terminaison occidentale du bassin lémanique (Suisse occidentale et France). *Eclogae Geologicae Helvetiae*, **91**: 185-201.
- Müller, C., Milkereit, B., Bohlen, T. and Theilen, F., 2002. Towards high-resolution 3D marine seismic surveying using Boomer sources. *Geophysical Prospecting*, **50** (5): 517-526.
- Musser, J.A., 2000. 3D seismic survey design: a solution. *First Break*, **18** (5): 166-171.
- Parkes, G. and Hatton, L., 1986. The Marine Seismic Source, *Seismology and Exploration Geophysics*. D. Reidel Publishing Company, Dordrecht, The Netherlands, 110 pp.
- Pasasa, L., Wenzel, F. and Zhao, P., 1998. Prestack Kirchhoff depth migration of shallow seismic data. *Geophysics*, **63** (4): 1241-1247.
- Pugin, A., Pullan, S.E., Burns, R.A., Douma, M. and Good, R.L., 1999. High-resolution multichannel, marine seismic surveying using a small airgun source. *Proceedings of the Symposium on the Application of Geophysics to Engineering & Environmental Problems*, Oakland, California, U.S.A.: 255-264.
- Rigassi, D., 1977. Subdivision et datation de la Molasse "d'eau douce inférieure" du Plateau suisse. *Paleolab News*, **1**: 1-42.
- Rowlett, R., 2001. How Many? A Dictionary of Units of Measurement, University of North Carolina, Chapel Hill, NC, U.S.A., <http://www.unc.edu/~rowlett/units/index.html>.
- Sanderson, D.J. and Marchini, W.R.D., 1984. Transpression. *Journal of Structural Geology*, **5**: 449-458.
- Sheriff, R.E. and Geldart, L.P. (Editors), 1982. Exploration Seismology (in 2 volumes), First Edition. Cambridge University Press, New York, U.S.A.

- Sheriff, R.E., 1991. Encyclopedic Dictionary of Exploration Geophysics, Third Edition, *Geophysical References Series*, 1. Society of Exploration Geophysicists, 384 pp.
- Sheriff, R.E. and Geldart, L.P., 1995. Exploration Seismology, Second Edition. Cambridge University Press, Cambridge, U.K., 592 pp.
- SODERA and Seismic Systems, Inc., 1990. T Water Gun Type S 15. *Instruction Handbook*, Houston, Texas, U.S.A.: 31 pp.
- SODERA and Seismic Systems, Inc., 1995. Mini G.I Gun. *Operation and Maintenance Manual*, Houston, Texas, U.S.A.: 46 pp.
- SODERA and Seismic Systems, Inc., 1997. G.I Gun. *Manual*, Houston, Texas, U.S.A.: 20 pp.
- Staller, L., 2002. Improving A/D Converter Resolution by Oversampling and Averaging. *Tech Note*, Cygnal Integrated Products, Inc., Austin, Texas, U.S.A., <http://www.chipcenter.com/TestandMeasurement/tn033.html>: 7 pp.
- Steeple, D.W. and Miller, R.D., 1998. Avoiding pitfalls in shallow seismic reflection surveys. *Geophysics*, **63** (4): 1213-1224.
- Stone, D.G., 1994. Designing Seismic Surveys in Two and Three Dimensions. In: Meeder, C. A. (Ed.). Society of Exploration Geophysicists, Tulsa, OK, 244 pp.
- Sullivan, K., 1998. Defining Accuracy with ENOB, Data Translation, Marlborough, MA, USA, www.sensormag.com/articles/0898/da0898/main.shtml: 5 pp.
- Tacchini, G. and Zingg, O., 2000. Etude Sismique Lacustre Haute Résolution du Delta du Rhône, Lac Léman, Suisse. *M.S. Thesis*, University of Lausanne, Lausanne, Switzerland: 151 pp.
- Taner, M.T. and Koehler, F., 1969. Velocity spectra - digital computer derivations and applications of velocity functions. *Geophysics*, **39** (6): 859-881.
- Telford, W.M., Geldart, L.P. and Sheriff, R.E., 1990. Applied Geophysics, Second Edition., New York, U.S.A.
- Thierry, P., Lambaré, G., Podvin, P. and Noble, M.S., 1999. 3-D preserved amplitude prestack depth migration on a workstation. *Geophysics*, **64** (1): 222-229.
- Van Rensbergen, P., De Batist, M., Beck, C. and Manalt, F., 1998. High-resolution seismic stratigraphy of late Quaternary fill of Lake Annecy (northwestern Alps): evolution from glacial to interglacial sedimentary processes. *Sedimentary Geology*, **117** (1-2): 71-96.
- Van Rensbergen, P., De Batist, M., Beck, C. and Chapron, E., 1999. High-resolution seismic stratigraphy of glacial to interglacial fill of a deep glacial lake: Lake Le Bourget, Northwestern Alps, France. *Sedimentary Geology*, **128** (1-2): 99-129.
- Verbeek, N.H. and McGee, T.M., 1995. Characteristics of high-resolution marine reflection profiling sources. *Journal of Applied Geophysics*, **33** (4): 251-269.
- Vermeer, G.J.O., 1991. Symmetric sampling. *The Leading Edge*, **10** (11): 21-29.
- Vermeer, G.J.O., 2001. Understanding the fundamentals of 3D seismic survey design. *First Break*, **19** (3): 130-134.

- Vermeer, G.J.O., 2002. 3-D Seismic Survey Design. In: Beasley, C. J. (Ed.), *Geophysical references*, **12**. Society of Exploration Geophysicists, Tulsa, OK, U.S.A.
- Vernet, J.-P., Horn, R., Badoux, H. and Scolari, G., 1974. Etude structurale du Léman par sismique réflexion continue. *Eclogae Geologicae Helvetiae*, **67** (3): 515-529.
- Weidmann, M., 1988. Feuille 1243 Lausanne. *Atlas Géol. Suisse* 1:25 000, Carte et Notice expl. 85.
- Weidmann, M. and Morend, D., 2002. Anciennes vallées dans la Molasse grise de Lausanne (Aquitaniens, USM, Suisse occidentale). *N. Jb. Geol. Paläont. Abh.*, **223** (2): 163-182.
- Yilmaz, Ö., 1987. Seismic Data Processing, Seventh Printing. In: Doherty, S. M. (Ed.), *Investigations in Geophysics*, **2**. Society of Exploration Geophysicists, Tulsa, 526 pp.
- Yilmaz, Ö., 2001. Seismic Data Analysis - Processing, Inversion, and Interpretation of Seismic Data, Second Edition,. In: Cooper, M. R. (Ed.), *Investigations in Geophysics*, **II**. Society of Exploration Geophysicists, Tulsa, 2025 pp.
- Zingg, O., Tacchini, G., Marillier, F., Scheidhauer, M. and Beres, M., 2003. Sédimentation récente sur le delta du Rhône à partir de profils sismiques réflexion à haute résolution. *Eclogae Geologicae Helvetiae*, **Supplement 1** (Lake Systems - From Ice Age to Industrial Time): 21-30.

APPENDIX

N	2^n	A_{\max}/A_{\min}	D	S/N ratio
1	2^1	2	6	7.79
2	2^2	4	12	13.81
3	2^3	8	18	19.83
4	2^4	16	24	25.85
5	2^5	32	30	31.87
6	2^6	64	36	37.89
7	2^7	128	42	43.91
8	2^8	256	48	49.93
9	2^9	512	54	55.95
10	2^{10}	1'024	60	61.97
11	2^{11}	2'048	66	67.99
12	2^{12}	4'096	72	74.01
13	2^{13}	8'192	78	80.03
14	2^{14}	16'384	84	86.05
15	2^{15}	32'768	90	92.07
16	2^{16}	65'536	96	98.09
17	2^{17}	131'072	102	104.11
18	2^{18}	262'144	108	110.13
19	2^{19}	254'288	114	116.15
20	2^{20}	1'048'576	120	122.17
21	2^{21}	2'097'152	126	128.19
22	2^{22}	4'194'304	132	134.21
23	2^{23}	8'388'608	138	140.23
24	2^{24}	16'777'216	144	146.25

Table A-1. Relationship between number of bits of the recording instrument (n), binary system level, total number of quantizing levels, theoretical dynamic range ($n*6\text{dB}$), and theoretical S/N ratio (in dB). Highlighted are the 20-bit and 22-bit values of the BISON and GEOMETRICS seismographs (section 3.3), respectively.

Acquisition statistics

Survey I

In September 1999, four days of single-streamer acquisition served as the final test of all components as they were going to be used for Survey I. Furthermore, we conducted the Mini G.I G30 / I30 signature test (see section 3.4.6 and Table A-8). Sample profiles were shot on the first 7 theoretical navigation lines of the acquisition preplot (Fig. 4-3 and Table A-9) and recorded with the BISON seismograph. Strong 100 Hz noise contaminated the resulting data induced by the recording instrument. This is why we decided to use the GEOMETRICS from the University of Geneva (section 3.3) to acquire sail lines 5, 6, 11 and 12 of Survey I (Fig. 5-2) at a sampling rate of 0.25 ms and a trace length of 500 ms. This time, data quality was satisfactory.

Survey I was planned to take place between October 12 and October 26, 1999, containing 11 working days. During the first two days “La Licorne” was loaded, the equipment installed and tested. The last two days served for water gun signature tests (see section 3.4.6 and Table A-6) and the recording of 2-D profile 140_30, which corresponds to the extension of sail line 55 of Survey I (see section 4.3 and Table A-12). On October 14, the shooting of navigation lines for the 3-D survey began. Table A-16 shows the acquisition sheet of sail line 5, the first in-line, containing notes on that specific line but also all general acquisition parameters. Table A-2 is an accumulation of the specific information from acquisition sheets of all navigated lines of Survey I.

The listing of every navigated line, their start and end time and the corresponding air pressure consumed and that remaining in the bottles, allowed some general statistics. It took an average of 16 minutes to shoot one line and 14 minutes to turn around to the beginning of the next. Some results of this table had already been used for calculations with regard to air consumption in section 3.4.3. The compressor was not always running during data recording, so that one average expresses the net air consumption with the compressor turned on (light grey) and the other expresses the real water gun air consumption without simultaneous air production (dark grey). While the average water gun air consumption with 25.69 NI/shot is slightly higher than the predicted 23.33 NI/shot, the average net air consumption with 4.71 NI/shot is a bit lower than the theoretical 6.67 NI/shot although the compressor produces an average of 245.19 NI/shot, which is about the same as the AP assumed in Table 3-B. The accuracy of reading the air pressure in the storage bottles on the control panel is limited to about 5 bars. Since the water gun’s net air consumption is based on small pressure differences, reading errors weigh more heavily. Overall, these measurements confirm the theory of section 3.4.3.

Each line of Survey I has an average length of about 240 shots, hence 1200 m and was thus slightly shorter than the 300 shots assumed for calculating the total number of lines per day in Fig. 3-15. However, the so predicted 12 lines for an average turning time of 14 minutes (see Fig. 3-15) correspond well to the actually obtained average number of lines per day, as is summarized in Table A-3. It was due to the longer turning time that the initial goal of 14 acquisition lines per day, thus 126 lines in 9 days, has not been reached. But although we shot only 4 lines on the first acquisition day in September, we acquired a total of 80 sail lines in 8 days, covering an area of 1200 m by 600 m and giving an in-line to cross-line length ratio of 2:1.

3-D Acquisition Survey I 15.10.-22.10.1999												
Day of Acquisition 1999	Direction Line Name	Line Start	Line End	Line Navigation Time [min]	Turning Time [min]	Pressure in Bottles Start [bar]	Pressure in Bottles End [bar]	Pressure Difference Start-End [bar]	Gained Pressure between Lines [bar]	Net Air Consumption on Line [NI/min]	Air Production on Turning [NI/min]	Net Air Consumption on Line [NI/shot]
17. Sept.	SE-NW 05	14:12	14:37	00:25	00:06	198	170	28		224.00		14.93
17. Sept.	NW-SE 11	14:43	14:56	00:13	00:11	178	178	0	12	0.00	218.18	0.00
17. Sept.	SE-NW 06	15:07	15:24	00:17	00:06	190	188	2	4	23.53	133.33	1.57
17. Sept.	NW-SE 12	15:30	15:46	00:16		192	190	2		25.00		1.67
14. Oct.	NW-SE 13	11:27	11:44	00:17	00:15	250	218	32	0	376.47		25.10
14. Oct.	SE-NW 23	11:59	12:15	00:16	01:07	218	190	28	100	350.00	298.51	23.33
14. Oct.	NW-SE 14	13:22	13:35	00:13	00:14	290	248	42	0	646.15		43.08
14. Oct.	SE-NW 24	13:49	14:03	00:14	00:10	248	215	33	0	471.43		31.43
14. Oct.	NW-SE 15	14:13	14:27	00:14	00:13	215	185	30	25	428.57	384.62	28.57
14. Oct.	SE-NW 25	14:40	14:55	00:15	00:13	210	202	8	18	106.67	276.92	7.11
14. Oct.	NW-SE 16	15:08	15:22	00:14	00:15	220	210	10	12	142.86	160.00	9.52
14. Oct.	SE-NW 26	15:37	15:48	00:11	00:20	222	191	31	0	563.64		37.58
14. Oct.	NW-SE 17	16:08	16:21	00:13	00:14	191	165	26	23	400.00	328.57	26.67
14. Oct.	SE-NW 27	16:35	16:50	00:15		188	180	8		106.67		7.11
15. Oct.	NW-SE 18	10:56	11:13	00:17	00:16	260	250	10	0	117.65		7.84
15. Oct.	SE-NW 28	11:29	11:44	00:15	00:16	250						
15. Oct.	NW-SE 19	12:00	12:17	00:17	01:25	240	240	0	10	0.00	23.53	0.00
15. Oct.	SE-NW 29	13:42	13:55	00:13	00:17	250	250	0	25	0.00	294.12	0.00
15. Oct.	NW-SE 20	14:12	14:28	00:16	00:17	275	240	35	0	437.50		29.17
15. Oct.	SE-NW 30	14:45	14:57	00:12	00:15	240	210	30	8	500.00	106.67	33.33
15. Oct.	NW-SE 20	15:12	15:29	00:17	00:13	218	218	0	12	0.00	184.62	0.00
15. Oct.	SE-NW 31	15:42	15:55	00:13	00:15	230	205	25	25	384.62	333.33	25.64
15. Oct.	NW-SE 21	16:10	16:27	00:17	00:14	230	195	35	23	411.76	328.57	27.45
15. Oct.	SE-NW 29	16:41	16:55	00:14	00:14	218	190	28	20	400.00	285.71	26.67
15. Oct.	NW-SE 22	17:09	17:25	00:16	00:14	210	180	30	20	375.00	285.71	25.00
15. Oct.	SE-NW 07	17:39	17:54	00:15		200						
18. Oct.	NW-SE 08	10:20	10:37	00:17	00:20	243	210	33	30	388.24	300.00	25.88
18. Oct.	SE-NW 16	10:57	11:07	00:10	00:17	240	200	40	25	800.00	294.12	53.33
18. Oct.	NW-SE 32	11:24	11:41	00:17	00:13	225	192	33	18	388.24	276.92	25.88
18. Oct.	SE-NW 09	11:54	12:09	00:15	01:00	210	186	24	24	320.00	80.00	21.33
18. Oct.	NW-SE 33	13:09	13:26	00:17	00:14	210	179	31	21	364.71	300.00	24.31
18. Oct.	SE-NW 10	13:40	13:55	00:15	00:19	200	175	25	15	333.33	157.89	22.22
18. Oct.	NW-SE 34	14:14	14:32	00:18	00:16	190	163	27	18	300.00	225.00	20.00
18. Oct.	SE-NW 44	14:48	15:04	00:16	00:17	181	157	24	23	300.00	270.59	20.00
18. Oct.	NW-SE 35	15:21	15:37	00:16	00:18	180	178	2	19	25.00	211.11	1.67
18. Oct.	SE-NW 45	15:55	16:11	00:16	00:18	197	197	0	18	0.00	200.00	0.00
18. Oct.	NW-SE 36	16:29	16:45	00:16	00:18	215	210	5	17	62.50	212.50	4.17
18. Oct.	SE-NW 46	17:00	17:15	00:15	00:16	227	221	6	9	80.00	112.50	5.33
18. Oct.	NW-SE 37	17:31	17:47	00:16		230	197	33		412.50		27.50
19. Oct.	NW-SE 47	11:04	11:20	00:16	00:15	238	205	33	25	412.50	333.33	27.50
19. Oct.	SE-NW 38	11:35	11:50	00:15	00:16	230	200	30	18	400.00	225.00	26.67
19. Oct.	NW-SE 48	12:06	12:26	00:20	00:16	218	190	28	20	280.00	250.00	18.67
19. Oct.	SE-NW 39	12:42	13:00	00:18	01:08	210	185	25	17	277.78	50.00	18.52
19. Oct.	NW-SE 49	14:08	14:26	00:18	00:18	202	200	2	3	22.22	33.33	1.48
19. Oct.	SE-NW 40	14:44	15:03	00:19	00:50	203	200	3	10	31.58	40.00	2.11
19. Oct.	SE-NW 50	15:53	16:11	00:18	00:16	210	192	18	13	200.00	162.50	13.33
19. Oct.	NW-SE 41	16:27	16:45	00:18	00:19	205	205	0	25	0.00	263.16	0.00
19. Oct.	SE-NW 51	17:04	17:22	00:18	00:14	230	230	0	18	0.00	257.14	0.00
19. Oct.	NW-SE 42	17:36	17:54	00:18		248						
20. Oct.	NW-SE 52	10:30	10:48	00:18	00:13	275	240	35	0	388.89		25.93
20. Oct.	SE-NW 43	11:01	11:13	00:12	00:20	240						
20. Oct.	NW-SE 43	11:33	11:51	00:18	00:14	238	203	35	17	388.89	242.86	25.93
20. Oct.	SE-NW 53	12:05	12:21	00:16	01:13	220						
20. Oct.	NW-SE 59	13:34	13:53	00:19	00:15	215	190	25	18	263.16	240.00	17.54
20. Oct.	SE-NW 54	14:08	14:25	00:17	00:17	208	178	30	22	352.94	258.82	23.53
20. Oct.	NW-SE 60	14:42	15:01	00:19	00:15	200						
20. Oct.	SE-NW 55	15:16	15:31	00:15	00:14	218	210	8	10	106.67	142.86	7.11
20. Oct.	NW-SE 61	15:45	16:05	00:20	00:15	220	220	0	20	0.00	266.67	0.00
20. Oct.	SE-NW 56	16:20	16:35	00:15	00:13	240						
20. Oct.	NW-SE 62	16:48	17:08	00:20	00:13	230						
20. Oct.	SE-NW 57	17:21	17:38	00:17		210	210	0		0.00		0.00
21. Oct.	NW-SE 58	10:20	10:38	00:18	00:12	250	225	25	15	277.78	250.00	18.52
21. Oct.	SE-NW 63	10:50	11:05	00:15	00:14	240	208	32	17	426.67	242.86	28.44
21. Oct.	NW-SE 68	11:19	11:39	00:20	00:10	225	192	33	15	330.00	300.00	22.00
21. Oct.	SE-NW 64	11:49	12:04	00:15	01:05	207	200	7	30	93.33	92.31	6.22
21. Oct.	NW-SE 69	13:09	13:27	00:18	00:24	230	225	5	13	55.56	108.33	3.70
21. Oct.	SE-NW 65	13:51	14:06	00:15	00:13	238	208	30	15	400.00	230.77	26.67
21. Oct.	NW-SE 70	14:19	14:35	00:16	00:11	223	190	33	10	412.50	181.82	27.50
21. Oct.	SE-NW 66	14:46	15:02	00:16	00:13	200	192	8	18	100.00	276.92	6.67
21. Oct.	NW-SE 71	15:15	15:32	00:17	00:13	210	205	5	20	58.82	307.69	3.92
21. Oct.	SE-NW 67	15:45	15:59	00:14	00:16	225	215	10	25	142.86	312.50	9.52
21. Oct.	NW-SE 72	16:15	16:34	00:19	00:13	240	232	8	18	84.21	276.92	5.61
21. Oct.	SE-NW 80	16:47	17:03	00:16	00:15	250	240	10	10	125.00	133.33	8.33
21. Oct.	NW-SE 73	17:18	17:37	00:19		250	212	38		400.00		26.67
22. Oct.	NW-SE 74	10:26	10:44	00:18	00:13	270	235	35	20	388.89	307.69	25.93
22. Oct.	SE-NW 79	10:57	11:12	00:15	00:12	255	220	35	18	466.67	300.00	31.11
22. Oct.	NW-SE 75	11:24	11:42	00:18	00:12	238	205	33	15	366.67	250.00	24.44
22. Oct.	SE-NW 81	11:54	12:10	00:16	01:09	220						
22. Oct.	NW-SE 76	13:19	13:36	00:17	00:12	220						
22. Oct.	SE-NW 82	13:48	14:04	00:16	00:13	230	220	10	15	125.00	230.77	8.33
22. Oct.	NW-SE 77	14:17	14:36	00:19	00:10	235	200	35	12	368.42	240.00	24.56
22. Oct.	SE-NW 83	14:46	15:02	00:16	00:12	212	205	7	15	87.50	250.00	5.83
22. Oct.	NW-SE 78	15:14	15:32	00:18	00:12	220	205	15	20	166.67	333.33	11.11
22. Oct.	SE-NW 84	15:44	15:59	00:15	00:16	225	218	7	17	93.33	212.50	6.22
22. Oct.	NW-SE 30	16:15	16:34	00:19	00:14	235	200	35	20	368.42	285.71	24.56
22. Oct.	SE-NW 29	16:48	17:03	00:15	00:17	220	207	13	23	173.33	270.59	11.56
22. Oct.	NW-SE 31	17:20	17:39	00:19		230						
MEAN				00:16	00:14			20	compr. on	70.70	245.19	4.71
									compr. off	385.39		25.69

Table A-2. Accumulation of information concerned with line navigation time, turning time and compressed air consumption gathered from all acquisition sheets of Survey I. Exceptional turning times underlain in dark grey are not included in mean calculation. Air consumption is considered separately with the compressor off (dark grey) or on (light grey). Line names underlain in dark grey were repeated later.

	Day	Start Time	End Time	Hours per day	No. Lines per day
	17. Sept.	13:53	15:46	1:53	4.0
	14. Oct.	11:27	16:50	5:23	10.0
	15. Oct.	10:56	17:54	6:58	12.0
	18. Oct.	10:20	17:47	7:27	13.0
	19. Oct.	11:04	17:54	6:50	10.0
	20. Oct.	10:30	17:38	7:08	12.0
	21. Oct.	10:20	17:37	7:17	13.0
	22. Oct.	10:26	17:39	7:13	13.0
TOTAL	8 days			50h09	87.0
MEAN				6:53	11.9

Table A-3. Table showing statistics on acquisition time and total number of lines per day as well as the total and the mean of the whole Survey I (excluding values in grey).

Survey II

After having conducted two more 2-D acquisitions in October 2000 and March 2001 (e.g. Table A-11) as well as a three-streamer acquisition that served as final test of all components in May (see section 3.2.2), 3-D Survey II took place in August 2001. Planned were a total of 13 working days between August 6 and August 22. During the first day “La Licorne” was loaded, all equipment installed, all three streamers connected and the new navigation software tested. The second day served for Mini G.I G15 / I15 signature tests (see section 3.4.6 and Table A-7) and the recording of the final portion of the 2-D lake traverse, which corresponds to the extension of sail line 55 of Survey I as well as to in-line 140 of Survey II (see section 4.3 and Table A-12). We began shooting the navigation lines for our second 3-D survey on August 9. Table A-17 shows the acquisition sheet of the first line, sail line1, containing notes on that specific line but also all general acquisition parameters of Survey II.

Table A-4 is an accumulation of this specific information from acquisition sheets of all navigated line. This listing of every sailed line, their start and end time, the corresponding air pressure used and that remaining in the bottles, allowed some general statistics. Compared to the 16 minutes for Survey I, it took an average of 22 minutes to shoot the 300 m longer sail lines. The parallel shooting technique required a full turn to get back to the beginning of the adjacent sail line, which necessarily took longer than the 14 minute U-turns of Survey I. The average of 35 minutes though proves that it takes only slightly more than double the U-turning time and comes close to the estimation from section 5.2.1. Some results of this table had already been used for calculations with regard to air consumption in section 3.4.3.

3-D Acquisition Survey II 9.8.-21.8.2001												
Day in August 2001	Line Name SE-NW	Line Start	Line End	Line Navigation Time [min]	Turning Time [min]	Pressure in Bottles Start [bar]	Pressure in Bottles End [bar]	Pressure Difference Start-End [bar]	Gained Pressure between Lines [bar]	Net Air Consumption on Line [NI/min]	Air Production on Turning [NI/min]	Net Air Consumption on Line [NI/shot]
9. Aug.	1	12:00	12:21	00:21	00:39	280	200	80		761.90		50.79
9. Aug.	2 old	13:00										0.00
9. Aug.	3	13:53	14:15	00:22	00:29	240	190	50	35	454.55	241.38	30.30
9. Aug.	4	14:44	15:06	00:22	00:41	225	165	60	45	545.45	219.51	36.36
9. Aug.	5	15:47	16:10	00:23	00:29	210	160	50	35	434.78	241.38	28.99
9. Aug.	6	16:39	17:04	00:25	00:26	195	150	45	25	360.00	192.31	24.00
9. Aug.	7	17:30	17:51	00:21		175	125	50		476.19		31.75
10. Aug.	8	11:32	11:54	00:22	00:24	270	200	70	40	636.36	333.33	42.42
10. Aug.	9	12:18	12:37	00:19	00:25	240	175	65	35	684.21	280.00	45.61
10. Aug.	10	13:02	13:21	00:19	00:22	210	150	60	30	631.58	272.73	42.11
10. Aug.	11	13:43	14:02	00:19	00:23	180	125	55	30	578.95	260.87	38.60
10. Aug.	12	14:25	14:44	00:19	00:26	155	105	50	30	526.32	230.77	35.09
10. Aug.	13	15:10	15:34	00:24	00:46	135	90	45	55	375.00	239.13	25.00
10. Aug.	14	16:20	16:43	00:23	00:44	145	90	55	60	478.26	272.73	31.88
10. Aug.	15	17:27	17:48	00:21		150	90	60		571.43		38.10
13. Aug.	16	10:49	11:10	00:21	00:34	280	200	80	50	761.90	294.12	50.79
13. Aug.	17	11:44	12:06	00:22	00:34	250	185	65	45	590.91	264.71	39.39
13. Aug.	18	12:40	13:01	00:21	00:29	230	165	65	35	619.05	241.38	41.27
13. Aug.	19	13:30	13:51	00:21	00:39	200	140	60	50	571.43	256.41	38.10
13. Aug.	20	14:30	14:52	00:22	00:31	190	140	50	35	454.55	225.81	30.30
13. Aug.	21	15:23	15:45	00:22	00:28	175	120	55		500.00		33.33
13. Aug.	22 old	16:13										
13. Aug.	23	16:49	17:11	00:22	00:33	145	95	50	35	454.55	212.12	30.30
13. Aug.	24 old	17:44	18:08	00:24		130	80	50		416.67		27.78
14. Aug.	25	10:34	10:56	00:22	00:32	220	153	67	39	609.09	243.75	40.61
14. Aug.	26	11:28	11:49	00:21	00:53	192	130	62	56	590.48	211.32	39.37
14. Aug.	27	12:42	13:04	00:22	00:27	186	130	56	30	509.09	222.22	33.94
14. Aug.	28	13:31	13:53	00:22	00:43	160	103	57	57	518.18	265.12	34.55
14. Aug.	29	14:36	14:59	00:23	00:31	160	100	60	35	521.74	225.81	34.78
14. Aug.	30	15:30	15:54	00:24	00:53	135	85	50	65	416.67	245.28	27.78
14. Aug.	31	16:47	17:11	00:24	00:42	150	90	60	60	500.00	285.71	33.33
14. Aug.	32	17:53	18:16	00:23		150	90	60		521.74		34.78
15. Aug.	33	10:44	11:08	00:24	00:42	280	200	80	60	666.67	285.71	44.44
15. Aug.	34	11:50	12:13	00:23	00:30	260	190	70	35	608.70	233.33	40.58
15. Aug.	35	12:43	13:05	00:22	01:06	225	160	65	95	590.91	287.88	39.39
15. Aug.	37	14:11	14:35	00:24		255	195	60		500.00		33.33
15. Aug.	140_15d	14:35	15:12	00:37	01:09	195	85	110	90	594.59	260.87	39.64
15. Aug.	36	16:21	16:42	00:21	00:30	175	120	55	35	523.81	233.33	34.92
15. Aug.	22	17:12	17:32	00:20		155	95	60		600.00		40.00
16. Aug.	38	11:07	11:31	00:24	00:37	275	205	70	50	583.33	270.27	38.89
16. Aug.	39 old	12:08	12:31	00:23	00:35	255	185	70	45	608.70	257.14	40.58
16. Aug.	40	13:06	13:27	00:21	01:13	230	161	69	47	657.14	128.77	43.81
16. Aug.	2	14:40	15:01	00:21	00:36	208	140	68	50	647.62	277.78	43.17
16. Aug.	41	15:37	16:03	00:26	00:32	190	130	60	40	461.54	250.00	30.77
16. Aug.	42	16:35	16:56	00:21	00:29	170	115	55	30	523.81	206.90	34.92
16. Aug.	43	17:25	17:45	00:20		145	90	55		550.00		36.67
17. Aug.	44	10:28	10:51	00:23	00:48	260	192	68	63	591.30	262.50	39.42
17. Aug.	45	11:39	12:02	00:23	00:58	255	185	70	65	608.70	224.14	40.58
17. Aug.	46	13:00	13:23	00:23	00:30	250	180	70	42	608.70	280.00	40.58
17. Aug.	47	13:53	14:13	00:20	00:27	222	157	65	28	650.00	207.41	43.33
17. Aug.	48	14:40	15:01	00:21	00:36	185	130	55	30	523.81	166.67	34.92
17. Aug.	49	15:37	15:56	00:19	00:26	160	110	50	30	526.32	230.77	35.09
17. Aug.	50	16:22	16:45	00:23	00:43	140	95	45	55	391.30	255.81	28.09
17. Aug.	39	17:28	17:51	00:23		150	95	55		478.26		31.88
20. Aug.	51	10:39	11:00	00:21	00:41	275	195	80	60	761.90	292.68	50.79
20. Aug.	52	11:41	12:02	00:21	00:40	255	190	65	55	619.05	275.00	41.27
20. Aug.	53	12:42	13:04	00:22	00:40	245	175	70	55	636.36	275.00	42.42
20. Aug.	54	13:44	14:05	00:21	00:34	230	165	65	45	619.05	264.71	41.27
20. Aug.	55	14:39	15:01	00:22	00:38	210	150	60	50	545.45	263.16	36.36
20. Aug.	56	15:39	16:01	00:22	00:54	200	145	55	35	500.00	129.63	33.33
20. Aug.	57	16:55	17:17	00:22	00:32	180	120	60	40	545.45	250.00	36.36
20. Aug.	58	17:49	18:08	00:19		160	108	52		547.37		36.49
21. Aug.	59	11:20	11:40	00:20	00:35	270	212	58	53	580.00	302.86	38.67
21. Aug.	60	12:15	12:37	00:22	00:28	265	195	70	45	636.36	321.43	42.42
21. Aug.	24	13:05	13:24	00:19		240	170	70		736.84		49.12
MEAN				00:22	00:35			61		560.22	248.46	37.13

Table A-4. Accumulation of information concerned with line navigation time, turning time and compressed air consumption gathered from all acquisition sheets of Survey II. Exceptional values underlain in dark grey are not included in mean calculations. Line names underlain in dark grey were repeated later.

In contrast to Survey I, it was in this survey essential for the compressor to run non-stop during the whole day in order to compensate for the much higher air consumption of the Mini G.I G15 / I15. Its average net air consumption of 37.13 NI/shot is not only much higher than the 4.71 NI/shot that had been measured for the water gun source (Table A-2) but also somewhat higher than the 28.56 NI/shot that have been predicted in Table 3-B. On some of the lines the net consumption came rather close to this theoretical value suggesting that the increased consumption could be due to problems with the compressor while shooting. Air production might sometimes have been interrupted or the purge interval increased. Since

consumption is rather high, small changes in air production play an important role on the net consumption along one line. However, compressor delivery on turning was only slightly less than the assumed 250 NI/shot. So it could also be the air gun's real air consumption that is more elevated than expected. If this is the case, then either the relationship of equation (3.2) is not exact, the actual chamber volumes had been a bit larger than 15 in³ or the gun was operated at a pressure exceeding slightly the desired 80 bars. Measurements, especially while reading the pressure at the control panel, are subject to errors in the order of 5%. Overall, these results confirm that the theory of section 3.4.3 can well be used to determine survey design parameters, such as the choice of the gun, the survey geometry and the expected total number of lines per day.

As stated above, each sail line of Survey II had a length of 301 shots, hence 1500 m, and thus exactly the length that had been assumed for calculating the total number of lines per day in Fig. 3-15. The predicted 8 lines for an average turning time of 35 minutes (see Fig. 3-15) correspond very well to the actually obtained average number of lines per day (excluding the last day), as summarized in Table A-5. On the one hand, it was due to the longer turning time (plus 5 minutes) that the initial goal of 9 acquisition lines a day and a total of 81 in 9 days has not been reached; on the other hand, it was because only three sail lines had been recorded on August 21 (Table A-5). Several additional 2-D profiles had been shot that same day. Nevertheless, we acquired 60 sail or 180 CMP lines in 9 days, covering a surface of about 1500 m by 675 m, an area bigger than that of Survey I but sampled at half the cross-line interval.

	Day	Start Time	End Time	Hours per day	No. Lines per day
	9. Aug.	12:00	17:51	5:51	7.0
	10. Aug.	11:32	17:48	6:16	8.0
	13. Aug.	10:49	18:08	7:19	9.0
	14. Aug.	10:34	18:16	7:42	8.0
	15. Aug.	10:44	17:32	6:48	7.5
	16. Aug.	11:07	17:45	6:38	7.0
	17. Aug.	10:28	17:51	7:23	8.0
	20. Aug.	10:39	18:08	7:29	8.0
	21. Aug.	11:20	13:24	2:04	3.0
TOTAL	9 days			57h30	65.5
MEAN				6:55	7.8

Table A-5. Table showing statistics on acquisition time and total number of lines per day as well as the total and the mean of the whole Survey II (last day excluded from mean calculation).

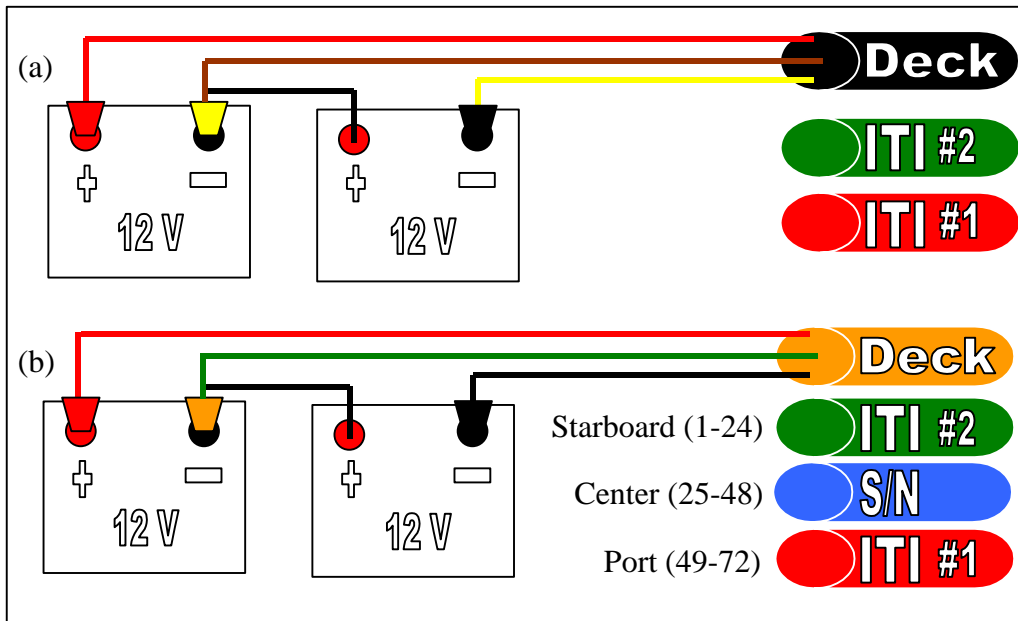


Fig. A-1. Connections of batteries to deck cable (a) Survey I: single streamer configuration - both interconnected ITI streamer sections mounted on ITI deck cable; (b) Survey II: multi-streamer configuration - both ITI streamer sections and S/N section connected to each of the three branches of the S/N deck cable. Color code indicates which streamer (streamer position) corresponds to what channels on the recording seismograph, see also Fig. 5-4.

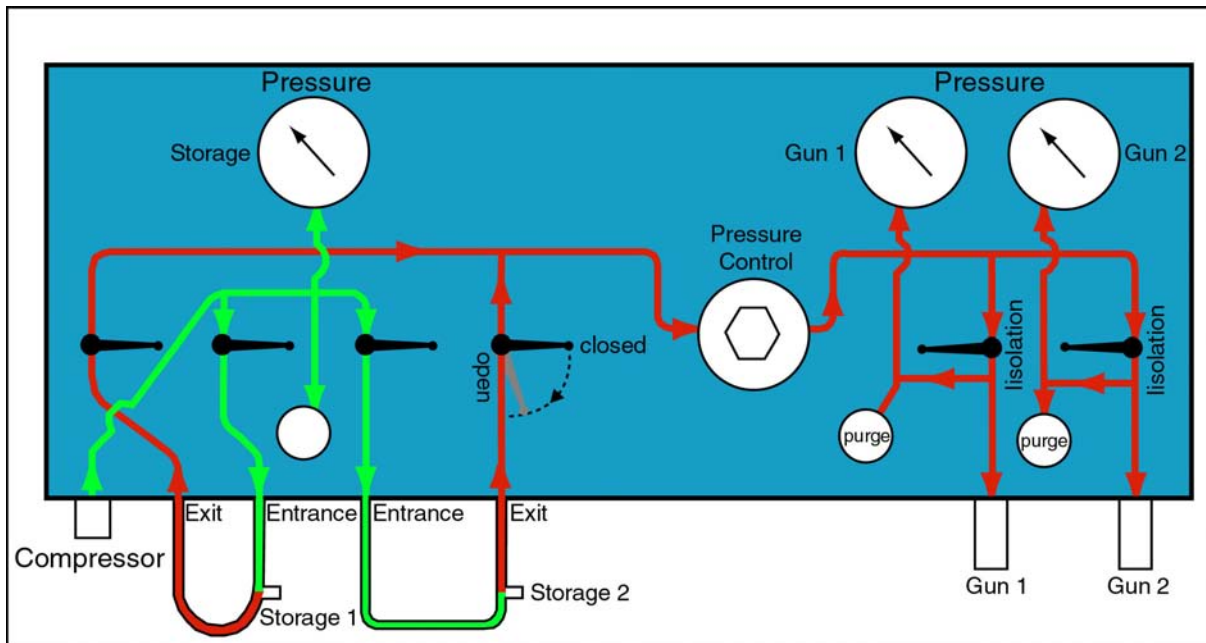


Fig. A-2. Detailed description of air flow through the control panel and its connection to the compressor, storage bottles and seismic sources.

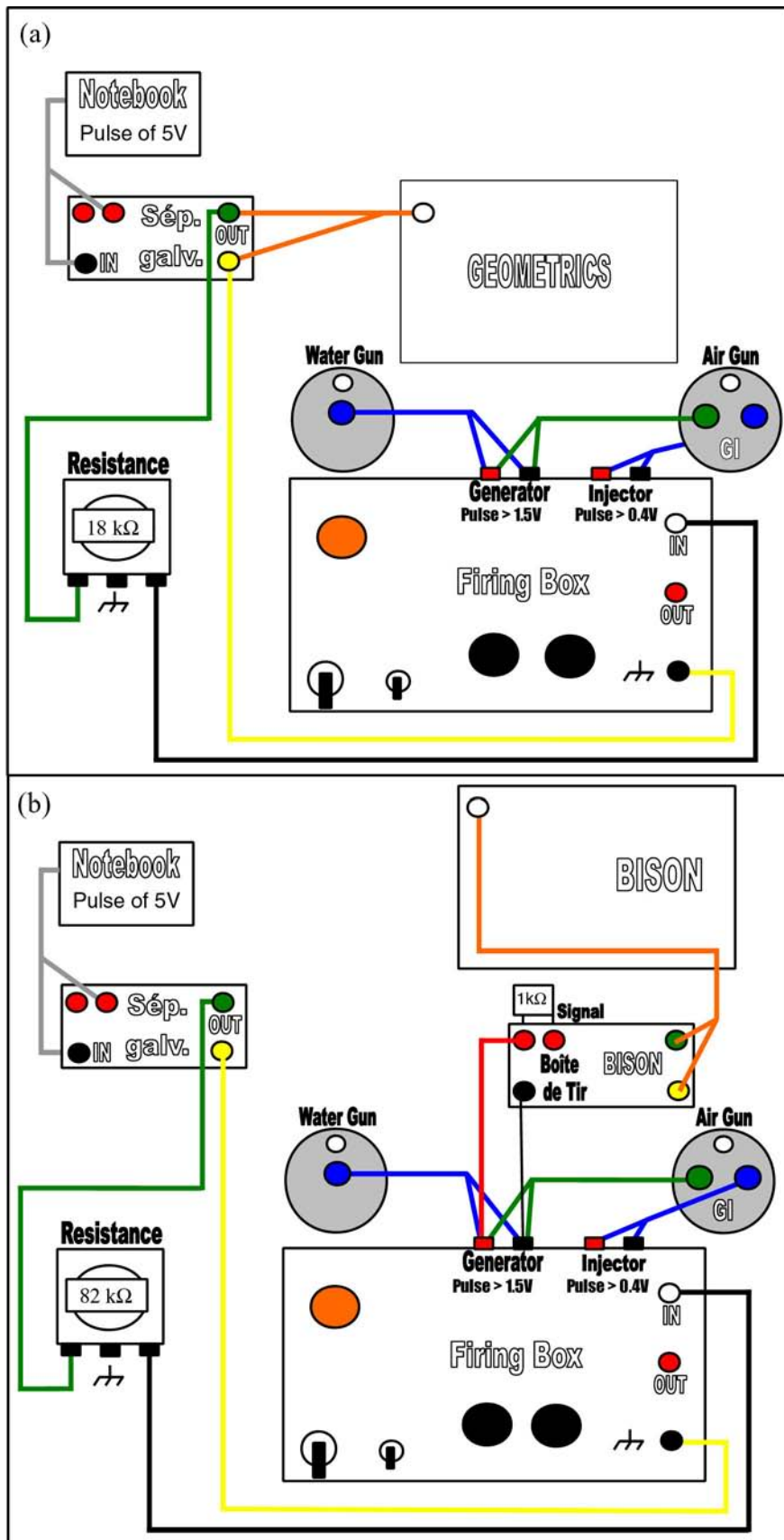


Fig. A-3. The firing box (precision ~ 0.25 ms) and its connection to (a) the Geometrics or (b) the BISON seismograph and to either water (Survey I) or air gun (Survey II).

Far-Field Signature Test		(Maren Scheidhauer, Milan Beres, François Marillier)			
General:		Source:		Position:	
Date:	26.10.1999	Time:	10:40	Type:	Water Gun
Weather:	cloudy, calm	Chamber Size [cuin]	15	Line:	%
Co-workers:	Emanuelle	Depth [m]	0.3	Location:	535782 / 147418
Geometry:		Shooting Frequency [s]:		Distance boat - water surface: 2m	
Minimum Offset [m]:	-57.25	Distance to Boat [m]:		Streamer #1 at Bottom, Streamer #2 at Top	
Maximum Offset [m]:	-174.75	Active length of Streamer [m]:		Trace Spacing [m]: 2.5	
Recording Parameters of GEOMETRICS:		Length of Lead-in Cable [m]:		Fold: %	
Directory:		below water surface?		System Setup/Boards:	
Files:	D:\waters2	System Setup/Boards:		change to 60 channels	
Segy-File Name:	001.DAT-020.DAT	Data:		Filter:	
DAT-File Name:	wsigfar.sgy	Sample Interval [ms]:		Nyquist Filter [Hz]	
		Recording Time [ms]:		Filter [Hz]:	
		Default Gain [db]:		Notch:	
		Total Channels:		No	
Trigger:					
Mode:	auto				
Standard Trigger:	both				
Recording Delay [ms]:	0				
TURN CHARGER OFF !!!					
Shot N°	set GI Delay [ms]	Depth (Sonar) [m]	Operating Pressure [bar]	Pressure in Bottles [bar]	Comments
1		306	140		
2		306	140		
3		306	140		
4		306	140		
5		306	140		
6		306	140		
7		306	140		
8		306	140		
9		306	140		
10		306	140		535774 / 147421
11		306	140		
12		306	140		
13		306	140		
14		306	140		
15		306	140		example of best signature -->
16		306	140		half the dominant period measured from
17		306	140		peak-to-peak: 69.75-69ms = 0.75ms
18		306	140		
19		306	140		
20		306	140		

Table A-6. Acquisition sheet of S15.02 Water Gun far-field signature test.

Signature and Time Delay Test		(Maren Scheidhauer, David Dupuy, François Marillier)				sig3
General:		Source:		Position:		
Date:	07.08.2001	Time:	11:45	Type:	Mini GI	
Weather:	windy	Chamber Size [cuin]	15/15	Line:	center of lake	
Co-workers:	Philippe L., Yvan, Alexandre	Depth [m]	1	Location:		
Geometry:		Shooting Frequency [s]:		Only streamer #1 used		
Minimum Offset [m]:	50.25	Distance to Boat [m]:		Trace Spacing [m]: 2.5		
Maximum Offset [m]:	112.75	Active length of Streamer [m]:		Fold: %		
Recording Parameters of BISON:		Length of Lead-in Cable [m]:		below water surface		
Survey Name:		System Setup/Boards:		change to 24 channels		
Tape:	sig3	Data:		Filter:		
Segy-File Name:	asig15_15a.sgy	Sample Interval [ms]:		Nyquist Filter [Hz]:		
DAT-File Name:	I9000013DSEISM.DAT	Recording Time [ms]:		Filter [Hz]:		
		Default Gain [db]:		Notch:		
		Total Channels:		No		
Trigger:						
Mode:	auto (manual)	Batch:		Gun Hydrophone: 25: channel		
Standard Trigger:	both	Batch Mode:		on, automatic triggering		
Recording Delay [ms]:	2.5	Marine Mode:		on		
		View Stack after each Shot:		on		
		Screen Update:		1		
TURN CHARGER OFF !!!						
Shot N°	set GI Delay [ms]	Depth (Sonar) [m]	Operating Pressure [bar]	Pressure in Bottles [bar]	Comments	
1		303	80		generator only	
2		303	80			
3		303	80			
4-8		303	80		bad shots	
9	29	303	80		with injector	
10	29	303	80			
11	29	303	80			
12	30	303	80			
13	30	303	80			
14	30	303	80			
15	31	303	80		engine and compressor off for shots 1-24	
16	31	303	80			
17	31	303	80			
18	32	303	80			
19	32	303	80			
20	28	303	80			
21	28	303	80		example of best signature -->	
22	27	303	80		half the dominant period measured from	
23	27	303	80		peak-to-peak: 81.5-80ms = 1.5ms	
24	26	303	80			

Signature and Time Delay Test					(Maren Scheidhauer, David Dupuy, François Marillier)	sig3
Recording Parameters of BISON: Survey Name: sig3 Tape: sig3 Sheet N°: 2						
Shot N°	set GI Delay [ms]	Depth (Sonar) [m]	Operating Pressure [bar]	Pressure in Bottles [bar]	Comments	
25	26	303	80		engine on for shots 25-82	
26	24	303	80			
27	24	303	80			
28	22	303	80			
29	22	303	80			
30	20	303	80			
31	20	303	80			
32	34	303	80			
33	34	303	80			
34	36	303	80			
35	36	303	80			
36	38	303	80			
37	38	303	80			
38	40	303	80			
39	40	303	80			
40	42	303	80			
41	42	303	80			
42	29	303	80		extra shot	
43	29	303	80		extra shot	
44	29	303	80		compressor back on	
45	29	303	80			
46	29	303	80			
47	29	303	80		lead-in: 5m below water surface	
48	29	303	80			
49	30	303	80			
50	30	303	80			
51	30	303	80			
52	31	303	80			
53	31	303	80			
54	32	303	80			
55	32	303	80			
56	28	303	80			
57	28	303	80			
58	27	303	80			
59	27	303	80			
60	26	303	80			
61	26	303	80			
62	24	303	80			
63	24	303	80			
64	22	303	80			

Signature and Time Delay Test					(Maren Scheidhauer, David Dupuy, François Marillier)	sig3
Recording Parameters of BISON: Survey Name: sig3 Tape: sig3 Sheet N°: 3						
Shot N°	set GI Delay [ms]	Depth (Sonar) [m]	Operating Pressure [bar]	Pressure in Bottles [bar]	Comments	
65	22	303	80			
66	20	303	80			
67	20	303	80			
68	34	303	80			
69	34	303	80			
70	36	303	80			
71	36	303	80			
72	38	303	80			
73	38	303	80			
74	40	303	80			
75	40	303	80			
76	42	303	80			
77	42	303	80			
78		303	80		extra shot	
79		303	80		generator only	
80		303	80			
81		303	80			
82		303	80			

Table A-7. Acquisition sheet of Mini G.I G15 / I15 far- and near-field signature test including gun hydrophone measurements; page 1, 2 and 3.

Signature and Time Delay Test			(Maren Scheidhauer, Milan Beres, François Marillier)		sign1
General:			Source:		Position:
Date:	14.9.1999	Time:	17:40	Type:	Mini GI
Weather:	sunny, no wind	Chamber Size [cuin]	30/30	Line:	%
Co-workers:	Yvan, Olivier, Gilles	Depth [m]	1.5	Location:	536100 / 147800
Geometry:			Shooting Frequency [s]:		Streamer #1 at Bottom, Streamer #2 at Top
Minimum Offset [m]	-59.25	Distance to Boat [m]		Active length of Streamer [m]	117.5
Maximum Offset [m]	-176.75	Length of Lead-in Cable [m]:	58-60	Trace Spacing [m]:	2.5
Recording Parameters of BISON:			below water surface?		Fold:
Survey Name:			System Setup/Boards:		change to 60 channels
Tape:	sign1	Data:		Sample Interval [ms]:	0.5
Segy-File Name:	asig.sgy	Recording Time [ms]:		1000	Filter:
DAT-File Name:		Default Gain [db]:		saturated !! 60	Nyquist Filter [Hz]
Trigger:			Total Channels:		60
Mode:	auto	Batch:		Batch Mode:	on, automatic triggering
Standard Trigger:	both	Marine Mode:		on	Gun Hydrophone:
Recording Delay [ms]:	2.5	View Stack after each Shot:		on	0-Offset Hydrophone:
NegDelay runs in the background			Screen Update:		1
					TURN CHARGER OFF !!!
Shot N°	set GI Delay [ms]	Depth (Sonar) [m]	Operating Pressure [bar]	Pressure in Bottles [bar]	Comments
81	18	303	100	203	
82	18	303	100	203	
83	18	303	100	203	
84	18	303	100	203	
85	18	303	100	203	
86	18	303	100	203	
87	18	303	100	203	
88	18	303	100	203	
89	18	303	100	203	
90	18	303	100	197	
91	24	303	100	197	
92	24	303	100	197	
93	24	303	100	197	
94	24	303	100	197	
95	24	303	100	197	
96	24	303	100	197	
97	24	303	100	197	
98	24	303	100	197	
99	24	303	100	197	
100	24	304	100	190	
Signature and Time Delay Test			(Maren Scheidhauer, Milan Beres, François Marillier)		sign1
Recording Parameters of BISON:			Survey Name:		sign1
			Tape:		sign1
			Sheet N°:		5
Shot N°	set GI Delay [ms]	Depth (Sonar) [m]	Operating Pressure [bar]	Pressure in Bottles [bar]	Comments
101	26-29	304	100	190	
102	26-29	304	100	190	
103	26-29	304	100	190	
104	26-29	304	100	190	
105	26-29	304	100	190	
106	26-29	304	100	190	
107	26-29	304	100	190	
108	26-29	304	100	190	
109	26-29	304	100	190	
110	26-29	304	100	182	
111	32	304	100	182	
112	32	304	100	182	
113	32	304	100	182	
114	32	304	100	182	
115	32	304	100	182	
116	32	304	100	182	
117	32	304	100	182	
118	32	304	100	182	example of best signature -->
119	32	304	100	182	half the dominant period measured on
120	32	304	100	182	zero-crossings: 90-86.5ms = 3.5ms
121	48	304	100	175	
122	48	304	100	175	
123	48	304	100	175	
124	48	304	100	175	
125	48	304	100	175	
126	48	304	100	175	
127	48	304	100	175	
128	48	304	100	175	
129	48	304	100	175	
130	48	304	100	168	

Table A-8. Acquisition sheet of Mini G.I G30 / I30 far-field signature test including near-field measured on gun hydrophone; page 1 and 2.

SAIL LINE	X START	Y START	X END	Y END	DIRECTION	DIRECTION
1						
2						
3						
4						
5	536472.16	148722.35	535982.40	149354.92	322.25	SE-NW
6	536466.23	148717.76	535976.47	149350.33	322.25	SE-NW
7	536460.30	148713.17	535970.54	149345.73	322.25	SE-NW
8	536454.37	148708.58	535964.61	149341.14	322.25	SE-NW
9	536448.44	148703.99	535958.68	149336.55	322.25	SE-NW
10	536442.51	148699.39	535952.75	149331.96	322.25	SE-NW
11	536436.57	148694.80	535946.82	149327.37	322.25	SE-NW
12	536430.64	148690.21	535940.89	149322.78	322.25	SE-NW
13	536424.71	148685.62	535934.96	149318.19	322.25	SE-NW
14	536418.78	148681.03	535929.03	149313.59	322.25	SE-NW
15	536412.85	148676.44	535923.10	149309.00	322.25	SE-NW
16	536406.92	148671.85	535917.17	149304.41	322.25	SE-NW
17	536400.99	148667.25	535911.24	149299.82	322.25	SE-NW
18	536395.06	148662.66	535905.31	149295.23	322.25	SE-NW
19	536389.13	148658.07	535899.38	149290.64	322.25	SE-NW
20	536383.20	148653.48	535893.45	149286.05	322.25	SE-NW
21	536377.27	148648.89	535887.52	149281.45	322.25	SE-NW
22	536371.34	148644.30	535881.59	149276.86	322.25	SE-NW
23	536365.41	148639.71	535875.66	149272.27	322.25	SE-NW
24	536359.48	148635.11	535869.73	149267.68	322.25	SE-NW
25	536353.55	148630.52	535863.79	149263.09	322.25	SE-NW
26	536347.62	148625.93	535857.86	149258.50	322.25	SE-NW
27	536341.69	148621.34	535851.93	149253.90	322.25	SE-NW
28	536335.76	148616.75	535846.00	149249.31	322.25	SE-NW
29	536329.83	148612.16	535840.07	149244.72	322.25	SE-NW
30	536323.90	148607.56	535834.14	149240.13	322.25	SE-NW
31	536317.97	148602.97	535828.21	149235.54	322.25	SE-NW
32	536312.04	148598.38	535822.28	149230.95	322.25	SE-NW
33	536306.11	148593.79	535816.35	149226.36	322.25	SE-NW
34	536300.18	148589.20	535810.42	149221.76	322.25	SE-NW
35	536294.25	148584.61	535804.49	149217.17	322.25	SE-NW
36	536288.32	148580.02	535798.56	149212.58	322.25	SE-NW
37	536282.39	148575.42	535792.63	149207.99	322.25	SE-NW
38	536276.46	148570.83	535786.70	149203.40	322.25	SE-NW
39	536270.53	148566.24	535780.77	149198.81	322.25	SE-NW
40	536264.60	148561.65	535774.84	149194.22	322.25	SE-NW
41	536258.67	148557.06	535768.91	149189.62	322.25	SE-NW
42	536252.74	148552.47	535762.98	149185.03	322.25	SE-NW
43	536246.81	148547.88	535757.05	149180.44	322.25	SE-NW
44	536240.87	148543.28	535751.12	149175.85	322.25	SE-NW
45	536234.94	148538.69	535745.19	149171.26	322.25	SE-NW
46	536229.01	148534.10	535739.26	149166.67	322.25	SE-NW
47	536223.08	148529.51	535733.33	149162.08	322.25	SE-NW
48	536217.15	148524.92	535727.40	149157.48	322.25	SE-NW
49	536211.22	148520.33	535721.47	149152.89	322.25	SE-NW
50	536205.29	148515.74	535715.54	149148.30	322.25	SE-NW
51	536199.36	148511.14	535709.61	149143.71	322.25	SE-NW
52	536193.43	148506.55	535703.68	149139.12	322.25	SE-NW
53	536187.50	148501.96	535697.75	149134.53	322.25	SE-NW
54	536181.57	148497.37	535691.82	149129.94	322.25	SE-NW
55	536175.64	148492.78	535685.89	149125.34	322.25	SE-NW
56	536169.71	148488.19	535679.96	149120.75	322.25	SE-NW
57	536163.78	148483.60	535674.03	149116.16	322.25	SE-NW
58	536157.85	148479.00	535668.09	149111.57	322.25	SE-NW
59	536151.92	148474.41	535662.16	149106.98	322.25	SE-NW
60	536145.99	148469.82	535656.23	149102.39	322.25	SE-NW
61	536140.06	148465.230	535650.304	149097.795	322.25	SE-NW
62	536134.129	148460.638	535644.374	149093.204	322.25	SE-NW
63	536128.199	148456.047	535638.443	149088.612	322.25	SE-NW
64	536122.269	148451.455	535632.513	149084.021	322.25	SE-NW
65	536116.339	148446.864	535626.583	149079.429	322.25	SE-NW
66	536110.408	148442.272	535620.652	149074.838	322.25	SE-NW
67	536104.478	148437.681	535614.722	149070.246	322.25	SE-NW
68	536098.548	148433.089	535608.792	149065.655	322.25	SE-NW
69	536092.617	148428.498	535602.862	149061.063	322.25	SE-NW
70	536086.687	148423.906	535596.931	149056.472	322.25	SE-NW
71	536080.757	148419.315	535591.001	149051.881	322.25	SE-NW
72	536074.826	148414.723	535585.071	149047.289	322.25	SE-NW
73	536068.896	148410.132	535579.140	149042.698	322.25	SE-NW
74	536062.966	148405.541	535573.210	149038.106	322.25	SE-NW
75	536057.036	148400.949	535567.280	149033.515	322.25	SE-NW
76	536051.105	148396.358	535561.349	149028.923	322.25	SE-NW
77	536045.175	148391.766	535555.419	149024.332	322.25	SE-NW
78	536039.245	148387.175	535549.489	149019.740	322.25	SE-NW
79	536033.314	148382.583	535543.558	149015.149	322.25	SE-NW
80	536027.384	148377.992	535537.628	149010.557	322.25	SE-NW
81	536021.454	148373.400	535531.698	149005.966	322.25	SE-NW
82	536015.523	148368.809	535525.768	149001.374	322.25	SE-NW
83	536009.593	148364.217	535519.837	148996.783	322.25	SE-NW
84	536003.663	148359.626	535513.907	148992.192	322.25	SE-NW

Table A-9. Acquisition preplot: theoretical start and end points for all 80 sail lines of Survey I calculated perpendicular to the average fault zone direction – 322.25° relative to geographical north.

SAIL LINE	X START	Y START	X END	Y END	DIRECTION	DIRECTION
1	536801.975	148345.364	535883.683	149531.424	322.25	SE-NW
2	536793.080	148338.477	535874.788	149524.537	322.25	SE-NW
3	536784.184	148331.589	535865.892	149517.650	322.25	SE-NW
4	536775.289	148324.702	535856.997	149510.763	322.25	SE-NW
5	536766.394	148317.815	535848.101	149503.875	322.25	SE-NW
6	536757.498	148310.928	535839.206	149496.988	322.25	SE-NW
7	536748.603	148304.041	535830.310	149490.101	322.25	SE-NW
8	536739.707	148297.153	535821.415	149483.214	322.25	SE-NW
9	536730.812	148290.266	535812.520	149476.327	322.25	SE-NW
10	536721.916	148283.379	535803.624	149469.440	322.25	SE-NW
11	536713.021	148276.492	535794.729	149462.552	322.25	SE-NW
12	536704.125	148269.605	535785.833	149455.665	322.25	SE-NW
13	536695.230	148262.717	535776.938	149448.778	322.25	SE-NW
14	536686.334	148255.830	535768.042	149441.891	322.25	SE-NW
15	536677.439	148248.943	535759.147	149435.004	322.25	SE-NW
16	536668.544	148242.056	535750.251	149428.116	322.25	SE-NW
17	536659.648	148235.169	535741.356	149421.229	322.25	SE-NW
18	536650.753	148228.282	535732.460	149414.342	322.25	SE-NW
19	536641.857	148221.394	535723.565	149407.455	322.25	SE-NW
20	536632.962	148214.507	535714.670	149400.568	322.25	SE-NW
21	536624.066	148207.620	535705.774	149393.680	322.25	SE-NW
22	536615.171	148200.733	535696.879	149386.793	322.25	SE-NW
23	536606.275	148193.846	535687.983	149379.906	322.25	SE-NW
24	536597.380	148186.958	535679.088	149373.019	322.25	SE-NW
25	536588.485	148180.071	535670.192	149366.132	322.25	SE-NW
26	536579.589	148173.184	535661.297	149359.244	322.25	SE-NW
27	536570.694	148166.297	535652.401	149352.357	322.25	SE-NW
28	536561.798	148159.410	535643.506	149345.470	322.25	SE-NW
29	536552.903	148152.522	535634.610	149338.583	322.25	SE-NW
30	536544.007	148145.635	535625.715	149331.696	322.25	SE-NW
31	536535.112	148138.748	535616.820	149324.808	322.25	SE-NW
32	536526.216	148131.861	535607.924	149317.921	322.25	SE-NW
33	536517.321	148124.974	535599.029	149311.034	322.25	SE-NW
34	536508.425	148118.086	535590.133	149304.147	322.25	SE-NW
35	536499.530	148111.199	535581.238	149297.260	322.25	SE-NW
36	536490.635	148104.312	535572.342	149290.373	322.25	SE-NW
37	536481.739	148097.425	535563.447	149283.485	322.25	SE-NW
38	536472.844	148090.538	535554.551	149276.598	322.25	SE-NW
39	536463.948	148083.650	535545.656	149269.711	322.25	SE-NW
40	536455.053	148076.763	535536.760	149262.824	322.25	SE-NW
41	536446.157	148069.876	535527.865	149255.937	322.25	SE-NW
42	536437.262	148062.989	535518.970	149249.049	322.25	SE-NW
43	536428.366	148056.102	535510.074	149242.162	322.25	SE-NW
44	536419.471	148049.215	535501.179	149235.275	322.25	SE-NW
45	536410.575	148042.327	535492.283	149228.388	322.25	SE-NW
46	536401.680	148035.440	535483.388	149221.501	322.25	SE-NW
47	536392.785	148028.553	535474.492	149214.613	322.25	SE-NW
48	536383.889	148021.666	535465.597	149207.726	322.25	SE-NW
49	536374.994	148014.779	535456.701	149200.839	322.25	SE-NW
50	536366.098	148007.891	535447.806	149193.952	322.25	SE-NW
51	536357.203	148001.004	535438.910	149187.065	322.25	SE-NW
52	536348.307	147994.117	535430.015	149180.177	322.25	SE-NW
53	536339.412	147987.230	535421.120	149173.290	322.25	SE-NW
54	536330.516	147980.343	535412.224	149166.403	322.25	SE-NW
55	536321.621	147973.455	535403.329	149159.516	322.25	SE-NW
56	536312.725	147966.568	535394.433	149152.629	322.25	SE-NW
57	536303.830	147959.681	535385.538	149145.741	322.25	SE-NW
58	536294.935	147952.794	535376.642	149138.854	322.25	SE-NW
59	536286.039	147945.907	535367.747	149131.967	322.25	SE-NW
60	536277.144	147939.019	535358.851	149125.080	322.25	SE-NW

Table A-10. Acquisition preplot: theoretical start and end points for all 60 sail lines of Survey II calculated perpendicular to the average fault zone direction – 322.25° relative to geographical north.

2-D Acquisition		(Imran Chaudhary, Maren Scheidhauer, David Dupuy, Milan Beres, François Marillier)			
General:		Source:		Position:	
Date:	16.10.2000	Time:	17:00	Type:	Mini GI
Weather:	sunny, calm	Chamber Size [cuin]	15/15	Line:	140_15a
Co-workers:	Francine, Philippe, Yvan	Depth [m]:	1	Location:	Lake Traverse
		GI Delay [ms]	27	Line Direction:	SE-NW
Geometry (single-streamer configuration):		Shooting Frequency [m]:	5	Trace Spacing [m]:	2.5
Minimum Offset [m]:	5	Distance to Boat [m]:	10	Cross Spacing [m]:	%
Maximum Offset [m]:	122.5			Fold:	12
No. of first Streamer:	2	Active Length of Streamer [m]:	117.5		
Recording Parameters of BISON:		Length of Lead-in Cable [m]:	13.75		
		Offset [m]:	5		
Survey Name:	ouch4	Data:		Filter:	
Tape:	ouch4	Sample Interval [ms]:	0.5	Nyquist Filter [Hz]:	1000
GPS-File Name:		Recording Time [ms]:	800	Filter [Hz]:	4-1000
SEGY-File Name:	imran2a.sgy	Default Gain [db]:	60	Notch [Hz]:	No
DAT-File Name:		Total Channels:	48		
TURN CHARGER OFF !!!					

Hour	Shot N° PC	Shot N° BISON	Gun Pressure [bar]	Pressure in Bottles [bar]	Depth Sonar [m]	Ship Coordinates GPS	Comments (measure voltage of hydrophone amplifiers!)
17:00							+ 200 mA -84 mA
							6 extra shots, no gun
17:52	1	7					
17:53	11	17	80	180			
17:55	41	47	80	180			
17:58	80	86	80	169			
18:01	119	125	80	153			
18:04	158	164	80	140			
18:07	192	198	80	128			
18:10	233	239	80	119			
18:13	278	284	80	107			
18:16	212	318	80	92			
18:19	342	348	80	94			
18:22	379	385	80	82			
18:25	418	424	77	77			
18:28	457	462	69	69	238		
18:31	497	503	62	62			
18:32	509	515	60	60			

2-D Acquisition		(Imran Chaudhary, Maren Scheidhauer, David Dupuy, Milan Beres, François Marillier)			
General:		Source:		Position:	
Date:	05.03.2001	Time:	13:50	Type:	Mini GI
Weather:	calm, cloudy	Chamber Size [cuin]	15/15	Line:	140_15b
Co-workers:	Philippe L., Yvan	Depth [m]:	1	Location:	Lake Traverse
		GI Delay [ms]	28	Line Direction:	NW-SE
Geometry (single-streamer configuration):		Shooting Frequency [m]:	5	Trace Spacing [m]:	2.5
Minimum Offset [m]:	5	Distance to Boat [m]:	10	Cross Spacing [m]:	%
Maximum Offset [m]:	122.5			Fold:	12
No. of first Streamer:	2	Active Length of Streamer [m]:	117.5		
Recording Parameters of BISON:		Length of Lead-in Cable [m]:	13.75		
		Offset [m]:	5		
Survey Name:	profil2	Data:		Filter:	
Tape:		Sample Interval [ms]:	0.5	Nyquist Filter [Hz]:	1000
GPS-File Name:		Recording Time [ms]:	900	Filter [Hz]:	4-1000
SEGY-File Name:	imran2b.sgy	Default Gain [db]:	60	Notch [Hz]:	No
DAT-File Name:	I9000023DSEISM.DAT	Total Channels:	48		
TURN CHARGER OFF !!!					

Hour	Shot N° PC	Shot N° BISON	Gun Pressure [bar]	Pressure in Bottles [bar]	Depth Sonar [m]	Ship Coordinates GPS	Comments (measure voltage of hydrophone amplifiers!)
13:50	1	2	80	275			13.28 V, +116 mA, -82 m -84 mA
13:53	43	44	80	250			one extra shot at beginning
13:56	83	84	80	239			compressor on
13:59	123	124	80	230			
14:05	167	168	80	221			
14:08	199	200	80	215			
14:11	235	236	80	210			
14:14	276	277	80	200			
14:17	307	308	80	195			
14:20	346	347	80	193			
14:23	381	382	80	181	308		
14:26	417	418	80	177	308		
14:29	553	454	80	168	308		
14:32	491	492	80	161	308		no GPS for a while
14:35	530	531	77	157	308		
14:38	570	571	69	150	308		
14:41	603	604	62	145	308		
14:44	654	652	60	140	308		
14:47	677	675		138	308		

3-D Acquisition		(Maren Scheidhauer, David Dupuy)		2
General:		Source:		Position:
Date: 15.08.2001	Time: 14:11	Type: Mini GI	Line: 140_15d	
Weather: sunny, calm		Chamber Size [cuin]: 15/15	Location: OUCHY	
Co-workers: Jochen, Mathieu, Philippe		Depth [m]: 1	Line Direction: SE-NW	
Geometry (multi-streamer configuration):		GI Delay [ms]: 28	Trace Spacing [m]: 2.5	
Minimum Offset [m]: 5		Shooting Frequency [m]: 5	Cross Spacing [m]: 3.75	
Maximum Offset [m]: 62.5		Distance to Boat [m]: 6.25	Fold: 6	
No. of Streamer, Starboard (green): 2		Active Length of Streamer [m]: 57.5		
No. of Streamer, Center (blue): S/N		Length of Center Lead-in [m]: 10		
No. of Streamer, Port (red): 1		Length of other Lead-ins [m]: 17		
Recording Parameters of BISON:		Offset [m]: 5	Filter:	
Survey Name: OUCHY1		Data:	Nyquist Filter [Hz]: 1000	
Tape: OUCHY37		Sample Interval [ms]: 0.5	Filter [Hz]: 25-1000	
GPS-File Name: 3D037		Recording Time [ms]: 1000	Notch [Hz]: No	
SEGY-File Name: sail37.sgy		Default Gain [db]: 24		
DAT-File Name: I1000373DSEISM.DAT		Total Channels: 72		
		Booms:		
		Distance Boom - End of Boat [m]: 7.9		
		Distance Boom - Streamer [m]: 0.9		TURN CHARGER OFF !!!

Hour	Shot N° PC	Shot N° BISON	Gun Pressure [bar]	Pressure in Bottles [bar]	Depth Sonar [m]	Ship Coordinates GPS	Comments (measure voltage of hydrophone amplifiers!)
14:37	320	326	80	185			
14:38	340	346	80				
14:40	360	366	80	180			
14:42	380	386	80				
14:44	400	406	80	170			
14:45	420	426	80				
14:46	440	446	80	160			
14:47	460	466	80				
14:49	480	486	80	155			
14:50	500	506	80				
14:52	520	526	80	150			
14:54	540	546	80				
14:55	560	566	80	140			
14:56	580	586	80				
14:57	600	606	80	130			
14:58	620	626	80				
14:59	640	646	80	120			
15:01	660	666	80				
15:02	680	686	80	110			

3-D Acquisition		(Maren Scheidhauer, David Dupuy)		3
General:		Source:		Position:
Date: 15.08.2001	Time: 14:11	Type: Mini GI	Line: 140_15d	
Weather: sunny, calm		Chamber Size [cuin]: 15/15	Location: OUCHY	
Co-workers: Jochen, Mathieu, Philippe		Depth [m]: 1	Line Direction: SE-NW	
Geometry (multi-streamer configuration):		GI Delay [ms]: 28	Trace Spacing [m]: 2.5	
Minimum Offset [m]: 5		Shooting Frequency [m]: 5	Cross Spacing [m]: 3.75	
Maximum Offset [m]: 62.5		Distance to Boat [m]: 6.25	Fold: 6	
No. of Streamer, Starboard (green): 2		Active Length of Streamer [m]: 57.5		
No. of Streamer, Center (blue): S/N		Length of Center Lead-in [m]: 10		
No. of Streamer, Port (red): 1		Length of other Lead-ins [m]: 17		
Recording Parameters of BISON:		Offset [m]: 5	Filter:	
Survey Name: OUCHY1		Data:	Nyquist Filter [Hz]: 1000	
Tape: OUCHY37		Sample Interval [ms]: 0.5	Filter [Hz]: 25-1000	
GPS-File Name: 3D037		Recording Time [ms]: 1000	Notch [Hz]: No	
SEGY-File Name: sail37.sgy		Default Gain [db]: 24		
DAT-File Name: I1000373DSEISM.DAT		Total Channels: 72		
		Booms:		
		Distance Boom - End of Boat [m]: 7.9		
		Distance Boom - Streamer [m]: 0.9		TURN CHARGER OFF !!!

Hour	Shot N° PC	Shot N° BISON	Gun Pressure [bar]	Pressure in Bottles [bar]	Depth Sonar [m]	Ship Coordinates GPS	Comments (measure voltage of hydrophone amplifiers!)
15:02	680	686	80	110			
15:03	700	706	80				
15:04	720	726	80	105			
15:05	740	746	80				
15:06	760	766	80	100			
15:07	780	786	80				
15:08	800	806	80	90			
15:10	820	826	70				
15:11	840	846	70	85			
15:12	860	866	70				
15:12	861	867	70	85			

Table A-11. Acquisition sheets of 2-D lake traverse, profile 140_15 portions a-d, shot with the Mini G.I G15 / I15 along extension of sail line 140 towards the southeast and northwest of Survey II.

2-D Acquisition		(Maren Scheidhauer, Milan Beres, François Marillier)					
General:		Source:		Position:			
Date: 25.10.1999	Time: 11:59	Type: Mini GI	Line: 55long	Location: OUCHY			
Weather: cloudy, small waves, rain		Chamber Size [cuin]: 30/30	Line Direction: NW-SE				
Co-workers: Olivier Z., Olivier, Manuelle, Gilles		Depth [m]: 1.5					
Geometry (single-streamer configuration):		GI Delay [ms]: (27 kOhm) 27	Shooting Frequency [s]: 5	Trace Spacing [m]: 2.5			
Minimum Offset [m]: 5		Distance to Boat [m]: 10		Cross Spacing [m]: %			
Maximum Offset [m]: 122.5				Fold: 12			
No. of first Streamer: 1		Active length of streamer [m]: 117.5					
		Length of lead-in cable [m]: 13.75					
Recording Parameters of GEOMETRICS:		Data:		Filter:			
Directory: D:\055long		Sample Interval [ms]: 0.5	Nyquist Filter [Hz]: 10-1000				
Files: 001.DAT-371.DAT		Recording Time [ms]: 1024	Filter [Hz]: 10-1000				
GPS-File Name: 55long.obs		Default Gain [db]: 36	Notch [Hz]: No				
SEGY-File Name: 55long.sgy		Total Channels: 48					
DAT-File Name:							
TURN CHARGER OFF !!!							

Hour	Shot N° GEOMETRICS	Shot N° PC	Gun Pressure [bar]	Pressure in Bottles [bar]	Depth Sonar [m]	Ship Coordinates GPS	Comments (measure voltage of hydrophone amplifiers!)
11:59	001	1	90	260	126	535 444 / 149 428	12.5 V
12:02	047	47	90		197	535 575 / 149 269	start of line
12:05	090	90	90		203	535 706 / 149 097	strong rain around shot 80
12:08	121	121	90		225	535 802 / 148 976	
12:11	160	160	90		239	535 915 / 148 825	
12:14	198	198	90		246	536 044 / 148 670	
12:17	237	237	90		251	536 964 / 148 515	almost no more rain
12:20	284	284	90	90	270	536 306 / 148 320	end of line
12:23	325	325	85	85	286	536 438 / 148 153	pressure starts to go below 90 at shot 290
12:26	370	370	70	70	294	536 555 / 148 004	compressor on since 100 bars in bottles
		371					extra shot

Table A-12. Acquisition sheet of Mini G.I G30 / I30 2-D profile 140_30 along sail line 55 of Survey I.

Processing Sheet 2-D		55LONG		Maren Scheidhauer	
Data:		Source:		Files:	
Sample Interval [ms]: 0.5		Type: Mini GI	Line: 55long	Date: 25.10.1999	
Recording Time [ms]: 1024		Chamber Size [cuin]: 30/30	Survey: OUCHY	Line Name: 55 LONG	
No. of first streamer: 1		SPs: 371 / 370	SEGY-File Name: 55long.sgy	DAT-File Name:	
Recording Instrument: GEOMETRICS		CMPs: 1524			

NO	JOB NAME	INPUT FILE [*.cst]	OUTPUT FILE [*.cst]	GEOVECTEUR MODULES	PROCESSING
1.	input		gathers55long	INPTR	input
				MODET	numbering of traces (1-48)
				BSORT	sorting of traces (WORD 17, 2)
				MODET	numbering of shotpoints (1-?)
				BSORT	sorting of traces (WORD 2, 17)
2.	neartracelong	gathers55long	PLOT	SELEC	selection of 21th trace of each SP
				FILTR	40 / 60 - 500 / 550 Hz filter length: 500
				REFOR	((t / 250)**2
				DYNQU	50 ms, mean amplitude: 5000
3.	inversion	gathers55long	temp1	MODET	renaming of the first 24 traces
4.	geometrylong	temp1	temp2	BSORT	resorting of traces (WORD 2 and 17)
				HISTA	shifting all traces 10 ms up
				LABEL	geometry / renumbering of SP
				SELEC	deletion of 4 SP (87, 127, 232, 371)
5.	editinglong	temp2	geometry55long	OUTST	trace elimination (24, 37), resorting of traces (WORD 2, 17)
				MODET	numbering of traces (1-46)
				MNGTY	setting y-flag in the sequence
6.	sortlong	geometry55long	sort55long	BSORT	CDP sorting (WORD 4, 20)
				MODET	renumbering of traces in CDP domain
7.	vespalong	sort55long	vespa55long.velcom	FILTR	40 / 60 - 500 / 550 Hz filter length: 500
				REFOR	((t / 250)**5
				MUTES	muting of water column: mute55long.lmu
				MUTES	muting of multiple: int55long.lmu
				DYNQU	50 ms, mean amplitude: 5000
				VESPA	semblance
8.	stacklong	sort55long	stack55long	FILTR	40 / 60 - 500 / 550 Hz filter length: 500
				REFOR	((t / 250)**5
				PANMO	NMO correction: ouchy55long.lvi
				STACK	stack
				MUTES	muting of water column: mute55long.lmu
				MUTES	muting of multiple: int55long.lmu
				DYNQU	1024 ms, mean amplitude: 5000
9.	migrlong	stack55long	migr55long	KIRCH	2D Kirchhoff migration (half-width = 200 traces)
					migration velocities: ouchy55long.vel
				DYNQU	1024 ms, mean amplitude: 5000

Table A-13. 2-D processing sheets for profile 140_30 using GéovecteurPlus. Gray areas indicate parameter differences between this profile and profile 140_15 and 140_w.

SAIL LINE	X START	Y START	X END	Y END	DIRECTION	DIRECTION	1. SP	LAST SP	TOTAL
1									
2									
3									
4									
5	536542.35	148571.07	535890.64	149465.90	323.93	SE-NW	55	275	221
6	536574.72	148549.95	535878.95	149465.15	322.76	SE-NW	1	235	235
7	536584.80	148565.80	535854.13	149499.45	321.95	SE-NW	1	239	239
8	535854.87	149490.11	536571.22	148561.32	322.36	NW-SE	14	252	239
9	536566.94	148554.20	535838.75	149481.23	321.85	SE-NW	1	232	232
10	536555.66	148548.72	535837.80	149479.66	322.36	SE-NW	1	232	232
11	535831.90	149470.25	536522.93	148575.20	322.33	NW-SE	1	224	224
12	535915.22	149355.67	536523.53	148581.27	321.85	NW-SE	42	235	194
13	535802.91	149441.13	536572.92	148534.21	319.67	NW-SE	17	243	227
14	535818.02	149472.91	536522.01	148513.07	323.74	NW-SE	2	232	231
15	535802.66	149447.50	536520.47	148534.31	321.83	NW-SE	1	233	233
16	535803.18	149458.00	536516.39	148522.50	322.68	NW-SE	1	234	234
17	535798.88	149451.85	536514.51	148521.75	322.42	NW-SE	1	232	232
18	535783.41	149449.55	536513.21	148518.76	321.90	NW-SE	17	258	242
19	535781.89	149451.75	536496.89	148505.25	322.93	NW-SE	3	249	247
20	535774.57	149444.23	536491.57	148500.46	322.78	NW-SE	1	242	242
21	535772.27	149439.50	536492.62	148496.74	322.62	NW-SE	1	242	242
22	535764.92	149437.94	536499.52	148496.92	322.02	NW-SE	1	239	239
23	536504.32	148502.88	535762.92	149422.88	321.14	SE-NW	1	238	238
24	536479.55	148482.06	535768.03	149420.24	322.82	SE-NW	1	233	233
25	536469.59	148473.84	535747.84	149403.21	322.17	SE-NW	1	240	240
26	536450.68	148486.58	535743.90	149412.50	322.64	SE-NW	7	243	237
27	536453.71	148461.36	535731.10	149394.88	322.26	SE-NW	1	243	243
28	536453.49	148460.50	535732.02	149400.28	322.49	SE-NW	1	226	226
29	536441.25	148461.91	535724.17	149391.43	322.35	SE-NW	1	230	230
30	535718.42	149391.06	536436.04	148462.53	322.30	NW-SE	1	242	242
31	535714.21	149387.44	536441.65	148460.93	321.86	NW-SE	1	251	251
32	535701.62	149384.21	536426.41	148450.35	322.18	NW-SE	1	239	239
33	535706.83	149375.39	536404.41	148431.99	323.52	NW-SE	1	242	242
34	535715.28	149341.79	536408.71	148436.16	322.56	NW-SE	9	241	233
35	535684.66	149363.62	536405.99	148432.07	322.25	NW-SE	1	237	237
36	535686.89	149350.00	536400.06	148426.88	322.31	NW-SE	1	236	236
37	535680.04	149359.56	536391.58	148421.28	322.83	NW-SE	1	237	237
38	536392.29	148414.24	535681.96	149356.52	322.99	SE-NW	1	233	233
39	536382.26	148411.71	535669.82	149347.05	322.70	SE-NW	1	235	235
40	536349.48	148462.10	535675.12	149321.96	321.89	SE-NW	14	239	226
41	535675.12	149321.96	536372.08	148409.53	322.63	NW-SE	7	237	231
42	535646.09	149332.96	536359.87	148398.81	322.62	NW-SE	1	238	238
43	535672.28	149288.44	536350.80	148394.29	322.81	NW-SE	22	250	229
44	536348.64	148390.48	536364.20	149327.87	322.69	SE-NW	1	235	235
45	536361.09	148391.48	53628.52	149318.57	321.68	SE-NW	1	239	239
46	536341.94	148380.48	535634.79	149325.26	323.19	SE-NW	1	230	230
47	535625.52	149306.47	536332.04	148387.41	322.45	NW-SE	23	254	232
48	535610.46	149311.78	536330.25	148377.84	322.38	NW-SE	1	239	239
49	535605.51	149309.01	536331.96	148374.98	322.13	NW-SE	1	236	236
50	536324.16	148366.68	535599.48	149296.95	322.08	SE-NW	2	235	234
51	536308.45	148353.30	535604.50	149296.46	323.26	SE-NW	1	240	240
52	535587.29	149289.31	536306.16	148360.36	322.27	NW-SE	18	250	233
53	536299.75	148352.22	535583.16	149280.46	322.33	SE-NW	1	236	236
54	536303.97	148354.91	535574.89	149277.41	321.68	SE-NW	1	235	235
55	536293.14	148345.73	535567.98	149271.87	321.94	SE-NW	1	228	228
56	536282.24	148345.49	535573.13	149276.36	322.70	SE-NW	1	231	231
57	536283.34	148337.58	535559.96	149262.85	321.98	SE-NW	1	231	231
58	535549.67	149267.27	536271.63	148339.67	322.11	NW-SE	18	256	239
59	535443.73	149254.96	536265.06	148324.69	322.21	NW-SE	1	243	243
60	535543.68	149256.34	536261.77	148321.80	322.46	NW-SE	1	242	242
61	535531.31	149247.61	536259.98	148321.57	321.80	NW-SE	1	243	243
62	535530.44	149245.09	536245.72	148322.98	322.20	NW-SE	1	245	245
63	536244.03	148315.35	535522.00	149235.04	321.87	SE-NW	1	233	233
64	536238.25	148303.49	535514.01	149229.37	321.97	SE-NW	1	233	233
65	536229.21	148300.42	535508.07	149222.27	321.96	SE-NW	3	231	229
66	536226.12	148295.86	535508.08	149226.23	322.34	SE-NW	1	237	237
67	536221.26	148291.37	535499.09	149218.23	322.08	SE-NW	1	232	232
68	535492.60	149218.21	536216.09	148286.77	322.16	NW-SE	1	240	240
69	535488.33	149209.72	536211.62	148282.79	322.03	NW-SE	1	237	237
70	535479.67	149208.05	536202.46	148274.55	322.25	NW-SE	1	241	241
71	535475.76	149190.67	536200.88	148274.01	321.65	NW-SE	1	239	239
72	535469.32	149194.93	536189.61	148270.67	322.07	NW-SE	1	242	242
73	535461.92	149190.73	536180.87	148254.96	322.47	NW-SE	1	246	246
74	535457.08	149187.96	536173.94	148254.38	322.48	NW-SE	8	245	238
75	535452.86	149180.99	536162.32	148248.17	322.75	NW-SE	1	242	242
76	535441.50	149177.86	536169.63	148252.53	321.80	NW-SE	1	239	239
77	535435.33	149170.20	536163.06	148246.88	321.76	NW-SE	1	248	248
78	535441.30	149173.34	536152.09	148241.28	322.67	NW-SE	2	240	239
79	536151.99	148232.25	535430.18	149165.74	322.29	SE-NW	1	236	236
80	536139.90	148228.86	535420.53	149157.39	322.23	SE-NW	1	226	226
81	536139.90	148226.62	535421.60	149155.99	322.30	SE-NW	1	228	228
82	536128.23	148225.30	535414.67	149147.09	322.26	SE-NW	1	232	232
83	536116.10	148234.05	535412.44	149152.91	322.56	SE-NW	8	237	230
84	536124.30	148215.07	535404.54	149144.42	322.24	SE-NW	1	231	231

Table A-14. Navigated start and end points for all 80 sail lines of Survey I, indicating acquisition direction between those points, corresponding shot point numbers and total number of shot points per line.

SAIL LINE	X START	Y START	X END	Y END	DIRECTION	DIRECTION	1. SP	LAST SP	TOTAL
1	536802.71	148345.93	535883.79	149531.61	322.22	SE-NW	1	301	301
2	536793.06	148338.74	535874.21	149524.16	322.22	SE-NW	1	301	301
3	536784.32	148331.78	535866.26	149518.02	322.26	SE-NW	1	301	301
4	536776.09	148325.42	535855.88	149510.05	322.16	SE-NW	1	301	301
5	536765.86	148317.48	535848.64	149504.35	322.30	SE-NW	1	301	301
6	536758.08	148311.43	535837.91	149496.05	322.16	SE-NW	1	301	301
7	536749.89	148305.29	535830.70	149490.54	322.21	SE-NW	1	301	301
8	536739.60	148297.18	535821.34	149483.20	322.25	SE-NW	1	301	301
9	536730.51	148290.14	535812.43	149476.41	322.26	SE-NW	1	301	301
10	536721.75	148283.45	535803.65	149469.78	322.26	SE-NW	1	301	301
11	536712.44	148276.13	535794.47	149462.62	322.27	SE-NW	1	301	301
12	536703.87	148269.63	535785.93	149455.78	322.26	SE-NW	1	301	301
13	536695.04	148262.63	535775.87	149448.17	322.21	SE-NW	1	301	301
14	536686.95	148256.36	535768.44	149442.21	322.24	SE-NW	1	301	301
15	536676.10	148247.96	535759.14	149435.01	322.32	SE-NW	1	301	301
16	536668.03	148241.75	535750.01	149428.02	322.26	SE-NW	1	301	301
17	536659.35	148234.97	535740.12	149420.49	322.21	SE-NW	1	301	301
18	536650.69	148228.45	535732.51	149414.54	322.26	SE-NW	1	301	301
19	536642.48	148222.00	535723.00	149407.20	322.20	SE-NW	1	301	301
20	536634.01	148215.39	535714.67	149400.75	322.20	SE-NW	1	301	301
21	536624.19	148207.88	535704.79	149393.05	322.20	SE-NW	1	301	301
22	536615.23	148200.84	535696.26	149386.58	322.22	SE-NW	1	301	301
23	536605.77	148193.53	535687.85	149379.90	322.27	SE-NW	1	301	301
24	536597.87	148187.34	535680.15	149373.87	322.28	SE-NW	1	301	301
25	536588.99	148180.48	535669.12	149365.45	322.18	SE-NW	1	301	301
26	536579.43	148173.24	535661.86	149359.84	322.29	SE-NW	1	301	301
27	536568.47	148164.61	535651.79	149352.01	322.33	SE-NW	1	301	301
28	536560.19	148158.35	535644.31	149346.16	322.37	SE-NW	1	301	301
29	536552.42	148152.34	535634.86	149338.81	322.28	SE-NW	1	301	301
30	536544.34	148145.92	535625.85	149331.87	322.24	SE-NW	1	301	301
31	536536.15	148139.56	535617.33	149325.26	322.23	SE-NW	1	301	301
32	536525.91	148131.67	535608.63	149318.48	322.30	SE-NW	1	301	301
33	536517.51	148125.30	535599.09	149311.28	322.25	SE-NW	1	301	301
34	536508.06	148117.96	535589.31	149303.74	322.23	SE-NW	1	301	301
35	536498.20	148110.35	535580.04	149296.54	322.26	SE-NW	1	301	301
36	536490.52	148104.48	535572.48	149290.74	322.26	SE-NW	1	301	301
37	536484.28	148097.41	535563.89	149281.89	322.15	SE-NW	1	301	301
38	536471.79	148089.89	535554.07	149276.32	322.28	SE-NW	1	301	301
39	536465.68	148085.07	535544.90	149269.36	322.14	SE-NW	1	301	301
40	536454.76	148076.67	535534.92	149261.41	322.17	SE-NW	1	301	301
41	536446.94	148070.52	535527.03	149255.51	322.18	SE-NW	1	301	301
42	536440.14	148065.25	535517.87	149248.51	322.07	SE-NW	1	301	301
43	536429.18	148056.97	535509.57	149242.04	322.19	SE-NW	1	301	301
44	536418.77	148048.85	535501.48	149235.57	322.30	SE-NW	1	301	301
45	536409.99	148042.05	535492.36	149228.56	322.28	SE-NW	1	301	301
46	536401.19	148035.26	535483.60	149221.90	322.29	SE-NW	1	301	301
47	536392.63	148028.55	535475.08	149215.33	322.29	SE-NW	1	301	301
48	536383.84	148021.83	535465.74	149208.00	322.26	SE-NW	1	301	301
49	536374.57	148014.72	535457.07	149201.29	322.29	SE-NW	1	301	301
50	536366.45	148008.35	535448.53	149194.55	322.27	SE-NW	1	301	301
51	536356.79	148000.78	535438.31	149186.67	322.24	SE-NW	1	301	301
52	536348.10	147994.20	535430.20	149180.38	322.27	SE-NW	1	301	301
53	536339.21	147987.14	535421.01	149173.31	322.26	SE-NW	1	301	301
54	536330.57	147980.54	535412.56	149166.77	322.26	SE-NW	1	301	301
55	536321.17	147973.36	535402.81	149159.18	322.24	SE-NW	1	301	301
56	536312.73	147966.77	535393.60	149152.22	322.21	SE-NW	1	301	301
57	536303.68	147959.72	535385.13	149145.44	322.24	SE-NW	1	301	301
58	536294.81	147952.94	535375.96	149138.43	322.22	SE-NW	1	301	301
59	536286.15	147946.19	535367.28	149131.61	322.22	SE-NW	1	301	301
60	536276.89	147938.92	535358.53	149125.16	322.25	SE-NW	1	301	301

Table A-15. Navigated start and end points for all 60 sail lines of Survey II, indicating acquisition direction between those points, corresponding shot point numbers and total number of shot points per line.

3-D Survey I							(Maren Scheidhauer, Milan Beres, Francois Marillier)	
General:			Source:			Position:		
Date:	17.09.1999	Time:	13:44	Type:	water gun	Line:	5	
Weather:	sunny, no wind	Shooting Frequency [m]:	5	Location:	OUCHY	Line Direction:	NW-SE	
Co-workers:	Yvan, Gilles, Olivier, André	Distance to Boat [m]:	10	Depth [m]:	0.3	Trace Spacing [m]:	2.5	
Geometry (single-streamer configuration):			Trace Spacing [m]:			Filter:		
Minimum Offset [m]:	5	Active length of streamer [m]:	117.5	Cross-Line Spacing [m]:	7.5			
Maximum Offset [m]:	122.5	Length of lead-in cable [m]:	13.75	Fold:	12			
No. of first Streamer:	1							
Recording Parameters of GEOMETRICS:			Data:			Filter:		
Survey Name:	ouchy5	Sample Interval [ms]:	0.25	Nyquist Filter [Hz]:	4-2000			
Tape:	CD	Recording Time [ms]:	500	Filter [Hz]:	10-2000			
GPS-File Name:	Ouchy05.obs	Default Gain [db]:	36	Notch [Hz]:	No			
Segy-File Name:	ouchy5.sgy	Total Channels:	48					
DAT-File Name:	I909005000000.DAT							
Trigger:			Batch:			TURN CHARGER OFF !!!		
Mode:	automatic	Batch Mode:	on, automatic triggering					
Standard Trigger:	both	Marine Mode:	on					
Recording Delay [ms]:	0	View Stack after each shot:	on					
NegDelay runs in the background			Screen Update:	5				
Hour	DIR PC	Shot N° PC	Gun Pressure [bar]	Pressure in Bottles [bar]	Depth Sonar [m]	Ship Coordinates GPS		Comments
13:53	105000	0	140	198	250	536570/148545		Compressor ON
14:12	105020	20	140	200	222	536408/148844		Compressor OFF STOP
14:22	105057	57	140	200	247	536523/148618		again Compressor OFF
14:24	105090	90	140	192	228	536441/148756		Start of Line
14:27	105135	135	140	185	217	536323/148922		
14:30	105186	186	140	180	200	536152/149127		
14:35	105249	249	140	175	192	535955/149388		End of Line
14:37	105280	280	140	170	185	535844/149544		

Table A-16. Acquisition sheet of sail line 5, the first navigation line of 3-D Survey I.

3-D Survey II							(Maren Scheidhauer, David Dupuy, François, Marillier)	
General:			Source:			Position:		
Date:	09.08.2001	Time:	12:00	Type:	Mini GI	Line:	1	
Weather:	cloudy, calm	Chamber Size [cuin]:	15/15	Location:	OUCHY	Line Direction:	SE-NW	
Co-workers:	Alexandre, Yvan	Depth [m]:	1	GI Delay [ms]:	28	Trace Spacing [m]:	2.5	
Geometry (multi-streamer configuration):			Shooting Frequency [m]:			Filter:		
Minimum Offset [m]:	5	Distance to Boat [m]:	6.25	Active Length of Streamer [m]:	57.5	Cross Spacing [m]:	3.75	
Maximum Offset [m]:	62.5	Length of Center Lead-in [m]:	10	Length of other Lead-ins [m]:	17	Fold:	6	
No. of Streamer, Starboard (green):	2	Offset [m]:	5					
No. of Streamer, Center (blue):	S/N				Filter:			
No. of Streamer, Port (red):	1				Nyquist Filter [Hz]:			
Recording Parameters of BISON:			Data:			Filter [Hz]:		
Survey Name:	OUCHY1	Sample Interval [ms]:	0.5	Notch [Hz]:	No	25-1000		
Tape:	OUCHY1	Recording Time [ms]:	1000					
GPS-File Name:	3D001	Default Gain [db]:	24					
SEG-Y-File Name:	sail01.sgy	Total Channels:	72					
DAT-File Name:	I1000013DSEISM.DAT				Booms:			
			Distance Boom - End of Boat [m]:	7.9				
			Distance Boom - Streamer [m]:	0.9	TURN CHARGER OFF !!!			
Hour	Shot N° PC	Shot N° BISON	Gun Pressure [bar]	Pressure in Bottles [bar]	Depth Sonar [m]	Ship Coordinates GPS		Comments (measure voltage of hydrophone amplifiers!)
								13.16 V, + 310 mA, - 280 mA
								10 extra shots
12:00	11	11	80	280				
12:01	25	24	80					
12:02	40	39	80	260				
12:04	60	59	80					
12:05	80	79	80	250				
12:06	100	99	80					
12:08	120	119	80	240				
12:09	140	139	80					
12:11	160	159	80	230				
12:12	180	179	80					
12:13	200	199	80	225				
12:15	220	219	80					
12:16	240	239	80	220				
12:17	260	259	80					
12:19	280	279	80	210				
12:20	300	299	80					
12:21	311	310	80	200				

Table A-17. Acquisition sheet of sail line 1, the first navigation line of 3-D Survey II.

Processing Sheet 3-D		OUCHY1999		Maren Scheidhauer 1	
Data: Sample Interval [ms]: 0.25 Source: Type: Water Gun Files: Date: Oct. 1999 Recording Time [ms]: 512 Chamber Size [cuin]: 15 Survey: OUCHY1 No. of first Streamer: 1 SPs per LINE: variable Line Name: 05-84 Recording Instrument: GEOMETRICS CMPs per LINE: 31-1112 / 119-1011 SEG-Y File Name: line05.sgy ; line84.sgy DAT File Convention: JOBN00SurveyNO0NO NO: 05-84 DAT-File Name: I1010053DSEISM.DAT ; I1010843DSEISM.DAT					
JOB NO	JOB NAME	INPUT FILE [*.cst]	OUTPUT FILE [*.cst] or other	GEOVECTEUR MODULES	PROCESSING
1.	input	I1010NO3DSEISM.DAT	gathersNO	INPTR MODET BSORT MODET BSORT	input (check WORD 01) numbering of traces (WORD 17=1-48) sorting of traces (WORDS 17, 02) numbering of shotpoints (1-max. number of SPs) sorting of traces (WORDS 02, 17)
2.	neartrace	gathersNO	PLOTX neartraceNO	SELEC FILTR REFOR DYNQU	selection of 21st trace of each SP 100 / 200 - 1500 / 1700 Hz operator length: 300 (t/250)**2 AGC: 50 ms, mean amplitude: 5000
3.	inversion	gathersNO	temp1	MODET	renaming of the first 24 traces
4.	shift	temp1	lineNO	MODET HISTA OUTST MODET MNGTY OUTBD	set WORD 01 = 511 shifting all traces 25 ms up resorting of traces (WORDS 02, 17) renumbering of traces (WORD 17=1-48) setting y-flag to WORD 02 writing files to stage
5.A	NAVIGATION/OUCHY	OUCHY0NO.OBS	UKO05-25.SAV UKO26-46.SAV UKO47-67.SAV UKO68-84.SAV UKO05-25.SAV UKO26-46.SAV UKO47-67.SAV UKO68-84.SAV	NAV WILOC OUTBD	navigation from GPS files OUCHY05-OUCHY25.OBS navigation from GPS files OUCHY26-OUCHY46.OBS navigation from GPS files OUCHY47-OUCHY67.OBS navigation from GPS files OUCHY68-OUCHY84.OBS creation of S.N.T. (Seismic Navigation Tape) trace headers containing the (X,Y) field positions in one trace per cable writing files to stage
5.B	GEOUNIX/grillith ASPRO/eqrid	I4010NO0000000.DAT I0005253DSEISM.DAT I0026463DSEISM.DAT I0047673DSEISM.DAT I0068843DSEISM.DAT	I5010NO3DSEISM.DAT grid1.lgr	IFTHN MODET EGRID BSORT	if WORD 07 = 9999 set WORD 30 = NO WORD 30 in seismic file set to NO merging of seismic and navigation data (change line in GSL) trace elimination (WORD 17 = 24, 37) sorting of traces (WORDS 04, 19, 20) make EGRID coverage table
6.	haben_035-076 haben_076-115	I501005-I501046 I501044-I501084	haben_035-077 haben_075-115	BSORT HABIN	sorting traces (WORDS 04, 19, 20) very important !!! harmonization of offset groups in 3D within a marco-bin of 3 bins in LINE direction and 1 bin in CMP direction make HABIN coverage table

Processing Sheet 3-D		OUCHY1999		Maren Scheidhauer 2	
Data: Sample Interval [ms]: 0.25 Source: Type: Water Gun Files: Date: Oct. 1999 Recording Time [ms]: 512 Chamber Size [cuin]: 15 Survey: OUCHY1 No. of first Streamer: 1 SPs per LINE: variable Line Name: 05-84 Recording Instrument: GEOMETRICS CMPs per LINE: 31-1112 / 119-1011 SEG-Y File Name: line05.sgy ; line84.sgy DAT File Convention: JOBN00SurveyNO0NO NO: 05-84 DAT-File Name: I1010053DSEISM.DAT ; I1010843DSEISM.DAT					
JOB NO	JOB NAME	INPUT FILE [*.cst]	OUTPUT FILE [*.cst] or other	GEOVECTEUR MODULES	PROCESSING
7A.	vespa11 vespa21 vespa31 vespa41	haben_04-27 haben_24-48 haben_42-65 haben_62-85	lines_06-24i.velcom lines_26-44i.velcom lines_46-62i.velcom lines_64-84i.velcom	BSORT FILTR REFOR MUTES DYNQU VESPA	resorting of traces (WORDS 19, 04, 20) selection of every 4th LINE: 06-24, 26-44, 46-62, 64-84 file output: velselect1, 2i, 3i, 4i 100 / 200 - 1500 / 1700 Hz operator length: 300 (t/250)**5 muting of water column: mute_04-85.lmu AGC: 50 ms, mean amplitude: 5000 semblance spectra calculation every 4th LINE and every 100th CMP for 1300-3000 m/s velocity analysis final velocity: 5000 m/s, density display: color shades semi-auto picking, scaling 120, 1200 color palette: velcom.cmp
7B.	dmofovespa1 dmofovespa2 dmofovespa3 dmofovespa4	haben_04-27 haben_24-48 haben_42-65 haben_62-85	vespainput1 vespainput2 vespainput3 vespainput4	FILTR REFOR FANMO KIDMO FANMO BSORT	100 / 200 - 1500 / 1700 Hz operator length: 300 (t/250)**5 NMO correction: wbstackold.lfd, iamute_preNMO.lmu v_04-27i.lvi, v_24-48i.lvi, v_42-65i.lvi, v_62-85i.lvi unstacked DMO (grid1.lgr) inverse NMO correction
	vespa1 vespa2 vespa3 vespa4	vespainput1 vespainput2 vespainput3 vespainput4	lines_06-24.velcom lines_26-44.velcom lines_46-62.velcom lines_64-84.velcom	BSORT VESPA	resorting of traces (WORDS 19, 04, 20) selection of every 2nd LINE: 06-24, 26-44, 46-62, 64-84 file output: velselect1, 2, 3, 4 semblance spectra calculation every 2nd LINE and every 50th CMP for 1300-3000 m/s velocity analysis final velocity: 5000 m/s, density display: color shades semi-auto picking, scaling 120, 1200 color palette: velcom.cmp
	EDIT/	vnew_04-27.lvi vnew_24-48.lvi vnew_46-62.lvi vnew_64-84.lvi	vnew_04-27.lvi vnew.lvi		combine all 4 files to vnew.lvi
	UTIL/Tabedit	vnew.lvi	vnew_001-145.lvi	Operation/Formula	add 31 to each LINE: \$5 = \$1+31 add 15 to each CMP: \$6 = \$2 + 15 add LINE 01 and 145
	EDIT	vnew_001-145.lvi	vnew_001-145.lvi		

Processing Sheet 3-D **OUCHY1999** Maren Scheidhauer 3

Data:
 Sample Interval [ms]: 0.25 **Source:** Type: Water Gun **Files:** Date: Oct. 1999
 Recording Time [ms]: 512 Chamber Size [cuin]: 15 Survey: OUCHY I
 No. of first Streamer: 1 SPs per LINE: variable Line Name: 05-84
 Recording Instrument: GEOMETRICS CMPs per LINE: 31-1112 / 119-1011 SEG-Y-File Name: line05.sgy - line84.sgy
 DAT File Convention: JOBN00SurveyNO0NO NO: 05-84 DAT-File Name: I1010053DSEISM.DAT
 I1010843DSEISM.DAT

JOB NO	JOB NAME	INPUT FILE [*.cst]	OUTPUT FILE [*.cst] or other	GEOVECTEUR MODULES	PROCESSING
8A.	stack_035-076i	haben_035-077	stack_035-076i	FILTR	100 / 200 - 1500 / 1700 Hz operator length: 300
	stack_077-115i	haben_075-115	stack-077-115i	REFOR	(t / 250)**5
				FANMO	NMO correction: v 04-27i.lvi, v 24-48i.lvi, v 42-65i.lvi, v 62-85i.lvi
				KIDMO	3D DMO stack (Kirchhoff): mute_04-85.lmu
				OUTST	selection of LINES 05-25, 26-44, 45-63, 64-84 resorting of traces (WORDS 04, 19)
				YDRIV	adding of blank traces: (WORD 04: 16-1097, WORD 19: 05-25, 26-44, 45-63, 64-84)
				DYNQU	AGC: 512 ms, mean amplitude: 5000
	UTIL/Tabedit	wbstackold.lfd	wbstack.lfd	Operation/Formula	add 31 to each LINE: \$5 = \$1+31 add 15 to each CDP: \$6 = \$2 + 15
	EDIT	wbstack.lfd	wbstack.lfd		add LINE 01 and 145
	UTIL/Tabedit	wbstack.lfd	iqmute.lmu	Operation/Statistics	in order to create iqmute.lmu find min and max water bottom values on field 4 for all records
	8B.	stacknohaben_036-076	I501005-I501046	I7036763DSEISM.DAT	BSORT
stacknohaben_077-115		I501044-I501084	I7771153DSEISM.DAT	FILTR	100 / 200 - 1500 / 1700 Hz operator length: 300
				REFOR	(t / 250)**5
				FANMO	NMO correction: vnew_001-145.lvi
				KIDMO	3D DMO stack (Kirchhoff): iqmute.lmu, wbstack.lfd
				OUTST	selection of LINES 036-76, 077-115 resorting of traces (WORDS 04, 19)
				YDRIV	adding of blank traces: (WORD 04: 31-1112, WORD 19: 036-076, 077-115)
				DYNQU	AGC: 512 ms, mean amplitude: 5000
				OUTBD	writing files to stage 1
stacknohaben		I7036763DSEISM.DAT	stacknohaben_035-115	INPTR	merging 4 files to 1
		I7771153DSEISM.DAT			

Processing Sheet 3-D **OUCHY1999** Maren Scheidhauer 4

Data:
 Sample Interval [ms]: 0.25 **Source:** Type: Water Gun **Files:** Date: Oct. 1999
 Recording Time [ms]: 512 Chamber Size [cuin]: 15 Survey: OUCHY I
 No. of first Streamer: 1 SPs per LINE: variable Line Name: 05-84
 Recording Instrument: GEOMETRICS CMPs per LINE: 31-1112 / 119-1011 SEG-Y-File Name: line05.sgy - line84.sgy
 DAT File Convention: JOBN00SurveyNO0NO NO: 05-84 DAT-File Name: I1010053DSEISM.DAT
 I1010843DSEISM.DAT

JOB NO	JOB NAME	INPUT FILE [*.cst]	OUTPUT FILE [*.cst] or other	GEOVECTEUR MODULES	PROCESSING
8.	stack_035-076	haben_035-077	I8036763DSEISM.DAT	FILTR	100 / 200 - 1500 / 1700 Hz operator length: 300
	stack_077-115	haben_075-115	I8771153DSEISM.DAT	REFOR	(t / 250)**5
				FANMO	NMO correction: vnew_001-145.lvi
				KIDMO	3D DMO stack (Kirchhoff): iqmute.lmu, wbstack.lfd
				OUTST	selection of LINES 036-076, 077-115 resorting of traces (WORDS 04, 19)
				YDRIV	adding of blank traces: (WORD 04: 30-1330, WORD 19: 36-076, 077-115)
				SCALE	if WORD 03 = 30146560 or 25952256 this trace is muted
				DYNQU	AGC: 512 ms, mean amplitude: 5000
				OUTBD	writing files to stage 1
	stack	I8036763DSEISM.DAT	stack_036-115	INPTR	merging 4 files to 1
		I8771153DSEISM.DAT			
stackmute	stack_036-115	stackmute_036-115	MUTES	muting of water bottom: iqmute.lmu, wbstack.lfd	
QC	CDPfoldfd	stackmute	8CDPfoldfd.list	RESTR	update of water bottom in WORD 47 (wbstack.lfd)
	stacknohaben	stacknohaben	8CDPfoldfd.list	OUTST	sorting of traces (WORDS 19, 04)
				LISTE	if WORD 43 = 0 output contents of WORDs 43 (bin center-X), 44 (bin center-Y), no decimal output!!! 04 (CMP), 19 (LINE), 08 (FOLD), 47
	EDIT/	8CDPfoldfd.list	UTILITIES/8CDPfoldfd		delete all other lines except data
	EDIT/	8CDPfoldfd.list	UTILITIES/8CDPfoldfdnohaben		delete all other lines except data
	UTILITIES/	UTILITIES/8CDPfoldfd	foldCDP.txt	foldlist.awk	create stacking charts with SURFER 7.0
		UTILITIES/8CDPfoldfdnohaben	foldCDPnohaben.txt		
			foldxy.txt		
			foldxynohaben.txt		
	qcdbu	stack	stack_ouchy	QCDBU	quality control database update
			stacknohaben.ouchy		precision problem while plotting due to the lack of decimals in X/Y coordinates of bin centers

Processing Sheet 3-D		OUCHY1999		Maren Scheidhauer		5
Data: Sample Interval [ms]: 0.25 Source: Type: Water Gun Files: Date: Oct. 1999 Recording Time [ms]: 512 Chamber Size [cuin]: 15 Survey: OUCHY I No. of first Streamer: 1 SPs per LINE: variable Line Name: 05-84 Recording Instrument: GEOMETRICS CMPs per LINE: 31-1112 / 119-1011 SEG-Y File Name: line05.sgy : line84.sgy DAT File Convention: JOBNO0SurveyNO0NO NO: 05-84 DAT-File Name: I1010053DSEISM.DAT - I1010843DSEISM.DAT						
JOB NO	JOB NAME	INPUT FILE [*.cst]	OUTPUT FILE [*.cst] or other	GEOVECTEUR MODULES	PROCESSING	
9.	migrphase1new	stack_036-115 [CDPs: 32-1330, LINES: 036-115]	stackmod_036-115 [CDPs: 32-1112, LINES: 36-115]	SELTR HISTA MODET	deselection of CDP 31 (does not exist for LINE 036-50) change trace length to 470 ms WORD 01 = 1879 (last sample) WORD 09 = 1000 (4 * SI), WORD 10 = 1880 (trace length).	
				LISTE BSORT	verification of header WORDs sorting of traces (WORDs 19, 04)	
				INMIG	selection of CDPs: 32-1112 and LINES: 36-115 creation of a 3D frequency volume, add padding of traces FCDP = 2, NCDP = 1141, FLINE = 6, NLINE = 145 frequencies: FMIN = 25 (100 / 4) - 425 (1700 / 4)	
	librimod	vnew_001-145.lvi	vnewtemp2.lvi	MODVI	modification of velocity library: velocities are reduced to 25 % do not use real trace length but less to avoid steep slopes	
	UTIL / Tabedit	vnewtemp2.lvi	vnewmod2.lvi	Operation/Formula	times are multiplied by 4: \$5 = \$3 * 4 apply formula to all records	
	Edit / Search / Replace	vnewmod2.lvi	vnewmod2.lvi	File/Export/LibraryVI	change field 3 to 5 T39996V5000 --> VF1250 library must also contain values for padded LINES/CMPs	
	UTIL / Tabedit	vnewmod2.lvi	vnewmod2.lvi	Operation/Statistics	field 4 for all records to find min and max velocity	
	velvolumemod	vnewmodcdp.lvi	velvolumemod	TRVEL	creation of velocity traces	
	velvolume	vnewwater.lvi	velvolumewat	TRVEL	creation of velocity traces	
	migrphase2	vnewmod2.lvi		TRVEL INMIG	creation of interval velocity traces creation of a 3D velocity volume	
	migrphase3			GTMIP	LCDP = 1142, ICDP = 10, LLINE = 140, ILINE = 2, TAU = 24 3D time migration after stack (about 5h)	
	migrphase4		[CDPs: 32-1112, LINES: 36-115], temp1 temp2	OUMIG SELTR	transposition of a volume of planes to a volume of traces selection of original unpadded traces	
				MODET	change back header WORDs 01, 09, 10	
				OUTST	sorting of traces (WORDs 04, 19)	
			migr_040-198	YDRIV	adding of blank traces: (WORDs 04: 30-1330, WORD 19: 036-115)	
				MODET	WORD 19 = WORD 19 * 2 - 32	

Processing Sheet 3-D		OUCHY1999		Maren Scheidhauer		6
Data: Sample Interval [ms]: 0.25 Source: Type: Water Gun Files: Date: Oct. 1999 Recording Time [ms]: 512 Chamber Size [cuin]: 15 Survey: OUCHY I No. of first Streamer: 1 SPs per LINE: variable Line Name: 05-84 Recording Instrument: GEOMETRICS CMPs per LINE: 31-1112 / 119-1011 SEG-Y File Name: line05.sgy : line84.sgy DAT File Convention: JOBNO0SurveyNO0NO NO: 05-84 DAT-File Name: I1010053DSEISM.DAT - I1010843DSEISM.DAT						
JOB NO	JOB NAME	INPUT FILE [*.cst]	OUTPUT FILE [*.cst] or other	GEOVECTEUR MODULES	PROCESSING	
9.	EXAM/ migrmute	migr_040-198 migr_040-198	migrmute_040-198	MUTES DYNQU	creation of a migration mute library: wbmigr.lfd muting of water bottom: iqmute.lmu, wbmigr.lfd AGC: 470 ms, mean amplitude: 5000	
QC	CDPfoldfd	migrmute	9CDPfoldfd.list	RESTR OUTST LISTE	update of water bottom in WORD 47 (wb3dmigr.lfd) sorting of traces (WORDs 19, 04) if WORD 43 = 0 output contents of WORDs 43 (CMP-X), 44 (CMP-Y), 04 (CMP), 19 (LINE), 08 (FOLD), 47	
	EDIT/ UTILITIES/	9CDPfoldfd.list UTILITIES/9CDPfoldfd	UTILITIES/9CDPfoldfd fdCDP fdxy	fdlist.awk	delete all other lines except data create contour plots with Surfer 7.0	
TKS	seqoutTKS	migrmute	P0000013DSEISM migrmute.sgy tempmigrmute	BSORT LISTE	sorting of traces (WORDs 19, 04) verification of header WORDs 04, 11, 19	
		tempmigrmute		SELTR HISTA MODET	selection of CMPs 119-1011 (all valid) and LINES 42-198 shifting all traces 250 ms up and cutting at 470 ms set WORD 05 = WORD 19 and WORD 19 = 1	
				RESTR LISTE SEGOU	update WORD 01, 06, 14 verification of header WORDs 01, 04, 05, 06, 10, 11, 19 sequential SEG-Y output (standard, 32-bit IBM) add parameter HTR7=CGG5(1,32) WORD 04 --> SEG-Y trace header WORD 06 (21 bit) WORD 05/19 --> SEG-Y trace header WORD 07 (25 bit)	

Table A-18. 3-D processing sheets 1-6 for Survey I using GéovecteurPlus. Gray areas indicate parameter differences between Survey I and II.

EGRID/HABIN COVERAGE TABLE			OUCHY 1999		Maren Scheidhauer	1	
Data:		Source:	Files:				
Sample Interval [ms]:	0.25	Type:	Water Gun	Date:	Oct. 1999		
Recording Time [ms]:	512	Chamber Size [cun]:	15	Survey:	OUCHY I		
No. of first Streamer:	1	SPs per LINE:	variable	Line Name:	05-84		
Recording Instrument:	GEOMETRICS	CMPs per LINE:	31-1112 / 119-1011	SEG-Y File Name:	line05.sgy-line84.sgy		
DAT File Convention:	JOBNO0SurveyNO0NO	CMP LINES:	36-115/40-198	DAT File Name:	11010053DSEISM.DAT-		
		NO:	05-84		11010843DSEISM.DAT		
SAIL NO	CMPs	SUBSURFACE LINES	CHOSEN SUBSURFACE LINES FOR HABIN	CHOSEN SAIL LINES FOR HABIN	HABIN OUTPUT LINES	MAX CMPs	CMPs
1							
2							
3							
4							
5	152-1025	35-42					
6	147-1112	36-41					
7	113-1108	37-39					
8	120-1027	38-40					
9	117-1107	39-41					
10	117-1105	40-42					
11	43-995	40-43					
12	211-991	42-44					
13	219-1046	41-46					
14	35-1030	43-47					
15	74-1019	45-48					
16	37-1024	46-48					
17	78-1025	46-48					
18	123-1025	47-49	35-76	05-46	?	?	
19	53-1026	49-51					
20	32-1027	49-52					
21	34-1030	50-53					
22	31-1033	51-53					
23	117-1109	50-55					
24	121-1086	53-55					
25	122-1052	55-57					
26	114-1093	56-58					
27	119-1110	57-59					
28	116-1110	58-60					
29	118-1104	60-61					
30	38-1023	60-61					
31	38-1027	61-62					
32	34-1026	62-64					
33	42-1028	63-67					
34	67-1026	64-66					
35	39-1028	65-68					
36	48-1028	66-68					
37	39-1028	67-69					
38	119-1110	68-70					

EGRID/HABIN COVERAGE TABLE			OUCHY 1999		Maren Scheidhauer	2	
SAIL NO	CMPs	SUBSURFACE LINES	CHOSEN SUBSURFACE LINES FOR HABIN	CHOSEN SAIL LINES FOR HABIN	HABIN OUTPUT LINES	MAX CMPs	MISSING CMPs
39	119-1107	69-71					
40	115-1059	69-72	35-76	05-46	?	?	
41	60-1025	71-72					
42	39-1026	72-74					
43	80-1025	74-75					
44	114-1103	75-77					
45	117-1109	74-77					
46	116-1107	75-58					
47	46-1020	77-78					
48	35-1025	78-79					
49	34-1027	79-80					
50	116-1107	80-83					
51	119-1107	81-84					
52	38-1024	82-83					
53	119-1104	84-85					
54	116-1104	83-86					
55	117-1104	85-87					
56	117-1100	86-88					
57	118-1105	87-89					
58	33-1020	88-89					
59	38-1027	89-91					
60	38-1027	89-91					
61	37-1026	91-93					
62	38-1018	92-93					
63	117-1100	93-95					
64	117-1105	94-96	77-115	44-84	?	?	
65	119-1102	95-97					
66	116-1103	96-07					
67	117-1103	96-98					
68	36-1027	97-99					
69	40-1027	99-100					
70	37-1028	99-101					
71	46-1027	101-103					
72	40-1024	102-104					
73	39-1030	103-105					
74	38-1027	104-106					
75	41-1025	105-107					
76	37-1026	106-108					
77	38-1026	107-109					
78	39-1024	108-110					
79	116-1108	109-111					
80	117-1103	111-112					
81	118-1102	111-112					
82	121-1100	113-114					
83	115-1089	112-114					
84	118-1105	114-115					
85							

Table A-19. EGRID / HABIN coverage table for Survey I. For each sail line, the minimum and maximum CMP and LINE number are indicated that were assigned in EGRID. On this basis, the input files to the subsequent two bin harmonization jobs (job *habin*, step 6, Table A-18) were chosen.

Processing Sheet 3-D		OUCHY2001		Maren Scheidhauer 1	
Data:		Source:		Files:	
Sample Interval [ms]	0.5	Type:	Air Gun	Date:	Aug. 2001
Recording Time [ms]	1000	Chamber Size [cuin]	15/15	Survey:	OUCHY II
No. of Streamer, Starboard (green)	2 [01-24]	SPs per LINE:	301	Line Name:	1-60
No. of Streamer, Center (blue)	S/N [25-48]	CMPs per LINE:	102-1328/105-1326	SEGY-File Name:	sail01.sgy ; sail60.sgy
No. of Streamer, Port (red)	1 [49-72]	CMP LINES:	29-210	DAT-File Name:	I1020013DSEISM.DAT ; I1020603DSEISM.DAT
Recording Instrument	BISON	NO=01-60			
JOB NO	JOB NAME	INPUT FILE [*.cst]	OUTPUT FILE [*.cst]	GEOVECTEUR MODULES	PROCESSING
1.	ASPRO/input3D	I1020NO3DSEISM.DAT	sail3dNO	INPTR	input (problem: MOT 01 is set to 500 instead of 999)
				MODET	numbering of traces (WORD 17 = 1-72)
				BSORT	sorting of traces (WORDS 02, 17)
2.	neartrace3D	sail3dNO	PLOTX	SELEC	selection of 4th trace of each SP
				FILTR	40 / 60 - 600 / 650 Hz operator length: 500
				REFOR	(t / 250)**2
				DYNQU	AGC: 50 ms, mean amplitude: 5000
				TRANS	polarity reversal (ITI streamers)
4.	ASPRO/shift3D	sail3dNO	shift3dNO	MODET	set WORD 30 (sail line number), set WORD 01 = 999
				SELEC	deletion of bad SPs (1-x); see ASPRO spreadsheet
				MODSP	subtraction of x from each SP number
				HISTA	shifting all traces 8 ms up
				TRANS	polarity reversal (for ITI streamers)
				OUTBD	writing three files to stage1
	NAVIGATION	3D0NO.txt	UK00160.SAV	program	navigation from GPS files 3D001-3D030.txt
		bleuNO.txt		Philippe	navigation from GPS files 3D031-3D060.txt
		rougeNO.txt			navigation from GPS files bleuNO.txt, rougeNO.txt, vertNO.txt
		vertNO.txt			
	wiloc3D	UK00160.SAV	I10001603DSEISM.DAT	WILOC	creation of S.N.T. (Seismic Navigation Tape) trace headers
		(K1UKOA90.SAV)	(I10001303DSEISM.DAT)		containing the (X,Y) field positions in one trace per cable
				LISTE	WORD 01/12 = acquisition line number
					WORD 02 = SP number
					WORD 07 = 9999 characterizes radionavigation tape
					WORD 08 = cable number
				OUTBD	writing file to stage1
5.	GEOUNIX/grillith		grid2.lgr		grid definition (see extra sheets)
	ASPRO/eGRID3D	I10001603DSEISM.DAT	eGRID3dNO	EGRID	merging of seismic and navigation data (change line in GSL)
		I4020NO3DSEISM.DAT		BSORT	trace elimination (WORD 17 = 13, 72)
					sorting of traces (WORDS 04, 19)
					make EGRID coverage table
				OUTBD	writing file to stage1
6.	habin3D 029-119	I502001-I502030	habin3d 029-121	BSORT	sorting traces (WORDS 04, 19, 20) very important !!!
	habin3D 120-210	I502030-I502060	habin3d 118-210	HABIN	harmonization of offset groups in 3D within a marco-bin
					of 3 bins in LINE direction and 1 bin in CDP direction
					make HABIN coverage table

Processing Sheet 3-D		OUCHY2001		Maren Scheidhauer 3	
Data:		Source:		Files:	
Sample Interval [ms]	0.5	Type:	Air Gun	Date:	Aug. 2001
Recording Time [ms]	1000	Chamber Size [cuin]	15/15	Survey:	OUCHY II
No. of Streamer, Starboard (green)	2 [01-24]	SPs per LINE:	301	Line Name:	1-60
No. of Streamer, Center (blue)	S/N [25-48]	CMPs per LINE:	102-1328/105-1326	SEGY-File Name:	sail01.sgy ; sail60.sgy
No. of Streamer, Port (red)	1 [49-72]	CMP LINES:	29-210	DAT-File Name:	I1020013DSEISM.DAT ; I1020603DSEISM.DAT
Recording Instrument	BISON	NO=01-60			
JOB NO	JOB NAME	INPUT FILE [*.cst]	OUTPUT FILE [*.cst]	GEOVECTEUR MODULES	PROCESSING
8A.	stack3D 029-119	habin3d 029-121	stack3d 029-119	FILTR	40 / 60 - 600 / 650 Hz operator length: 500
	stack3D 120-210	habin3d 118-210	stack3d 120-210	REFOR	(t / 250)**5
				FANMO	NMO correction: vnew3d_001-240.lvi
				KIDMO	3D DMO stack (Kirchhoff): imute3d_001-240.lmu,
					selection of LINES 029-119, 120-210
				OUTST	resorting of traces (WORDS 04, 19)
				YDRIV	adding of blank traces: (WORD 04: 102-1328,
					WORD 19: 029-119, 120-210)
				DYNQU	AGC: 1000 ms, mean amplitude: 5000
	EXAM	stack3d_029-119	wbstack3d.lfd		creation of a water bottom library and iqmute3d.lmu
		stack3d_120-210			coded in IQ, watch out not to delete lateral reflections !!!
					extend LINE bounds to those of HABIN files (029-210)
	UTIL/Tabedit	wbstack3d.lfd	iqmute3d.lmu	Operation/Statistics	in order to create iqmute3d.lmu find min and max water
					bottom values on field 4 for all records
8B.	stacknohabin3D 029-119	I502001-I502030	stacknohabin3d 029-119	BSORT	sorting of traces (WORDS 04, 19, 20)
	stacknohabin3D 120-210	I502030-I502060	stacknohabin3d 120-210	FILTR	40 / 60 - 600 / 650 Hz operator length: 500
				REFOR	(t / 250)**5
				FANMO	NMO correction: vnew3d_001-240.lvi
				KIDMO	3D DMO stack (Kirchhoff): iqmute3d.lmu, wbstack3d.lfd
					selection of LINES 029-119, 120-210
				OUTST	resorting of traces (WORDS 04, 19)
				YDRIV	adding of blank traces: (WORD 04: 102-1328,
					WORD 19: 029-119, 120-210)
				DYNQU	AGC: 1000 ms, mean amplitude: 5000
				OUTBD	writing files to stage 1
	stacknohabin3D	I7291193DSEISM.DAT	stacknohabin3d	INPTR	merging both files to 1
		I7120213DSEISM.DAT		HISTA	change trace length to 800 ms
				MODET	set WORD 01= 799 ms
	stacknohabinmute3D	stacknohabin3d	stacknohabinmute3d	MUTES	muting of water bottom: iqmute3d.lmu, wbstack3d.lfd
				MUTES	muting of multiples: iqintmute3d.lmu
				DYNQU	AGC: 800 ms, mean amplitude: 5000

Processing Sheet 3-D **OUCHY2001** Maren Scheidhauer 4

Data:	Source:	Files:
Sample Interval [ms]: 0.5	Type: Air Gun	Date: Aug. 2001
Recording Time [ms]: 1000	Chamber Size [cuin]: 15/15	Survey: OUCHY II
No. of Streamer, Starboard (green): 2 [01-24]	SPs per LINE: 301	Line Name: 1-60
No. of Streamer, Center (blue): S/N [25-48]	CMPs per LINE: 102-1328/105-1326	SEG-Y-File Name: sai01.sgy ; sai60.sgy
No. of Streamer, Port (red): 1 [49-72]	CMP LINES: 29-210	DAT-File Name: 11029013DSEISM.DAT - 11020603DSEISM.DAT
Recording Instrument: BISON	NO=01-60	

JOB NO	JOB NAME	INPUT FILE [*.cst]	OUTPUT FILE [*.cst]	GEOVCTEUR MODULES	PROCESSING
8.	stack3D_029-120	habin_029-121	stack3d_029-119	FILTR	40 / 60 - 600 / 650 Hz operator length: 500
	stack3D_120-210	habin_118-210	stack3d_120-210	REFOR	(t / 250)**5
				FANMO	NMO correction: vnew3d_001-240.lvi,
				KIDMO	3D DMO stack (Kirchhoff), igmute3d.lmu, wbstack3d.lfd
				OUTST	selection of LINES 029-119, 120-210
				YDRIV	resorting of traces (WORDS 04, 19)
					adding of blank traces: (WORD 04: 30-1330, WORD 19: 029-119, 120-210)
			I8291193DSEISM.DAT	DYNQU	AGC: 1000 ms, mean amplitude: 5000
			I8120213DSEISM.DAT	OUTBD	writing files to stage 1
	stack3D	I8291193DSEISM.DAT	stack3d	INPTR	merging both files to 1
		I8120213DSEISM.DAT		HISTA	change trace length to 800 ms
				MODET	set WORD 01 = 799 ms
	stackmute3D	stack3d	stackmute3d	MUTES	muting of water bottom: igmute3d.lmu, wbstack3d.lfd
				MUTES	muting of multiples: iqintmute3d.lmu, wbstack3d.lfd
QC	CDPfoldfd3D	stackmute3d	8CDPfoldfd3d.list	DYNQU	AGC: 800 ms, mean amplitude: 5000
		stacknohabin3d	8CDPfoldfd3d.list	RESTR	update of water bottom in WORD 47 (wbstack3d.lfd)
				OUTST	selection of CMPs 102-1328
				LISTE	sorting of traces (WORDS 19, 04)
					if WORD 43 = 0 output contents of WORDs
					43 (bin center-X), 44 (bin center-Y), no decimal output!!!
					04 (CMP), 19 (LINE), 08 (FOLD), 47
	EDIT/	8CDPfoldfd3d.list	UTILITIES/8CDPfoldfd3d		delete all other lines except data
	EDIT/	8CDPfoldfd3d.list	UTILITIES/8CDPfoldfdnohabin3d		delete all other lines except data
	UTILITIES/	UTILITIES/8CDPfoldfd3d	foldCDP3d.txt	foldlist.awk	create stacking charts with SURFER 7.0 (see extra sheet)
		UTILITIES/	foldCDPnohabin3d.txt		
		8CDPfoldfdnohabin3d	foldxy3d.txt		
			foldxynohabin3d.txt		
	qcdbu3d	stack3d	stack3d_ouchy	QCDBU	quality control database update
			stacknohabin3d_ouchy		precision problem while plotting due to the lack of decimals in XY coordinates of bin centers

Processing Sheet 3-D **OUCHY2001** Maren Scheidhauer 5

Data:	Source:	Files:
Sample Interval [ms]: 0.5	Type: Air Gun	Date: Aug. 2001
Recording Time [ms]: 1000	Chamber Size [cuin]: 15/15	Survey: OUCHY II
No. of Streamer, Starboard (green): 2 [01-24]	SPs per LINE: 301	Line Name: 1-60
No. of Streamer, Center (blue): S/N [25-48]	CMPs per LINE: 102-1328/105-1326	SEG-Y-File Name: sai01.sgy ; sai60.sgy
No. of Streamer, Port (red): 1 [49-72]	CMP LINES: 29-210	DAT-File Name: 11029013DSEISM.DAT - 11020603DSEISM.DAT
Recording Instrument: BISON	NO=01-60	

JOB NO	JOB NAME	INPUT FILE [*.cst]	OUTPUT FILE [*.cst]	GEOVCTEUR MODULES	PROCESSING
9.	migr3Dphase1	stack3d	stackmod3d	MUTES	muting of multiples: iqintmute3d.lmu, wbstack3d.lfd
		[CDPs: 102-1328, LINES: 029-210]	[CDPs: 102-1328, LINES: 029-210]	MODET	WORD 01 = 1599 (last sample)
					WORD 09 = 1000 (4 * SI), WORD 10 = 1600 (trace length),
				LISTE	verification of header WORDs
				BSORT	sorting of traces (WORDS 19, 04)
				INMIG	selection of CMPs: 102-1328 and LINES: 29-210
					creation of a 3D frequency volume, add padding of traces
					FCDP = 70, NCDP = 1291, FLINE = 1, NLINE = 240
					frequencies: FMIN = 10 (40 / 4) - 163 (650 / 4)
	librimod3D	vnew3d_001-240.lvi	vnewtemp3d.lvi	MODVI	modification of velocity library: velocities are reduced to 50 %
					do not use real trace length but less to avoid steep slopes
	UTIL / Tabedit	vnewtemp3d.lvi	vnewmod3d.lvi	Operation/Formu	times are multiplied by 2: \$5 = \$3 * 2
				File/Export/LibraryVI	apply formula to all records
	Edit / Search / Replace	vnewmod3d.lvi	vnewmod3d.lvi		change field 3 to 5
					T19998V5000 --> VF2500
					library must also contain values for padded LINES/CMPs
					add LINE 01 +240
	velvolumemod3D	vnewmod3d.lvi	velvolumemod3d	TRVEL	creation of velocity traces
	velvolume3D	vwaternew3d.lvi	velvolumewat3d	TRVEL	creation of velocity traces
	migr3Dphase2	vnewmod3d.lvi		TRVEL	creation of interval velocity traces
				INMIG	creation of a 3D velocity volume
					LCDP = 1360, ICDP = 10, LLINE = 240, ILINE = 2, TAU = 24
	migr3Dphase3			GTMP	3D time migration after stack (about 6h)
	migr3Dphase4			OUMIG	transposition of a volume of planes to a volume of traces
			temp1 [CDPs: 102-1328, LINES: 29-210]	SELTR	selection of original unpadding traces
			temp2	MODET	change back header WORDs 01, 09, 10
				OUTST	sorting of traces (WORDS 04, 19)
			migr3d	YDRIV	adding of blank traces: (WORD 04: 30-1330, WORD 19: 029-210)

Processing Sheet 3-D		OUCHY2001		Maren Scheidhauer		6
Data:		Source:		Files:		
Sample Interval [ms]:	0.5	Type:	Air Gun	Date:	Aug. 2001	
Recording Time [ms]:	1000	Chamber Size [cun]:	15/15	Survey:	OUCHY II	
No. of Streamer, Starboard (green):	2 [01-24]	SPs per LINE:	301	Line Name:	1-60	
No. of Streamer, Center (blue):	S/N [25-48]	CMPs per LINE:	102-1328/105-1326	SEGY-File Name:	sail01.sdy - sail60.sgy	
No. of Streamer, Port (red):	1 [49-72]	CMP LINES:	29-210	DAT-File Name:	H020013DSEISM.DAT - H020603DSEISM.DAT	
Recording Instrument:	BISON	NO=01-60				
JOB NO	JOB NAME	INPUT FILE [*.cst]	OUTPUT FILE [*.cst]	GEOVECTEUR MODULES	PROCESSING	
9.	EXAM/ miqmute3D	miqr3d miqr3d	miqmute3d	MUTES	creation of a migration mute library: <i>wbmiqr3d.lfd</i>	
				MUTES	muting of water bottom: <i>iqmte3d.lmu, wbmiqr3d.lfd</i>	
				HISTA	muting of multiples: <i>iqintmute3d.lmu, wbmiqr3d.lfd</i>	
QC				DYNQU	shifting traces 2 ms up to adapt to survey I	
	CDPfold3D	miqmute3d	9CDPfold3d.list	RESTR	AGC: 800 ms, mean amplitude: 5000	
				OUTST	update of water bottom in WORD 47 (<i>wbmiqr3d.lfd</i>)	
				LISTE	selection of CMPs 102-1328	
					sorting of traces (WORDS 19, 04)	
					if WORD 43 = 0 output contents of WORDs	
	EDIT/ UTILITIES/	9CDPfold3d.list UTILITIES/9CDPfold3d	UTILITIES/9CDPfold3d fdCDP3d		43 (CMP-X), 44 (CMP-Y), 04 (CMP), 19 (LINE), 08 (FOLD), 47	
			fdxy3d	fdlist.awk	delete all other lines except data	
					create contour plots with SURFER 7.0	
	camprep	file	filecam	SELEC	selection of line to print	
				MODET	validate all trace: set WORD 11 = 7	
TKS	segout3DTKS	miqmute3d	P0000023DSEISM miqmute3d.sgy tempmiqmute3d	BSORT	sorting of traces (WORDS 19, 04)	
				LISTE	verification of header WORDs 04, 11, 19	
				SELTR	selection of CMPs 105-1324 (all valid) and LINES 30-210	
				HISTA	shifting all traces 250 ms up and cutting at 470 ms	
				MODET	set WORD 05 = WORD 19 and WORD 19 = 1	
				RESTR	update WORD 01, 06, 14	
				LISTE	verification of header WORDs 01, 04, 05, 06, 10, 11, 19	
			seqmiqmute3d	SEGOU	sequential SEG-Y output (standard, 32-bit IBM)	
					add parameter HTR7=CGG5(1,32)	
					WORD 04 --> SEG-Y trace header WORD 06 (21 bit)	
					WORD 05/19 --> SEG-Y trace header WORD 07 (25 bit)	

Table A-20. 3-D processing sheets 1, 2-6 for Survey II using GéovecteurPlus. Gray areas indicate parameter differences between Survey I and II.

H0100	SURVEY AREA	LEMAN 3D AOUT 2001							
H0101	SURVEY DETAILS	SINGLE VESSEL, SINGLE SOURCE, 3 STREAMERS							
H0102	VESSEL DETAILS	La Licorne	1						
H0103	SOURCE DETAILS	Air Gun	1	1					
H0104	STREAMER DETAILS	STB (green) 24 chan	1	1	1				
H0104	STREAMER DETAILS	CENT (blue) 24 chan	1	2	2				
H0104	STREAMER DETAILS	PORT (red) 24 chan	1	3	3				
H0200	SURVEY DATE	08-2001							
H0201	TAPE DATE	03-2001							
H0202	TAPE VERSION	PhL							
H0300	CLIENT	University of Lausanne							
H0400	GEOPHYSICAL CONTRACTOR	UNIL							
H0500	POSITIONING CONTRACTOR	UNIL / EPFL							
H0600	POS PROCESSING CONTRACTOR	UNIL / EPFL							
H0700	POSITIONING SYSTEM	LEICA 500 2-FREQ PHASE DIFF GPS ON VESSEL							
H0700		ASHTECH 1-FREQ CODE DIFF GPS ON TAILBUOYS							
H0800	SHOTPOINT LOCATION	CENTER OF SOURCE							
H0900	OFFSET ANTENNA TO SOURCE	1 2 0.00 -12.60							
H0901	TO STB TAILBUOY	1 2 7.50 -76.35							
H0902	TO CENT TAILBUOY	1 2 0.00 -73.85							
H0903	TO PORT TAILBUOY	1 2 -7.50 -76.35							
H0904	TO STB G24	1 2 7.50 -75.10							
H0905	TO CENT G24	1 2 0.00 -75.10							
H0906	TO PORT G24	1 2 -7.50 -75.10							
H1000	CLOCK TIME	GMT							
H1100	RECEIVER GROUPS PER SHOT	72							
H1400	GEODETTIC DATUM AS SURVEY	CH1903	BESSEL 1841	6377397.155	299.1528130				
H1401	H1400 TO WGS84 TRANSFORM								
H1500	GEODETTIC DATUM AS PROCESS	CH1903	BESSEL 1841	6377397.155	299.1528130				
H1501	H1500 TO WGS84 TRANSFORM								
H1600	H1400 TO H1500 TRANSFORM	0.0 0.0 0.0	0.000	0.000	0.000	0.0000000			
H1700	VERTICAL DATUM	ES				ECHO SOUNDER			
H1800	PROJECTION CODE	999 LABORDE							
H1900	PROJECTION ZONE	NORTH HEMISPHERE							
H2000	GRID UNITS	1 INTERNATIONAL METER	1.0						
H2001	HEIGHT UNITS	1 INTERNATIONAL METER	1.0						
H2002	ANGULAR UNITS	1 DEGREE							
H2200	CENTRAL MERIDIAN	72622.500E							
H2301	GRID ORIGIN	72622.500E465708.660N							
H2302	GRID COORD AT ORIGIN	600000.00 200000.00							
H2401	SCALE FACTOR	1.0000000000							
H2507	CIRC BEARING OF L.O.P	900000.0000	DEGREES						

H2600	FORMAT OF SHOT RECORDS
H2600	COLUMN DESCRIPTION
H2600	1 'V', 'S', OR 'T'
H2600	V=VESSEL REFERENCE POINT,
H2600	S=CENTER OF SOURCE POSITION
H2600	T=TAILBUOY POSITION
H2600	2-13 LINE NAME
H2600	17-19 IDENTIFIER(VESSELCODE, GUNCODE, STREAMERCODE)
H2600	20-25 SHOT POINT NUMBER
H2600	26-35 LATITUDE
H2600	36-46 LONGITUDE
H2600	47-55 X COORDINATE
H2600	56-64 Y COORDINATE
H2600	65-70 WATER DEPTH
H2600	71-73 JULIAN DAY
H2600	74-79 TIME HHMMSS
H2600	
H2600	FORMAT OF RECEIVER RECORDS
H2600	COLUMN DESCRIPTION
H2600	1 'R'
H2600	2-5 RECEIVER NUMBER
H2600	6-14 X COORDINATE OF RECEIVER POSITION
H2600	15-23 Y COORDINATE OF RECEIVER POSITION
H2600	24-27 RECEIVER DEPTH
H2600	28-31 RECEIVER NUMBER
H2600	32-40 X COORDINATE OF RECEIVER POSITION
H2600	41-49 Y COORDINATE OF RECEIVER POSITION
H2600	50-53 RECEIVER DEPTH
H2600	54-57 RECEIVER NUMBER
H2600	58-66 X COORDINATE OF RECEIVER POSITION
H2600	67-75 Y COORDINATE OF RECEIVER POSITION
H2600	76-79 RECEIVER DEPTH
H2600	80 STREAMER CODE
H2600	*****
V3D001	11 1462904.97N 63659.19E 536802.6 148346.0 0.0 0100155
T3D001	11 1 1462903.54N 63702.12E 536864.6 148301.0 0.0 0100155
T3D001	11 2 1462903.37N 63701.74E 536856.4 148296.0 0.0 0100155
T3D001	11 3 1462903.18N 63701.64E 536854.3 148290.2 0.0 0100155
S3D001	111 1462904.66N 63659.56E 536810.4 148336.1 0.0 0100155
R	1 536820.9 148339.9 0.0 2 536822.8 148338.2 0.0 3 536824.6 148336.6 0.01
R	4 536826.5 148334.9 0.0 5 536828.4 148333.3 0.0 6 536830.2 148331.6 0.01
R	7 536832.1 148330.0 0.0 8 536833.9 148328.3 0.0 9 536835.8 148326.6 0.01
R	10 536837.7 148325.0 0.0 11 536839.5 148323.3 0.0 12 536841.4 148321.7 0.01
R	13 536843.2 148320.0 0.0 14 536845.1 148318.4 0.0 15 536847.0 148316.7 0.01
R	16 536848.8 148315.1 0.0 17 536850.7 148313.4 0.0 18 536852.5 148311.8 0.01
R	19 536854.4 148310.1 0.0 20 536856.3 148308.5 0.0 21 536858.1 148306.8 0.01
R	22 536860.0 148305.2 0.0 23 536861.8 148303.5 0.0 24 536863.7 148301.8 0.01
R	25 536815.4 148334.1 0.0 26 536817.2 148332.4 0.0 27 536819.1 148330.7 0.02
R	28 536820.9 148329.0 0.0 29 536822.7 148327.3 0.0 30 536824.5 148325.6 0.02
R	31 536826.3 148323.9 0.0 32 536828.2 148322.2 0.0 33 536830.0 148320.5 0.02
R	34 536831.8 148318.8 0.0 35 536833.6 148317.2 0.0 36 536835.5 148315.5 0.02
R	37 536837.3 148313.8 0.0 38 536839.1 148312.1 0.0 39 536840.9 148310.4 0.02
R	40 536842.7 148308.7 0.0 41 536844.6 148307.0 0.0 42 536846.4 148305.3 0.02
R	43 536848.2 148303.6 0.0 44 536850.0 148301.9 0.0 45 536851.9 148300.3 0.02
R	46 536853.7 148298.6 0.0 47 536855.5 148296.9 0.0 48 536857.3 148295.2 0.02
R	49 536810.6 148329.0 0.0 50 536812.4 148327.4 0.0 51 536814.3 148325.7 0.03
R	52 536816.2 148324.1 0.0 53 536818.0 148322.4 0.0 54 536819.9 148320.8 0.03
R	55 536821.7 148319.1 0.0 56 536823.6 148317.4 0.0 57 536825.5 148315.8 0.03
R	58 536827.3 148314.1 0.0 59 536829.2 148312.5 0.0 60 536831.0 148310.8 0.03
R	61 536832.9 148309.2 0.0 62 536834.8 148307.5 0.0 63 536836.6 148305.9 0.03
R	64 536838.5 148304.2 0.0 65 536840.3 148302.6 0.0 66 536842.2 148300.9 0.03
R	67 536844.1 148299.3 0.0 68 536845.9 148297.6 0.0 69 536847.8 148295.9 0.03
R	70 536849.6 148294.3 0.0 71 536851.5 148292.6 0.0 72 536853.4 148291.0 0.03
V3D001	11 2462905.10N 63659.04E 536799.4 148350.0 0.0 0100159
T3D001	11 1 2462903.66N 63701.95E 536860.9 148304.9 0.0 0100159
T3D001	11 2 2462903.49N 63701.57E 536852.9 148299.6 0.0 0100159
T3D001	11 3 2462903.29N 63701.49E 536851.0 148293.7 0.0 0100159
S3D001	111 2462904.78N 63659.42E 536807.3 148340.1 0.0 0100159
R	1 536817.4 148343.9 0.0 2 536819.3 148342.2 0.0 3 536821.1 148340.6 0.01
R	4 536823.0 148338.9 0.0 5 536824.8 148337.2 0.0 6 536826.7 148335.6 0.01
R	7 536828.5 148333.9 0.0 8 536830.4 148332.3 0.0 9 536832.2 148330.6 0.01
R	10 536834.1 148328.9 0.0 11 536835.9 148327.3 0.0 12 536837.8 148325.6 0.01
R	13 536839.6 148324.0 0.0 14 536841.5 148322.3 0.0 15 536843.3 148320.6 0.01
R	16 536845.2 148319.0 0.0 17 536847.0 148317.3 0.0 18 536848.9 148315.7 0.01
R	19 536850.7 148314.0 0.0 20 536852.6 148312.3 0.0 21 536854.4 148310.7 0.01
R	22 536856.3 148309.0 0.0 23 536858.1 148307.4 0.0 24 536860.0 148305.7 0.01
R	25 536812.3 148338.0 0.0 26 536814.1 148336.3 0.0 27 536815.9 148334.6 0.02
R	28 536817.7 148332.9 0.0 29 536819.5 148331.2 0.0 30 536821.3 148329.5 0.02
R	31 536823.1 148327.8 0.0 32 536824.9 148326.1 0.0 33 536826.7 148324.4 0.02
R	34 536828.5 148322.7 0.0 35 536830.3 148321.0 0.0 36 536832.1 148319.3 0.02
R	37 536834.0 148317.5 0.0 38 536835.8 148315.8 0.0 39 536837.6 148314.1 0.02
R	40 536839.4 148312.4 0.0 41 536841.2 148310.7 0.0 42 536843.0 148309.0 0.02
R	43 536844.8 148307.3 0.0 44 536846.6 148305.6 0.0 45 536848.4 148303.9 0.02
R	46 536850.2 148302.2 0.0 47 536852.0 148300.5 0.0 48 536853.8 148298.8 0.02
R	49 536807.5 148332.7 0.0 50 536809.3 148331.0 0.0 51 536811.2 148329.3 0.03
...	

Table A-21. Example of a UKOOA P1/90 file showing the ship, tail buoy, shot and receiver positions for the first two shot points of Survey II. Line name and the shot number are highlighted in grey. This file is the result of processing step 5A in Table A-20.

ASPRO SPREADSHEET		OUCHY2001		SHIFT3D		Maren Scheidhauer		1	
Data:		Source:		Files:					
Sample Interval [ms]	0.5	Type:	Air Gun	Date:	Aug. 2001				
Recording Time [ms]	1000	Chamber Size [cuin]	15/15	Survey:	OUCHY				
No. of Streamer, Starboard (green)	1	SPs per LINE	301	Line Name:	1-60				
No. of Streamer, Center (blue)	S/N	CMPs per LINE	102-1328/105-1326	SEGY-File Name	sail01.sgy - sail60.sgy				
No. of Streamer, Port (red)	2	CMP LINES	29-210	DAT-File Name:	11000013DSEISM.DAT - 11000603DSEISM.DAT				
Recording Instrument	BISON								
SAIL NO REG. #1#	REGISTER #2# LAST SHOT TO DELETE	TOTAL NUMBER OF SHOTS	COMMENTS	CORRECTIONS					
1	10	310	1 shot lost within first 14 shots	shot 11 duplicated and added as shot 10					
2	5	306							
3	5	306							
4	5	306							
5	5	306							
6	5	306							
7	5	306	booms shortened by 30 cm by end of the day						
8	20	321							
9	5	306							
10	5	305	1 shot lost within first 14 shots	shot 6 duplicated and added as shot 5					
11	5	306							
12	5	306							
13	5	306							
14	5	306							
15	5	306							
16	5	306							
17	5	306	nothing/noise on 4th channel of first 9 shots	delete 4th trace on first 9 shots (editing)					
18	5	306	nothing/noise on 4th channel of first 34 shots	delete 4th trace on first 34 shots (editing)					
19	5	306							
20	5	306							
21	5	306							
22	5	306	first 9 shots without amplification	mute shots 1-9 (editing)					
23	5	306							
24	5	306							
25	6	307							
26	5	306							
27	5	306							
28	5	306							
29	5	306							
30	5	306							
31	6	307	first 3 shots at about 100 bars						
32	5	306							
33	5	306							
34	5	306							
35	5	306							

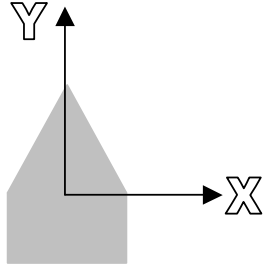
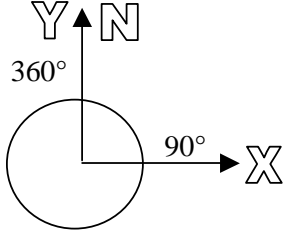
ASPRO SPREADSHEET		OUCHY2001		SHIFT3D		Maren Scheidhauer		2	
Data:		Source:		Files:					
Sample Interval [ms]	0.5	Type:	Air Gun	Date:	Aug. 2001				
Recording Time [ms]	1000	Chamber Size [cuin]	15/15	Survey:	OUCHY				
No. of Streamer, Starboard (green)	1	SPs per LINE	301	Line Name:	1-60				
No. of Streamer, Center (blue)	S/N	CMPs per LINE	102-1328/105-1326	SEGY-File Name	sail01.sgy - sail60.sgy				
No. of Streamer, Port (red)	2	CMP LINES	29-210	DAT-File Name:	11000013DSEISM.DAT - 11000603DSEISM.DAT				
Recording Instrument	BISON								
SAIL NO REG. #1#	REGISTER #2# LAST SHOT TO DELETE	TOTAL NUMBER OF SHOTS	COMMENTS	CORRECTIONS					
36	6	307							
37	5	306							
38	5	306							
39	5	306							
40	5	306							
41	5	306							
42	5	306							
43	5	306							
44	5	306							
45	5	306							
46	5	306							
47	5	306							
48	5	306							
49	5	306							
50	5	306							
51	10	311							
52	5	306							
53	5	306							
54	5	306							
55	5	306							
56	10	311							
57	5	306	piece of wood under center GPS raft						
58	6	307	maybe 6 extra shots: 307 shots recorded!!!	change last shot to delete from 5 to 6					
59	5	306							
60	5	306							

Table A-22. ASPRO spreadsheet for job *shift3D*, step 4 (Table A-20) of Survey II. The sail line number is represented by register #1#, the number of the last test shot to delete by register #2#.

EGRID/HABIN COVERAGE TABLE			OUCHY 2001		Maren Scheidhauer		1	
Data:			Source:		Files:			
Sample Interval [ms]: 0.5			Type:		Date:		Aug. 2001	
Recording Time [ms]: 1000			Chamber Size [cuin]:		Survey:		OUCHY II	
No. of Streamer, Starboard (green): 2 [01-24]			SPs per LINE:		Line Name:		1-60	
No. of Streamer, Center (blue): S/N [25-48]			CMPs per LINE:		SEGY-File Name:		sail01.sgy - sail60.sgy	
No. of Streamer, Port (red): 1 [49-72]			CMP LINES:		DAT-File Name:		H020013DSEISM.DAT -	
Recording Instrument: BISON			NO-01-60		H020003DSEISM.DAT			
SAIL NO	CMPs	SUBSURFACE LINES	CHOSEN SUBSURFACE LINES FOR HABIN	CHOSEN SAIL LINES FOR HABIN	HABIN OUTPUT LINES	MAX CMPs	CMPs on CMP line	
1	104-1327	29-33						
2	103-1327	33-37						
3	104-1326	34-39						
4	104-1327	38-42						
5	103-1327	43-45						
6	103-1327	43-48						
7	102-1328	46-51						
8	103-1327	51-55						
9	103-1327	54-58						
10	103-1327	57-61						
11	104-1327	60-64						
12	103-1327	63-67						
13	104-1327	67-70	029-119	01-30	28-?	?		
14	104-1326	69-73						
15	103-1326	72-76						
16	104-1327	76-79						
17	104-1327	79-82						
18	103-1326	81-85						
19	104-1327	84-87						
20	103-1326	86-90						
21	104-1326	89-93						
22	103-1327	93-97						
23	103-1327	96-99						
24	104-1326	98-102						
25	104-1327	103-106						
26	103-1327	105-109						
27	104-1327	108-112						
28	103-1327	111-115					1290-1326	
29	104-1326	114-117					120-1326	
30	103-1327	118-121					104-1326	
31	103-1327	120-124					104-1326	
32	104-1327	124-127					104-1325	
33	103-1327	126-130					103-1326	
34	104-1327	129-133	120-210	30-60			103-1327	
35	103-1327	132-136					103-1327	
36	103-1327	135-138					103-1327	
37	105-1328	138-142						
38	104-1327	141-145						
EGRID/HABIN COVERAGE TABLE			OUCHY 2001		Maren Scheidhauer		2	
SAIL NO	CMPs	SUBSURFACE LINES	CHOSEN SUBSURFACE LINES FOR HABIN	CHOSEN SAIL LINES FOR HABIN	HABIN OUTPUT LINES	MAX CMPs	MISSING CMPs	
39	103-1327	144-148						
40	103-1327	147-150						
41	104-1327	149-154						
42	103-1328	152-157						
43	103-1327	156-159						
44	103-1327	159-163						
45	104-1327	162-165						
46	103-1327	165-169						
47	104-1327	169-172						
48	104-1327	172-175						
49	104-1327	175-178	120-210	30-60	?	?		
50	103-1327	178-181						
51	104-1326	180-184						
52	104-1327	184-186						
53	104-1327	187-190						
54	104-1327	189-192						
55	103-1327	191-195						
56	103-1327	195-198						
57	104-1327	198-201						
58	104-1327	201-204						
59	103-1326	204-207						
60	103-1326	206-210						
61								
62								
63								
64								
65								
66								
67								
68								
69								
70								
71								
72								
73								
74								
75								
76								
77								
78								
79								
80								
81								
82								
83								
84								
85								

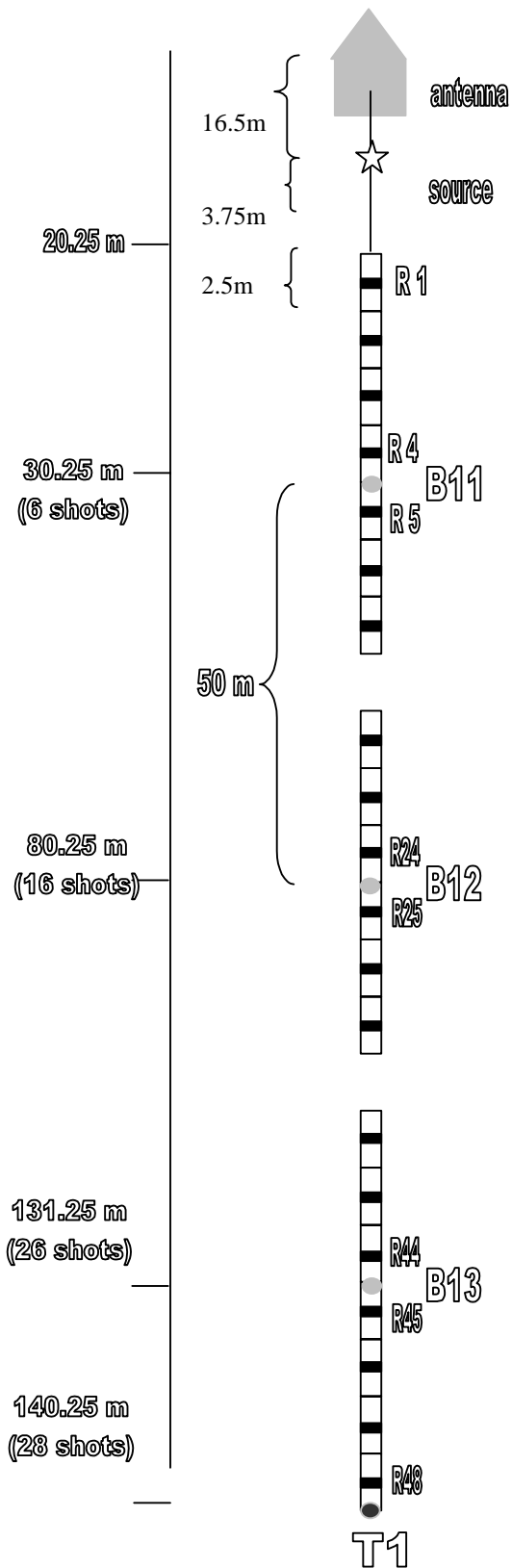
Table A-23. EGRID / HABIN coverage table for Survey II. For each sail line, the minimum and maximum CMP and LINE number are indicated that were assigned after EGRID. On this basis, the input files to the subsequent two bin harmonization jobs (job *habin3D*, step 6, Table A-20) were chosen.

Table A-24. Navigation Processing for Survey I in form of a separate instruction document.

Navigation Processing for Survey I <i>Using Radionavigation Modules of GéovecteurPlus, Version 6.2</i>	
<p>Ship coordinate system (SCS):</p> <p>TRAX: X-position of a point offset relative to boat antenna</p> <p>TRAY: Y-position of a point offset relative to boat antenna</p> <p>TRLO: Longitude of a point offset relative to boat antenna</p> <p>TRLA: Latitude of a point offset relative to boat antenna</p>	
<p>Geographical coordinate system:</p> <p>VHDG: Theoretical heading Values given by the Gyro-compass onboard (boat's axis relative to geographical north)</p> <p>CPFL: Shot point course Real navigation relative to ground</p> <p>ANTX: X-position of boat antenna</p> <p>ANTY: Y-position of boat antenna</p> <p>ANLO: Longitude of boat antenna</p> <p>ANLA: Latitude of boat antenna</p> <p>CAP: direction between two extreme points of a line</p>	
<p>Magnetic coordinate system (measured relative to magnetic N, then corrected)</p> <p>BSL1: Reading of compass 1 on streamer (90° for east)</p> <p>BSL2: Reading of compass 2 on streamer</p> <p>BSL3: Reading of compass 3 on streamer</p> <p>ALEPH: Invalidation</p>	

Acquisition Geometry:

Definition: The receiver is located in the center of the 2.5 m element



Preparation of dGPS coordinate files

Run Fortran 77 program **gvtlibrary.f** in /home/mscheidh/seis/navigation/OUCHY (see appendix) to create **V1-ANTEN.SAV** file in NAVP1 format and navigation libraries for groups of 21 lines respectively (5-25, 26-46, 47-67, 68-84). Put file **V1-ANTEN.SAV** in Géovecteur's **SAVE** directory and the libraries in the **NAVIGATION** folder organized by groups of lines (**NAV5-25**, **NAV26-46**, etc.). The dGPS data files for all lines have to be stored in the **/obsfiles** subdirectory (**OUCHY05.OBS-OUCHY84.OBS**).

bsmap5000_05-84_job0a

**** CREATION OF A MAP OF BOAT POSITIONS BY USING FILE V1-ANTEN.SAV TO GET ****
**** AN OVERVIEW OF NAVIGATION DATA QUALITY ****

```
* BOUCL          1
* BSMAP          PF=V1-ANTEN, ID=OUCHY, LANG0,
                  TITLE1=OFFSHORE 3D SURVEY 1999,
                  TITLE2=LAKE GENEVA,
                  TITLE3=P,
                  TITLE4=BOAT POSITION,
                  CLIENT=I.G.L/UNIL,
                  CREW=3DSEISM,
                  AUTHOR=M. SCHEIDHAUER,
                  REC,
                  MARGE2, RECOOR,
                  NUM5-84, ANO2, ANN20,
                  SYMBANO1, HSAÑO0.02,
                  HSANN.02, DECNUM0.05
                  ANGNUM315,
                  SIZNUM0.07, SIZE.15,
                  NAME50, PEN1, IPLOT3,
                  XPAS0.5, YPAS0.5,
                  XSCALE5000,
                  PROJ4, ELIP6, CM72622.5, CLA465708.66,
                  CX600000.0, CY200000.0, CK1.0, CU1, DEGRAD1.

* FINBO
* PROCS          1 (B1)
```

bsmap2000_05-84_job0b

**** CREATION OF A MAP OF BOAT POSITIONS AT A SMALLER SCALE ****

```
* BOUCL          1
* BSMAP          PF=V1-ANTEN, ID=OUCHY, LANG0,
                  TITLE1=OFFSHORE 3D SURVEY 1999,
                  TITLE2=LAKE GENEVA,
                  TITLE3=P,
                  TITLE4=BOAT POSITION,
                  CLIENT=I.G.L/UNIL,
                  CREW=3DSEISM,
                  AUTHOR=M. SCHEIDHAUER,
                  REC,
                  MARGE2, RECOOR,
                  NUM5-84, ANO1, ANN10,
                  SYMBANO1, HSAÑO0.05,
                  SIZNUM0.12, SIZE.15,
                  NAME10, PEN1, IPLOT3,
                  XPAS0.25, YPAS0.25,
                  XMIN535.35, XMAX536.82, YMIN147.9, YMAX149.55,
                  XSCALE2000,
                  PROJ4, ELIP6, CM72622.5, CLA465708.66,
                  CX600000.0, CY200000.0, CK1.0, CU1, DEGRAD1.

* FINBO
* PROCS          1 (B1)
```

LIST MT05-84 (file linelist)

Creation of a list that contains the CAP and the first and last shot points (FSTSP, LSTSP) for every line by using file MT05-84 created by a series of 6 jobs:

INIT.SAV (Initialization file)

```
2
/*Gerneral parameters*/
3D OUCHY          UNIL          99          3D
10/1999          LAUSANNE       XX          XX
0.0
/*Vessel parameters*/
LA LICORNE       V1           1           1           0           0           0
2              3
0
0
0
/*HEAD BUOYS*/
F1              0           0           0           0           -16.5       0
F2              0           0           0           0           -20.25      0
/*Parameters streamer number 1*/
C1              3           0           0           0           48          1
0              -20.25      0.0         1           1
N1  0.0  A4  2.5  B11  0.0  A20  2.5
B12  0.0  A20  2.5  B13  0.0  A4  2.5
N2  0.0  T1  0.0
/*Parameters source number 1*/
1
G1  0  0  0  0  -16.5-0.3
/*Projection parameters*/
SUISSE          BESSEL18416      0           0
LABORDE         4           72622.5      465708.66
0.0             600000      200000      1           465708.66  1           1
900000
```

nvp1-binloc_05-84_job1

```
* NVINI          INIT=INIT, ID=OUCHY,
* NVFOR          INFILE=V1-ANTEN, INFORM=NAVPI, ID=OUCHY,
                  OUTFORM=BINLOC, OUTLOC=V1-BIN, ID=OUCHY,
                  POSTYP1=A,
                  PLIST500,
                  COMMENT=NVFOR-NAVPI-BINLOC,
                  FLOG5,
* NVEND
* DLOOP          1
* DAGEN SN       EB          RL1000, SI4, F50,
* ENDLF
* PROCS          1B1
```

nvgeo-xylola_05-84_job2

```
* NVINI          INIT=INIT, ID=OUCHY, PRINT,
* LIBRI NV 01     CHANG, NUM5-NUM84, CPFL, ADD322.4, MULT0.0,
                  CHANG, NUM5-NUM84, VHDG, ADD322.4, MULT0.0,
* LIBRI NV 02     BINTY, V1, V1,
** CREATION OF BINLOC VESSEL FILE - HAS TO BE EXPLICITLY CREATED **
* NVCOR          INLOC=V1-BIN, ID=OUCHY,
                  OUTLOC=EA,
                  LNV01,
* NVEDI          INLOC=EA,
                  OUTLOC=EB,
                  LNV02,
* NVGEO          INLOC=EB,
                  OUTLOC=V1A05-84, ID=OUCHY,
                  XYLOLA,
```

```

* NVEND
* BOUCL          1
* DAGEN SN      EB      F50,RL1000,SI4,
* FINBO
* PROCS          1B1

nvgeo-deport-buoy-05-84_job3
* NVINI          INIT=INIT, ID=OUCHY, PRINT,
* LIBRI NV 01    PERMU, ANTX, TRAX,
                  PERMU, ANTY, TRAY,
                  PERMU, ANLO, TRLO,
                  PERMU, ANLA, TRLA,
                  BINTY, V1, C1,
* LIBRI NV 02
** CREATION OF A BINLOC CABLE FILE - THIS FILE MUST CONTAIN SOME INFORMATION **
** THE TAIL BUOY POSITION IS NOT USED IN FURTHER PROCESSING **
** WILL BE INVALIDATED IN JOB 5 **
* LIBRI NV 03    WCOPY, VHDG, BSL1,
                  WCOPY, VHDG, BSL2,
                  WCOPY, VHDG, BSL3,
* NVGEO          INLOC=V1A05-84, ID=OUCHY,
                  OUTLOC=EA,
                  HEADING,
                  OFLON-140.25,
                  OFLAT0,
                  PLIST100,
* NVEDI          INLOC=EA,
                  OUTLOC=C1A05-84, ID=OUCHY,
                  LNV01, LNV02, LNV03,
* NVEND
* BOUCL          1
* DAGEN SN      EB      F50,RL1000,SI4,
* FINBO
* PROCS          1B1

nvbou1c1_05-84_job4
* NVINI          INIT=INIT, ID=OUCHY, PRINT,
* NVBOU          INLOC=C1A05-84, ID=OUCHY,
                  BSL1-3, BSLBQ3,
                  DTIR5.0, INDCAB1,
                  PLIST50,
                  SPAMIX10, FILOPT0,
                  SPACAL40, SPAITER3
                  FILWIN4,
                  NOPLOT,
                  FILEN0=7,
                  CALMOY1,
* NVCAL          INLOC=C1A05-84, ID=OUCHY,
* NVBOU          OUTLOC=C1B05-84, ID=OUCHY,
                  BSL1-3, BSLBQ3,
                  DTIR5.0, INDCAB1,
                  PLIST50,
                  SPAMIX10, FILOPT0,
                  SPACAL40, SPAITER3
                  FILWIN4,
                  FILEN0=7,
                  COMMENT=CABLE 1,
* NVEND
* BOUCL          1
* DAGEN SN      EB      F50,RL1000,SI4,
* FINBO
* PROCS          1B1

```

nvcab-offxy_05-84_job5

```
* NVINI                               INIT=INIT, ID=OUCHY,
* LIBRI NV 01                          WCOPY, VHDG, BSL1,
                                        WCOPY, VHDG, BSL2,
                                        WCOPY, VHDG, BSL3,
                                        CHANG, NUM5-NUM84, DXHEAD, ADD13.10, MULT0,
                                        CHANG, NUM5-NUM84, DYHEAD, ADD-17.00, MULT0,
* LIBRI NV 02                          CHANG, NUM5-NUM84, DXSOUR, ADD10.00, MULT0,
                                        CHANG, NUM5-NUM84, DYSOUR, ADD-13.00, MULT0,
* LIBRI NV 64                          CHANG, ANLO, ALEPH,
                                        CHANG, ANLA, ALEPH,
* NVCOR                                INLOC=C1B05-84, ID=OUCHY,
                                        OUTLOC=EA,
                                        LNV01, LNV64,
* NVCOR                                INLOC=V1A05-84, ID=OUCHY,
                                        OUTLOC=EB,
                                        LNV02,
* NVCAB                                INLOC=EB,
                                        INST1=EA,
                                        SRCBIN,
                                        HEADBIN,
                                        TBBIN,
                                        NUM5-84,
                                        PLOT3,
                                        OUTUK=UKO05-84, ID=OUCHY,
                                        HEADER=HEAD-001, ID=OUCHY,
* NVEND
* BOUCL                                1
* DAGEN SN                             EB   F50, RL1000, SI4,
* FINBO
* PROCS                                1B1
```

wiloc_05-84_job6

```
* LIBRI BD 1                           CREW(3DSEISM), B000584(RW), STG,
* BOUCL                                1
* WILOC                                EA   PFUK=UKO05-84, IDUK=OUCHY,
                                        FORM9, ASCII,
                                        TIR48, BRN1, INCSP1,
                                        NLINE5, INCR1,
                                        UDFILE=MT05-84,
                                        PF=NAV05-84, ID=OUCHY,
                                        NAVQC,
                                        SHAPE, MAXPT5000,
                                        INCS10,
                                        XSCALE500,
                                        YSCALE1000,
* LISTE SS                             EA   STEP2001
* OUTBD                                EA   LBD1, STEPWD12
* FINBO
* PROCS                                X(B1)
**
** GO INTO LIBRIS DIRECTORY AND TYPE THE FOLLOWING COMMAND TO CREATE LIST: **
** cut -c 1-57 MT05-84 >! linelist **
```

Unix: cut -c 1-57 MT05-84 >! linelist

White areas in linelist (see table below) are filled with information from GPS (SPGPS) and seismic data (SPTOTAL) and with navigation results (for line 16: deletion of SP 145 and 163 in OBS-file).

LINES NAMES	SPGPS	LOGIC	CAP	NAVFSTSP	FSTSP	LSTSP	DR FSTSP	WFOLD	DR LSTSP	SEISFSTSP	SEISLSTSP	SPTOTAL
OUCHY 5	280 - 3	5	324	55	1	275	-0.62	221	-0.62	55	275	277
OUCHY 6	237	6	322	1	1	235	-0.61	235	-0.68	1	235	237
OUCHY 7	241	7	321	1	1	239	-0.55	239	-0.56	1	239	241
OUCHY 8	243 + 11	8	141	14	1	252	-0.62	239	-0.62	3	241	243
OUCHY 9	234	9	321	1	1	232	-0.55	232	-0.55	1	232	234
OUCHY10	234	10	322	1	1	232	-0.66	232	-0.66	1	232	234
OUCHY11	500 - 725 = 226	11	142	1	1	224	-0.69	224	-0.66	1	224	226
OUCHY12	237	12	144	42	1	235	1.33	194	1.36	42	235	237
OUCHY13	229 + 16	13	194	17	1	243	51.82	227	51.79	1	227	229
OUCHY14	234 - 1	14	143	1	1	231	0.72	231	0.75	2	232	234
OUCHY15	235	15	141	1	1	233	-1.16	233	-1.19	1	233	235
OUCHY16	238 + 3	16	142	1	1	234	-0.31	234	-0.31	1	234	235
OUCHY17	234	17	142	1	1	232	-0.6	232	-0.6	1	232	234
OUCHY18	244 + 16	18	137	17	1	258	-5.55	242	-5.55	1	242	244
OUCHY19	249 + 2	19	141	3	1	249	-1.37	247	-1.37	1	247	249
OUCHY20	244	20	142	1	1	242	-0.25	242	-0.22	1	242	244
OUCHY21	244	21	142	1	1	242	-0.37	242	-0.4	1	242	244
OUCHY22	241	22	142	1	1	239	-1	239	-1	1	239	241
OUCHY23	240	23	321	1	1	238	-1.86	238	-1.86	1	238	240
OUCHY24	235	24	322	1	1	233	-0.17	233	-0.2	1	233	235
OUCHY25	242	25	322	1	1	240	-0.85	240	-0.85	1	240	242
OUCHY26	245	26	322	7	1	243	-0.38	237	-0.35	7	243	245
OUCHY27	245 + 1 end	27	322	1	1	243	-0.73	243	-0.73	1	243	244
OUCHY28	228	28	322	1	1	226	-0.51	226	-0.51	1	226	228
OUCHY29	232	29	322	1	1	230	-0.67	230	-0.67	1	230	232
OUCHY30	244	30	142	1	1	242	-0.73	242	-0.73	1	242	244
OUCHY31	253	31	141	1	1	251	-1.16	251	-1.16	1	251	253
OUCHY32	241	32	142	1	1	239	-0.84	239	-0.84	1	239	241
OUCHY33	244	33	143	1	1	242	0.53	242	0.53	1	242	244
OUCHY34	243	34	142	9	1	241	-0.29	233	-0.26	9	241	243
OUCHY35	239	35	142	1	1	237	-0.77	237	-0.74	1	237	239
OUCHY36	238	36	142	1	1	236	-0.68	236	-0.68	1	236	238
OUCHY37	239	37	142	1	1	237	-0.2	237	-0.17	1	237	243 + 6 end
OUCHY38	235	38	322	1	1	233	-0.03	233	-0.03	1	233	235
OUCHY39	237	39	322	1	1	235	-0.32	235	-0.32	1	235	237
OUCHY40	241	40	322	14	1	239	-0.6	226	-0.6	14	239	241
OUCHY41	239	41	143	7	1	237	0.93	231	0.93	7	237	239
OUCHY42	240	42	142	1	1	238	-0.41	238	-0.41	1	238	242 + 2 end
OUCHY43	243 + 9 beg.	43	141	22	1	250	-1.19	229	-1.16	13	241	243
OUCHY44	237	44	322	1	1	235	-0.31	235	-0.31	1	235	237
OUCHY45	241	45	321	1	1	239	-1.31	239	-1.31	1	239	241
OUCHY46	232	46	323	1	1	230	0.19	229	0.16	1	230	232
OUCHY47	236 + 20 beg.	47	142	23	1	254	-0.64	232	-0.64	3	234	236
OUCHY48	241	48	142	1	1	239	-0.61	239	-0.64	1	239	241
OUCHY49	238	49	142	1	1	236	-0.9	236	-0.87	1	236	238
OUCHY50	236 + 1 beg.	50	320	2	1	235	-2.35	234	-2.35	1	234	236
OUCHY51	242	51	323	1	1	240	0.27	240	0.24	1	240	242
OUCHY52	235 + 17 beg.	52	142	18	1	250	-0.61	233	-0.61	1	233	235
OUCHY53	238	53	322	1	1	236	-0.69	236	-0.69	1	236	238
OUCHY54	237	54	321	1	1	235	-1.34	235	-1.34	1	235	237
OUCHY55	230	55	321	1	1	228	-1.09	228	-1.06	1	228	230
OUCHY56	233	56	322	1	1	231	-0.3	231	-0.33	1	231	233
OUCHY57	233	57	321	1	1	231	-1.01	231	-1.04	1	231	233
OUCHY58	241 + 17 beg.	58	202	18	1	256	59.38	239	59.38	1	239	241
OUCHY59	245	59	142	1	1	243	-0.82	243	-0.79	1	243	245
OUCHY60	244	60	142	1	1	242	-0.56	242	-0.53	1	242	244
OUCHY61	245	61	141	1	1	243	-1.22	243	-1.19	1	243	245
OUCHY62	247	62	142	1	1	245	-0.83	245	-0.79	1	245	247
OUCHY63	235	63	321	1	1	233	-1.16	233	-1.16	1	233	235
OUCHY64	235	64	321	1	1	233	-1.03	233	-1.03	1	233	235
OUCHY65	231 + 2	65	324	3	1	231	1.16	229	1.16	1	229	231
OUCHY66	239	66	322	1	1	237	-0.65	237	-0.68	1	237	239
OUCHY67	234	67	322	1	1	232	-0.92	232	-0.95	1	232	234
OUCHY68	242	68	142	1	1	240	-0.86	240	-0.83	1	240	242
OUCHY69	239	69	142	1	1	237	-0.99	237	-0.96	1	237	239
OUCHY70	243	70	142	1	1	241	-0.77	241	-0.77	1	241	243
OUCHY71	241	71	141	1	1	239	-1.34	239	-1.37	1	239	241
OUCHY72	244	72	142	1	1	242	-0.95	242	-0.92	1	242	244
OUCHY73	248	73	142	1	1	246	-0.56	246	-0.53	1	246	251 + 3 end
OUCHY74	240 + 7 beg.	74	145	8	1	245	2.46	238	2.46	1	238	240

Due to a difference in navigation and seismic data, the first shot number (SHPT) has to be adjusted in job 5b for black lines in table.

Run jobs 2-6 for groups of 21 lines (5-25, 26-46, 47-67, 68-84) respectively (a maximum of 600 text lines per GSL file cannot be exceeded).

nvgeo-xylola_05-25_job2 (for 21 lines)

```

* NVINI                               INIT=INIT, ID=OUCHY, PRINT,
* LIBRI NV 31                          ELIMN, NUM26-84,
*READ /data/proj/9008/3DSEISM/NAVIGATION/OUCHY/NAV05-25/HEADING/LIBNV01
*READ /data/proj/9008/3DSEISM/NAVIGATION/OUCHY/NAV05-25/HEADING/LIBNV02
*READ /data/proj/9008/3DSEISM/NAVIGATION/OUCHY/NAV05-25/HEADING/LIBNV03
*READ /data/proj/9008/3DSEISM/NAVIGATION/OUCHY/NAV05-25/HEADING/LIBNV04
*READ /data/proj/9008/3DSEISM/NAVIGATION/OUCHY/NAV05-25/HEADING/LIBNV05
*READ /data/proj/9008/3DSEISM/NAVIGATION/OUCHY/NAV05-25/HEADING/LIBNV06
*READ /data/proj/9008/3DSEISM/NAVIGATION/OUCHY/NAV05-25/HEADING/LIBNV07
*READ /data/proj/9008/3DSEISM/NAVIGATION/OUCHY/NAV05-25/HEADING/LIBNV08
*READ /data/proj/9008/3DSEISM/NAVIGATION/OUCHY/NAV05-25/HEADING/LIBNV09
*READ /data/proj/9008/3DSEISM/NAVIGATION/OUCHY/NAV05-25/HEADING/LIBNV10
*READ /data/proj/9008/3DSEISM/NAVIGATION/OUCHY/NAV05-25/HEADING/LIBNV11
*READ /data/proj/9008/3DSEISM/NAVIGATION/OUCHY/NAV05-25/HEADING/LIBNV12
*READ /data/proj/9008/3DSEISM/NAVIGATION/OUCHY/NAV05-25/HEADING/LIBNV13
*READ /data/proj/9008/3DSEISM/NAVIGATION/OUCHY/NAV05-25/HEADING/LIBNV14
*READ /data/proj/9008/3DSEISM/NAVIGATION/OUCHY/NAV05-25/HEADING/LIBNV15
*READ /data/proj/9008/3DSEISM/NAVIGATION/OUCHY/NAV05-25/HEADING/LIBNV16
*READ /data/proj/9008/3DSEISM/NAVIGATION/OUCHY/NAV05-25/HEADING/LIBNV17
*READ /data/proj/9008/3DSEISM/NAVIGATION/OUCHY/NAV05-25/HEADING/LIBNV18
*READ /data/proj/9008/3DSEISM/NAVIGATION/OUCHY/NAV05-25/HEADING/LIBNV19
*READ /data/proj/9008/3DSEISM/NAVIGATION/OUCHY/NAV05-25/HEADING/LIBNV20
*READ /data/proj/9008/3DSEISM/NAVIGATION/OUCHY/NAV05-25/HEADING/LIBNV21
* LIBRI NV 33                          BINTY, V1, V1,
** CREATION OF BINLOC VESSEL FILE - HAS TO BE EXPLICITLY CREATED **
* NVCOR                               INLOC=V1-BIN, ID=OUCHY,
                                       OUTLOC=EA,
                                       LNV31,
* NVEDI                               INLOC=EA,
                                       OUTLOC=EB,
                                       LNV1, LNV2, LNV3, LNV4, LNV5, LNV6, LNV7, LNV8, LNV9,
                                       LNV10, LNV11, LNV12, LNV13, LNV14, LNV15, LNV16, LNV17,
                                       LNV18, LNV19, LNV20, LNV21,
                                       LNV33,
* NVGEO                               INLOC=EB,
                                       OUTLOC=V1A05-25, ID=OUCHY,
                                       XYLOLA,
                                       PLIST100,
* NVEND
* BOUCL                               1
* DAGEN SN                            EB          F50, RL1000, SI4,
* FINBO
* PROCS                               1B1

```

nvgeo-deport-buoy_05-25_job3 (for 21 lines)

```

* NVINI                               INIT=INIT, ID=OUCHY,
* LIBRI NV 01                          PERMU, ANTX, TRAX,
                                       PERMU, ANTY, TRAY,
                                       PERMU, ANLO, TRLO,
                                       PERMU, ANLA, TRLA,
* LIBRI NV 02                          BINTY, V1, C1,
** CREATION OF A BINLOC CABLE FILE - THIS FILE MUST CONTAIN SOME INFORMATION **
** THE TAIL BUOY POSITION IS NOT USED IN FURTHER PROCESSING **
** WILL BE INVALIDATED IN JOB 5A **
* NVGEO                               INLOC=V1A05-25, ID=OUCHY,
                                       OUTLOC=EB,
                                       HEADING,
                                       OFLON-140.25,
                                       OFLAT0,

```



```

* NVEDI                                PLIST100 ,
                                        INLOC=EB ,
                                        OUTLOC=C1A05-25 , ID=OUCHY ,
                                        LNV01 , LNV02 ,

* NVEND
* BOUCL                                1
* DAGEN SN                            EB      F50,RL1000,SI4,
* FINBO
* PROCS                                1B1

nvbou1c1_05-25_job4a (for 21 lines)
* NVINI                                INIT=INIT, ID=OUCHY ,
** CORRECTION COMPASS 1 **
*READ /data/proj/9008/3DSEISM/NAVIGATION/OUCHY/NAV05-25/BSL1/LNV01
*READ /data/proj/9008/3DSEISM/NAVIGATION/OUCHY/NAV05-25/BSL1/LNV02
*READ /data/proj/9008/3DSEISM/NAVIGATION/OUCHY/NAV05-25/BSL1/LNV03
*READ /data/proj/9008/3DSEISM/NAVIGATION/OUCHY/NAV05-25/BSL1/LNV04
*READ /data/proj/9008/3DSEISM/NAVIGATION/OUCHY/NAV05-25/BSL1/LNV05
*READ /data/proj/9008/3DSEISM/NAVIGATION/OUCHY/NAV05-25/BSL1/LNV06
*READ /data/proj/9008/3DSEISM/NAVIGATION/OUCHY/NAV05-25/BSL1/LNV07
*READ /data/proj/9008/3DSEISM/NAVIGATION/OUCHY/NAV05-25/BSL1/LNV08
*READ /data/proj/9008/3DSEISM/NAVIGATION/OUCHY/NAV05-25/BSL1/LNV09
*READ /data/proj/9008/3DSEISM/NAVIGATION/OUCHY/NAV05-25/BSL1/LNV10
*READ /data/proj/9008/3DSEISM/NAVIGATION/OUCHY/NAV05-25/BSL1/LNV11
*READ /data/proj/9008/3DSEISM/NAVIGATION/OUCHY/NAV05-25/BSL1/LNV12
*READ /data/proj/9008/3DSEISM/NAVIGATION/OUCHY/NAV05-25/BSL1/LNV13
*READ /data/proj/9008/3DSEISM/NAVIGATION/OUCHY/NAV05-25/BSL1/LNV14
*READ /data/proj/9008/3DSEISM/NAVIGATION/OUCHY/NAV05-25/BSL1/LNV15
*READ /data/proj/9008/3DSEISM/NAVIGATION/OUCHY/NAV05-25/BSL1/LNV16
*READ /data/proj/9008/3DSEISM/NAVIGATION/OUCHY/NAV05-25/BSL1/LNV17
*READ /data/proj/9008/3DSEISM/NAVIGATION/OUCHY/NAV05-25/BSL1/LNV18
*READ /data/proj/9008/3DSEISM/NAVIGATION/OUCHY/NAV05-25/BSL1/LNV19
*READ /data/proj/9008/3DSEISM/NAVIGATION/OUCHY/NAV05-25/BSL1/LNV20
*READ /data/proj/9008/3DSEISM/NAVIGATION/OUCHY/NAV05-25/BSL1/LNV21
** CORRECTION COMPASS 2 **
*READ /data/proj/9008/3DSEISM/NAVIGATION/OUCHY/NAV05-25/BSL2/LNV31
*READ /data/proj/9008/3DSEISM/NAVIGATION/OUCHY/NAV05-25/BSL2/LNV32
*READ /data/proj/9008/3DSEISM/NAVIGATION/OUCHY/NAV05-25/BSL2/LNV33
*READ /data/proj/9008/3DSEISM/NAVIGATION/OUCHY/NAV05-25/BSL2/LNV34
*READ /data/proj/9008/3DSEISM/NAVIGATION/OUCHY/NAV05-25/BSL2/LNV35
*READ /data/proj/9008/3DSEISM/NAVIGATION/OUCHY/NAV05-25/BSL2/LNV36
*READ /data/proj/9008/3DSEISM/NAVIGATION/OUCHY/NAV05-25/BSL2/LNV37
*READ /data/proj/9008/3DSEISM/NAVIGATION/OUCHY/NAV05-25/BSL2/LNV38
*READ /data/proj/9008/3DSEISM/NAVIGATION/OUCHY/NAV05-25/BSL2/LNV39
*READ /data/proj/9008/3DSEISM/NAVIGATION/OUCHY/NAV05-25/BSL2/LNV40
*READ /data/proj/9008/3DSEISM/NAVIGATION/OUCHY/NAV05-25/BSL2/LNV41
*READ /data/proj/9008/3DSEISM/NAVIGATION/OUCHY/NAV05-25/BSL2/LNV42
*READ /data/proj/9008/3DSEISM/NAVIGATION/OUCHY/NAV05-25/BSL2/LNV43
*READ /data/proj/9008/3DSEISM/NAVIGATION/OUCHY/NAV05-25/BSL2/LNV44
*READ /data/proj/9008/3DSEISM/NAVIGATION/OUCHY/NAV05-25/BSL2/LNV45
*READ /data/proj/9008/3DSEISM/NAVIGATION/OUCHY/NAV05-25/BSL2/LNV46
*READ /data/proj/9008/3DSEISM/NAVIGATION/OUCHY/NAV05-25/BSL2/LNV47
*READ /data/proj/9008/3DSEISM/NAVIGATION/OUCHY/NAV05-25/BSL2/LNV48
*READ /data/proj/9008/3DSEISM/NAVIGATION/OUCHY/NAV05-25/BSL2/LNV49
*READ /data/proj/9008/3DSEISM/NAVIGATION/OUCHY/NAV05-25/BSL2/LNV50
*READ /data/proj/9008/3DSEISM/NAVIGATION/OUCHY/NAV05-25/BSL2/LNV51
* LIBRI NV 60                          ELIMN,NUM5,PT1-54,
                                        ELIMN,NUM8,PT1-13,
                                        ELIMN,NUM12,PT1-41,
                                        ELIMN,NUM13,PT1-16,
                                        ELIMN,NUM18,PT1-16,
                                        ELIMN,NUM19,PT1-2,
* NVCOR                                INLOC=C1A05-25, ID=OUCHY,
                                        LNV1, LNV2, LNV3, LNV4, LNV5, LNV6, LNV7, LNV8, LNV9,
                                        LNV10, LNV11, LNV12, LNV13, LNV14, LNV15, LNV16, LNV17,
                                        LNV18, LNV19, LNV20, LNV21,
                                        LNV31, LNV32, LNV33, LNV34, LNV35, LNV36, LNV37, LNV38,

```

```

LNV39,LNV40,LNV41,LNV42,LNV43,LNV44,LNV45,LNV46,
LNV47,LNV48,LNV49,LNV50,LNV51,
LNV60,
OUTLOC=C1B05-25,ID=OUCHY,
* NVEND
* BOUCL          1
* DAGEN SN      EB      F50,RL1000,SI4,
* FINBO
* PROCS          1B1

nvbou1c1_05-25_job4b (for 21 lines)
** BEFORE RUNNING THIS JOB ALWAYS DELETE FILES CMOY.SAV AND QBOUC1.SAV **
** RUN THIS JOB AND JOB 4C FIRST WITHOUT SHOT ELIMINATION, AFTER HAVING **
** LOOKED AT RESULTS DECIDE ON WHICH SHOTPOINTS TO DELETE **
** CORRECT ALSO ALL THREE COMPASS LIBRARIES FOR EACH LINE AS FOLLOWS **
** DELETE ALL ENTRIES BEFORE SHOT NUMBER IN HEADING LIBRARY **
** +5 FOR BSL1, +15 FOR BSL2, +25 FOR BSL3 **
** THEN RERUN JOBS 4A, 4B AND 4C **
**
* NVINI          INIT=INIT,ID=OUCHY,
* LIBRI NV 01    FILTR,VHDG,
                  WCOPY,VHDG,CPFL,
** APPLICATION OF GLOBAL FILTER - DEFAULT FILTER LENGTH 10 SHOTS **
** 5 BEFORE AND 5 AFTER THE FILTERED VALUE **
* NVCOR          INLOC=C1B05-25,ID=OUCHY,
                  LNV01,
                  OUTLOC=EA,
* NVBOU          INLOC=EA,
                  NUM5-25,
                  BSL1-3,BSLBQ3,
                  DTIR5.0,INDCAB1,
                  PLIST50,
                  FLOPT0,
                  SPACAL85,SPAITER6,SPAMIX35,
                  FILWIN10,
                  FILEN0=5,
** 1.) APPLICATION OF A TIME FILTER: **
** a) REGRESSION OF ALL SHOTPOINTS OF EACH COMPASS **
** b) FILWIN = 10 WIDTH IN DEGREES OF THE TOTAL WINDOW USED FOR REMOVING **
** ANOMALOUS VALUES - SHOTPOINTS OUTSIDE THIS WINDOW ARE REPLACED BY **
** THE REGRESSION VALUE CALCULATED IN a) **
** c) SMOOTHING IS PERFORMED BY AVERAGING OVER FILEN = 5 PRECEEDING SHOTPOINTS **
** 2.) APPLICATION OF A SPATIAL FILTER: **
** SPACAL = PERCENTAGE OF SMOOTHING FOR SPATIAL CALIBRATION **
** SPAITER = NUMBER OF ITERATIONS FOR COMPUTING SPATIAL CALIBRATION **
** SPAMIX = PERCENTAGE OF MIXING BETWEEN COMPASS AND THE VALUE COMPUTED **
** BY SPATIAL SMOOTHING **
** IT IS ASSUMED THAT THE CONDITION OF THE ACQUISITION DOES NOT CHANGE. **
** WHEN THE COMPASSES STAY IN THE WATER IT IS POSSIBLE TO APPLY A STATISTICS **
** (CURRENTS, DRIFT SAVED IN FILE QBOUC1.SAV) ON THE CORRECTIONS (CALIBRATION). **
** CREATION OF FILE CMOY.SAV CONTAINING COMPASS CORRECTIONS (CALIBRATION) **
* NVCAL          CALMOY1,
* NVEND
* BOUCL          1
* DAGEN SN      EB      F50,RL1000,SI4,
* FINBO
* PROCS          1B1
**
** IN FILE CMOY.SAV CHANGE CALIBRATION FOR THE THREE COMPASSES FROM 0.0 TO .01 **

nvbou1c1_05-25_job4c (for 21 lines)
** RUN THIS JOB FIRST WITHOUT SHOT ELIMINATION, AFTER HAVING LOOKED AT **
** RESULTS DECIDE ON WHICH SHOTPOINTS TO DELETE **
** CORRECT ALSO ALL THREE COMPASS LIBRARIES FOR EACH LINE AS FOLLOWS **
** DELETE ALL ENTRIES BEFORE SHOT NUMBER IN HEADING LIBRARY **
** +5 FOR BSL1, +15 FOR BSL2, +25 FOR BSL3 **
** THEN RERUN JOBS 4A, 4B AND 4C **

```

```

**
* NVINI                               INIT=INIT, ID=OUCHY,
** CORRECTION COMPASS 3 **
*READ /data/proj/9008/3DSEISM/NAVIGATION/OUCHY/NAV05-25/BSL3/LNV61
*READ /data/proj/9008/3DSEISM/NAVIGATION/OUCHY/NAV05-25/BSL3/LNV62
*READ /data/proj/9008/3DSEISM/NAVIGATION/OUCHY/NAV05-25/BSL3/LNV63
*READ /data/proj/9008/3DSEISM/NAVIGATION/OUCHY/NAV05-25/BSL3/LNV64
*READ /data/proj/9008/3DSEISM/NAVIGATION/OUCHY/NAV05-25/BSL3/LNV65
*READ /data/proj/9008/3DSEISM/NAVIGATION/OUCHY/NAV05-25/BSL3/LNV66
*READ /data/proj/9008/3DSEISM/NAVIGATION/OUCHY/NAV05-25/BSL3/LNV67
*READ /data/proj/9008/3DSEISM/NAVIGATION/OUCHY/NAV05-25/BSL3/LNV68
*READ /data/proj/9008/3DSEISM/NAVIGATION/OUCHY/NAV05-25/BSL3/LNV69
*READ /data/proj/9008/3DSEISM/NAVIGATION/OUCHY/NAV05-25/BSL3/LNV70
*READ /data/proj/9008/3DSEISM/NAVIGATION/OUCHY/NAV05-25/BSL3/LNV71
*READ /data/proj/9008/3DSEISM/NAVIGATION/OUCHY/NAV05-25/BSL3/LNV72
*READ /data/proj/9008/3DSEISM/NAVIGATION/OUCHY/NAV05-25/BSL3/LNV73
*READ /data/proj/9008/3DSEISM/NAVIGATION/OUCHY/NAV05-25/BSL3/LNV74
*READ /data/proj/9008/3DSEISM/NAVIGATION/OUCHY/NAV05-25/BSL3/LNV75
*READ /data/proj/9008/3DSEISM/NAVIGATION/OUCHY/NAV05-25/BSL3/LNV76
*READ /data/proj/9008/3DSEISM/NAVIGATION/OUCHY/NAV05-25/BSL3/LNV77
*READ /data/proj/9008/3DSEISM/NAVIGATION/OUCHY/NAV05-25/BSL3/LNV78
*READ /data/proj/9008/3DSEISM/NAVIGATION/OUCHY/NAV05-25/BSL3/LNV79
*READ /data/proj/9008/3DSEISM/NAVIGATION/OUCHY/NAV05-25/BSL3/LNV80
*READ /data/proj/9008/3DSEISM/NAVIGATION/OUCHY/NAV05-25/BSL3/LNV81
* LIBRI NV 01                          FILTR,VHDG,
                                         WCOPY,VHDG,CPFL,
* LIBRI NV 02                          FILTR,BSL1,
                                         FILTR,BSL2,
                                         FILTR,BSL3,
* NVCOR                                INLOC=C1B05-25, ID=OUCHY,
                                         LNV61, LNV62, LNV63, LNV64, LNV65, LNV66, LNV67, LNV68,
                                         LNV69, LNV70, LNV71, LNV72, LNV73, LNV74, LNV75, LNV76,
                                         LNV77, LNV78, LNV79, LNV80, LNV81,
                                         LNV01, LNV02,
                                         OUTLOC=EB,
* NVBOU                                INLOC=EB,
                                         NUM5-NUM25,
                                         OUTLOC=C1C05-25, ID=OUCHY,
                                         BSL1-3,BSLBQ3,
                                         DTIR5.0, INDCAB1,
                                         PLIST50,
                                         FILOPT0,
                                         SPACAL85, SPAITER6, SPAMIX35,
                                         FILWIN10,
                                         FILEN1=2,
                                         FILEN2=4,
                                         FILEN3=6,
                                         COMMENT=CABLE 1,
* NVEND
* BOUCL                                1
* DAGEN SN                            EB          F50,RL1000,SI4,
* FINBO
* PROCS                                1B1

```

nvcab-offxy_05-25_job5a (for 21 lines)

```

* NVINI                               INIT=INIT, ID=OUCHY,
** CORRECTION DX DY OF STREAMER HEAD **
*READ /data/proj/9008/3DSEISM/NAVIGATION/OUCHY/NAV05-25/DXDYHEAD/LNV31
*READ /data/proj/9008/3DSEISM/NAVIGATION/OUCHY/NAV05-25/DXDYHEAD/LNV32
*READ /data/proj/9008/3DSEISM/NAVIGATION/OUCHY/NAV05-25/DXDYHEAD/LNV33
*READ /data/proj/9008/3DSEISM/NAVIGATION/OUCHY/NAV05-25/DXDYHEAD/LNV34
*READ /data/proj/9008/3DSEISM/NAVIGATION/OUCHY/NAV05-25/DXDYHEAD/LNV35
*READ /data/proj/9008/3DSEISM/NAVIGATION/OUCHY/NAV05-25/DXDYHEAD/LNV36
*READ /data/proj/9008/3DSEISM/NAVIGATION/OUCHY/NAV05-25/DXDYHEAD/LNV37
*READ /data/proj/9008/3DSEISM/NAVIGATION/OUCHY/NAV05-25/DXDYHEAD/LNV38
*READ /data/proj/9008/3DSEISM/NAVIGATION/OUCHY/NAV05-25/DXDYHEAD/LNV39
*READ /data/proj/9008/3DSEISM/NAVIGATION/OUCHY/NAV05-25/DXDYHEAD/LNV40

```

```

*READ /data/proj/9008/3DSEISM/NAVIGATION/OUCHY/NAV05-25/DXDYHEAD/LNV41
*READ /data/proj/9008/3DSEISM/NAVIGATION/OUCHY/NAV05-25/DXDYHEAD/LNV42
*READ /data/proj/9008/3DSEISM/NAVIGATION/OUCHY/NAV05-25/DXDYHEAD/LNV43
*READ /data/proj/9008/3DSEISM/NAVIGATION/OUCHY/NAV05-25/DXDYHEAD/LNV44
*READ /data/proj/9008/3DSEISM/NAVIGATION/OUCHY/NAV05-25/DXDYHEAD/LNV45
*READ /data/proj/9008/3DSEISM/NAVIGATION/OUCHY/NAV05-25/DXDYHEAD/LNV46
*READ /data/proj/9008/3DSEISM/NAVIGATION/OUCHY/NAV05-25/DXDYHEAD/LNV47
*READ /data/proj/9008/3DSEISM/NAVIGATION/OUCHY/NAV05-25/DXDYHEAD/LNV48
*READ /data/proj/9008/3DSEISM/NAVIGATION/OUCHY/NAV05-25/DXDYHEAD/LNV49
*READ /data/proj/9008/3DSEISM/NAVIGATION/OUCHY/NAV05-25/DXDYHEAD/LNV50
*READ /data/proj/9008/3DSEISM/NAVIGATION/OUCHY/NAV05-25/DXDYHEAD/LNV51
* LIBRI NV 64          FILTR,DXHEAD,
                      FILTR,DYHEAD,
                      CHANG,ANLO,ALEPH,
                      CHANG,ANLA,ALEPH,
** NVCAB USES ONLY GEOGRAPHICAL COORDINATES, THAT IS WHY ONLY ANLO AND ANLA **
** ARE INVALIDATED **
* NVCOR              INLOC=C1C05-25, ID=OUCHY,
                      OUTLOC=EA
                      LNV31, LNV32, LNV33, LNV34, LNV35, LNV36, LNV37, LNV38,
                      LNV39, LNV40,
* NVCOR              INLOC=EA
                      OUTLOC=C1D05-25, ID=OUCHY,
                      LNV41, LNV42, LNV43, LNV44, LNV45, LNV46,
                      LNV47, LNV48, LNV49, LNV50, LNV51,
                      LNV64,
* NVEND
* BOUCL              1
* DAGEN SN          EB          F50,RL1000,SI4,
* FINBO
* PROCS              1B1

```

nvcab-offxy_05-25_job5b (for 21 lines)

```

* NVINI              INIT=INIT, ID=OUCHY,
* LIBRI NV 30        FILTR,VHDG,
                      WCOPY,VHDG,CPFL,
* LIBRI NV 31        ELIMN,NUM5,PT1-54,
                      ELIMN,NUM8,PT1-13,
                      ELIMN,NUM12,PT1-41,
                      ELIMN,NUM13,PT1-16,
                      ELIMN,NUM18,PT1-16,
                      ELIMN,NUM19,PT1-2,
* LIBRI NV 32        CHANG,NUM8,SHPT,ADD-11,MULT1.0,
                      CHANG,NUM13,SHPT,ADD-16,MULT1.0,
                      CHANG,NUM14,SHPT,ADD+1,MULT1.0,
                      CHANG,NUM18,SHPT,ADD-16,MULT1.0,
                      CHANG,NUM19,SHPT,ADD-2,MULT1.0,
** CORRECTION OF SHOTPOINT NUMBERS IN NAVIGATION DATA SO THAT THEY **
** CORRESPOND TO SEISMIC DATA **
** CORRECTION DX AND DY OF SOURCE CENTER **
*READ /data/proj/9008/3DSEISM/NAVIGATION/OUCHY/NAV05-25/DXDYSOURCE/LNV01
*READ /data/proj/9008/3DSEISM/NAVIGATION/OUCHY/NAV05-25/DXDYSOURCE/LNV02
*READ /data/proj/9008/3DSEISM/NAVIGATION/OUCHY/NAV05-25/DXDYSOURCE/LNV03
*READ /data/proj/9008/3DSEISM/NAVIGATION/OUCHY/NAV05-25/DXDYSOURCE/LNV04
*READ /data/proj/9008/3DSEISM/NAVIGATION/OUCHY/NAV05-25/DXDYSOURCE/LNV05
*READ /data/proj/9008/3DSEISM/NAVIGATION/OUCHY/NAV05-25/DXDYSOURCE/LNV06
*READ /data/proj/9008/3DSEISM/NAVIGATION/OUCHY/NAV05-25/DXDYSOURCE/LNV07
*READ /data/proj/9008/3DSEISM/NAVIGATION/OUCHY/NAV05-25/DXDYSOURCE/LNV08
*READ /data/proj/9008/3DSEISM/NAVIGATION/OUCHY/NAV05-25/DXDYSOURCE/LNV09
*READ /data/proj/9008/3DSEISM/NAVIGATION/OUCHY/NAV05-25/DXDYSOURCE/LNV10
*READ /data/proj/9008/3DSEISM/NAVIGATION/OUCHY/NAV05-25/DXDYSOURCE/LNV11
*READ /data/proj/9008/3DSEISM/NAVIGATION/OUCHY/NAV05-25/DXDYSOURCE/LNV12
*READ /data/proj/9008/3DSEISM/NAVIGATION/OUCHY/NAV05-25/DXDYSOURCE/LNV13
*READ /data/proj/9008/3DSEISM/NAVIGATION/OUCHY/NAV05-25/DXDYSOURCE/LNV14
*READ /data/proj/9008/3DSEISM/NAVIGATION/OUCHY/NAV05-25/DXDYSOURCE/LNV15
*READ /data/proj/9008/3DSEISM/NAVIGATION/OUCHY/NAV05-25/DXDYSOURCE/LNV16
*READ /data/proj/9008/3DSEISM/NAVIGATION/OUCHY/NAV05-25/DXDYSOURCE/LNV17

```

```

*READ /data/proj/9008/3DSEISM/NAVIGATION/OUCHY/NAV05-25/DXDYSOURCE/LNV18
*READ /data/proj/9008/3DSEISM/NAVIGATION/OUCHY/NAV05-25/DXDYSOURCE/LNV19
*READ /data/proj/9008/3DSEISM/NAVIGATION/OUCHY/NAV05-25/DXDYSOURCE/LNV20
*READ /data/proj/9008/3DSEISM/NAVIGATION/OUCHY/NAV05-25/DXDYSOURCE/LNV21
* LIBRI NV 65          FILTR,DXSOUR,
                      FILTR,DYSOUR,
* NVCOR              INLOC=V1A05-25, ID=OUCHY,
                      OUTLOC=EB,
                      LNV01, LNV02, LNV03, LNV04, LNV05, LNV06, LNV07, LNV08,
                      LNV09, LNV10,
* NVCOR              INLOC=EB,
                      OUTLOC=V1B05-25, ID=OUCHY,
                      LNV11, LNV12, LNV13, LNV14, LNV15, LNV16,
                      LNV17, LNV18, LNV19, LNV20, LNV21,
                      LNV30, LNV31, LNV32, LNV65,
* NVCOR              INLOC=C1D05-25, ID=OUCHY,
                      LNV32,
                      OUTLOC=EC,
* NVCAB              INLOC=V1B05-25, ID=OUCHY,
                      INST1=EC,
                      SRCBIN,
                      HEADBIN,
                      TBBIN,
                      NUM5-25,
                      PLOT3,
                      OUTUK=UKO05-25, ID=OUCHY,
                      HEADER=HEAD-001, ID=OUCHY,

* NVEND
* BOUCL              1
* DAGEN SN          EB          F50,RL1000,SI4,
* FINBO
* PROCS              1B1

```

wiloc_05-25_job6 (for 21 lines)

```

* LIBRI BD 1          CREW(3DSEISM),B000525(RW),STG,
* BOUCL              1
* WILOC              EA          PFUK=UKO05-25, IDUK=OUCHY,
                                FORM9,ASCII,
                                TIR48, BRN1, INCSP1,
                                NLINE5, INCRT1,
                                UDFILE=MT05-25,
                                PF=NV05-25, ID=OUCHY,
                                NAVQC,
                                SHAPE,MAXPT5000,
                                INCS10,
                                XSCALE500,
                                YSCALE1000,
* LISTE SS          EA          STEP2001
* OUTBD              EA          LBD1,STEPWD12
* FINBO
* PROCS              X(B1)

```

wiloc-nvp1itr48_05-25_job6b (for 21 lines)

```

** CALCULATES POSITION OF TRACE 48 **
* BOUCL              1
* WILOC              EA          PFUK=UKO05-25, IDUK=OUCHY,
                                FORM9,ASCII,
                                TIR48, BRN1, INCSP1,
                                NLINE5, INCRT1,
                                UDFILE=MT05-25,
                                PF=NVITR-48, ID=OUCHY,
                                ITR48, ITR1,
                                SHAPE,MAXPT5000,
                                INCS10,
                                XSCALE500,
                                YSCALE1000,

```

```

* LISTE SS      EA                STEP2001
* FINBO
* PROCS                X(B1)
**
** IN OUCHY DIRECTORY TYPE COMMAND TABEDIT & **
** IN FILE / IMPORT / NAVP1 READ FILE NVITR-48 **
** IN EDIT / DELETE FIELD, DELETE FIELDS 8,9,10 **
** IN OPERATION / FORMULA TYPE $8 = $3 + 1000 **
** IN FILE / EXPORT / NAVP1 REPLACE FIELD 3 BY FIELD 8 **
** SAVE FILE UNDER THE NAME NVITR.SAV **
** IN OUCHY DIRECTORY TYPE: grep S11 < NV05-25.SAV > templ **
** THEN: cat templ NVITR.SAV > SG05-25.SAV **
** DELETE templ **

```

bsmap2000_05-25_job7a

```

* BOUCL                1
* BSMAP                PF=SG05-25, ID=OUCHY, LANG0,
                        TITLE1=OFFSHORE 3D SURVEY,
                        TITLE2=LAKE GENEVA,
                        TITLE3=P,
                        TITLE4=SOURCE POSITION & TRACE 48,
                        TITLE5=LINES 5-25 UNEVEN,
                        CLIENT=I.G.L/UNIL,
                        CREW=3DSEISM,
                        AUTHOR=M. SCHEIDHAUER,
                        REC,
                        MARGE2, RECOOR,
                        NUM1-99999, ANO99999, ANN99999,
** NO LINES ARE DISPLAYED, NO SYMBOL AND NO ANNOTATION **
                        NUM5-25, I2, ANO1, ANN10,
                        SYMBANO1, SYMBANN1, HSANO0.02, HSANN0.04,
                        SIZNUM0.12, SIZE.15,
                        NAME10, PEN1, Iplot3,
** SHOT POSITION OF EVERY SECOND LINE ARE DISPLAYED **
                        NUM1005-1025, I2, ANO1, ANN10,
                        SYMBANO3, SYMBANN3, HSANO0.02, HSANN0.04,
                        SIZNUM0.12, SIZE.15,
                        NAME10, PEN2, Iplot3,
** POSITIONS OF TRACE 48 OF EVERY SECOND LINE ARE DISPLAYED **
                        XSCALE3300,
                        PROJ4, ELIP6, CM72622.5, CLA465708.66,
                        CX600000.0, CY200000.0, CK1.0, CU1, DEGRAD1.
* FINBO
* PROCS                1(B1)
**
** XSCALE 3300 = PAPER FORMAT A1 **
** XSCALE 2000 = PAPER FORMAT A0 **

```

bsmap2000_05-25_job7b

```

* BOUCL                1
* BSMAP                PF=SG05-25, ID=OUCHY, LANG0,
                        TITLE1=OFFSHORE 3D SURVEY,
                        TITLE2=LAKE GENEVA,
                        TITLE3=P,
                        TITLE4=SOURCE POSITION & TRACE 48,
                        TITLE5=LINES 5-25 EVEN,
                        CLIENT=I.G.L/UNIL,
                        CREW=3DSEISM,
                        AUTHOR=M. SCHEIDHAUER,
                        REC,
                        MARGE2, RECOOR,
                        NUM1-99999, ANO99999, ANN99999,
** NO LINES ARE DISPLAYED, NO SYMBOL AND NO ANNOTATION **
                        NUM6-25, I2, ANO1, ANN10,
                        SYMBANO1, SYMBANN1, HSANO0.02, HSANN0.04,
                        SIZNUM0.12, SIZE.15,
                        NAME10, PEN1, Iplot3,

```

```

** SHOT POSITION OF EVERY SECOND LINE ARE DISPLAYED **
      NUM1006-1025,I2,ANO1,ANN10,
      SYMBANO3,SYMBANN3,HSANOO.02,HSANN0.04,
      SIZNUM0.12,SIZE.15,
      NAME10,PEN2,IPL0T3,
** POSITIONS OF TRACE 48 OF EVERY SECOND LINE ARE DISPLAYED **
      XSCALE3300,
      PROJ4,ELIP6,CM72622.5,CLA465708.66,
      CX600000.0,CY200000.0,CK1.0,CU1,DEGRAD1.

* FINBO
* PROCS              1(B1)
**
** XSCALE 3300 = PAPER FORMAT A1 **
** XSCALE 2000 = PAPER FORMAT A0 **

```

Use ASPRO to create an **EGRID**-job for each line using the following model job.

egrid.mod

```

* LIBRI TR 01              CREW3DSEISM,
                          C00#4##5#,
                          F1,
                          SELEC=MOT12=(#1#),
                          STG,
                          CREW3DSEISM,
                          C4010#1#,
                          F1,
                          SELEC=MOT2=(#2#-#3#),
                          STG,
**/data/proj/9008/3DSEISM/LIBRIS/grid1.lgr
* LIBRI GR 01              XOR   536003.11,YOR   149769.21,
                          AZX   5.37125077,AZY   3.80045445,
                          DCDP   1.25,DLINE   7.50
* LIBRI BD 01              B5010#1#(RW),STG1,
                          BLOCK,UNLIMITD,
* DLOOP                    1
* INPTR                    ++      LTR01,RL512,SI0.25,EGRID,
                          Y=MOT7,K1,
                          SELEC=MOT7=(99999),
* IFTHN                    ==
* ELSE                      ==
* MODET                    ==      ++      *MOT30=#1#,
* ENDIF
* EGRID                    ==      ++      NSP260,NPRO=(#1#),BRN1,TIR48,INCSP1,WORDSPT2,
                          WORDSPS2,MOT30,
                          LGR01,
                          FCDP1,NCDP1500,NLINE41,INCCDP0,INCLINO,
                          OPT1,
                          NOTESTC,EDITE,
* BSORT                    ==      02      SELEC=MOT17=(1-23),
                          (25-36),
                          (38-48),
                          SORT=ONE4,TWO19,THREE20,NT15000,PACK32,OC,YTWO,
                          PROCS=YB2,
* ENDLP
* DLOOP                    2
* OUTBD                    ==
* ENDLP
* PROCS                    X(YB1)

```


APPENDIX

```

1      program gvtlibrary
*****
* VARIABLE DECLARATION
*****
2      parameter (size=400)
3      integer a,d,shot,n,line,line1,line2,total
4      integer shotno(size),dgps(size),speed(size),loc1(size),loc2(size)
5      character in*25,navpl*14,heading*20,BSL1*20,BSL2*20,BSL3*20
6      character dxdyhead*20,dxdysource*20
7      double precision diff,crit,alpha,beta,dx,dy,DXHEAD(size),DYHEAD(size),DXSOUR(size)
8      double precision lat(size),long(size),latmin(size),longmin(size)
9      double precision swissn(size),swisse(size),shotn(size),shote(size)
10     double precision coeff(size),dist(size),shotdist(size),DYSOUR(size)
11     double precision interval(size),shottime(size),timec(size),coortime(size)
12     double precision antn(size),ante(size),antdist(size),VHDG(size)
*****
* DATA INPUT
*****
13     print*, 'First line number (RETURN) and last line number (RETURN)?'
14     read*, line1, line2
19     write(navpl, '(A,A)') 'V1-ANTEN', '.SAV'
20     open(2, file=navpl, status='unknown')
21     write(2, '(A1,A3,A50)') 'H', '104', '3-D SURVEY OUCHY, OCTOBER 1999'
*****
***** START OF DO LOOP 1 *****
*****
22     DO 381 line=line1, line2
23         shot=1
25         write (heading, '(A,I2.2)') 'HEADING/LIENV', line-line1+1
26         write (BSL1, '(A,I2.2)') 'BSL1/LNV', line-line1+1
27         write (BSL2, '(A,I2.2)') 'BSL2/LNV', line-line1+31
28         open(10, file=heading, status='unknown')
29         open(11, file=BSL1, status='unknown')
30         open(12, file=BSL2, status='unknown')
31         write(10, '(A1,I2.2)') '* LIBRI NV ', line-line1+1
32         write(11, '(A1,I2.2)') '* LIBRI NV ', line-line1+1
33         write(12, '(A1,I2.2)') '* LIBRI NV ', line-line1+31
34         write (BSL3, '(A,I2.2)') 'BSL3/LNV', line-line1+61
35         write (dxdyhead, '(A,I2.2)') 'DXDYHEAD/LNV', line-line1+31
36         write (dxdysource, '(A,I2.2)') 'DXDYSOURCE/LNV', line-line1+1
37         open(15, file=BSL3, status='unknown')
38         open(14, file=dxdyhead, status='unknown')
39         open(13, file=dxdysource, status='unknown')
40         write(13, '(A1,I2.2)') '* LIBRI NV ', line-line1+1
41         write(14, '(A1,I2.2)') '* LIBRI NV ', line-line1+31
42         write(15, '(A1,I2.2)') '* LIBRI NV ', line-line1+61
43         write(in, '(A,I3.3,A)') 'obsfiles/OUCHY', line, '.OBS'
44         open(1, file=in, status='old')
45         CONTINUE
46         read(1, *, err=57, end=70) shotno(shot), interval(shot), shottime(shot), timec(shot), dgps(shot), lat(shot),
47             long(shot), speed(shot)
*****
* MEANING OF VARIABLES:
*
* shotno(shot) = shot number
* interval(shot) = shot interval [s]
*
* shottime(shot) = shot time [s after midnight]
* timec(shot) = DGPS coordinate time before next shot [hr/min/s] *
* dgps(shot) = (2) differential, (1) no diff.
* lat(shot) = latitude N [degrees,min,decimal] *
* long(shot) = longitude W [degrees,min,decimal]
* speed(shot) = speed [km/s] *
*
* CONVERSION FROM DEGREES TO MINUTES AND FROM HOURS TO SECONDS, THEN COORDINATE
*
* TRANSFORMATION FROM LATITUDE/LONGITUDE TO SWISS COORDINATES
*****
59     latmin(shot)=DINT(lat(shot)/100)*60+(lat(shot)-DINT(lat(shot)/100)*100)
60     longmin(shot)=DINT(long(shot)/100)*60+(long(shot)-DINT(long(shot)/100)*100)
61     coortime(shot)=DINT(timec(shot)/10000)*3600+DINT((timec(shot)-
62         -(DINT(timec(shot)/10000)*10000)/100)*60+(((timec(shot)-
63         (DINT(timec(shot)/10000)*10000))/100)-(DINT((timec(shot)-
64         (DINT(timec(shot)/10000)*10000))/100)))*100
65     CALL GEOTOSWISS(longmin(shot), latmin(shot), swisse(shot), swissn(shot))
66     print*, shot, longmin(shot), latmin(shot), swisse(shot), swissn(shot)
67     print '(F8.4,F11.4,F13.4,F15.6)', long(shot), lat(shot), swisse(shot), swissn(shot)
68     print '(I3,F6.2,F10.2,F10.1,F9.1,I3,F12.5,F11.5,I3)', shotno(shot), interval(shot), shottime(shot), timec(shot),
69         coortime(shot), dgps(shot), lat(shot), long(shot), speed(shot)
70     shot=shot+1
71     goto 57
72     CONTINUE
73     total=shot-1
*****
* longmin(shot) = longitude W [min]
* latmin(shot) = latitude N [min]
* swisse(shot) = swiss coordinates E
* swissn(shot) = swiss coordinates N
* coortime(shot) = DGPS coordinate time before next shot [s]
*
* INTERPOLATIONS
*****
* SORTING (FIND COORDINATE TIMES THAT LIE AROUND SHOTTIME FOR EACH SHOT, SEE FIGURE 1)
*****
90     shot=1
91     crit=1000000
*****
***** START OF DO LOOP 2 *****
*****
100    DO 130 shot=1, total
101        shottime(shot)=shottime(shot)+0.01
*****
* CORRECTION OF SHOTTIME (+ 0.01 seconds)
*****
102        loc2(shot)=1
103    DO 120 n=1, total

```

```

104      diff=shottime(shot)-coortime(n)
105      IF (diff.gt.0) THEN
106          IF (diff.lt.crit) THEN
107              crit=diff
108              loc1(shot)=n
109          END IF
*110      print*, 'end of first if', shot, n, diff, crit, loc1(shot)
111          crit=1000000
112      ELSE
113          diff=diff*(-1)
114          IF (diff.lt.crit) THEN
115              crit=diff
116              loc2(shot)=n
117          END IF
*118      print*, 'end of second if', shot, n, diff, crit, loc2(shot)
119      END IF
120      CONTINUE
*125      print*, shot, loc1(shot), loc2(shot)
130      CONTINUE
*****
***** END OF DO LOOP 2 ***** (116)
***** (118)
* diff/crit = time difference between shot time and coordinate time *
* loc1(shot) = shot number of coordinate time closest before shot time *
* loc2(shot) = location of coordinate time closest after shot time *
*
* CALCULATION OF ANTENNA AND SHOTPOINT POSITIONS (SEE FIGURE 1) *
* ANTE/ANTN ANTENNA POSITION; SHOTE/SHOTN GUN POSITION *
***** (125)
***** START OF DO LOOP 3 ***** (127)
141      DO 195 shot=1, total-2
145          diff=coortime(loc2(shot))-coortime(loc1(shot))
150          crit=shottime(shot)-coortime(loc1(shot))
155          coeff(shot)=crit/diff
*158      print ' (I3,F13.4,F13.4,F13.4,F13.4) ', shot, swisse(loc1(shot)), swissn(loc1(shot)), swisse(loc2(shot)),
*          A          swissn(loc2(shot))
160      CALL DISTANCE(swissn(loc2(shot)), swissn(loc1(shot)), swisse(loc2(shot)), swisse(loc1(shot)), dist(shot))
*170      print ' (I3,F17.8,F13.4,F10.4,F10.4,F10.4) ', shot, shottime(shot), coortime(loc1(shot)), diff, crit,
*          A          coeff(shot), dist(shot)
174      antn(shot)=swissn(loc1(shot))+coeff(shot)*(swissn(loc2(shot))-swissn(loc1(shot)))+140.92
179      ante(shot)=swisse(loc1(shot))+coeff(shot)*(swisse(loc2(shot))-swisse(loc1(shot)))+64.65
*184      CALL DISTANCE(antn(shot), antn(shot-1), ante(shot), ante(shot-1), antdist(shot))
*175      shotn(shot)=swissn(loc1(shot))+coeff(shot)*
*          A          (swissn(loc2(shot))-swissn(loc1(shot)))-(16.5/dist(shot))*
*          A          (swissn(loc2(shot))-swissn(loc1(shot)))
*180      shote(shot)=swisse(loc1(shot))+coeff(shot)*
*          A          (swisse(loc2(shot))-swisse(loc1(shot)))-(16.5/dist(shot))*
*          A          (swisse(loc2(shot))-swisse(loc1(shot)))
*185      CALL DISTANCE(shotn(shot), shotn(shot-1), shote(shot), shote(shot-1), shotdist(shot))
*186      diff=ABS(antdist(shot)-shotdist(shot))
*189      print*, line, shot, loc1(shot), loc2(shot), shottime(shot), coortime(shot)
*189      print*, shot, antn(shot)
190      write(2, '(A4,A5,I2,A13,I8,I8,F11.2,F11.2) ', 'S ', 'OUCHY', line, ', line, shot, ante(shot), antn(shot)
195      CONTINUE
*****
***** END OF DO LOOP 3 ***** (160)
***** (162)
* diff = P2-P1 = difference in the coordinate time closest before and after the shot time *
* crit = t1-P1 = difference between the shot time and the coordinate time closest before the shot time *
*
* coeff(shot) = crit/diff *
* dist(shot) = distance between two consecutive coordinate points P1 and P2 *
* antn(shot) = swiss coordinate N for boat antenna at moment of shot *
*
* ante(shot) = swiss coordinate E for boat antenna at moment of shot *
*
*
* HEADING CALCULATION FOR EACH SHOT AS AN AVERAG OF THE DIRECTION OF THE 5 PRECEDING SHOT POINTS (SEE FIGURE 2) *
***** (171)
***** START OF DO LOOP 4 ***** (173)
206      DO 375 shot=1, total-2
210          alpha=0
215          IF (shot.gt.5) THEN
220              DO 245 a=0,4
225                  dx=ante(shot-4+a)-ante(shot-4+a-1)
230                  dy=antn(shot-4+a)-antn(shot-4+a-1)
*231          print*, line, shot, a, dx, dy
235                  alpha=alpha+ATAN(ABS(dx)/ABS(dy))
245              CONTINUE
250          ELSE
255              DO 275 a=1,5
260                  dx=ante(1+a)-ante(1+a-1)
265                  dy=antn(1+a)-antn(1+a-1)
*266          print*, line, shot, a, dx, dy
270                  alpha=alpha+ATAN(ABS(dx)/ABS(dy))
275              CONTINUE
280          END IF
281          beta=alpha/5
285          alpha=alpha*(360/(5*2*3.1415927))
*286          print*, line, shot, alpha
***** (194)
* FOUR CASES ARE DISTINGUISHED TO CALCULATE VARIABLES VHDG, DXHEAD, DYHEAD, DXSOUR AND DYSOUR (SEE FIGURE 2 AND 3) *
***** (196)
290          IF (dx.lt.0) THEN ! CASE I
295              IF (dy.gt.0) THEN
296                  VHDG(shot)=360-alpha
297                  DXHEAD(shot)=20.25*SIN(beta)
298                  DYHEAD(shot)=-20.25*COS(beta)
299                  DXSOUR(shot)=16.5*SIN(beta)
300                  DYSOUR(shot)=-16.5*COS(beta)
305              ELSE ! CASE II

```

```

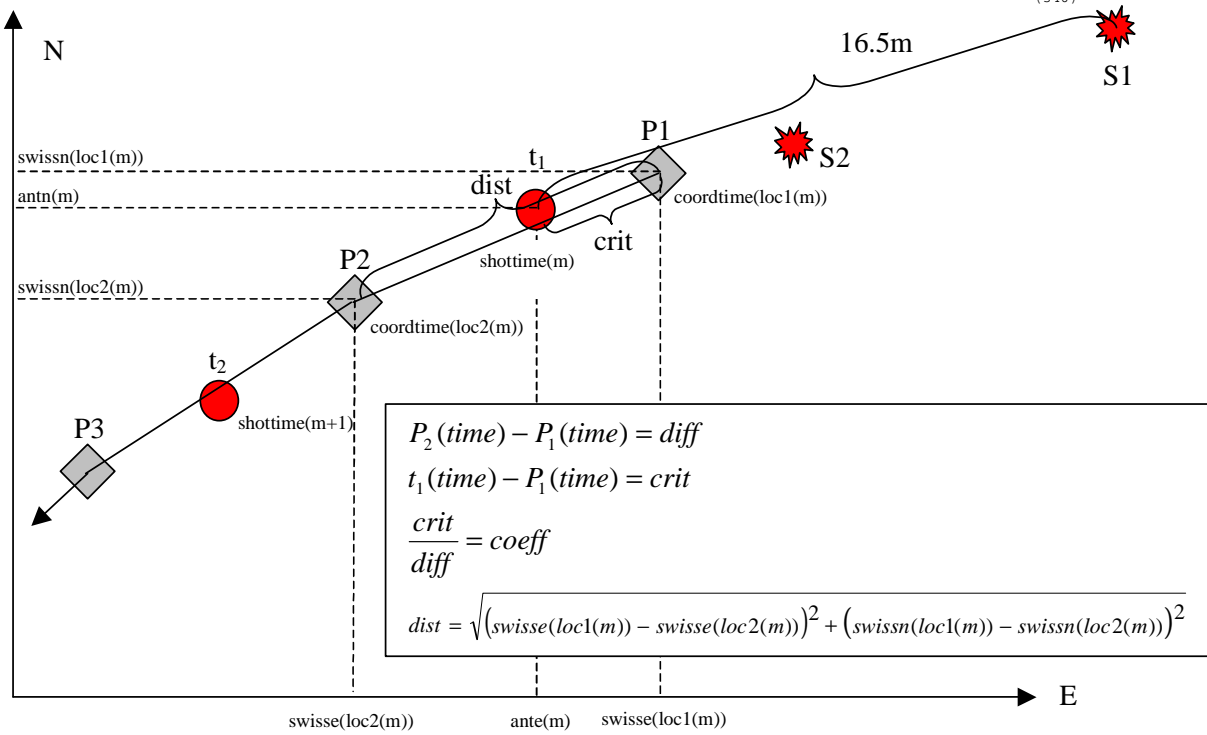
310      VHDG(shot)=180+alpha
311      DXHEAD(shot)=20.25*SIN(beta)
312      DYHEAD(shot)=20.25*COS(beta)
313      DXSOUR(shot)=16.5*SIN(beta)
314      DYSOUR(shot)=16.5*COS(beta)
315      END IF
320      ELSE
325      IF (dy.gt.0) THEN          ! CASE III
330      VHDG(shot)=alpha
331      DXHEAD(shot)=-20.25*SIN(beta)
332      DYHEAD(shot)=-20.25*COS(beta)
333      DXSOUR(shot)=-16.5*SIN(beta)
334      DYSOUR(shot)=-16.5*COS(beta)
335      ELSE          ! CASE IV
339      VHDG(shot)=180-alpha
340      DXHEAD(shot)=-20.25*SIN(beta)
341      DYHEAD(shot)=20.25*COS(beta)
342      DXSOUR(shot)=-16.5*SIN(beta)
343      DYSOUR(shot)=16.5*COS(beta)
344      END IF
345      END IF
*346      print*,line,shot,VHDG(shot)
***** (227)
* alpha = average angle of boat course relative to ship coordinate system (SCS) in rad *
* beta = average angle of boat course relative to SCS in degrees *
* VHDG = theretical heading (Gyro compass) *
* DXHEAD = distance of streamer head relative to SCS in x-direction *
* DYHEAD = distance of streamer head relative to SCS in y-direction *
* DXSOUR = distance of source relative to SCS in x-direction *
* DYSOUR = distance of source relative to SCS in y-direction *
*
* OUTPUT TO LIBRARY DIRECTORIES VHDG, BSL1, BSL2, BSL3, DXDYHEAD, DXDYSOURCE *
* For the compass heading libraries (BSL1, BSL2, BSL3) of each line, boat headings are shifted 5,15, and 25 *
* number of shot points up and 5, 15, and 25 shot points are deleted at the end *
***** (239)
347      write(10,'(A30,A9,I2,A3,I3,A9,F5.1,A9)', ' ', 'CHANG,NUM',line,' ',PT',shot,
A      ',VHDG,ADD',VHDG(shot)',MULT0.0,')
348      IF (shot.lt.total-6) THEN
349      IF (shot.eq.1) THEN
350      write(11,'(A30,A9,I2,A3,A3,A9,F5.1,A9)', ' ', 'CHANG,NUM',line,' ',PT', '1-6',
A      ',BSL1,ADD',VHDG(shot)',MULT0.0,')
351      ELSE
352      write(11,'(A30,A9,I2,A3,I3,A9,F5.1,A9)', ' ', 'CHANG,NUM',line,' ',PT',shot+5,
A      ',BSL1,ADD',VHDG(shot)',MULT0.0,')
353      END IF
354      END IF
355      IF (shot.lt.total-16) THEN
356      IF (shot.eq.1) THEN
357      write(12,'(A30,A9,I2,A3,A4,A9,F5.1,A9)', ' ', 'CHANG,NUM',line,' ',PT', '1-16',
A      ',BSL2,ADD',VHDG(shot)',MULT0.0,')
358      ELSE
359      write(12,'(A30,A9,I2,A3,I3,A9,F5.1,A9)', ' ', 'CHANG,NUM',line,' ',PT',shot+15,
A      ',BSL2,ADD',VHDG(shot)',MULT0.0,')
360      END IF
361      END IF
363      IF (shot.lt.total-26) THEN
364      IF (shot.eq.1) THEN
365      write(15,'(A30,A9,I2,A3,A4,A9,F5.1,A9)', ' ', 'CHANG,NUM',line,' ',PT', '1-26',
A      ',BSL3,ADD',VHDG(shot)',MULT0.0,')
366      ELSE
367      write(15,'(A30,A9,I2,A3,I3,A9,F5.1,A9)', ' ', 'CHANG,NUM',line,' ',PT',shot+25,
A      ',BSL3,ADD',VHDG(shot)',MULT0.0,')
368      END IF
369      END IF
370      write(14,'(A30,A9,I2,A3,I3,A11,F5.1,A9)', ' ', 'CHANG,NUM',line,' ',PT',shot,
A      ',DXHEAD,ADD',DXHEAD(shot)',MULT0.0,')
371      write(14,'(A30,A9,I2,A3,I3,A11,F5.1,A9)', ' ', 'CHANG,NUM',line,' ',PT',shot,
A      ',DYHEAD,ADD',DYHEAD(shot)',MULT0.0,')
372      write(13,'(A30,A9,I2,A3,I3,A11,F5.1,A9)', ' ', 'CHANG,NUM',line,' ',PT',shot,
A      ',DXSOUR,ADD',DXSOUR(shot)',MULT0.0,')
373      write(13,'(A30,A9,I2,A3,I3,A11,F5.1,A9)', ' ', 'CHANG,NUM',line,' ',PT',shot,
A      ',DYSOUR,ADD',DYSOUR(shot)',MULT0.0,')
375      CONTINUE
***** (278)
***** END OF DO LOOP 4 ***** (280)
*376      print*,line,shot-1,loc1(shot-1),loc2(shot-1),' last value is not supposed to be 1!'
close(1,status='keep')
378      close(10,status='keep')
379      close(11,status='keep')
380      close(12,status='keep')
close(13,status='keep')
close(14,status='keep')
close(15,status='keep')
381      CONTINUE
***** (290)
***** END OF DO LOOP 1 ***** (292)
382      close(2,status='keep')
390      END
***** (296)
400      SUBROUTINE GEOTOSWISS(Xi,Yi,x,y)
***** (298)
410      DOUBLE PRECISION x,y, Xi,Yi
420      DOUBLE PRECISION x1,x3,x5,y,y0,y2,y4
430      DOUBLE PRECISION P,P1,P2,P3,P4,P5, L,L2,L3,L4,L5
***** (302)
*      get (x,y) in meters from (Xi,Yi) in minutes *
***** (304)
440      P = ( Yi*60D0 - 169028.66 ) * 1D-4          ! latitude in seconds E-4
450      L = ( 26782.5D0 - Xi*60D0 ) * 1D-4          ! longitude in seconds E-4
460      P1 = P*1D6

```

```

470 P2 = P1*P
480 P3 = P2*P
490 P4 = P3*P
500 P5 = P4*P
510 L2 = L*L
520 L3 = L2*L
530 L4 = L3*L
540 L5 = L4*L
550 X1 = 0.211428534D6 - 0.010939609D0*P1 - 0.000002658D0*P2
560 A X3 = -0.00008539D0*P3 - 0.00000003D0*P4 - 0.00000008D0*P5
570 X5 = 0.00000002D6 - 0.00000004D0*P1
580 A Y0 = 0.308770746D0*P1 + 0.000075028D0*P2 + 0.000120435D0*P3
590 A Y2 = 0.003745409D6 - 0.000193793D0*P1 + 0.000004341D0*P2
600 A Y4 = -0.000000376D0*P3 + 0.000000004*P4
610 x = X1*L + X3*L3 + X5*L5
620 y = Y0 + Y2*L2 + Y4*L4
630 x = 60000D0 - x
640 y = y + 20000D0
660 END
*****
700 SUBROUTINE DISTANCE(X2,X1,Y2,Y1,DIST)
***** (332)
710 double precision X1,X2,Y1,Y2,DIST
***** (334)
720 DIST=SQRT((X2-X1)**2+(Y2-Y1)**2)
***** (336)
*725 print '(F20.4,F20.4,F20.4,F20.4,F15.4)',X1,X2,Y1,Y2,DIST
730 END
***** (340)

```



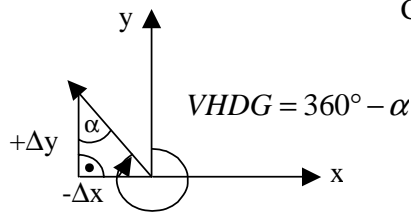
$$\begin{aligned}
 P_2(\text{time}) - P_1(\text{time}) &= \text{diff} \\
 t_1(\text{time}) - P_1(\text{time}) &= \text{crit} \\
 \frac{\text{crit}}{\text{diff}} &= \text{coeff} \\
 \text{dist} &= \sqrt{(\text{swisse}(\text{loc1}(\text{m})) - \text{swisse}(\text{loc2}(\text{m})))^2 + (\text{swissn}(\text{loc1}(\text{m})) - \text{swissn}(\text{loc2}(\text{m})))^2}
 \end{aligned}$$

$$\begin{aligned}
 \text{ante}(\text{m}) &= \text{swisse}(\text{loc1}(\text{m})) + \text{coeff} * (\text{swisse}(\text{loc2}(\text{m})) - \text{swisse}(\text{loc1}(\text{m}))) \\
 \text{antn}(\text{m}) &= \text{swissn}(\text{loc1}(\text{m})) + \text{coeff} * (\text{swissn}(\text{loc2}(\text{m})) - \text{swissn}(\text{loc1}(\text{m}))) \\
 \text{shote}(\text{m}) &= \text{swisse}(\text{loc1}(\text{m})) + \text{coeff} * (\text{swisse}(\text{loc2}(\text{m})) - \text{swisse}(\text{loc1}(\text{m}))) - \frac{16.5\text{m}}{\text{dist}} (\text{swisse}(\text{loc2}(\text{m})) - \text{swisse}(\text{loc1}(\text{m}))) \\
 \text{shotn}(\text{m}) &= \text{swissn}(\text{loc1}(\text{m})) + \text{coeff} * (\text{swissn}(\text{loc2}(\text{m})) - \text{swissn}(\text{loc1}(\text{m}))) - \frac{16.5\text{m}}{\text{dist}} (\text{swissn}(\text{loc2}(\text{m})) - \text{swissn}(\text{loc1}(\text{m})))
 \end{aligned}$$

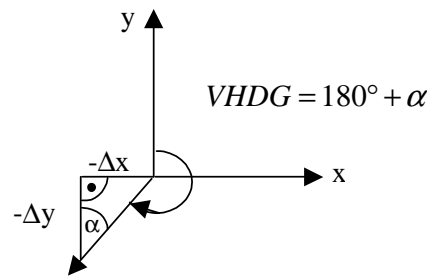
Figure 1: Calculation of antenna and shot point coordinates. **S1, S2:** gun positions; **P1, P2:** antenna positions at coordinate times; **t1, t2:** shot times; **m:** shot number; **loc1, loc2:** determines closest coordinate time before / after shot time; **swisse, swissn:** Swiss coordinates of P; **antn, ante:** Swiss coordinates of antenna.

Geographical Coordinate System:

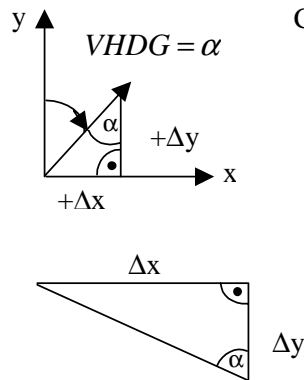
Case I:



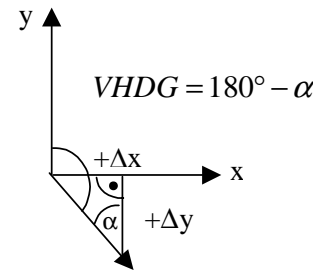
Case II:



Case III:



Case IV:



$$\tan \alpha = \frac{\Delta x}{\Delta y}$$

$$\alpha = \arctan \frac{\Delta x}{\Delta y}; \quad \frac{rad}{2\pi} = \frac{\alpha}{360^\circ}$$

Figure 2: The boat's **HEADING** (variable **VHDG**) is calculated by taking the average direction of the 5 preceding shot points. There exist four different cases to calculate the average heading.

Case I:

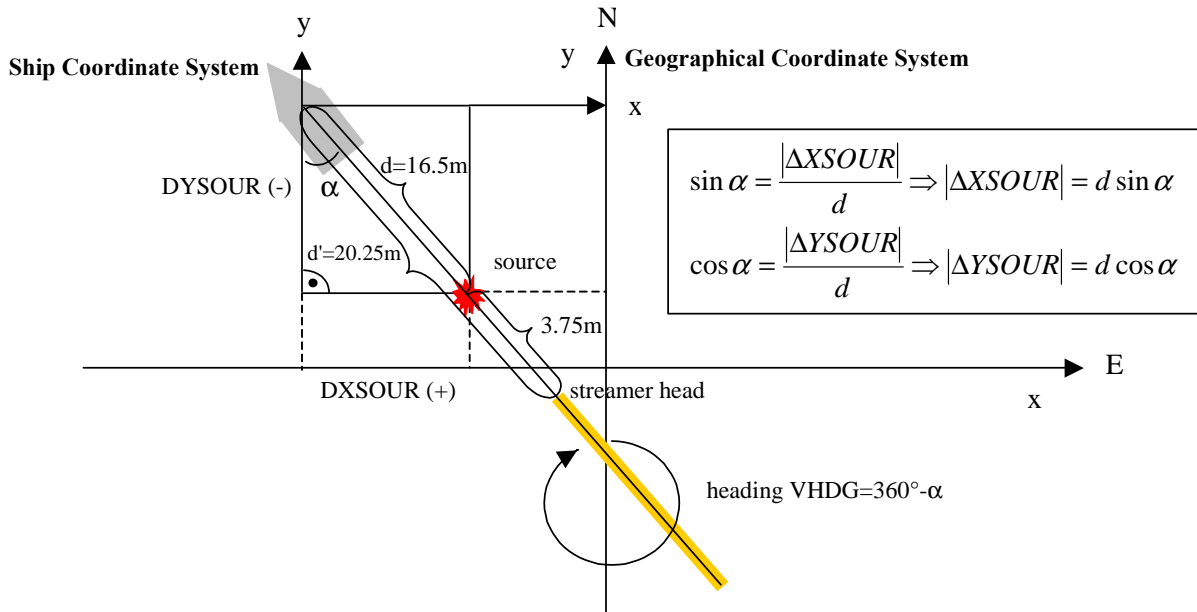


Figure 3: Calculation of variables **DXSOUR**, **DYSOUR**, **DXHEAD**, **DYHEAD** containing the source and streamer head positions relative to the ship coordinate system (SCS).

Table A-25 Navigation processing for Survey II: FORTRAN 77 code *gvt3Dnav*.

```

program gvt3Dnav
*****
* VARIABLE DECLARATION
*****
integer size
parameter (size=50000)
integer a,shot,line,line1,line2,totalb,totalr,totalv,n,limit
integer bhour(size),bmin(size),bsec(size),rhour(size),rmin(size),rsec(size),vhour(size),vmin(size),vsec(size)
integer bloc1(size),bloc2(size),rloc1(size),rloc2(size),vloc1(size),vloc2(size)
character ina*64,inb*64,inc*64,ind*64,navpla*64,navplb*64,navplc*64,navpld*64,navple*64,heading*20
double precision time(size),shottime(size),track(size)
double precision antn(size),ante(size),bn(size),be(size),bleun(size),bleue(size)
double precision rn(size),re(size),rougen(size),rougee(size),vn(size),ve(size),vertn(size),verte(size)
double precision bgpstime(size),rgpstime(size),vgpstime(size)
double precision diffb,diffr,diffv,critb,critr,critv,coeffb(size),coeffv(size)
double precision distb(size),distr(size),distv(size),alpha,VHDG(size)
*****
* DATA INPUT
*****
print*, 'First line number (RETURN) and last line number (RETURN)?'
read*,line1,line2
write(navpla,'(A,A)') 'V1-ANTEN','.SAV'
write(navplb,'(A,A)') 'B-GPS','.SAV'
write(navplc,'(A,A)') 'R-GPS','.SAV'
write(navpld,'(A,A)') 'V-GPS','.SAV'
write(navple,'(A,A)') 'QC','.txt'
open(22,file=navpla,status='unknown')
open(33,file=navplb,status='unknown')
open(44,file=navplc,status='unknown')
open(55,file=navpld,status='unknown')
open(66,file=navple,status='unknown')
write(22,'(A1,A3,A50)'),'H','104','3-D SURVEY OUCHY, AUGUST 2001'
write(33,'(A1,A3,A50)'),'H','104','3-D SURVEY OUCHY, AUGUST 2001'
write(44,'(A1,A3,A50)'),'H','104','3-D SURVEY OUCHY, AUGUST 2001'
write(55,'(A1,A3,A50)'),'H','104','3-D SURVEY OUCHY, AUGUST 2001'
write(66,*),'QUALITY CONTROL: MORE THAN 60 SECONDS BETWEEN TWO CONSECUTIVE COORDINATE TIMES'
write(66,*),'GPS ','LINE',' SHOT',' SHOTTIME ','BEFORE/AFTER SHOTTIME',' BEFORE & SHOTTIME'
*****
***** START OF DO LOOP 1 *****
*****
DO 900 line=line1,line2
shot=1
write(ina,'(A,I3.3,A)') 'obsfiles/3D',line,'.txt'
write(inb,'(A,I2.2,A)') 'obsfiles/bleu',line,'.txt'
write(inc,'(A,I2.2,A)') 'obsfiles/rouge',line,'.txt'
write(ind,'(A,I2.2,A)') 'obsfiles/vert',line,'.txt'
write(heading,'(A,I2.2)') 'HEADING/LIBNV',line-line1+1
open(10,file=ina,status='old')
open(11,file=inb,status='old')
open(12,file=inc,status='old')
open(13,file=ind,status='old')
open(14,file=heading,status='unknown')
write(14,'(A11,I2.2)'),'* LIBRI NV ',line-line1+1
50 CONTINUE
read(10,*,err=50,end=100) xbid,ante(shot),antn(shot),xbid,xbid,xbid,time(shot),
A xbid,xbid,xbid,xbid,xbid,xbid,xbid,xbid,track(shot)
*****
* MEANING OF VARIABLES:
*****
* time(shot) = UTC shot time [HMS]
* ante(shot) = swiss coordinate E for boat antenna at moment of shot
* antn(shot) = swiss coordinate N for boat antenna at moment of shot
*****
* CONVERSION FROM HOURS TO SECONDS AFTER MIDNIGHT
*****
shottime(shot)= AINT(time(shot)/10000)*3600+AINT((time(shot)-(AINT(time(shot)/10000)*10000))/100)*60
A +((time(shot)-(AINT(time(shot)/10000)*10000))/100)
A -(AINT((time(shot)-(AINT(time(shot)/10000)*10000))/100))*100
* print*,shot,time(shot),shottime(shot)
shot=shot+1
goto 50
100 CONTINUE

DO i=1, 15 ! skips 15 lines
read(11,*)
read(12,*)
read(13,*)
END DO

shot=1
CONTINUE
read(11,FMT=160,err=150,end=175) be(shot),bn(shot),bhour(shot),bmin(shot),bsec(shot)
* print*,shot,be(shot),bn(shot),bhour(shot),bmin(shot),bsec(shot)
160 format(15X,F10.3,5X,F10.3,40X,I2,1X,I2,1X,I2)
bgpstime(shot)=bhour(shot)*3600+bmin(shot)*60+bsec(shot)
* print*,shot,bhour(shot),bmin(shot),bsec(shot),bgpstime(shot)
shot=shot+1
goto150
175 CONTINUE
totalb=shot-1
print*,totalb
shot=1
CONTINUE
read(12,FMT=210,err=200,end=225) re(shot),rn(shot),rhour(shot),rmin(shot),rsec(shot)
210 format(15X,F10.3,5X,F10.3,40X,I2,1X,I2,1X,I2)
rgpstime(shot)=rhour(shot)*3600+rmin(shot)*60+rsec(shot)
* print*,shot,re(shot),rn(shot),rhour(shot),rmin(shot),rsec(shot)
shot=shot+1
goto200
225 CONTINUE
totalr=shot-1
shot=1

```

```

250 CONTINUE
    read(13,FMT=260,err=250,end=275) ve(shot),vn(shot),vhour(shot),vmin(shot),vsec(shot)
260 format(15X,F10.3,5X,F10.3,40X,I2,1X,I2,1X,I2)
    vgpstime(shot)=vhour(shot)*3600+vmin(shot)*60+vsec(shot)
    shot=shot+1
    goto250
275 CONTINUE
    totalv=shot-1
*****
* shottime(shot) = UTC shot time [s after midnight] *
* bgpstime(shot) = UTC time of GPS recordings on blue streamer [s after midnight] *
* rgpstime(shot) = UTC time of GPS recordings on red streamer [s after midnight] *
* vgpstime(shot) = UTC time of GPS recordings on green streamer [s after midnight] *
*
* INTERPOLATIONS
*****
* SORTING (FIND GPS COORDINATE TIMES THAT LIE AROUND SHOTTIME FOR EACH SHOT) *
*****
***** START OF DO LOOP 2 *****
*****
DO 350 shot=1,301
* print*, 'DO 350', shot
DO 325 n=1,totalb
    diffb=shottime(shot)-bgpstime(n)
    print*,n,diffb
    IF (diffb.gt.0) THEN
        bloc1(shot)=n
        bloc2(shot)=n+1
        print*,n,diffb,bloc1(shot),bloc2(shot)
    *
    END IF
325 CONTINUE
DO 330 n=1,totalr
    diffr=shottime(shot)-rgpstime(n)
    IF (diffr.gt.0) THEN
        rloc1(shot)=n
        rloc2(shot)=n+1
    *
    END IF
330 CONTINUE
DO 340 n=1,totalv
    diffv=shottime(shot)-vgpstime(n)
    IF (diffv.gt.0) THEN
        vloc1(shot)=n
        vloc2(shot)=n+1
    *
    END IF
340 CONTINUE
* print*,shot,bloc1(shot),bloc2(shot),be(bloc1(shot)),be(bloc2(shot)),bn(bloc2(shot))
350 CONTINUE
*****
***** END OF LOOP 2 *****
*****
* diff = time difference between shot time and GPS time on streamer
*
* loc1(shot) = shot number of GPS coordinates recorded closest before shot time
*
* loc2(shot) = shot number of GPS coordinates recorded closest after shot time
*
*
*
*****
* CALCULATION OF ANTENNA POSITIONS ON STREAMERS (SEE FIGURE 1) *
*****
***** START OF DO LOOP 3 *****
*****
DO 800 shot=1,301
    diffb=bgpstime(bloc2(shot))-bgpstime(bloc1(shot))
    diffr=rgpstime(rloc2(shot))-rgpstime(rloc1(shot))
    diffv=vgpstime(vloc2(shot))-vgpstime(vloc1(shot))
    critb=shottime(shot)-bgpstime(bloc1(shot))
    critr=shottime(shot)-rgpstime(rloc1(shot))
    critv=shottime(shot)-vgpstime(vloc1(shot))
    coeffb(shot)=critb/diffb
    coeffr(shot)=critr/diffr
    coeffv(shot)=critv/diffv
* CALL DISTANCE(bn(bloc2(shot)),bn(bloc1(shot)),be(bloc2(shot)),be(bloc1(shot)),distb(shot))
* CALL DISTANCE(rn(rloc2(shot)),rn(rloc1(shot)),re(rloc2(shot)),re(rloc1(shot)),distr(shot))
* CALL DISTANCE(vn(vloc2(shot)),vn(vloc1(shot)),ve(vloc2(shot)),ve(rloc1(shot)),distv(shot))
    limit=60
*****
* QUALITY CONTROL - CHANGE VARIABLE limit FOR THE MAXIMUM AMOUNT OF SECONDS USED BETWEEN TWO INTERPOLATED VALUES *
*****
IF (diffb.gt.limit) THEN
* bleun(shot)=149250
* bleue(shot)=536500
    bleun(shot)=bn(bloc1(shot))+coeffb(shot)*(bn(bloc2(shot))-bn(bloc1(shot)))
    bleue(shot)=be(bloc1(shot))+coeffb(shot)*(be(bloc2(shot))-be(bloc1(shot)))
    write(66,'(A5,I4,I5,F11.1,F22.1,F18.1)', 'BLEU ',line,shot,time(shot),diffb,critb)
ELSE
    bleun(shot)=bn(bloc1(shot))+coeffb(shot)*(bn(bloc2(shot))-bn(bloc1(shot)))
    bleue(shot)=be(bloc1(shot))+coeffb(shot)*(be(bloc2(shot))-be(bloc1(shot)))
END IF
IF (diffr.gt.limit) THEN
* rougen(shot)=149250
* rougee(shot)=536500
    rougen(shot)=rn(rloc1(shot))+coeffr(shot)*(rn(rloc2(shot))-rn(rloc1(shot)))
    rougee(shot)=re(rloc1(shot))+coeffr(shot)*(re(rloc2(shot))-re(rloc1(shot)))
    write(66,'(A5,I4,I5,F11.1,F22.1,F18.1)', 'ROUGE ',line,shot,time(shot),diffr,critr)
ELSE
    rougen(shot)=rn(rloc1(shot))+coeffr(shot)*(rn(rloc2(shot))-rn(rloc1(shot)))
    rougee(shot)=re(rloc1(shot))+coeffr(shot)*(re(rloc2(shot))-re(rloc1(shot)))
END IF
IF (diffv.gt.limit) THEN
* vertn(shot)=149250
* verte(shot)=536500

```



```

      vertn(shot)=vn(vloc1(shot))+coeffv(shot)*(vn(vloc2(shot))-vn(vloc1(shot)))
      verte(shot)=ve(vloc1(shot))+coeffv(shot)*(ve(vloc2(shot))-ve(vloc1(shot)))
      write(66,'(A5,I4,I5,F11.1,F22.1,F18.1)','VERT ',line,shot,time(shot),diffv,critv
ELSE
      vertn(shot)=vn(vloc1(shot))+coeffv(shot)*(vn(vloc2(shot))-vn(vloc1(shot)))
      verte(shot)=ve(vloc1(shot))+coeffv(shot)*(ve(vloc2(shot))-ve(vloc1(shot)))
END IF
***** OUTPUT FOR FURTHER NAVIGATION PROCESSING *****
      write(22,'(A4,A5,I2.2,A13,I8,I8,F11.2,F11.2)','A ', '3D0',line,' ',line,shot,ante(shot),antn(shot)
      write(33,'(A4,A5,I2.2,A13,I8,I8,F11.3,F11.3)','B ', '3D0',line,' ',line,shot,bleue(shot),bleun(shot)
      write(44,'(A4,A5,I2.2,A13,I8,I8,F11.3,F11.3)','R ', '3D0',line,' ',line,shot,rougee(shot),rougen(shot)
      write(55,'(A4,A5,I2.2,A13,I8,I8,F11.3,F11.3)','V ', '3D0',line,' ',line,shot,verte(shot),vertn(shot)
***** OUTPUT FOR QUALITY CONTROL PURPOSES *****
      write(22,'(A4,A5,I2.2,A13,I8,I8,F11.2,F11.2)','S11 ', '3D0',line,' ',line+3000,shot,ante(shot),antn(shot)
      write(33,'(A4,A5,I2.2,A13,I8,I8,F11.3,F11.3)','S11 ', '3D0',line,' ',line,shot,bleue(shot),bleun(shot)
      write(44,'(A4,A5,I2.2,A13,I8,I8,F11.3,F11.3)','S11 ', '3D0',line,' ',line+1000,shot,rougee(shot),rougen(shot)
      write(55,'(A4,A5,I2.2,A13,I8,I8,F11.3,F11.3)','S11 ', '3D0',line,' ',line+2000,shot,verte(shot),vertn(shot)
800 CONTINUE
***** END OF DO LOOP 3 *****
* diff = P2-P1 = difference in the GPS times closest before and after the shot time
* crit = t1-P1 = difference between the shot time and the GPS coordinate time closest before the shot time
* coeff(shot) = crit/diff
* dist(shot) = distance between two consecutive GPS coordinate points P1 and P2
* bleun(shot) = swiss coordinate N for blue GPS antenna at moment of shot
* bleue(shot) = swiss coordinate E for blue GPS antenna at moment of shot
*
* HEADING CALCULATION FOR EACH SHOT POINT AS AN AVERAGE OF THE DIRECTION OF THE 5 PRECEDING SHOT POINTS (SEE FIGURE 2)
***** START OF DO LOOP 4 *****
      DO 870 shot=1,301
        alpha=0
        IF (shot.gt.4) THEN
          DO 850 a=1,5
            alpha=alpha+track(shot-5+a)
950 CONTINUE
            VHDG(shot)=alpha/5
          ELSE
            DO 860 a=1,shot
              alpha=alpha+track(a)
860 CONTINUE
              VHDG(shot)=alpha/shot
            END IF
            beta=VHDG(shot)*(2*3.1415927/360)
            print*,shot,track(shot),VHDG(shot)
*****
            * VHDG = theoretical heading (Gyro compass)
            * DXHEAD = distance of streamer head relative to SCS in x-direction
            * DYHEAD = distance of streamer head relative to SCS in y-direction
            * DXSOUR = distance of source relative to SCS in x-direction
            * DYSOUR = distance of source relative to SCS in y-direction
            *
            * OUTPUT TO LIBRARY DIRECTORIES VHDG, BSL1, BSL2, BSL3, DXDYHEAD, DXDYSOURCE
            write(14,'(A30,A9,I2,A3,I3,A9,F5.1,A9)',' ', 'CHANG,NUM',line,'PT',shot,
A ' ',VHDG,ADD',VHDG(shot),' ,MULT0.0,'
870 CONTINUE
***** END OF DO LOOP 4 *****
      close(10,status='keep')
      close(11,status='keep')
      close(12,status='keep')
      close(13,status='keep')
      close(10,status='keep')
900 CONTINUE
***** END OF DO LOOP 1 *****
      close(22,status='keep')
      close(33,status='keep')
      close(44,status='keep')
      close(55,status='keep')
      close(66,status='keep')
950 END
*****
1000 SUBROUTINE DISTANCE(X2,X1,Y2,Y1,DIST)
*****
      double precision X1,X2,Y1,Y2,DIST
*****
      DIST=SQRT((X2-X1)**2+(Y2-Y1)**2)
1100 END
*****

```